Enhancing treatment response to neo-adjuvant radiation therapy in oesophageal cancer using novel dual action drugs targeting tumour energy metabolism and angiogenesis

Amy M. Buckley

Student No. 15301770

Ph.D. Thesis

Submitted to Trinity College Dublin for the degree of Doctor of Philosophy

June 2019

Department of Surgery, Trinity Translational Medicine Institute, Trinity College Dublin

Thesis Supervisors: Prof. Jacintha O'Sullivan[1] (Primary Supervisor), Prof. Breandán Kennedy[2] (Secondary Supervisor)

1. Trinity Translational Medicine Institute, Trinity College Dublin
2. School of Biomolecular and Biomedical Science, Conway Institute, University College Dublin

Declaration

I declare that this thesis has not been submitted as an exercise for a degree at this or any other university and it is entirely my own work. I agree to deposit this thesis in the University's open access institutional repository or allow the library to do so on my behalf, subject to Irish Copyright Legislation and Trinity College Library conditions of use and acknowledgement.

(Amy Buckley) (Date)

Thesis Abstract

Oesophageal cancer is an aggressive malignancy associated with a poor 5-year survival of <20%, accounting for over 400,000 deaths each year. The current standard of care for oesophageal adenocarcinoma (OAC) is neo-adjuvant therapy with chemotherapy or chemoradiation therapy to debulk the tumour prior to surgery. However, only 30% of patients achieve a complete pathological response to neo-adjuvant treatment. Currently there are no approved biomarkers which can be used in the clinic to stratify patients into good and poor responders prior to treatment. In addition, there are currently no approved radiosensitisers in the neo-adjuvant space which can be administered with the standard of care to enhance radioresponse. The radioresistant phenotype is polymodal and influenced by multiple biological processes. Altered energy metabolism and mitochondrial function were previously linked with the radioresistant phenotype in OAC. In this thesis we evaluated the action of our novel small molecule patented compounds on angiogenesis, energy metabolism and inflammatory secretions to enhance radioresponse.

Through phenotype-based screens we identified Pyrazinib (P3), a pyrazine phenol small molecule drug with anti-angiogenic and anti-metabolic activity *in-vivo* in zebrafish and *in-vitro* isogenic models of OAC radioresistance. Pyrazinib (P3) significantly inhibited intersegmental vessel development in zebrafish embryos. *In-vivo*, in zebrafish Pyrazinib (P3) significantly inhibited both oxygen consumption rate (OCR) and extracellular acidification rate (ECAR), measures of oxidative phosphorylation and glycolysis respectively, when evaluated using seahorse technology. *In-vitro*, in an isogenic model of OAC radioresistance, Pyrazinib (P3) significantly reduced OCR in both OE33P (radiation-sensitive) and OE33R (radiation-resistant) cells, in addition Pyrazinib (P3) produced a simultaneous reduction in ECAR in OE33R cells.

The ability of Pyrazinib (P3) to alter radiosensitivity was evaluated by clonogenic assay. Pyrazinib (P3) significantly reduced the surviving fraction in OE33P; radiation-sensitive and OE33R; radiation-resistant cells following 2, 4 and 6 Gy irradiation. Under hypoxic conditions Pyrazinib (P3), significantly reduced the surviving fraction of OE33R cells following 4 Gy irradiation. Pyrazinib (P3) did not significantly alter the sensitivity of cisplatin sensitive OE33 Cis P and cisplatin resistant OE33 Cis R cells to cisplatin treatment nor did it alter sensitivity of OE33P or OE33R cells to 5-flouracil.

Inflammation has previously been linked with the radioresistant phenotype in OAC. Proteomic profiling of 184 proteins found leukaemia inhibitory factor (LIF), to be significantly elevated in radioresistant OAC cells. Furthermore, significantly higher circulating levels of LIF were present

in the serum of treatment-naive OAC patients who had a subsequent poor pathological response to neo-adjuvant therapy. Quantitative PCR analysis revealed expression of LIF receptor (LIFR) may function as a predictive indicator of response to neo-adjuvant chemoradiation therapy in OAC. LIF was demonstrated to be actively secreted from human OAC treatment-naïve biopsies and significantly correlated with the secretion of bFGF, VEGF-A and IL-8. Importantly, LIF secretion negatively correlated with the percentage of tumour infiltrating lymphocytes in matched pre-treatment OAC patient biopsies. Elevated circulating LIF is a marker of poor response to neo-adjuvant treatment in OAC and secretion of this chemokine from the tumour is tightly linked with pro-tumorigenic mediators including bFGF, VEGF-A and IL-8. Targeting this pathway may reveal a novel mechanism to enhance neo-adjuvant treatment responses in OAC. Further investigation of the inflammatory secretions from our isogenic model of OAC radioresistance by multiplex ELISA showed 11 of 30 detected inflammatory and angiogenic factors were secreted at significantly higher levels in OE33R than OE33P cells; IL-2, IL-4, IL-6, IL-8, IL-12p70, IL-10, MCP-1, IP-10, ICAM. Pyrazinib (P3) significantly reduced the secretions of IL-4, IL-6, IL-8 and IL-13 in OE33R cells.

Furthermore, in this thesis for the first time we have demonstrated in real-time using the Seahorse Biosciences XFe24 analyser and human *ex-vivo* biopsies, OAC tumour biopsies have a significantly higher OCR, a measure of oxidative phosphorylation compared to ECAR, a measure of glycolysis highlighting the importance of aerobic respiration in OAC. Pyrazinib (P3), an anti-metabolic small molecule radiosensitiser significantly inhibited oxygen consumption rate in OAC biopsies. Furthermore, biopsies from OAC tumours can quickly adapt their metabolic rate to their environment to cope with hypoxia. Under conditions of hypoxia, Pyrazinib (P3) produced a simultaneous and significant reduction in both OCR and ECAR in OAC treatment-naïve biopsies. We demonstrated that the inflammatory secretome profile of OAC treatment-naïve biopsies is highly heterogeneous. OCR was significantly correlated with three secreted factors in the tumour conditioned media: VEGF-A, IL-1RA and TSLP. ECAR was significantly correlated with VEGF-A, IL-1RA, TSLP, IL-13, MIP-3α and TNF-α. Pyrazinib (P3) significantly inhibited IL-1β secretion and increased IL-3 and IL-17B secretions from treatment-naïve OAC patient tumour biopsies. Critically, Pyrazinib (P3) did not directly alter the expression of dendritic cell maturation markers.

The findings of this thesis have identified the small molecule compound Pyrazinib (P3) with anti-angiogenic, anti-metabolic and anti-inflammatory action which can enhance radiosensitivity both under normoxic and hypoxic conditions *in-vitro* in isogenic model of OAC radioresistance. Further pre-clinical development of this small molecule compound will been required in different *in-vivo* models to track radiosensitivity more precisely.

Acknowledgements

Firstly, I would like to sincerely thank my supervisor Prof. Jacintha O'Sullivan for her invaluable support, encouragement and guidance throughout my Ph.D. Thank you for always being there whenever I needed anything, I couldn't have asked for a better supervisor it has been a pleasure to work with you. Thank you to my second supervisor Prof. Breandán Kennedy for your continued support and guidance from the very beginning of this project and your constructive feedback throughout.

I would also like to thank Dr Joanne Lysaght, Dr Stephen Maher and Prof. John Reynolds for all of their constructive input and support throughout my Ph.D. Thank you to all of the members of the Dept. of Surgery; post-docs, Ph.D. students and biobank managers, past and present for all of your help and support throughout. It has been a pleasure to work in such a fun, friendly and supportive environment.

In addition, I would especially like to thank Dr Niamh Lynam-Lennon for her continued guidance and advice through my Ph.D. and for providing the isogenic cell line for my research. I would especially like to thank her for her endless time for all of my questions, especially at the start of my project.

I would like to acknowledge all of the patients who consented to participate in this research, which would have been impossible otherwise. Thank you to the Irish Cancer Society for funding this research.

To my parents, Jennifer and Colm, I could not have done this without you. Thank you for always believing in me and supporting me in everything I do. Thanks to my brother Ben for always being there and giving me a laugh whenever I needed it.

Finally, to Sam, thank you for your continuous support and for always being there for me no matter what part of the world we were in.

Ph.D. Outputs

Publications

Buckley, A. M., Bibby, B. AS., Dunne, M. R., Kennedy, S. A., Davern, M. B., Kennedy, B.N., Maher, S.G., and O'Sullivan, J. (2019). Characterisation of an isogenic model of cisplatin resistance in oesophageal adenocarcinoma cells. *Pharmaceuticals*. 12(1): p. 33.

Buckley, A. M., Dunne, M. R., Lynam-Lennon, N., Kennedy, S. A., Cannon, A., Reynolds, A. L., Maher, S.G., Reynolds, J.V., Kennedy, B.N. and O'Sullivan, J. (2019). Pyrazinib (P3),[(E)-2-(2-Pyrazin-2-yl-vinyl)-phenol], a small molecule pyrazine compound enhances radiosensitivity in oesophageal adenocarcinoma. *Cancer letters*, 447, 115-129.

Buckley, A. M., Lynam-Lennon, N., Kennedy, S. A., Dunne, M. R., Aird, J. J., Foley, E. K., Clarke, N., Ravi, N., O'Toole, D., Reynolds, J. V., Kennedy, B. N., and O'Sullivan, J. (2018). Leukaemia inhibitory factor is associated with treatment resistance in oesophageal adenocarcinoma. *Oncotarget*, 9(72), 33634-33647.

Butler, C.T., Kennedy A. S., **Buckley, A. M.**, Doyle, R., Conroy, E., Gallagher, W.M., O'Sullivan, J. and Kennedy, B.N. (2019). 1,4-dihydroxy Quininib Attenuates Growth of Colorectal Cancer Cells and Xenografts and Regulates the TIE-2 Signalling Pathway in Patient Tumours. *Oncotarget*, 10(38), 3725-3744.

Slater, K., Hoo, P. S., **Buckley, A. M.**, Piulats, J. M., Villanueva, A., Portela, A., and Kennedy, B. N. (2018). Evaluation of oncogenic cysteinyl leukotriene receptor 2 as a therapeutic target for uveal melanoma. *Cancer and Metastasis Reviews*, 37(2-3), 335-345.

Under Review

Buckley, A. M., Lynam-Lennon, N., O'Neill, H. and O'Sullivan, J. Novel strategies to enhance radiosensitivity in gastrointestinal cancer (Review Article) (*Nature Reviews Gastroenterology and Hepatology*).

In preparation

Buckley A. M., , Dunne, M. R, Morrissey M, Kennedy, S. A., Foley, E. K., Clarke, N., Ravi, N., O'Toole, D., Reynolds, J. V., Kennedy, B. N. and O'Sullivan, J. Real-time metabolic profiling reveals an altered and adaptive metabolic phenotype of oesophageal adenocarcinoma tumours (Research Article) (Target Journal – *Nature Metabolism*).

Oral Presentations

Invited Speaker at 'The Seahorse Technology Workshop' held in Trinity Biomedical Science Institute, Dublin, June 2016. Title of talk: '*Screening Metabolic Changes in Zebrafish'.*

Invited Speaker at the 'Young Cancer Researchers Networking Conference', Cork, June 2018. Title of talk: '*The action of P3, a novel radiosensitiser in Oesophageal Adenocarcinoma tumour microenvironment'.*

Invited Speaker at 'The Seahorse Technology Workshop', held in Trinity Biomedical Science Institute, Dublin, June 2018. Title of talk: '*Screening Metabolic Changes in Human treatment-naïve OAC patient biopsies'.*

Invited speaker at the 'Association for Radiation Research Conference', Belfast, June 2018. Title of talk: '*The action of a novel radiosensitiser within the Oesophageal Adenocarcinoma tumour microenvironment'*.

Invited speaker at the 'Irish Association for Cancer Research Conference', Belfast, February 2019. Title of talk*: 'Investigating the action of a novel radiosensitiser, Pyrazinib, in the oesophageal adenocarcinoma tumour microenvironment'.*

Poster Presentations

International *(Presenting Author)*

European Association of Cancer Research Conference, Manchester, July 2016. Title: Identification of novel dual action anti-angiogenic and anti-metabolic small molecule compounds to enhance radiosensitivity in oesophageal adenocarcinoma. Authors: Amy M. Buckley [1], Niamh Lynam-Lennon [1], Aoife Cannon [1], Roisin Dunne [1], Alison L. Reynolds [2], Breandán N. Kennedy [2] and Jacintha O'Sullivan [1].

European Association of Cancer Research: Radiation Breakthrough Conference, Oxford, March 2018. Title: The action of a novel radiosensitiser within the oesophageal adenocarcinoma tumour microenvironment**.** Authors: Amy M. Buckley [1], Niamh Lynam-Lennon [1], Susan A. Kennedy [1], Aoife Cannon [1], Maria Morrissey [1], Alison L. Reynolds [2], Breandán N. Kennedy [2] and Jacintha O'Sullivan [1].

National (*Presenting Author*)

Irish Association of Cancer Research, Cork, February 2016 Title: Identification of novel dual action anti-angiogenic and anti-metabolic small molecule compounds to enhance radiosensitivity in oesophageal adenocarcinoma**.** Amy M. Buckley [1], Niamh Lynam-Lennon [1], Aoife Cannon [1], Roisin Dunne[1], Alison L. Reynolds [2], Breandán N. Kennedy [2] and Jacintha O'Sullivan [1].

10th International Cancer Conference, Dublin, October 2016. Title: Identification of novel dual action anti-angiogenic and anti-metabolic small molecule compounds to enhance radiosensitivity in oesophageal adenocarcinoma. Authors; Amy M. Buckley [1], Niamh Lynam-Lennon [1], Aoife Cannon [1], Roisin Dunne [1], Alison L. Reynolds [2], Breandán N. Kennedy [2] and Jacintha O'Sullivan [1].

Irish Radiation Research Meeting, Dublin, November 2016. Title: Identification of novel dual action anti-angiogenic and anti-metabolic small molecule compounds to enhance radiosensitivity in oesophageal adenocarcinoma Authors; Amy M. Buckley [1], Niamh Lynam-Lennon [1], Aoife Cannon [1], Alison L. Reynolds [2], Breandán N. Kennedy [2] and Jacintha O'Sullivan [1].

Irish Association of Pharmacologists Conference, Dublin, November 2016. Title: Identification of novel dual action anti-angiogenic and anti-metabolic small molecule compounds to enhance radiosensitivity in oesophageal adenocarcinoma**.** Authors: Amy M. Buckley [1], Niamh Lynam-Lennon [1], Aoife Cannon [1], Roisin Dunne [1], Alison L. Reynolds [2], Breandán N. Kennedy [2] and Jacintha O'Sullivan [1].

Irish Association of Cancer Research Meeting, Kilkenny, February 2017. Title: Dual action anti-angiogenic and anti-metabolic compounds enhance radiosensitivity in an isogenic model of oesophageal adenocarcinoma radioresistance. Authors: Amy Buckley [1], Niamh Lynam-Lennon [1], Aoife Cannon [1], Roisin Dunne [1], Alison Reynolds [2], Breandán Kennedy [2] and Jacintha O'Sullivan [1].

Irish Immunological Society Conference, Dublin 2017. Title: A novel anti-metabolic, anti-angiogenic and anti-inflammatory small molecule compound can enhance radiosensitivity in oesophageal adenocarcinoma. Authors: Amy Buckley [1], Niamh Lynam-Lennon [1], Susan Kennedy [1], Aoife Cannon [1], Alison L. Reynolds [2], David Gomez-Matallanas [3], Dermot O'Toole [1], John V. Reynolds [1], Breandán N. Kennedy [2], Jacintha O'Sullivan [1].

Affiliations:

[1] Trinity Translational Medicine Institute, St James Hospital Campus, Trinity College Dublin.

[2] School of Biomolecular and Biomedical Science, Conway Institute, University College Dublin.

[3] Systems Biology Ireland, University College Dublin.

Courses and Credits

LAST- Laboratory Animal Science and Training – September 2015 (Certificate Awarded)

Good Clinical Practice Course November 2015

Molecular Medicine Techniques Course –December 2015, UCD Conway Institute

Module 13 Tumour Microenvironment -Translational Oncology MSc Module – Feb-April 2016, Trinity Translational Medicine Institute – 5 ECTS (Awarded a Distinction)

SMART Futures Course – 15th August 2016, Trinity Translational Medicine Institute

Irish Cancer Society Media Training Workshop, August 2016, Irish Cancer Society Offices, Dublin

Module 4 Radiation, Chemotherapy and Molecular Targeted Therapies - Translational Oncology MSc Module – Oct-Dec 2016, Trinity Translational Medicine Institute – 5 ECTS (Awarded a Distinction)

Awards

Best poster Award at the 10th International Cancer Conference, Dublin, 2016.

Travel Bursary Award from Don Whitley Scientific to attend the Irish Association of Cancer Research Conference February, Dublin, 2018.

Travel Bursary from European Association of Cancer Research to attend Radiation Breakthrough conference, Oxford, 2018.

Travel bursary award from the association of radiation research to attend Association of Radiation Research conference, Belfast 2018.

Table of Contents

List of Figures

List of Tables

Abbreviations

2-DG	2-deoxy-D-glucose
5-FU	Fluorouracil
α-KG	Alpha ketoglutarate
Abs	Absorbance
Acetyl CoA	Acetyl coenzyme A
AMPK	Adenosine monophosphate-activated protein kinase
ANG	Angiopoietin
ANOVA	Analysis of variance
ARCON	Accelerated radiotherapy with carbogen and nicotinamide
ATM	Ataxia telangiectasia mutated
ATP	Adenosine tri-phosphate
ATP5B	Adenosine triphosphate synthase, H+ transporting, mitochondrial F1 complex, β polypeptide
ATR	ATM-Rad3-related
Bcl-2	B-cell lymphoma-2
Bcl-xL	B-cell lymphoma-extra-large
BER	Base excision repair
B-FGF	Basic fibroblast growth factor
BMI	Body mass index
BRCA1/2	Breast cancer type 1 susceptibility protein
BrdU	5-bromo-2'deoxyuridine
BSA	Bovine serum albumin
cDNA	Complementary deoxyribonucleic acid
Chk1/2	Checkpoint kinases 1/2
Ct	Threshold cycle
CT	Computerised tomography
CTLA-4	cytotoxic T-lymphocyte-associated protein 4
CRC	Colorectal Cancer
CRT	Chemoradiation therapy
CysLT1	Cysteinyl leukotriene receptor 1
DCF	Dichlorofluorescein
DMSO	Dimethyl sulfoxide
DMEM	Dulbecco's Modified Eagle's medium
DNA	Deoxyribonucleic acid
DNA-PK	DNA-dependent protein kinase

dNTPs	Deoxyribose nucleotide triphosphates
Dpf	Days post fertilisation
DSB	Double strand break
ECAR	Extracellular acidification rate
EGF	Epidermal growth factor
EGFR	Epidermal growth factor receptor
ELISA	Enzyme-linked immunosorbent assay
EM	Embryo medium
EUS	Endoscopic ultrasound
$FADH_2$	Flavin adenine dinucleotide
FCCP	Carbonylcyanide p-trifluoromethoxyphenylhydrazone
FBS	Foetal bovine serum
FDG	Fluorodeoxyglucose
GFP	Green fluorescent protein
GORD	Gastro-oesophageal reflux disease
Gy	Gray, radiation units
HER2	Human epidermal growth factor receptor 2
HIF	Hypoxia inducible factor
Hpf	Hours post fertilisation
HR	Homologous recombination
HRP	Horseradish peroxidise
IFN-γ	Interferon gamma
IL	Interleukin
LIF	Leukaemia Inhibitory factor
LIFR	Leukaemia Inhibitory factor receptor
LPS	Lipopolysaccharide
MCP-1	Monocyte chemoattractant protein-1
MFI	Mean nuclear fluorescence intensity
miR/miRNA	MicroRNA
MLH1	MutL homologue 1
MMP	Matrix metalloproteinase
MMR	Mismatch repair
MMS19	Nucleotide excision repair protein homolog
mRNA	Messenger RNA
N	Node/nodal
n	Sample size
NADH	Nicotinamide adenine dinucleotide

Neo-CT	Neo-adjuvant chemotherapy
Neo-CRT	Neo-adjuvant chemoradiation therapy
NFκβ	Nuclear factor κ-light-chain-enhancer of activated B cells
NHEJ	Non-homologous end joining
OCR	Oxygen Consumption Rate
OAC	Oesophageal adenocarcinoma
OE33P	OE33 parental
OE33R	OE33 radioresistant
PARP	Poly-ADP ribose polymerase
PDL-1	Programmed death-ligand 1
PBS	Phosphate buffered saline
pCR	Pathological complete response
PDGF	Platelet derived growth factor
PE	Plating efficiency
PET	Positron emission tomography
PFA	Paraformaldehyde
PGC-1α	Peroxisome proliferator-activated receptor γ coactivator-1α
PI3K	Phosphoinositide 3-kinase
PKcs	Protein kinase catalytic subunit
qPCR	Quantitative polymerase chain reaction
ROS	Reactive oxygen species
RPMI-1640	Roswell park memorial institute-1640
RT	Room Temperature
SCC	Squamous cell carcinoma
SEM	Standard error of the mean
SF	surviving fraction
SMUG1	Single-strand-selective mono-functional uracil-DNA glycosylase 1
SSB	Single strand break
TAMs	Tumour associated macrophages
TCA	The tricarboxylic acid cycle
TCM	Tumour conditioned media
TNF-α	Tumour necrosis factor alpha
TNM	Tumour node metastasis
TRG	Tumour regression grade
TSLP	Thymic stromal lymphopoietin
VEGF-A	Vascular endothelial growth factor A
VEGF-R2	Vascular endothelial growth factor receptor 2

XIAP	X-linked inhibitor of apoptosis protein

1. Chapter 1 – General Introduction

1.1. Oesophageal cancer

1.1.1. *Epidemiology and incidence*

Oesophageal cancer is the eighth most common cancer worldwide and the 6th most common cause of cancer related death, accounting for approximately 400,000 deaths annually [1]. Oesophageal cancer is primarily classified into two histological subtypes, squamous cell carcinoma (SCC) and oesophageal adenocarcinoma (OAC) [1]. SCC and OAC have distinct pathological characteristics. SCC can occur in all subsections of the oesophagus, but predominantly occurs in the middle and upper third whilst the majority of OAC's are located in the distal oesophagus or gastro-oesophageal junction **(Figure 1-1)** [2-4].

Whilst SCC is the predominant subtype globally, in western populations, the incidence of OAC has increased by approximately 48% over the past 15 years **(Figure 1-2)** [1, 5]. Critically, over the next 10 years, the incidence of oesophageal cancer is expected to increase by 140% [6]. In Ireland, the average number of new oesophageal cancer cases diagnosed each year is 182 in women and 301 in men [7]. The incidence of each subtype is highly variable depending on geographical location **(Figure 1-3)**. The highest incidence rates for OAC are in the UK, Netherlands and Ireland [5]. The highest incidence rates for SCC occur in Asia and east Africa [5]. The prognosis of oesophageal cancer remains poor with the overall five-year survival rate less than 20% in most developed countries, the best outcomes are associated with early disease diagnosis [1, 5]. In Ireland, between 2005-2009, oesophageal cancer accounted for 7.62 deaths per 100,000 people annually [8].

The incidence of OAC is 3-9 times higher in men than women, depending on geographical location [5]. To date there is insufficient evidence to explain the vast difference in gender risk. For females, breastfeeding may reduce OAC risk as female sex hormones may provide a protective effect against disease development [9]. Male and female obesity rates are similar in the West, however visceral adipose tissue around the abdomen is more often observed in males and may contribute to increased risk of disease development [10].

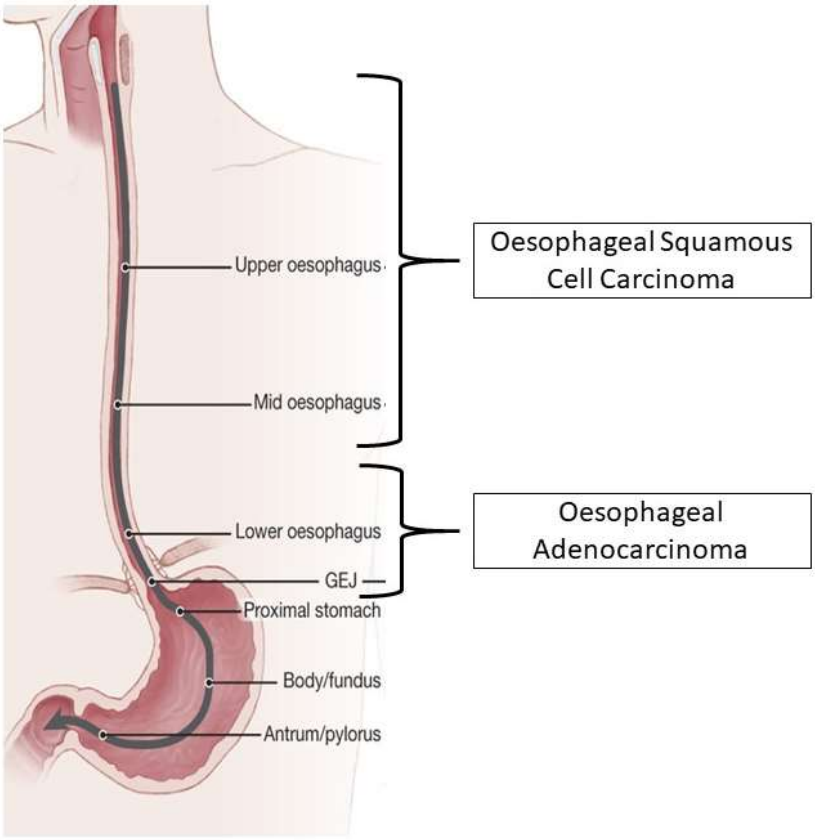

Figure 1-1 Location of SCC and OAC tumours.
Figure outlining the physical location of SCC and OAC tumours within the oesophagus. SCC tumours are predominantly located in the middle and upper third of the oesophagus. OAC tumours are predominantly located in the distal third of the oesophagus and at the gastro-oesophageal junction. *Image adapted from www.cancer.gov*.

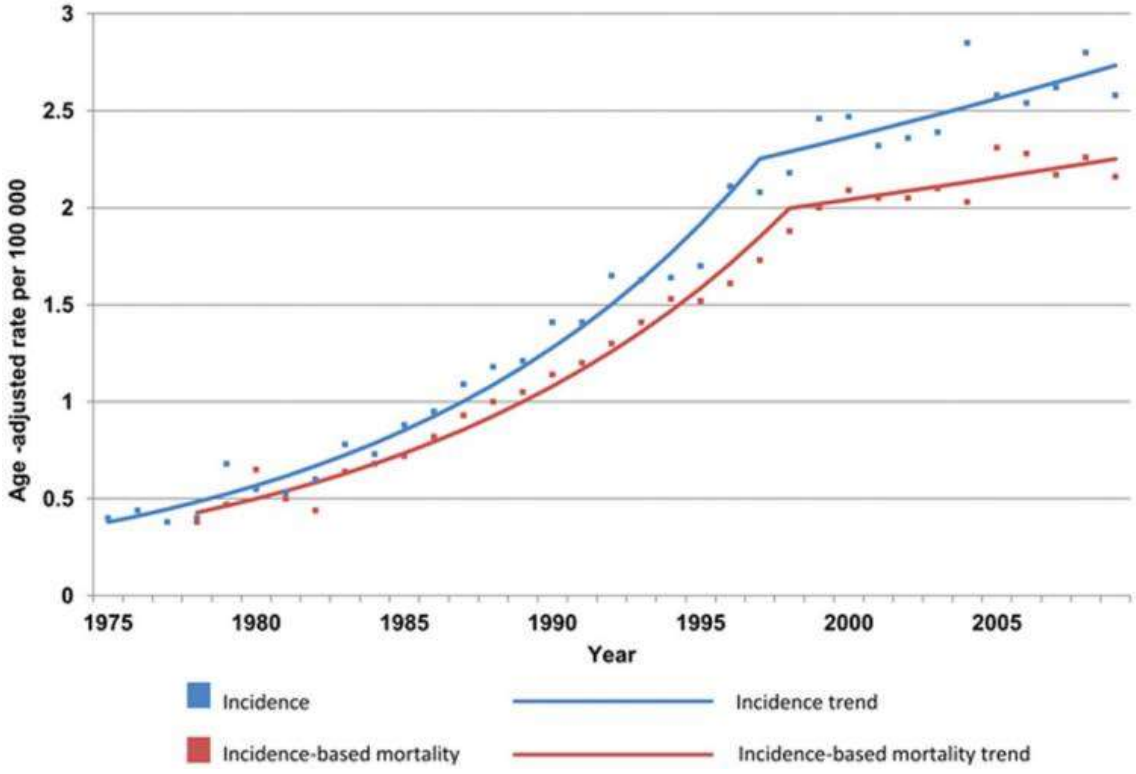

Figure 1-2 OAC incidence and incidence-based mortality, 1975 to 2009.
This figure outlines both the incidence of OAC and the incidence-based mortality of OAC between 1975 and 2009. *Image taken from Hur et al.* [11].

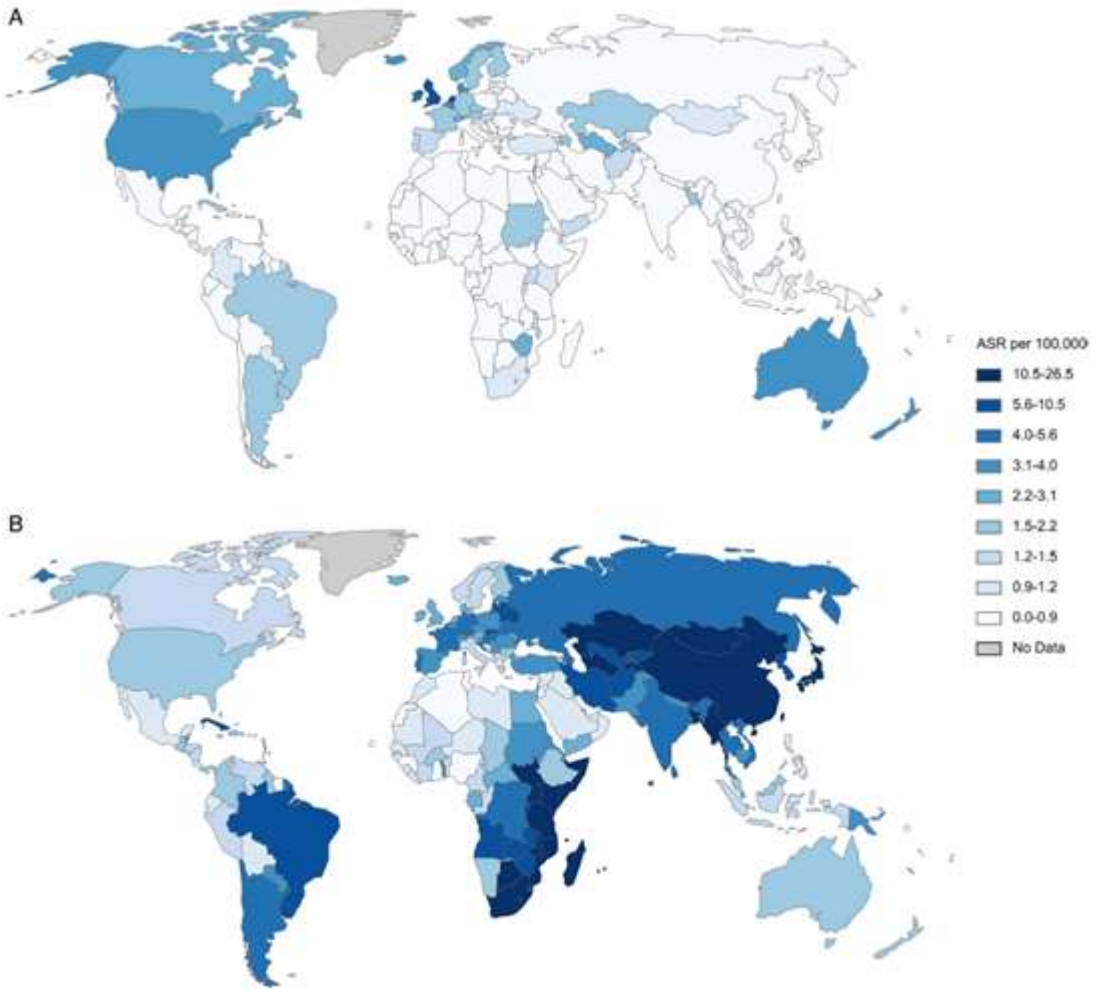

Figure 1-3 Global incidence rates of OAC and SCC and global distribution of disease in men. Figure illustrating the age standardised incidence rate (ASR) of **(A)** OAC and **(B)** SSC per 100,000 men. *Image taken from Arnold et al.* [5].

1.1.2. *Risk factors of oesophageal adenocarcinoma*

There are three major risk factors for the development of OAC including gastro-oesophageal reflux disease (GORD), the pre-disposing condition Barrett's oesophagus and obesity.

GORD is a common clinical condition and heartburn is the most frequent symptom. GORD induces oesophageal inflammation and consequent oxidative stress leading to DNA damage [12, 13]. Both acid and bile can activate oncogenic pathways. Bile acid induces DNA damage, decreases proliferation and increases apoptosis whilst bile salts induce DNA damage and affect proliferation in a pH-dependent manner and promote resistance to apoptosis [12, 13].

Barrett's oesophagus is characterised by chronic tissue inflammation which results in the transition of the stratified normal epithelium of the oesophagus to a single layered mucin-secreting columnar epithelium [14]. Tissue inflammation and a dysregulated immune response provide the ideal microenvironment for OAC development [15]. Barrett's oesophagus is considered the strongest risk factor for OAC, increasing the risk of incidence by 30-40 fold over the normal population [16]. The development of OAC occurs in step-wise progression from no reflux disease to GORD to Barrett's oesophagus to OAC [17]. Only approximately 10% of patients will progress from GORD to Barrett's oesophagus [18]. The overall risk of cancer developing in Barrett's oesophagus patients is estimated to be approximately 0.12–0.5% per year [19-21]. Interestingly a study by Drahos *et al*. found that the metabolic syndrome increases the risk of Barrett's oesophagus in the absence of gastroesophageal reflux [22]. Supporting this, our group has shown that patients with Barrett's oesophagus commonly display symptoms of the metabolic syndrome, characterised by visceral obesity, blood lipid disorders, insulin resistance and type II diabetes [23]. This study by Ryan *et al.* demonstrated that 46% of the Barrett's oesophagus patients in their cohort had the metabolic syndrome and this was significantly correlated with the length of intestinal metaplasia [23]. The step-wise progression from GORD to Barrett's oesophagus to OAC over ~10 years should provide the opportunity for early diagnosis and prevention of OAC [24]. However, disease progression is relatively asymptomatic and less than 5% of patients diagnosed with OAC have a precancerous diagnosis of Barrett's oesophagus [24].

The dramatic increase in the incidence of OAC in the Western World has paralleled with increasing rates of obesity. A meta-analysis of 14 studies found that a body mass index of greater than 25 was associated with an increased risk of OAC in both males and females [25]. In addition as body mass index increased the relative risk of OAC increased [25]. Another meta-analysis of 22 studies found a nearly threefold increase in risk with a body mass index greater than 30 kg/m^2 [26]. Altered secretion of adipokines such as leptin produced by visceral adipose tissue, often

observed in men, has been suggested to contribute to markedly differential incidence of OAC by sex [27]. This has been supported by the observation that patients with Barrett's oesophagus have a greater waist circumference than population controls [28].

1.1.3. *Diagnosis and staging of oesophageal adenocarcinoma*

Early stage OAC is often asymptomatic and as a result approximately 50% of patients present with locally advanced disease at first diagnosis [29]. Diagnosis of OAC is commonly coupled with patients presenting with common symptoms including dysphagia and unexplained weight loss [30]. Three diagnostic tests are commonly used in the diagnosis of OAC including endoscopic ultrasound (EUS), a computed tomographic (CT) scan and positron-emission tomography (PET). EUS is used to determine tumour (T) stage and has been shown to be the most accurate method for nodal (N) staging [31, 32]. A CT scan is used to assess the primary tumour and can detect lymph node metastasis, if the appearance of the node is enlarged [32]. A CT scan is limited to defining the local extent and nodal involvement in OAC but is useful in identifying the presence of distant disease such as liver or lung metastases [32]. PET with fludeoxyglucose (^{18}F-FDG) is used to detect tissues with high metabolic activity [33]. The detection of ^{18}F-FDG uptake depends on the capacity of the PET detector to detect the natural radioactive decay of fluorine-18 attached to this glucose analogue. [34] PET scans improve staging by detecting previously unsuspected metastatic disease in up to 15-20% of patients and should be considered when the CT scan does not show metastatic disease [33, 35]. However, PET scans are not without their limitations and have been associated with both false positive and false negative results which can limit their sensitivity and specificity and as a result their clinical efficacy [34]. The clinical efficacy of PET scans is influenced by multiple factors including tumour size, tumour stage and the cellular content of the tumour [34].

Oesophageal cancer staging is based on the depth of tumour invasion, involvement of regional lymph nodes, and the presence or absence of metastatic disease [36]. Clinical staging of OAC is carried out using the TNM system which was developed by the American Joint Committee on Cancer (AJCC) [37]. The staging system that establishes tumour-node-metastasis (TNM) sub-classifications based on the depth of invasion of the primary tumour (T), lymph node involvement (N), and extent of metastatic disease (M) **(Table 1-1) (Table 1-2)**. Accurate pre-treatment staging of OAC and subsequent stage-appropriate treatment is crucial to optimise OAC patient outcomes.

Table 1-1 TNM classification and histological grading for OAC.
This table outlines the scoring system used to give an OAC a tumour, node and metastasis score (TNM) based on tumour invasion, nodal involvement and the presence or absence of metastases. Histological grades can also be determined based on the level of tumour differentiation.

T classification	
Tis	High grade dysplasia
T1	Tumour invades lamina propria, muscularis mucosa (T1a) or submucosa (T1b)
T2	Tumour invades muscularis propria
T3	Tumour invades adventitia
T4	Tumour invades adjacent structures; T4a resectable, T4b unresectable
N classification	
N0	No regional lymph node metastasis
N1	1 to 2 positive lymph node metastasis
N2	3 to 6 positive lymph node metastasis
N3	≥7 positive lymph node metastasis
M classification	
M0	No distant metastasis
M1	Distant metastasis
Histological grade	
G1	Well differentiated
G2	Moderately differentiated
G3	Poorly differentiated
G4	Undifferentiated

Table 1-2 OAC tumour stage classification based on TNM.
This table outlines how a tumour stage is determined based on the tumour node and metastasis score described in **Table 1-1**.

Stage	**Tumour**	**Node**	**Metastasis**	**Therapeutic options**
0	Tis	N0	M0	Local ablative therapy
I	T1	N0	M0	Surgery
IIA	T2	N0	M0	Surgery
	T3	N0	M0	
IIB	T1	N1	M0	Neo-adjuvant therapy with or without surgery
	T2	N1	M0	
III	T3	N1	M0	Neo-adjuvant therapy with or without surgery
	T4	Any N	M0	
IVA	Any T	Any N	M1a	Chemotherapy or radiation therapy with or without surgery
IVB	Any T	Any N	M1b	Palliative treatment

1.1.4. *Treatment of oesophageal adenocarcinoma*

Treatment options for OAC tumours include local mucosal resection, ablation therapies, oesophagectomy, chemotherapy and chemoradiation therapy both pre- and post-operatively [38]. The recommended treatment for each patient is dependent on multiple factors including tumour stage, tumour location, and the patients' medical fitness for receiving a particular therapeutic modality.

Patients with T1-2N0 OAC tumour are typically recommended to undergo surgery without the induction treatment [38]. The standard treatment for patients with locally advanced operable OAC is neo-adjuvant therapy and surgical resection. The neo-adjuvant therapies are utilised to debulk the primary tumour prior to surgery [39]. Surgery offers the best chance of loco-regional control and neo-adjuvant treatment aims to reduce tumour burden prior to surgery to improve post-operative outcome, neo-adjuvant chemoradiation therapy in combination with surgery has been associated with higher rates of overall survival [40-42]. In addition surgical resection aims to reduce local reoccurrence and systemic disease [43].

In Ireland, the current standard of care for OAC focuses on neo-adjuvant treatment with chemotherapy (neo-CT) alone or in combination with radiation; neo-adjuvant chemoradiation (neo-CRT) for locally advanced tumours, prior to surgery [40]. The Cancer Trials Ireland-sponsored Neo-AEGIS randomised, phase III clinical trial, is comparing neo-CT (MAGIC protocol) to neo-CRT (CROSS protocol) in OAC **(Figure 1-4)** [44]. The MAGIC chemotherapy protocol consists of administration of epirubicin, cisplatin or oxaliplatin, and 5-Fluorouracil (5-FU) or capecitabine chemotherapy pre- and post-operatively, the CROSS protocol consists of administration of carboplatin and paclitaxel chemotherapy with fractionated radiotherapy of 41.4 Gy over five weeks [45, 46]. Since the initiation of the Neo-AEGIS trial, the perioperative chemotherapy protocol FLOT, which includes treatment with docetaxel, oxaliplatin , leucovorin and 5-FU prior to surgery was found to significantly improve patient outcome compared to the combination of epirubicin, cisplatin and 5-FU (MAGIC) in a phase III randomised controlled trial [47]. As a result, the FLOT protocol is now offered as an option in addition to MAGIC as standard treatment regimen of chemotherapy in the Neo-AEGIS trial. The primary end-point of the Neo-AEGIS trial is overall survival with 3 year follow up [44]. The secondary endpoints of this trial are disease-free survival, recurrence rates, clinical and pathological response rates, toxicities of induction regimens, post-operative pathology and tumour regression grade, operative in-hospital complications, and health-related quality of life **(Figure 1-4)** [44].

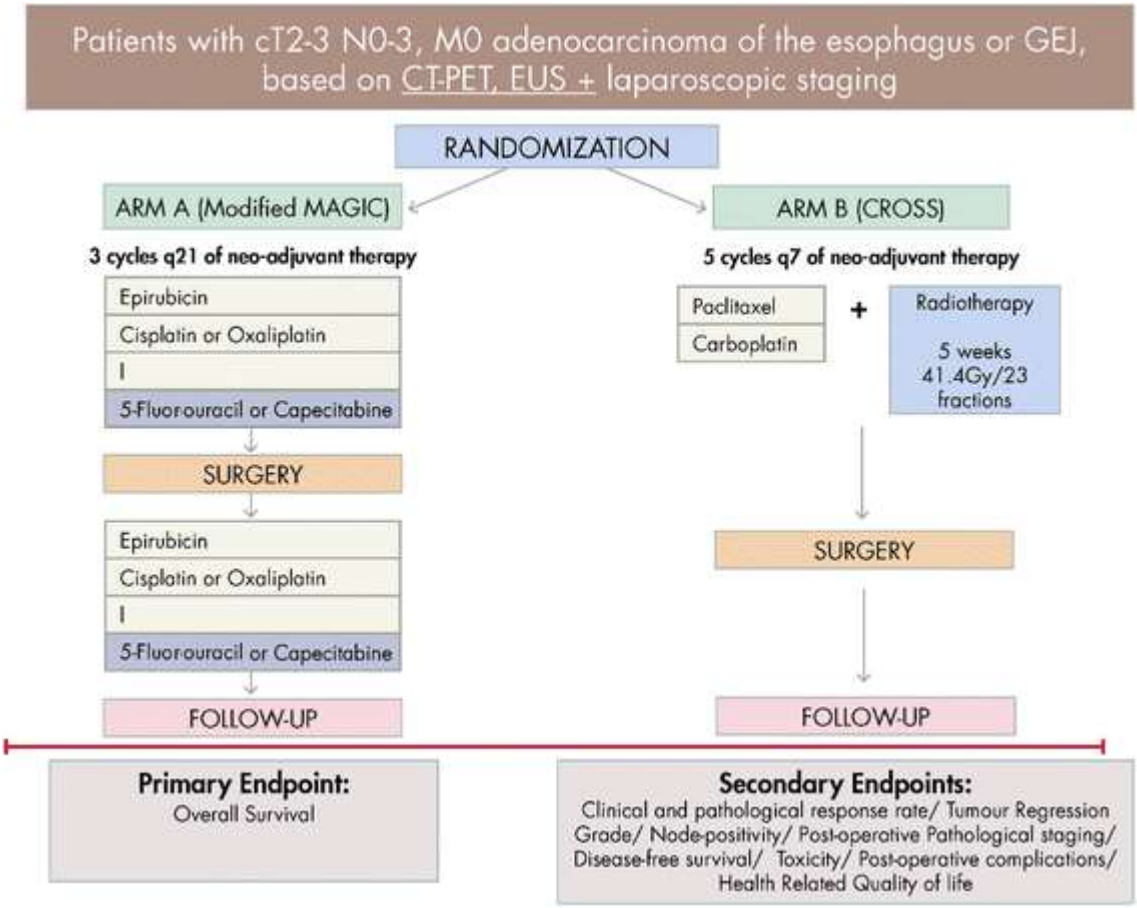

Figure 1-4 Neo-AEGIS trial schematic.
This figure illustrates the two treatment arms of the neo-AEGIS trial, the modified MAGIC regimen and the CROSS regimen, and outlines both the primary and secondary endpoints of the trial. *Image taken from Reynolds et al.* [44].

The cytotoxic chemotherapies which are administered pre- or post-operatively to OAC patients are classified based on their cytotoxic effect into alkylating agents, anti-metabolites, anti-microtubule agents, topoisomerase inhibitors and cytotoxic antibiotics.

Cisplatin, carboplatin and oxaliplatin are platinum-based alkylating agents which form covalent bonds with DNA resulting in DNA intercalation and the formation of DNA adducts [48]. These DNA adducts disrupt DNA replication and transcription and result in the induction cell death. Importantly, alkylating agents are cell cycle independent as they can bind to the DNA during all stages of the cell cycle [49].

Paclitaxel is an anti-microtubule taxane agent which stabilises microtubules and inhibits microtubule disassembly [50]. During cell division microtubules form the mitotic spindle, paclitaxel inhibits normal microtubule function and induces mitotic catastrophe and cell death during G_2/M phase of the cell cycle [49].

Anti-metabolite agents capecitabine and 5-FU are pyrimidines which are incorporated into DNA and RNA. The thymidine synthase enzyme is the only source of *de novo* thymine base production in the cell, inhibition of thymine synthase inhibits DNA synthesis [51]. The cytotoxic effects of 5-FU are S phase cell cycle dependent [52]. The metabolites of 5-FU interfere with RNA function, induce DNA damage and interfere with DNA replication and transcription to induce cell death [52].

Epirubicin is an anthracycline and topoisomerase inhibitor [53]. The topoisomerase II enzyme relieves supercoiled DNA during replication by inducing temporary double strand DNA breaks which are immediately repaired. Epirubicin inhibits topoisomerase II and interferes with DNA replication during S phase of the cell cycle [54].

Ionising radiation is a crucial treatment modality used to exert local tumour control in over 50% of solid cancers [55]. Irradiation aims to exert local control through the induction of double strand breaks (DSB) to induce cellular DNA damage [55].

A number of patients are not suitable for neo-adjuvant treatment and surgical resection. Approximately 50% of patients have evidence of distant metastatic disease at the time of diagnosis [36]. Palliative therapy is recommended for patients with metastatic disease and can include chemotherapy, clinical trial enrolment if available and suitable, or best supportive care [36].

1.1.5. *Oesophageal adenocarcinoma tumour response to treatment*

Despite major advances in the multimodal approach to treat locally advanced OAC, the 5-year survival of patients treated with curative intent remains poor [56, 57]. Unfortunately, on average only 20-30% of patients show a complete pathological response (pCR) to neo-adjuvant therapy with 70-80% of patients receiving a toxic treatment with little to no therapeutic gain and a subsequent delay to surgery [43, 55, 58]. Importantly, there are currently no clinico-pathological markers available to stratify patients who will achieve a beneficial response to neo-adjuvant therapy. Tumour response to neo-CT/CRT is the best predictor of both disease-free and overall survival [59]. Five-year survival rates are increased up to 60% for patients achieving a pCR, irrespective of treatment protocol, tumour histology or stage [60, 61].

Several classification systems for grading tumour response to neo-adjuvant therapy have been developed, but the most widely used is the Mandard system, which is divided into 5 tumour regression grades (TRG) 1-5 **(Figure 1-5)** [62]. TRG 1 represents a complete response and is

characterised by fibrosis within the oesophageal wall with no viable residual tumour cells. TRG 2 is characterised by rare residual tumour cells within the fibrosis. TRG 3 is characterised by predominant fibrosis with residual tumour cells [62]. TRG 4 represents residual tumour cells outgrowing fibrosis, whilst TRG 5 represents a complete absence of regression change. A TRG of 1-3 was significantly associated with disease-free survival, when compared to TRG 4-5 [62].

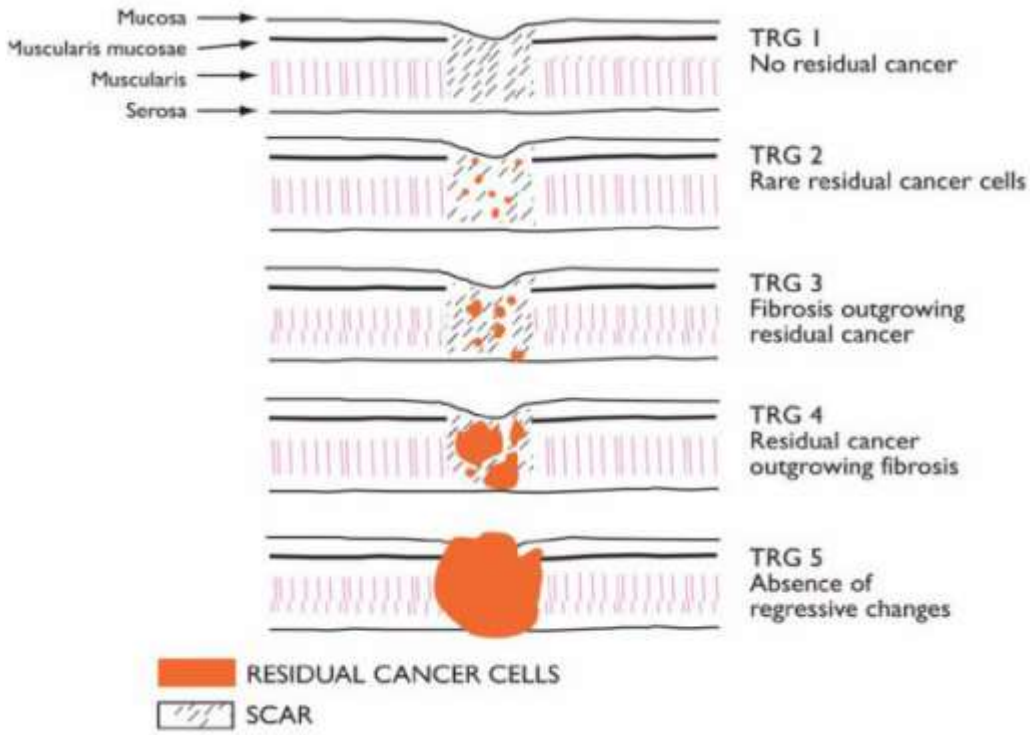

Figure 1-5 Mandard's Tumour Regression Grade (TRG) scoring system for tumour response to radiation.
Diagrammatic representation of Mandard's tumour regression grade scoring system. TRG 1 indicates that no viable tumour cells remain after treatment, TRG 2 indicates rare residual cancer cells remain, TRG 3 indicates fibrosis outgrows residual cancer, TRG 4 indicates residual cancer outgrows fibrosis and TRG 5 indicates that there is no evidence of tumour regression. *Image taken from Mandard et al*. [62].

Combination therapies aim to overcome resistance by challenging the tumour with a variety of cytotoxic mechanisms to overwhelm the repair and survival pathways to exceed the sublethal threshold of cellular damage of cancer cells to subsequently induce cell death [63]. Randomised clinical trials continue to inform best clinical practice in order to identify the best treatment combinations for improved response and overall survival, the key clinical trials informing clinical practice based on pathological complete response and overall 5 year survival are outlined in **Table 1-3**.

Table 1-3 Key clinical trials informing the treatment of oesophageal cancer.
This table details the trial name, oesophageal tumour type, patient number, treatment arms, pathological complete response rates (pCR), median survival and 5-year survival in key clinical trials which have informed clinical treatment of oesophageal cancer.

Trial	Tumour Type and Patient number	Treatment arms	pCR rate (%)	Median Survival (Months)	5-year Survival (%)
OE02 [64]	SCC (n=269)	Surgery	2	13	17
	OAC (n=533)	Neo-CT	4	17	23
MAGIC [45]	OAC/Junctional (n=503)	Surgery	0	20	23
		Peri-operative chemotherapy	0	24	36
ACCORD 07 FNCLCC-FFCD 9703 [57]	OAC (n=224)	Surgery	0	N/A	24
		Peri-operative chemotherapy	3	N/A	38
CROSS [56]	SCC (n=96)	Surgery	0	24	33
	OAC (n=270)	Neo-CRT	29	49	47
FLOT4 [65]	OAC (n=716)	MAGIC CT	Not yet reported	35	Not yet reported
		FLOT CT	Not yet reported	50	Not yet reported

1.1.6. *Targeted therapies which have been previously investigated in OAC*

As previously described the primary treatment modality for OAC patients with advanced disease is combination chemotherapy administered in conjunction with radiotherapy. Oesophageal cancers are associated with a high mutational burden and as a result a number of alternative targeted therapies have been investigated for the treatment of oesophageal cancer with varying success [66].

HER2 is overexpressed in approximately 24% of OAC patient tumours [67]. Trastuzumab, an anti-HER2 monoclonal antibody, was the first targeted agent approved for the treatment of advanced oesophageal and gastroesophageal patients in combination with first-line chemotherapy for patients with ERBB2/HER2-positive disease [66]. A phase III randomised control trial evaluated 594 patients with gastric or gastro-oesophageal junction cancer with HER2 overexpressing tumours [68]. Patients were randomised to either combination chemotherapy or combination chemotherapy in combination with trastuzumab, median overall survival was significantly higher (13.8 months v 11.1 months) in the patient cohort that received trastuzumab plus chemotherapy compared to patients who received chemotherapy alone [68]. Whether anti-HER2 targeted treatment strategies are of added value in patients with resectable OAC is currently being investigated in a phase I/II clinical trial (NCT02120911) [69]. Given the relative improved overall survival with trastuzumab, additional HER2 targeting agents were also evaluated in clinical trials but have led to disappointing results. A phase III clinical trial comparing the

antibody–drug conjugate ado-trastuzumab emtansine (T-DM1) to taxane monotherapy in the second-line setting failed to meet its primary endpoint of improved overall survival. In addition, the administration of the dual EGFR/HER2 small molecule inhibitor lapatinib, in combination with chemotherapy as part of first- or second line-treatment did not improve overall survival [70, 71]. **(Figure 1-6)**

In addition to HER2, EGFR is another ERBB1 family protein found to be overexpressed in oesophageal tumours [66]. However, EGFR targeting therapies such as the monoclonal antibodies cetuximab or panitumumab or small molecule inhibitors such as gefitinib did not show any survival benefit when evaluated in gastro-oesophageal cancer patients in phase III clinical trials **(Figure 1-6)** [72, 73].

Furthermore, vascular endothelial growth factor (VEGF) and its receptors have been shown to be overexpressed in approximately 30-40% of all gastroesophageal carcinomas. Ramucirumab, a monoclonal antibody against VEGFR-2 has been approved for second-line therapy in OAC patients with advanced disease both as monotherapy and in combination with paclitaxel. A Phase III randomised controlled study of 355 patients demonstrated an increase in median overall survival to 5.2 months versus 3.8 months in patients treated with ramucirumab versus placebo respectively [74]. In another trial, the addition of ramucirumab to paclitaxel also improved survival (9.6 months v 7.4 months). Importantly, analysis of tumour biopsies and serum from patients enrolled on the trial did not identify any significant markers that were predictive of sensitivity to ramucirumab [75]. Following the improved survival benefit demonstrated with ramucirumab, the anti-VEGF antibody bevacizumab was evaluated as part of first-line therapy in combination with chemotherapy in a phase III clinical trial [76]. However, the addition of bevacizumab to capecitabine-cisplatin did not improve overall survival or progression-free survival of oesophageal cancer patients [76]. **(Figure 1-6)**

The amplification of the hepatocyte growth factor receptor, MET, was identified in 2% of gastroesophageal adenocarcinomas and was associated with an aggressive tumour subtype [77] . Therapeutic targeting of this receptor was evaluated in clinical trials, however, similar to a number of the trials previously described in this section the addition of MET targeting antibodies to combination chemotherapy in the first-line setting for patients with advanced MET-positive gastric or gastroesophageal junction adenocarcinomas did not improve overall survival [78, 79].

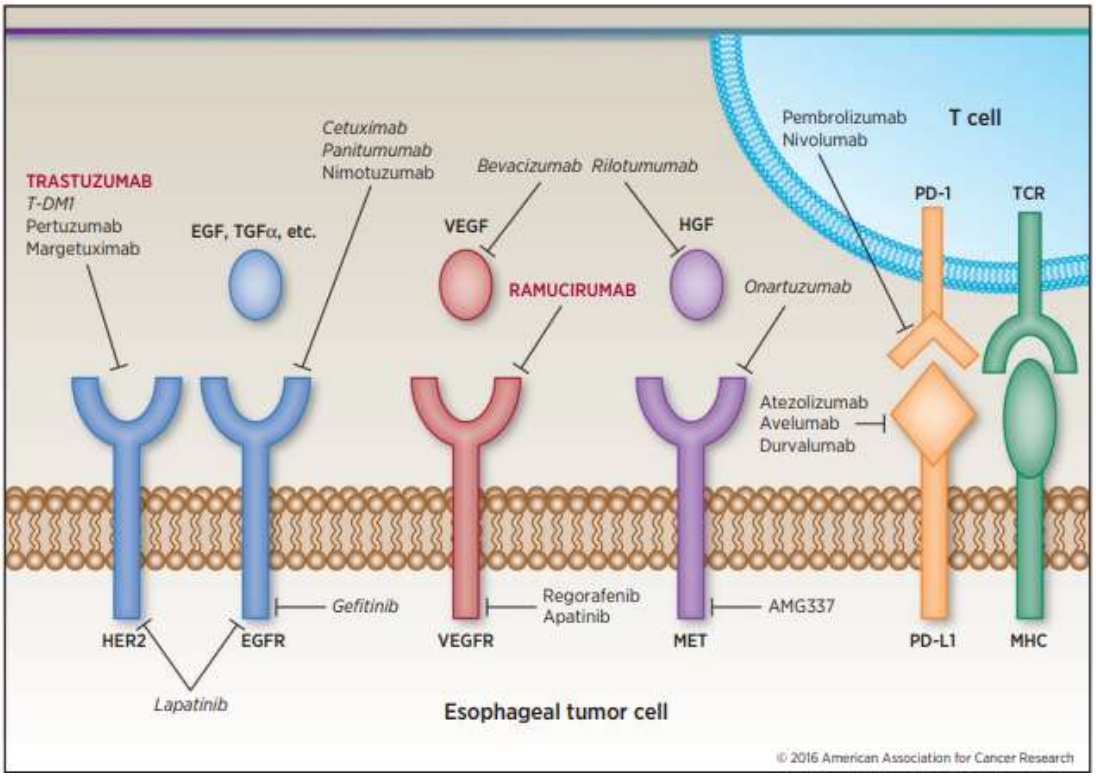

Figure 1-6 Schematic of several of the most well-studied therapeutic targets in oesophageal cancer.
Figure illustrating molecular targeted agents which have been or are currently being evaluated for the treatment of oesophageal cancer. Agents in red upper-case letters represent approved drugs for this indication; agents in Roman type (no italics) are currently undergoing evaluation and final study results are not yet available; agents in italic type were previously evaluated in clinical trials with negative results. TCR; T cell receptor. *Image taken from Wang et al.* [66].

More recently, there has been a shift in molecular targeted clinical trials in the OAC advanced disease setting towards the evaluation of immune targeted agents. Early stage clinical trials have shown initial promise such as the phase I/II CHECKMATE-032 trial which evaluated the combination of anti-PD-1 antibody nivolumab and the anti–CTLA-4 antibody ipilimumab in patients with locally advanced or metastatic chemotherapy-refractory gastric, oesophageal, or gastroesophageal junctional tumours showed a response rate of 26% [80] . In the neoadjuvant setting the combination of neo-CRT with immunotherapies is currently being investigated in multiple clinical trials and this is discussed further in section 1.6.15.

A major limitation of a number of studies which have evaluated novel molecular targeting agents in oesophageal cancer is that often studies do not recruit for one subtype of oesophageal cancer alone and studies often include gastric cancer as well, and as there are distinct histological and genetic differences between the subtypes this can impact on the primary outcomes of the trials. In the future it will be crucial to ensure robust pre-selection of patients based on the expression levels of proteins of interest and their specific tumour histological subtype for optimal treatment evaluation and patient outcomes.

1.2. Radiation therapy and the development of resistance to radiation therapy

Radiation therapy is the targeted administration of X-rays to destroy cancer cells and tumour tissue. The X-rays penetrate the tumour tissues inducing cytotoxic damage in proliferating cells through both direct and indirect mechanisms **(Figure 1-7)**. Radiotherapy X-rays are targeted to the site of the tumour to minimise off-target effects on the normal healthy tissue. The sensitivity of OAC tumours to irradiation is inversely correlated to tumour burden [81]. Resistance to radiation therapy is multifactorial and associated with a number of biological processes both within the tumour itself and the surrounding microenvironment, including dysregulated cellular energetics, angiogenesis and inflammation which are discussed further in the next sections, section 1.3 -1.5 [82-84]. Radiation-mediated cell death is induced by direct and indirect damage effects **(Figure 1-7)**. Radiation directly induces single and double strand breaks in the DNA. In addition, radiation induces ROS and free radicals which induce DNA damage, cell stress and indirectly alter cellular signalling pathways [85]. The accumulation of radiation-mediated DNA breakages and ROS damage ultimately induce cell death [85]. Radiotherapy is a mainstay treatment for many types of cancer, although it is still a large challenge to enhance radiation damage to tumour tissue and reduce side-effects to healthy tissue. Radiosensitisers are promising agents that enhance injury to tumour tissue by accelerating DNA damage and producing free radicals. Several strategies have been exploited to develop highly effective and low-toxicity radiosensitisers.

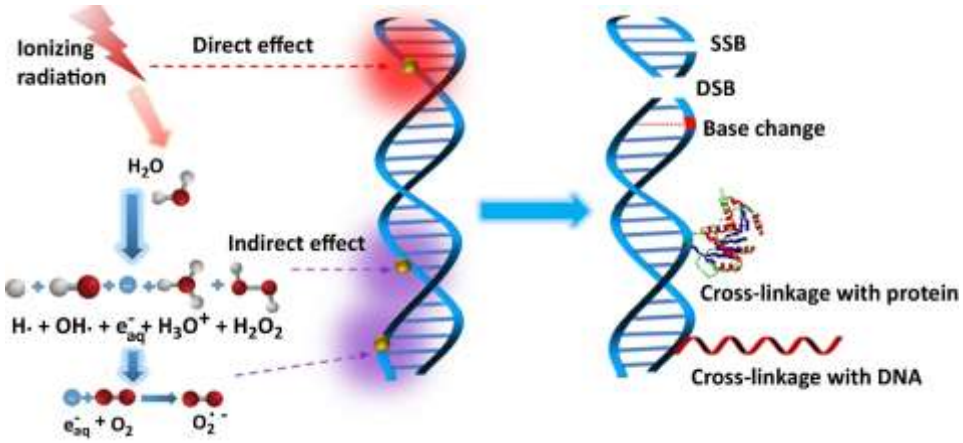

Figure 1-7 Direct and indirect effects of radiation therapy.
Ionising radiation induces DNA damage through both direct and indirect effects. Radiation directly damages DNA (direct effect) through the induction of both single and double DNA strand breaks. In addition radiation damages DNA by indirect effects through the cleavage of the water molecules to generate ROS, and then ROS subsequently damages DNA. There are several types of DNA damage, such as single-strand breaks (SSBs), double-strand breaks (DSBs), base damage, cross-linking with protein or another DNA molecule. *Image adapted from Wang et al.* [85].

Currently no radiosensitisers are approved for clinical use in the treatment of oesophageal cancer and there is an unmet clinical need for novel radiosensitising agents given the large number of patients (~70%) who do not have a complete pathological response to neo-CRT.

As oxygen is a potent radiosensitiser a large body of work has focused on oxygen mimetics or oxygen promoting agents to improve radiosensitivity in the clinic. Oxygen mimetic drugs often contain a nitro group which has electron affinity and can fix the free radical damage similar to oxygen [86]. Nicotinamide is a vasoactive substance which has been combined with accelerated radiotherapy and inhalation of carbogen to enhance radiosensitivity (ARCON) [86]. In a phase III laryngeal cancer clinical trial, 5-year regional tumour control was significantly better with ARCON compared to accelerated radiotherapy alone specifically in patients with hypoxic tumours compared to well-oxygenated tumours [86]. Other nitro compounds such as misonidazole which showed promise in pre-clinical trials failed in the clinic due to limiting neurotoxicity and less toxic modified compounds such as etanidazole and pimonidaole failed to show clinical efficacy [87, 88]. Nimorazole, is part of a class of nitroimidazoles with anti-microbial activity and has been shown to enhance radiosensitivity in clinical trials, and has been recommended for clinical use in the treatment of head and neck cancers in Denmark, especially for patients with high concentrations of osteopontin in their plasma [89, 90].

Tirapazamine (TPZ) is a hypoxia-activated prodrug that selectively acts in hypoxic tumour cells through a bio-reductive mechanism, administration of TPZ was associated with mixed results in clinical trials whereby selection of patients on the basis of tumour oxygenation was deemed critical to the success of the drug [91]. TPZ was also associated with poor diffusion and as such an analogue of TPZ is currently under investigation in clinical trial. [91]. One major limitation of the evaluation of bio-reductive prodrugs in the clinic is the failure to identify patients who will have an optimal response to such therapies. Stratification of patients most likely to benefit from these therapies is difficult due to the variability in the incidence and severity of tumour hypoxia, in patient populations with the same tumour type [91].

A number of chemotherapies including 5-FU, capecitabine, gemcitabine, paclitaxel, docetaxel and cisplatin are commonly combined with radiotherapy in a bid to enhance tumour sensitivity [92]. However the results of the combined therapy are often mixed and fail to enhance radiosensitivity in a large percentage of the patient population [92]. Nonetheless they remain the standard treatment of care in combination with radiotherapy in the absence of any superior targeted therapies [92].

A number of novel targeted therapies to enhance radiosensitivity are currently under investigation at both pre-clinical and clinical trial level and are discussed in depth in section 1.6.

1.3. Angiogenesis and cancer

Having extensively discussed the difficulty in treating OAC and high rate of treatment failure, in this section we begin to discuss key molecular processes and hallmarks of cancer which have previously been linked with radiation resistance including angiogenesis. Sustained angiogenesis is a well-established hallmark of cancer, which refers to vessel sprouting and development from pre-existing blood vessels [93]. Blood vessels supply oxygen and nutrients to growing tumours and provide a route for tumour cells to enter the circulation and metastasise [94]. It was first reported in 1971 by Folkman *et al*. that tumour growth and metastasis are angiogenesis-dependent and inhibiting angiogenesis could arrest tumour growth [95].

The development of new blood vessels relies on the availability of pro-angiogenic factors such as VEGF, Platelet Derived Growth Factor (PDGF), Fibroblast Growth Factor (FGF), Epidermal Growth Factor (EGF), Transforming Growth Factor (TGF), Tumour Necrosis Factor (TNF) and Angiopoietins (Ang) and anti- angiogenic mediators such as thrombospondin-1 (TSP-1) and interferon beta which govern the angiogenic switch [96, 97]. Angiogenic growth factors can be secreted from numerous cell types including endothelial cells, fibroblasts, smooth muscle cells, platelets, inflammatory cells, and cancer cells [96]. In addition, growth factors such as FGF-2, or basic fibroblast growth factor (b-FGF), are sequestered in the extracellular matrix (ECM), and serve as reservoirs for sustained cell-demanded growth factor release [96].

The 'angiogenic switch' is 'off' when pro-angiogenic molecules are balanced by anti-angiogenic molecules and is 'on' when the balance is tipped in favour of pro-angiogenic mediators [93, 98]. When the angiogenic switch is 'on' this results in the initiation of a number of steps which lead to angiogenic sprouting including perivascular detachment and vessel dilation, angiogenic sprouting, new vessel creation and development, and recruitment of the perivascular cells **(Figure 1-8)** [99].

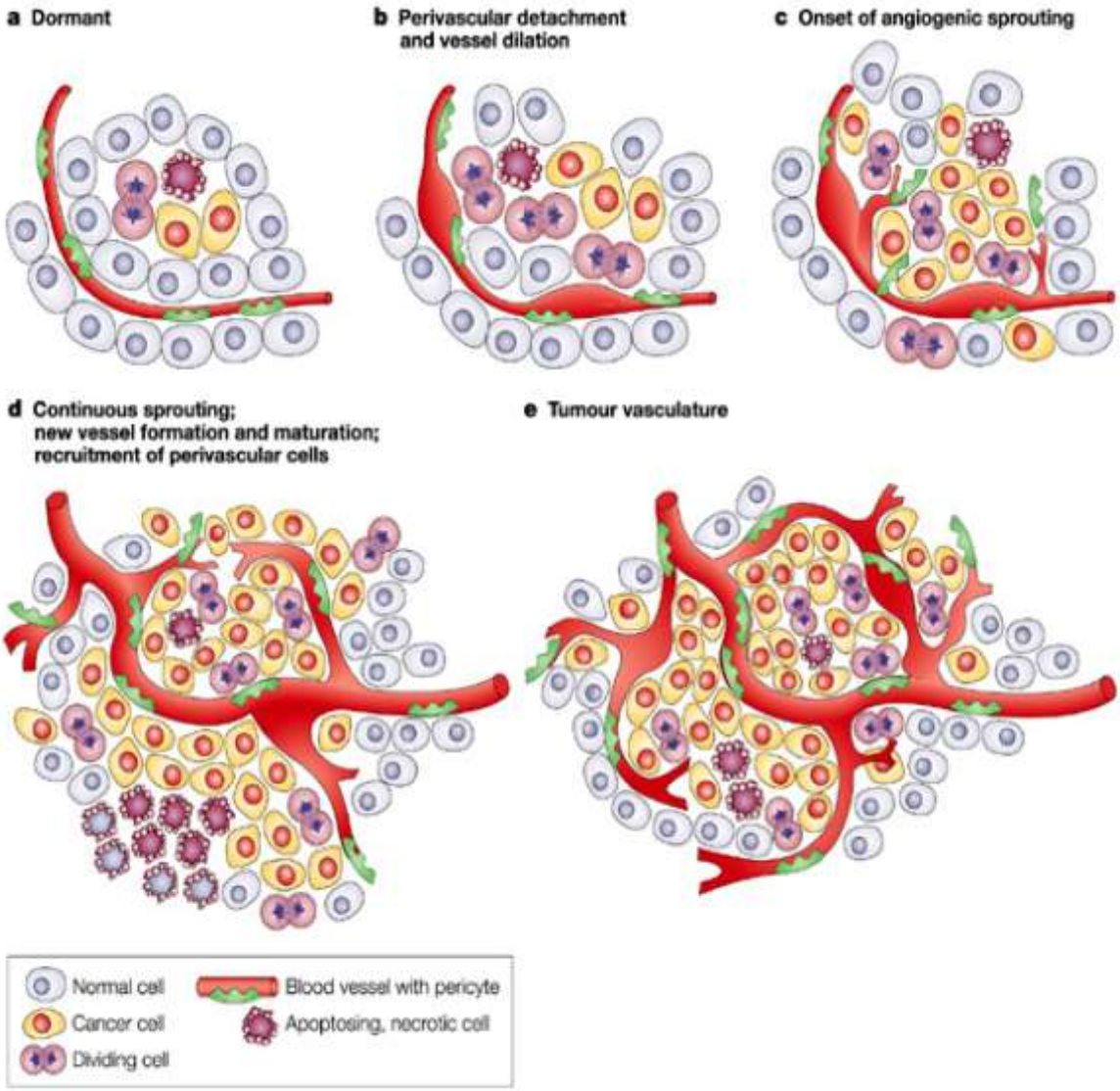

Figure 1-8 The angiogenic "switch" from dormant vasculature to tumour vasculature.
This figure illustrates the step wise process of the 'angiogenic switch' which occurs during tumour development and progression including **(A)** dormant tumours have avascular nodules (dormant), and **(B)** the initiation of angiogenesis, or the 'angiogenic switch' begins with perivascular detachment and vessel dilation, **(C)** this is then followed by angiogenic sprouting, (**D**) and subsequently new vessel formation and maturation, and the recruitment of perivascular cells. (**E**) Finally, blood-vessel formation will continue as long as the tumour continues to grow. *Image adapted from Bergers et al.* [99].

The process of angiogenic vessels sprouting begins when endothelial cells become activated and motile in response to pro-angiogenic signals. The activated endothelial cells have filopodia which guide the vessel development as tip cells. The tip cells lead the new sprouting vessels in response to guidance cues from their surrounding environment. Stalk cells follow the tip cell and continue to proliferate to support sprout elongation. Tip cells anastomose with cells from neighbouring sprouts to build vessel loops. The initiation of blood flow, the establishment of a basement membrane and the recruitment of mural cells stabilise new connections. Vessel sprouting continues until the balance of pro- and anti-angiogenic signals is restored **(Figure 1-9)**. [99]

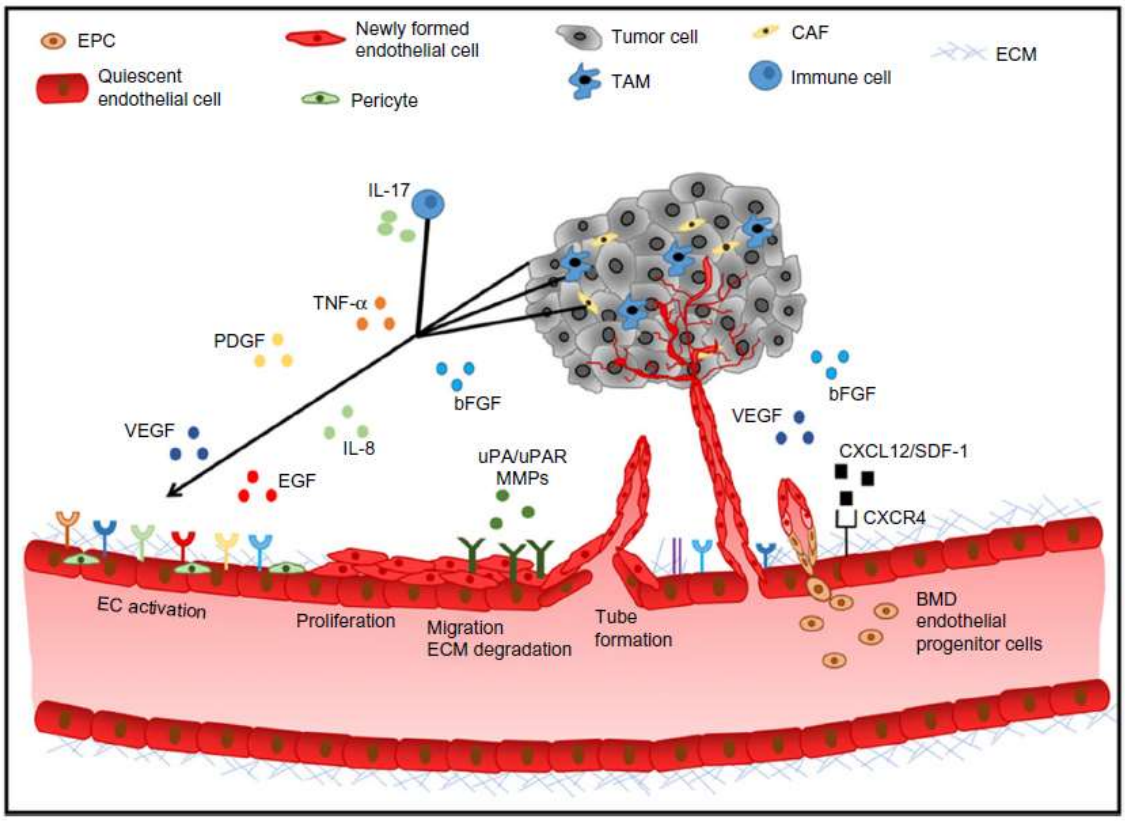

Figure 1-9 The angiogenic cascade.
This figure illustrates the angiogenic cascade following endothelial cell activation. Quiescent endothelial cells are activated when stromal, tumour and immune cell-derived pro-angiogenic factors are secreted into the tumour site leading to proliferation, migration, ECM degradation and tube formation from existing capillaries. Bone marrow derived (BMD) endothelial progenitor cells (EPCs) are recruited to the tumour site and differentiate into endothelial cells, forming *de-novo* vessels. The resulting tumour blood vessels are morphologically and functionally distinct from normal vasculature. *Image* a*dapted from Bejarano et al.* [100].

Under normal tissue homeostasis endothelial cells which line blood vessels are responsible for tissue growth and repair however the development of abnormal and uncontrolled vascular growth contributes to cancer growth and progression through pathological angiogenesis [94]. A number of environmental and genetic factors influence the development of angiogenesis in the tumour including low oxygen and pH which can induce metabolic stress, the response of infiltrating immune cells into the tumour, genetic mutations which alter angiogenic regulators and the mechanical stress of rapidly proliferating cancer cells [101, 102]. Tumour vessels are structurally and functionally abnormal [103]. Unlike normal vasculature, tumour vasculature is highly disorganised and permeable and associated with altered structures and blood flow with uneven diameters, dilated lumens and excessive branching [103]. As a result tumour blood flow is chaotic and variable and leads to hypoxic and acidic regions in tumours [103]. A hypoxic environment promotes the secretion of pro-angiogenic signals, vessel sprouting and tumour growth through the upregulation of HIF-1α [99]. In addition, abnormal tumour vasculature is associated with an

immunosuppressive tumour microenvironment which does not support anti- tumour immunity **(Figure 1-10)** [104].

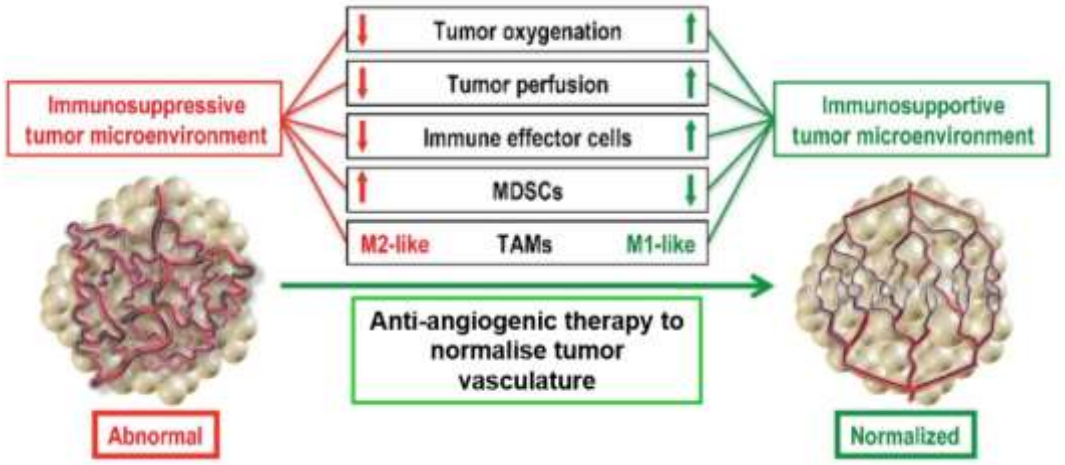

Figure 1-10 Impact of tumour vasculature normalisation on the tumour microenvironment. The abnormal tumour vasculature creates a hypoxic tumour microenvironment which hinders the infiltration of T effector cells into tumours and polarises tumour associated macrophages (TAMs) to an immune inhibitory M2-like phenotype which suppresses T cell function. Vascular normalising therapies generate homogeneous distribution of tumour vessels which facilitate the infiltration of T cells. In addition, improved vascular perfusion polarises TAMs to an immunostimulatory M1-like phenotype. *Image adapted from Huang et al.* [104].

Examples of anti-angiogenic agents include bevacizumab, a monoclonal antibody which targets the VEGF pathway [105]. Targeting endothelial cells in cancer is thought to have a number of advantages including the easy accessibility of endothelial cells by anti-angiogenic/vascular targeting agents compared with drugs that act directly on tumour cells found in bulky masses [106]. Vascular targeting agents may avoid resistance mechanisms because they are directly cytotoxic to endothelial cells [106]. The biological process of angiogenesis is limited in normal body homeostasis limiting normal tissue toxicities and each tumour capillary supplies a large number of tumour cells, therefore targeting of the tumour vasculature should lead to a potentiation of the anti-tumorigenic effect [106]. Despite these advantages resistance to anti-angiogenic agents is extremely common in the clinic. An alternative to monotherapy with anti-angiogenic agents is the combined administration of anti-angiogenic agents with radiation for an enhanced anti-tumour effect [107]. Combining anti-angiogenic agents with radiation has been shown to improve response to radiation [105]. Sustained tumour angiogenesis is associated with the formation of hypoxic regions within the tumour. Anti-angiogenic agents are thought to create a window of vascular normalisation during which there is a transient increase of tumour oxygenation and decrease of tumour interstitial pressure which has been supported by pre-clinical studies [108, 109]. Winkler *et al.* demonstrated that the administration of the VEGF-R2 inhibitor DC-101 alone did not significantly decrease tumour cell growth significantly, and irradiation only had a modest effect but the combination of both treatments produced a synergistic effect when

irradiation was performed 4–6 days after the administration of DC-101. This interval corresponded to a significant and transient increase of tumour oxygenation, and it is precisely during this window that radiation was the most effective highlighting the importance of this vascular normalisation window and treatment scheduling [110]. The potential of combining anti-angiogenic agents with radiation is discussed further in section 1.6.10.

As previously mentioned, the process of angiogenesis does not function in isolation, it is interconnected with other biological processes within the tumour microenvironment including tumour metabolism **(Figure 1-11)** [111]. Blood vessels supply oxygen and nutrients required to fuel metabolic pathways. In addition, endothelial cells can secrete mediators which promote mitochondrial biogenesis [111]. High levels of VEGF-B, are found in metabolically active tissues, where it is co-expressed with mitochondrial proteins and stimulates mitochondrial biogenesis and controls endothelial uptake distribution of fatty acids into other tissues [112]. Cross-talk also exists in the opposite direction whereby metabolism can affect vascular growth. Metabolic sensors and regulators (PGC1α, LKB1, AMPK, FOXOs, and SIRT1) can control vascular growth and stimulate angiogenesis in conditions of nutrient deprivation [111]. In conditions of oxygen and nutrient starvation, PGC1α stimulates angiogenesis by upregulating VEGF through interaction with the estrogen receptor alpha (ERRα) resulting in both angiogenesis and mitochondrial biogenesis which prepares the low oxygen tissue for oxidative metabolism upon revascularization [111]. In addition, under conditions of metabolic stress upregulation of AMPK can induce VEGF-mediated angiogenesis [111].

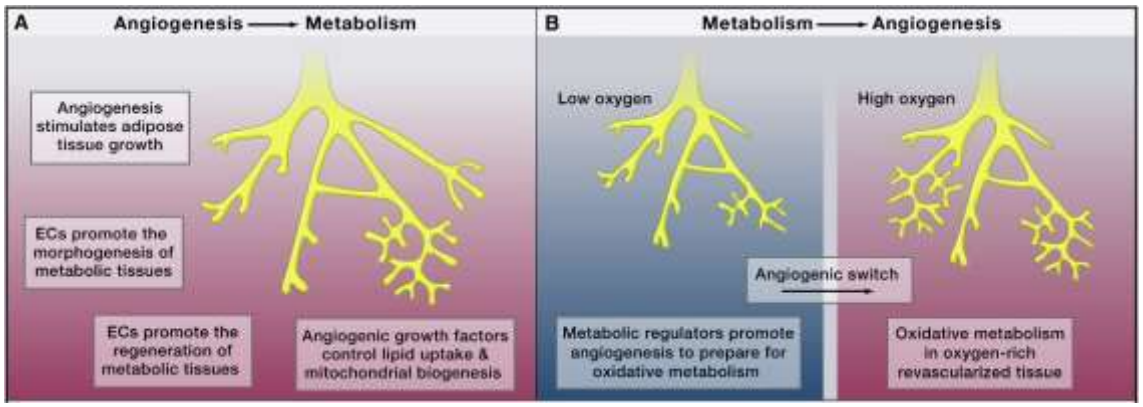

Figure 1-11 Angiogenesis and metabolism crosstalk.
(A) Endothelial cells (ECs) promote growth and repair of metabolically active tissues and angiogenic molecules stimulate *trans*-endothelial transport of fuel to surrounding tissues. **(B)** Metabolic sensors and regulators stimulate angiogenesis and mitochondrial biogenesis in order to prepare the ischemic tissue for oxidative metabolism upon repletion of oxygen and nutrients following revascularization. *Image adapted from Potente et al.* [94].

The cross talk which exist between the two biological processes of angiogenesis and metabolism highlights the therapeutic potential of targeting both biological processes for anti-tumour effect. The main aim of this thesis was to evaluate the potential of anti-angiogenic and anti-metabolic agents to enhance radiosensitivity in OAC.

1.4. Energy metabolism and cancer

As previously mentioned, energy metabolism is tightly linked with angiogenesis as metabolic pathways rely on the oxygen and nutrients being brought to the tumour by blood vessels. In this section we discuss the importance of energy metabolism as a mediator of tumour growth and treatment resistance in OAC. Metabolism can be defined as a series of chemical reactions whereby cells carry out a series of catabolic reactions to meet their energy requirements. A number of metabolic pathways exist and the use of a certain metabolic pathway is often determined by the availability of metabolic pathway substrates including glucose, glutamine, amino acids and fatty acids in addition to oxygen [113]. The main metabolic pathways of interest in this study were oxidative phosphorylation, the tricarboxylic acid (TCA) cycle and glycolysis.

Glycolysis is an anaerobic process which takes place in the cytosol **(Figure 1-12)**. During this process, one molecule of glucose is converted into two molecules of pyruvate in a series of chemical reactions, with the net production of two molecules of ATP [114].

The TCA cycle is a cyclic mitochondrial pathway which takes places in the mitochondrial matrix **(Figure 1-12).** Pyruvate formed by glycolysis is converted to acetyl coenzyme A (acetyl-CoA), the start point of the TCA cycle and is responsible for the oxidisation of the acetyl moiety of acetyl-CoA to CO_2 which in turn results in the generation of NADH and $FADH_2$, whose electrons fuel the electron transport chain of the oxidative phosphorylation pathway for ATP generation. The TCA cycle begins with the condensation of acetyl-CoA with oxaloacetate to form citrate, catalysed by citrate synthase. Citrate can be exported to the cytoplasm, where it is used as precursor for lipid biosynthesis or remains in the mitochondria, where it is converted to isocitrate by aconitase. In the next step, α-ketoglutarate (α-KG), formed by the oxidative decarboxylation of isocitrate catalysed by isocitrate dehydrogenase (IDH) and is converted to succinyl-CoA by a further decarboxylation by the α-KG dehydrogenase complex. Succinyl-CoA is then transformed to succinate by the succinyl-CoA synthetase. Fumarate which is produced by succinate oxidation and catalysed by the succinate dehydrogenase complex, is then hydrated to malate by fumarase. Oxidation of malate by malate dehydrogenase, results in the regeneration oxaloacetate, thus ensuring the completion of the cycle. [115]

The oxidative phosphorylation pathway takes place in the inner mitochondrial membrane and involves the transfer of electrons from NADH or $FADH_2$ from the TCA cycle to oxygen (O_2) by a series of electron carriers to form ATP **(Figure 1-12)**. Electrons are transferred by electron carriers NADH via three protein complexes: NADH-Q oxidoreductase (Complex I), Q-cytochrome c oxidoreductase (Complex III) and cytochrome c oxidase (Complex IV). Another protein complex, succinate-Q reductase (Complex II) transfers electrons from $FADH_2$ instead of NADH. Complex I accepts two electrons and transfers them through FeS clusters to ubiquinone to form ubiquinol. Complex II also functions during the TCA cycle to convert succinate to fumarate, generating $FADH_2$. The electrons then get transferred from $FADH_2$ to ubiquinone. Complex III accepts electrons from ubiquinol generated by Complexes I and II and transfers them to cytochrome c protein. Cytochrome c transfers electrons to Complex IV which then pass to O_2, reducing it to two water molecules. The electron transport by complexes I, III and IV drives the transport of protons through the protein complexes out of the mitochondrial matrix, creating a pH gradient. This pH gradient then forces protons through ATP synthase back into the mitochondrial matrix. This energy drives the rotation of ATP synthase to generate ATP. [116]

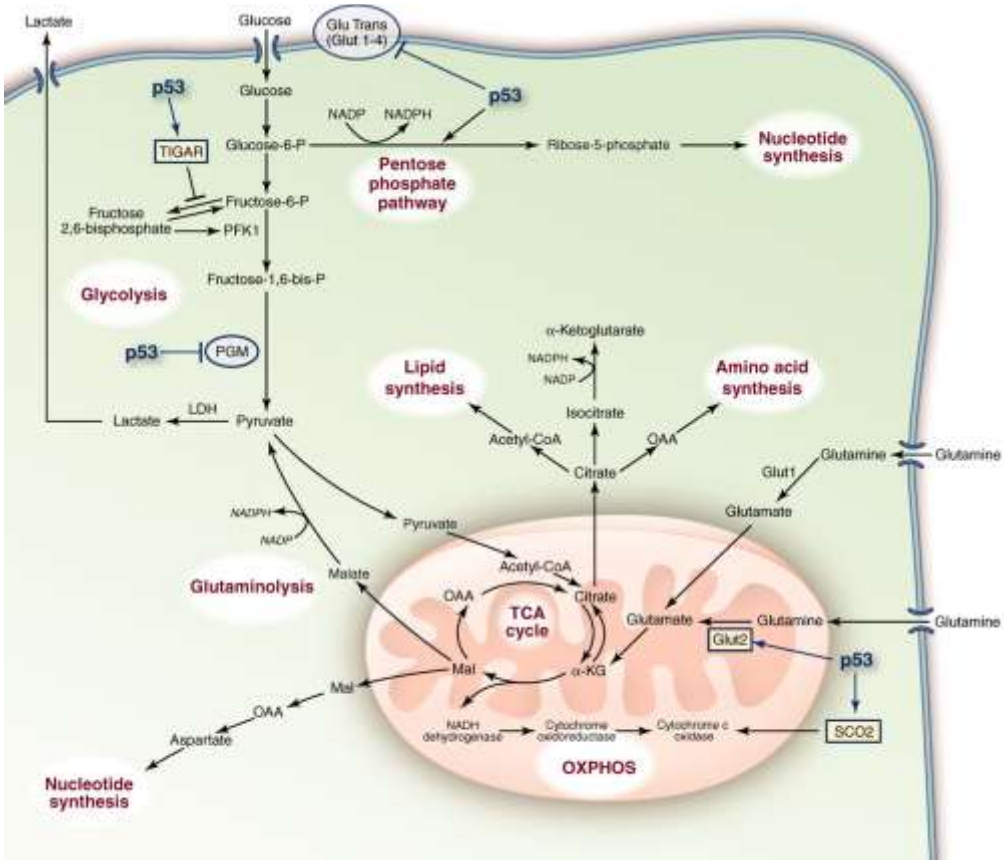

Figure 1-12 Schematic of cellular metabolism pathways.
This figure illustrates metabolic pathways in proliferating cells including glycolysis; lactate production; TCA cycle; oxidative phosphorylation, the pentose phosphate pathway, glutaminolysis and the biosynthesis of nucleotides, lipids, and amino acids. Glucose is metabolised through the glycolytic pathway for production of ATP and pyruvate. Pyruvate can

either be used in the formation of lactate or enter the TCA cycle. Glucose-derived citrate is exported to the cytosol and processed to acetyl-CoA, oxaloacetate (OAA), or α-ketoglutarate (α-KG). Glutamine is deaminated to form glutamate, which is processed to generate α-ketoglutarate and maintain the TCA cycle. Glut Trans indicates glucose transporters; Glut 1, glutaminase 1, Glut 2, glutaminase 2, LDH, lactate dehydrogenase; Mal, malate, and OXPHOS, oxidative phosphorylation. *Image* a*dapted from Levine et al.* [117].

It is critical to understand normal cellular metabolism to be able to understand changes to cellular metabolism in cancer cells. Dysregulated cellular energetics has been identified as an emerging hallmark of cancer whereby cancers cells have adapted to sustain rapid growth and proliferation through altering their metabolism [118]. The first tumour-specific alteration in metabolism was reported by Otto Warburg [119]. Warburg demonstrated that cancer cells rely on an increased glycolytic flux, whereby cancer cells were found to constitutively take up glucose even in the presence of oxygen, an effect which is now commonly referred to as "aerobic glycolysis" or the "Warburg effect" [119]. The increase in glycolytic flux was thought to fulfil the metabolic demands of proliferating cells [120]. Whilst the Warburg effect has been repeatedly reported in multiple studies it has also been well established in recent years that cancer cells also require mitochondrial respiration [121]. As such, metabolic reprogramming of tumours is complex and can now be divided in six distinct hallmarks including (1) dysregulated uptake of glucose and amino acids, (2) use of opportunistic modes of nutrient acquisition, (3) use of glycolysis/TCA cycle intermediates for biosynthesis and NADPH production, (4) increased demand for nitrogen, (5) alterations in metabolite-driven gene regulation and (6) metabolic interactions with the microenvironment [122].

There is now accumulating evidence in the literature which suggests certain subpopulations of tumours exhibit a high dependence on oxidative phosphorylation and reduced glycolytic dependence [122]. Examples of such populations are stem-like sub-clones and circulating tumour cells (CTCs) [123]. In pancreatic ductal carcinoma xenografts where tumours had regressed, relapse occurred 4-5 months later following doxycycline withdrawal, tumour relapse was attributed to cancer stem cells surviving the ablation of mutant K-Ras [123]. Of importance, the remaining cancer stem cells had increased oxidative phosphorylation and mitochondrial biogenesis and relapsing tumours were responsive to the complex V inhibitor, oligomycin [123]. In MCF-7 breast cancer stem cells atovaquone treatment was shown to inhibit cancer stem-cell proliferation through the inhibition oxygen-consumption [124]. In a study by Le Bleu *et al.* invasive mammary carcinoma cells were shown to enhance mitochondrial biogenesis and oxygen consumption rate via the use transcription co-activator, PGC-1α. Silencing of PGC-1α in cancer cells suspended their invasive potential and attenuated metastasis without affecting proliferation [125]. In addition, in patient invasive breast cancer samples a strong correlation was identified

between PGC-1α expression in invasive cancer cells and the formation of distant metastases [125]. In a previous study by our department, OAC radioresistant cells were found to have a significantly higher oxygen consumption rate, a measure of oxidative phosphorylation when compared to matched OAC radiosensitive cells [82]. ATP5B, a surrogate marker of oxidative phosphorylation was found to be expressed at significantly higher levels in OAC treatment-naïve biopsies which had a subsequent poor response to neo-CRT compared to biopsies of patients who had a subsequent good response to neo-adjuvant treatment [82].

An altered metabolic phenotype confers a survival advantage in cancer cells, the findings reported both here and in literature report the dysregulated metabolic phenotype of cancer cells and highlight the important link between mitochondrial respiration and tumour progression and treatment response. A major focus of our study is targeting mitochondrial respiration to improve radiation response and this is discussed further in section 1.6.12.

1.5. Inflammation and cancer

The link between inflammation and cancer was originally identified in 1863, by Rudolf Ludwig and Carl Virchow, who identified the inflammatory process as a predisposing condition for tumour development [126]. Cancer-related inflammation is a hallmark of cancer and contributes to proliferation and survival of cancerous cells, tumour angiogenesis, tumour metastasis, altered immune response and treatment resistance [93]. Inflammation contributes to tumour development and progression through the promotion of a pro-tumourigenic tumour microenvironment [93]. In addition, inflammation and metabolism are tightly linked biological processes as inflammatory cells rely on metabolites generated from the metabolic cycle to maintain their function. The balance of cytokines in a tumour is critical for regulating the type and extent of inflammatory infiltrate that forms. The inflammatory infiltrate is diverse and can consist of multiple cell types including neutrophils, dendritic cells, macrophages, eosinophils, mast cells and lymphocytes. The heterogeneous inflammatory infiltrate can produce a wide array of factors including cytokines, MMPs, cytokine mediators and reactive oxygen species (ROS) which can influence tumour progression [127]. C3a and C4a, components of the complement system, were previously found to be upregulated in the pre-treatment serums of OAC patients having a subsequent poor pathological response to neo-CRT, when compared to patients having a good response to treatment [15].

Inflammatory mediators can promote cell differentiation and tumour cell responses. For example, GM-CSF and interleukin 4 (IL-4) can cause monocytes to differentiate into immature dendritic cells [128]. Dendritic cells migrate into inflamed peripheral tissue where they capture antigens

and, after maturation, migrate to lymph nodes to stimulate T lymphocyte activation. Interestingly, dendritic cells found in tumour infiltrates are frequently immature and defective in T cell stimulatory capacity [129]. Soluble factors such as IL-6 and CSF-1, derived from malignant cells, push myeloid precursors towards a macrophage-like phenotype [129].

TAMs are recruited to the tumour site predominantly by monocyte chemotactic proteins (MCP-1). TAMs make up a large amount of the inflammatory cell infiltrate and are associated with both pro- and anti-tumourigenic activity. TAMs can produce a number of potent angiogenic and lymphangiogenic growth factors, cytokines and proteases which promote tumour progression [130]. TAMs and tumour cells also produce IL-10, which blunts the anti-tumour response by cytotoxic T cells. TAMs can also kill neoplastic cells following activation by IL-2, interferon and IL-12 [131].

Interleukin-6 (IL-6), one of the major cytokines in the tumour microenvironment and is an important factor that is found at high concentrations and known to be deregulated in cancer [132]. The main sources of this cytokine are monocytes, fibroblasts and endothelial cells [133]. IL-6 functions as a modulator of tumour cell growth and has previously been shown to be expressed constitutively in cervical cancer cells [134]. IL-6 has been found to be overexpressed in multiple tumour types and interestingly IL-6 was shown to be overexpressed in the pre-malignant disease of OAC, Barrett's oesophagus and promote apoptosis resistance [135]. IL-6 protects cancer cells from therapy-induced DNA damage, oxidative stress and apoptosis by facilitating the repair and induction of countersignalling antioxidant and anti-apoptotic/pro-survival pathways [132]. IL-6 derived from cancer-associated fibroblasts was shown to promote chemoresistance in oesophageal SSC by upregulating C-X-C motif chemokine receptor 7 (CXCR7) expression through signal transducer and activator of transcription 3/nuclear factor-κB (STAT3/NFκB) pathway [136]. Knockdown of CXCR7 resulted in the inhibition of IL-6-induced proliferation and chemoresistance [136].

Interleukin-8 (IL-8) is pro-inflammatory cytokine found in abundance in the tumour microenvironment [137]. Expression of IL-8 is primarily regulated by the NFκB pathway and is secreted in response to inflammatory cytokines such as TNF-α and IL-1β [137]. In addition exposure of cancer cells to chemotherapies, regions of hypoxia and steroid hormones have been shown to increase IL-8 expression [137, 138]. Importantly, the secretion of IL-8 from cancer cells can promote tumour growth and survival through the upregulation of autocrine signalling pathways such as the PI3K pathway [139]. Tumour derived IL-8 can activate endothelial cells and promote angiogenesis and induce a chemotactic infiltration of neutrophils into the tumour site [139]. IL-8 secretion has also been shown to induce TAMs to secrete growth factors which

further stimulate cancer cell proliferation. Targeting IL-8 has been shown to enhance response to chemotherapeutics and radiation [138, 140].

TNF-α is a multifunctional cytokine that is synthesized from various cell types, including macrophages, monocytes, fibroblasts, endothelial cells, adipocytes, B cells, and some tumour cell types. The binding of TNF-α to its receptor can result in the activation of the NFκB and MAPK pathways [141]. TNF-α has been shown to have a paradoxical role in cancer whereby on the one hand it can induce cancer death and on the other hand, TNF-α stimulates proliferation, survival, migration, and angiogenesis in most cancer cells that are resistant to TNF-induced cytotoxicity, resulting in tumour promotion [141].

IL-1β is a pro-inflammatory cytokine which can be secreted from immune, stromal and cancer cells and binds to the IL-1 receptor. Activation of the IL-1 pathway is associated with tumour infiltrating myeloid cell recruitment, angiogenesis and skewing and suppression of anti-tumour immunity. In an oesophageal SCC patient cohort IL-1β was significantly overexpressed at both the mRNA and protein level in cancer specimens when compared to non-malignant tissues [142]. IL-1β expression significantly correlated with higher clinical stage, lower response rate to concurrent CRT and tumour recurrence [142]. In addition, inhibition of IL-1β signalling significantly reduced tumour growth, invasion ability and treatment resistance *in-vitro* [142]. In a study by Li *et al*. IL-1β was shown to promote self-renewal of colon cancer cells and induce cancer stem cells [143, 144] .

In this section we have only discussed a very small number of inflammatory mediators which play a role in tumour progression and may influence response to radiation therapy. Inflammation is an important driver of tumorigenesis. Numerous pro-inflammatory cytokines, including those discussed in this section and many others are secreted from the tumour cells and cells of the surrounding tumour microenvironment which promote tumour growth and progression and can attenuate response to treatment. The potential of targeting inflammatory mediators to augment radiation response is discussed further in section 1.6.13.

In the previous three sections we have extensively discussed the role of three key biological processes; angiogenesis, metabolism and inflammation in OAC tumour progression and their potential in governing resistance to radiation. In the next section we discuss the potential of targeting different biological processes in combination with radiotherapy to enhance radioresponse.

1.6.Current strategies under investigation to enhance radiation response

1.6.1. *Overview*

Resistance to radiation therapy is polymodal and associated with a number of biological alterations both within the tumour itself and the surrounding microenvironment including; altered cell cycle [145], accelerated repopulation [146, 147], hypoxia [148], evasion of apoptosis [149], altered DNA damage response and enhanced DNA repair [150], inflammation [84] and altered mitochondrial function and cellular energetics [82] **(Figure 1-13)**.

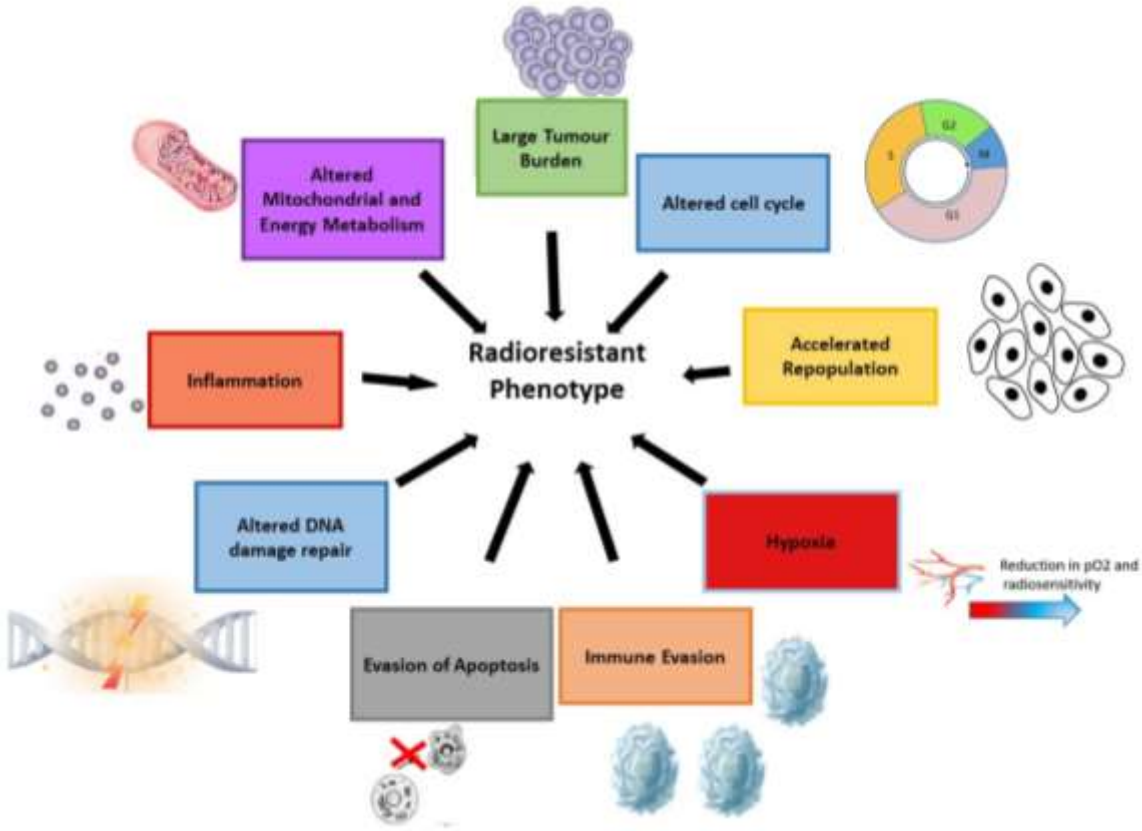

Figure 1-13 Molecular mechanisms contributing to radioresistance.
The radiation-resistant phenotype is commonly associated with large tumour burden, altered cell cycle, accelerated repopulation, hypoxia and inflammation, evasion of apoptosis, altered DNA damage repair and immune cell function.

Combining radiotherapy with conventional chemotherapies such as cisplatin and 5-FU has produced improved response to radiation in the clinic in a number of different tumour types including gastrointestinal cancers such as gastric and rectal cancers [151, 152] . These chemotherapy drugs generally enhance radiosensitivity through increasing the amount of DNA damage induced by radiotherapy thereby increasing cell death. However, conventional chemotherapies do not specifically target tumour cells, they can increase toxicity in normal tissues

and importantly resistance is an inherent problem. There is currently a significant unmet clinical need for novel targeted agents which can enhance radiosensitivity of gastrointestinal cancers.

The next sub-sections review the current literature evaluating the potential of targeting the key hallmarks of cancer in combination with radiation to improve response to radiation treatment in gastrointestinal cancers, in *in-vitro* studies, *in-vivo* studies and in patients through clinical data.

1.6.2. *Targeting altered DNA repair and genome instability to enhance radiosensitivity in gastrointestinal cancer*

DNA is a primary target for ionising radiation and the therapeutic efficacy of radiation therapy relies on its ability to induce lethal DNA damage in cancer cells [153]. A cells ability to repair this radiation-induced DNA damage will ultimately affect its decision to undergo cell death. Alterations in the DNA Damage Response (DDR) and DNA repair are associated with tumour resistance to ionising radiation [150], suggesting that targeting of the DDR and/or DNA repair pathways is a viable therapeutic approach to boost the efficacy of ionising radiation in cancer.

1.6.3. *PARP, ATM and ATR inhibitors in combination with radiotherapy*

DNA lesions induced by radiotherapy lead to the activation of ataxia telangiectasia-mutated (ATM) and ATM-Rad3-related (ATR) protein kinases in response to DSBs and replication stress, respectively [154, 155].

In colorectal cancer, the selective ATR inhibitor VE-821, was shown to significantly sensitise a panel of colorectal cancer cell lines to radiation [156]. VE-821 was also demonstrated to inhibit hypoxia-induced ATR signalling, increase DNA damage and inhibit HIF-1-mediated signalling. Importantly, VE-821 was demonstrated to significantly radiosensitise cells under physiologically-hypoxic conditions, which is a common mechanism of radioresistance *in-vivo*. This is also supported in oesophageal cancer, where combined treatment with the ATR inhibitor VX-970 and radiation significantly reduced viability of oesophageal cell lines under normoxic and hypoxic conditions [157]. The radiosensitising effects of VX-970 were also demonstrated in a murine oesophageal cancer model where the combination of this ATR inhibitor with ionising radiation produced a significant tumour growth delay in xenografts [157] . In a separate study, the selective ATR inhibitor VE-822 was demonstrated to inhibit Chk1 phosphorylation and sensitise pancreatic ductal adenocarcinoma cells to radiation *in-vitro* [158]. Importantly VE-822 did not significantly alter normal tissue radiosensitivity *in-vitro* in HFL-1 fibroblast cells. *In-vivo* growth delay experiments demonstrated VE-822 was capable of sensitising tumours to both single and fractionated radiation in a dose dependant manner [158]. **(Figure 1-14)**

A Phase I trial investigating the maximum tolerated dose of an ATR inhibitor AZD6738 and its potential as a radiosensitiser in patients with advanced solid tumours receiving palliative radiotherapy was suspended due to a potential serious breach **(Table 1-4)** [159].

Targeting ATM has been investigated as a radiosensitising approach in colorectal cancer. The flavanol quercetin, was demonstrated to sensitise colon cancer to radiation *in-vitro* and *in-vivo* [160]. Quercetin prolonged IR-induced γH2AX foci, and inhibited IR-induced activation of ATM, suggesting impairment of the DDR [160]. Supporting this, the radiosensitising effects of quercetin were lost in ATM-deficient cells, highlighting the potential of quercetin as a novel radiosensitiser via its abrogation of ATM signalling following irradiation. *In-vivo*, administration of quercetin enhances radiosensitivity in DLD-1 xenografts demonstrating a significant increase in mean tumour doubling time [160]. **(Figure 1-14)**

Poly ADP-ribose polymerase 1 (PARP1) is the best studied PARP enzyme and plays a critical role in the repair of DNA damage [161]. PARP1 is primarily involved in the repair of single strand DNA breaks but a role for PARP1 in the repair of other DNA lesions has also been implicated [162]. A number of PARP1 inhibitors have been developed and assessed clinically as a single agent therapy for cancer, which exploit BRCA1/BRCA2 deficiencies in mammary tumours [163]. However, increasing evidence also supports the potential of PARP inhibition as a combination therapy in cancer. Radiation exposure results in the rapid activation and recruitment of PARP1 to damaged DNA [164] suggesting that a combination approach of PARP inhibition and ionising radiation could deliver synergistic effects.

A study in hepatocellular cancer, demonstrated that a panel of liver cancer cells have different sensitivities to the PARP-1 inhibitor ABT-888 as a single agent, potentially due to differences in DNA repair capacities. Interestingly, ABT-888 significantly sensitised two hepatocellular cancer cell lines (with differing ABT-888 sensitivities) to radiation, with radiosensitisation greatest in the cell line most sensitive to ABT-888. This highlights the potential use of PARP inhibitors as a radiosensitising approach but suggests that efficacy of this combined approach may depend on inherent DNA repair capabilities of tumours [165]. **(Figure 1-14)**

This approach is also supported in colon cancer [166], the PARP1 and PARP2 inhibitor olaparib significantly sensitised colon cancer cells to radiation *in-vitro* at doses as low as 0.01 μM at 2 h following irradiation. Combined treatment significantly increased induction of γH2AX foci, when compared to radiation alone. The addition of the topoisomerase I inhibitor camptothecin, to olaparib and ionising radiation also significantly radiosensitised cells, significantly inducing

γH2AX foci and G2/M arrest, when compared to olaparib and ionising radiation treatment [166]. Thus, combination therapy of PARP and topoisomerase inhibitors may be a promising strategy for enhancing the effects of radiotherapy.

In 2000 a phase I clinical trial, evaluated the maximal tolerated dose of combining the topoisomerase inhibitor irinotecan with radiation in patients with locally advanced, unresectable gastric, gastroesophageal junction, or oesophageal cancer [167]. The combination was tolerated but doses of irinotecan above 250mg/m^2 combination with ionising radiation were associated with more grade 3 and 4 hematologic and gastrointestinal toxicities [167]. Treatment response to combination of irinotecan and ionising radiation was reported in 12 patients where 7 patients responded of which 2 had a complete response, 4 patients had no response and 1 patient progressed on treatment [167]. An additional clinical trial combining topoisomerase inhibitor camptothecin with radiation in rectal cancer patients is currently ongoing [168].

In pancreatic cancer [169], pre-treatment (1 day prior to ionising radiation) with the PARP inhibitor rucaparib, was demonstrated to sensitise pancreatic cancer cells to radiation *in-vitro*. Pre-treatment with rucaparib also sensitised cells to combined ionising radiation and gemcitabine treatment. Interestingly, this sensitisation effect was independent of BRCA mutation status. Combined rucaparib and ionising radiation treatment induced similar levels of DSBs (γH2AX) in both BRCA mutated and WT cell lines, however, induction of apoptosis was only observed in the BRCA mutated pancreatic cell line. This approach is supported by a separate study in pancreatic cancer [170], which demonstrated that the PARP inhibitor, LT626, significantly radiosensitised pancreatic cells, increasing levels of γH2AX and 53BP1 foci following ionising radiation, highlighting PARP inhibitor as a potential radiosensitising approach in pancreatic cancer. Of note in a separate study, the sensitivity of two patient-derived pancreatic cancer xenografts which expressed either a truncated or wild type BRCA2, to ionising radiation alone or in combination with olaparib was evaluated [171]. In this four arm animal experiment, treatments involved the following; 7 days of olaparib, a single dose of 12 Gy or 7 days of olaparib followed by a single dose of 12 Gy. The BRCA-2 mutated and wild type tumours showed similar radiation sensitivity, and treatment with olaparib did not further sensitise either model when compared to ionising radiation alone suggesting PARP inhibition is not beneficial in BRCA2 related pancreatic tumours [171].

One clinical trial is currently underway assessing the effect of olaparib as a radiosensitiser in oesophageal cancer [172]. The ROCOCO trial is currently recruiting in the UK for Phase I dose escalation testing of olaparib with radical radiotherapy in oesophageal cancer patients unsuitable for platinum-based chemotherapy **(Table 1-4)**. This 5 arm study will compare oral olaparib twice

daily at either 25 mg, 50 mg, 100 mg or 200 mg commencing three days before irradiation (50 Gy in 25 fractions) until the last day of radiotherapy to radiotherapy alone. This study will also use local tumour regression and blood-borne pharmacodynamic markers to assess for any response to treatment [172].

1.6.4. *Targeting non-homologous end joining (NHEJ) in combination with radiation*

DNA-dependent protein kinase (DNA-PK) is a protein essential for non-homologous end joining (NHEJ), a major mechanism for repair of DNA double strand breaks (DSB) [173]. A study by Li and colleagues [174], profiled a panel of pancreatic cancer cell lines and demonstrated that inhibition of DNA-PK by shRNA and the DNA-PK inhibitor NU7026 reduced cell growth and increased DNA damage and apoptosis, suggesting a dependence on NHEJ for normal viability and proliferation in pancreatic cancer cells. Interestingly, inhibition of DNA-PK significantly decreased repair of radiation-induced DSB in three pancreatic cancer cell lines and significantly sensitised cells to radiation, suggesting NHEJ as the predominant repair mechanism for IR-induced DSB in pancreatic cancer, and supporting inhibition of NHEJ as a potential therapeutic radiosensitising approach [174].

This is approach was also supported in colon cancer. Sun *et al*. developed BTW3, a novel small fusion peptide that targets the auto-phosphorylation of DNA-PK, inhibiting its activation in response to DNA damage [175]. *In-vitro* in colon cancer cells, BTW3 significantly decreased the induction and repair of IR-induced DSB (as assessed by γH2AX foci) and significantly sensitised cells to radiation *in-vitro* [175]. A separate study by Zhao *et al*. [176], demonstrated that another DNA-PK specific inhibitor, NU7441, significantly sensitised two colon cancer cell lines to radiation when used at non-cytotoxic doses, an effect which was independent of p53 status. NU7441 treatment increased IR-induced G2/M phase arrest and persistence of IR-induced γH2AX foci, suggesting impairment of DSB repair as a mechanism of NU7441-mediated radiosensitisation, **(Figure 1-14).** The potential of DNA-PK inhibitors has not yet been investigated in oesophageal cancer specifically.

A DNA-PK inhibitor is currently being tested in clinical trial in combination with radiation therapy in patients with solid malignancies, administration of M3814 in combination with palliative dose radiotherapy has been associated with an acceptable toxicity profile **(Table 1-4)** [177].

1.6.5. *Homologous recombination (HR)*

Using high-throughput screening, Stachelek *et al.* developed YU238259, a novel small molecule that demonstrated synthetic lethality in HR-deficient colorectal cancer cells and colorectal mouse xenografts [178]. YU238259 was demonstrated to specifically inhibit homologous-dependant DNA repair with no effect on NHEJ efficiency *in-vitro*. This effect on HR was also independent of PARP activity. YU238259 was demonstrated to inhibit the repair of IR-induced DSB and significantly sensitised DLD-1 BRCA knockout colorectal cancer cell lines to radiation, with radiosensitisation greatest in BRCA2 deficient cells, suggesting a potential role for YU238259 as a novel radiosensitiser in BRCA2-negative tumours [178].

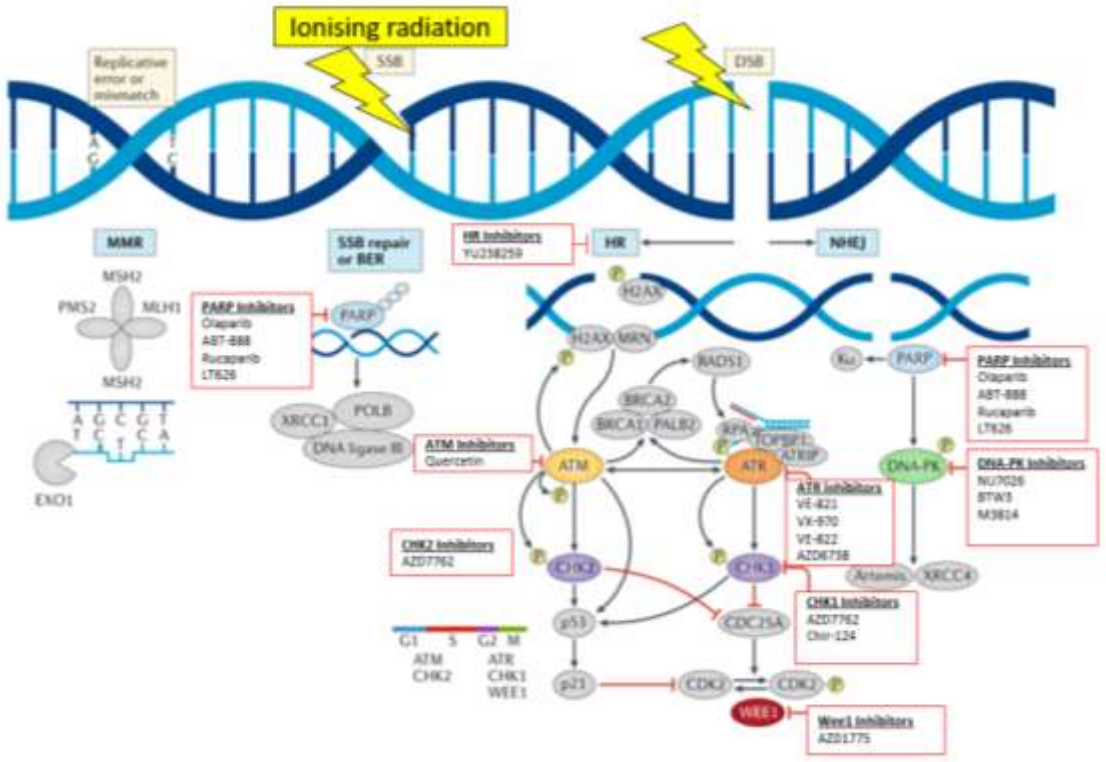

Figure 1-14 Schematic of DNA damage response pathway inhibitors
The induction of DNA damage results in the activation of specific DNA damage repair pathways. This figure illustrates the molecular targets of specific inhibitors of the DNA damage response which have been shown to enhance radiation induced cell death when administered in combination with radiotherapy in gastrointestinal cancers. *Image adapted from Pilié et al.* [179].

1.6.6. *Dual targeting of HR and NHEJ*

A study in pancreatic cancer, demonstrated that treatment with the MEK inhibitor GSK212 significantly sensitised a panel of pancreatic cell lines to X-ray radiation [180]. This radiosensitisation was mediated by inhibiting both HR and NHEJ repair pathways and decreased expression of proteins involved in the DNA damage response and DSB repair pathways [180].

This dual targeting approach is also supported in oesophageal cancer. Valproic acid is a histone deacetlyase inhibitor (HDACi) which is approved for the treatment of epilepsy. A study in oesophageal SCC demonstrated a valproic acid-mediated radiosensitising effect on four SCC cell lines [181]. This was accompanied by an increase in radiation-induced DSB and suppression of the HR protein RAD-51. A further study demonstrated that valproic acid treatment resulted in acetylation of the NHEJ protein Ku70 following radiation in SCC cells [182], suggesting that the radiosensitising effects of valproic acid in SCC is mediated via inhibition of the HR and NHEJ DNA repair pathways.

A phase I clinical trial is currently testing the potential of combining a MEK-1/2 inhibitor; trametinib with neo-adjuvant chemoradiation therapy for locally advanced rectal adenocarcinoma. The trial is assessing 3 dose levels of the MEK-1/2 inhibitor trametinib in combination with 5-FU: 0.5 mg, 1.0 mg, and 2.0 mg daily **(Table 1-4)** [183]. Patients receive standard CRT (5-FU 225 mg/m^2 per day by continuous infusion during radiotherapy, and 50.4 Gy in 28 fractions, 5 days/ week) in combination with trametinib (5 days/week) [183]. Patients have total mesorectal excision (TME) 6-10 weeks after completion of CRT [183].

Table 1-4 Summary of clinical trials targeting DNA repair and genome instability to enhance radiosensitivity.
Table detailing registered clinical trials investigating the potential of targeting DNA repair and genome instability in combination with radiotherapy in gastrointestinal cancers. *estimated enrolment.

Drug Class	Drug Name	Year	Phase	N	Cancer Type	Conclusion	Ref
PARP Inhibitor	Olaparib	Ongoing	Phase I	36*	Oesophageal	No published results.	[172]
Proteosome Inhibitor	Bortezomib	2010	Phase I	9	Colorectal	Maximum tolerated dose when combined with chemoradiotherapy may not be clinically relevant.	[184]
ATR Inhibitor	AZD6738	Ongoing	Phase I	100*	Solid tumours	Suspended	[159]
Topoisomerase I Inhibitor	Irinotecan	2000	Phase I	12	Upper GI	Combining irinotecan with radiotherapy is feasible from a toxicity perspective. Good response noted in this small cohort.	[167]
Topoisomerase I Inhibitor	Camptothecin	Ongoing	Phase Ib/II	32*	Rectal	No published results.	[168]
DNA-PK inhibitor	M3814	2018	Phase Ia/Ib	10	Solid tumours	Acceptable toxicity profile up to doses of 200mg QDS when combined with palliative dose radiotherapy.	[177]
MEK1/2 Inhibitor	Trametinib	Ongoing	Phase I	19*	Rectal (neo-adjuvant)	No published results.	[183]

1.6.7. *Targeting the cell cycle*

A study by Kleiman and colleagues [185], screened a panel of 28 small molecule inhibitors *in-vitro* for radiosensitising effects in rectal cancer. They identified AZD7762, a checkpoint kinases 1 and 2 (Chk1/2) inhibitor as a potent radiosensitiser in a panel of 4 rectal cancer cell lines. AZD7762 also inhibited the ionising radiation-induced G2 arrest and increased ionising radiation-induced γH2AX foci and apoptosis *in-vitro*. Interestingly, 5-FU a chemotherapeutic commonly combined with radiation therapy in the clinic to treat rectal cancer, was demonstrated to enhance

the radiosensitising effects of AZD7762, suggesting Chk1/2 inhibitors as a potential novel combination therapeutic approach for rectal cancer.

This approach is also supported in colon cancer, where a study demonstrated that the selective Chk1 inhibitor Chir-124, abrogated the IR-induced G2 arrest in HCT116 cells, increased apoptosis and significantly sensitised cells to 2 Gy radiation. Interestingly, these effects were independent of p53 mutational status [186]. **(Figure 1-14)**

The potential of targeting cell cycle checkpoints in combination with radiation was also investigated in a pancreatic xenograft model using AZD7762, a Chk1/2 targeted agent [187]. This combination significantly extended the median tumour volume doubling time [187]. Enhanced radiosensitivity status was seen with this combination and was associated with abrogation of the G2 checkpoint and inhibition of Rad51 focus formation, inhibition of homologous recombination repair, and persistent gamma-H2AX expression [187]. In another study with colorectal xenografts where HT29 xenografts exposed to five daily radiation fractions and to two daily AZD7762 doses there was a significant increase in radiation response compared with radiation alone [188]. The potential of Chk1/2 inhibitors in combination with radiotherapy has not yet been extensively investigated in OAC.

Wee1 is a tyrosine kinase which phosphorylates cyclin-dependent kinase 1 (CDK1, CDC2) to inactivate the CDC2/cyclin B complex. Inhibition of Wee1 activity prevents the phosphorylation of CDC2 and impairs the G2 DNA damage checkpoint which may cause apoptosis following treatment with DNA damaging agents. A Wee1 inhibitor AZD1775 sensitised BRAC2 wild type cells but not BRCA2 mutant pancreatic cancer cells to gemcitabine-radiation therapy *in-vitro* [189]. In both wild type and mutant cells Wee1 inhibition was associated with CDK1 phosphorylation and G2 checkpoint abrogation but sensitisation by AZD1775 in BRCA2 wild type only cells was specifically associated with persistent formation of γH2AX foci and reduction of RAD51 foci formation. *In-vivo*, AZD1775 in combination with gemcitabine-radiation therapy significantly inhibited tumour growth in patient-derived pancreatic xenografts and which was associated with the inhibition of RAD51 foci formation [189]. Wee1 inhibition in combination with gemcitabine-radiation therapy may be a novel strategy in pancreatic patients with no defects in HR. **(Figure 1-14, Figure 1-15)**

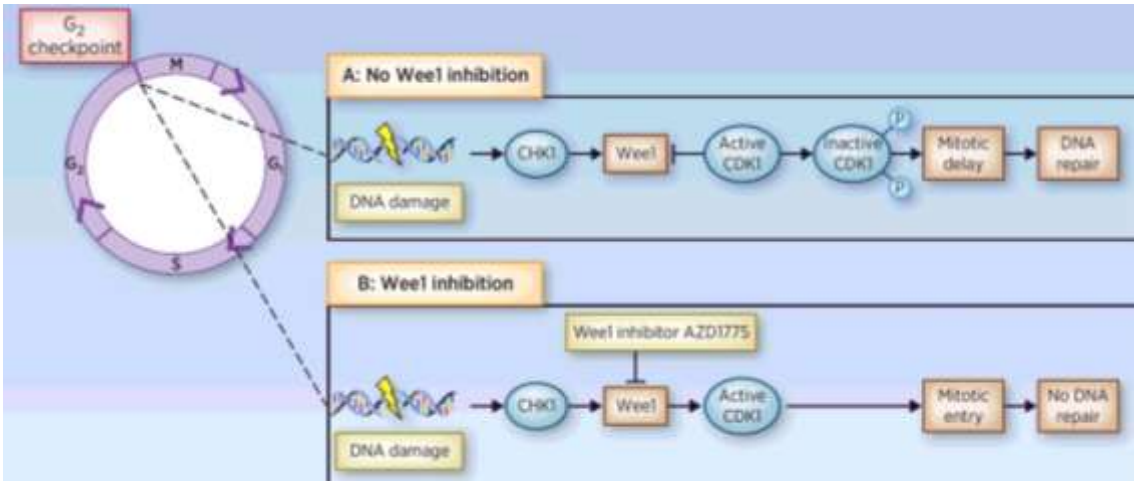

Figure 1-15 Wee1 inhibition in combination with radiotherapy enhances radiation-induced cell death.
Figure demonstrating **(A)** the role of Wee1 in G2–M regulation **(B)** Wee1 inhibition using the Wee1 inhibitor (AZD1775) in combination with radiotherapy results in increased mitotic entry and reduced DNA repair. *Image adapted from Geenan et al.* [190].

Furthermore, dual targeting of both Wee1 and PARP in pancreatic cancer produced a greater effect than either agent alone *in-vitro* and *in-vivo* [191]. AZD1775 in combination with the PARP inhibitor olaparib was associated with abrogation of the G2 checkpoint and persistent DNA damage in pancreatic cancer cells. *In-vivo*, pancreatic MiaPaCa-2-derived xenografts, AZD1775 in combination with olaparib significantly enhanced radiosensitivity as demonstrated by a 13-day delay in tumour volume doubling and an eradiation of 20% of tumours when compared to radiation alone [191]. Importantly, in the xenograft model olaparib alone did not enhance radiosensitivity and AZD1775 alone could only modestly enhance radiosensitivity when compared the dual targeting with the Wee1 and PARP inhibitors [191]. This study suggests the potential of targeting both Wee1 tyrosine kinase and PARP enzyme to modulate radiosensitivity in pancreatic cancer.

1.6.8. *Targeting replicative immortality with telomerase inhibitors*

Another radiosensitising therapeutic approach that has been investigated is the targeting of telomeres or the ribonucleoprotein telomerase to boost radioresponse. Telomeres are nucleoprotein structures located at the end of chromosomes and their primary role is to maintain chromosome integrity and ultimately genomic stability [192]. Several studies have demonstrated that telomere dysfunction is associated with increased sensitivity to genotoxic agents such as ionising radiation, suggesting that targeting of telomere function may provide a novel radiosensitising approach **(Figure 1-16)** [193, 194]. A study in SSC [195], investigated the radiosensitising effects of zidovudine, abacavir and lamivudine, which are frequently used in the

treatment of HIV and have been demonstrated to inhibit telomerase activity [196]. All 3 drugs were demonstrated to inhibit telomerase activity and increase ionising radiation-induced telomere shortening in SSC cells. This was accompanied by a significant increase in ionising radiation-induced DNA damage and apoptosis. Treatment with either zidovudine, abacavir or lamivudine for 48 hours prior to radiation was demonstrated to significantly increase sensitivity to radiation in two OSSC cell lines [195]. This is supported by another study in SCC [197], which demonstrated that a 40 day pre-treatment with the telomerase inhibitor imetelstat, significantly sensitised KYSE-410 and KYSE-520 OSCC cells to X-ray radiation *in-vitro*. Combined treatment also delayed tumour growth *in-vivo* in xenograft murine models, which was accompanied by increased apoptosis.

This approach is also supported in liver cancer. Wang and colleagues [198] treated HepG2 liver cancer cells with a telomerase inhibitor MST-312. MST-312 treatment inhibited basal and IR-induced telomerase activity. Pre-treatment with MST-312 significantly sensitised HepG2 cells to 2 Gy radiation and increased radiation-induced DNA damage and apoptosis, whilst reducing RAD51 foci, suggesting impairment of HR repair of radiation-induced DSB.

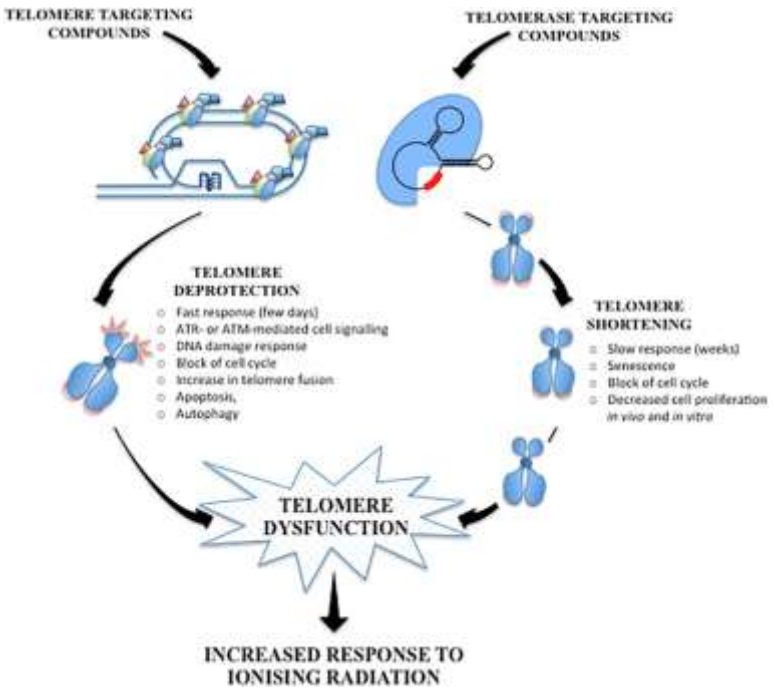

Figure 1-16 Targeting telomere and telomerase to enhance radioresponse.
Inhibition of telomeres and telomerase results in the activation of cellular responses such as the DNA damage response, alterations to cell cycle, apoptosis and senescence resulting in telomere dysfunction, enhanced radiosensitivity of malignant cells. *Image adapted from Berardinelli et al.* [199].

In colon cancer, a bipartite vector strategy was employed to disrupt one allele of *hTERT*, the catalytic subunit of telomerase in HCT116 cells [200]. *hTERT* heterozygous HCT116 cells

demonstrated 50% reduced telomerase activity and were more sensitive to radiation at 2, 4, 6 and 8 Gy. Interestingly, no alterations in cell cycle or apoptosis was observed following ionising radiation in hTERT-targeted cells. However, these cells demonstrated significantly higher levels of senescence-associated-beta galactosidase following irradiation, suggesting a potential mechanism explaining the radiosensitising effects.

1.6.9. *Targeting growth signalling pathways*

Radiation has been shown to induce PI3K/AKT activation and activation of the PI3K/AKT signalling pathway is correlated with radioresistance in a number of cancers [201], suggesting inhibition of PI3K/AKT as a novel radiosensitising approach. In pancreatic cancer [202], the novel PI3K inhibitor HS-173 significantly sensitised pancreatic cell lines to X-ray radiation, which was associated with an increased G2/M arrest and apoptosis **(Figure 1-17)**. Treatment with HS-173 significantly reduced radiation-induced levels of both phosphorylated-AKT and the major regulator of the DNA damage response, ATM, suggesting an impaired DNA damage response. Supporting this, HS-173 also inhibited radiation-induced activation of DNA-PKcs, suggesting that the radiosensitising effect of HS-173 may be due to inhibition of repair of radiation-induced DNA damage in pancreatic cancer cells. This was also supported *in-vivo*, using pancreatic cancer xenograft models. Treatment with HS-173 significantly sensitised tumours to radiation, significantly inhibiting tumour growth and was demonstrated to significantly inhibit the phosphorylation of ATM and DNA-PKcs [202]. This approach was also supported in colorectal cancer. Pal *et al*. demonstrated that combined treatment with the COX-2 inhibitor celecoxib and the AKT-inhibitor BI-69A11, significantly sensitised colon cancer cells to radiation [203]. Treatment was demonstrated to attenuate radiation-induced G2/M phase arrest and increase cells in sub-G1 phase **(Figure 1-17)**. Combined treatment inhibited radiation-induced ATM and DNA-PK phosphorylation, which was accompanied by prolonged radiation-induced γH2AX foci formation, suggesting that BI-69A11 and celecoxib-mediated radiosensitisation is via abrogation of DDR and DNA repair following IR.

The EGFR pathway is the pathway that has been most extensively studied so far in human trials. Following initial promising phase I studies by Machiels *et al.* proving the safety and possible efficacy of panitumumab as a neo-adjuvant single agent radiosensitiser in human rectal cancer, Mardjuadi *et al*. performed a Phase II trial, published in 2015 **(Table 1-5)** [204, 205] . This study evaluated response to neo-adjuvant concomitant panitumumab and radiotherapy in 19 patients with KRAS wild type locally advanced rectal cancer (LARC). Traditionally only used in the metastatic setting, this was one of the first trials that attempted to assess the ability of panitumumab to act as a potent radiosensitiser in the neo-adjuvant setting. The primary endpoint

was pCR. Unfortunately, the trial was closed prematurely due to failure to meet this endpoint. Despite this, some interesting observations were made. The investigators noted tumour regression in 17 patients despite a lack of pCR, an acceptable rate of side-effects and a high rate of colorectal anastomosis. Investigators admitted that the primary endpoint of pCR was optimistic however given the great impact pCR has on DFS and OS in rectal cancer they felt it was justified and necessary. The SAKK 41/07 trial published in 2013 also incorporated panitumumab into standard neo-adjuvant chemo radiotherapy for LARC [206]. This followed on from a Phase I/II study by Roedel *et al.* which demonstrated safety in the combination of cetuximab, oxaliplatin and radiotherapy **(Table 1-5)**. 68 patients received cetuximab and chemoradiotherapy and 28 received chemoradiotherapy alone [207]. Results showed pCR in 10% and 14% of patients respectively. More interestingly the near-complete pathological response favoured the panitumumab group at 43% compared to 14% in the chemoradiotherapy alone group. There was a slightly higher rate of grade 3 and 4 side-effects in the panitumumab arm with an anastomotic leakage rate of 18% vs. 7%. Although this study was small it showed an interesting improvement in near complete pathological response suggesting that panitumumab may increase the radiosensitising effects of chemotherapy in humans. A new phase III clinical trial is currently recruiting patients with HER2-positive metastatic gastric or gastroesophageal junction adenocarcinoma (KEYNOTE 811) to compare trastuzumab plus chemotherapy and pembrolizumab or placebo as first-line treatment.

Table 1-5 Summary of clinical trials targeting growth signalling to enhance radiosensitivity
Table detailing registered clinical trials which investigated the effect of targeting growth signalling pathways in combination with radiotherapy in gastrointestinal cancers.

Drug Name	Year	Phase	N	Cancer Type	Conclusion	Ref
Cetuximab	2007	Phase I/II	60	Rectal (neo-adjuvant)	Safety of combining cetuximab with capecitabine, oxaliplatin and radiotherapy confirmed. Further investigation into optimum sequencing of treatments required.	[207]
Panitumumab	2013	Phase II	68	Rectal (neo-adjuvant)	Combination panitumumab and chemoradiotherapy resulted in a good pNC/CR rate, however was associated with increased toxicity.	[206]
Panitumumab	2015	Phase II	19	Rectal (neo-adjuvant)	Modest tumour regression noted in combining panitumumab and preoperative radiotherapy. Primary endpoint not met-unable to recommend this combination outside research setting.	[204]
Panitumumab	2017	Phase II	54	Rectal (neo-adjuvant)	Tumour regression noted not significant enough to justify further trial. Favourable toxicity profile observed.	[208]

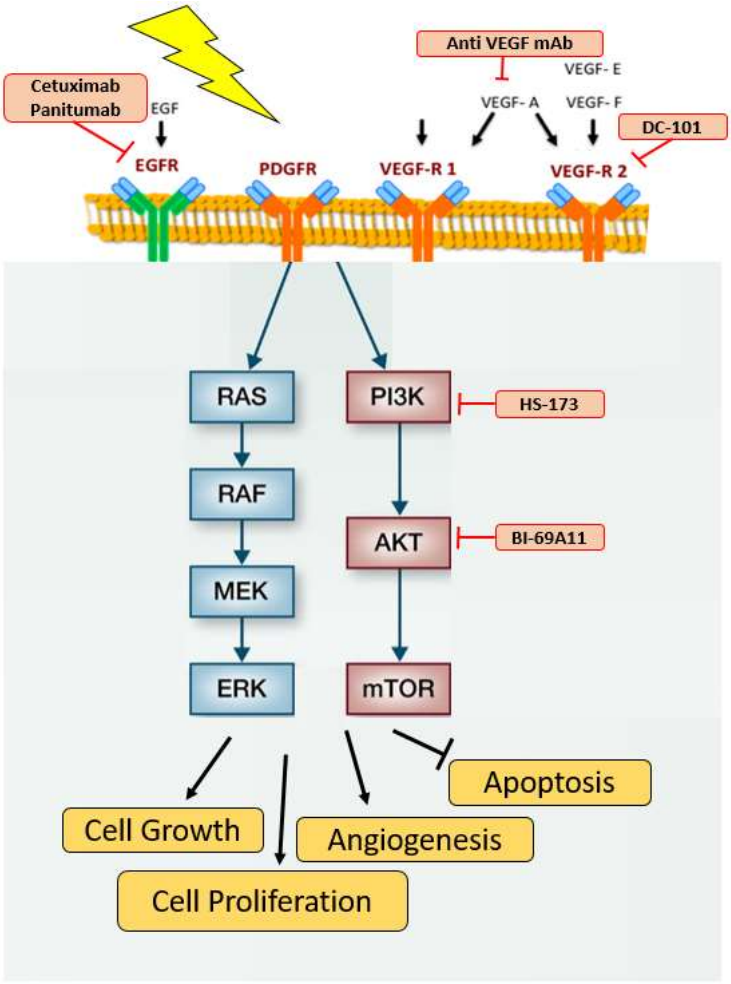

Figure 1-17 Inhibition of cellular proliferation and angiogenic growth factor receptors and downstream mediators in combination with radiotherapy.
This figure illustrates specific inhibitors of receptor tyrosine kinase growth factor receptors and downstream mediators. Inhibition in combination with radiotherapy results in inhibition of cellular growth, cellular proliferation and/or angiogenesis and enhanced radioresponse. *Image adapted from Simone et al.* [209].

1.6.10. *Targeting angiogenesis to enhance radiosensitivity*

Pathological angiogenesis is thought to play a critical role in governing response to ionising radiation [210]. A number of chemotherapeutic agents and radiation therapy alike rely on the formation of oxygen radical species to exert their cytotoxic effects; oxygen is a potent radiosensitiser, with oxygenated cells killed more readily than hypoxic cells [210]. As oxygen is required for maximal response to radiation it may be of concern that combining anti-angiogenic agents with radiation may compromise tumour vasculature and result in a more hypoxic environment with reduced sensitivity to radiation [210]. Despite this concern, anti-angiogenic agents have previously been shown to enhance tumour response when combined with single dose radiotherapy in oesophageal SCC xenografts and in pancreatic and colorectal cancer patients [105, 107, 211, 212]. Anti-angiogenic agents may enhance radio-sensitivity through normalisation of the tumour vasculature and augmenting endothelial cell response to injury

creating a more favourable environment for response to radiation therapy [105, 210]. It is also critical to understand the effect of radiation on endothelial cell function for maximising the effect of radiotherapy. Radiation-induced changes of tumour vasculature is dependent on dose, fraction, tumour location and tumour size [213].

In an oesophageal SCC xenograft model the pre-treatment with recombinant endostain (rh-Endo) prior to one dose of 8 Gy irradiation significantly delayed tumour growth when compared to radiation or rh-Endo treatment alone. Treatment with rh-Endo in combination with radiation was associated with remodelling of the tumour vasculature and a reduction in tumour hypoxia in xenografts demonstrated by reduction on in HIF-1α and VEGF expression *in-vivo* [211]. In colon xenografts, an anti-VEGF monoclonal antibody administered every second day for 11 days prior to radiation had an additive effect **(Figure 1-17)**. The anti-VEGF antibody induced a significant tumour growth delay which was associated with a reduction in tumour micro vessel density and interstitial fluid pressure. Interestingly the significant delay in tumour growth was found to be independent of oxygenation status. The results of this study suggested that the increase in tumour growth delay observed under both normoxic and hypoxic conditions suggests that anti-VEGF mAb treatment can compensate for the resistance to radiation induced by hypoxia [109]. Another study investigated the potential of targeting the VEGF receptor VEGFR-2 using an anti-VEGFR2 monoclonal antibody DC-101. Pre-treatment with either low or high doses of DC-101 before radiation significantly delayed tumour growth by an average 7.9 days compared to radiation alone in a pancreatic xenograft [214]. The increase in tumour growth delay in tumours treated with DC-101 in combination with radiation tumours was strongly associated with changes in tumour perfusion compared to tumours treated with radiation alone **(Figure 1-17)** [214].

The radiation-enhancing effects of VEGF-targeted therapies may occur through a number of mechanisms including the normalisation of tumour vascular and subsequent re-oxygenation of the tumour and directly increasing the radiosensitivity of cancer cells; the killing of endothelial cells in the tumour vasculature causing indirect killing of cancer cells; and the reduction of the number of blood endothelial and progenitor cells supporting the tumour.

1.6.11. *Overcoming resistance to cell death to enhance radiosensitivity*

Proteins which are responsible for the inhibition of apoptosis, known as Inhibitor of apoptosis protein (IAP) play a crucial role in radiation response. One member of this family is X chromosome linked inhibitor of apoptosis (XIAP) which functions as an endogenous caspase inhibitor which targets caspase 3 and caspase 9. An advantage of targeting this particular protein is its higher expression in cancer tissue when compared to normal tissue. Targeting XIAP has

been found to inhibit proliferation and invasion of tumour cells and enhance apoptosis. Inhibition of XIAP by siRNA in an oesophageal SCC xenograft model EC9706 cells in combination with one dose of 15 Gy radiation reduced tumour growth. This study demonstrated reduced XIAP expression significantly suppressed tumour growth and enhanced radiosensitivity [215].

An additional IAP which plays an important role in response to radiation is survivin, a key regulator of apoptosis inhibition. Therapeutic targeting of this protein with a miR-338-5p mimic delivered by direct injection into the tumour mass significantly enhanced radiosensitivity in an oesophageal SCC xenograft model [216].

1.6.12. *Targeting cellular bioenergetics to enhance radiosensitivity*

Targeting energy metabolism pathways is increasingly being investigated in combination with radiation therapy as a means to enhance radiosensitivity. Metformin is a well-tolerated an anti-diabetic drug which is prescribed for type II diabetes which safely lowers blood glucose levels. Metformin targets complex I of the mitochondrial electron transport chain and inhibits mitochondrial respiration **(Figure 1-18)**. Increasing evidence supports the anti-cancer effects of metformin, which along with its well established safety profile, supports the repurposing of metformin as an anti-cancer drug [217].

Several studies support the combined use of metformin and radiation therapy in oesophageal, colorectal, pancreatic and hepatocellular cancers. Metformin was demonstrated to significantly sensitise oesophageal cancer cells to radiation *in-vitro* through targeting the AMPK/mTOR/HIF-1α pathway [218]. The enhanced radiosensitivity of oesophageal cells was associated with an induction of G0/G1 arrest, apoptosis and delayed repair of DSBs following ionising radiation and activation of AMPK, serine/threonine kinase which functions as a cellular metabolism sensor. In colorectal cancer [219], pre-treatment with metformin significantly sensitised cells and xenografts to radiation. Metformin was demonstrated to prolong IR-induced G2/M phase arrest, inhibit repair of DNA damage and decrease expression of DNA repair proteins. Interestingly, these effects were more pronounced in p53-deficient colorectal cells, highlighting metformin as a potential novel radiosensitiser in p53-deficient tumours. However, a study by Jin and colleagues [220], demonstrated that metformin induced activation of AMPK, which enhanced radioresistance in colorectal cells, suggesting that metformin may play a dual role in the radioresponse in colorectal cancer and may be dependent on the molecular background of the tumour.

In contrast, in pancreatic cancer [221], the radiosensitising effects of metformin were abrogated when AMPK was inhibited, suggesting that AMPK is important for metformin-mediated

radiosensitisation. Importantly, this metformin-mediated radiosensitisation was demonstrated at clinically-relevant doses of radiation and in a cancer stem-like population of pancreatic cells, highlighting the clinical potential of metformin as a novel radiosensitiser in pancreatic cancer. Metformin also radiosensitised hepatocellular cancer cell lines [222], significantly enhancing radiation-induced G2/M arrest, radiation-induced DNA damage and a decrease in DNA repair of radiation-induced damage. Interestingly, combined treatment of metformin and ionising radiation was demonstrated to alter energy metabolism. Metformin treatment significantly decreased mitochondrial respiratory chain complex I activity, which was accompanied by a significant increase in lactate and activity of the key glycolysis enzyme LDH, suggesting a switch from oxidative phosphorylation to glycolysis in these cells. ATP levels were significantly decreased in cells treated with metformin and ionising radiation, ATP is known to function in DNA repair and the reduction in ATP levels may be one mechanism underlying metformin-mediated radiosensitisation.

To improve metformin targeting in pancreatic cancer, Cheng and colleagues developed a panel of metformin analogues that are specifically targeted to the mitochondria (Mito-Mets), using an alkyl substituent containing a triphenylphosphonium cation [223]. One of these Mito-Met analogues, Mito-Met_{10}, was nearly 1,000 times more effective at inhibiting proliferation in pancreatic cancer cells and also significantly inhibited tumour growth in a murine model of pancreatic cancer, when compared to metformin. Mito-Met_{10} demonstrated enhanced radiosensitising effects in pancreatic cells, when compared to metformin, which was associated with G1 arrest. Mito-Met_{10} was also demonstrated to be a more potent inducer of AMPK activation and inhibitor of mitochondrial respiratory complex I, suggesting that direct targeting of the mitochondria may be a viable approach for radiosensitisation. In contrast, a study in pancreatic cancer demonstrated that the flavanol (-)-epicatechin selectively stimulates mitochondrial respiration in pancreatic cancer cells and significantly sensitises K-ras mutant pancreatic cells to cells to radiation *in-vitro*. This combination treatment stimulated p21 expression, phosphorylation of Chk2 and caspase 3 cleavage, suggesting possible mechanisms underlying the radiosensitising effects. Interestingly, no radiosensitisation was demonstrated in normal human fibroblasts, suggesting (-)-epicatechin as a novel, selective radiosensitiser in pancreatic cancer [224].

In-vivo, in HCT-116 xenografts administration of metformin 30 mins before the tumours were excised was found to produce a 7% reduction in oxygen consumption rate and to improve tumour reoxygenation *in-vivo*. HCT-116 colon cancer xenografts were administered one dose of metformin 30 minutes before receiving one dose of 15 Gy radiation. Metformin treated tumours were found to have significantly increased tumour growth delay compared to ionising radiation

only treated animals but one dose alone did not alter tumour growth, a number of pre-treatment doses of metformin may be required to enhance radiosensitivity and inhibit tumour growth especially given the fact in a non-gastrointestinal xenograft study when metformin was administered twice a day at 25 mg/Kg prior and following one dose of 20 Gy radiation, tumour growth was significantly inhibited [225] .

Metformin also enhanced radiosensitivity by reducing Rad51 and ERCC1 proteins *in-vivo*, especially in p53-deficient colorectal xenografts [226]. Thus, metformin does influence oxygen levels and DNA repair gene expression and may enhance radiosensitivity in gastrointestinal cancers *in-vivo.* In addition to targeting complex I of the ETC, metformin has also been shown to produce anti-tumoural effects through activation of AMPK and subsequent inhibition of mTOR, a known mediator of tumour progression and radioresistance [227, 228]. In addition, the reduction of circulating insulin levels may also reduce growth signals available to insulin receptor expressing tumour cells. Given the widespread use of metformin and the potential benefits in cancer therapy further studies investigating the potential of metformin as a radiosensitiser are warranted. An early phase I clinical trial is currently recruiting to evaluate the tolerability and preliminary activity of the combination of stereotactic body radiation therapy with metformin for resectable and locally-advanced pancreatic/periampullary cancers. (ClinicalTrials.gov Identifier: NCT02153450). A phase II, randomized study of placebo versus metformin in addition to chemotherapy with capecitabine and radiation in the neo-adjuvant treatment of locally advanced rectal carcinomas was terminated due to slow recruitment (ClinicalTrials.gov Identifier: NCT02473094).

In addition to metformin other compounds targeting cellular energetics are also currently under investigation in combination with radiotherapy to enhance radioresponse. Papaverine is mitochondrial complex I inhibitor which was shown significantly reduce the demand for oxygen [229]. The reduction in oxygen demand of tumour cells was directly linked to increased tumour oxygenation and radiation response [229]. **(Figure 1-18)**

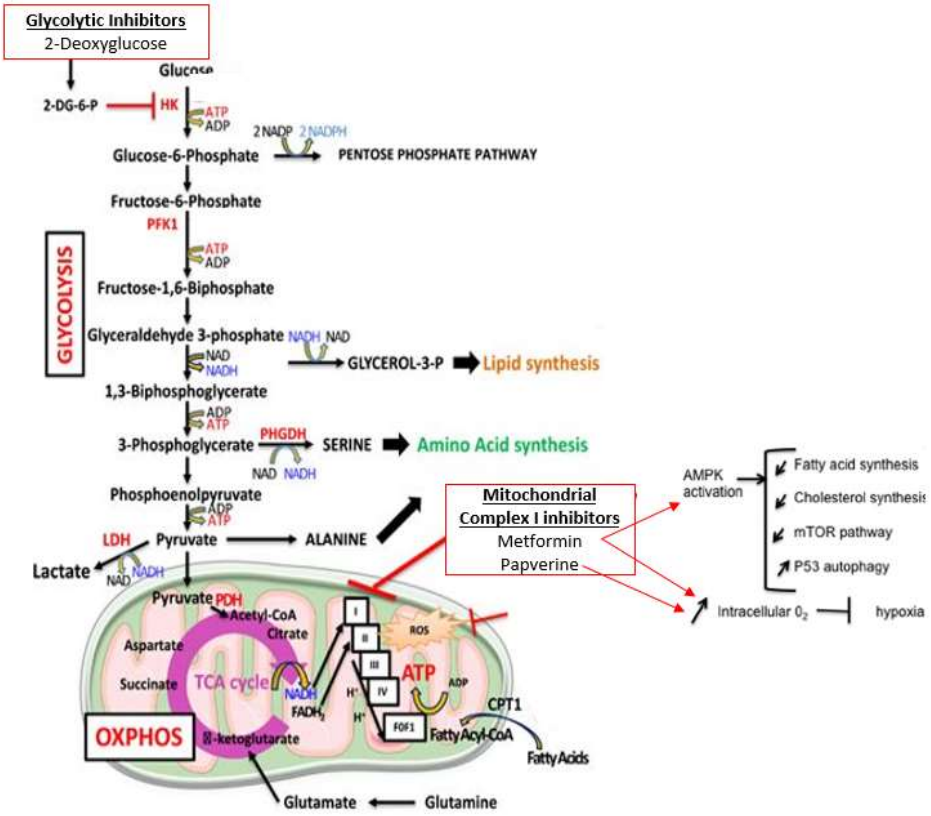

Figure 1-18 Targeting cellular energetics to enhance to radiosensitivity.
2-Deoxyglucose inhibits glycolysis, it is phosphorylated by the hexokinase (HK) to produce 2-deoxglucose-6-phosphate (2-DG-6-P). Metformin and papaverine inhibit complex I of the electron transport chain. The glycolysis pathway converts glucose in pyruvate via a sequence of enzymatic reactions. The lactate dehydrogenase (LDH) catalyses the conversion of pyruvate into lactate. Pyruvate can also enter the mitochondria where it is converted into acetyl-CoA by the pyruvate dehydrogenase (PDH), acetyl-CoA is then processed by the tricarboxylic acid (TCA) cycle. The TCA produces important intermediates but also cofactors (NADH and $FADH_2$) required by the electron transport chain. Inhibition of complex I by metformin and papaverine reduces oxygen consumption resulting in increased cellular O_2. Metformin has also been shown to induce AMPK activation which results in reduced fatty acid, cholesterol synthesis and mTOR activation. *Image adapted from images by Bost et al. and Van De Voorde et al*. [230, 231].

Inhibition of glucose metabolism with 2-Deoxyglucose, a glycolytic inhibitor in combination with ionising radiation was also demonstrated to enhance radiosensitivity *in-vivo* in a pancreatic xenografts [232]. The combination of 2-DG with x-ray radiation resulted in greater inhibition of tumour growth and increased survival versus either agent alone. The enhanced radiosensitivity seen with this combination occurred via the inhibition of glucose metabolism resulting in cytotoxicity of human pancreatic cancer cells via metabolic oxidative stress and disruptions in thiol metabolism. **(Figure 1-18)**

1.6.13. *Targeting inflammation and inflammation-associated hypoxia*

Inflammation plays a pivotal role in modulating response of tumours to radiation. NF-κB, STAT-3, and HIF-1 play a crucial role in radiation-induced inflammatory responses thus therapeutic

targeting of these factors may be a novel mechanism to overcome inflammation-induced radioresistance [233]. Of note, OAC, an inherently radioresistant cancer has been identified as an inflammatory-driven upper gastrointestinal cancer and previous studies have reported the role of inflammation as a negative regulator of response to radiation treatment in OAC [15, 234]. Inflammatory cytokines are been increasingly reported to play a role in radioresistance, LIF is an IL-6 type cytokine and has previously been linked with radioresistance in nasopharyngeal carcinoma and OAC [228, 235].

A study by Chen *et al*. investigated the manipulation of the STAT-3 pathway to enhance radiosensitivity in oesophageal SCC through targeting IL-6. In CE81T oesophageal SCC cells, down regulation IL-6 expression significantly inhibited tumour growth *in-vitro* and *in-vivo* and increased radiation sensitivity. *In-vivo,* IL-6 inhibition was associated with delayed tumour growth enhanced DNA damage as a result of reduced STAT3 activation [236].

Hypoxia often develops as a result of inflammation in tumours which promotes the stabilisation of HIF-1α. Oxygen is a potent radiosensitiser and solid tumours with areas of hypoxia are the most aggressive and difficult tumours to treat [237]. Hypoxia is heterogeneous across tumours and can change following radiation treatment [238]. Hypoxic cancer cells are generally more resistant to both chemotherapy and radiotherapy than their normoxic counterparts and contribute largely to the development of treatment resistance and thus may serve as a novel target to enhance radiosensitivity [238].

In gastric cancer [239], the RNA polymerase inhibitor TAS106 was demonstrated to radiosensitise gastric cancer cells and xenografts to X-ray radiation. TAS106 enhanced IR-induced apoptosis and suppressed HIF-1α both *in-vitro* and *in-vivo.* Inhibition of HIF-1α was demonstrated to enhance radiation-induced apoptosis in hypoxic gastric cancer cells, suggesting that the induction of apoptosis via inhibition of HIF-1α is a mechanism underlying TAS106-mediated radiosensitisation in gastric cancer.

Another approach for targeting hypoxia is the use of nitroimidazole radiosensitisers, a class of chemical compounds that react with radiation-induced DNA radicals and cause DNA strand breaks in a manner similar to oxygen [240]. Bonnet and colleagues developed a panel of novel nitroimidazole alkylsulfonamides and demonstrated their radiosensitising potential in anoxic colorectal cancer both *in-vitro* and *in-vivo* [241].

In a pancreatic xenograft, the selective HIF-1α inhibitor PX-478 was found to potentiate the effect of fractioned chemoradiation therapy [242]. Alternative dosing schedules indicate he optimal treatment schedule of either adjuvant or concurrent administration of this inhibitor with radiation therapy [242]. It is important to note PX-478 was toxic to mice when given concurrently with 5-FU and radiation causing myelosuppression, a 50% decrease in the maximum tolerated daily dose was required to safely administer this combination. This is a novel approach of targeting radioresistance in pancreatic cancer given inherently high rate of radioresistance associated with tumour hypoxia in pancreatic cancer.

1.6.14. *Targeting invasion activation and metastasis proteins*

Invasion and metastasis are well-defined hallmarks of cancer and importantly metastasis has been reported to account for over 90% of cancer-related deaths [118, 243]. Epithelial to mesenchymal transition (EMT) is a fundamental biological process during which epithelial cells lose their polarity and change to a mesenchymal phenotype [244]. The role of EMT in tumour invasion and metastasis is well established [118]. Emerging evidence suggests that EMT plays an important role in cancer radiation resistance [245, 246]. Targeting key proteins involved in the invasion and metastasis process may be a novel mechanism to enhance radiosensitivity in gastrointestinal cancers. An EMT-like phenotype has been identified in a number of radioresistant cells including in an oesophageal SCC model of radioresistance [247]. KYSE-150R radioresistant oesophageal SCC cells were shown to have an irregular shape and loss of cell-cell adhesion proteins [247]. Targeting KYSE-150R cells with FH535, a Wnt/β-catenin pathway inhibitor could reverse the EMT phenotype and enhance radiosensitivity [247].

In addition Bcl-xL has been previously shown to enhance metastatic potential in numerous cancer types such as breast cancer where Bcl-xL could increase metastatic activity by inducing resistance to apoptosis and enhancing anchorage-independent growth [248]. The potential targeting of Bcl-xL was evaluated in a colorectal cancer model [249]. Adenovirus-mediated siRNA targeting Bcl-xL was shown to inhibit proliferation, reduce invasion and enhance radiosensitivity of human colorectal cancer cells [249]. SiRNA targeting of Bcl-xL was shown to enhance radiosensitivity both *in-vitro* and *in-vivo* by increasing caspase-dependant apoptosis **(Figure 1-19)** [249]**.** This strategy has not yet been investigated in OAC.

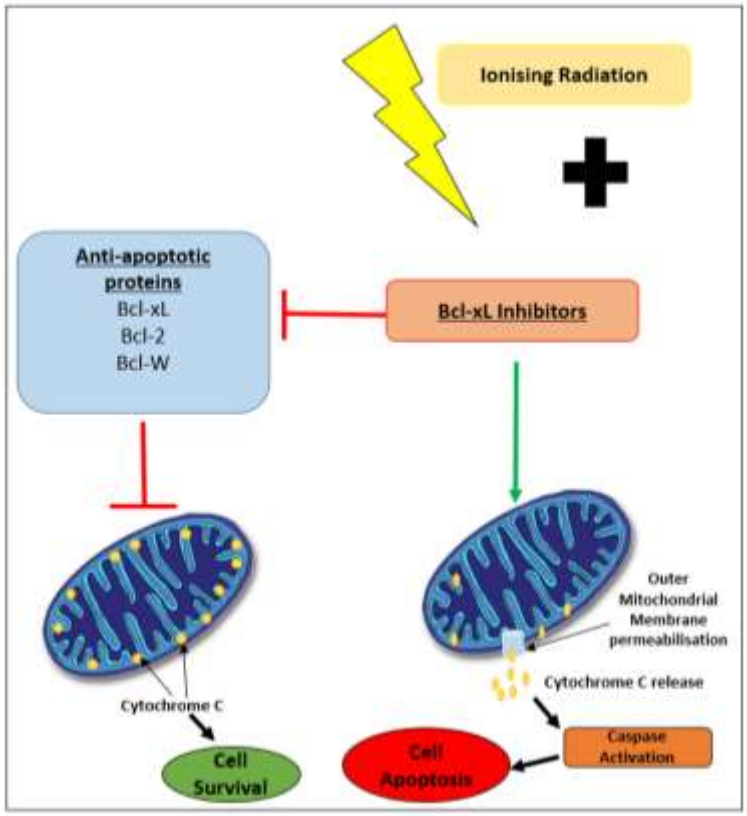

Figure 1-19 Targeting Bcl-xL in combination with radiotherapy to enhance radioresponse. Administration of a Bcl-xL inhibitor in combination with radiotherapy results in outer membrane polarisation and the release of cytochrome C from the mitochondria and caspase activation and subsequent cellular apoptosis.

1.6.15. *Immunotherapy in combination with radiation*

The potential of combining immunotherapy with radiation for improved treatment response has been increasingly investigated in recent years with the increasing clinical use of targeted immunotherapies. Radiation therapy can activate the immune system and increase T cell trafficking to the tumour. In addition, radiation triggers an anti-tumour immune response following cytotoxic death and subsequent release of immune-stimulating signals. The biologic premise behind such a strategy is that the tumour-antigen release and change in the tumour microenvironment achieved by localised radiotherapy will promote specific tumour targeting by the adaptive immune system, which can be augmented further by systemic immune-stimulating agents [250].

In pancreatic ductal adenocarcinoma xenograft model the combination of an anti-PD-L1 therapy with 12 Gy radiation significantly enhanced tumour growth delay when compared to radiation therapy alone **(Figure 1-20)** [251]. Furthermore, the addition the chemotherapeutic gemcitabine to this combination produced an additive effect in a JAK/Stat1-dependent manner [251].

Enhanced radiation response following PD-L1 blockade and ionising radiation was associated with a reduction in $CD11b^{+}Gr1^{+}$ myeloid cell infiltration and enhanced $CD45^{+}$ $CD8^{+}$ T cell infiltration coupled with an upregulation of T-cell activation markers including CD69, CD44, and FasL, and increased CD8:Treg ratio. Interestingly the depletion of $CD8^{+}$ T cells diminished the radiosensitisation effect by anti-PD-L1 in this study [251]. Given that pancreatic cancer is inherently resistant to treatment and pancreatic ductal adenocarcinoma is non-immunogenic this study offers new possibilities in cancers where the response to immunotherapies is minimal.

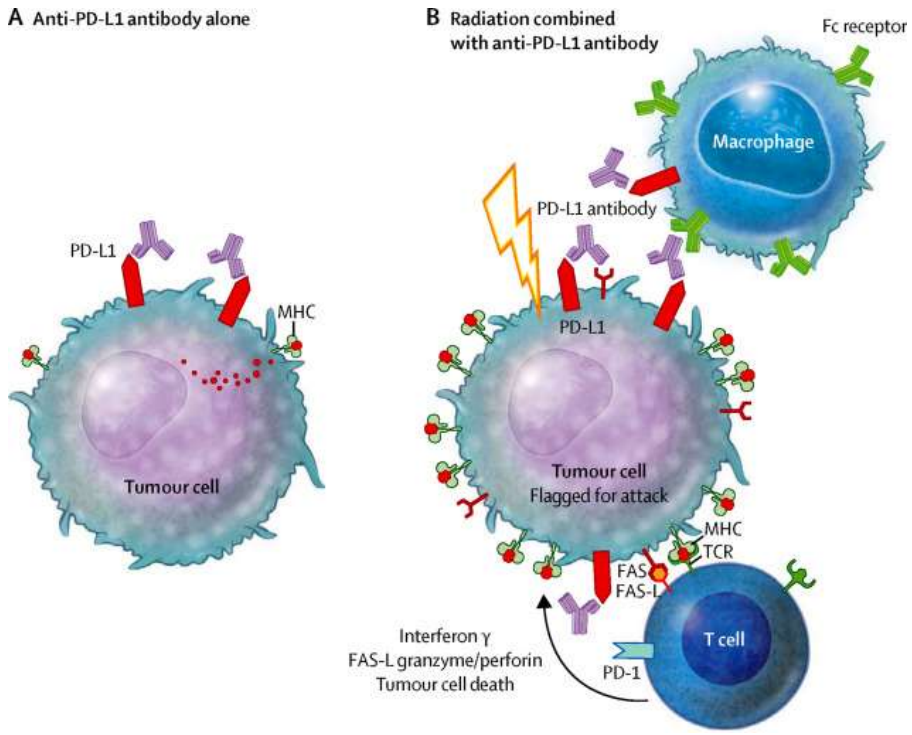

Figure 1-20 Combining radiation with immune check point inhibitors increases tumour cell susceptibility to immune-mediated cell death.
(A) Anti-PD-L1 alone is not predominantly cytotoxic. **(B)** Radiation combined with anti-PD-L1 upregulates MHC and FAS on tumour cells, increasing susceptibility to T-cell-mediated cytotoxicity. TCR=T cell receptor. *Image adapted from Sharabi et al.* [252].

Furthermore, in a study by Son *et al*. the potential of combining anti-CTLA-4 with the injection of immature dendritic cells and radiation was investigated in a colon cancer xenograft model. This combination was developed on the basis that the combined administration of anti-CTLA-4 with the immature dendritic cells to potentiate tumour response and overcome tumour tolerance to the immature dendritic cells and irradiation seen in previous studies by the group [253]. This combination was associated with inhibition of metastatic tumour growth and improved survival when compared to control and other treatment groups [254].

A study by Dewan *et al*. investigated the potential synergistic effects of combining anti-CTLA-4 therapy with radiation in a colon cancer xenograft model both locally and at secondary sites [255].

CTLA-4 blockade alone had no effect on tumour growth whilst radiation induced tumour growth delay at the local site. Importantly, when anti-CTLA-4 therapy was combined with fractionated radiotherapy both primary and secondary tumour growth was significantly inhibited when compared to radiation alone. The growth inhibition of the secondary tumour was proportional to the frequency of tumour-specific T cells. Importantly, anti-CTLA-4 blockade in combination with a single large fraction of radiation at 20 Gy failed to significantly enhance the inhibition of primary tumours highlighting the importance of radiation dose and frequency when combining with immunotherapy for best outcomes.

A study by Welsh *et al*. investigated the potential of combining ipilimumab with radiation in 100 patients with different metastatic cancers, importantly the outcomes of this trial indicated favourable toxicity profile and supported the sequential treatment of ipilimumab and radiotherapy for the best responses, supporting the development of further clinical trials combining immunotherapy approaches with radiation [256]. A number of clinical trials investigating the potential of combining immunotherapy approaches with radiation for improved outcomes in gastrointestinal cancers do not have updated results available **(Table 1-6)**. A novel approach under investigation for oesophageal cancer involves the use of adoptive cellular therapy in combination with radiation in oesophageal cancer patients using cytokine induced killer cells, cytokine-induced killer (CIK) cells show cytolytic activity against tumour. It is hypothesised that combining radiation therapy with adoptive cellular therapy after surgery may produce improved responses compared to treatment with radiation alone, the estimated completion for the primary end point of this study is December 2019 [257].

Table 1-6 List of clinical trials combining immunotherapies with radiation for improved outcome in gastrointestinal cancer.

Table outlining registered clinical trials investigating immunotherapies in combination with radiotherapy in gastrointestinal cancers. *denotes estimated enrolment.

Drug Class	Drug Name	Year	Phase	N	Cancer Type	Conclusion	Ref
Immunotherapy	Ipilimumab	2017	Phase II	100	Various Metastatic Cancers	Toxicity profile acceptable. Trial supports sequential treatment of ipilimumab and radiotherapy for best response.	[256]
Immunotherapy	DC-CIK	Ongoing	N/A	40*	Oesophageal	No published results to date.	[257]
Immunotherapy	DC-CIK	Ongoing	N/A	50*	Oesophageal	No published results to date.	[258]
Immunotherapy	Pembrolizumab	Ongoing	Phase I	18*	Oesophageal	No published results to date.	[259]
Immunotherapy	Pembrolizumab	Ongoing	Phase II	14*	Oesophageal/ Gastric/Junctional	No published results to date.	[260]
Immunotherapy	Durvalumab	Ongoing	Phase I/II	75*	Oesophageal	No published results to date.	[261]

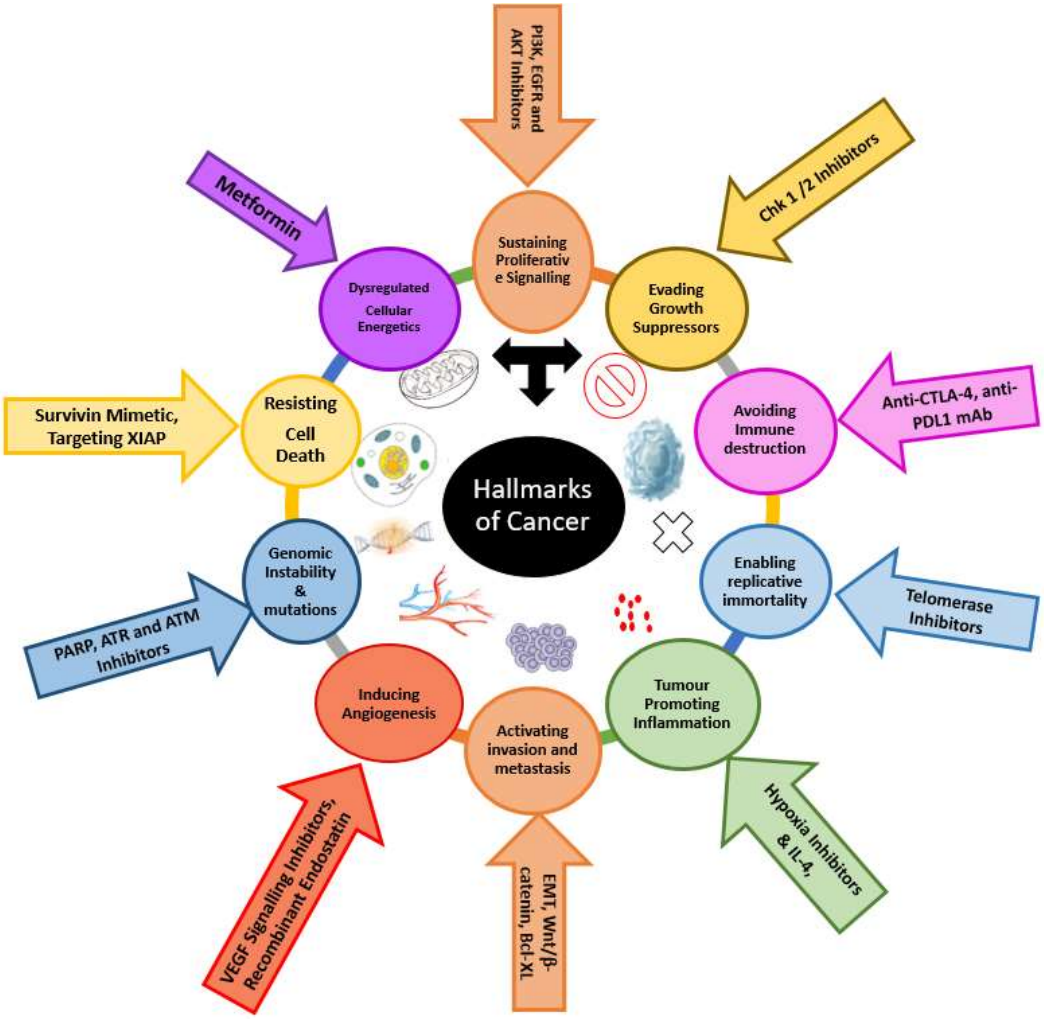

Figure 1-21 Figure summarising potential therapeutics targeting processes associated with the hallmarks of cancer to enhance radiosensitivity in gastrointestinal cancers.
Schematic illustrating the different treatments which have been tested at the preclinical and/or the clinical level targeting the hallmarks of cancer in combination with radiotherapy to enhance radiosensitivity in gastrointestinal cancers.

In conclusion, there are a wide number of molecular targets and biological processes currently being investigated to enhance radiosensitivity **(Figure 1-21)** and it will be crucial to monitor the development of these therapies from pre-clinical to clinical testing. In addition, in the future for any new experimental therapeutics, it will be essential to define not only effects on the tumour but also effects on normal tissues when given in combination with radiation to enhance radiosensitivity. In this thesis we present our findings of the effect of a pyrazine compound (Pyrazinib (P3)) with anti-angiogenic, anti-metabolic and anti-inflammatory activity on radiosensitivity in OAC.

1.7. Aims and objectives

1.7.1. *Overall hypothesis*

Dual inhibition of both angiogenesis and metabolism in the form of oxidative phosphorylation enhances response to radiation therapy in oesophageal adenocarcinoma. Novel dual action drugs which inhibit both angiogenesis and metabolism will enhance radiosensitivity in oesophageal adenocarcinoma.

1.7.2. *Overall aim*

The overall aim of this thesis was to identify a novel small compound with anti-angiogenic and anti-metabolic activity *in-vivo* in zebrafish and *in-vitro* in an isogenic model of OAC radioresistance and determine if this compound could enhance radiosensitivity of OAC radiosensitive and radioresistant cells.

1.7.3. *Specific aims of thesis*

1. Assess the anti-angiogenic and anti-metabolic activity of Pyrazinib (P3) and P series compounds *in-vivo* using a zebrafish model.
2. Determine the effect of our P series compounds on metabolism, mitochondrial function, radiosensitivity and cellular proliferation using a novel *in-vitro* isogenic model of OAC radioresistance.
3. Evaluate the activity of our lead compound on metabolism and radiosensitivity under hypoxic conditions of 0.5% O_2 and determine its effect on chemosensitivity.
4. Evaluate the inflammatory secretions of our isogenic model of OAC radioresistance and determine the effect of our lead compound on inflammatory protein secretions.
5. Investigate the activity of our lead compound on metabolic rate and inflammatory protein secretions *ex-vivo* in OAC treatment-naïve patient biopsies.

2. Chapter 2 Evaluation of the anti-angiogenic and anti-metabolic activity of Pyrazinib (P3) and P series compounds *in-vivo* in Tg*(fli1:*EGFP*) Danio Reiro* zebrafish

2.1. Introduction

Blood vessels deliver oxygen and nutrients to every part of the body, but also nourish diseases such as cancer. Vascular growth can occur through a number of processes including angiogenesis, vasculogenesis, angiogenic sprouting and vessel branching [262]. New blood vessel development is regulated by a number of pro-angiogenic and anti-angiogenic factors [263]. Example proteins which play a pivotal role in new blood vessel development include the proangiogenic factors VEGF-A, b-FGF, Angiopoietin-2 (ANG-2), PDGF and anti-angiogenic factors angiostatin, endostatin and thrombospondin [263].

Pathological angiogenesis may occur when a quiescent vessel is activated in response to pro-angiogenic factors released by hypoxic or inflammatory cells [263]. Pro-angiogenic signals can promote endothelial cell proliferation, differentiation, chemotaxis and angiogenic remodelling [263]. Angiogenic sprouting can facilitate angiogenic remodelling through the selection of tip-cells which lead the sprouting vessel [262]. The growing sprout is guided by VEGF gradients and extracellular matrix cues where tip-cells migrate and stalk cells proliferate [262]. Interaction of two vessel sprouts may eventually lead to mature endothelial tube formation [262]. Inappropriate activation of quiescent vessels and resulting development of new vasculature can promote pathological angiogenesis [264].

Importantly, pathological angiogenesis is thought to play a critical role in governing response to X-ray radiation [210]. A number of chemotherapeutic agents and radiation therapy alike rely on the formation of oxygen radical species to exert their cytotoxic effects; oxygen is a potent radiosensitiser, with oxygenated cells killed more readily than hypoxic cells [210]. As oxygen is required for maximal response to radiation it may be of concern that combining anti-angiogenic agents with radiation may compromise tumour vasculature and result in a more hypoxic environment with reduced sensitivity to radiation [210]. Despite this concern, anti-angiogenic agents have previously been shown to enhance tumour response when combined with single dose radiotherapy [107, 212, 265]. Anti-angiogenic agents may enhance radio-sensitivity through normalisation of the tumour vasculature creating a more favourable environment for response to radiation therapy [105, 210].

In addition to angiogenesis, altered energy metabolism is an emerging hallmark of cancer, and a feature of cancer cells which was originally eluded to in 1956 by Otto Warburg [266] . Cells produce energy primarily through two interconnected pathways; glycolysis and oxidative phosphorylation, which involve the catabolism of glucose to pyruvate and the production of energy from glucose via the mitochondrial tricarboxylic acid cycle respectively [266]. Novel

therapeutics which target oxidative phosphorylation could reduce oxygen consumption and in turn allow more oxygen to be available to act as a radiosensitiser. This may in turn reduce tumour hypoxia and create a more oxygen-rich radiation-sensitive tumour microenvironment [229]. Given the critical role of angiogenesis in supplying critical nutrients such as glucose and oxygen for metabolism and the role of both angiogenesis and metabolism in tumourigenesis and treatment response we hypothesise that targeting both processes may enhance radio-response in OAC.

For our angiogenic and metabolic screening studies we initially used a zebrafish *in-vivo* model, which offers the advantages of a whole organism model. We chose to use a whole model organism for our initial screening as they are a superior screening tool to *in-vitro* cell lines such as endothelial cell line models, the benefits and limitations of this model are discussed in the following sections.

2.1.1. *Zebrafish as a model organism*

Zebrafish (*Danio Reiro*) are an important model organism used in drug discovery and cancer research. Zebrafish have a number of advantages which position them as an attractive model organism and are an invaluable tool for phenotypic based drug discovery [267]. A number of advantages of this cost-effective small vertebrate organism include their small size, rapid development and high reproduction rates [267]. An adult zebrafish is only approximately 2 cm long and as a result large numbers of zebrafish can be housed at a relatively low cost. Furthermore, a mating pair of zebrafish can produce over 200 embryos per week which undergo rapid development *ex-vivo*. In addition, the rapid development of zebrafish embryos means the progenitors of major organs can be seen by 36 hours post fertilisation and embryos are able to dechorniate and feed independently by 5 days post fertilisation (dpf). The small and transparent nature of zebrafish embryos makes them suitable for optical imaging. [267]

Zebrafish are an invaluable tool for drug screening which have a broad range of accessible biological targets and can provide an early insight into toxicity including developmental and cardiotoxicity [268]. A large number of phenotypic drug screens are carried out using cell-based assays thus limiting these screens to cell-autonomous phenotypes. Zebrafish screens use living zebrafish embryos that possess fully integrated vertebrate organ systems meaning a much broader range of phenotypes can be assayed when compared to *in-vitro* cell culture assays [269]. A number of disease relevant phenotypes can currently be assessed in zebrafish including tumour metastasis, vascular development, pain, sedation, gut motility and vision [270]. Furthermore, drug screening in zebrafish can often provide an early insight into toxicity as zebrafish larvae have functional kidneys, livers and blood–brain barriers [268]. Obvious phenotypic changes that are

easily visualised are often produced in zebrafish embryos following treatment with a toxic compound, for example developmental toxicity is often exhibited by curving of the trunk of the embryo [268]. Furthermore, drug screening in zebrafish can provide initial pharmacological insight. In order for a compound to induce a particular phenotype *in-vivo* in zebrafish, the compound must have the ability to be absorbed, distributed to the target tissue, avoiding rapid metabolism and excretion prior to reaching its target tissue providing important pharmacokinetic insight [270]. This can provide valuable information for later studies in rodents as several compounds that were discovered in zebrafish screens were rapidly translated to *in-vivo* mammalian models with minimal optimisation of the pharmacological properties of the compound [271, 272].

Importantly, for cancer research, zebrafish possess a high level of genetic similarity to humans, where 71% of human proteins and more importantly 82% of disease-causing human proteins have an obvious orthologue in zebrafish where they appear to be reasonably similar to their human counterparts, notably within the functional domains [273]. The conservation rate of pharmacological effect from zebrafish to humans is relatively high and this is possibly attributable to the fact that the active sites of enzymes, cell channels and receptors which are often drug targets have retained the ability to bind to the same metabolites, ions and other biomolecules [273]. It is important to note that hepatic drug metabolism enzymes are not fully characterised in zebrafish thus the understanding of drug metabolism in this organism is limited.

2.1.2. *Zebrafish and angiogenic screens*

Transgenic zebrafish are an important model used in drug discovery screens, especially in the identification of anti-angiogenic agents. In our studies we used Tg(*fli1*:EGFP) zebrafish which drive enhanced green fluorescent protein (EGFP) using the *fli1* promotor. *Fli1* is the earliest known endothelial cell marker in zebrafish embryos which is present until 2 dpf [274]. Morphological changes in blood vessels can be observed using fluorescent microscopy making Tg(*fli1*:EGFP) embryos an ideal *in-vivo* model for early anti-angiogenic screens. Importantly, the zebrafish vascular system exhibits functional conservation with the human vascular system [275]. An important study by Stoletov *et al.* demonstrated that human VEGF-A could promote zebrafish angiogenesis [275]. A number of small molecule anti-angiogenic hits identified in zebrafish have been validated in mammalian models such as 3-PO which was shown to have anti-angiogenic activity in zebrafish embryos, endothelial cell spheroids and in the retina of a mouse model [271].

2.1.3. *Zebrafish and metabolic screens*

Although rodent models are widely used as animal models for metabolism studies, the use of zebrafish is emerging as an interesting alternative option. Zebrafish possess key organs also involved in the metabolic processes of humans including the appetite circuits of the hypothalamus, pancreas and insulin-sensitive tissues including the liver, white adipose tissue and muscle [276]. It is important to note that zebrafish are substantially smaller than other animal models and are poikilothermic thus their body temperature varies with the ambient temperature [276]. Therefore, the study of pathways that are activated by non-shivering thermogenesis, for example the β-adrenergic system, will be more limited in zebrafish than in mice [277]. Nonetheless, zebrafish are emerging as a novel model for studying metabolism, especially for the screening of pharmacological inhibitors of oxidative phosphorylation and glycolysis in real-time using the Seahorse analyser [278] which is demonstrated in this chapter.

In summary, angiogenesis and metabolism are thought to play a critical role in both the pathogenesis and treatment response of OAC to neoadjuvant CRT as discussed in depth in Chapter 1. Zebrafish are a well-established tool for the identification of novel anti-angiogenic agents through the use of transgenic strains such as Tg*(fli1*:EGFP*)* zebrafish which express green fluorescent protein in developing blood vessels which can be examined using fluorescent microscopy. More recently the popularity of zebrafish as tool for metabolic studies has increased [278], the use of zebrafish as a model for the identification of novel anti-angiogenic and anti-metabolic agents is demonstrated in our work.

2.1.4. *Quininib, Pyrazinib and P series compounds and their activity*

Previously, screening of a DIVERSET™ chemical library of over 50,000 small molecule compounds (<500kDa) identified Quininib (Q1), a small molecule compound which could significantly inhibit developmental angiogenesis in Tg(*fli1*:EGFP) zebrafish embryos at 2 dpf. Quininib (Q1) was also shown to reduce endothelial tube cell formation, but not endothelial cell migration or proliferation. Treatment of human colorectal explants with Quininib (Q1) reduced the secretions of VEGF, IL-6, IL-8, IL-1β, GRO-α, MCP-1 and TNF-α. In addition, treatment of Balb/C *nu/nu* mice injected with HT29-LUC CRC cells with Quininib (Q1), reduced tumour development and metastasis [272]. Immunohistochemical analysis demonstrated CD31, a marker of blood vessels, was significantly reduced by 5 mg/kg, 25 mg/kg and 50 mg/kg of Quininib (Q1) and VEGF was reduced following treatment with 25 mg/kg of Quininib (Q1). Quininib (Q1) was also shown to inhibit ocular angiogenesis whereby a sustained release formulation of novel quininib-hyaluronan microneedles inhibited angiogenesis and retinal vascular permeability *in-vivo* [279].

Structural analogues of Quininib (Q1), the parent compound, were designed and synthesised with the expectation of developing small molecules which could inhibit angiogenesis more effectively than Quininib (Q1) including Pyrazinib (P3). Quininib (Q1) has previously been shown to act as a cyteinyl leukotriene receptor antagonist however the mechanism of action of Pyrazinib (P3) and P series compounds is not currently known. A priority patent application for the novel use of Pyrazinib (P3) and P series compounds was filed in February 2011, progressed to a National Phase PCT (Patent Cooperation Treaty) in 2013 (PCT/IE2012/000002) and has now been nationally and regionally filed and published in Europe and in the USA. Pyrazinib (P3) and P series compounds were tested in this project to investigate their effect angiogenesis, metabolism and inflammation and their ability to enhance radiosensitivity.

It was critical to investigate both the anti-angiogenic and the anti-metabolic activity of Pyrazinib (P3) and P series compounds to determine if by targeting both these biological processes could enhance radiosensitivity in OAC. The parent compound Quininib (Q1) was previously shown to inhibit angiogenesis and tumour growth, however, to enhance radiosensitivity it may be critical to inhibit oxidative phosphorylation in addition to angiogenesis in OAC. A previous study by our group demonstrated a significant association between oxidative phosphorylation and treatment response both *in-vitro* and *ex-vivo,* whereby radioresistant cells have a significantly higher rate of oxygen consumption and ATP5B a marker of oxidative phosphorylation is significantly higher in patients who have a subsequent poor response to neoCRT. Angiogenesis fuels the metabolic cycle through the provision of oxygen and nutrients to the mitochondria via the blood supply. Targeting both angiogenesis and metabolism is hypothesised to both normalise tumour vasculature and limit oxygen consumption respectively to increase intra-tumoural oxygen levels and thus enhance radioresponse in OAC.

Following initial screening *in-vivo* in zebrafish 5 potent anti-angiogenic compounds and 2 non-anti-angiogenic compounds were carried forward for further screening. Both anti-angiogenic and non-anti-angiogenic compounds were carried forward to determine whether compounds with or without anti-angiogenic activity also had anti-metabolic activity and if only compounds which inhibited both angiogenesis and oxidative phosphorylation could enhance radiosensitivity.

2.2. Overall objective and specific aims of chapter 2

The overall objective of chapter 2 was to evaluate the anti-angiogenic activity of Pyrazinib (P3) and P series compounds (n=23) in an *in-vivo* model of developmental angiogenesis in Tg*(fli1*:EGFP*)* zebrafish and determine the anti-metabolic activity of Quininib (Q1), the 5 most potent and 2 least potent anti-angiogenic compounds of the P series of compounds in Tg*(fli1*:EGFP) zebrafish.

The specific aims of this chapter were:

1. Evaluate and rank the anti-angiogenic activity of quinoline compound Quininib (Q1) and Pyrazinib (P3) and 22 P series compounds in an *in-vivo* model of developmental angiogenesis in Tg(*fli1*:EGFP) zebrafish using an intersegmental vessel assay screen.
2. Evaluate the anti-metabolic activity of Quininib (Q1) and our 5 most potent anti-angiogenic P series compounds on energy metabolism including oxidative phosphorylation and glycolysis in Tg(*fli1*:EGFP) zebrafish using the Seahorse Biosciences XFe24 Analyser.
3. Evaluate the effect of our 2 least potent P series compounds which show no anti-angiogenic activity *in-vivo* on energy metabolism in Tg*(fli1:*EGFP) zebrafish.
4. Rank compounds based on dual anti-angiogenic and anti-metabolic activity *in-vivo.*

2.3. Methods

2.3.1. *Small molecule compounds*

Quininib (Q1), (parent compound) 2-[(e)-2-(quinolin-2-yl)vinyl]phenol, Pyrazinib (P3), (E)-2-(2-Pyrazin-2-yl-vinyl)-phenol and P series compounds were synthesised by Celtic Catalysts (Ireland) and Onyx Scientific (UK). Analogues were dissolved in 100% DMSO to make 10 mM stock solutions for experimental use and stored at -20°C. Pyrazinib (P3) and 22 P series compounds are listed below in **Table 2-1**.

2.3.2. *Ethical approval*

The intersegmental vessel assay screen was approved by the UCD Animal Research Ethics Committee under protocol number AREC-P-14-69 prior to commencement of this study. The zebrafish metabolic profilling assay was approved by TCD Animal Research Ethics Committee prior to commencement of the study.

2.3.3. *Zebrafish husbandry*

Tg*(fli1:*EGFP*)* zebrafish were maintained on a 14 hour (h) light /10 h dark cycle at 28°C in a recirculating aquaculture system, according to standard procedures [280]. Embryos were obtained through natural spawning and developmental stages were determined using time and morphological criteria [281]. Fertilised eggs were obtained from mating adult Tg*(fli1:*EGFP*)* zebrafish and were stored in an incubator at 28°C. Embryos were analysed under an Olympus-SZX16 at time of collection, undeveloped-embryos were removed to prevent a delay to development of other embryos

Compound	Compound Chemical Name	A	C2	C3	C4	C5	C6	X	Y	R1	R2	Salt	Chemical Structure Skeleton
P1	(E)-2-(2-Pyridin-2-yl-vinyl)-phenol	-	N	-	-			alkene		OH			
P2	(E)-2-(2-Pyridin-2-yl-vinyl)-phenol HCl salt	-	N	-	-			alkene		OH		HCl	
P3	(E)-2-(2-Pyrazin-2-yl-vinyl)-phenol	-	N	-	-	N		alkene		OH			
P4	(E)-2-(2-Pyrazin-2-yl-vinyl)-phenol HCl salt	-	N	-	-	N		alkene		OH		HCl	
P5	(E)-2-(2-pyridin-4-yl-vinyl)-phenol	-	-	-	N			alkene		OH			
P6	(E)-2-(2-pyridin-4-yl-vinyl)-phenol HCl salt	-	-	-	N			alkene		OH		HCl	
P7	(E)-2-[2-(6-Methyl-pyridin-2-yl)-vinyl]-phenol	Me	N	-	-			alkene		OH			
P8	(E)-2-[2-(6-Methyl-pyridin-2-yl)-vinyl]-phenol HCl salt	Me	N	-	-			alkene		OH		HCl	
P9	(E)-2-(2-(pyridin-3-yl)vinyl)phenol	-	-	N	-			alkene		OH			
P10	(E)-2-(2-(pyridin-3-yl)vinyl)phenol hydrochloride	-	-	N	-			alkene		OH		HCl	
P11	(E)-2-(2-Pyraxin-2-yl-properyl)-phenol	-	N	-	-	N		alkene	Me	OH			
P12	(E)-2-(2-Pyraxin-2-yl-properyl)-phenol HCl salt	-	N	-	-	N		alkene	Me	OH		HCl	
P13	(E)-4-Methyl-2-(2-pyrazin-2-yl-yl-vinyl)-phenol	-	N	-	-	N		alkene		OH	Me		
P14	(E)-4-Methyl-2-(2-pyrazin-2-yl-yl-vinyl)-phenol HCl salt	-	N	-	-	N		alkene		OH	Me	HCl	
P15	(E)-2-(2-Pyrimidin-2-yl-vinyl)-phenol HCl salt	-	N	-	-		N	alkene		OH		HCl	
P16	(E)-2-(2-Pyridin-2-yl-vinyl)-pyrazine HCl salt	-	N	-	-	N		alkene		C=N		HCl	
P17	(E)-2-(2-Pyrazin-2-yl-vinyl)-benzamide HCl salt	-	N	-	-	N		alkene		CON2		HCl	
P18	2-[2-(Pyrazin-2-yl)ethynyl]phenol	-	N	-	-	N		alkyne		OH			
P19	2-[2-(2-Methoxyphenyl) ethynyl]pyrazine	-	N	-	-	N		alkyne		Ome			
P20	2-[2-(Pyrazin-2-yl)ethynyl]phenol hydrochloride	-	N	-	-	N		alkyne		OH		HCl	
P21	(Z)-2-[2-(Pyrazin-2-yl)vinyl]phenol	-	N	-	-	N		z-alkene		OH			
P22	(E)-2-(2-(IH-imidazol-2-yl)vinyl)phenol	-	N	-	-	N	-	alkene		OH			
P23	(E)-2-(2-(IH-imidazol-2-yl)vinyl)phenol hydrochloride	-	N	-	-	N	-	alkene		OH		HCl	

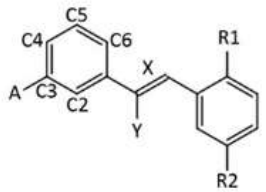

Table 2-1 Structures of P Series Compounds.
Table listing differences in chemical structures of P series compounds indicating where modifications were made to groups C2-C6, R1-R2, A, X and Y to yield P series of compounds.

2.3.4. *Intersegmental vessel assay*

6 hours post fertilisation (hpf) Tg*(fli1:EGFP)* zebrafish embryos were plated 5 per well in a 48-well plate, and visualised using an Olympus-SZX16 microscope in 400 µL Embryo medium (EM) (5 mM NaCl, 0.17 mM KCl, 0.4 mM $CaCl_2$ and 0.16 mM $MgSO_4$). 100 µM solutions dissolved in dH_2O/1% DMSO of Quininib (Q1), Pyrazinib (P3) and 22 P series compounds were stored at -20°C. Compounds were defrosted to room temperature (RT) and vortexed before use. EM was removed and 400 µL containing EM and test compound was added to each well. Drug treatments were carried out in duplicate and repeated three times at 1, 5 and 10 µM. Sunitinib (10 µM) was used as a positive control. Drug treated larvae were incubated until 48 hpf at 28°C on a 14 h light/10 h dark cycle.

After incubation, larvae were placed in 400 µL of Phosphate-Buffered-Saline (PBS) (Lonza, Basal, Switzerland) and dechorionated under an Olympus-SZX16 microscope. Larvae were euthanized and fixed in 400 µL of 4% para-formaldehyde (PFA) in PBS in a parafilm-covered plate at RT for 2 h. 400 µL of PFA was removed and larvae were washed three times at 10 minute intervals with 400 µL PBS. Larvae were stored in 400 µL of PBS in a parafilm-covered 48-well plate at 4°C until analysis. **(Figure 2-1)**

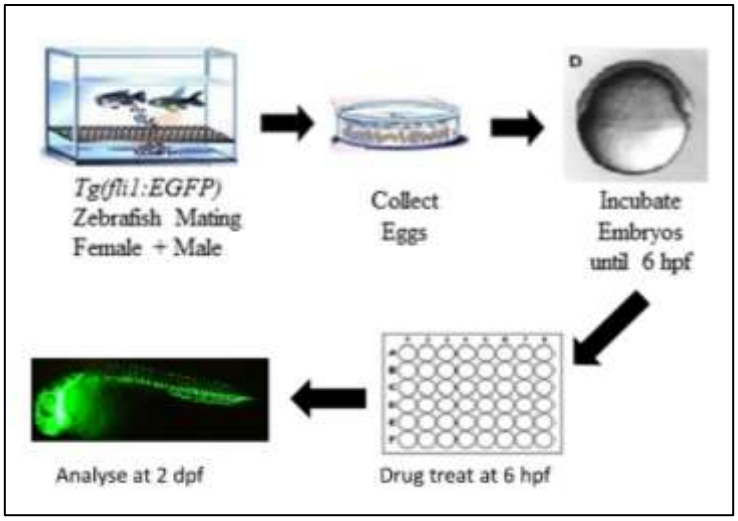

Figure 2-1 Schematic of intersegmental vessel assay in Tg(fli1:EGFP) zebrafish embryos.
Intersegmental vessel assay schematic; Embryos were collected following mating and placed in incubator at 28°C, 6 hour post fertilisation (hpf) embryos were plated 5 per well in 48 well plate and treated with novel compounds at either 1, 5 or 10 µM and fixed and analysed at 2 days post fertilisation (dpf).

2.3.5. *Quantification of intersegmental vessels and imaging*

Prior to analysis of intersegmental vasculature, larvae were screened using an Olympus-SZX16 microscope for gross morphological defects. Larvae were placed on a depression slide on their side with their head in a left pointing orientation. Anti-angiogenic activity was determined on the basis of (a) the total inhibition of intersegmental vessel (ISV) growth and (b) incomplete sprouting of the intersegmental vessel (ISV) from the dorsal aorta (DA) to the dorsal longitudinal anastomotic vessel (DLAV). Intersegmental vasculature was viewed by epi-fluorescence under an Olympus-SZX16 microscope using a GFP filter. The number of complete intersegmental vessels was quantified for each larvae which were imaged using cell^F software (Olympus, Europe). **(Figure 2-2)**

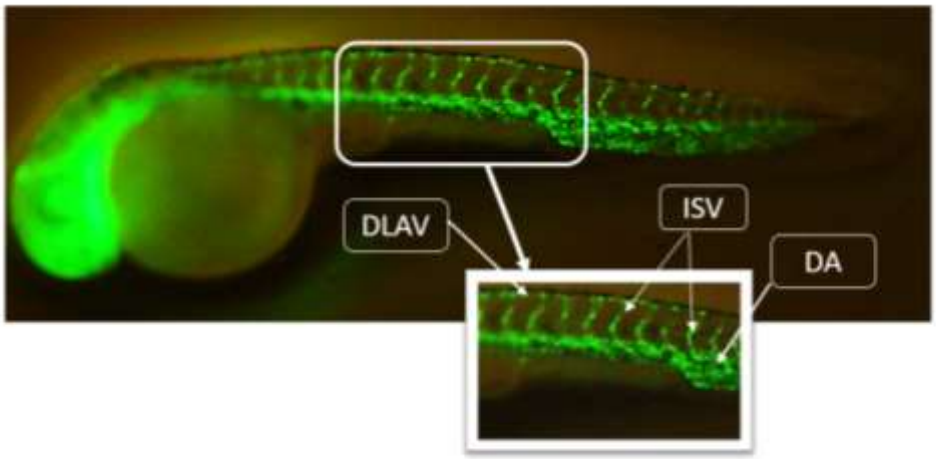

Figure 2-2 Intersegmental vasculature of Danio Rerio zebrafish.
Schematic illustrating zebrafish intersegmental vasculature highlighting major structures including the dorsal longitudinal anastomotic vessel (DLAV), intersegmental vessel (ISV) and the dorsal aorta (DA).

2.3.6. *Optimisation of zebrafish metabolic profiling assay.*

To optimise the most suitable number of embryos per well for our zebrafish metabolic profiling assay, 26 hpf Tg*(fli1*:EGFP*)* zebrafish embryos were plated 1, 2 , 3, 4 or 5 per well in a 24-well islet cell microplate (Agilent Technologies, Santa Clara, CA, USA) using an Olympus-SZX16 microscope in 700 µL EM. Larvae were incubated for 24 h at 28°C on a 14 h light/10 h dark cycle until 50 hpf. At 50 hpf, an islet screen (Agilent Technologies, Santa Clara, CA, USA) was inserted above the embryos in each well to prevent the embryos coming in contact with the sensor probe during the course of the assay. The Seahorse Biosciences XFe24 analyser (Agilent Technologies, Santa Clara, CA, USA) couples a sensor cartridge with a custom cell plate. Sensor probes that lie close to the islet screen to sense changes in the levels of dissolved oxygen and free protons in this micro-chamber at indicated intervals, giving a read-out of Oxygen Consumption Rate (OCR) and Extracellular Acidification rate (ECAR), a measure of oxidative phosphorylation and glycolysis respectively. Prior to the assay the XFe24 cartridge plate (Agilent Technologies, Santa Clara, CA, USA) was hydrated overnight at 28°C in a non-CO_2 incubator. At 50 hpf three measurements were taken over 24 minutes (min) consisting of three repeats of mix (3 min) / wait (2 min) / measurement (3 min) to establish basal respiration. Upon completion of assay, drug treatment was aspirated off and larvae were euthanized and fixed in 400 µL of 4% PFA in PBS in a parafilm-covered plate at RT for 2 h.

2.3.7. *Zebrafish metabolic profiling assay*

26 hpf Tg*(fli1*:EGFP*)* zebrafish embryos were plated 3 per well (as determined from optimisation) in a 24-well islet cell microplate (Agilent Technologies, Santa Clara, CA, USA) using an Olympus-SZX16 microscope in 700 µL EM containing a final concentration of 10 µM of test compounds; Quininib (Q1), Pyrazinib (P3), P2, P4, P18, P20, P8 and P23, with 5 wells per treatment group. Four wells contained EM only to identify temperature fluctuations across the plate. Drug treated larvae were incubated for 24 h at 28°C on a 14 h light/10 h dark cycle until 50 hpf. At 50 hpf, an islet screen (Agilent Technologies, Santa Clara, CA, USA) was inserted above the embryos in each well. Prior to the assay the XFe24 cartridge plate (Agilent Technologies, Santa Clara, CA, USA) was hydrated overnight in 28°C non-CO_2 incubator. At 50 hpf three measurements were taken over 24 min consisting of three repeats of mix (3 min) / wait (2 min) / measurement (3 min) to establish basal respiration. Upon completion of assay, drug treatment was aspirated off and larvae were euthanized and fixed in 400 µL of 4% PFA in PBS in a parafilm-covered plate at RT for 2 h **(Figure 2-3).**

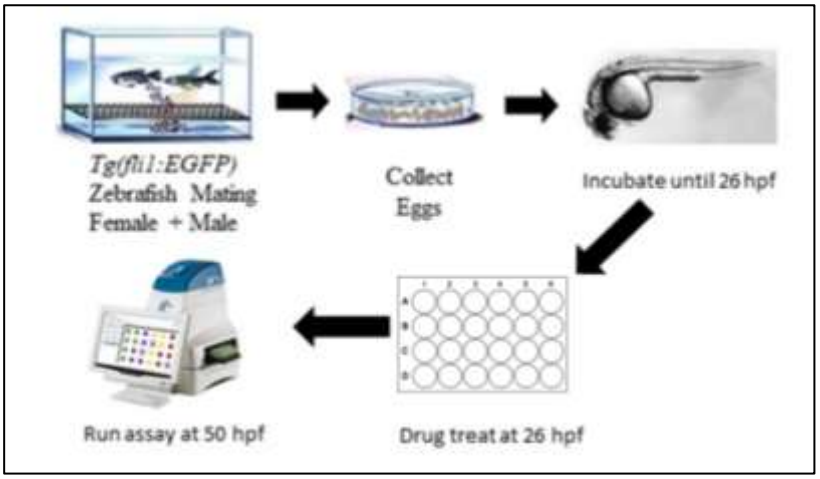

Figure 2-3 Real-time metabolic profile analysis in zebrafish.
Embryos were collected and placed in incubator at 28°C. 26 hpf embryos were plated in a XFe24 islet cell microplate and treated with 10 µM novel compounds or 0.1% DMSO control. Metabolic profile was analysed at 50 hpf using the Seahorse Biosciences XFe24 analyser.

2.3.8. *Statistical analysis*

Statistical analysis was performed using GraphPad Prism 5 software (GraphPad Software, CA, USA). Scientific data were expressed as mean ± standard error of the mean (SEM). SEM was calculated as the standard deviation of the original samples divided by the square root of the sample size. Statistical test used indicated in relevant figure legends.

2.4. Results

2.4.1. *Pyrazinib (P3) and P series compounds inhibit developmental angiogenesis in Tg(fli1:EGFP) zebrafish.*

Using Tg(*fli1:*EGFP) embryos, Pyrazinib (P3) & P series compounds were screened for anti-angiogenic activity in a phenotype based approach using the intersegmental vessel assay illustrated in **Figure 2-1**. Compounds were tested at 1, 5 and 10 µM and their anti-angiogenic activity assessed by quantification of intersegmental vessel number at 48 hpf **(Figure 2-2)**. This screen was carried out to identify if Pyrazinib (P3) and 22 P series compounds **(Table 2-2)** produced greater anti-angiogenic effects compared to the quinoline series compound Quininib (Q1) from which Pyrazinib (P3) was derived. Quininib (Q1) has previously been shown to inhibit both ocular and tumour angiogenesis *in-vitro* and *in-vivo* [272, 282]. A dose response profile was conducted at 1, 5 and 10 µM, with the most potent anti-angiogenic effect seen at 10 µM. Pyrazinib (P3) and P series compounds P2, P4 and P18 produced the most potent anti-angiogenic activity (p<0.0001) compared to vehicle control **(Figure 2-4A-C)**. The most potent anti-angiogenic compound Pyrazinib (P3), reduced ISV number by ~67% at 10 µM , whereas the quinoline compound Quininib (Q1) produced a reduction in ISV number of ~35% in this screen. Furthermore, the P series compounds, Pyrazinib (P3) and P4 produced significantly greater anti-angiogenic activity when compared directly to the quinoline compound Quininib (Q1) when tested at 10 µM (p<0.001 and p<0.01) respectively **(Figure 2-4C)**. Fluorescent images **(Figure 2-5)** illustrate the potent reduction in ISV number and loss of vessel integrity following treatment with Pyrazinib (P3) (white arrows indicate incomplete sprouting and absence of vessel growth) and P series compounds (P2, P4, P18, P20), compared to control and quinoline series compound Quininib (Q1). No gross morphological defects or toxicities were observed following treatment with Pyrazinib (P3) or any other P series compounds tested in this assay, although there were some alterations to skin pigmentation following treatment **(Figure 2-5).**

Based on this anti-angiogenic screening of Pyrazinib (P3) and 22 P series compounds, it was decided to further test P series compounds which produced significant (P2, P4, Pyrazinib (P3), P18 and P20) or no (P8 and P23) anti-angiogenic activity *in-vivo* to determine if these compounds could also inhibit metabolism, in particular oxidative phosphorylation, which is strongly associated with radioresistance in OAC.

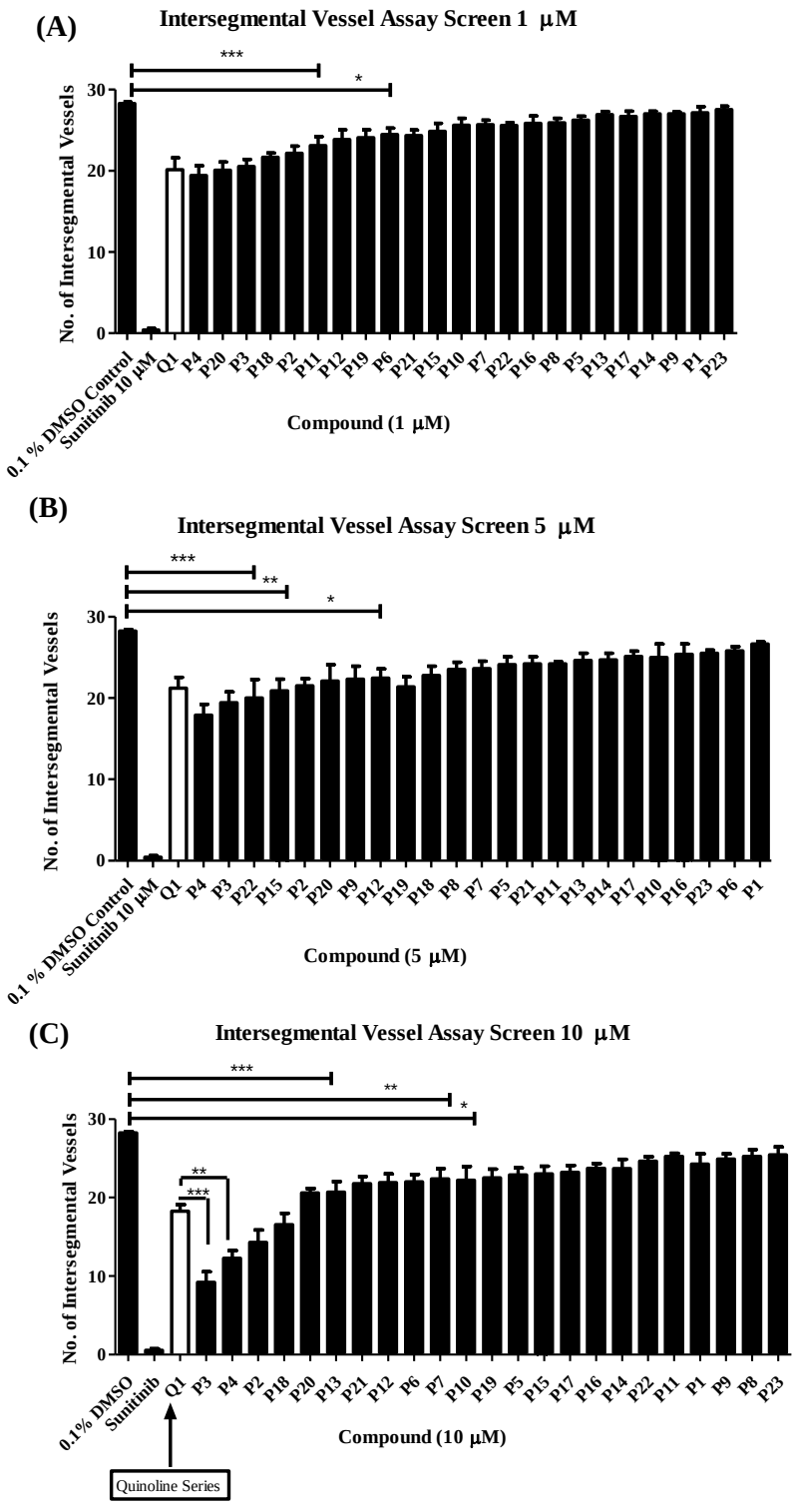

Figure 2-4 Inhibition of intersegmental vasculature growth in Tg(fli1:EGFP) zebrafish at 1, 5 and 10 µM.

6 hpf zebrafish embryos were treated with 0.1% DMSO control, 10 µM Sunitinib (positive control), parent compound Quininib (Q1), P3 and 22 P series compounds at **(A)** 1, **(B)** 5 and **(C)** 10 µM. Number of intersegmental vessels was quantified at 2 dpf. One-way ANOVA with Tukey post-tests (n=3). *p<0.05, **p<0.01 and ***p<0.001. Data expressed as mean +SEM.

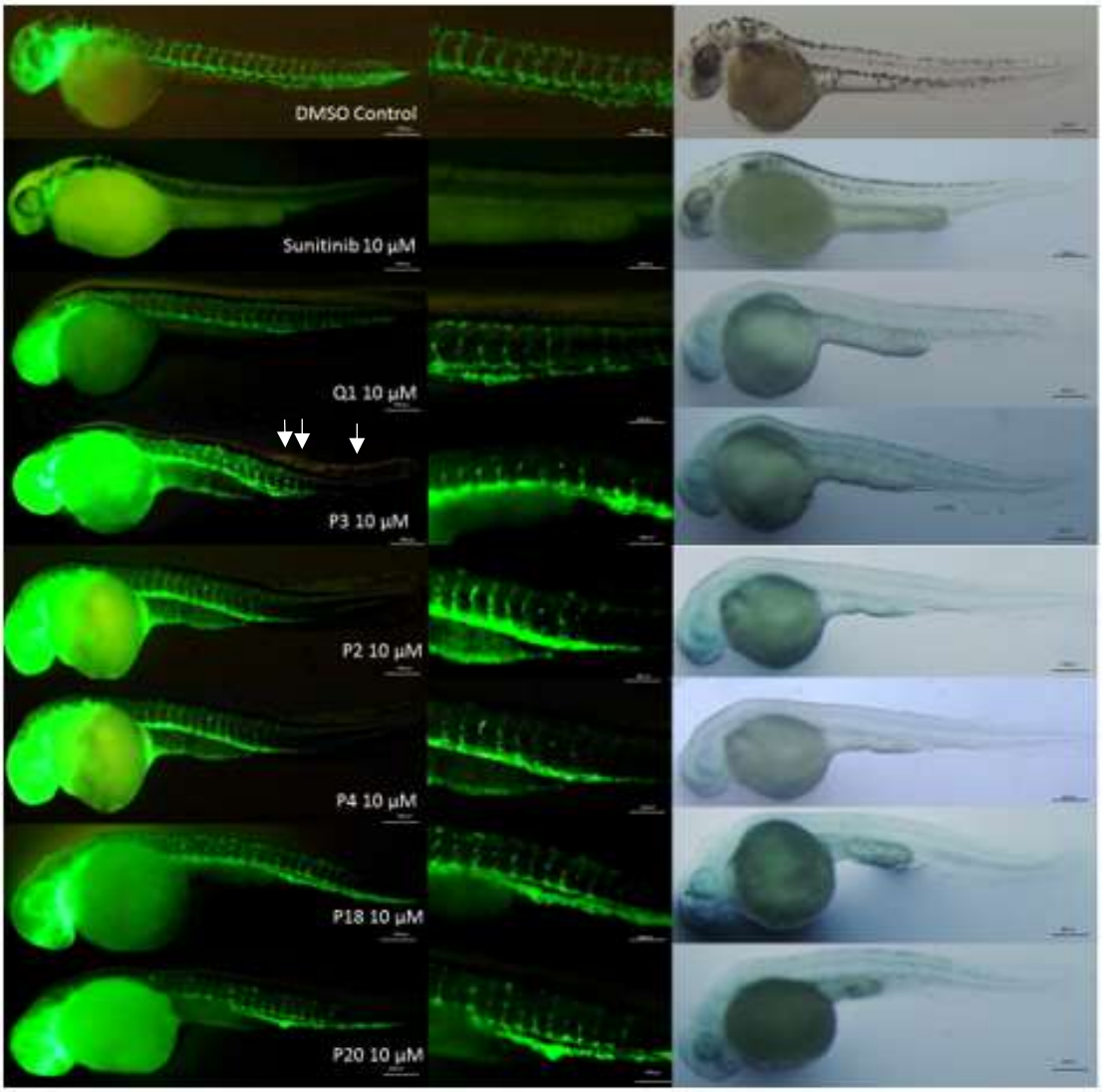

Figure 2-5 GFP and brightfield images showing Pyrazinib (P3) and P series compounds inhibit developmental angiogenesis in Tg(fli1:EGFP) zebrafish.
Representative fluorescent images illustrating GFP-positive intersegmental vessels at low and high magnification and brightfield images of whole larvae at 2 dpf in Tg*(fli1:*EGFP*)* zebrafish treated with 0.1% DMSO vehicle control, 10 µM sunitinib (positive control), Quininib (Q1) 10 µM, Pyrazinib (P3) 10 µM, P4 10 µM, P18 10 µM and P20 10 µM. White arrows highlight areas of incomplete vessel sprouting and absence of vessel growth.

2.4.2. *Measuring metabolic rate in real-time in Tg(fli1:EGFP) zebrafish embryos*

As previously mentioned we sought to identify novel compounds which could inhibit both angiogenesis and metabolism as both biological processes are tightly interlinked and are mediators of radioresistance. Zebrafish are becoming an increasingly popular model for cancer research and the use of this model for metabolic screening and profiling is continuing to emerge. Previous studies carried out by Gibert *et al*. reported using one embryo per well for metabolic screening using the Seahorse Biosciences XFe24 Seahorse Analyser [278].

We determined the optimal number of embryos to plate per well to obtain an optimal metabolic readout. When embryos were plated at either 1, 2, 3, 4 or 5 per well we found that 3 embryos per well produced a strong metabolic readout of both OCR (~218 pmol/min) and ECAR (~20 mpH/min) and was sufficient to detect a change in metabolic readout following drug treatment if present **(Figure 2-6A,B).** One and 2 embryos per well produced a much lower metabolic readout as expected and were thought to be too low to efficiently detect changes in metabolic rate where OCR was ~100-120 pmol/min and ECAR was ~5 mpH/min. Furthermore we determined when we increased the embryos in the well above 3 to 4 or 5, the embryos did not have enough space in the well and at 5 embryos the variability between wells increased. Thus, on the basis of these optimisation studies we used 3 embryos per well for our further experiments.

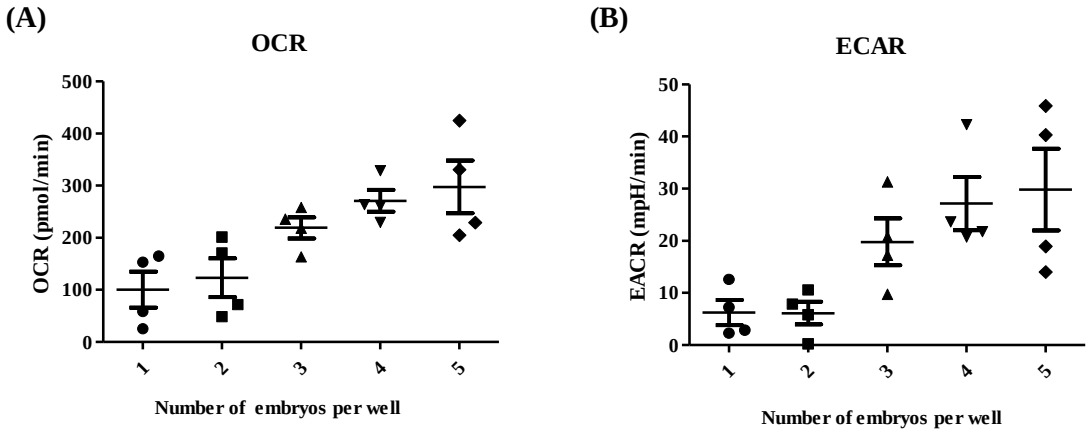

Figure 2-6. Evaluation of optimal number of zebrafish emrbyos per well to measure metabolic rate in Tg(fli1:EGFP) zebrafish embryos.

26 hpf embryos were plated 1, 2, 3, 4 or 5 per well and at 50 hpf basal metabolic rate was measured using the Seahorse Biosciences XFe24 Analyser. **(A)** Oxygen Consumption Rate (OCR) in zebrafish embryos at 50 hpf measured using the Seahorse Biosciences XFe24 Analyser, (n=1). **(B)** Extracellular acidification rate (ECAR) in 50 hpf zebrafish embryos measured using the Seahorse Biosciences XFe24 Analyser, (n=1). Data expressed as mean ±SEM.

2.4.3. *Pyrazinib (P3) and P series compounds inhibit metabolism in Tg(fli1:EGFP) zebrafish*

Following on from our angiogenic screens in zebrafish we sought to evaluate the potential of Pyrazinib (P3) and P series compounds to inhibit metabolism *in-vivo* in zebrafish embryos. Using Tg*(fli1:*EGFP*)* embryos, Pyrazinib (P3), 6 P series compounds and Quininib (Q1) of the quinoline series were screened for anti-metabolic activity as illustrated in **Figure 2-3**. 26 hpf embryos were treated with vehicle control or 10 µM of test compound and anti-metabolic activity assessed at 50 hpf using the Seahorse XFe24 Biosciences analyser. Pyrazinib (P3), P2 and P4 significantly reduced OCR (p=0.0076, p=0.0088 and p=0.0194 respectively), a measure of oxidative phosphorylation, producing a reduction of between ~16-18% **(Figure 2-7A)**, with both Pyrazinib (P3) and P2 producing a simultaneous and significant reduction in ECAR, a measure of glycolysis, (p=0.0059, p=0.0352) respectively **(Figure 2-7B)**. This significant reduction of both OCR and ECAR following treatment with 10 µM of Pyrazinib (P3) and P2 illustrates the ability of these P series compounds to target the two major metabolic pathways, oxidative phosphorylation and glycolysis.

In summary, *in-vivo* in zebrafish we identified three compounds of the P series; Pyrazinib (P3), P2 and P4 which inhibit both angiogenesis and metabolism, a significant finding given the well reported role of angiogenesis and metabolism, particularly oxidative phosphorylation in radioresponse in OAC [82].

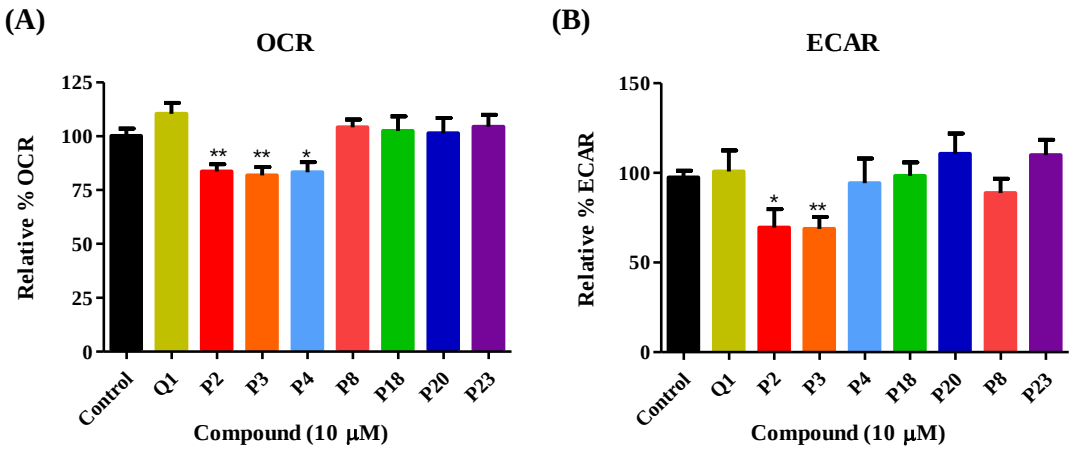

Figure 2-7 Pyrazinib (P3) and P series compounds inhibit metabolism in Tg(fli1:EGFP) zebrafish.

(A) OCR in zebrafish embryos treated with 0.1% DMSO vehicle control or 10 µM of Quininib (Q1), Pyrazinib (P3), P2, P4, P18, P20, P8 and P23, (n=5). **(B)** ECAR in zebrafish embryos treated with 10 µM of Quininib (Q1), P3, P2, P4, P18, P20, P8 and P23, (n=5). Unpaired two-tailed t-test. *p<0.05, **p<0.01. Data expressed as mean +SEM.

2.4.4. *Ranking of Pyrazinib (P3) and P series compounds following in-vivo screens in zebrafish*

Following our *in-vivo* screening of the anti-angiogenic and anti-metabolic activity of Pyrazinib (P3) and P series compounds in Tg(*fli1*:EGFP) embryos we ranked the compounds evaluated in both assays based on their activity **Table 2-2**.

Pyrazinib (P3) was identified as the most active compound in this model producing both robust anti-angiogenic and anti-metabolic activity inhibiting both OCR and ECAR. The parent compound of Pyrazinib (P3), Quininib (Q1) significantly inhibited blood vessel growth in zebrafish embryos as seen in previous studies but did not significantly alter real-time metabolic rate in this model. P2 and P4 in addition to Pyrazinib (P3) significantly inhibited blood vessel growth, OCR and ECAR and were ranked 2nd and 3rd respectively, notably P4 is a HCl salt of Pyrazinib (P3) and thus it is not surprising that it has similar activity to Pyrazinib (P3). Importantly not all compounds which significantly inhibited angiogenesis (P18, P20) inhibited metabolic rate. The P series compounds P8 and P23 which produced no significant anti-angiogenic activity did not significantly inhibit real-time metabolic rate either. Our initial findings have identified novel dual acting anti-angiogenic and anti-metabolic compounds in this zebrafish model.

Table 2-2 Ranking Table of Pyrazinib (P3) and P series compounds based on their anti-angiogenic and anti-metabolic activity in-vivo in zebrafish embryos.
Table ranking P series compounds based on their anti-angiogenic anti-metabolic activity, a greater weighting was given for inhibition of oxygen consumption rate than inhibition of extracellular acidification rate.

Rank	Hit	% ISV Reduction at 10 µM	% Reduction OCR at 10 µM	% Reduction ECAR at 10 µM	Chemical Name
Quinoline Compound	Q1	35.4	0	0	2-[2-(2-quinolinyl)vinyl]phenol
1	P3	67.4	18.19	31.3	(E)-2-(2-Pyrazin-2-yl-vinyl)-phenol
2	P4	56.6	16.8	5.8	(E)-2-(2-Pyrazin-2-yl-vinyl)-phenol HCl salt
3	P2	49.5	16.4	30.5	(E)-2-(2-Pyridin-2-yl-vinyl)-phenol HCl salt
4	P18	41.5	0	1.6	2-[2-(Pyrazin-2-yl)ethynyl]phenol
5	P20	27	0	0	2-[2-(Pyrazin-2-yl)ethynyl]phenol hydrochloride
6	P8	9.9	0	0	(E)-2-[2-(6-Methyl-pyridin-2-yl)-vinyl]-phenol HCl salt
7	P23	9.9	0	0	(E)-2-(2-(IH-imidazol-2-yl)vinyl)phenol hydrochloride

2.5. Summary of main findings of chapter 2

- Pyrazinib (P3), P2, P4, P18 and P20 significantly inhibited blood vessel development in zebrafish embryos following 10 μM treatment.

- Pyrazinib (P3) and the P series compound P4 produced a significantly greater inhibition of intersegmental blood vessel development than the parent compound of Pyrazinib (P3), Quininib (Q1) following 10 μM treatment.

- Pyrazinib (P3), P2 and P4 significantly reduced OCR, a measure of oxidative phosphorylation in zebrafish embryos with Pyrazinib (P3) and P2 producing a simultaneous reduction in ECAR, a measure of glycolysis.

2.6. Discussion

Two of twenty-three of our P series compounds tested; Pyrazinib (P3) and P4, demonstrated greater anti-angiogenic activity than the quinoline series compound Quininib, (Q1) in the ISV assay. Pyrazinib (P3) produced the most potent anti-angiogenic activity with a ~67% reduction in vessel number compared to control. The enhanced anti-angiogenic activity produced by Pyrazinib (P3) and P4 of the P series was an important finding given that Quininib (Q1), a quinoline compound from which Pyrazinib (P3) was derived was previously shown to inhibit ocular and tumoural angiogenesis using *in-vitro* and *in-vivo* models and produces a potent anti-tumoural response in a colorectal murine xenograft model [272, 282]. Thus, our initial findings indicate our novel small molecule compounds have more potent anti-angiogenic activity than quinoline series compound, Quininib (Q1), and warrant further investigation in other model systems.

The potent anti-angiogenic activity of our novel compounds is an important finding given that tumour vasculature has been recognised as a critical component of radiation response [83]. Aberrant tumour vasculature and dysregulated blood flow through tumour vasculature can promote the development of hypoxic regions which are associated with radioresistance [83]. Cells irradiated in the presence of oxygen are thought to be ~3 times more sensitive to irradiation than those located in regions of severe hypoxia [83]. In an oesophageal SCC xenograft model the administration of anti-angiogenic recombinant endostatin (rh-Endo) in combination with one dose of 8 Gy irradiation significantly delayed tumour growth which was associated with remodelling of the tumour vasculature and a reduction in tumour hypoxia in xenografts [211]. In a colon cancer xenograft model, an anti-VEGF monoclonal antibody in combination with radiation had an additive effect. The anti-VEGF antibody induced a significant tumour growth delay which was associated with a reduction in tumour microvessel density and interstitial fluid pressure [109]. These studies strongly support the development of a novel anti-angiogenic to enhance radiosensitivity. It is important to consider that the *Tg(fli1:*EGFP*)* zebrafish model used in this assay to identify our potent anti-angiogenic compounds is a model of developmental angiogenesis, and not pathological angiogenesis. Both developmental and pathological angiogenesis occur through very similar processes to drive the development of new blood vessels in response to an increased demand for oxygen and nutrients. However, pathological angiogenesis unlike developmental angiogenesis is not resolved upon the establishment of vascular perfusion. Despite this, a large number of agents currently used in the clinic such as sorafenib and regorafenib have also previously been shown to inhibit angiogenic activity in this zebrafish model [283]. In order to identify novel radiosensitisers with potential therapeutic benefit, it is likely that such agents will need to affect more than one biological process including metabolism to counteract the complex polymodal OAC radioresistant phenotype [82, 150]. Thus, in addition to

the anti-angiogenic activity produced by Pyrazinib (P3) and other P series compounds, we investigated whether these compounds could also inhibit two major metabolic pathways, oxidative phosphorylation and glycolysis *in-vivo* given the important association between oxidative phosphorylation and treatment response previously reported in OAC whereby oxidative phosphorylation was significantly upregulated in radioresistant OAC cells compared to matched radiation-sensitive OAC cells [82].

Zebrafish are becoming an increasingly popular model for cancer research and the use of this model for metabolic screening and profiling is continuing to emerge [278]. Pyrazinib (P3), P2 and P4 significantly reduced OCR, a measure of oxidative phosphorylation in zebrafish embryos, where Pyrazinib (P3) and P2 produced a simultaneous reduction in ECAR, a measure of glycolysis. These findings suggest Pyrazinib (P3) and P2 may be exerting their effect at an earlier point common to both metabolic pathways. Notably, Pyrazinib (P3) and P4, two of the most active compounds in both zebrafish assays have the same structural features including a (E)-2-(2-Pyridin-2-yl-vinyl)-phenol backbone where unlike Pyrazinib (P3), P4 is a HCl salt, thus, the highly potent activity produced by these P3 and P4 is likely to be attributable to these common structural features. *In-vitro* studies cannot recapitulate the complexity that exists in *in-vivo* systems thus whole-animal approaches are required to study metabolism. Zebrafish are a good model in which to study metabolism because they possess all the key organs required for metabolic control in humans, from the appetite circuits that are present in the hypothalamus, through to the pancreas and insulin-sensitive tissues. This highlights the unique and robust approach we have taken to identify novel anti-metabolic agents in our initial screen. Previous studies have shown the reproducibility of metabolic studies carried out in zebrafish using different housing facilities and instrumentation and highlighted the enhanced sensitivity of the Seahorse Biosciences XFe24 analyser further supporting our method and findings using our zebrafish model [284]. Whilst the current literature is limited on the use of whole zebrafish for pharmacological screening of metabolic inhibitors some studies do report validation of pharmacological manipulation of metabolic rate in zebrafish in mammalian model systems [284]. In OAC, previous studies have highlighted the importance of oxidative phosphorylation in radioresponse whereby ATP5B, a marker of oxidative phosphorylation was upregulated in patients with a subsequent poor response to chemoradiation therapy and *in-vitro,* in an OAC model of radioresistance, OCR in OE33R; radiation-resistant cells OCR was significantly higher than OCR in OE33P; radiation-sensitive cells. Targeting oxidative phosphorylation has been found to enhance radiosensitivity in multiple cancer models, *in-vivo,* in HCT-116 xenografts, administration of metformin was found to produce a 7% reduction in oxygen consumption rate and to improve tumour re-oxygenation [225]. In addition, in these xenografts, pre-treatment with metformin before one dose of 15 Gy irradiation produced a significant tumour growth delay [225].

In summary, in this chapter we have identified three compounds, Pyrazinib (P3), P2 and P4 which can significantly inhibit both angiogenesis and metabolism in zebrafish embryos. The effect of Pyrazinib (P3) and P series compounds on metabolic rate and radiosensitivity *in-vitro* in an isogenic model of OAC radioresistance is discussed in chapter 3.

Aspects of this chapter have been published in *Cancer Letters*, see **Figure 2-8**.

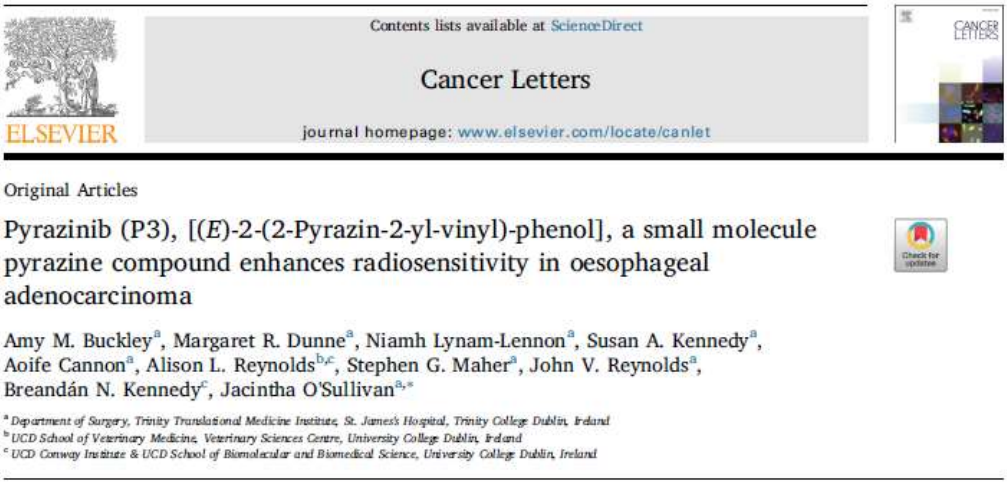

Figure 2-8 Pyrazinib (P3), [(E)-2-(2-Pyrazin-2-yl-vinyl)-phenol], a small molecule pyrazine compound enhances radiosensitivity in oesophageal adenocarcinoma.
Aspects of this chapter have been published in *Cancer Letters* [285].

3. Chapter 3 - Effect of Quininib (Q1), Pyrazinib (P3) and P series compounds on energy metabolism, mitochondrial function, radiosensitivity and cytotoxicity *in-vitro* in our isogenic model of OAC radioresistance

3.1. Introduction

In Chapter 2, we previously identified Pyrazinib (P3) and P2 which produced a greater anti-angiogenic effect than Quininib (Q1) *in-vivo* in zebrafish embryos. In addition, we found Pyrazinib (P3), P2 and P4 could also inhibit oxidative phosphorylation *in-vivo* in zebrafish embryos with Pyrazinib (P3) and P2 producing a simultaneous reduction in glycolysis. Thus, we sought to investigate the effect of Pyrazinib (P3) and P series compounds on metabolism, mitochondrial function, radiosensitivity and DNA repair gene expression *in-vitro* using our isogenic model of OAC, consisting of OE33P; radiation-sensitive cells and OE33R; radiation-resistant cells [150].

Cells produce energy primarily through two interconnected pathways; glycolysis and oxidative phosphorylation [286]. Glycolysis is an anaerobic process which involves the catabolism of glucose to pyruvate and ATP in the cytosol [286]. The pyruvate generated during glycolysis can be reduced to lactate in the absence of oxygen by lactate dehydrogenase or enters the mitochondria to be oxidised to acetyl-CoA in the presence of oxygen [286]. Oxidative phosphorylation is an aerobic process which involves the production of energy from glucose via the mitochondrial tricarboxylic acid cycle [266]. Novel therapeutics which target oxygen consumption in the tumour could reduce tumour hypoxia and create a more oxygen-rich radiation-sensitive tumour microenvironment. A common characteristic of aggressive malignant tumours is their ability to metabolise more glucose to lactic acid than normal non-malignant tissues allowing for a selective growth advantage [114].

Altered energy metabolism is an emerging hallmark of cancer [118] and feature of cancer cells which was originally alluded to in 1956 by Otto Warburg [119]. Warburg reported that cancer cells predominantly produce energy via the glycolytic pathway, even in the presence of oxygen due to defective oxidative phosphorylation, termed aerobic glycolysis [119]. Whilst in the past it was believed that aerobic glycolysis occurred in cancer cells due to permanent impairment of the oxidative phosphorylation pathway, a number of recent studies have challenged this demonstrating that in a number of cancers, the oxidative phosphorylation pathway is still intact. As a result emerging reports have suggested that the presence of aerobic glycolysis in cancers is the combined result of numerous factors such as oncogenes, hypoxia, tumour suppressors, mitochondrial DNA mutations and the genetic background of the cancer [286, 287]. Lactate reuse known as metabolic symbiosis can also occur in tumour cells where lactate can function as a medium to carry energy from highly glycolytic/hypoxic transformed cells to more oxidative cancer cells [288, 289].

Recent studies have reported the reverse Warburg effect to further describe tumour metabolism, the reverse Warburg effect proposes that cancer cells secrete hydrogen peroxide to induce the Warburg effect in stromal cells [290, 291]. Furthermore, cancer associated fibroblasts export the lactate produced by this aerobic glycolysis, which is then converted into pyruvate to be used in oxidative phosphorylation by the cancer cells [292].

Altered energy metabolism is a hallmark of cancer which is tightly linked to treatment resistance. Elevated glycolysis has previously been linked to enhanced radioresistance. In a study by Bhatt *et al*. transient stimulation of glycolysis was found to enhance radioresistance in cerebral glioma and oral carcinoma cell lines through enhanced DNA repair [293]. Inhibition of glycolysis is thought to enhance radioresponse through a reduction in DNA repair and energy production and subsequent increase in cell death [293, 294].

Oxidative phosphorylation has also been linked to radioresistance in cancer [82, 295]. A previous publication by Lynam-Lennon *et al.*, which evaluated the metabolic profile of radiation-sensitive and radiation-resistant OAC cells demonstrated that radio-resistant OAC cancer cells have an altered metabolic phenotype when compared to isogenic radiosensitive cells [82]. Radio-resistant cells were found to have a significantly higher rate of oxidative phosphorylation with no significant differences observed in glycolytic rate between the isogenic OAC cell lines [82]. In addition, radioresistant cells were also shown to have altered mitochondrial function [82]. Examination of metabolic markers in treatment-naïve patient samples of OAC found ATP5B, a surrogate marker of oxidative phosphorylation to be significantly upregulated in the patient cohort with a poor response to radiation therapy [82]. Interestingly, in a xenograft study using a cervical cancer isogenic model, tumours derived from cells with a higher intrinsic level of oxidative phosphorylation were more radioresistant when compared to matched radiosensitive cells which were predominantly glycolytic [295].

Ionising radiation is a crucial treatment modality used to exert local tumour control in over 50% of human malignancies [55]. Response to radiation plays a central role in patient outcome in OAC, with sensitivity to ionising radiation inversely correlated with tumour burden [81]. Resistance to radiation therapy is polymodal and associated with a number of biological alterations both within the tumour itself and the surrounding microenvironment including; altered cell cycle [145] accelerated repopulation [146, 147], hypoxia [148], evasion of apoptosis [149], altered DNA damage response and enhanced DNA repair [150] and altered mitochondrial function and cellular energetics [82]. Altered cellular energetics and DNA repair have been specifically linked to the radio-resistant phenotype in OAC [82, 150].

A fibrosarcoma xenograft study showed that administration of metformin, a mitochondrial complex I inhibitor twice a day at 25 mg/Kg prior and following one dose of 20 Gy ionising radiation tumour significantly inhibited tumour growth when compared to ionising radiation alone [225]. The potential of compounds which target oxidative phosphorylation as radiosensitisers are warranted. It will be important to consider the plasticity of tumour metabolism as inhibition of one pathway may result in the upregulation of another.

This chapter aimed to identify compounds with anti-metabolic activity specifically targeting oxidative phosphorylation, which in turn may enhance radiosensitivity in both radiosensitive and radioresistant OAC cells from a series of small molecule compounds consisting of Pyrazinib (P3), a pyrazine compound, and P series compounds P2, P4, P18, P20, P8 and P23. Pyrazinib (P3) was synthesised as an analogue of Quininib (Q1) and we sought to determine if Pyrazinib (P3) or compounds of the P series could produce more potent anti-cancer activity than its parent compound Quininib (Q1) in OAC. Quininib (Q1) is an anti-angiogenic quinoline compound which was previously discovered to produce significant anti-angiogenic activity and inhibit tumour growth both *in-vitro* and *in-vivo* respectively [272, 282]. The findings presented in this chapter demonstrate that *in-vitro*, in an isogenic model of OAC radioresistance, Pyrazinib (P3) significantly reduced OCR and ECAR. Pyrazinib (P3) significantly enhanced the radiosensitivity of OE33P; radiation-sensitive and OE33R; radiation-resistant cells to increasing doses of X-ray radiation.

3.2. Overall objective and specific aims of chapter 3

The overall objective of chapter 3 was to evaluate the anti-metabolic activity of Pyrazinib (P3) and P series compounds *in-vitro* using an isogenic model of radioresistance previously generated in our department. The specific aims of this chapter was to assess the effect of Quininib (Q1), the 5 most potent and 2 least potent anti-angiogenic compounds of the P series compounds previously identified in Chapter 2 in Tg(*fli1*:EGFP) zebrafish embryos on energy profiles, mitochondrial function, radiosensitivity, cytotoxicity and DNA repair gene expression *in-vitro* in our OE33P; radiation-sensitive and OE33R; radiation-resistant cells.

The specific aims of chapter 3 were:

1. Evaluate the anti-metabolic activity of Quininib (Q1) , Pyrazinib (P3), P2, P4, P18, P20, P8 and P23 on energy metabolism including oxidative phosphorylation and glycolysis *in-vitro* using our isogenic OAC cell line and the Seahorse Biosciences XFe24 Analyser.
2. Investigate the effects of Quininib (Q1), Pyrazinib (P3), P2, P4, P18, P20, P8 and P23 on ATP levels in OE33P and OE33R cell lines using the ATP luminescence assay.
3. Evaluate the effect of Quininib (Q1), Pyrazinib (P3), P2, P4, P18, P20, P8 and P23 on mitochondrial function *in-vitro* including mitochondrial membrane potential, mitochondrial mass and ROS levels in OE33P and OE33R cells.
4. Evaluate the effect of Quininib (Q1), Pyrazinib (P3), P2, P4, P18, P20, P8 and P23 on radiosensitivity and cytotoxicity *in-vitro* in OE33P and OE33R cells.
5. Evaluate the effect of Quininib (Q1), Pyrazinib (P3), P2, P4, P18, P20, P8 and P23 on cell proliferation *in-vitro* in OE33P and OE33R cells.
6. Evaluate the effect of Quininib (Q1), Pyrazinib (P3), P2, P4 on the expression of *MLH1*, *SMUG1, PARP1* and *MMS19* in OE33P and OE33R cells.
7. Carry out a dose response to investigate the effect of Pyrazinib (P3) on radiosensitivity in OE33P and OE33R cells at 1, 5 and 10 μM.
8. Evaluate the effect of Pyrazinib (P3) on radiosensitivity at increasing doses of irradiation in our isogenic model of OAC radioresistance.

3.3. Methods

3.3.1. *Generation of the OE33P and OE33R cell lines*

The human OE33 oesophageal adenocarcinoma cell line was obtained from the European Collection of Authenticated Cell Cultures. The isogenic model of radioresistant OAC; OE33P (radiosensitive) and OE33R (radioresistant) cells was generated as previously described [150].

3.3.2. *Cell sub-culture*

Cells were examined daily using an inverted phase contrast Nikon microscope (Nikon Corporation, Tokyo, Japan) and sub-cultured upon reaching 70-80% confluency. Both OE33P and OE33R cells were cultured in Roswell Park Memorial Institute (RPMI) 1640 medium supplemented with 10% fetal bovine serum (FBS) (Lonza, Basal, Switzerland) and 1% penicillin-streptomycin (Lonza, Basal, Switzerland). Growth media was decanted and cells were washed with 3 mL PBS. 2 mL trypsin ethylene-diamine tetra acetic acid (EDTA) (0.5% trypsin, 0.02% EDTA) was added to the flask and cells were incubated for 3-5 min at 37°C in 5% CO_2/95% air until they had detached from the surface. 6 mL complete medium was added to inactivate the trypsin, cell pellets were collected in 15 mL tubes after centrifugation at 180 x g for 3 min, cells were seeded at appropriate densities in vented 75 cm^2 culture flasks.

3.3.3. *Preparation of frozen cell stocks*

Frozen cell stocks were prepared from cell lines growing in the exponential phase at 70-80% confluency. The flask of cells was trypsinised and 10 mL complete medium was added to inactivate the trypsin. Cells were centrifuged at 180 x g for 3 min, the supernatant was decanted, and the pelleted cells were resuspended in 3 mL FBS containing 10% DMSO. The cell suspension was divided into 1 mL aliquots in cryovials and placed in a -80°C freezer for short-term storage or under liquid nitrogen for long-term storage.

3.3.4. *Reconstitution of frozen cells*

Frozen stocks were thawed rapidly in a water-bath at 37°C, added to 5 mL complete medium and centrifuged at 180 x *g* for 3 min. The supernatant was decanted and the cell pellet was resuspended in 5 mL complete medium and transferred to a vented 25 cm^2 culture flask. Once the cells were 70-80% confluent, they were trypsinised and transferred to a 75 cm^2 flask.

3.3.5. *Cell counting*

Cell counting was carried out using a Bright Line haemocytometer (Hausser Scientific, PA, USA). Cells pellets were collected as previously described. The supernatant was decanted and the cell pellet was resuspended in 1 mL complete medium. 20 µL of the cell suspension was added to 180 µL of trypan blue solution (0.4%), mixed by pipetting, and 20 µL was added to the

haemocytometer. Viable cells were unstained due to their active exclusion of trypan blue, whereas dead cells were stained blue due to their disrupted cell membranes. The number of viable cells in each of the five squares at the corners of the grid and the square in the centre of the grid was counted excluding cells touching the edges of the grid. The number of cells per mL was calculated using the following equation:

(Total number of cells/5) x 10^4 x 10 (dilution factor) = number of cells/mL where;

5=number of squares counted, 4= Haemocytometer constant and 10=Trypan blue dilution factor.

3.3.6. *OCR and ECAR measurements in OE33P and OE33R cells*

OE33P and OE33R cells were seeded in triplicate at a density of 11,000 and 13,000 cells/well, respectively in 24-well cell culture XFe24 microplates (Agilent Technologies, Santa Clara, CA, USA) at a volume of 100 μL in complete RPMI-1640 and allowed to adhere at 37°C in 5% CO_2/95% air. Following 5 h incubation, an additional 150 μL/well complete RPMI-1640 medium was added. Twenty four hours later, OE33P and OE33R cells were treated with either 0.1% DMSO control or 10 μM of Quininib (Q1), Pyrazinib (P3), P2, P4, P18, P20, P8 and P23. Following 24 h treatment, media was removed and cells were washed with unbuffered Dulbecco's Modified Eagle's medium (DMEM) supplemented with 10 mM glucose (Sigma-Aldrich) and 10 mM sodium pyruvate (Sigma-Aldrich) (pH 7.4) and incubated for 1 h at 37°C in a CO_2-free incubator. OCR and ECAR were measured using a Seahorse Biosciences XFe24 Analyser (Agilent Technologies, Santa Clara, CA, USA). Three basal measurements of OCR and ECAR were taken over 24 min consisting of three repeats of mix (3 min) / wait (2 min) / measurement (3 min) to establish basal respiration. Three additional measurements were obtained following the injection of 3 mitochondrial inhibitors including oligomycin (Sigma Aldrich), an uncoupling agent carbonyl cyanide 4-(trifluoromethoxy) phenylhydrazone (FCCP) (Sigma-Aldrich) and antimycin-A (Sigma-Aldrich). ATP turnover was calculated by subtracting the OCR post oligomycin injection from baseline OCR prior to oligomycin addition. Maximal respiration was calculated by subtracting OCR post antimycin A addition from OCR post FCCP addition. Spare respiratory capacity was calculated by subtracting basal OCR from maximal respiration. All measurements were normalised to cell number using the crystal violet assay, transferring the eluted stain to a 96-well plate before reading.

3.3.7. *Crystal violet assay*

Cells were fixed with 1% glutaraldehyde (Sigma-Aldrich) for 15 min at RT. The fixative was removed and cells were washed with PBS and stained with 0.1% crystal violet in dH_20 for 30 min at RT. Plates were left to air dry and incubated with 50 μL 1% Triton X-100 in PBS on a plate

shaker for 30 min at RT. Absorbance was read at 595nm on a VersaMax microplate reader (Molecular Devices, Sunnyvale, CA, USA).

3.3.8. *ATPlite assay*

ATP levels were measured using the ATPlite™ Luminescence Assay System (Perkin Elmer, Waltham, MA, USA). ATP levels are measured on the basis of the production of light caused when ATP reacts with luciferase and D-luciferin, with the emitted light proportional to ATP concentration. This assay was carried out in a low lit area in 96-well white-walled plates (Perkin Elmer, Waltham, MA, USA). OE33P and OE33R cells were seeded at a density of 8,000 cells/well in 96-well plates in triplicate and allowed to adhere overnight. Twenty-four hours later, OE33P and OE33R cells were treated with 0.1% DMSO control or 10 μM Quininib (Q1), Pyrazinib (P3), P2, P4, P18, P20, P8 and P23 by removal of 50 μL of cell media and addition of 50 μL of novel compound diluted in complete media. 24 h later, 50 μL/well Mammalian Cell Lysis Solution (Perkin Elmer, Waltham, MA, USA) was added. The plate was incubated with vigorous shaking for 5 min at RT. The ATP Lyophilised Substrate (Perkin Elmer, Waltham, MA, USA) was resuspended in 5 mL Substrate Buffer and 50 μL/well was added. The plate was incubated with vigorous shaking for 5 min at RT. The plate was dark adapted for 10 min at RT and luminescence was read on a FLx800 Fluorescence Microplate Reader (Mason Technology Dublin, Ireland). Luminescence values were normalised to cell numbers using the crystal violet assay in section 3.3.7.

3.3.9. *Reactive oxygen species (ROS) levels*

Reactive oxygen species (ROS) levels were measured using 2,7-dichlorofluorescein (DCF) which emits a fluorescent signal linearly linked to the intracellular H_2O_2. OE33P and OE33R cells were seeded at a density of 8,000 cells/well in triplicate and allowed to adhere overnight. Following 24 h incubation after seeding, OE33P and OE33R cells were treated with for 24 h with 10 μM Quininib (Q1), Pyrazinib (P3), P2, P4, P18, P20, P8 and P23 or 0.1% DMSO control dissolved in RPMI-1640, 24 h later media was removed from wells. 50 μL of 5 μM 2,7-DCF in PBS Mg^{++} (Sigma-Aldrich) was added to each well and incubated for 30 min at 37°C in 5% CO_2/95% air. The stain was removed and 100 μL PBS was added to each well, fluorescence was measured on a FLx800 fluorescence microplate reader (Mason Technology Dublin, Ireland). Fluorescence was normalised to cell number using the crystal violet assay, as previously described in section 3.3.7.

3.3.10. *Mitochondrial membrane potential*

To assess mitochondrial membrane potential, the fluorescent probe rhodamine 123 (5 μM) was used, which is selectively taken up by mitochondria and its uptake dependent on mitochondrial membrane potential. OE33P and OE33R cells were seeded at a density of 8,000 cells/well in triplicate and allowed to adhere overnight. 24 h later, OE33P and OE33R cells were treated with 0.1% DMSO control or 10 μM of Quininib (Q1), Pyrazinib (P3), P2, P4, P18, P20, P8 and P23 for 24 h. Following 24 h incubation, the media was removed from wells and cells were washed with 100 μL of PBS. 50 μL of 5 μM rhodamine 123 in PBS Mg^{++} solution was added to each well and incubated for 30 min at 37°C in 5% CO_2/95% air. The stain was removed and 100 μL of PBS added to each well. Fluorescence was measured on a FLx800 fluorescence microplate reader (Mason Technology Dublin, Ireland). Fluorescence was normalised to cell number using the crystal violet assay, as previously described in section 3.3.7.

3.3.11. *Mitochondrial mass*

MitoTracker Green (0.3 μM, Invitrogen, Carlsbad, CA, USA), a mitochondrial selective dye was used to evaluate mitochondrial mass in OE33P and OE33R cells treated with 10 μM of our novel compounds. OE33P and OE33R cells were seeded at a density of 8,000 cells/well in triplicate in 100 μL complete RPMI-1640 and allowed to adhere overnight. Following 24 h incubation after seeding, OE33P and OE33R cells were treated with 0.1% DMSO or 10 μM Quininib (Q1), Pyrazinib (P3), P2, P4, P18, P20, P8 and P23. Following 24 h treatment, media was removed and 50 μL of 0.3 μM MitoTracker Green in PBS Mg++ and incubated for 30 min at 37°C in 5% CO_2/95% air. The stain was removed and 100 μL PBS was added to each well and fluorescence was measured on a FLx800 fluorescence microplate reader (Mason Technology Dublin, Ireland). Fluorescence was normalised to cell number using the crystal violet assay, as previously described section 3.3.7.

3.3.12. Clonogenic assay

OE33P and OE33R cells were trypsinised, counted and seeded at the optimised densities of 1 - 11 x 10^3 in 1.5 mL complete RPMI-1640 in triplicate in 6 well plates and allowed to adhere overnight. 24 h later OE33P and OE33R cells were treated with 0.1% DMSO control or 10 μM of Quininib (Q1), Pyrazinib (P3), P2, P4, P18, P20, P8 and P23. Following 24 or 72 h incubation, OE33P and OE33R cells were either irradiated at 2 Gy or mock irradiated (0 Gy). OE33P and OE33R cells were additionally treated with either 0.1% DMSO or Pyrazinib (P3) at 1, 5 or 10 μM for 24 h prior to 2, 4 or 6 Gy irradiation or mock irradiation. Colonies were allowed to grow for 7-14 days at which point they were stained and fixed with ~200 μL crystal violet (0.5%/ 25% v/v methanol) per well and allowed to air dry. Colonies consisting of 50 cells or more were counted

using a colony counter (ColCountTM, Oxford Optronix, Oxford, UK). Plating efficiency (PE), fraction of colonies formed by untreated cells, was calculated using the formula: PE = No. colonies/No. cells seeded. The surviving fraction (SF), the number of colonies formed by treated cells, expressed in terms of PE, was calculated using the formula: SF = No. colonies/(No. cells seeded x PE).

3.3.13. *Irradiation*

Irradiation was performed using a Gulmay Medical X-ray generator, (RS225) (Gulmay Medical), at a dose rate of 3.25 Gray (Gy) per min.

3.3.14. *BrdU ELISA*

Proliferation was assessed using the BrdU cell proliferation enzyme-linked immunosorbent assay (ELISA) (Roche Diagnostics, Sussex, UK). The pyrimidine analogue 5-bromo-2'deoxyuridine (BrdU) is incorporated in the place of thymine in the newly synthesised DNA of proliferating cells during the S phase of the cell cycle, and is bound by the BrdU anti-POD antibody. The antibody complexes are then detected by a substrate reaction. As DNA is only synthesised in proliferating cells, this assay gives a measurement of cell proliferation. Cells were seeded in triplicate at a density of 5,000 cells/well in complete RPMI-1640 in 96-well plates and allowed to adhere overnight, followed by treatment with 0.1% DMSO control or 10 μM Quininib (Q1), Pyrazinib (P3), P2, P4, P18, P20 , P8 and P23 for 24 or 72 h. 10 μM BrdU labelling solution was added (except for background control wells) and cells were incubated for 1 hour at 37°C in 5% CO_2/95% air. The media was removed and cells were fixed by adding 200 μL FixDenat and incubating for 30 min at RT. FixDenat was removed, 100 μL/well Anti-BrdU-POD working solution was added (1:100 dilution of Anti-BrdU-POD stock solution in antibody dilution solution) and cells were incubated for 90 min at RT. Cells were washed three times with 250 μL washing solution. 100 μL/well substrate solution was added and cells were incubated for 5-10 min at RT until colour was sufficient for photometric detection. 25 μL/well sulfuric acid (H_2SO_4) was added to stop the reaction and absorbance was measured at 450nm on a VersaMax microplate reader (Molecular Devices, Sunnyvale, CA, USA).

3.3.15. *RNA isolation*

OE33P and OE33R cells were seeded at a density of 2.5 x 10^5 cells/well in complete RPMI-1640 in 6-well plates and allowed to adhere overnight. Following drug treatment with 10 μM of Quininib (Q1), Pyrazinib (P3), P2, P4 or 0.1% DMSO control for 24 h, RNA was isolated from cell lines using the TRI Reagent® method. The RNA pellet was re-suspended in 30 μL RNAase free molecular grade H_20 and stored at -80°C.

3.3.16. *RNA quantification*

RNA quantification was determined spectrophotometrically, using a Nanodrop 1000 spectrophotometer (version 3.1.0, Nanodrop technologies, DE, USA). 1 µL RNase-free water was used to blank the instrument prior to RNA analysis. 1 µL of each sample of isolated RNA was loaded onto the instrument and concentration was measured in ng/µL. 260:280 and 260:230 ratios were also recorded to evaluate RNA quality.

3.3.17. *cDNA synthesis*

For cell line samples, total RNA (1 µg total RNA) was reverse transcribed to cDNA using the following method. To anneal the primers to the RNA, the sample was heated for 10 min at 70°C, and immediately chilled for at least 1 min at 4°C. A master mix containing RNaseOUT (Invitrogen, Carlsbad, CA, USA) recombinant ribonuclease inhibitor (1unit/µL), dNTPs (Invitrogen, Carlsbad, CA, USA) (10 mM, prepared as a 1:1:1:1 ratio of dATP, dGTP, dTTP and dCTP), Bioscript reverse transcriptase (200units/µL) (Bioline, Kilkenny, Ireland) and 5X Bioscript Reaction Buffer (Bioline, Kilkenny, Ireland) in RNase-free water was added to each sample. Samples were incubated for 1 h at 37°C then 10 min at 70°C and held at 4°C. The resulting cDNA was stored at -20°C.

3.3.18. *Quantitative real-time PCR (RT-PCR)*

Mastermix was prepared with 10 µL Taqman® Universal Master Mix (2X, Applied Biosystems, CA, USA) and 8 µL nuclease-free H_2O per sample to be amplified. 1 µL cDNA and 1 µL RealTime Ready Custom Single Assay probes for *MLH1, SMUG1, PARP1, MMS19* (Roche) and *18S* (Applied Biosystems) were added in triplicate to a 96-well MicroAmp™ Optical reaction plate (Applied Biosystems, CA, USA). A non-template control using 1 µL H_2O instead of cDNA template was also included. The plate was sealed using an optical adhesive cover (Applied Biosystems, CA, USA), and the plate was centrifuged briefly to pool reagents and eliminate any bubbles. Quantitative real-time PCR (qPCR) detections were performed using an ABI Quant Studio 5 real-time thermal cycler (Applied Biosystems, CA, USA). The plate was heated for 2 min at 50°C, then 10 min at 95°C, followed by 40 cycles of 15 seconds at 95°C and 1 min at 60°C for 1 min.

3.3.19. *Quantitative real-time PCR data analysis*

Data analysis was performed using Thermofisher Scientific Connect qPCR application software. The threshold cycle (Ct) for each well was calculated and the expression levels of target genes

were normalised to expression levels of an endogenous control gene (18S ribosomal RNA). Analysis of gene expression data was performed using the 2-ΔΔCt relative quantification method, which describes the change in expression of a target gene relative to the expression of a reference group, such as an untreated control. One sample was set as the calibrator for the analysis. Gene expression changes were only reported if the transcript was amplified before 35 cycles.

3.3.20. *Statistical analysis*

Statistical analysis was performed using GraphPad Prism version 5 software (GraphPad Software, CA, USA). Scientific data were expressed as mean ±SEM. SEM was calculated as the standard deviation of the original samples divided by the square root of the sample size. Specific statistical tests used are indicated in figure legends. For all statistical analysis, differences were considered statistically significant at $p<0.05$.

3.4. Results

3.4.1. *Pyrazinib (P3) significantly alters metabolic rates in OE33P (radiation-sensitive) and OE33R (radiation-resistant) isogenic OAC cells*

In chapter 2 we previously identified 3 compounds Pyrazinib (P3), P2 and P4 which significantly inhibited metabolic rate *in-vivo* in zebrafish embryos. In this chapter we investigated if Pyrazinib (P3) and P series compounds altered OCR and ECAR when tested in an *in-vitro* model, we used an isogenic OAC cell line model of radioresistance, OE33P; radiation-sensitive and OE33R; radiation-resistant, cells which was previously generated in our department [150]. The effect of our novel compounds on two major metabolic pathways; oxidative phosphorylation and glycolysis was assessed using the Seahorse Biosciences XFe24 analyser. Following 24 h treatment of OE33P and OE33R cells with our novel P series compounds, simultaneous measurements of OCR and ECAR were recorded in live cells. Radioresistant OE33R cells produced a significantly higher OCR at baseline when compared to OE33P cells ($p<0.05$) but no significant difference in ECAR was observed **(Figure 3-1A, B).** 24 h treatment with Pyrazinib (P3) significantly reduced OCR in OE33P (7.8%) and OE33R (22.1%) cells ($p=0.0262$, $p=0.0044$) (**Figure 3-1C, E**), with a simultaneous reduction in ECAR in OE33R cells ($p=0.0162$) **(Figure 3-1F)**. Treatment with P2 produced a reduction in OCR alone in OE33R cells ($p=0.0169$). Interestingly, the non-anti angiogenic analogue P8 increased OCR in OE33P cells ($p=0.0175$) **(Figure 3-1C)** and Quininib (Q1) significantly reduced ECAR in OE33P cells only **(Figure 3-1D)**. Interestingly, no significant effect was seen following treatment with P4, the HCl salt of Pyrazinib (P3), which was previously shown to have anti-angiogenic and anti-metabolic activity in zebrafish embryos **(Figure 2-5, Figure 2-7)**. This screen demonstrated the novel anti-metabolic action of Pyrazinib (P3) *in-vitro* through the production of a significant reduction in OCR in both OE33P and OE33R cells and ECAR in OE33R cells only. P series compounds; P8 and P23 which produced no effect on angiogenesis or metabolism *in-vivo* in zebrafish embryos also produced no anti-metabolic activity when tested *in-vitro* in the isogenic OAC model (**Figure 3-1C,D,E,F).** In summary, Pyrazinib (P3) a novel small molecule compound can significantly inhibit oxidative phosphorylation in radiation-sensitive (OE33P) and radiation-resistant (OE33R) OAC cells, with a simultaneous reduction in glycolysis in radiation-resistant OE33R cells.

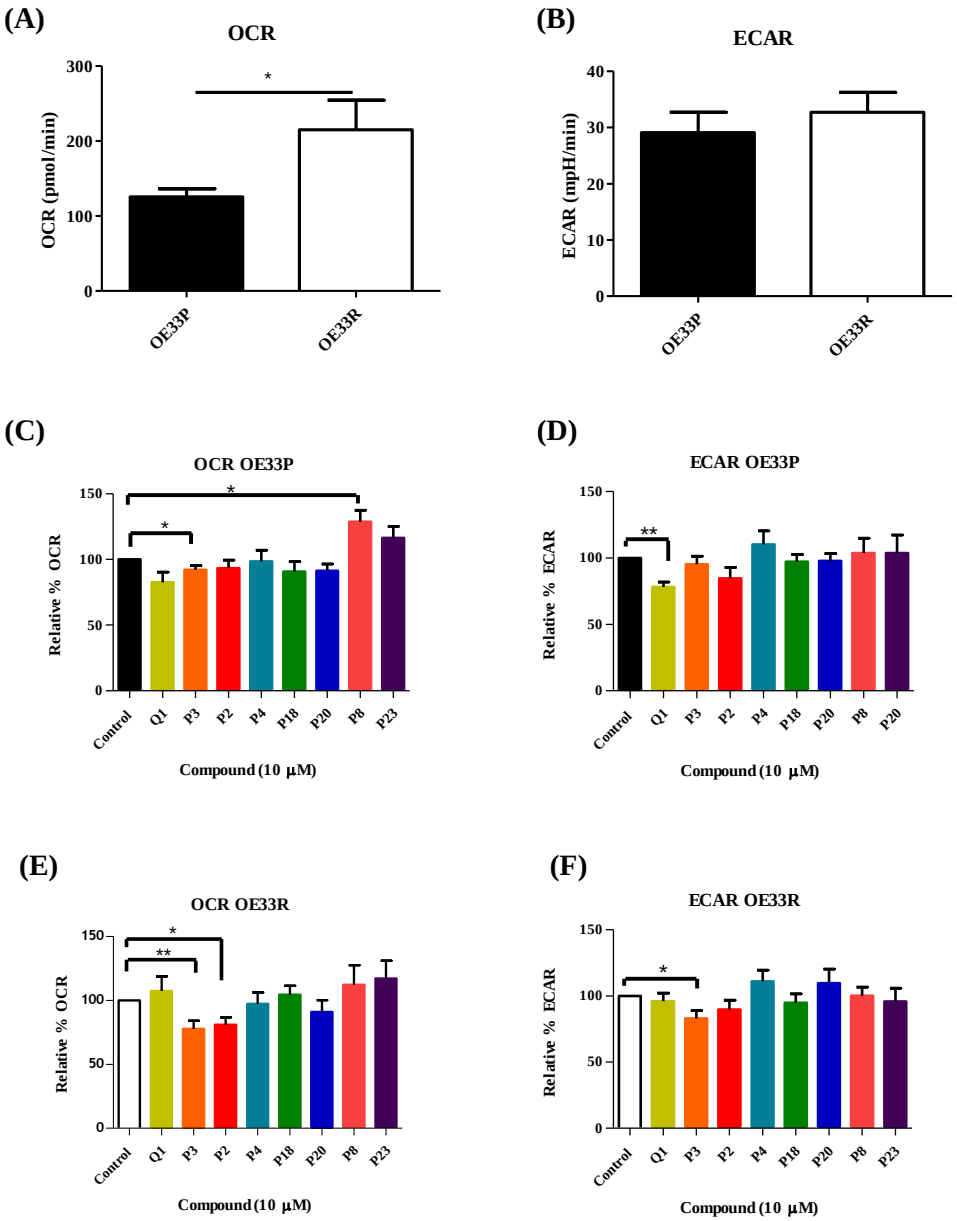

Figure 3-1 Pyrazinib (P3) treatment reduced oxidative phosphorylation and glycolysis in OE33R; radioresistant OAC cells.

(A) OCR, a measure of oxidative phosphorylation was evaluated in OE33P and OE33R cells using the Seahorse Biosciences XFe24 analyser. OE33R; radiation-resistant cells have a significantly higher OCR when compared to OE33P; radiation-sensitive cells, (n=13). **(B)** ECAR, a measure glycolysis was evaluated in OE33P and OE33R cells using the Seahorse Biosciences XFe24 analyser, (n=13). **(C)** Relative percentage OCR in OE33P cells following treatment with 0.1% DMSO control, Quininib (Q1), Pyrazinib (P3), P2, P4, P18, P20, P8 and P23 at 10 µM, (n=7, except Pyrazinib (P3) n=12). **(D)** ECAR in OE33P cells following treatment with 0.1% DMSO control, Quininib (Q1) or P series compounds at 10 µM (n=7, except Pyrazinib (P3) n=12). **(E)** Relative percentage OCR in OE33R cells following treatment with 0.1% DMSO control, Quininib (Q1), or P series compounds at 10 µM, (n=7, except Pyrazinib (P3) n=12). **(F)** Relative percentage ECAR in OE33R cells following treatment with 0.1% DMSO control, Quininib (Q1) or P series compounds at 10 µM (n=7 except Pyrazinib (P3) n=12). Statistical analysis was carried out using an unpaired t-test to compare different cell lines and a paired t-test to compare within the same cell line, *p<0.05, **p<0.01. Data was normalised to cell number, as assessed by crystal violet assay. Data are expressed as mean +SEM.

3.4.2. *ATP levels are significanty higher in OE33R cells compared to OE33P cells*

To further investigate the anti-metabolic activity of our P series compounds we investigated the effect of treatment on ATP levels in OE33P and OE33R cells using an ATPlite luminescence assay. OE33P and OE33R cells were treated with 0.1% DMSO control, 10 μM of Quininib (Q1), Pyrazinib (P3) or P series compounds for 24 or 72 h and ATP levels were measured using an ATP luminescence assay. Interestingly there was no significant difference observed in ATP levels in OE33P compared OE33R cells at 24 h **(Figure 3-2A)** but ATP levels were significantly higher in OE33R cells compared to OE33P cells at 72 h, **(Figure 3-2A),** *$p<0.05$. In addition, no significant changes in ATP levels were observed following treatment with Pyrazinib (P3), which was previously shown to inhibit OCR in OE33P and OE33R cells **(Figure 3-2B,C,D,E).** Interestingly, P20 which was previously shown to inhibit angiogenesis *in-vivo* but had no effect on metabolic rate *in-vivo* or *in-vitro* was found to significantly increase ATP levels in OE33R cells following 72 h treatment ($p=0.0420$) **(Figure 3-2E).** In addition, treatment with P8 for 72 h, a compound which was previously shown to have no anti-angiogenic activity *in-vivo* and increased OCR in OE33P cells, significantly increased ATP levels in both OE33P ($p=0.0220$) and OE33R ($p=0.0190$) cells **(Figure 3-2E)**. In summary, P series compounds which were previously shown to inhibit metabolic rate did not significantly alter ATP levels in OE33P or OE33R cells following 24 or 72 h treatment whilst 2 compounds which were previously shown to have no anti-metabolic activity, P20 and P8 significantly increased ATP levels following 72 h treatment.

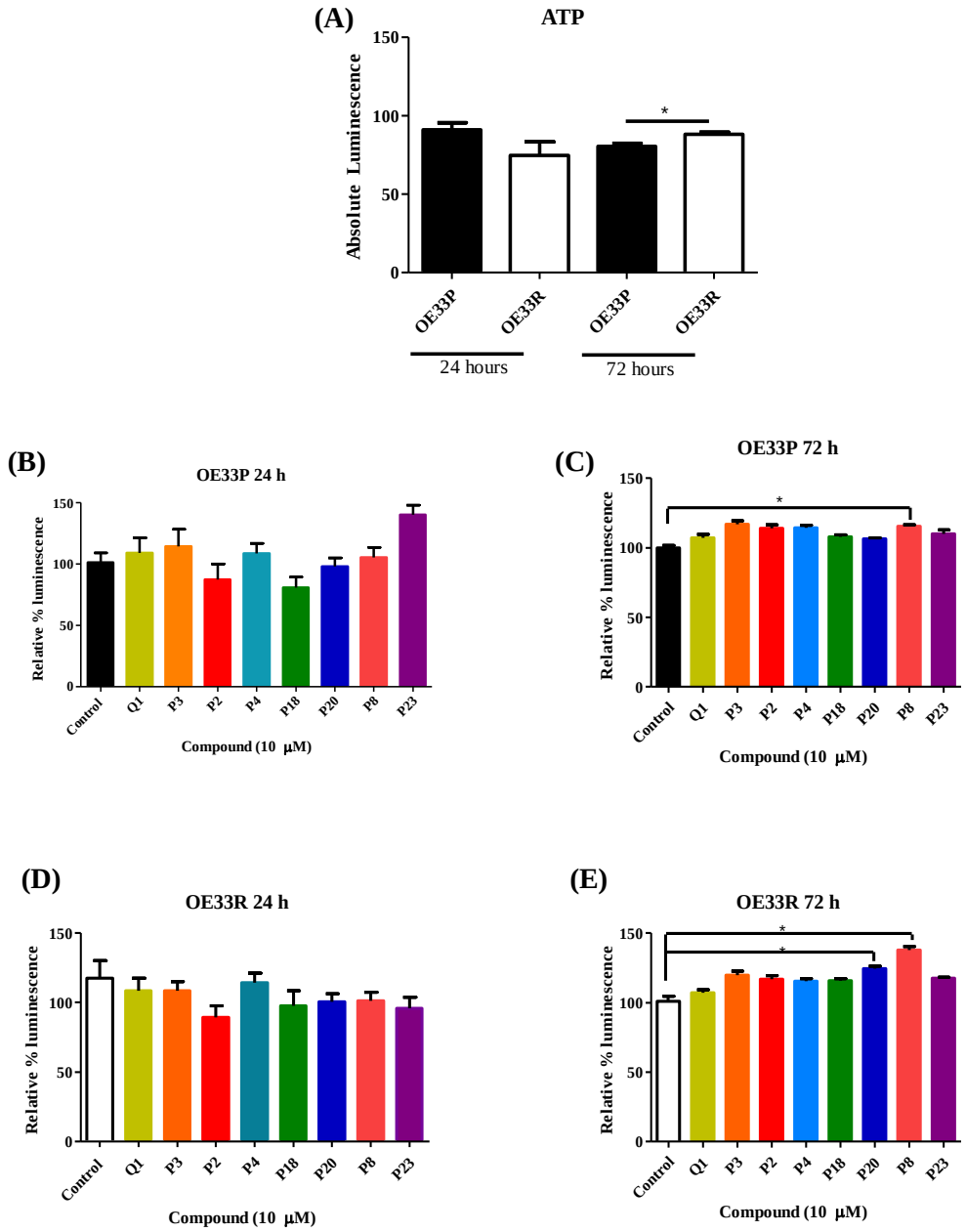

Figure 3-2 The effect of 24 and 72 h treatment with P series compounds on ATP levels in OE33P and OE33R cells.

Difference in ATP levels were assessed using an ATP luminescence assay, at **(A)** 24 h and 72 h in OE33P and OE33R cells, two-tailed, unpaired t-test, (n=4). ATP levels in OE33P cells following treatment with 10 µM of Quininib (Q1), Pyrazinib (P3) and P series compounds for **(B)** 24 h and **(C)** 72 h (n=4). ATP levels in OE33R cells following treatment with 10 µM of Quininib (Q1), Pyrazinib (P3) and P series compounds for **(D)** 24 h and **(E)** 72 h, two-tailed, unpaired t-test, (n=3). Paired t-tests used to compare same cell lines, unpaired t-tests used to compare different cell lines. *p<0.05. Data was normalised to cell number, as assessed by crystal violet assay. Data expressed as mean +SEM.

3.4.3. *Pyrazinib (P3) reduces ROS levels in radiation-sensitive OE33P cells with no effect on mitochondrial mass and mitochondrial membrane potential*

Treatment with Pyrazinib (P3) and P2 was previously shown to reduce metabolic rate in the isogenic model of OAC, thus, we investigated if this reduction in metabolic rate was accompanied by changes in mitochondrial function following treatment with our novel compounds. To investigate if treatment with our novel compounds induced changes in mitochondrial function we assessed alterations in ROS levels, mitochondrial membrane potential and mitochondrial mass, three surrogate markers of mitochondrial function.

OE33R cells were associated with significantly higher basal levels of ROS (p=0.0151) when compared to age and passage matched OE33P cells (**Figure 3-3A**). Treatment with our novel compounds had a notable effect on ROS production in OE33P cells (**Figure 3-3B**) but no changes in ROS were observed following treatment in OE33R cells (**Figure 3-3C**). 24 h treatment with Pyrazinib (P3), P2 and P18, P20 significantly reduced ROS levels in OE33P cells (p<0.01) with P4 and P8 also inducing a modest but significant reduction in ROS levels (p<0.05) in radiation-sensitive OE33P cells **(Figure 3-3B)**. There were no significant differences in the other two surrogate markers of mitochondrial function; mitochondrial membrane potential and mitochondrial mass either between the two cell lines at baseline or following treatment with 10 μM of novel compounds **(Figure 3-3D-I)**.

In summary, the potent anti-metabolic activity of Pyrazinib (P3) in OE33R cells is independent of changes to mitochondrial function including ROS production, mitochondrial membrane potential and mitochondrial mass.

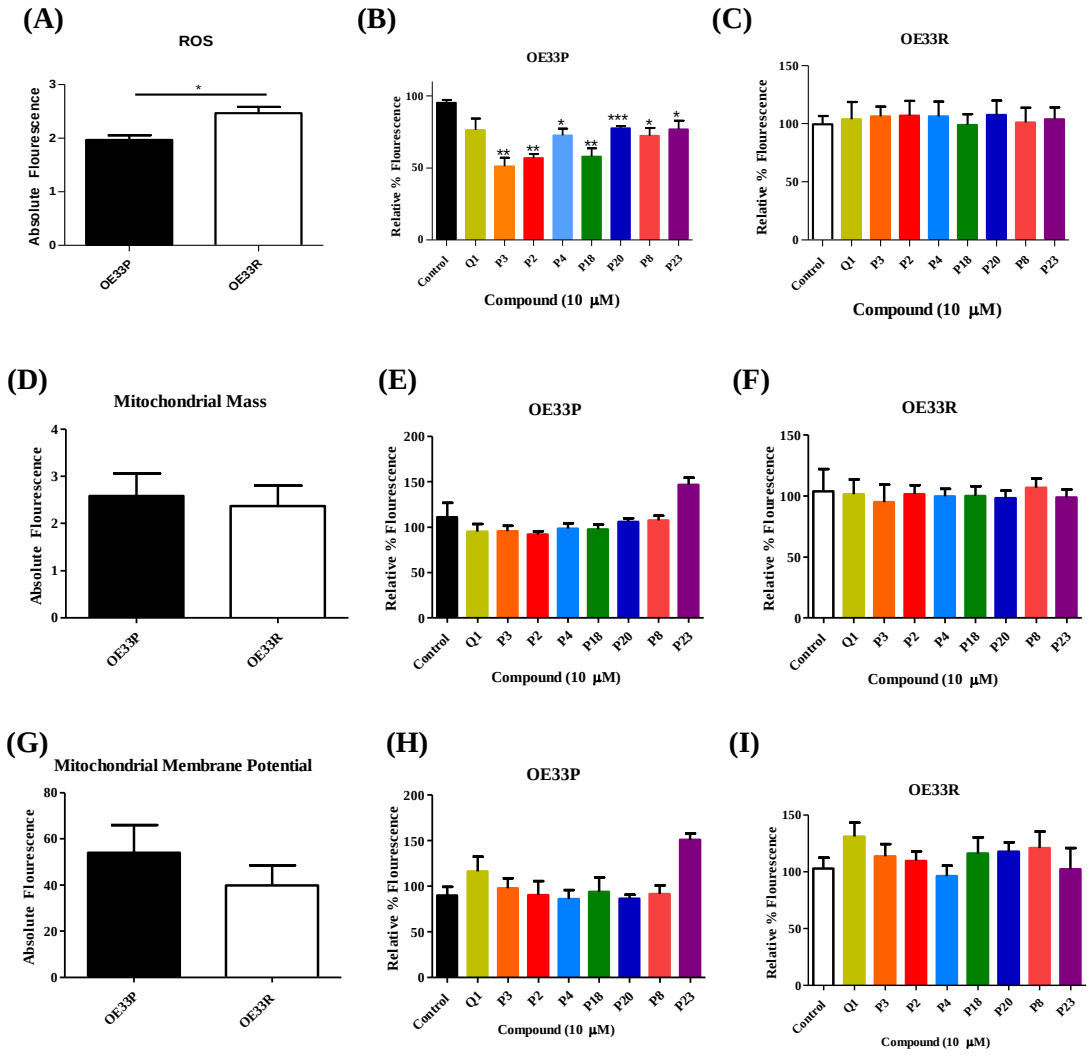

Figure 3-3 Pyrazinib (P3) and P series compounds can reduce ROS levels in the radiation-sensitive OE33P cells with no effect on mitochondrial mass and mitochondrial membrane potential.

(A) ROS levels are significantly higher in radiation-resistant OE33R cells compared OE33P; radiation-sensitive cells, (n=4). **(B)** 24 h treatment with 10 µM Pyrazinib (P3) or P series compounds significantly reduced ROS in OE33P cells, (n=4). **(C)** Pyrazinib (P3) and other P series compounds tested did not significantly alter ROS levels in OE33R cells following treatment at 10 µM, (n=4). **(D)** Mitochondrial mass was not significantly different between OE33P and OE33R cells, (n=4). **(E)** 24 h treatment with 10 µM of Q1 or P series compounds did not significantly alter mitochondrial mass in OE33P cells, (n=4) **(F)** 24 h treatment with 10 µM of Quininib (Q1) or P series compounds did not significantly alter mitochondrial mass in OE33R cells, (n=4). **(G)** Mitochondrial membrane potential was not significantly different between OE33P and OE33R cells, unpaired t-test, (n=4). **(H)** 24 h treatment with 10 µM of P series compounds had no effect on mitochondrial membrane potential in OE33P cells, (n=4). **(I)** 24 h treatment with 10 µM of Q1 or P series compounds had no effect on mitochondrial membrane potential in OE33R cells, (n=4). Statistical analysis was carried out using an unpaired t-test to compare different cell lines and paired t-test to compare within same cell line, *p<0.05, **p<0.01, ***p<0.001. Data was normalised to cell number, determined by crystal violet assay. Data are expressed as mean +SEM.

3.4.4. *Pyrazinib (P3) significantly enhances radio-sensitivity in-vitro in an isogenic model of oesophageal adenocarcinoma*

Angiogenesis and metabolism are interconnected processes, tightly linked to the radioresistant phenotype [82, 109]. We investigated the ability of our small molecule compounds with anti-angiogenic and anti-oxidative phosphorylation activity, Pyrazinib (P3) and other P series compounds (P2, P4), and the parent compound Quininib (Q1) to sensitise OAC cells to radiation.

We carried out a clonogenic assay, the gold standard for assessing radiosensitivity [296], following 24 h treatment with 10 μM of Quininib (Q1), Pyrazinib (P3), P2, P4 OE33P and OE33R cells were either irradiated (2 Gy) or mock irradiated (0 Gy). We also tested other P series compounds which had previously been shown to be anti-angiogenic and have no anti-metabolic activity; P18 and P20 and two compounds which were neither anti-angiogenic or anti-metabolic; P8 and P23. Quininib (Q1), which produced significant anti-angiogenic activity and a modest but significant reduction in ECAR in OE33P cells had no effect on the surviving fraction in either cell line **(Figure 3-4B,F**) indicating that targeting OCR as opposed to ECAR may be more important to overcome radioresistance in OAC cells.

Notably, Pyrazinib (P3), which produced the most potent anti-angiogenic activity *in-vivo* in zebrafish embryos and significant anti-metabolic effect activity both *in-vivo* and *in-vitro*, could significantly reduce the surviving fraction in both radiation-sensitive (p=0.0395) and radiation-resistant cells (p=0.0342) following 24 h treatment **(Figure 3-4C,G**). Pyrazinib (P3) treatment produced a sensitisation enhancement ratio of 23% and 25% in OE33P and OE33R cells to 2 Gy radiation respectively. In addition, P4, the HCl salt of Pyrazinib (P3), which was previously shown to have potent anti-angiogenic and anti-metabolic activity *in-vivo* produced a significant reduction in surviving fraction in both OE33P (p=0.0373) and OEE3R cells (p=0.0220) **(Figure 3-4E, I**). P2, a HCl salt which has a similar but distinct different IUPAC structure from Pyrazinib (P3) and P4, could significantly reduce surviving fraction in OE33P cells (p=0.0246) **(Figure 3-4D)** and showed a trend, although not significant, towards a reduction in surviving fraction in the radioresistant line **(Figure 3-4H**). This result indicated that small molecule compounds which were previously shown to inhibit angiogenesis *in-vivo* and inhibit oxidative phosphorylation either *in-vivo* or *in-vitro* or both could radio-sensitise OAC cells to radiation, whereas compounds which were anti-angiogenic but do not inhibit OCR, a measure of oxidative phosphorylation (Q1, P18 and P20) could not induce this effect **(Figure 3-4B,F,J,K,N,O)** nor could compounds P8 and P23, which had neither anti-angiogenic or anti-metabolic activity **(Figure 3-4L,M,P,Q)**.

To further investigate the ability of Pyrazinib (P3) and P series compounds to enhance radioresponse in OE33P and OE33R cells we investigated the effect of 72 h treatment with our P series compounds at 10 μM on colony formation with/without 2 Gy irradiation. The extended treatment period of 72 h from 24 h did not further enhance the activity of any of the P series compounds. Surprisingly the radio-sensitising effect of P2 and P4 **(Figure 3-5D,E,I)** was lost following the extended treatment incubation time. Pyrazinib (P3) could only enhance radiosensitivity in OE33R cells (p=0.0402) **(Figure 3-5G)** but the effect in OE33P cells previously seen following 24 h of treatment was diminished **(Figure 3-5C,E).**

These results indicate that repeated treatment may be required to maintain the radio-sensitising effect if there is an extended time period between drug treatments and ionising radiation administration. No significant changes in the surviving fraction were seen following treatment for 72 h with Quininib (Q1), P18, P20, P8 and P23 similar to results obtained following 24 h treatment.

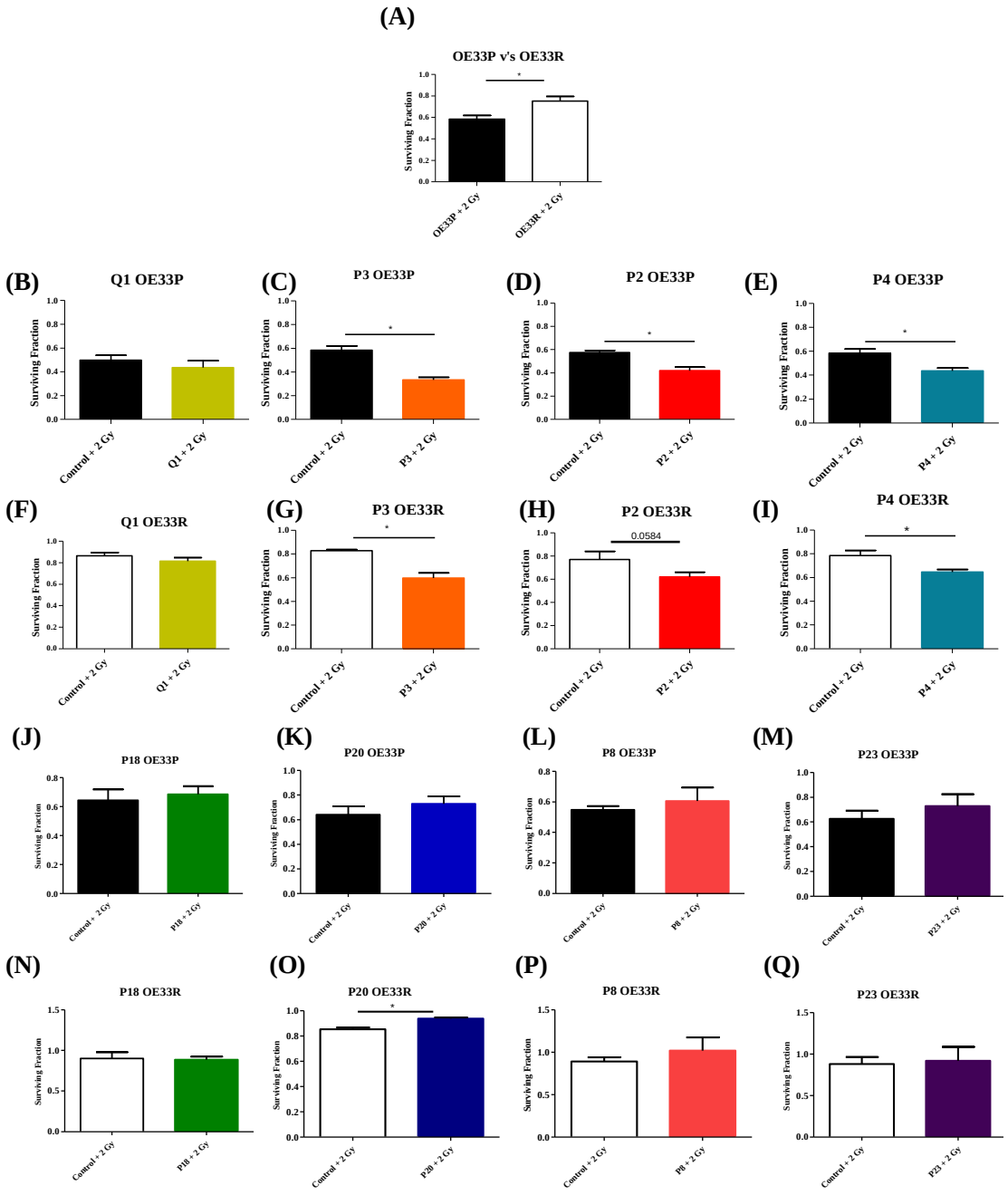

Figure 3-4. Dual action compounds Pyrazinib (P3), P2 and P4 can enhance radio-sensitivity in-vitro in an isogenic model of oesophageal adenocarcinoma.

The effect of our novel small molecule compounds following 24 h treatment on radiosensitivity *in-vitro* was assessed by clonogenic assay. **(A)** Surviving Fraction of OE33P and OE33R cells following 2 Gy radiation, OE33R radioresistant cells have a significantly higher surviving fraction when compared to OE33P radiation-sensitive cells, (n=3), unpaired t-test, **p*<0.05. Surviving Fraction of OE33P cells following treatment with 0.1% DMSO or 10 µM of **(B)** Quininib; Q1 + 2 Gy, (n=3), **(C)** P3 + 2Gy, (n=3), (**D)** P2 + 2 Gy, (n=3) and **(E)** P4 + 2 Gy, (n=3). Surviving Fraction of OE33R cells following treatment with **(F)** Quininib; Q1 + 2 Gy, (n=3), **(G)** P3 + 2Gy, (n=3), (**H)** P2 + 2 Gy, (n=4) and **(I)** P4 + 2 Gy, (n=4). Surviving Fraction of OE33P cells following treatment with 0.1% DMSO or 10 µM of **(J)** P18 + 2Gy, (n=3), **(K)** P20 + 2Gy, (n=3), (**L)** P8 + 2 Gy, (n=3) and **(M)** P23 + 2 Gy, (n=3). Surviving Fraction of OE33R cells following treatment with 0.1% DMSO or 10 µM of **(N)** P18 + 2Gy, (n=3), **(O)** P20 + 2Gy, (n=3) **(P)** P8 + 2 Gy, (n=4) and **(Q)** P23 + 2 Gy, (n=3). Statistical analysis by two-tailed paired t-test, **p*<0.05. Data expressed as mean +SEM.

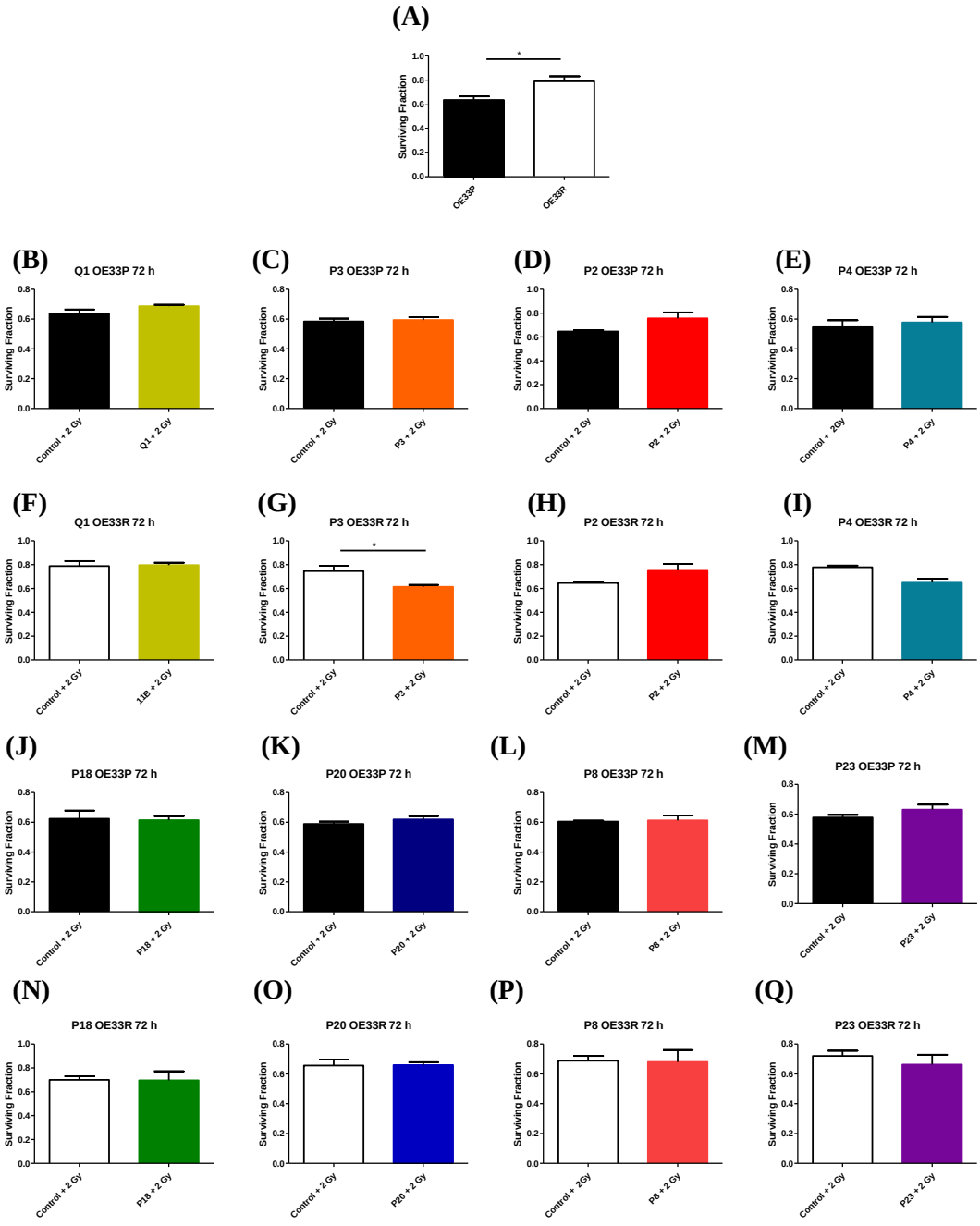

Figure 3-5 The effect of P series compounds on radio-sensitivity in-vitro in an isogenic model of oesophageal adenocarcinoma following treatment for 72 h.

The effect of 72 h treatment with our novel small molecule compounds on radiosensitivity *in-vitro* was assessed by clonogenic assay. **(A)** Surviving Fraction of OE33P and OE33R cells following 2 Gy radiation, OE33R radioresistant cells have a significantly higher surviving fraction when compared to OE33P radiation-sensitive cells, (n=3), unpaired t-test, **p*<0.05. Surviving Fraction of OE33P cells following treatment with 0.1% DMSO or 10 µM of **(B)** Quininib; Q1 + 2 Gy, (n=3), **(C)** P3 + 2Gy, (n=3), **(D)** P2 + 2 Gy, (n=3) and **(E)** P4 + 2 Gy, (n=3). Surviving Fraction of OE33R cells following treatment with **(F)** Quininib; Q1 + 2 Gy, (n=3), **(G)** P3 + 2Gy, (n=3) **(H)** P2 + 2 Gy, (n=4) and **(I)** P4 + 2 Gy, (n=4). Surviving Fraction of OE33P cells following treatment with 0.1% DMSO or 10 µM of **(J)** P18 + 2Gy, (n=3), **(K)** P20 + 2Gy, (n=3), **(L)** P8 + 2 Gy, (n=3) and **(M)** P23 + 2 Gy, (n=3). Surviving Fraction of OE33R cells following treatment with 0.1% DMSO or 10 µM **(N)** P18 + 2Gy, (n=3), **(O)** P20 + 2Gy, (n=3) **(P)** P8 + 2 Gy, (n=4) and **(Q)** P23 + 2 Gy, (n=3). Statistical analysis by two-tailed paired t-test, **p*<0.05. Data expressed as mean +SEM.

3.4.5. *The effect of Quininib (Q1), Pyrazinib (P3) and P series on cellular proliferation and cytotoxicity in-vitro*

To investigate if Quininib (Q1), Pyrazinib (P3) and P series compounds alter cell proliferation in our isogenic model of OAC radio-resistance, two assays were performed: the BrdU assay and the clonogenic assay.

The BrdU assay was used to assess the ability of OE33P and OE33R cells to proliferate following treatment with our P series compounds and compared to that of 0.1% DMSO treated cells. OE33P and OE33R cells were treated with 10 μM of Quininib (Q1), Pyrazinib (P3), P2, P4, P18, P20, P8 and P23 for 24 and 72 h and the effect on cellular proliferation was determined by photometric detection. Following treatment with Quininib (Q1), Pyrazinib (P3) and P series compounds in OE33P and OE33R cells no significant change was seen in cellular proliferation when compared to control in either OE33P or OE33R cells following 24 h treatment **(Figure 3-6A,B)**. A longer treatment period of 72 h did not significantly alter cellular proliferation following treatment with Pyrazinib (P3) and P series compounds **(Figure 3-6C,D).**

In addition the effect of Pyrazinib (P3) and P series compounds on cellular cytotoxicity was evaluated using the gold standard clonogenic assay. There were no significant differences in the surviving fraction of OE33P and OE33R isogenic OAC cells following treatment with our P series compounds for 24 or 72 h **(Figure 3-7A-D)**. Following treatment for 72 h, Quininib (Q1) significantly reduced cell survival in OE33P and OE33R cells (**p<0.01, ***p<0.001), this was in line with previous findings by our group **(Figure 3-7C,D)**.

Interestingly these studies indicate Pyrazinib (P3) and P series compounds don't significantly alter cell growth or inhibit cellular proliferation thus the enhanced radiosensitivity seen upon treatment with Pyrazinib (P3), P2 and P4 previously is not mediated by cellular cytotoxicity or the inhibition of cellular proliferation

.

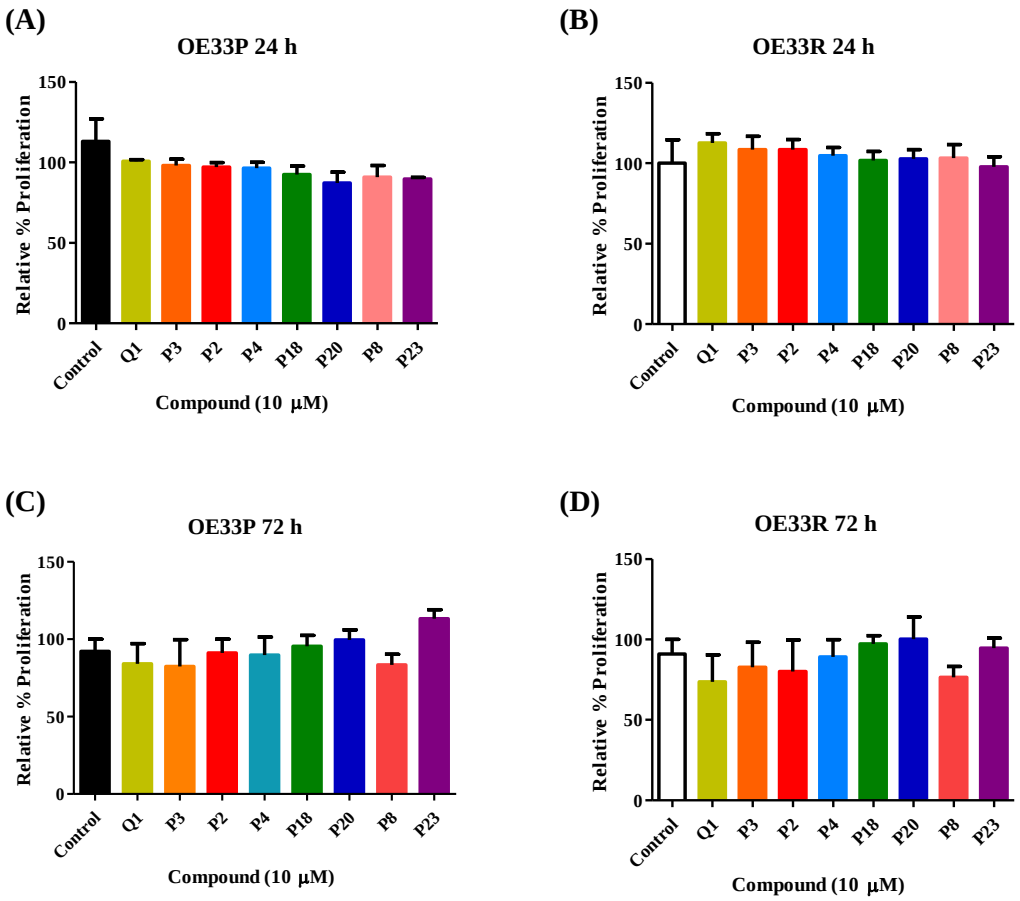

Figure 3-6 Proliferation of OE33P and OE33R cells following treatment with Quininib (Q1) and P series compounds for 24 and 72 h.

Proliferation of OE33P and OE33R cells was assessed by BrdU assay following 24 h treatment with Quininib (Q1), Pyrazinib (P3) and P series compounds at 10 µM in **(A)** OE33P **(B)** OE33R OAC cells and following 72 h treatment in **(C)** OE33P and **(D)** OE33R cells (n=3); Paired t-test. Data are expressed as mean +SEM.

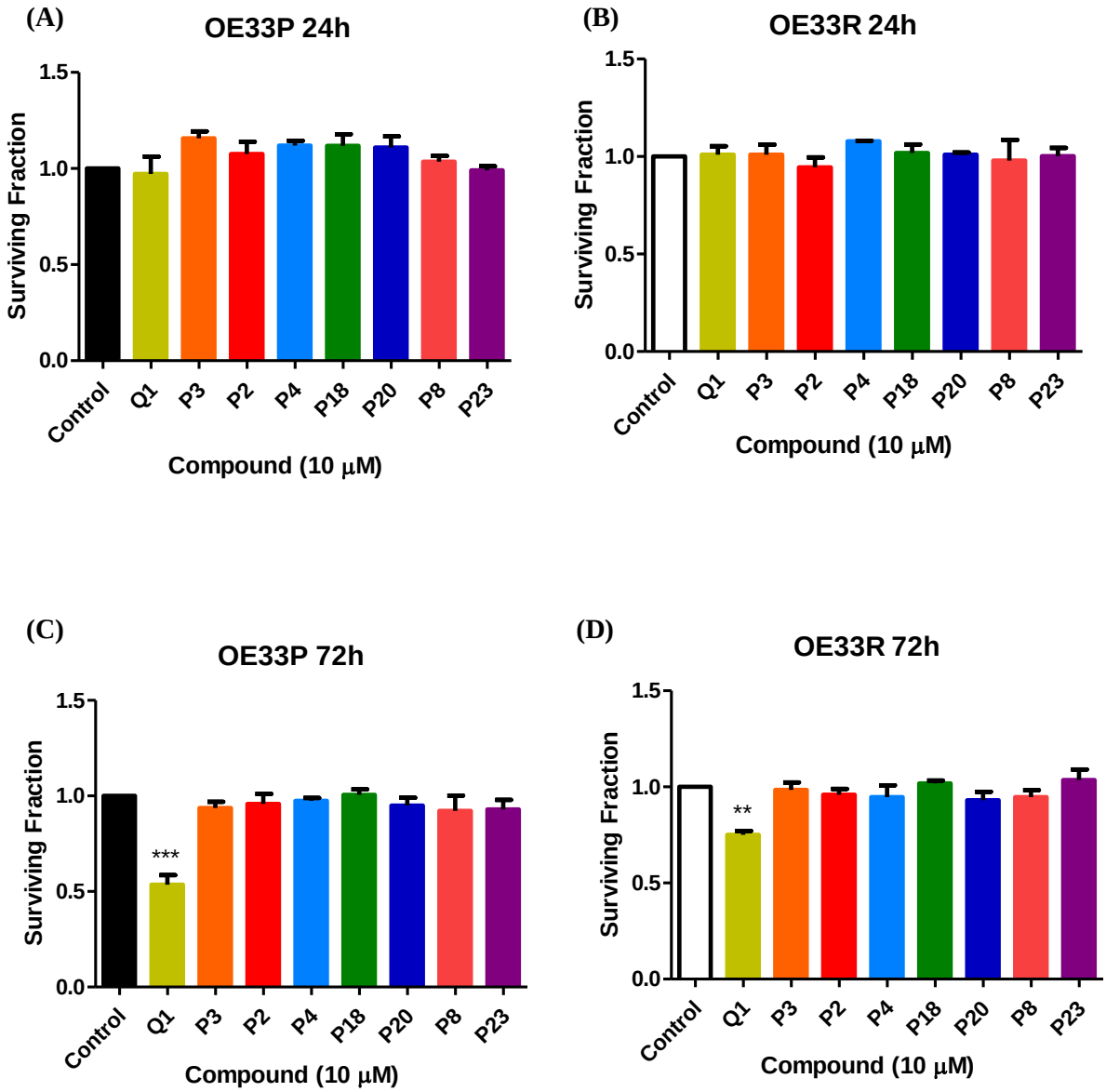

Figure 3-7 Differences in survival of OE33P and OE33R cells following treatment with our novel drugs.

Survival of OE33P and OE33R cells were assessed by clonogenic assay following 24 h treatments with 10 μM of Quininib (Q1), Pyrazinib (P3) and P series compounds in **(A)** OEE3P (n=3) and **(B)** OE33R (n=3) OAC and following 72 h treatment in **(C)** OE33P (n=4) and **(D)** OE33R cells (n=4). One-way ANOVA with Bonferroni post-tests, $^{**}p<0.01$, $^{***}p<0.001$. Data are expressed as mean +SEM.

3.4.6. *Investigating the effect of Quininib (Q1), Pyrazinib (P3), P2 and P4 on the expression of DNA repair genes in OE33P and OE33R cells*

To further investigate the mechanism by which Pyrazinib (P3) and P series compounds P2 and P4 can enhance the response of OE33P and OE33R cells to radiation we investigated the effect of Quininib (Q1), Pyrazinib (P3), P2 and P4 on the expression of DNA repair genes (*MMS19, SMUG1, PARP1,MLH1*) by quantitative real-time PCR.

Previously, our group identified four DNA repair genes (*MMS19, SMUG1, PARP1* and *MLH1*) whose increased expression in OAC patient samples was associated with poor treatment response [150].

We investigated if the expression of these genes was altered in OE33R cells when compared to the parental OE33P cells. Expression levels of *MMS19, SMUG1, PARP1* and *MLH1* were not significantly altered in OE33R cells when compared to OE33P cells **(Figure 3-8A-D)**. In addition treatment with Quininib (Q1), Pyrazinib (P3), P2 and P4 for 24 h at 10 μM did not significantly alter expression of *MMS19, SMUG1, PARP1* and *MLH1* in OE33P **(Figure 3-9A-D)** or OE33R cells **(Figure 3-10A-D)**. Of note, P4 produced a trend towards increased expression of all four DNA repair genes specifically in OE33P cells but this effect was not significant.

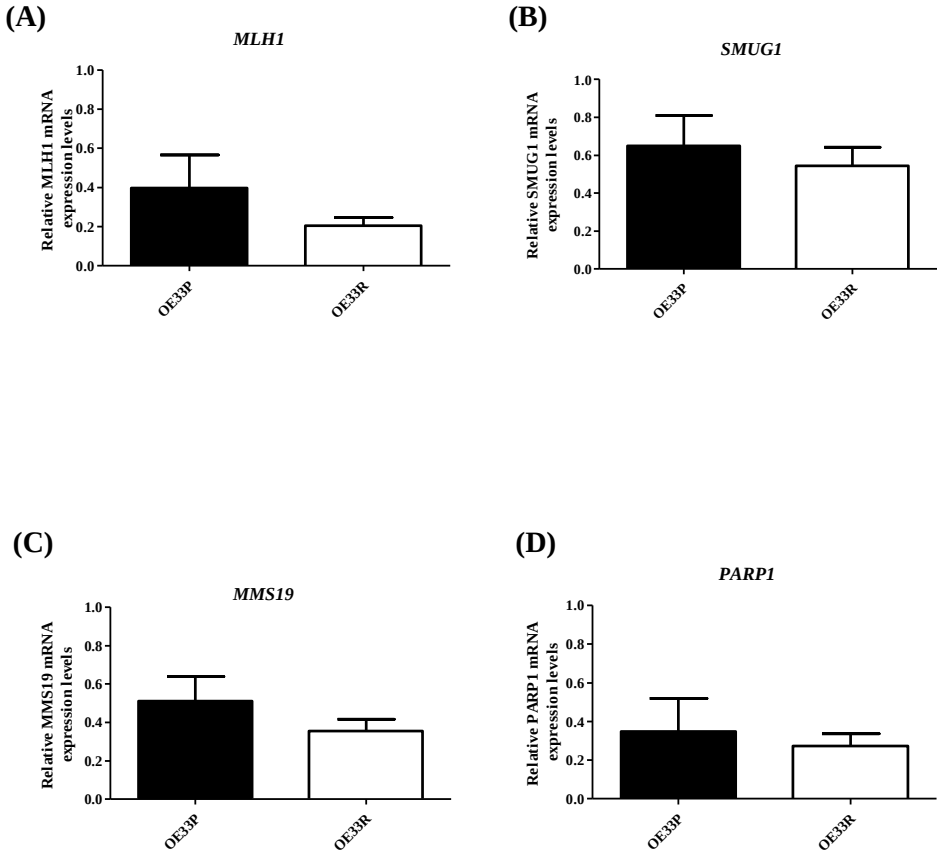

Figure 3-8 Expression of MLH1, SMUG1, MMS19 and PARP1 in OE33P and OE33R cells.
Relative expression of **(A)** *MLH1*, ***(B)*** *SMUG1*, ***(C)*** *MMS19* and **(D)** *PARP1* in OE33P and OE33R cells (n=3). Unpaired t-test. Data are expressed as mean +SEM.

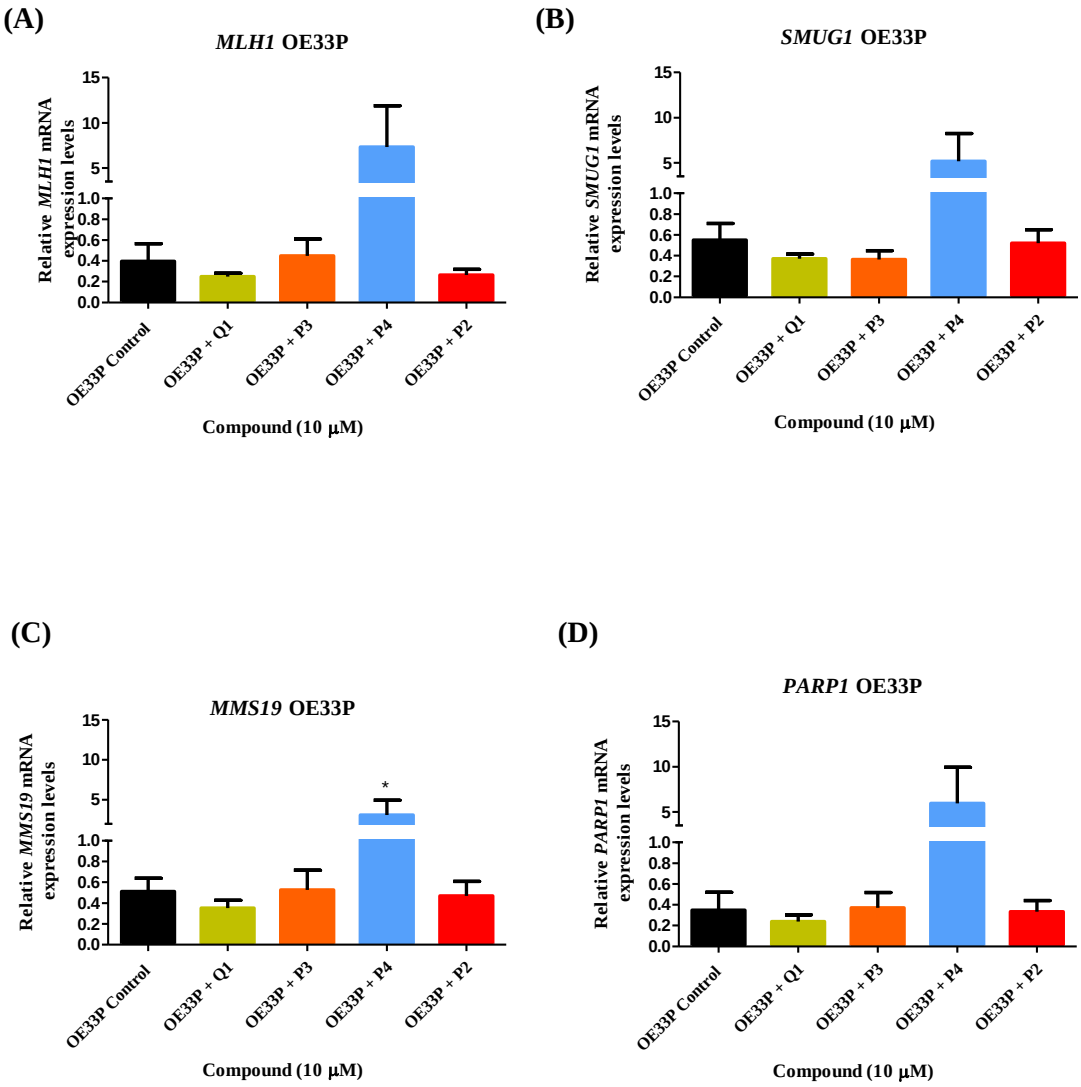

Figure 3-9 Expression of MLH1, SMUG1, MMS19 and PARP1 in OE33P cells following treatment with Quininib (Q1), Pyrazinib (P3), P2 and P4.

Gene expression of **(A)** MLH1, **(B)** SMUG1, **(C)** MMS19 and **(D)** PARP1 was assessed in OE33P cells by quantitative real-time PCR following 24 h treatments with 10 µM of Quininib (Q1), Pyrazinib (P3), P2 and P4 (n=3). Paired t-tests. Data are expressed as mean +SEM.

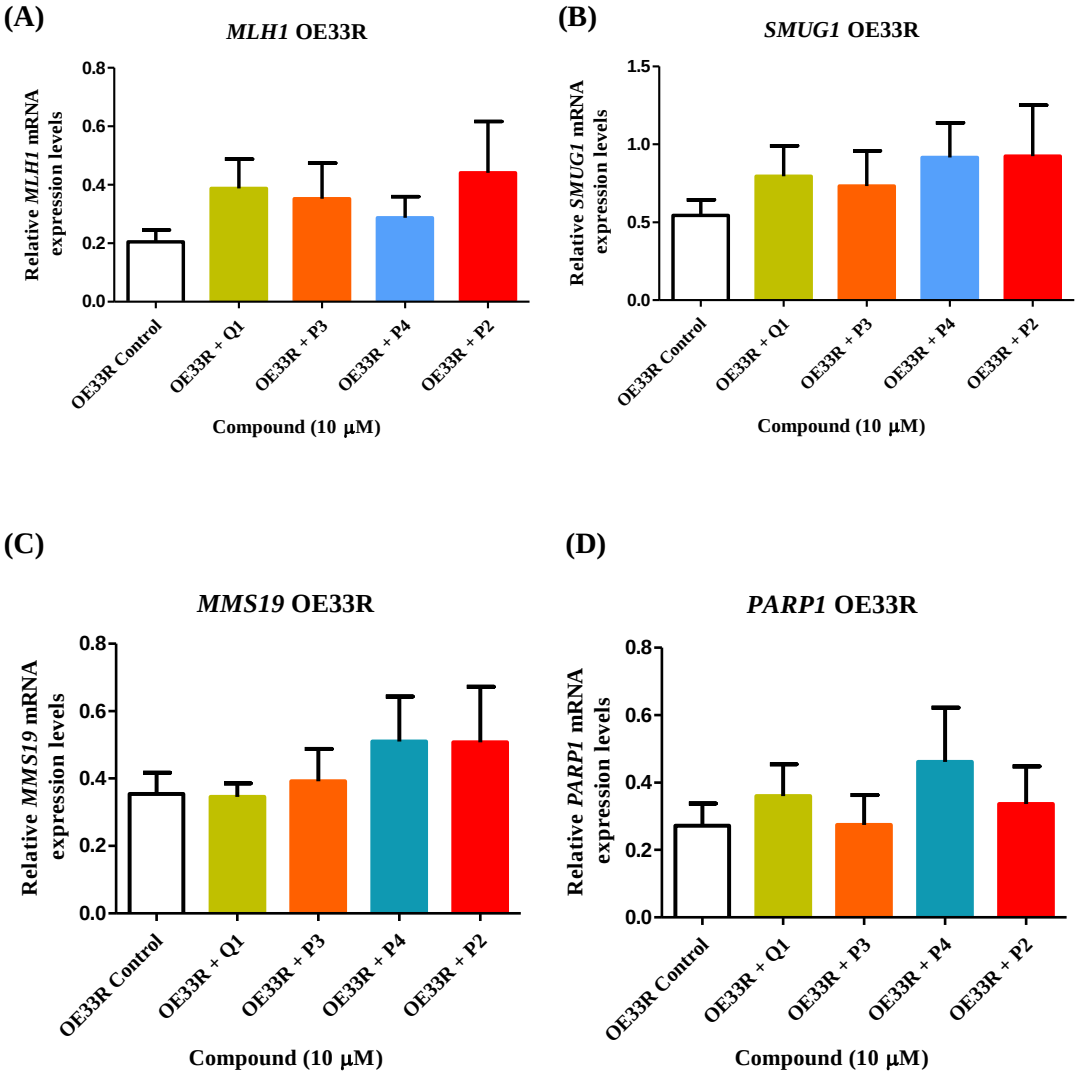

Figure 3-10 Expression of MLH1, SMUG1, MMS19 and PARP1 in OE33R cells following treatment with Quininib (Q1), Pyrazinib (P3), P2 and P4.
Gene expression of **(A)** MLH1, **(B)** SMUG1, **(C)** MMS19 and **(D)** PARP1 was assessed in OE33R cells by quantitative real-time PCR following 24 h treatments with 10 µM of Quininib (Q1), P3, P2 and P4 (n=3). Paired t-tests. Data are expressed as mean +SEM.

3.4.7. *Ranking of P series compounds following in-vitro screening experiments*

In chapter 2 we ranked the P series compounds on their ability to inhibit angiogenesis and two measures of metabolic rate; oxidative phosphorylation and glycolysis *in-vivo* in Tg(*fli1*:EGFP) zebrafish embryos, following which we brought the 5 most potent P series compounds Pyrazinib (P3), P2, P4, P18 and P20 and 2 least active compounds, P8 and P23 forward for *in-vitro* screening in this chapter.

In this chapter we have outlined the results of our extensive *in-vitro* screening where we evaluated the effect of the P series compounds on real-time metabolic rate including oxygen consumption rate and extracellular acidification rate, surrogate markers of mitochondrial function including ATP levels, ROS levels, mitochondrial mass and mitochondrial membrane potential. In addition we evaluated the effect of P series compounds on radiosensitivity, cellular proliferation and cellular cytotoxicity following 24 h and 72 h treatments.

The key aim of our extensive screening was to evaluate if any of our P series compounds could significantly enhance radiosensitivity in our isogenic model of radiosensitivity and if these compound's also inhibited oxidative phosphorylation which has been previously specifically linked to radioresistance in OAC. The activity and ranking of these compounds in these assays is outlined in **Table 3-1**. Three of our compounds, Pyrazinib (P3), P2 and P4 significantly enhanced radiosensitivity in OE33P cells, whilst Pyrazinib (P3) and P4 also significantly enhanced radiosensitivity of OE33R cells.

Based on our findings Pyrazinib (P3) was selected as our lead compound as it produced the most robust reduction in surviving fraction of OE33P (42.2%) and OE33R (27.9%) cells and in addition it was the only compound which could significantly reduce oxidative phosphorylation in both OE33P and OE33R cells, producing the greatest reduction of OCR in OE33R cells of 22.1%.

Table 3-1 Ranking of P series compounds following in-vitro screening in our isogenic model of OAC radioresistance.

A ranking table showing the ranking of P series compounds based on their effect on metabolic rate and radiosensitivity *in-vitro* in OE33P and OE33R cells. The greatest weighting was given for their effect on radiosensitivity, followed by their effect on OCR. Inhibition of OCR was of more importance in terms of weighting than ECAR. Pyrazinib (P3) achieved the highest ranking as a result of its robust radiosensitising activity and significant inhibition of OCR in both OE33P and OE33R cells.

Rank	**Hit**	***In-vitro* metabolism OE33P**		***In-vitro* metabolism OE33R**		**Radio-sensitivity OE33P @ 24 h**	**Radio-sensitivity OE33R @ 24 h**
		OCR % reduction	**ECAR % reduction**	**OCR % reduction**	**ECAR % reduction**	**Percentage reduction in surviving fraction**	**Percentage reduction in surviving fraction**
Quinoline Compound	**Q1**	17.5	21.7	**0**	3.8	12.7	5.8
1	**P3**	7.8	4.7	22.1	17	42.2	27.9
2	**P2**	6.5	15.2	18.8	10.2	27.16	19.5
3	**P4**	11.3	0	2.5	0	25.1	17.3
4	**P18**	9.2	2.8	0	5.1	0	2
5	**P20**	7.7	2.2	8.9	0	0	0
6	**P8**	0	0	0	0	0	0
7	**P23**	0	0	0	4	0	0

3.4.8. *Treatment with Pyrazinib (P3) at 10 μM is the optimal dose to enhance radio-sensitivity in-vitro in an isogenic model of OAC radioresistance at 2 Gy irradiation*

In the previous section we identified Pyrazinib (P3) as our lead radiosensitising compound, to further investigate the ability of Pyrazinib (P3) to enhance radiosensitivity in our isogenic model of OAC radioresistance we carried out a dose response clonogenic assay where we treated OE33P and OE33R cells with 1, 5 and 10 μM for 24 h prior to 0 or 2 Gy irradiation.

Pyrazinib (P3) significantly enhanced radiosensitivity in OE33P cells at 10 μM (p=0.0062) but there was no significant difference in surviving fraction following treatment with 1 or 5 μM and 2 Gy irradiation **(Figure 3-11A)**. Pyrazinib significantly enhance radiosensitivity in OE33R cells both at 5 (p=0.0008) and 10 μM (p=0.0031) to 2 Gy irradiation but there was no significant difference in surviving fraction following treatment with 1 μM and 2 Gy irradiation **(Figure 3-11B).** There was no significant difference in the surviving fraction of OE33R cells treated with either 5 or 10 μM of Pyrazinib **(Figure 3-11B)**.

Based on our findings we selected 10 μM of Pyrazinib (P3) as our optimal dose to enhance radiosensitivity in both OE33P and OE33R cells to 2 Gy irradiation.

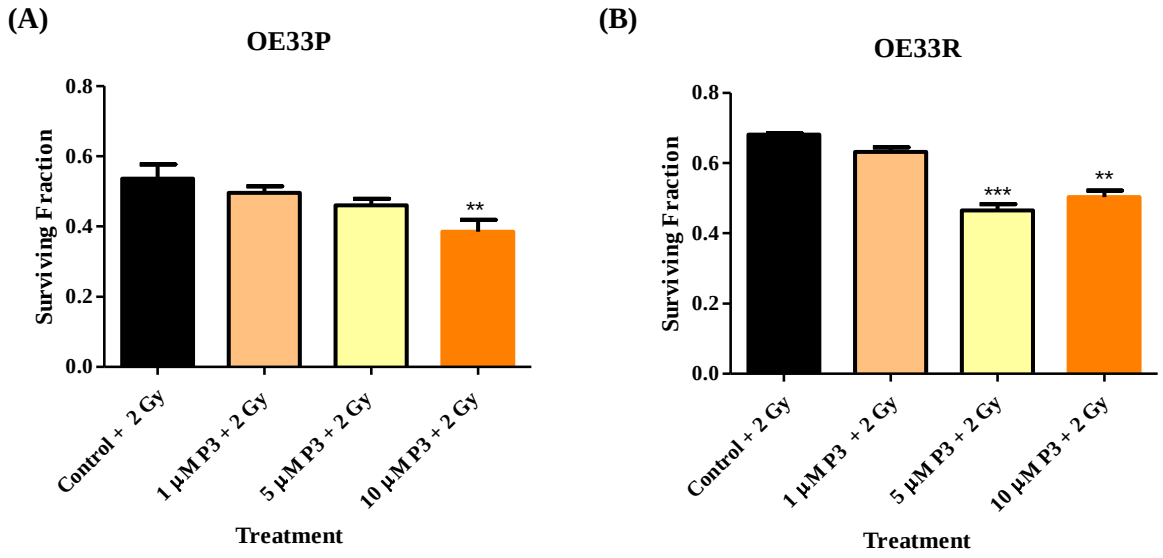

Figure 3-11 Increasing doses of Pyrazinib (P3) significantly enhance radiosensitivity in OE33P and OE33R cells.

The effect of 1, 5 and 10 µM treatment of Pyrazinib (P3) on radiosensitivity was assessed by clonogenic assay *in-vitro* in **(A)** OE33P and **(B)** OE33R oesophageal adenocarcinoma cells, (n=3). Paired t-test, **p*<0.05, ***p*<0.01, (n=3). Data expressed as +SEM.

3.4.9. *Pyrazinib (P3) enhances radio-sensitivity in-vitro in an isogenic model of oesophageal adenocarcinoma at 2, 4 and 6 Gy X-ray radiation*

To further investigate the ability of Pyrazinib (P3) to enhance radiosensitivity in OAC we evaluated the ability of Pyrazinib (P3) to radio-sensitise OE33P and OE33R cells to radiation therapy at increasing doses of radiation (0, 2, 4 and 6 Gy) by clonogenic assay.

Similar to our findings shown previously in this chapter, Pyrazinib (P3) significantly enhanced the radiosensitivity in OE33P and OE33R cells (p=0.0043, p=0.0051) respectively to 2 Gy irradiation **(Figure 3-12A,B)**. In addition, Pyrazinib (P3) significantly enhanced radiosensitivity following irradiation at 4 Gy in OE33P (p=0.0081) and OE33R cells (p=0.0139) and 6 Gy in OE33P and OE33R cells (p=0.0093, p=0.0141 respectively) **(Figure 3-12A,B)**.

Pyrazinib (P3) produced a ~30% reduction in surviving fraction of OE33P cells following 2, 4 and 6 Gy X-ray radiation. In OE33R cells Pyrazinib (P3) produced a ~25% reduction following 2 and 4 Gy X-ray radiation and ~20% reduction following 6 Gy X-ray radiation.

Our findings demonstrate the robust ability of Pyrazinib (P3) to significantly enhance radiosensitivity of both radiosensitive and radioresistant OAC cells to increasing doses of radiation including 2, 4 and 6 Gy and highlight the robust radiosensitising activity of our lead small molecule compound.

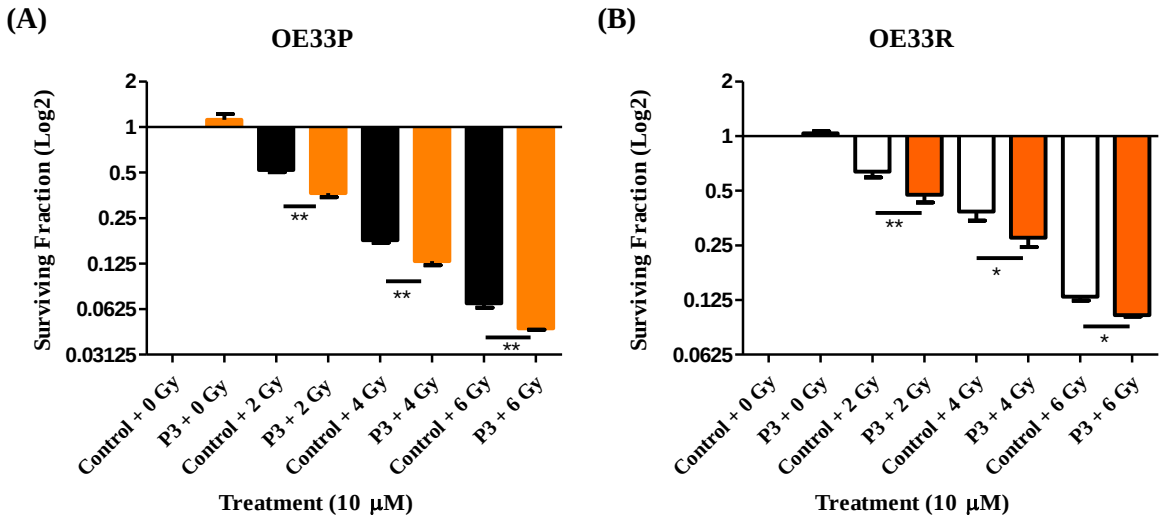

Figure 3-12 Pyrazinib (P3) significantly enhances radio-sensitivity in-vitro in an isogenic model of oesophageal adenocarcinoma at increasing fractionated doses of irradiation.
The effect treatment with our novel small molecule compound Pyrazinib (P3) on radiosensitivity *in-vitro* was assessed by clonogenic assay. **(A)** Surviving Fraction of OE33P cells following treatment with 0.1% DMSO control or 10 µM Pyrazinib (P3) and 0, 2, 4 and 6 Gy radiation, (n=3), paired t-test, **p*<0.05, ***p*<0.01. **(B)** Surviving Fraction of OE33R cells following treatment with 0.1% DMSO control or 10 µM Pyrazinib (P3) and 0, 2, 4 and 6 Gy radiation, (n=3), paired t-test, **p*<0.05, ***p*<0.01. Data expressed as mean +SEM.

3.5. Summary of main findings of chapter 3

- Pyrazinib (P3) significantly inhibited OCR, a measure of oxidative phosphorylation in both OE33P (radiation-sensitive) and OE33R (radiation-resistant) isogenic OAC cells

- ATP levels are significantly higher in OE33R cells compared to OE33P cells, Pyrazinib (P3) and P series compounds do not significantly alter ATP levels.

- Treatment with Pyrazinib (P3), P2 and P18, P20 significantly reduced ROS levels in OE33P but not OE33R cells.

- Pyrazinib (P3) and P4 significantly enhanced radio-sensitivity *in-vitro* in an isogenic model of oesophageal adenocarcinoma following 2 Gy X-ray radiation.

- Pyrazinib (P3) and P series compounds did not significantly alter cellular proliferation.

- Treatment with Quininib (Q1), Pyrazinib (P3), P2 and P4 did not significantly alter expression of *MMS19*, *SMUG1*, *PARP1* and *MLH1* in OE33P or OE33R cells.

- Pyrazinib (P3) was selected as our lead compound based on its ability to robustly enhance radiosensitivity in OE33P and OE33R cells following 2 Gy X-ray radiation.

- Pyrazinib significantly enhanced radiosensitivity in both OE33P and OE33R cells following 2, 4 and 6 Gy X-ray radiation doses.

3.6. Discussion

In our initial screens in zebrafish we identified 3 novel small molecule compounds (Pyrazinib (P3), P2 and P4) with significant anti-angiogenic and anti-metabolic activity *in-vivo*. For this chapter our goal was to investigate if Pyrazinib (P3) and P series compounds which were previously shown to inhibit angiogenesis and metabolism *in-vivo* in zebrafish could also inhibit metabolism *in-vitro* and enhance radiosensitivity in our isogenic model of radioresistance. Furthermore we also sought to investigate the effect of our P series compounds on surrogate markers of mitochondrial function and DNA repair gene expression.

In-vitro, Pyrazinib (P3) and P2 produced a significant reduction in OCR a measure of oxidative phosphorylation of ~22% and ~18% respectively in OE33R cells with Pyrazinib (P3) producing a simultaneous reduction in ECAR, a measure of glycolysis. Notably, only Pyrazinib (P3) produced significant anti-metabolic activity in both the radiosensitive OE33P and radioresistant OE33R cell lines. We have previously shown that OAC radio-resistant cells have an increased rate of oxidative phosphorylation when compared to radiosensitive OAC cells, thus, the potent inhibition of oxidative phosphorylation produced by our novel compounds is a significant finding in this model [82]. The higher rate of oxidative phosphorylation in OE33R radioresistant cells may indicate these cells consume more oxygen than radiosensitive cells and is thought to be a contributing factor promoting the radioresistant phenotype. Given the importance of oxygen in the radioresponse especially and that ATP5B, a marker of oxidative phosphorylation, is expressed at significantly higher levels in OAC patients with a subsequent poor response to neo-CRT the inhibition of OCR by Pyrazinib (P3) is a significantly important effect [82]. Metformin was demonstrated to significantly sensitise oesophageal cancer cells to radiation *in-vitro* [218]. This was associated with an induction of G0/G1 arrest, apoptosis and delayed repair of DSB's following ionising radiation and activation of AMPK, serine/threonine kinase which functions as a cellular metabolism sensor. As mentioned earlier, *in-vivo*, in HCT-116 xenografts, administration of metformin was found to produce a 7% reduction in oxygen consumption rate and to improve tumour re-oxygenation [225]. In addition, in these xenografts, pre-treatment with metformin before one dose of 15 Gy irradiation produced a significant tumour growth delay [225]. Targeting oxidative phosphorylation *in-vivo* with papaverine was found to enhance tumour oxygenation and sensitise tumours to radiation therapy [229]. These findings in the literature support our results and highlight the potential of our novel anti-metabolic agents to enhance radiosensitivity. ATP levels were modestly but significantly higher in OE33R cells when compared to OE33P cells, supporting previous findings by our group but P series compounds had no effect on ATP levels [82].

The more potent anti-angiogenic and anti-metabolic activity produced by Pyrazinib (P3) than its parent compound Quininib (Q1) may be attributable to their different structural features and molecular targets, Quininib (Q1), a quinoline compound, is a known cysteinyl leukotriene receptor 1 and receptor 2 antagonist whereas binding studies have shown Pyrazinib, a pyrazine phenol does not target this molecular pathway [272]. Furthermore, previous studies have indicated that cancer cells can switch from a predominant glycolytic phenotype to an oxidative phenotype following radiation to promote cancer cell survival under genotoxic stress via mTOR-mediated hexokinase II inhibition [297] and p53-independent mitochondrial biogenesis, which is counter-regulated by HIF1α [298] . Thus, dual inhibition of both oxidative phosphorylation and glycolysis by Pyrazinib (P3) in combination with anti-angiogenic activity is favourable. The lack of feedback upregulation of ECAR following OCR inhibition suggests Pyrazinib (P3) is acting at an early point common to both pathways or there is a dysregulated compensatory mechanism in this isogenic model. In a pancreatic study inhibition of OCR with oligomycin was not found to cause an upregulation in ECAR [123]. Furthermore, metabolism is tightly linked to angiogenesis, as tumour vasculature supplies glucose to the tumour which is used to fuel the tricarboxylic acid cycle [299]. Thus, the use agents targeting both angiogenesis and oxidative phosphorylation may be a novel approach that could be utilised to overcome radiation resistance.

Elevated levels of ROS have been reported in a number of cancer types [300]. *In-vitro*, OE33R cells were found to have significantly higher levels of ROS when compared to their matched OE33P cells which supports previous findings by our group and may be linked to the increased levels of mitochondrial mutagenesis in these cells [82]. The higher levels of ROS in the OE33R line may be a product of the extensive radiation exposure these cells underwent to become radioresistant but also highlights the altered mitochondrial function in radiation-resistant cells when compared to radiation-sensitive cells. Treatment with our novel compounds Pyrazinib (P3), P2, P4, P18, P20 and P8 significantly reduced ROS levels in the OE33P cells but no effect was seen in the treated OE33R cells. This inhibition of ROS specifically in our OE33P but not OE33R line was interesting and may indicate Pyrazinib (P3) and other P series compounds (P2, P4, P18, P20, P8) can only alter inherently lower levels of ROS, as seen in OE33P cells, with no activity on the higher ROS levels in OE33R cells. Notably only Pyrazinib (P3), which produced a reduction in ROS levels in OE33P cells, could also reduce oxidative phosphorylation in OE33P cells, potentially indicating that these compounds are targeting ROS generated from other processes outside the metabolic cycle, given no simultaneous reduction in metabolism is seen despite robust reductions in ROS produced by the other compounds (P2, P4, P18, P20 and P8) in OE33P cells. This result indicated that the previous reduction in metabolic rate in the OE33R cells is independent of changes to ROS and other mediators of mitochondrial function including mitochondrial membrane potential and mitochondrial mass and the reduction of either OCR or

ECAR or both by Pyrazinib (P3) and P2 is possibly occurring through an alternative mechanism. ROS is critical to the DNA damage response induced by irradiation, but on the contrary can promote cellular signalling and proliferation, thus a reduction of the higher levels of ROS in the OE33R cells following treatment may confer a favourable advantage [301]. ROS can function as tumourigenic mediators which promote cellular proliferation, survival and migration [302]. Furthermore ROS have been reported to function as second messengers in intracellular signalling cascades to further promote tumourigenesis [302]. On the other hand, it is also known that ROS can induce cellular senescence and cell death and can therefore function as anti-tumorigenic agents [300]. ROS is produced as a by-product of oxidative phosphorylation and elevated ROS levels in the tumour and surrounding microenvironment can be a result of a number of processes including increased metabolic activity and mitochondrial dysfunction [302]. A disproportional increase in intracellular ROS can also induce cancer cell cycle arrest, senescence and apoptosis which can be exploited by chemotherapy and may also occur due to the generation of ROS by immune cells [300]. In summary, our results suggest that our P series compounds may be acting directly on these metabolic pathways, independent of significant changes to mitochondrial function.

Pyrazinib (P3) and P4, significantly enhanced radiosensitivity in both radiation-sensitive and radiation-resistant OAC cells. P2 could only enhance radiosensitivity in the radiation-sensitive OAC cells. Importantly, the quinoline compound Quininib, (Q1) and the P series compounds which can inhibit angiogenesis but not OCR, a measure of oxidative phosphorylation could not enhance radioresponse. Furthermore, the enhanced radiosensitising effect was independent of changes to cellular proliferation or cellular cytotoxicity. These were significant findings which demonstrated that our lead small molecule compound; Pyrazinib (P3), could enhance radiosensitivity in an isogenic model of OAC radioresistance as similar agents currently do not exist in this space. Irradiation is a critical treatment modality which is used in the treatment of over 50% of human malignancies with response to radiation often inversely correlated to a reduction in tumour size [55]. This further highlights the importance of our identification of novel small molecule compounds which can enhance radiosensitivity in an isogenic model of OAC radioresistance. Importantly, clonogenic studies have been previously used to identify radiosensitising compounds *in-vitro* which have been later translated to radiosensitising agents in the clinic, an example of which is gemcitabine [189]. Thus, the clonogenic assay is a useful tool for the identification of potential novel radiosensitising agents, but it is important to note such assays lack the complexity of the heterogeneous tumour microenvironment.

In addition to metabolism and mitochondrial function, DNA repair plays a critical role in radiosensitivity. Pyrazinib (P3) significantly enhances radiosensitivity in OE33P and OE33R cells

independent of baseline changes to the expression of DNA repair genes *MLH1, SMUG1, MMS19* and *PARP1* which have been previously linked to radiation resistance in OAC [150]. Treatment of OE33P and OE33R cells with Quininib (Q1), Pyrazinib (P3), P2 and P4 had no effect on the expression four DNA repair genes; *MLH1, PARP1, MMS19* or *SMUG1*, these findings indicated that Pyrazinib (P3) is not enhancing radioresponse through the inhibition of these DNA repair genes specifically but may do so through alternative DNA damage/repair pathways and/or mechanisms. Importantly, the expression levels of these 4 DNA repair genes are not significantly different in OE33P versus OE33R cells at baseline indicating these genes may not be the only factors promoting the radio-resistant phenotype in these cells despite the apparent role of these genes in radiosensitivity in OAC, highlighting possibly the difference in biological importance of these genes *in-vitro* versus *in-vivo*. As mentioned previously ionising radiation primarily aims to exert local control through the induction of cellular DNA damage including critical double strand breaks (DSB) and the level repair of these DSB often confers the level of radiosensitivity within the tumour. In a previous study by our group, it was found there was significantly higher expression of DNA repair genes; *MLH1, SMUG1, PARP1* and *MMS19* in treatment-naïve OAC patient biopsies from patients who failed to respond to neo-CRT when compared to those obtained from patients with a good response to neo-CRT, highlighting the importance of DNA damage repair in treatment response in OAC [303]. Furthermore, additional studies in our lab have also demonstrated that microRNA; miR-31 was downregulated in OE33R cells and subsequent expression was associated with increased radiosensitivity and decreased expression of a number of genes involved in DNA repair including *MMS19, SMUG1, PARP1* and *MLH1* highlighting the role of these genes in radioresponse in OAC [303]. *MMS19*, Methyl-methanesulfonate sensitivity 19, which plays a crucial role in genomic stability has been identified as a potential new predictor of metastasis and CRT response in SCC [304]. Mut L homologue-1 (*MLH1*) protein which is a necessary component of DNA mismatch repair (MMR), in G2-M cell cycle checkpoint has been previously linked with radiosensitivity in CRC and inhibition of *MLH1* via c-MYC has been shown to enhance radiosensitivity in melanoma [305-307]. In a pancreatic xenograft model, the combination of a PARP1 inhibitor and Wee1 inhibitor significantly enhanced radiosensitivity and produced a 20 % eradication of tumours [308]. In addition silencing SMUG1, a DNA glycosylase which plays a role in the base excision repair pathway was shown to increase sensitivity to γ-radiation in mouse embryonic fibroblasts [309]. Notably, cisplatin and gemcitabine, two of the most widely used radio-sensitising agents exert their effects through the induction of DNA damage through the disruption of two common DNA repair pathways; non-homologous end joining and homologous recombination respectively. It will be of interest in the future to assess the levels of DNA damage induced by Pyrazinib (P3) treatment using the comet assay as our previous studies only focused on 4 specific DNA repair genes whereas this assay will allow us to assess the actual DNA damage levels induced in the cells following treatment and may provide

further information to aid investigation into the relationship between Pyrazinib (P3) and the DNA damage response pathway.

Pyrazinib (P3) significantly enhanced radiosensitivity of OE33P and OE33R cells to increasing doses of radiation including 2, 4 and 6 Gy. In our initial experiments in this we investigated the ability of Pyrazinib (P3) to enhance radiosensitivity at the clinically relevant dose of 2 Gy. In order to further investigate the clinical utility of Pyrazinib (P3) we investigated its potential to increase radiosensitivity at higher doses of radiation. OE33R cells have previously been shown to more resistant to 2, 4 and 6 Gy fractions of X-ray radiation than OE33P cells [150]. The ability of Pyrazinib (P3) to enhance radiosensitivity to higher doses of radiation further highlights in clinical potential as a radiosensitiser.

In summary from our findings in this chapter we have identified Pyrazinib (P3) as our lead compound which can significantly inhibit OCR, a measure of oxidative phosphorylation and enhance radiosensitivity in OE33P and OE33R cells. Pyrazinib (P3) will be the only drug taken into further studies detailed in the following chapters.

Aspects of this chapter have been published in *Cancer Letters*, see **Figure 3-13**.

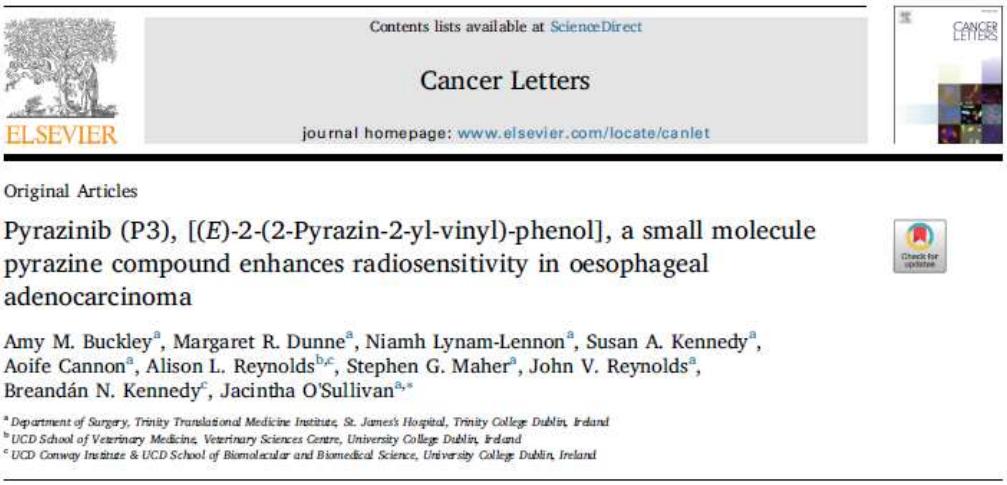

Figure 3-13 Pyrazinib (P3), [(E)-2-(2-Pyrazin-2-yl-vinyl)-phenol], a small molecule pyrazine compound enhances radiosensitivity in oesophageal adenocarcinoma.
Aspects of this chapter have been published in *Cancer Letters* [285].

4. Chapter 4. Evaluating the effect of Pyrazinib (P3) on metabolism and radiosensitivity under normoxic and hypoxic conditions and its effect on chemosensitivity in OAC

4.1. Introduction

In chapter 3 we identified Pyrazinib (P3) as our lead compound from our drug screening analysis with robust anti-angiogenic, anti-metabolic and radiosensitising activity. In this chapter we further investigated the anti-metabolic and radiosensitising activity of Pyrazinib (P3) under normoxic and hypoxic conditions. Furthermore, we investigated the action of Pyrazinib (P3) in an OAC isogenic model of cisplatin resistance and investigated the interactions between Pyrazinib (P3) and the well-known chemotherapy 5-FU in our OAC model of radioresistance.

Aerobic mitochondrial respiration is fuelled by a number of metabolic substrates including glucose/pyruvate, fatty acids and glutamine [310]. Pyruvate formed by glycolysis is converted to acetyl CoA, the starting point of the TCA cycle [310]. The TCA cycle is also the entry point for fatty acid and amino acid oxidation, which enter the cycle as acetyl CoA [310]. Fatty acids can then move through this pathway as acetyl CoA derivatives utilising NADH and $FADH_2$ [310]. Glutaminolysis involves the initial deamination of glutamine by glutaminase, yielding glutamate and ammonia. Glutamate is then converted via a second deamination step to a Krebs cycle intermediate, α-ketoglutarate (α-KG) [311]. In this chapter we sought to investigate the aerobic mitochondrial metabolic substrate dependency of OE33P and OE33R cells.

Increased levels of oxidative phosphorylation in tumours promote the development of hypoxic regions. Hypoxia can be defined as an oxygen deficiency. Hypoxic tumour cells are inherently resistant to radiation therapy and tumour hypoxia is a negative prognostic marker in head and neck SCC tumours treated with X-ray radiation [148, 312]. A number of studies which have previously investigated the potential of targeting tumour oxygenation levels before radiation to enhance radiation response have utilised hyperbaric oxygen or carbogen, an oxygen rich gas in combination with vasodilation therapies [313]. Although these studies have shown clinical benefit their application in the clinic is limited due to practical implications of applying such treatment [314]. An alternative approach is to molecularly target oxidative phosphorylation to reduce the amount of oxygen consumed and enhance the amount of oxygen available to function as a radiosensitiser in the tumour. Thus, given the elevated levels of oxidative phosphorylation in our OAC radioresistant cells and the role of oxygen in radioresponse we sought to evaluate the potential of Pyrazinib (P3) to inhibit oxygen consumption rate in our isogenic OAC model of radioresitance under conditions of normoxia and hypoxia and evaluate its ability to enhance radiosensitivity under both conditions.

Cisplatin is a platinum-based chemotherapy which is used to treat a wide number of solid cancers [315]. Cisplatin is administered as part of a neo-adjuvant chemotherapy regimen referred to as

MAGIC for the treatment of OAC [44]. The MAGIC chemotherapy protocol consists of administration of etoposide, cisplatin and 5-FU chemotherapy pre- and post-operatively [45, 46]. One mechanism by which cisplatin exerts its anti-cancer effect is through the generation of DNA lesions resulting in the activation of the DNA damage response and the subsequent induction of mitochondrial apoptosis [315]. Initial responses to cisplatin are often quite promising, however chemoresistance to cisplatin develops leading to treatment failure. A poor response to neo-adjuvant treatment is associated with poor outcome thus it is critical to understand the molecular mechanisms governing resistance to cisplatin in OAC and the effect of Pyrazinib (P3), if any on cisplatin sensitive and cisplatin resistant cells in terms of metabolism, cell survival, chemosensitivity and radiosensitivity.

5-FU is an anti-metabolite drug which is a pyrimidine nucleoside analogue [316]. 5-FU, is rapidly taken into cells via the same transport mechanism as uracil [316]. Intracellularly, 5-FU is converted into a number of active metabolites including, fluorodeoxyuradine monophosphate (FdUMP), fluorodeoxyuradine triphosphate (FdUTP) and fluorouradine triphosphate (FUTP) [52]. 5-FU is thought to exert its cytotoxic effect through both the misincorporation of fluoronucleotides into RNA and DNA and the inhibition of the nucleotide synthetic enzyme thymidylate synthase [52]. FdUMP binds to the nucleotide synthetic enzyme thymidylate synthase which results in the depletion of the thymidine nucleotide pool, and subsequently hinders nucleic acid synthesis. The delay in thymidine synthesis results in the misincorporation of uracil and subsequent DNA damage [317, 318]. 5-FU is given as a chemotherapy-based treatment alone or in combination with other chemotherapies or radiation to enhance radioresponse. 5-FU may enhance radiosensitisation through a number of mechanisms including cellular redistribution of cells to radiosensitive phases of the cell cycle, inappropriate progression through the radiation-resistant S-phase of the cell cycle and inhibition of DNA repair following radiation-induced damage [319-321]. In an *in-vitro* model of CRC, the down regulation of NAD^+-dependent deacetylase sirtuin-7 (SIRT7) by 5-FU was shown to enhance radiosensitivity [322]. 5-FU is commonly used clinically in conjunction with radiation for the treatment of malignant neoplasms of the gastrointestinal tract. In 2001, the INT-0116 study demonstrated an improvement in overall survival for patients with gastric cancer who underwent resection followed by adjuvant 5-FU chemotherapy and X-ray radiation compared to patients who were treated with surgical resection alone [323]. However, 5-FU is not currently administered in combination with radiation to OAC patients, 5-FU is administered as part of the chemotherapy only arm of the trial, the MAGIC regimen [44]. In this chapter we sought to investigate the effect of 5-FU on cellular cytotoxicity and radiosensitivity in our isogenic model of OAC radioresistance. Furthermore, we investigated the interaction of Pyrazinib (P3) and 5-FU when administered in combination to OE33P and OE33R cells. It is important to not only understand how Pyrazinib (P3) interacts with radiation

but also with other treatments such as chemotherapies and whether it can sensitise OAC cells to these chemotherapies.

In this chapter we sought to further investigate the anti-metabolic activity of Pyrazinib (P3) under both normoxic and hypoxic conditions and investigate the specific mitochondrial fuels that OE33P and OE33R cells rely on. We also wanted to explore the ability of Pyrazinib (P3) to inhibit metabolism and alter radioresponse under hypoxic conditions. Furthermore, we investigated the action of Pyrazinib (P3) in isogenic model of OAC cisplatin resistance and investigated the action of Pyrazinib (P3) in combination with 5-FU in our isogenic model of OAC radioresistance.

4.2. Overall objective and specific aims of chapter 4

Our overall objective of chapter 4 was to further investigate the ability of Pyrazinib (P3) to inhibit metabolism and enhance radiosensitivity in our isogenic model of OAC radioresistance under hypoxic conditions. In addition, we investigated the effect of Pyrazinib (P3) on chemosensitivity.

The specific aims of chapter 4 were:

1. Investigate the dependency of OE33P and OE33R cells on the metabolic substrates; pyruvate, fatty acids and glutamine for aerobic respiration.
2. Evaluate the effect of Pyrazinib (P3) treatment on the mitochondrial apoptosis proteins Cytochrome C and Caspase 3 secretion from OE33P and OE33R cells.
3. Evaluate the anti-metabolic activity of Pyrazinib (P3) on energy metabolism including oxidative phosphorylation and glycolysis in OE33P and OE33R cells cultured under normoxia and hypoxia (0.5% O_2).
4. Evaluate the effect of Pyrazinib (P3) on three surrogate markers of mitochondrial function; ROS, mitochondrial mass and mitochondrial membrane potential in OE33P and OE33R cells cultured under normoxia and hypoxia.
5. Evaluate the effect of Pyrazinib (P3) on radiosensitivity and cellular proliferation under hypoxic conditions of 0.5% O_2 in OE33P and OE33R cells.
6. Evaluate the anti-metabolic activity of Pyrazinib (P3) on energy metabolism in an OAC isogenic model of acquired cisplatin resistance.
7. Evaluate the effect of Pyrazinib (P3) on chemosensitivity and radiosensitivity in our isogenic model of OAC acquired cisplatin resistance.
8. Investigate the effect of Pyrazinib (P3) in combination with 5-FU on chemosensitivity and radiosensitivity in OE33P and OE33R cells.

4.3. Methods

4.3.1. *Generation of cell lines*

The human OE33 oesophageal adenocarcinoma cell line was obtained from the European Collection of Authenticated Cell Cultures and generated as previously described in section 3.3.1 [150]. The isogenic model of cisplatin resistant OAC; OE33 Cis P (cisplatin-sensitive) and OE33 Cis R (cisplatin-resistant) cells was generated as previously described [324]. Briefly, to generate the isogenic model of OAC cisplatin resistance, OE33 cells were treated with 1 µM cisplatin or PBS (NaCl) vehicle control for 72 h. Treatment was then discarded and replaced with complete media for 72 h, and this cyclic treatment regimen was repeated for approximately 6-months. During this time, cells were subcultured at 80-90% confluence and cisplatin sensitivity was assessed throughout the 6-month period via clonogenic assay. The IC50 of OE33 Cis P and OE33 Cis R cells was determined to be 1.3 µM and 2.8 µM respectively. OE33 Cis R cells maintain their resistance to cisplatin in cisplatin free media.

4.3.2. *Cell culture*

Cell culture was carried out as per section 3.3.2.

4.3.3. *Preparation and storage of Pyrazinib (P3)*

Pyrazinib (P3), (*E*)-2-(2-Pyrazin-2-yl-vinyl)-phenol was synthesised by Celtic Catalysts (Ireland). Pyrazinib (P3) was dissolved in 100% DMSO to make 10 mM stock solutions for experimental use and stored at -20°C.

4.3.4. *Metabolic pathway dependency analysis*

OE33P and OE33R cells were seeded at a density of 11,000 and 13,000 cells/well, respectively in 24-well cell culture XFe24 microplates (Agilent Technologies, Santa Clara, CA, USA) in a volume of 100 µL and allowed to adhere at 37°C in 5% CO_2/95% air. 5 hours later, an additional 150 µL/well complete cell culture RPMI-1640 medium was added. Cells were cultured for 24 h prior to running pathway dependency assay. Three specific inhibitors were used to evaluate the dependency of OE33P and OE33R cells on glutamine oxidation, fatty acid oxidation and glucose oxidation using the Seahorse Mito Fuel Flex Test (Agilent Technologies, Santa Clara, CA, USA). The Mito Fuel Flex Test inhibits import of three major metabolic substrates (pyruvate, fatty acids, and/or glutamine) with mitochondrial pyruvate carrier inhibitor UK5099 (2 µM), carnitine palmitoyltransferase 1A inhibitor etomoxir (4 µM), or glutaminase inhibitor BPTES (3 µM) **(Figure 4-1)**. This test determines cellular dependence on each metabolite to fuel mitochondrial metabolism by inhibiting the individual substrate import or the capacity for utilising that substrate when the others are blocked. Baseline OCR was monitored for 24 min followed by sequential

inhibitor injections of either Treatment 1 or Treatment 2 with OCR readings taken 6 times over 8 min following the addition of each treatment. The inhibitor treatments and calculations are shown in **Table 4-1**.

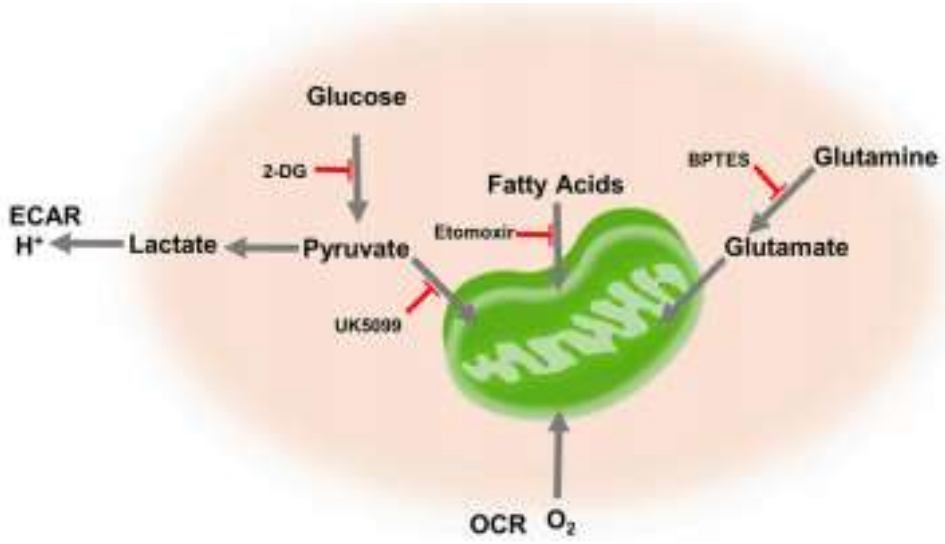

Figure 4-1 Schematic of metabolites and drug targets.
Schematic illustrating targets of three inhibitors used in pathway dependency assay; UK5099, BPTES and etomoxir. *Image adapted from Smallwood et al.* [325].

Table 4-1 Metabolic tests and associated inhibitors
Table detailing treatments used to carry out pyruvate, glutamine and fatty acid dependency and capacity tests. Formulas used to calculate percentage capacity, dependency and flexibility following metabolic tests are detailed in last three rows of table.

Metabolite Test	Treatment 1	Treatment 2
Pyruvate dependency	UK5099	Etomoxir + BPTES
Pyruvate capacity	Etomoxir + BPTES	UK5099
Glutamine dependence	BPTES	Etomoxir + UK5099
Glutamine capacity	Etomoxir + UK5099	BPTES
Fatty acid dependence	Etomoxir	BPTES + UK5099
Fatty acid capacity	BPTES + UK5099	Etomoxir
Percentage Capacity	$[1-\frac{(Baseline\ OCR - OCR\ following\ other\ 2\ inhibitors)}{(Baseline\ OCR - OCR\ following\ all\ inhibitors)}]*100$	
Percentage Dependency	$[\frac{(Baseline\ OCR - OCR\ following\ target\ inhibitor)}{(Baseline\ OCR - OCR\ following\ all\ inhibitors)}]*100$	
Percentage Flexibility	Percentage Capacity – Percentage Dependency	

4.3.5. *Caspase 3 ELISA*

Caspase 3 levels were assessed in OE33P and OE33R cell supernatants which were collected following 24 and 72 h treatment of 250,000 cells/well with 10 μM Pyrazinib (P3) or 0.1% DMSO by ELISA (LifeSpan Biosciences Inc.) using a human caspase 3 sandwich ELISA kit. The assay principle was based on specific binding of caspase 3 in 100 μL of standards or samples binding to target specific capture antibody on coated wells following incubation for 1 h at 37°C in 5% CO_2/95% air. Any unbound standard or samples were washed away following incubation. 100 μL of biotin-conjugated detection antibody was added and bound to capture antigen following incubation for 1 h at 37°C in 5% CO_2/95% air, any unbound detection antibody was washed away following incubation. 100 μL Avidin-Horseradish Peroxidase (HRP) which binds to biotin was added and incubated for 1 h at 37°C in 5% CO_2/95% air and any unbound HRP was washed away following incubation. 3,3',5,5'-Tetramethylbenzidine (TMB) substrate which reacts with HRP enzyme was added and colour change was induced following incubation for 10-20 min at 37°C in 5% CO_2/95% air. 50 μL sulfuric acid solution was added to terminate colour development and absorbance was read at 450 nm on a VersaMax microplate reader (Molecular Devices, Sunnyvale, CA, USA). Absorbance values were normalised to protein levels following BCA assay as described in section 4.3.7.

4.3.6. *Cytochrome C ELISA*

Cytochrome C levels were assessed in OE33P and OE33R cell supernatants which were collected following 24 and 72 h treatment with 10 μM Pyrazinib (P3) or 0.1% DMSO by ELISA (LifeSpan Biosciences Inc.) using a human Cytochrome C sandwich ELISA kit. The assay principle was based on specific binding of Cytochrome C in 100 μL standards or samples to target specific capture antibody on coated wells following incubation for 2 h at 37°C in 5% CO_2/95% air. Any unbound standard or samples were aspirated off. 100 μL biotin-conjugated detection antibody was added and bound to capture antigen following incubation for 1 h at 37°C in 5% CO_2/95% air, any unbound detection antibody was washed away. 100 μL HRP which binds to biotin was added and incubated for 1 h at 37°C in 5% CO_2/95% air. Any unbound HRP was removed following aspiration and 5 wash cycles. 90 μL TMB substrate which reacts with HRP enzyme was added for 15-30 min and incubated at 37°C in 5% CO_2/95% air until sufficient colour change was induced. The stop solution sulfuric acid was added at 50 μL/well to terminate colour development and absorbance was read at 450nm on a VersaMax microplate reader (Molecular Devices, Sunnyvale, CA, USA). Absorbance values were normalised to protein levels following BCA assay as described in next section 4.3.7.

4.3.7. *Bicinchoninic acid (BCA) assay*

Protein content was determined using the Pierce bicinchoninic acid (BCA) Protein Assay Kit (Thermo Fischer Scientific, Waltham, MA, USA). The highest standard used was 2 mg/mL albumin. A 2-fold serial dilution was made and 25 µL/well standard or sample was added in duplicate. 200 µL/well working reagent (50:1 BCA reagent A: BCA reagent B) was added and mixed. The plate was incubated for 30 min at 37°C. The plate was cooled to RT and absorbance was read at 562 nm on a VersaMax microplate reader (Molecular Devices, Sunnyvale, CA, USA). A standard curve was generated and sample values were interpolated to determine unknown protein concentration of samples.

4.3.8. *Evaluation of metabolic rate of OE33P and OE33R cells cultured under 0.5% O_2*

Cells cultured under normoxic conditions were cultured as follows, OE33P and OE33R cells were seeded at a density of 11,000 and 13,000 cells/well, respectively in 24-well cell culture XFe24 microplates (Agilent Technologies, Santa Clara, CA, USA) in a volume of 100 µL and allowed to adhere at 37°C in 5% CO_2/95% air. Following 5 h incubation, an additional 150 µL/well complete cell culture RPMI-1640 medium was added. Cells cultured under hypoxia of 0.5% O_2 were seeded at a density of 15,000 and 18,000 respectively, cells were allowed to adhere at 37°C in 5% CO_2/95% air for 6 h before being placed under hypoxic conditions in the H35 Whitley workstation. 24 h later, OE33P and OE33R cells were treated with 10 µM Pyrazinib (P3) or 0.1% DMSO control, treatment was carried out under normoxia or hypoxia conditions as required. Following 24 h treatment, media was removed and cells were washed with DMEM supplemented with 10 mM glucose and 10 mM sodium pyruvate (pH 7.4) and incubated for 1 h at 37°C in a CO_2-free incubator. OCR and ECAR were measured using a Seahorse Biosciences XFe24 Extracellular Flux Analyser (Agilent Technologies, Santa Clara, CA, USA). Three basal measurements of OCR and ECAR were taken over 24 min consisting of three repeats of mix (3 min) / wait (2 min) / measurement (3 min) to establish basal respiration. Three additional measurements were obtained following the injection of three mitochondrial inhibitors including oligomycin (2 µg·mL−1, Sigma Aldrich), FCCP (5 µM, Sigma Aldrich) and antimycin-A (2 µM, Sigma Aldrich). ATP turnover was calculated by subtracting the OCR post oligomycin injection from baseline OCR prior to oligomycin addition. Proton leak was calculated by subtracting OCR post antimycin-A addition from OCR post oligomycin addition. Maximal respiration was calculated by subtracting OCR post antimycin-A addition from OCR post FCCP addition. Non-mitochondrial respiration was determined as OCR value post antimycin A addition. All measurements were normalised to cell number using the crystal violet assay, transferring the eluted stain to a 96-well plate before reading as previously described in section 3.3.7.

4.3.9. *Measuring ROS levels, mitochondrial mass and mitochondrial membrane potential in OE33P and OE33R cells cultured under 0.5% O_2*

OE33P and OE33R cells were seeded at 8,000 cells/well for normoxic culture and 10,000 cells/well for hypoxic culture. Cells for hypoxic culture were allowed to adhere at 37°C in 5% CO_2/95% air for 6 h before being transferred to the Whitley H35 hypoxystation at 37°C in 5%CO_2/0.5%O_2. Following 24 h incubation under normoxic or hypoxic conditions (0.5% O_2) OE33P and OE33R cells were treated with 10 μM of Pyrazinib (P3) or 0.1% DMSO control whilst being maintained under specific culture conditions. Following 24 h treatment, ROS levels, mitochondrial mass and mitochondrial membrane potential were evaluated as previously described in sections 3.3.9 - 3.3.11 whilst being maintained under normoxic or hypoxic conditions of 0.5% O_2.

4.3.10. *Clonogenic assay with OE33P and OE33R OAC cells*

OE33P and OE33R cells were trypsinised, counted and seeded at the optimised densities of 1 - 3 x 10^3 in 1.5 mL complete RPMI-1640 in triplicate in 6 well plates and allowed to adhere overnight. Following 24 h incubation, OE33P and OE33R cells were treated with either 0.1% DMSO or Pyrazinib (P3) at 10 μM for 24 h prior to receiving 0 or 2 Gy irradiation. Clonogenics carried out under hypoxic conditions were seeded and allowed to adhere at 37°C in 5% CO_2/95% air for 6 h before being transferred to the Whitley H35 hypoxystation at 37°C in 5%CO_2/0.5%O_2. Following 24 h incubation under hypoxic conditions (0.5% O_2) OE33P and OE33R cells were maintained at 0.5% O_2 and treated with 10 μM of Pyrazinib (P3) or 0.1% DMSO control and irradiated 24 h later at 5% CO_2/0.5% O_2. Following 24 h incubation following irradiation, plates were returned to 37°C in 5% CO_2/95% air. Colonies were allowed to grow for 7-14 days, at which point they were fixed and stained with 250 μL 0.05 % crystal violet (25% Methanol in dH_20) and allowed to air dry. Colonies consisting of 50 cells or more were counted using a colony counter (ColCountTM, Oxford Optronix, Oxford, UK). Plating efficiency (PE), fraction of colonies formed by untreated cells, was calculated using the formula: PE = No. colonies/No. cells seeded. The surviving fraction (SF), the number of colonies formed by treated cells, expressed in terms of PE, was calculated using the formula: SF = No. colonies/(No. cells seeded x PE).

4.3.11. *Irradiation*

Irradiation was performed using a Xstrahl X-ray generator, (RS225) (Xstrahl), at a dose rate of 2.85 Gray (Gy) per min.

4.3.12. *BrdU proliferation assay in OE33P and OE33R cells cultured under 0.5% O_2*

OE33P and OE33R cells were seeded at 8,000 cells/well for normoxic culture and 10,000 cells/well for hypoxic culture. Cells for hypoxic culture were allowed to adhere at 37°C in 5% CO_2/95% air for 6 h before being transferred to the Whitley H35 hypoxystation at 37°C in 5%CO_2/0.5%O_2. Following 24 h incubation under normoxic or hypoxic conditions (0.5% O_2) OE33P and OE33R cells were maintained at 0.5% O_2 and treated with 10 μM of Pyrazinib (P3) or 0.1% DMSO control, following 24 h treatment BrdU labelling solution was added and BrdU assay was carried out as previously described in section 3.3.14.

4.3.13. *Preparation of chemotherapeutic drugs*

Stock solutions of cis-diamminedichloroplatinum (cisplatin) and 5-FU were prepared in PBS and dimethyl sulfoxide (DMSO), respectively. Solutions were sterile filtered and then aliquoted and stored at -20°C. Prior to use the solution was incubated at 37°C and mixed thoroughly.

4.3.14. *Metabolic rate measurements in OE33 Cis P and OE33 Cis R cells*

OE33 Cis P and OE33 Cis R cells were seeded in 5 wells per treatment group at a density of 18,000 and 20,000 cells/well, respectively in 24-well cell culture XFe24 microplates (Agilent Technologies, Santa Clara, CA, USA) at a volume of 100 μL and allowed to adhere at 37°C in 5% CO_2/95% air. 5 hours later, an additional 150 μL/well complete cell culture RPMI-1640 medium was added. Following 24 h incubation cells were treated with 10 μM Pyrazinib (P3) or 0.1% DMSO, 24 h later media was removed and cells were washed with DMEM supplemented with 10 mM glucose and 10 mM sodium pyruvate, (pH 7.4) and incubated for 1 h at 37°C in a CO_2-free incubator. OCR and ECAR were measured using a Seahorse Biosciences XFe24 Analyser (Agilent Technologies, Santa Clara, CA, USA). Three basal measurements of OCR and ECAR were taken over 24 min consisting of three repeats of mix (3 min) / wait (2 min) / measurement (3 min) to establish basal respiration ATP turnover, proton leak, maximal respiration, non-mitochondrial respiration was determined as previously described in section 4.3.5. All measurements were normalised to cell number using the crystal violet assay as previously described in section 3.3.7. For seahorse experiments carried out under 0.5% O_2 hypoxia, cells were seeded under normoxic conditions and allowed to adhere for 6 h at 37°C 5% CO_2/95 % air following which they were placed at 37°C 5% CO_2/0.5% O_2, in the H35 Whitley hypoxystation for 48 h and seahorse measurements were carried out under hypoxia in the i2 Whitley station using the same protocol for measuring rate as described for normoxic conditions.

4.3.15. *Clonogenic assay with OE33 Cis P and OE33 Cis R cells*

OE33 Cis P and OE33 Cis R cells were trypsinised, counted and seeded at the optimised densities of 1 – 2.5 x 10^3 in 1.5 mL complete RPMI-1640 in triplicate in 6 well plates and allowed to adhere overnight. For chemosensitivity assays, cells were allowed to adhere for 24 h following which they were treated with PBS control, 1.3 µM or 2.8 µM of cisplatin or 1.3 µM or 2.8 µM cisplatin in combination with 10 µM Pyrazinib (P3). OE33 Cis P cells were treated with 1.3 µM cisplatin and OE33 Cis R cells were treated with either 1.3 µM or 2.8 µM of cisplatin. For radiosensitivity assays, cells were seeded and allowed to adhere for 24 h following which OE33 Cis P and OE33 Cis R cells were treated with control or 10 µM Pyrazinib (P3) for 24 h following which cells were either irradiated at 2 Gy or mock irradiated. Colonies were allowed to grow for 7-14 days at which point they were fixed, stained and counted as described in section 3.3.12.

4.3.16. *Clonogenic assay with OE33P and OE33R cells treated with 5-FU*

OE33P and OE33R cells were trypsinised, counted and seeded at the optimised densities of 1 – 2.5 x 10^3 in 1.5 mL complete RPMI-1640 in triplicate in 6 well plates and allowed to adhere overnight. Following 24 h incubation, OE33P and OE33R cells were treated with either 0.1% DMSO, 10 µM of Pyrazinib (P3), 0.3511 or 0.8982 µM of 5-FU (Sigma-Aldrich) alone or in combination with 10 µM Pyrazinib (P3) for 24 h following which cells were either mock irradiated or received 2 Gy irradiation and were grown for 7-14 days until sufficient colonies had formed. Colonies were fixed, stained and counted as described in section 3.3.12.

4.3.17. *Statistical analysis*

Statistical analysis was performed using GraphPad Prism version 5 software (GraphPad Software, CA, USA). Scientific data were expressed as mean ±SEM. SEM was calculated as the standard deviation of the original samples divided by the square root of the sample size. Specific statistical tests used are indicated in figure legends. For all statistical analysis, differences were considered statistically significant at $p<0.05$.

4.4. Results

4.4.1. *Investigating the dependency of OE33P and OE33R cells on the glutamine, fatty acid and glucose/pyruvate metabolic pathways*

To further understand the anti-metabolic activity of Pyrazinib (P3) demonstrated in chapter 3 we investigated potential metabolic reprogramming which may occur as a result. As this has not yet been explored in our isogenic model of OAC radioresistance we initially investigated the cellular dependence on each of the mitochondrial metabolites, pyruvate, fatty acids and glutamine to fuel mitochondrial respiration of OE33P and OE33R cells when the other 2 are blocked using the Mito Fuel Flex test. OE33P cells are significantly more dependent on the glutamine pathway to fuel mitochondrial respiration compared to OE33R cells (p=0.0009) **(Figure 4-2A)**. There was no significant difference in the dependence of OE33P and OE33R cells on fatty acid oxidation and pyruvate oxidation **(Figure 4-2B,C)**.When the dependence on each metabolite was compared in both OE33P and OE33R cells, both cell lines relied on glutamine to fuel mitochondrial oxidation significantly more than pyruvate (p=0.0098, p=0.0464) respectively **(Figure 4-2D,E)**.

Our initial findings indicated that of the three pathways tested, OE33P and OE33R cells predominantly rely on the glutamine pathway to fuel OCR although they are not totally dependent on any one pathway. Thus, we sought to investigate the dependence, capacity and flexibility of OE33P and OE33R cells treated with Pyrazinib (P3) or 0.1% DMSO control on the glutamine pathway using the Mito Fuel Flex test.

Pyrazinib (P3) had very little impact on mitochondrial dependence of OE33P and OE33R cells on the import of glutamine into the mitochondria, the capacity for import of glutamine or metabolic flexibility when fatty acid oxidation and pyruvate oxidation were both inhibited in OE33P and OE33R cells **(Figure 4-3A,B,C)**. Furthermore, Pyrazinib (P3) had no effect on fatty acid import or capacity for import when pyruvate oxidation and glutaminolysis were both inhibited in OE33R cells **(Figure 4-3D,E,F)**.

In summary, OE33P and OE33R cells appear to utilise the glutamine oxidation pathway as the predominant pathway to fuel mitochondrial respiration however they are not reliant on this pathway alone, furthermore Pyrazinib (P3) does not significantly alter the dependence or capacity for glutamine import of OE33P and OE33R cells.

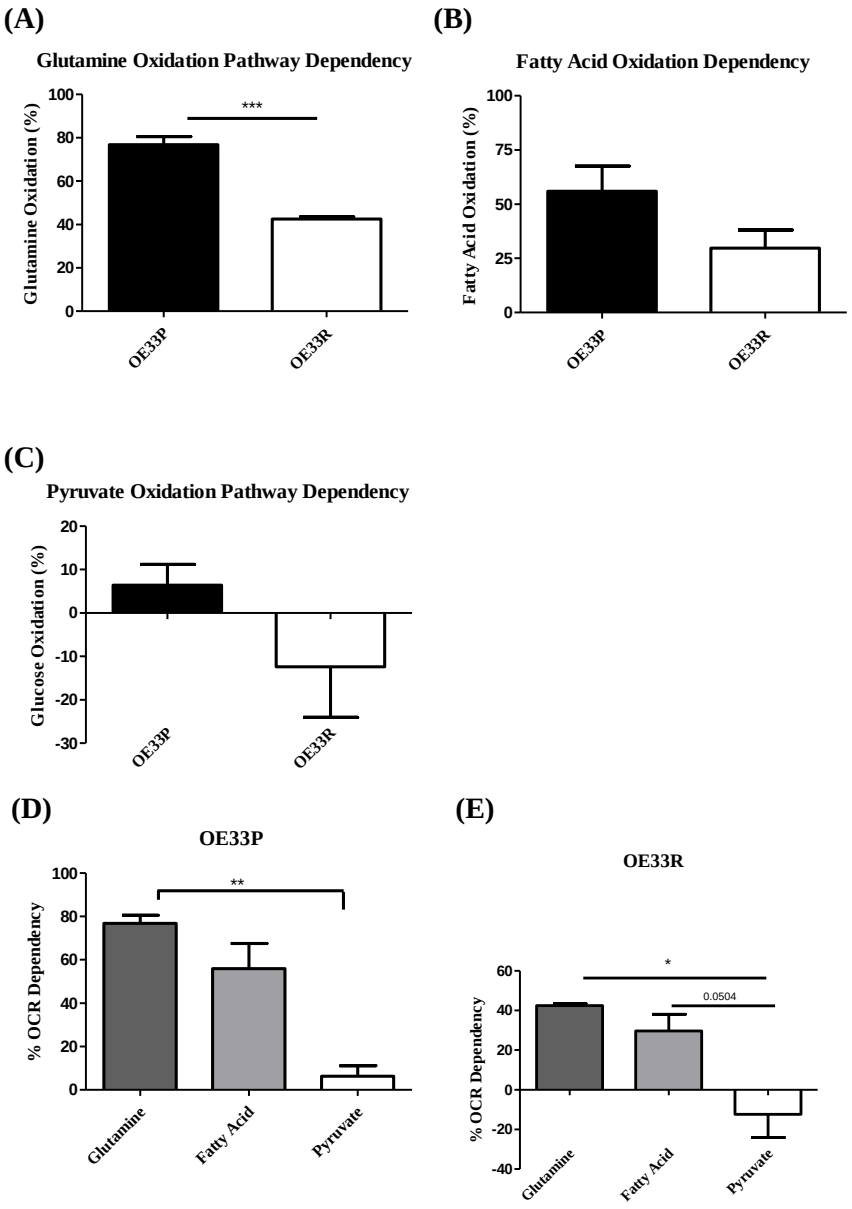

Figure 4-2 OE33P cells are significantly more dependent on the glutamine oxidation pathway compared to OE33R cells.

Percentage glutamine, fatty acid and glucose/pyruvate pathway dependency was assessed in OE33P and OE33R cells using the Seahorse Biosciences XFe24 analyser. Following 24 h culture of OE33P and OE33R cells, the Mito Fuel Flex test was run to evaluate **(A)** glutamine pathway dependency, (n=4), **(B)** fatty acid oxidation pathway dependency, (n=3), and **(C)** glucose/pyruvate oxidation pathway dependency, (n=3). Percentage pathway dependency of the three pathways was compared in **(D)** OE33P cells, (n=3), and **(E)** OE33R cells, (n=3). Unpaired t-test used compare different cell lines, paired t-test used to compare within same cell line, $^{**}p<0.01$, $^{***}p<0.001$. Data are expressed as mean +SEM.

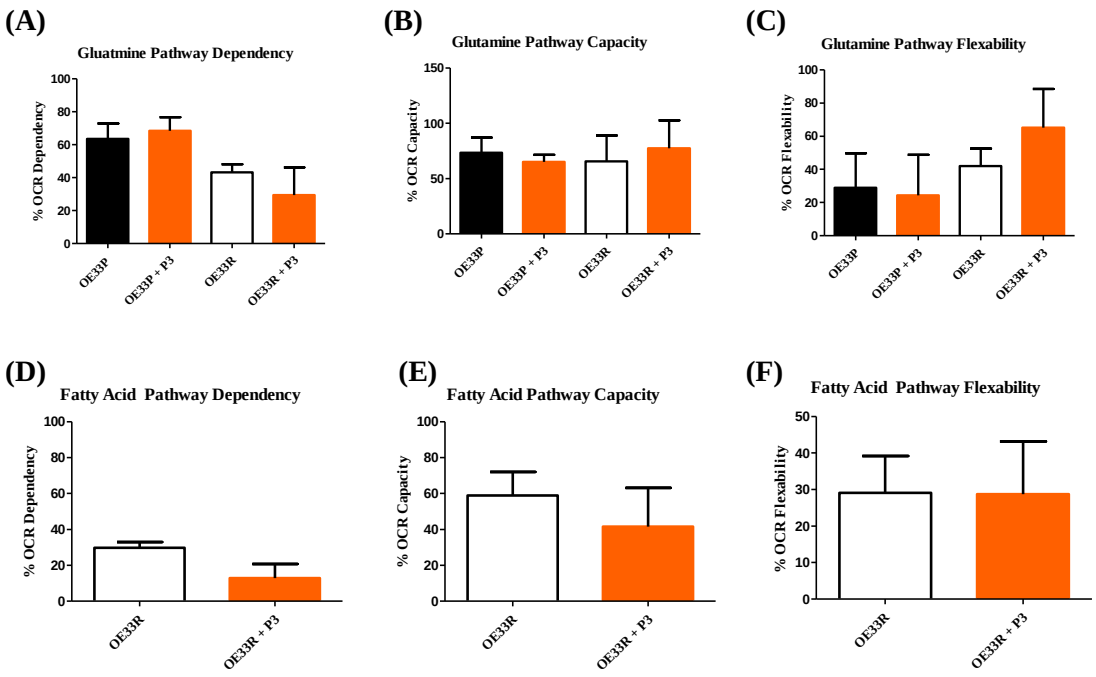

Figure 4-3 Pyrazinib (P3) does not significantly alter the percentage dependency, capacity or flexibility of OE33P and OE33R cells on the glutamine metabolic pathway.
Percentage glutamine pathway dependency, capacity and flexibility was assessed in OE33P and OE33R cells using the Seahorse Biosciences XFe24 analyser. Fatty acid pathway dependency, capacity and flexibility was measured in OE33R cells. OE33P and OE33R cells were treated for 24 h with either 0.1% DMSO or 10 µM Pyrazinib (P3) before the Mito Fuel Flex test was run to evaluate **(A)** glutamine pathway dependency, (n=4), **(B)** glutamine pathway capacity, (n=3), and **(C)** glutamine pathway flexibility, (n=3). OE33R cells were treated with either 0.1% DMSO or 10 µM of Pyrazinib (P3) for 24 h following which a Mito Fuel Flex test was carried out to evaluate **(D)** fatty acid pathway dependency, (n=3), **(E)** fatty acid pathway capacity, (n=3) and **(F)** fatty acid pathway flexibility, (n=3). Unpaired t-test used compare different cell lines, paired t-test used to compare within same cell line. Data are expressed as mean +SEM.

4.4.2. *Pyrazinib (P3) does not alter the secretion of cytochrome C or caspase 3 from OE33P or OE33R cells*

To further investigate the mechanism by which Pyrazinib (P3) inhibits OCR under normoxic conditions in OE33P and OE33R cells we evaluated the effect of treatment with Pyrazinib (P3) on mitochondrial apoptosis proteins, cytochrome C and caspase 3 secretions by ELISA. OE33P and OE33R cells were treated with 10 μM of Pyrazinib (P3) for 24 and 72 h.

Following treatment, the levels of both cytochrome C and cleaved caspase 3 were assessed in cell supernatants. At baseline the secreted levels of cytochrome C were not significantly different at 24 h **(Figure 4-4A)** however following 72 h incubation the secreted levels of cytochrome C were significantly lower in OE33R cells when compared to the parental OE33P cells **(Figure 4-4C)** ($p<0.05$). Treatment with Pyrazinib (P3) had no effect on the secreted levels of cytochrome C in either cell line at either time point **(Figure 4-4B, D).**

In addition caspase 3 levels did not significantly differ between the two cell lines at either time point **(Figure 4-4E, G)** or following treatment with Pyrazinib (P3) **(Figure 4-4F, H).** The lower cytochrome C levels following 72 h incubation in the OE33R cells would have thought to also result in lower levels of secreted caspase 3 in OE33R cells but this was not seen but this may be time dependent as the secreted levels of cleaved caspase 3 were very low in all samples tested **(Figure 4-4E-H)**.

These results indicated that the anti-metabolic activity previously seen following treatment with Pyrazinib (P3) is not being mediated through altered secretion of mitochondrial apoptosis proteins; cytochrome C and cleaved caspase 3 which have been previously shown to play a role in reduced metabolic activity and tumoural radio-sensitivity.

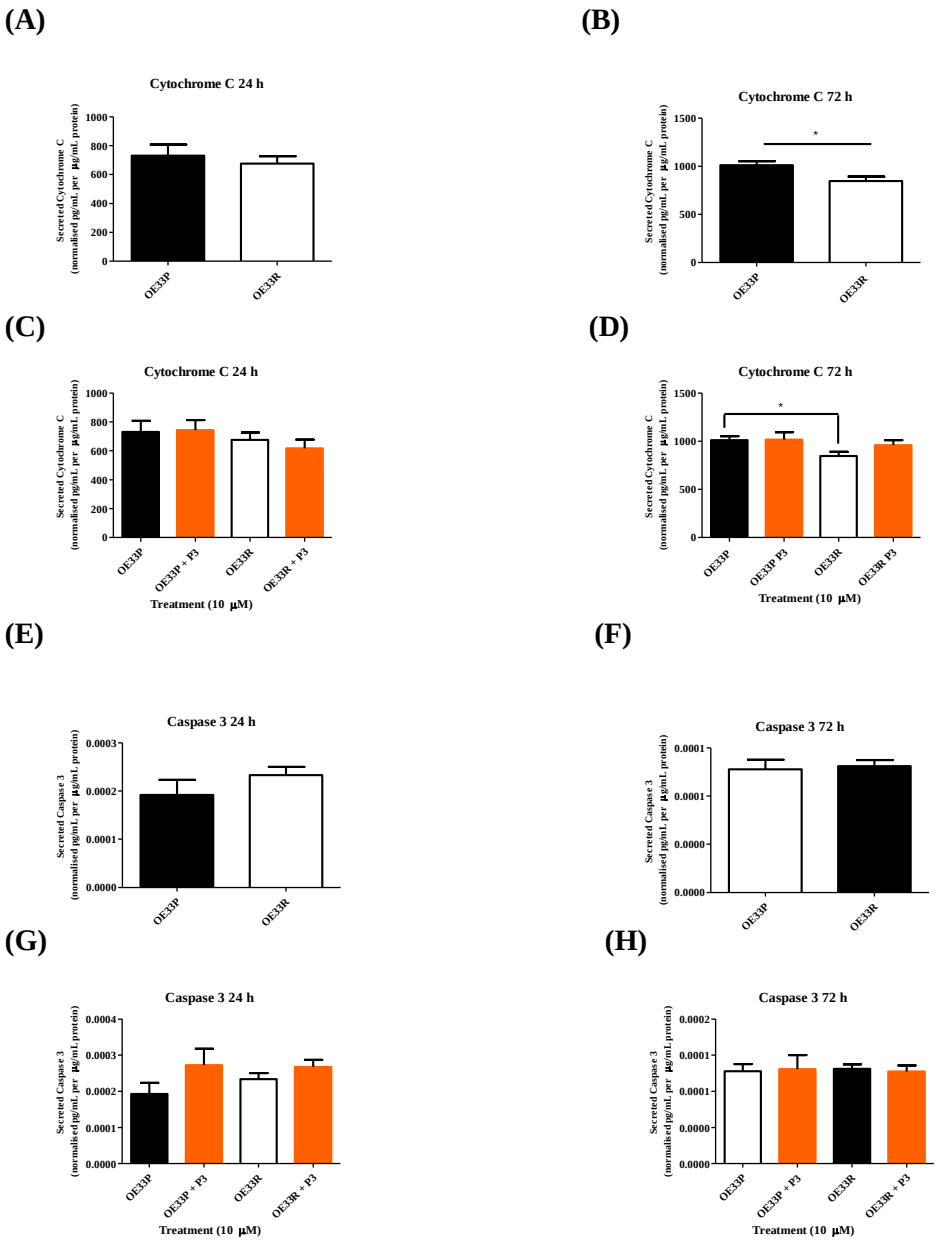

Figure 4-4 Secreted levels of cytochrome C and caspase 3 following treatment with Pyrazinib (P3) for 24 or 72 h.

(A) Difference in cytochrome C levels in OE33P and OE33R cells at 24 h, (n=3) **(B)** Difference in secreted levels of cytochrome C in OE33P and OE33R cells at 72 h (n=4) **(C)** Secreted levels of cytochrome C in OE33P and OE33R cells following 24 h treatment with 10 µM Pyrazinib (P3). **(D)** Secreted levels of cytochrome C in OE33P and OE33R cells following treatment with 10 µM of Pyrazinib (P3) for 72 h. **(E)** Difference in caspase 3 levels in OE33P and OE33R cells at 24 h **(F)** Difference in secreted levels of caspase 3 in OE33P and OE33R cells at 72 h **(G)** Secreted levels of caspase 3 in OE33P and OE33R cells following 24 h treatment with 10 µM Pyrazinib (P3). **(H)** Secreted levels of caspase 3 in OE33P and OE33R cells following treatment with Pyrazinib (P3) for 72 h. Unpaired t-test, *p<0.05, (n=3). Data are expressed as mean +SEM.

4.4.3. *Pyrazinib (P3) significantly inhibits ATP turnover in OE33R cells*

Previously in chapter 3 we have shown Pyrazinib (P3) can significantly inhibit OCR in OE33P and OE33R cells. In this chapter we further investigated the anti-metabolic activity of Pyrazinib (P3) in OE33P and OE33R cells under both normoxic and hypoxic conditions (0.5% O_2). Using the Seahorse Biosciences XFe24 analyser we investigated the effect of Pyrazinib (P3) treatment on ATP turnover, proton leak, spare respiratory capacity, maximal respiration and non-mitochondrial respiration in OE33P and OE33R cells cultured under both normoxic and hypoxic conditions (0.5% O_2).

OCR was significantly higher in OE33R cells compared to OE33P cells cultured under normoxia (p=0.0307) however under hypoxic conditions, there was no significant difference in oxygen consumption rate between OE33P and OE33R cells **(Figure 4-5A).** OCR was significantly higher in OE33P cells cultured under hypoxia compared to OE33P cells cultured under normoxia (p=0.0494). OCR was significantly higher in OE33R cells cultured hypoxia compared to OE33R cells cultured under normoxia (p=0.0259). As previously seen in chapter 3, Pyrazinib (P3) significantly reduced OCR in OE33P and OE33R cells cultured under normoxic conditions (p=0.0193, p=0.0183) respectively **(Figure 4-5A)**. Pyrazinib (P3) produced a non-significant ~10% decrease in OCR in OE33R cells cultured under hypoxic conditions (p=0.0877) **(Figure 4-5A)**.

As previously seen in chapter 3 there was no significant difference in ECAR between OE33P and OE33R cells cultured under normoxic conditions **(Figure 4-5B)**. Pyrazinib (P3) produced a non-significant reduction of 11.6% in ECAR in OE33R cells cultured under normoxic conditions **(Figure 4-5B)**. ECAR was significantly higher in OE33R cells cultured under hypoxia compared to those cultured under nomoxia, (p=0.0411) **(Figure 4-5B)**. In addition, ECAR was significantly higher in OE33R cells compared to OE33P cells cultured under hypoxic conditions (p=0.0466) **(Figure 4-5B)**.

Under normoxic conditions ATP turnover was found to be significantly higher in OE33R cells compared to OE33P cells (p=0.0236) **(Figure 4-5C)**. Furthermore, treatment with Pyrazinib (P3) was found to significantly decrease ATP turnover in OE33R cells cultured under normoxic conditions. There was no significant difference in ATP turnover between OE33P and OE33R cells cultured under hypoxia and treatment with Pyrazinib (P3) did not alter ATP turnover in either OE33P or OE33R cells cultured under hypoxia **(Figure 4-5C)**.

There was no significant difference in proton leak, spare respiratory capacity or non-mitochondrial respiration between OE33P and OE33R cells cultured under normoxia or hypoxia **(Figure 4-5D-F)**. Furthermore, treatment with Pyrazinib (P3) did not significantly alter any of

these 3 parameters in OE33P and OE33R cells cultured under normoxic and hypoxic conditions **(Figure 4-5D-F)**.

Maximal respiration decreased by ~67% in OE33R cells cultured under hypoxia compared to those cultured under normoxia but this was not significant, (p=0.0666) **(Figure 4-5G)**.

In summary, Pyrazinib (P3) can significantly inhibit OCR and ATP turnover in OE33R cells. OE33R cells adapt to the hypoxic environment through the significant upregulation of ECAR under hypoxic conditions. Pyrazinib (P3) does not significantly alter metabolic rate under hypoxic conditions.

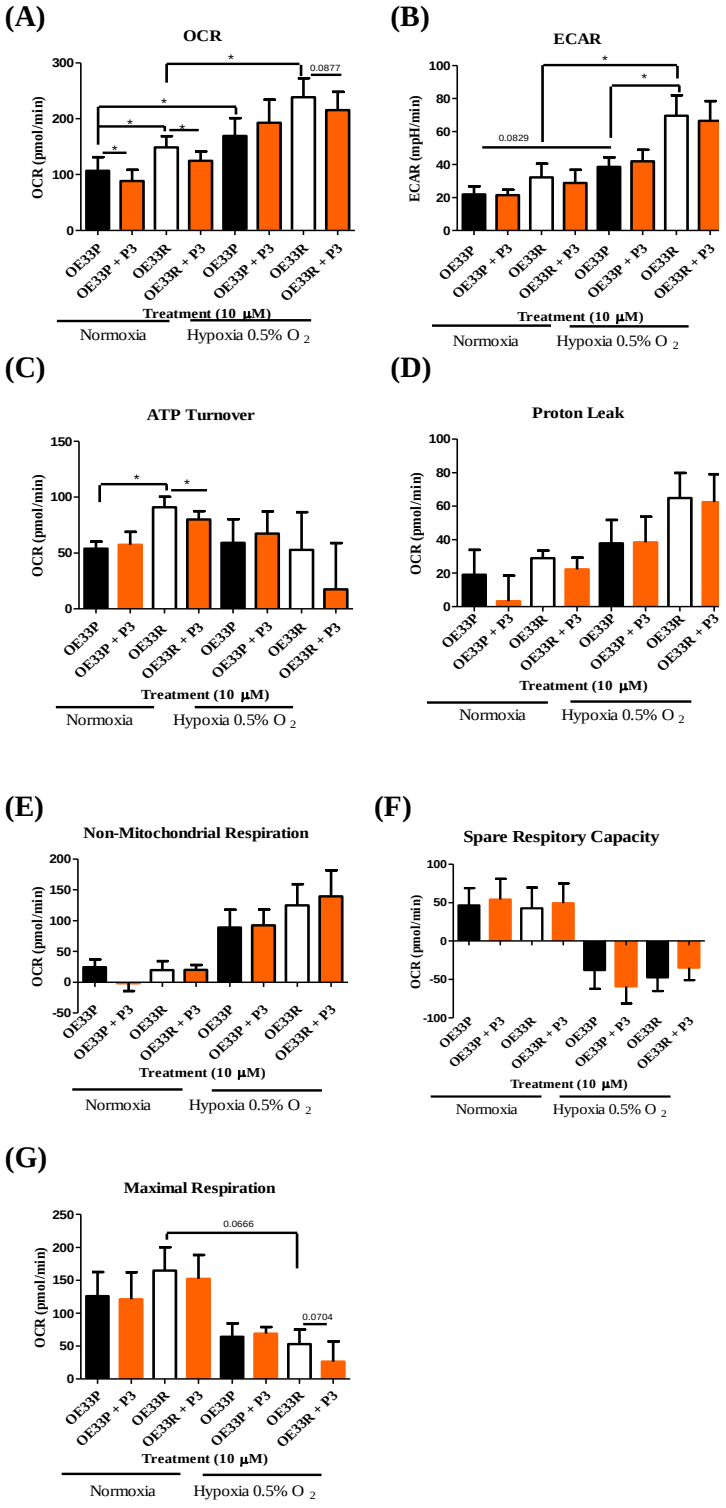

Figure 4-5 Pyrazinib (P3) significantly inhibits ATP turnover in OE33R cells.
Metabolic profiling of OE33P and OE33R cells was carried out using the Seahorse Biosciences XFe24 analyser. OE33P and OE33R cells were cultured under normoxic or hypoxic conditions and treated with either 0.1% DMSO or 10 µM Pyrazinib (P3) for 24 h following which they were analysed to assess **(A)** oxygen consumption rate, **(B)** extracellular acidification rate, **(C)** ATP turnover, **(D)** proton leak, **(E)** non-mitochondrial respiration, **(F)** spare respiratory capacity and **(G)** maximal respiration, (n=6). Statistical analysis was carried out using an unpaired t-test to compare different cell lines and paired t-test to compare within same cell line, *p<0.05, **p<0.01. Data was normalised to cell number, determined by crystal violet assay. Data are expressed as mean +SEM.

4.4.4. *Pyrazinib (P3) inhibits ROS under hypoxic conditions in OE33R cells*

To further understand the metabolic phenotype of OE33P and OE33R cells cultured under hypoxia and the action of Pyrazinib (P3) under these conditions we evaluated three surrogate markers of mitochondrial function including ROS levels, mitochondrial membrane potential and mitochondrial mass in cells treated with either 0.1% DMSO or 10 μM Pyrazinib (P3).

As previously seen, in chapter 3 ROS levels were significantly higher in OE33R cells compared to OE33P cells cultured under normoxia. ROS levels were significantly higher in OE33P cells cultured under hypoxia (0.5% O_2) compared to OE33P cells cultured under normoxia (p=0.0108) **(Figure 4-6A).** Pyrazinib (P3) treatment significantly reduced ROS levels in OE33R cells cultured under hypoxia **(Figure 4-6A).**

There were no significant differences in mitochondrial membrane potential in OE33P and OE33R cells cultured under normoxic or hypoxic conditions (0.5% O_2). Furthermore treatment with Pyrazinib (P3) for 24 h did not significantly alter mitochondrial membrane potential in either OE33P or OE33R cells **(Figure 4-6B)**.

Mitochondrial mass was significantly higher in OE33P cells cultured under hypoxia (0.5% O_2) compared to OE33P cells cultured under normoxia, (p=0.0081) **(Figure 4-6C)**. Pyrazinib (P3) did not alter mitochondrial mass in OE33P or OE33R cells cultured under normoxia or hypoxia **(Figure 4-6C).**

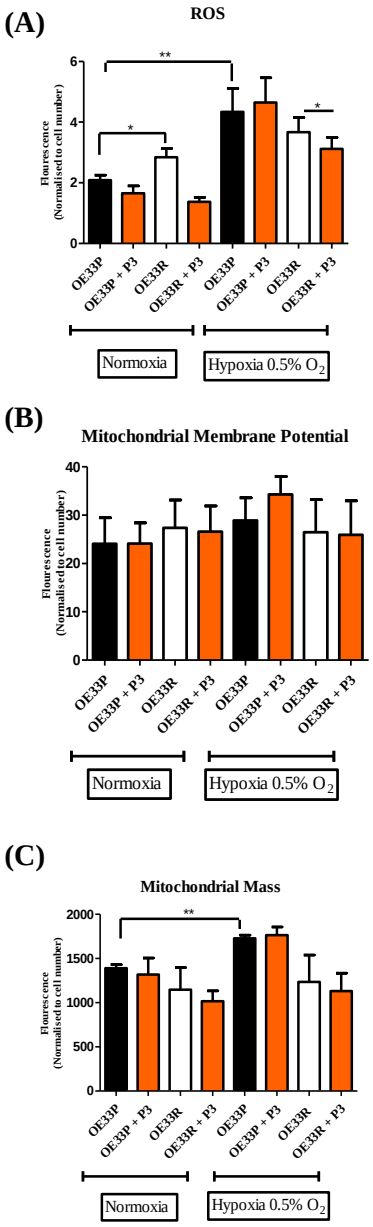

Figure 4-6 ROS levels, mitochondrial membrane potential and mitochondrial mass in OE33P and OE33R cells cultured under normoxic and hypoxic conditions.

(A) 24 h treatment with 10 µM Pyrazinib (P3) significantly reduced ROS in OE33R under hypoxic conditions, (n=4 for all except, OE33P and OE33R under normoxia n=8). **(B)** 24 h treatment with 10 µM Pyazinib (P3) did not significantly alter mitochondrial membrane potential in OE33P or OE33R cells under normoxic or hypoxic conditions, (n=3). **(C)** Mitochondrial mass is significantly higher in OE33P cells cultured under hypoxic conditions compared to OE33P cells cultured under normoxic conditions (n=3). Statistical analysis was carried out using an unpaired t-test to compare different cell lines and paired t-test to compare within same cell line, *p<0.05, **p<0.01. Data was normalised to cell number, determined by crystal violet assay. Data are expressed as mean +SEM.

4.4.5. *Pyrazinib (P3) can enhance radiosensitivity in-vitro in an isogenic model of oesophageal adenocarcinoma under hypoxic conditions*

We have previously shown in chapter 3 that Pyrazinib (P3) can significantly enhance radiosensitivity to increasing doses of radiation under normoxic conditions. Hypoxic tumours are inherently radioresistant [238], and OAC tumours have been shown to have hypoxic regions thus we investigated to ability of Pyrazinib (P3) to enhance radiosensitivity in an environment of low oxygen (0.5% O_2).

Both OE33P and OE33R cells were significantly more radioresistant to both 2 and 4 Gy radiation when cultured under hypoxic conditions (0.5% O_2) when compared to matched cells cultured under normoxic conditions **(Figure 4-7A,B)**. To determine the effect of 0.5% hypoxia quantitatively on the radiosensitivity of OE33P and OE33R cells, the oxygen enhancement ratio (OER) was determined for each cell line following increasing doses of irradiation by dividing the average surviving fraction of cells in hypoxia by number of surviving cells in normoxia. The OER of OE33P cells was 1.84 following 2 Gy irradiation and 3.45 following 4 Gy irradiation highlighting the importance of oxygen for the radiosensitivity of these cells. In OE33R cells the oxygen enhancement ratio was 1.43 and 1.32 following 2 and 4 Gy irradiation respectively.

Pyrazinib (P3) did not alter the radiosensitivity of OE33P cells cultured under hypoxic conditions of 0.5% O_2 but could enhance radiosensitivity under normoxic conditions following 2 and 4 Gy irradiation similar to results previously shown **(Figure 4-7C,E)**. Pyrazinib (P3) could significantly enhance radiosensitivity of OE33R cells cultured under normoxic conditions following 2 and 4 Gy X-ray radiation and hypoxic conditions following 4 Gy irradiation (p=0.0216) **(Figure 4-7D,F)**.

The radiosensitising activity of Pyrazinib (P3) is maintained when OE33R cells are cultured under either normoxic or hypoxic conditions (0.5 % O_2).

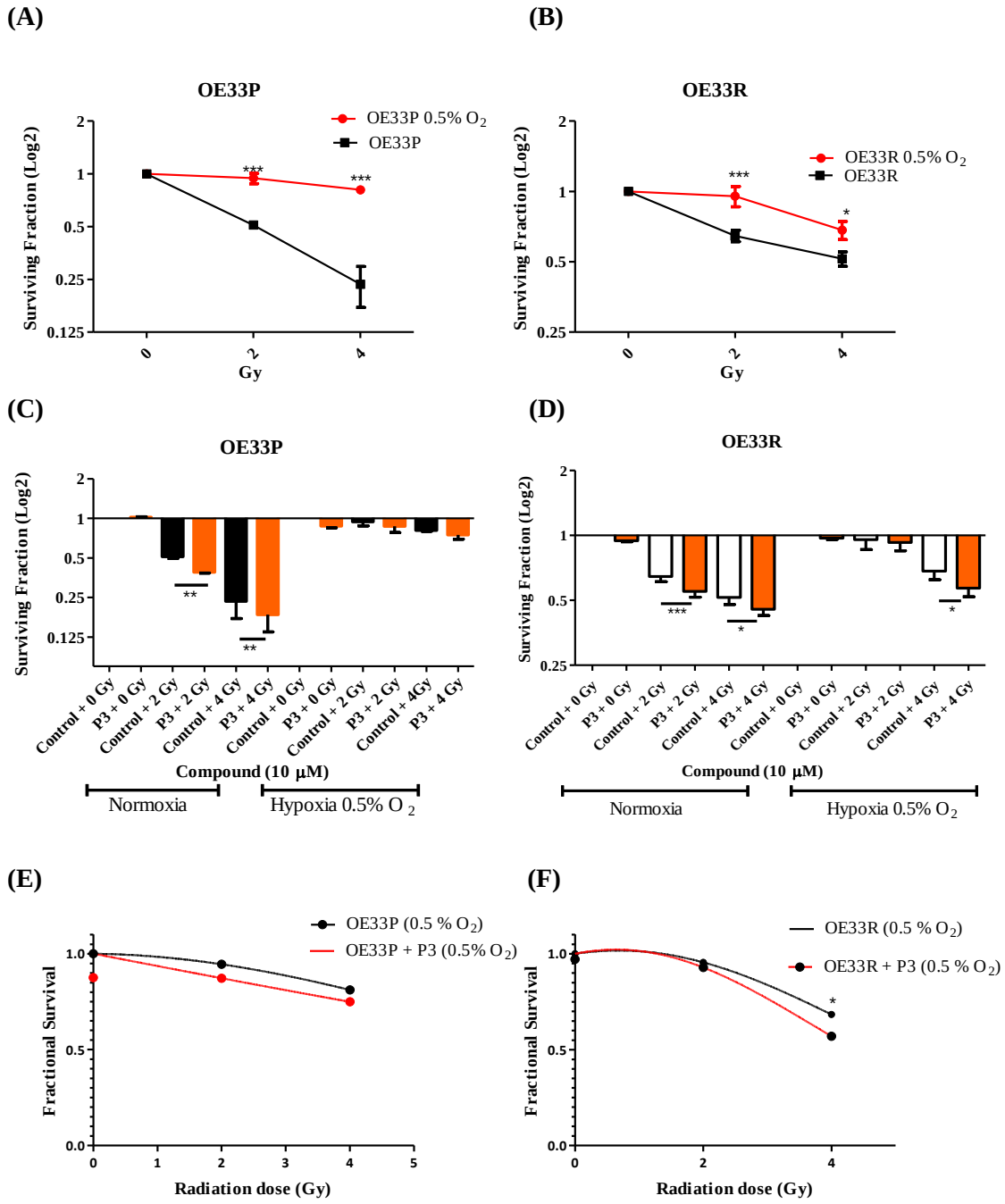

Figure 4-7 Pyrazinib (P3) can significantly enhance radiosensitivity under hypoxic conditions (0.5% O_2) in OE33R; OAC radioresistant cells.

The ability of Pyrazinib (P3) to enhance radiosensitivity was evaluated by clonogenic assay under normoxia and hypoxia (0.5% O_2) using the Whitley H35 hypoxystation. Surviving Fraction following culture under normoxic and hypoxic conditions following 0, 2 and 4 Gy irradiation of (A) OE33P and**(B)** OE33R cells, (n=3). **(C)** Surviving Fraction of OE33P cells cultured under normoxia and hypoxia following treatment with 0.1% DMSO control or 10 µM Pyrazinib (P3) and 0, 2, and 4 Gy irradiation, (n=3). **(D)** Surviving Fraction of OE33R cells cultured under normoxia or hypoxia following treatment with 0.1% DMSO control or 10 µM Pyrazinib (P3) and 0, 2, and 4 Gy irradiation, (n=3). Linear quadratic fit curves of **(E)** OE33P and **(F)** OE33R cells cultured under hypoxia following treatment with 0.1% DMSO or Pyrazinib (P3) and 0, 2 and 4 Gy radiation. Paired t-test used to compare within same cell line, unpaired t-test used to compare different cell lines, *p<0.05, **p<0.01, ***p<0.001. Data presented as the mean ±SEM.

4.4.6. *Pyrazinib (P3) significantly inhibits proliferation of OE33P cells cultured under hypoxic conditions following 2 Gy radiation*

To investigate if the radiosensitising effect of Pyrazinib (P3) treatment was accompanied by changes in cellular proliferation, we assessed cellular proliferation in OE33P and OE33R cells cultured under normoxic and hypoxic conditions which were either mock irradiated (0 Gy) or irradiated with 2 Gy X-ray radiation.

The proliferation rate of OE33P cells cultured under hypoxic conditions was significantly lower than OE33P cells cultured under normoxia, (p=0.0486) **(Figure 4-8A)**. There was no significant difference in proliferation rate of OE33P cells which received 2 Gy radiation compared to mock irradiated cells grown under normoxic or hypoxic conditions. Furthermore, there was no significant difference between OE33R cells grown under normoxic or hypoxic conditions which received 0 or 2 Gy radiation.

Pyrazinib (P3) treatment in combination with 0 or 2 Gy radiation did not significantly alter OE33P cell proliferation under normoxic conditions. Under hypoxic conditions of 0.5% O_2 OE33P cells treated with Pyrazinib (P3) and 2 Gy radiation had a significantly lower rate of cellular proliferation compared to OE33P cells treated with 2 Gy radiation alone, (p=0.0293) **(Figure 4-8B).**

Pyrazinib (P3) treatment in combination with 0 or 2 Gy radiation did not significantly alter OE33R cell proliferation under normoxic or hypoxic conditions (0.5% O_2) **(Figure 4-8C)**.

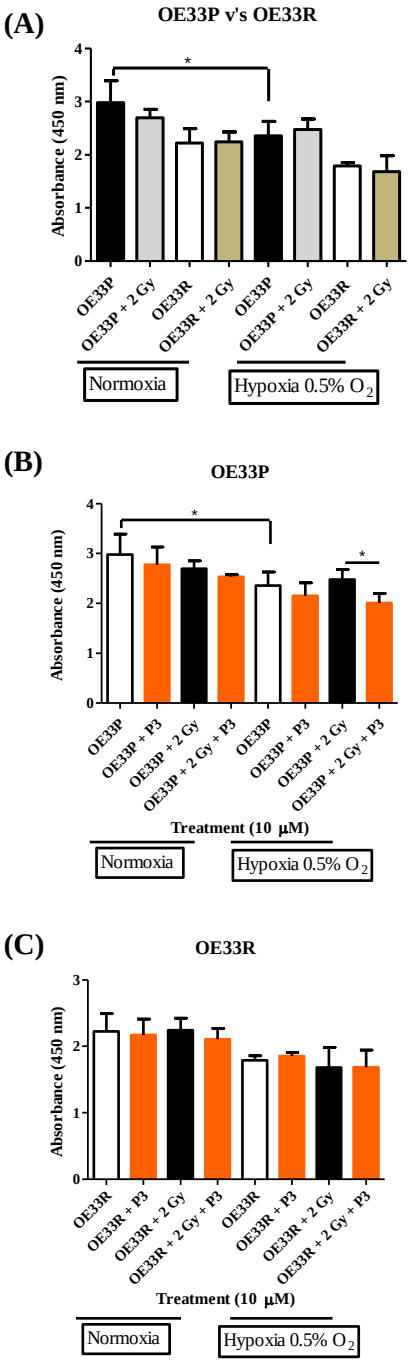

Figure 4-8 Pyrazinib (P3) significantly inhibits cellular proliferation of OE33P cells cultured under hypoxia following 2 Gy irradiation.

Proliferation of OE33P and OE33R cells was assessed by BrdU assay. **(A)** Proliferation of OE33P and OE33R cells treated with 0 or 2 Gy irradiation and cultured under normoxic or hypoxic conditions. Proliferation following 24 h treatment with Pyrazinib (P3) at 10 µM and 0 Gy or 2 Gy irradiation in **(B)** OE33P and **(C)** OE33R OAC cells cultured under normoxic and hypoxic (0.5% O_2) conditions. Paired t-test used to compare within same cell line, unpaired t-test used to compare different cell lines (n=3). *p<0.05. Data are expressed as mean +SEM.

4.4.7. *OE33 Cis R cells have an altered metabolic phenotype compared to the parental OE33 Cis P cells*

In addition to the radiosensitising action of Pyrazinib (P3) in OAC we investigated the potential of Pyrazinib (P3) to enhance chemosensitivity and radiosensitivity in a cisplatin sensitive and cisplatin resistant OAC isogenic cell line. Altered mitochondrial function has previously linked with radiation resistance in OAC thus we investigated the association between cisplatin resistance and metabolism in our model of OAC acquired cisplatin resistance [82].

To investigate if cisplatin resistant OE33 Cis R cells have altered energy metabolism, we measured the two major energy pathways, oxidative phosphorylation and glycolysis, in both OE33 Cis P and OE33 Cis R OAC cells treated with control or 10 µM of Pyrazinib (P3) using the Seahorse Biosciences XFe24 analyser. The metabolic profile of OE33 Cis P and OE33 Cis R cells was assessed under normoxic and hypoxic conditions (0.5% O_2) to investigate if the metabolic phenotype of cisplatin resistant cells can adapt to different environmental settings. OE33 Cis R cells have a significantly higher OCR, when compared to OE33 Cis P cells, p=0.0040 under normoxia however the OCR of OE33 Cis R cells was significantly lower than OE33 Cis P cells under low oxygen conditions of 0.5% O_2, p=0.0078, **(Figure 4-9A).**

Pyrazinib (P3) did not significantly alter metabolic rate in OE33 Cis P or OE33 Cis R cells under normoxia. Pyrazinib (P3) significantly inhibited OCR in OE33 Cis P cells under hypoxia (p=0.0260),**(Figure 4-9A)**. There was no significant difference in ECAR, a measure of glycolysis, between the two cell lines under normoxic or hypoxic conditions **(Figure 4-9B)**.

To further investigate cellular energetics of OE33 Cis P compared to OE33 Cis R cells, both OE33 Cis P and Cis R cells were treated with oligomycin, FCCP and antimycin A which inhibit specific processes in the electron transport chain. Oligomycin and antimycin A produced a similar levels of OCR inhibition in both OE33 Cis P and OE33 Cis R cells, and there was no significant difference in the rate of ATP production or proton leak between cisplatin sensitive and cisplatin resistant cells under normoxic or hypoxic conditions (**Figure 4-9C,D**). Furthermore, treatment of OE33 Cis P and OE33 Cis R cells with FCCP showed no significant difference maximal respiration rate between the two cell lines (**Figure 4-9E**). In addition, the rate of non-mitochondrial respiration was not significantly altered between the two cell lines (**Figure 4-9F**). In summary OE33 Cis R cells have an alerted metabolic phenotype whereby they have a significantly elevated OCR compared to parental OE33 Cis P cells under normoxia and OE33 Cis R cells have significantly lower OCR under hypoxic conditions.

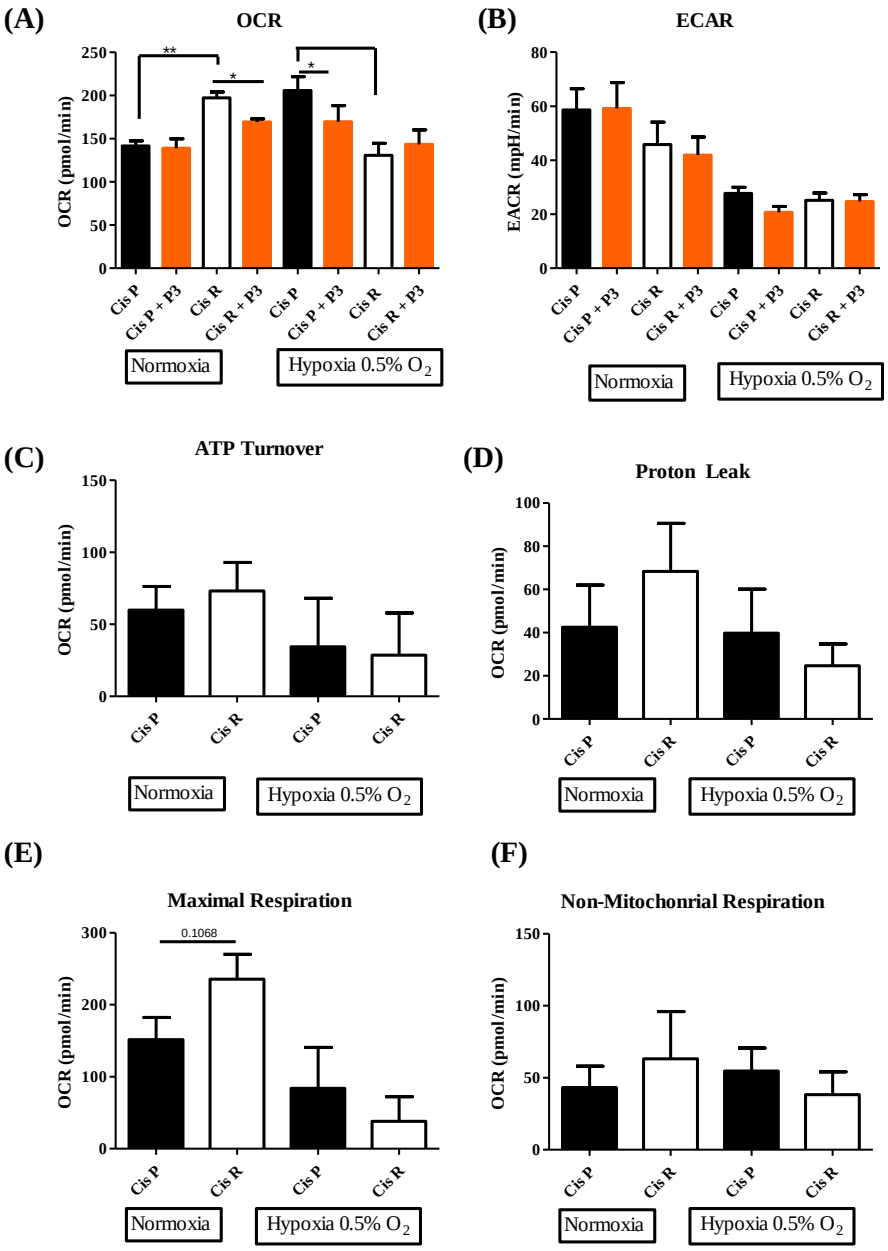

Figure 4-9 Cisplatin resistant (OE33 Cis R) oesophageal adenocarcinoma cells have altered metabolic phenotype compared to cisplatin sensitive (OE33 Cis P) cells under normoxic and hypoxic conditions (0.5% O_2).

(A) OE33 Cis R cells have a significantly higher OCR when compared to Cis P; cisplatin sensitive cells, under normoxic conditions (n=5). **(B)** ECAR was evaluated in OE33 Cis P and OE33 Cis R cells cultured under normoxic and hypoxic conditions (0.5% O_2), (n=5), unpaired t-test. **(C)** Difference in rate of ATP production in Cis P and Cis R cells cultured under normoxic and hypoxic conditions (0.5% O_2), (n=5), unpaired t-test. **(D)** Difference in rate of proton leak in OE33 Cis P and OE33 Cis R cells cultured under normoxic and hypoxic conditions (0.5% O_2), (n=5), unpaired t-test. **(E)** Difference in maximal respiration rate in OE33 Cis P and OE33 Cis R cells cultured under normoxic and hypoxic conditions (0.5% O_2), (n=5), unpaired t-test. **(F)** Difference in non-mitochondrial respiration in OE33 Cis P and OE33 Cis R cells cultured under normoxic and hypoxic conditions (0.5% O_2), (n=5). Paired t-test used to compare within same cell line, unpaired t-test used to compare different cell lines, *p<0.05, **p<0.01. Data presented as the mean +SEM.

4.4.8. *Pyrazinib (P3) does not enhance the sensitivity of OE33 Cis P or OE33 Cis R cells to cisplatin*

In the previous section we found Pyrazinib (P3) does not significantly alter the metabolic rate of OE33 Cis P or OE33 Cis R cells. In this section we investigated whether Pyrazinib (P3) can alter the sensitivity of an isogenic model of OAC cisplatin resistance to cisplatin treatment. Cisplatin is administered as part of the MAGIC treatment regimen to OAC patients and is associated with high rates of treatment resistance. Sensitivity of cisplatin sensitive OE33 Cis P and cisplatin resistant OE33 Cis R OAC cells to cisplatin treatment alone and in combination with 10 µM of Pyrazinib (P3) was evaluated by clonogenic assay. Treatment of cisplatin sensitive OAC cells with 1.3 µM of cisplatin significantly reduced the surviving fraction of OE33 Cis P cells to 0.303 when compared to untreated OE33 Cis P cells, p=0.0108 **(Figure 4-10A)**. Pyrazinib (P3) did not significantly enhance the sensitivity of OE33 Cis P cells to cisplatin but importantly it did not reduce the activity of cisplatin either when both drugs were administered in combination.

Treatment of cisplatin resistant OAC cells OE33 Cis R with 1.3 µM of cisplatin did not significantly reduce the surviving fraction of these cells only reducing the surviving fraction to 0.944 when compared to untreated OE33 Cis R cells, which was significantly higher than the surviving fraction of the OE33 Cis P cells at this concentration, p=0.0011 **(Figure 4-10A)**. More than double the concentration of cisplatin was required to significantly reduce colony formation in OE33 Cis R cells. Treatment of Cis R cells with 2.8 µM cisplatin significantly reduced the surviving fraction of Cis R cells to 0.604, a reduction of ~39%, p=0.0043 **(Figure 4-10A)**, OE33 Cis P cells were not viable following treatment with 2.8 µM of cisplatin **(Figure 4-10A)**. Pyrazinib (P3) significantly reduced the surviving fraction of OE33 Cis R cells by ~17%, (p=0.0094). An important finding from this experiment was the administration of 2.8 µM of cisplatin in combination with Pyrazinib (P3) attenuated the cytotoxic effect of cisplatin which would have to be further evaluated if these treatments were to be given in combination with one another.

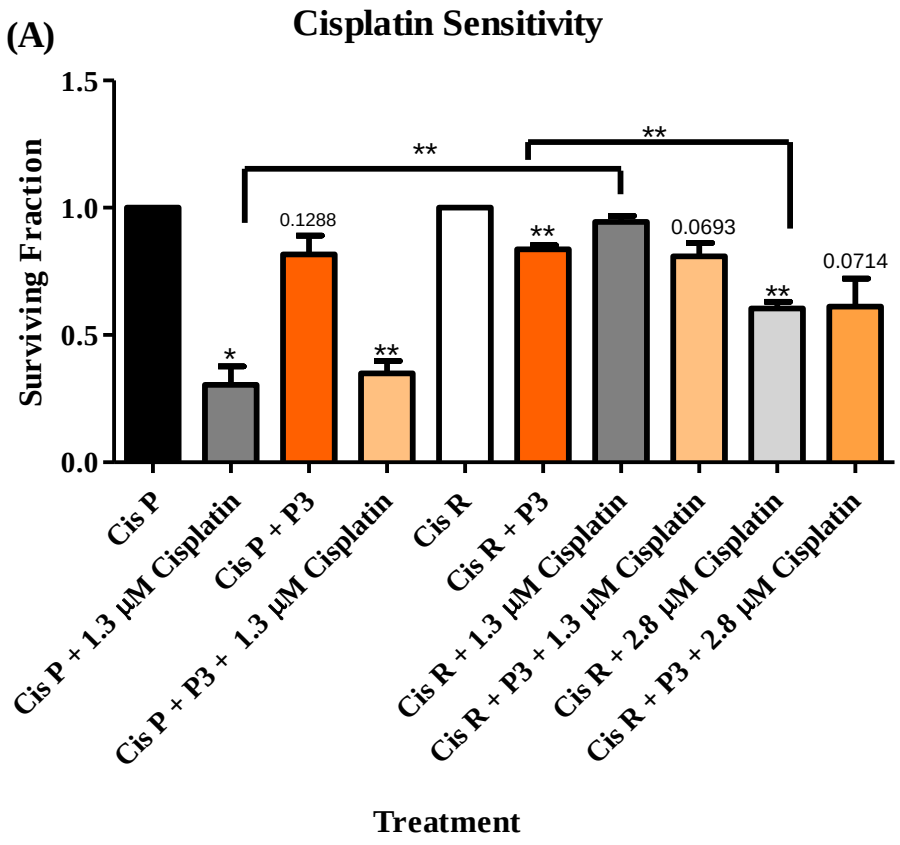

Figure 4-10 Pyrazinib (P3) does not enhance cisplatin sensitivity in an isogenic model OAC acquired cisplatin resistance.

The chemosensitivity of cisplatin-sensitive (OE33 Cis P) and cisplatin-resistant (OE33 Cis R) OAC cells to cisplatin alone and in combination with 10 µM of Pyrazinib (P3) was assessed by clonogenic assay. **(A)** Treatment of cisplatin-sensitive cells with 1.3 µM of cisplatin produced a significant reduction in surviving fraction of Cis P cells, treatment of cisplatin-resistant cells with 2.8 µM but not 1.3 µM of cisplatin produced a significant reduction in surviving fraction of Cis R cells, (n=3). Unpaired t-test between different cells lines, paired t-test between same cell line, *p<0.05, ******p<0.01. Data presented as the mean +SEM

4.4.9. *OE33 Cis R cells are more sensitive to 2 Gy radiation*

To investigate if OE33 cells with acquired cisplatin resistance have altered sensitivity to other treatments we investigated the response of OE33 Cis P cells to radiation compared to OE33 Cis R cells.

Radiosensitivity of OE33 Cis P cells and OE33 Cis R OAC cells was assessed by clonogenic assay. Initially, basal cell survival was assessed in OE33 Cis P and OE33 Cis R to determine if in the absence of any irradiation was there a difference in surviving fraction. No significant differences were seen at baseline in clonogenic survival between the two cell lines, indicating there is no longer term proliferation differences between these cell lines **(Figure 4-11A)**.

To assess if acquired cisplatin resistance conferred altered radiosensitivity, OE33 Cis P and OE33 Cis R cells were either mock irradiated or given one dose of 2 Gy irradiation. OE33 Cis P cells were significantly more radioresistant than OE33 Cis R OAC cells to one fraction of 2 Gy irradiation, (p=0.0055) **(Figure 4-11B).** To investigate if Pyrazinib (P3) altered radiosensitivity of a model acquired cisplatin resistance we treated OE33 Cis P and OE33 Cis R cells with 10 μM of Pyrazinib (P3) or 0.1% DMSO control for 24 h prior to 2 Gy irradiation. Pyrazinib (P3) significantly enhanced the radiosensitivity of OE33 Cis P (p=0.0425) but not OE33 Cis R cells **(Figure 4-11C)**. In summary OE33 Cis P cells are more radioresistant than OE33 Cis R cells, independent of differences in basal proliferation and Pyrazinib (P3) significantly enhanced the radioresponse of OE33 Cis P cells.

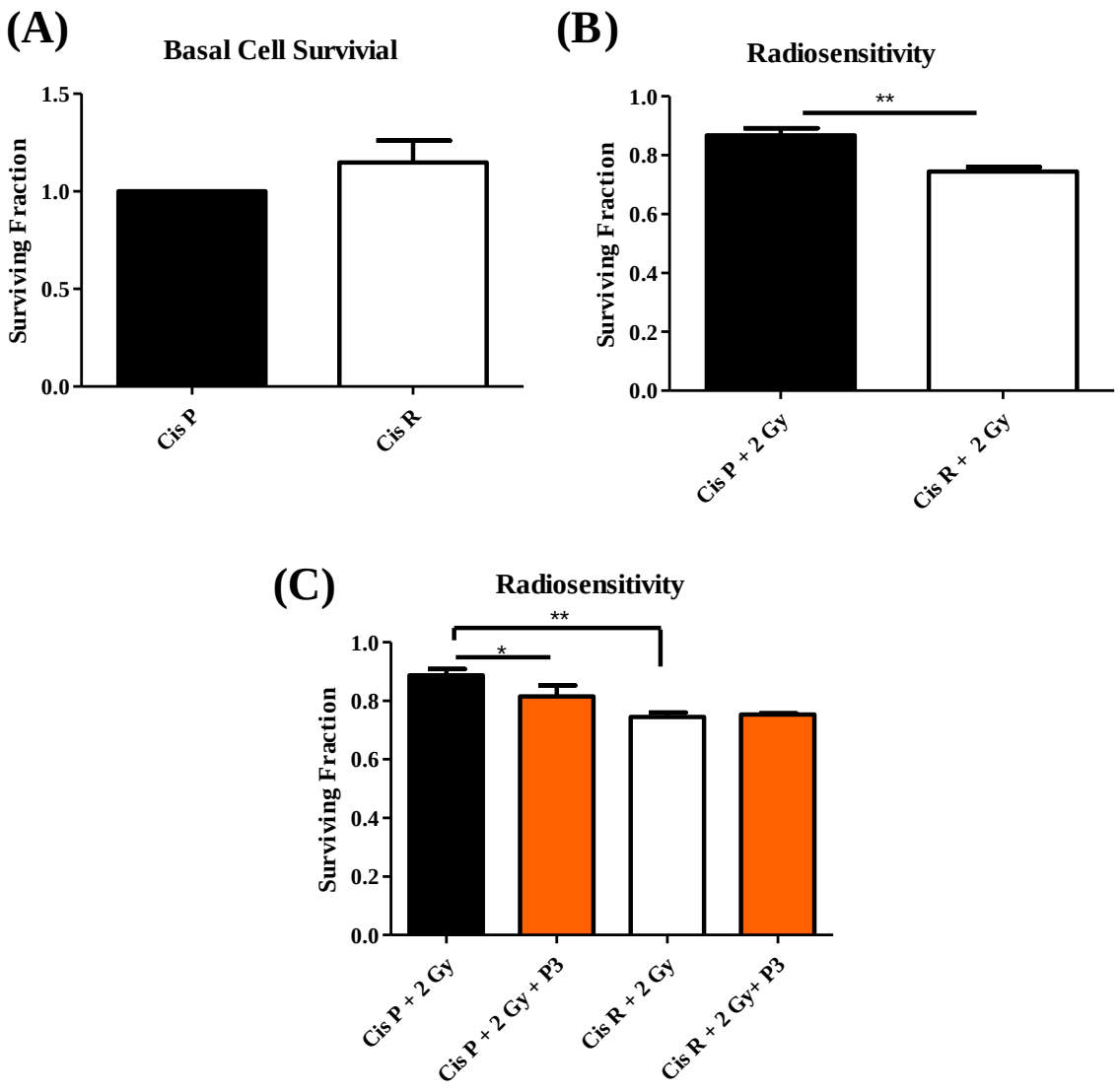

Figure 4-11 Pyrazinib (P3) significantly reduces the surviving fraction of OE33 Cis P cells following 2 Gy irradiation.

The radiosensitivity of cisplatin sensitive (OE33 Cis P) and cisplatin resistant (OE33 Cis R) OAC cells was assessed by clonogenic assay. **(A)** There is no difference in basal cell surviving fraction of cisplatin sensitive and cisplatin resistant OAC cells, (n=3). **(B)** Surviving fraction of Cis P and Cis R OAC cells following treatment with 2 Gy fraction of irradiation, (n=3). **(C)** Treatment with 10 µM of Pyrazinib (P3) significantly reduces the surviving fraction of OE33 Cis P cells, (n=3), unpaired t-test used to compare between different cell lines, paired t-test used to compare between same cell line. *p<0.05, **p<0.01. Data presented as the mean +SEM.

4.4.10. *Pyrazinib (P3) does not enhance the sensitivity of OE33P or OE33R cells to 5-FU*

To investigate if Pyrazinib (P3) altered the sensitivity of OE33P and OE33R cells to 5-FU, another chemotherapy administered to OAC patients as part of the MAGIC treatment regimen we treated OE33P and OE33R cells with two different doses of 5-FU (0.3511 and 0.8982 μM) alone and in combination with 10 μM of Pyrazinib (P3).

The surviving fraction of OE33P cells following treatment with 0.8982 μM of 5-FU was significantly reduced, (p=0.0351). The surviving fraction of OE33R cells was significantly reduced following treatment with both 0.3511 and 0.8982 μM of 5-FU (p=0.0042,p=0.0024) **(Figure 4-12A)**. There was no significant difference in the surviving fraction of OE33P compared to OE33R cells following treatment with either 0.3511 or 0.8982 μM of 5-FU. Pyrazinib (P3) treatment alone did not significantly alter the surviving fraction of OE33P or OE33R cells. Treatment with Pyrazinib (P3) in combination with 0.3511 of 5-FU significantly reduced the surviving fraction of OE33P cells, (p=0.0092) but there was no significant difference in surviving fraction between this combination and 0.3511 μM of 5-FU alone **(Figure 4-12A)**. Importantly when Pyrazinib (P3) was given in combination with 0.8982 μM of 5-FU in OE33P the cytotoxic effect of 5-FU was lost **(Figure 4-12A)**.

Similarly in OE33R cells, when Pyrazinib (P3) was given in combination with 0.3511 μM of 5-FU the cytotoxic effect of 5-FU was lost, however when Pyrazinib (P3) was given in combination with 5-FU at the higher dose in OE33R cells the cytotoxic effect was seen (p=0.0129) **(Figure 4-12A)**.

5-FU did not enhance the radioresponse of OE33P or OE33R cells to 2 Gy radiation **(Figure 4-12B)**. As previously seen, Pyrazinib (P3) significantly enhanced radiosensitivity of OE33P and OE33R cells to 2 Gy X-ray radiation, (p=0.0431, p=0.0459) respectively **(Figure 4-12B)**.When Pyrazinib (P3) was administered in combination with 5-FU the radiosensitising activity of this compound was lost in OE33P cells and OE33R cells, with the exception of the combination of 0.3511 μM 5-FU and Pyrazinib (P3) **(Figure 4-12B)**.

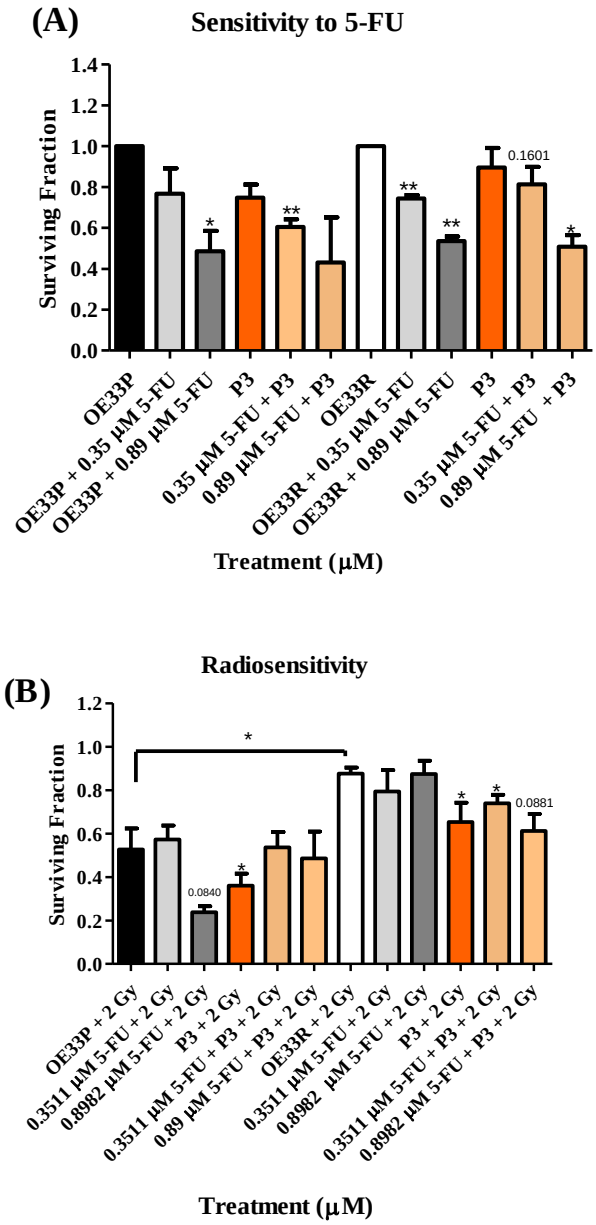

Figure 4-12 Pyrazinib (P3) does not significantly alter sensitivity to 5-FU in OE33P and OE33R cells.

(A) The effect of Pyrazinib (P3) and 5-FU on cellular cytotoxicity both alone and in combination was assessed in OE33P and OE33R cells, (n=3). **(B)** The effect of Pyrazinib (P3) and 5-FU on surviving fraction both alone and in combination with one another was assessed in both 0 and 2 Gy irradiated OE33P and OE33R cells, (n=4). Statistical analysis by unpaired t-test used to compare between different cell lines, paired t-test used to compare between same cell line. *p<0.05, **p<0.01.Data presented as the mean +SEM.

4.5. Summary of main findings of chapter 4

- OE33P and OE33R cells predominantly rely on the glutamine metabolic pathway and Pyrazinib (P3) treatment did not significantly alter the dependency of OE33P and OE33R cells on glutamine, pyruvate or fatty acid metabolism.

- Treatment of OE33P and OE33R cells with Pyrazinib (P3) did not significantly alter the secretion of mitochondrial apoptosis pathway proteins cytochrome C and caspase 3.

- Pyrazinib (P3) significantly inhibited ATP turnover in OE33R cells under normoxic conditions, the significant anti-metabolic activity of Pyrazinib (P3) was lost under hypoxic conditions of 0.5% O_2.

- Pyrazinib (P3) significantly inhibited ROS levels in OE33R but not OE33P cells cultured under 0.5% O_2.

- Pyrazinib (P3) treatment significantly reduced the surviving fraction of OE33R cells cultured under 0.5% O_2 following 4 Gy X-ray radiation.

- The enhanced radiosensitivity of OE33R cells following treatment with Pyrazinib (P3) to 4 Gy X-ray radiation cultured under hypoxia was not associated with significant changes in cellular proliferation.

- OE33 Cis R cisplatin resistant OAC cells have an altered metabolic phenotype.

- Treatment with Pyrazinib (P3) did not significantly enhance the sensitivity of cisplatin sensitive or cisplatin resistant cells to cisplatin.

- The sensitivity of OE33P and OE33R cells to 5-FU was not significantly enhanced when administered in combination with Pyrazinib (P3).

4.6. Discussion

In this chapter we further investigated the anti-metabolic and radiosensitising action of our lead compound, Pyrazinib (P3), under both hypoxic and normoxic conditions. In addition, we investigated the action of Pyrazinib (P3) in an isogenic model of OAC cisplatin resistance.

Anti-metabolic agents targeting mitochondrial respiration may target one specific substrate leading to metabolic reprogramming whereby cells can adapt to fuel mitochondrial respiration using other substrates. In this chapter we investigated the effect of Pyrazinib (P3) treatment on metabolic substrate dependency. OE33P and OE33R cells have a higher dependency on the glutamine metabolic substrate pathway than the pyruvate pathway to fuel mitochondrial respiration. Pyrazinib (P3) treatment did not significantly alter the dependence of OE33P or OE33R cells on the glutamine pathway or OE33R cells on the fatty acid oxidation pathway. Several studies have shown that glutamine is a major nutrient involved in multiple aspects of cancer metabolism and numerous cancer cell types have been shown to be addicted to glutamine [326, 327]. Glutamine is the second most abundant amino acid in blood and functions as a carbon source for energy production and anabolic processes [326]. Glutamine has been shown to be essential to mitochondrial metabolism in rapidly dividing cells supporting our findings in this chapter [327]. In particular glutamine has been shown to be of particular importance to cancer cells which have been altered by either c-MYC or KRAS [328-330]. Inhibiting glutamine metabolism using glutamate analogues demonstrated clinical activity however they were discontinued due to dose-limiting neurotoxicity, gastrointestinal toxicity and myelosuppression indicating the that lack of effect of Pyrazinib (P3) on glutamine metabolism is clinically favourable due to the importance of glutamine metabolism in normal tissue physiology [331].

To investigate if the inhibition of oxidative phosphorylation by Pyrazinib (P3) previously shown in chapter 3 was associated with changes in mitochondrial apoptosis protein secretions we investigated the levels of cytochrome C and caspase 3 following treatment with Pyrazinib (P3). Pyrazinib (P3) did not significantly alter the secretion of cytochrome C or caspase 3 from OE33P or OE33R cells. Cytochrome C and caspase 3 are mediators of the mitochondrial apoptosis pathway which have been previously shown to play a role in tumoral radio-sensitivity [332]. It has previously been shown that reduced levels of caspase 3 in tumour cells or surrounding stroma can enhance sensitivity to radiotherapy in xenograft *in-vivo* studies [332]. In addition, elevated levels of active caspase 3 in patient tumour tissues have been correlated with an increased rate of recurrence and mortality [332]. Furthermore, mitochondrial apoptosis is also associated with an increase in mitochondrial oxidative stress which results in cytochrome C release, an irreversible event which leads to the activation of caspases, such as caspase 3 and subsequent cell death [333,

334]. The anti-metabolic activity of Pyrazinib (P3) was independent of changes to surrogate markers of mitochondrial apoptosis, this supports our previous findings in chapter 3 where Pyrazinib (P3) treatment did not significantly alter mitochondrial mass.

As previously shown in chapter 3, OCR was significantly higher in OE33R cells compared to OE33P cells under normoxia, however under hypoxic conditions this significant difference was lost. OE33R cells were sensitive to and adapted to the low oxygen environment through the significant upregulation of ECAR in hypoxic compared to normoxic cells to meet their metabolic requirements. Metabolic changes in response to hypoxia are elicited through both direct and non-direct mechanisms. Indirect mechanisms of metabolic changes include the reduction of ATP generation by oxidative phosphorylation and inhibition of fatty-acid desaturation [335]. Indirect mechanisms include changes in isozyme expression through hypoxia inducible factor (HIF) activation [335]. A study in malignant glioma cells previously demonstrated the variability in oxygen consumption as a result of hypoxia induction [335]. Under conditions of low oxygen, hypoxia-tolerant glioma cells were shown to decrease their oxygen consumption rate in contrast to hypoxia-sensitive cells which continue to consume oxygen at a relatively steady rate until the oxygen supply becomes exhausted [335, 336]. In contrast in our study, both OE33P and OE33R cells increase OCR in response to hypoxic conditions but OE33R cells were able to adapt to the hypoxic environment through a significant upregulation in ECAR.

Pyrazinib (P3) significantly inhibited OCR in OE33P and OE33R cells cultured under normoxic conditions but under hypoxia Pyrazinib (P3) only produced a modest non-significant reduction in OCR in OE33R cells cultured under hypoxia. Hypoxia and HIF have been shown to increase glucose/carbon flux through the glycolytic pathway while minimising input into the TCA cycle and oxidative phosphorylation [337]. This result may be due to the rapid metabolic reprogramming of OE33R cells in response to hypoxia causing a reduction in the ability of Pyrazinib (P3) to alter metabolic rate whereby the metabolic shift due to hypoxic stress may alter multiple cellular processes including cellular differentiation and subsequently may alter the activity of Pyrazinib (P3). ATP turnover was significantly higher in OE33R cells when compared to OE33P cells, supporting previous findings by our group [82]. Pyrazinib (P3) could significantly inhibit ATP turnover in OE33R cells. This is an important finding given that a previous study demonstrated that the maintenance of intracellular ATP levels following irradiation was associated with a radioresistant phenotype in head and neck cancer [338]. This suggests that the ability of Pyrazinib (P3) to reduce ATP turnover may contribute to its ability to enhance radiosensitivity.

Whilst OCR significantly increased in OE33P and OE33R cells following hypoxic culture, the administration of the uncoupling agent FCCP, demonstrated maximal respiration is significantly decreased in OE33R cells cultured under hypoxic compared to cells cultured under normoxic conditions. FCCP results in the uninhibited flow of electrons through the electron transport chain resulting in maximal possible consumption of oxygen through complex IV [339]. The significant decrease in maximal respiration in OE33R cells cultured under hypoxia is not surprising in the low oxygen conditions further highlighting how the resistant cells can adapt to cope with the hypoxic environment. It is of importance to note, in contrast to its action on OCR, Pyrazinib (P3) treatment did not significantly alter maximal respiration under normoxic or hypoxic conditions, highlighting that in the presence of an uncoupling agent the anti-metabolic activity of Pyrazinib (P3) may be lost.

ROS levels were significantly increased in OE33P cells cultured under hypoxia compared to matched cells cultured under normoxic conditions. This result is in line with findings in the literature whereby induction of hypoxia has been shown to produce an increase in ROS production [340]. ROS is known to promote carcinogenesis from tumour initation to progression [340]. Hypoxia is thought to result in an increase in ROS levels through its effect on the electron transport chain particularly at complex I,II and III [340]. Pyrazinib (P3) significantly inhibited ROS in OE33R cells under hypoxic conditions which may be contribute to its radiosensitising activity. In a breast cancer xenograft model the administration of a potent scavenger of reactive oxygen and nitrogen species, was shown to enhance radiosensitivity through the inhibition of angiogenesis by altering the density of micro vessels and the proliferation rate of endothelial cells [341]. Furthermore, in a lung cancer model, inflammation was found to enhance radiation resistance in a ROS dependent manner [84]. It is important to note there are inconsistent reports on the role of ROS in radioresponse as whilst some studies mentioned a decrease in ROS is favourable, other studies have shown an increase in ROS to be linked with enhanced radiosensitivity. The overexpression of miR-200c in an *in-vitro* lung cancer model was shown to enhance radiosensitivity through increasing ROS, inhibiting DNA damage and upregulating p21 [342].

Mitochondrial membrane potential was not significantly altered in OE33P and OE33R cells cultured under normoxia compared to matched cells cultured under hypoxia which were treated with vehicle control of Pyrazinib (P3). Hypoxia tolerant glioma cell lines were previously found to maintain a constant mitochondrial membrane potential in response to changes in oxygen tension [336]. OE33P and OE33R cells do not need to alter the mitochondrial membrane potential to cope with a low oxygen environment.

Mitochondrial mass was significantly increased in OE33P cells cultured under normoxia compared to those cultured under hypoxia. The significant increase in mitochondrial biogenesis of OE33P may account for the increase in OCR in OE33P cells cultured under hypoxia. This result highlights the hypoxia sensitive nature of these cells whereby the change in oxygen tension has resulted in an increase mitochondrial mass. This response was similar to findings shown by Tohme *et al.* who found an increase in mitochondrial biogenesis in 2 hepatocellular carcinoma cell lines in response to hypoxia [343]. Interestingly, in this study when mitochondrial biogenesis was attenuated through the silencing of PGC-1a, cellular proliferation was significantly decreased [343]. The upregulation of mitochondrial biogenesis may allow our OAC cells to cope with the harsh hypoxic conditions by maintaining oxidative phosphorylation through increased mitochondria. The lack of upregulation of mitochondrial mass in OE33R cells following hypoxia further highlights the resilient and resistant nature of these cells as they appear to be better able to cope with changes oxygen tension without the need to increase mitochondrial biogenesis.

Pre-treatment with Pyrazinib (P3) significantly enhanced radiosensitivity of OE33R radioresistant cells to 4 Gy X-ray radiation cultured under hypoxic conditions. Oxygen is a potent radiosensitiser and solid tumours with areas of hypoxia are the most aggressive and difficult tumours to treat [237]. Hypoxia is heterogeneous across tumours and can change following treatment with radiation [238]. Hypoxic cancer cells are generally more resistant to both chemotherapy and radiotherapy than their normoxic counterparts and contribute largely to the development of treatment resistance and thus may serve as a novel target to enhance radiosensitivity. A number of studies have reportedly developed hypoxia-targeting agents as a mechanism to enhance radioresponse, thus the ability of Pyrazinib (P3) to maintain its radiosensitising effect under these conditions is a critical finding. The potential anti-metabolic agents which inhibit oxygen consumption rate to enhance radiosensitivity under hypoxic conditions is supported in the literature in a study by Ashton *et al*, using the anti-malarial compound atovaquone [344]. Ashton *et al,* demonstrated that a reduction of the oxygen consumption rate was associated with a significant reduction in tumour hypoxia and tumour growth when administered in combination with radiotherapy *in-vivo* in FaDu and HCT116 xenografts. In gastric cancer, the RNA polymerase inhibitor TAS106 was demonstrated to radiosensitise gastric cancer cells and xenografts to irradiation [239]. TAS106 enhanced IR-induced apoptosis and suppressed HIF-1α both *in-vitro* and *in-vivo.* Inhibition of HIF-1α was demonstrated to enhance radiation-induced apoptosis in hypoxic gastric cancer cells, suggesting that the induction of apoptosis via inhibition of HIF-1α is a mechanism underlying TAS106-mediated radiosensitisation in gastric cancer. The ability of Pyrazinib (P3) to radiosensitise OAC radioresistant cells under normoxic and hypoxic conditions further highlights the potential of this compound to function as a novel radiosensitiser in OAC.

Furthermore, Pyrazinib (P3) treatment could significantly inhibit cellular proliferation of OE33P cells under hypoxic conditions. This was interesting as Pyrazinib (P3) could not enhance the radiosensitivity of OE33P cells cultured under hypoxia. The result also indicates the radiosensitising effect of Pyrazinib (P3) on OE33R cells cultured under hypoxia is independent of change to cellular proliferation. Hypoxia-inducible factor-1 (HIF-1) is strongly associated with cancer cell growth and survival [345]. Most cell types have been shown to downregulate proliferation in response to hypoxia to cope with hypoxic stress, so it is expected that OE33P cells have a significantly lower cellular proliferation under hypoxic conditions [346]. No significant differences were seen in the cellular proliferation of OE33R cells cultured under normoxic versus hypoxic conditions further highlighting the resistant and resilient nature of these cells. Although proliferation was assessed 42 h following hypoxic induction, perhaps evaluating proliferation at an earlier time point following hypoxic induction may have shown differences in cellular proliferation.

Cisplatin is a widely used chemotherapeutic drug for the treatment of solid cancers, including OAC as part of the MAGIC treatment regimen, however the development of chemoresistance, to cisplatin hinders the success of this agent [315]. Previous studies in cisplatin resistant cancer cell lines of various tissue origin report multiple mechanisms responsible for enhanced resistance, and that cisplatin resistant phenotype is the result of multiple microRNA, gene and protein expression changes [347-349]. Molecular mechanisms commonly associated with cisplatin resistance include alterations in DNA repair, drug influx/efflux, drug detoxification, cell cycle dysregulation and evasion of apoptosis [350]. In this study we sought to characterise the key differences linked to resistance in an isogenic model of OAC cisplatin resistance, including relative chemosensitivity and radiosensitivity and metabolic phenotype.

Chemoresistant OE33 Cis R cells have a significant acquired resistance to cisplatin compared to cisplatin sensitive OE33 Cis P cells. Interestingly, cisplatin resistant OE33 Cis R cells are more radiosensitive than matched OE33 Cis P cells. Cisplatin is often administered in combination with radiation for the treatment of numerous solid cancers, including oesophageal, head and neck and cervical cancer [351-354]. Cisplatin has been widely shown to enhance radiosensitivity potentially through the disruption of the NHEJ DNA repair pathway [355, 356]. As cisplatin is often given in combination with radiation to improve response it was surprising that OE33 Cis R cells are more radiosensitive than OE33 Cis P cells. Our data suggest the pathways that OE33 Cis R cells employ to repair DNA damage induced by either radiation or cisplatin treatment are different. OE33 Cis R cells which can overcome cytotoxic insult from cisplatin to a greater degree than OE33 Cis P cells but cannot overcome radiation induced DNA damage as efficiently as they

could before the acquisition of cisplatin resistance. Pyrazinib (P3) could significantly enhance the radiosensitivity of OE33 Cis P but not OE33 Cis R cells indicating the mechanism of cisplatin resistance may attenuate the effect of this compound.

Cisplatin resistant OE33 Cis R cells have an altered metabolic phenotype compared to matched OE33 Cis P cisplatin sensitive cells. OE33 Cis R cells have ~40% higher rate of oxygen consumption rate than OAC cisplatin sensitive cells. Interestingly a previous study by Lynam-Lennon *et al*. demonstrated that increased OCR was linked with a radioresistant phenotype in OAC [82]. However, to date the role of oxidative phosphorylation in cisplatin resistance in OAC has been underexplored. In a human ovarian cancer model of cisplatin resistance, SKOV3/DPP cisplatin resistant cells had a significantly higher oxygen consumption rate when compared to SKOV3 cisplatin sensitive cells, similar to our findings in our OAC model of cisplatin resistance [357]. Treatment of ovarian cisplatin resistant cells with a Bcl-2 inhibitor was found to reduce OCR and enhance cisplatin sensitivity in the ovarian cancer cisplatin resistant cells [357]. Additionally, a study by Catanzaro *et al*. demonstrated that the inhibition of glucose-6-phosphate dehydrogenase sensitised cisplatin resistant ovarian cancer cells to cytotoxic death further highlighting the role of the oxidative phosphorylation pathway in cisplatin resistance [358]. Elevated OCR has also been linked to chemoresistance with other chemotherapies such 5-FU. A study by Denise *et al*. showed that 5-FU resistant colorectal cancer cells have a significantly higher oxygen consumption rate compared to parental 5-FU sensitive cells. Furthermore, increased OCR has also been linked to chemoresistance in docetaxel resistant prostate cancer cells, where treatment with metformin to inhibit OCR was found to increase chemosensitivity [359]. Thus, it would be of interest in the future to target oxidative phosphorylation in OAC OE33 Cis R cells as a potential mechanism to enhance cisplatin sensitivity in OAC. Metabolism is tightly influenced by environmental conditions, low oxygen conditions can result in the upregulation of hypoxia inducible glucose transporters thus we also investigated the metabolic rate of OE33 Cis P and Cis R cells under hypoxic conditions [360]. The metabolic profile of OE33 Cis R cells is significantly altered under hypoxic conditions, where OE33 Cis R cells have a significantly lower oxygen consumption rate than parental OE33 Cis P cells when cultured under 0.5 % O_2. This result highlights the flexible nature of OE33 Cis R cells whereby they are able to adopt to their environmental conditions and reduce their oxygen consumption rate in low oxygen conditions. Hypoxia plays a critical role in cisplatin resistance and hypoxic tumours often display a high level of resistance to cisplatin. Studies in lung cancer have reported that hypoxia can promote the activation of autophagy resulting in chemoresistance [361]. In addition cisplatin resistant lung cancer cells have hypoxia induced upregulation of p53 resulting in activation of p21 transcription resulting in arrest of the cell cycle at the G1-G0 phase reducing the effect of cisplatin [362]. As regions of hypoxia are found in most solid tumours including OAC, it is critical

to understand how OE33 Cis R cells adapt to their tumour microenvironment to determine the best method to target this cell population. OE33 Cis R cells may have a reduced OCR under hypoxic conditions as they have slowed their cell cycle as a means of protection from cytotoxic insult, this is something which needs to be further evaluated in future studies. Pyrazinib (P3) significantly inhibited OCR in OE33 Cis R but not OE33 Cis P cells, this surprising result further highlighting the different metabolic phenotype of the two cell lines which respond very differently to our anti-metabolic agent.

5-FU induces significantly enhanced cellular cytotoxicity of OE33P and OE33R cells. Pyrazinib (P3) does not significantly alter the sensitivity of OE33P and OE33R cells to 5-FU. The cytotoxic effects of 5-FU are S phase cell cycle dependent [51]. 5-FU is a broadly used chemotherapeutic which is administered as part of the MAGIC regimen to OAC patients and has previously been shown to enhance radioresponse in gastric cancers. We investigated the interaction between 5-FU and Pyrazinib (P3). Both previously and in our studies, OE33P and OE33R cells have been shown to have similar sensitivities to 5-FU, Pyrazinib (P3) does not significantly alter the sensitivity of OE33P and OE33R cells to 5-FU but of clinical importance the combined administration of 5-FU and Pyrazinib (P3) appears to slightly reduce the cytotoxic effect of 5-FU in some cases. This result may be due to a drug influx/efflux pressure and thus if both drugs were to be given in combination an optimal dosing schedule would be required.

5-FU does not significantly enhance the radioresponse of OE33P and OE33R cells. Importantly, the administration of 5-FU in combination with Pyrazinib (P3) reduces the ability of Pyrazinib (P3) to act as a radiosensitiser. This is an important clinical finding which indicates that 5-FU and Pyrazinib (P3) should not be administered at the same time for optimal response. Pre-treatment of OE33P and OE33R cells with concentrations of 5-FU which can induce 25-50% cellular cytotoxicity cannot enhance radioresponse to 2 Gy X-ray radiation. 5-FU has previously been shown to enhance radiosensitivity in numerous cancer types [363-365]. It would be of interest in the future to investigate if 5-FU can enhance radiosensitivity if given continuously or following radiation to OE33P and OE33R cells.

In summary in this chapter we have demonstrated the robust radiosensitising activity of Pyrazinib (P3) under both normoxic and hypoxic conditions. Furthermore, Pyrazinib (P3) does not significantly enhance the chemosensitivity of OE33P or OE33R cells to cisplatin or 5-FU, highlighting Pyrazinib (P3) acts specifically to enhance radiosensitivity. Importantly the combined administration of Pyrazinib (P3) with either of these chemotherapies can reduce the activity of Pyrazinib (P3), 5-FU and cisplatin highlighting the need for the development of dosing schedules if these drugs were to be given in combination with each other.

Aspects of this chapter have been published in *Pharmaceuticals*, see **Figure 4-13.**

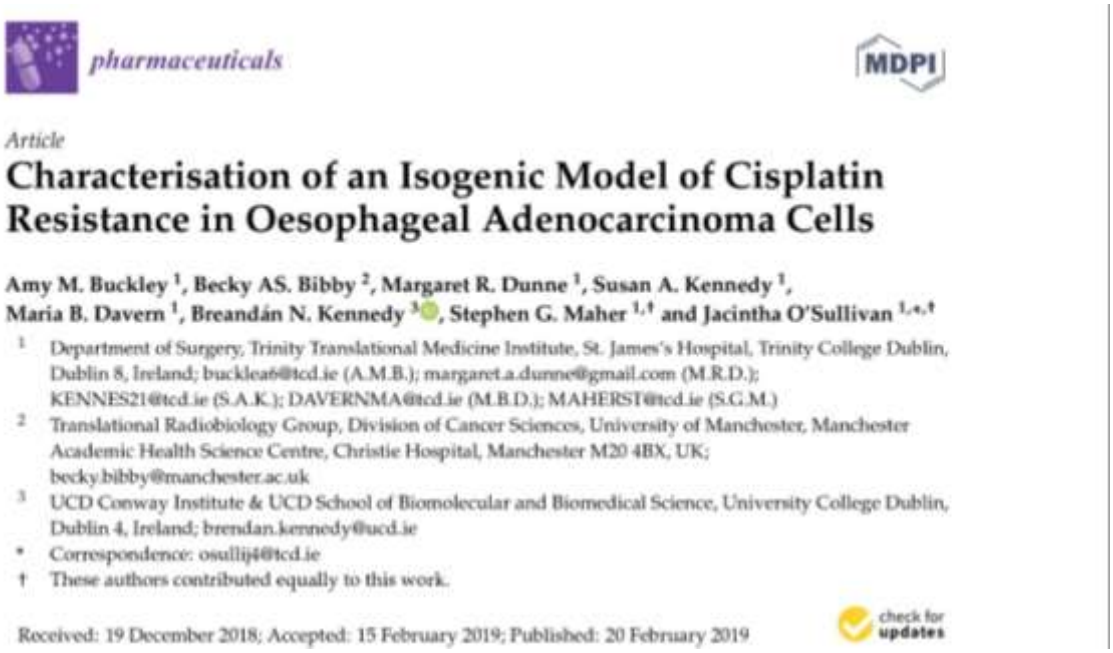

pharmaceuticals

MDPI

Article

Characterisation of an Isogenic Model of Cisplatin Resistance in Oesophageal Adenocarcinoma Cells

Amy M. Buckley [1], Becky AS. Bibby [2], Margaret R. Dunne [1], Susan A. Kennedy [1], Maria B. Davern [1], Breandán N. Kennedy [3], Stephen G. Maher [1,†] and Jacintha O'Sullivan [1,*,†]

1 Department of Surgery, Trinity Translational Medicine Institute, St. James's Hospital, Trinity College Dublin, Dublin 8, Ireland; buckleaб@tcd.ie (A.M.B.); margaret.a.dunne@gmail.com (M.R.D.); KENNES21@tcd.ie (S.A.K.); DAVERNMA@tcd.ie (M.B.D.); MAHERST@tcd.ie (S.G.M.)
2 Translational Radiobiology Group, Division of Cancer Sciences, University of Manchester, Manchester Academic Health Science Centre, Christie Hospital, Manchester M20 4BX, UK; becky.bibby@manchester.ac.uk
3 UCD Conway Institute & UCD School of Biomolecular and Biomedical Science, University College Dublin, Dublin 4, Ireland; brendan.kennedy@ucd.ie
* Correspondence: osullij4@tcd.ie
† These authors contributed equally to this work.

Received: 19 December 2018; Accepted: 15 February 2019; Published: 20 February 2019

check for updates

Figure 4-13 Characterisation of an Isogenic Model of Cisplatin Resistance in Oesophageal Adenocarcinoma Cells.
Aspects of this chapter have been published in *Pharmaceuticals* [366].

5. Chapter 5 Investigating inflammatory secretions from an isogenic model of OAC radioresistance and the anti-inflammatory action of Pyrazinib (P3)

5.1. Introduction

OAC has been identified as an inflammatory-driven upper gastrointestinal cancer and previous studies have reported the role of inflammation as a negative regulator of response to radiation treatment in OAC [15, 234]. C3a and C4a, components of the complement system, were previously found at higher levels in the pre-treatment serums of OAC patients who had a subsequent poor pathological response to neo-CRT, when compared to patients who had a good pathological response to treatment [15]. Inflammatory cytokines are being increasingly reported to play a role in radioresistance, leukaemia inhibitory factor (LIF) is an IL-6 type cytokine that has previously been linked with radioresistance in nasopharyngeal carcinoma [228, 235].

Inflammation plays a pivotal role in modulating response of tumours to radiation. NF-κB, STAT-3, and HIF-1 play a crucial role in radiation-induced inflammatory responses thus therapeutic targeting of these factors may be a novel mechanism to overcome inflammation-induced radioresistance [233]. Furthermore as previously mentioned, response to radiation plays a central role in patient outcome in OAC, sensitivity to ionising radiation is inversely correlated to tumour burden [81]. Inflammation does not promote tumourigenesis and radioresistance in isolation, it is tightly linked with other biological processes including angiogenesis and metabolism which we have previously investigated in earlier chapters. Inflammation is tightly linked to angiogenesis, with angiogenic networks responsible for sustaining inflammation through the supply of oxygen and nutrients to the inflammatory cells [367]. Inflammation is also tightly linked to metabolism as inflammatory cells rely on metabolites generated from the metabolic cycle to maintain their function. Thus, tumour inflammation, angiogenesis and metabolism form an interdependent network which plays a crucial role in radiation resistance.

A study by Liu *et al*., reported a potential role of the inflammatory LIF pathway in radioresistance of nasopharyngeal cancer (NPC), elevated serum levels of LIF were associated with significantly poorer recurrence-free survival [228]. LIF is an IL-6 type cytokine which signals through the leukaemia inhibitory factor receptor (LIFR) and glycoprotein (gp)-130 [368]. Other members of this family include IL-6, IL-11, cardiotrophin-1, cardiotrophin-like cytokine, ciliary neurotrophic factor and oncostatin M [368]. Activation of the LIFR pathway is associated with the activation of a number of downstream pathways including the ERK1/2, JAK/STAT3, MAPK and PI3K/AKT pathways [228, 369, 370]. Differential expression of LIF and/or LIFR is reported in a number of cancers including breast cancer, colorectal cancer (CRC), NPC, osteosarcoma, pancreatic cancer, melanoma, cholangiocarcinoma and cervical cancer [228, 369, 371-376].

LIF is a multifunctional protein and its role is often context-dependent. For example, in non-pathological conditions LIF plays an important role in embryonic implantation where dysregulated LIF expression is associated with implantation failure [377]. Furthermore in cancer, the role of LIF is complex and linked to both pro- and anti-tumorigenic functions dependent on the cancer type [371, 372, 374]. In breast cancer, LIF can promote tumour growth and migration *in-vitro* and *in-vivo* [369]. In addition, ectopic over-expression of LIF in CRC reduces chemotherapy-induced apoptosis in a p53-dependent manner [372]. In contrast, in cervical cancer, elevated LIF expression is associated with a reduction in cellular proliferation mediated by the downregulation of human papillomavirus-16 (HPV-16) oncogene expression [374]. However the role of LIF in OAC disease progression and treatment response has not yet been explored.

In this chapter we carried out a proteomics-based screen to identify molecular markers associated with radioresistance in OAC. We investigated the association of the pro-inflammatory cytokine LIF with response to neo-adjuvant treatment in OAC, both *in-vitro* and in pre-treatment OAC patient serum and biopsies. We profiled the expression and secretion of LIF *in-vitro, in-vivo* and *ex-vivo*. LIF expression and secretion was upregulated in radioresistant cells of an isogenic model of OAC radioresistance *in-vitro*. *In-vivo*, circulating LIF was significantly elevated in pre-treatment serum from OAC patients with a subsequent poor response to neo-adjuvant treatment. *Ex-vivo*, LIF secretions from treatment-naïve biopsies were positively correlated with secretions of IL-8, bFGF and VEGF-A. LIF secretions *ex-vivo* were negatively correlated with percentage lymphocyte infiltration into the tumour biopsies. In addition to LIF, downregulated LIFR expression is significantly associated with poor response to neo-CRT in OAC pre-treatment biopsies. Our findings both *in-vitro* and in patient samples strongly implicate the LIF/LIFR pathway in treatment response in OAC.

In this chapter we also investigated the effect of Pyrazinib (P3) on the inflammatory secretome in addition to its effects on two primary hallmarks of cancer, angiogenesis and dysregulated metabolism. At the protein level we investigated the action of our radiosensitiser Pyrazinib (P3) on inflammatory protein secretions from our isogenic model of OAC radioresistance. Pyrazinib (P3) significantly reduced the secretions of IL-6, IL-8, IL-4 and IL-13 *in-vitro* in OE33R cells.

5.2. Overall objective and specific aims of chapter 5

In this chapter we investigated the differences in inflammatory protein expression and secretion *in-vitro* using an isogenic model of OAC radioresistance. In addition we investigated the effect of Pyrazinib (P3) treatment on inflammatory protein secretions.

The specific aims of chapter 5 were:

1. Investigate the differences in protein expression using specific inflammatory and oncology panels in OE33P and OE33R cell lysates and supernatants using multiplex proteomics-based approach.
2. Validate lead hits of proteomic multiplex assay; LIF and LIFR *in-vitro*.
3. Evaluate the levels of circulating LIF and intra-tumoural expression of *LIF* and *LIFR* in OAC treatment-naïve patient serum and patient tumour biopsies respectively.
4. Correlate the levels secreted LIF with the secretion of a panel of inflammatory and angiogenic factors from tumour conditioned media (TCM) of matched OAC treatment-naïve biopsies.
5. Correlate secreted LIF with immune cell infiltrate score in matched human OAC pre-treatment biopsies.
6. Evaluate the effect of Pyrazinib (P3) treatment on protein secretions from OE33P and OE33R cells.

5.3. Methods

5.3.1. *Generation of the cell lines*

The OAC model of radioresistance was generated as previously described [150].

5.3.2. *Cell sub-culture*

Cell culture was carried out as previously described in section 3.3.2.

5.3.3. *Preparation of OE33P and OE33R cell supernatants and lysates for OLINK Proseek Proteomics Analysis*

OE33P and OE33R cells were seeded at a density of 2.5 x 10^5 in 6 well plates in 1.5 mL complete RPMI-1640 at 37°C in 5% CO_2/95% air. At 48 h supernatant was removed and stored at -20°C. Cells were washed twice with 300 µL of ice-cold PBS. NP40 cell lysis buffer (Invitrogen) was supplemented on day of use with 100 µL Phenylmethylsulfonyl fluoride (PMSF) (Sigma-Aldrich) per 10 mL cell lysis buffer and 1 mL protease inhibitor (Sigma-Aldrich) per 10 mL cell lysis buffer. Supplemented ice-cold NP40 cell lysis buffer (200 uL) was added to each well and left on ice for 20 min. Cell lysate solutions were pipetted up and down following incubation to aid lysis process. Lysis buffer solute was centrifuged for 20 min at 13,400 x g at 4°C. Lysates was aspirated off and stored at - 80°C. 20 µL of each supernatant and cell lysate of equal protein concentration was determined using the BCA assay (Pierce) as previously described in section 4.3.7 and were placed in a MicroAmp plate (Applied Biosystems) and sealed and shipped on dry ice to OLINK proteomics (Uppsala, Sweden).

5.3.4. *Proseek proteomics assay*

OLINK proteomics conducted a proseek proteomics screen of our samples, including supernatants and cell lysates from 3 independent experiments obtained from OE33P and OE33R cells. Samples were run on both their inflammatory I and oncology II platform, with samples screened for expression of a total of 184 proteins (92 per panel). All samples were of equal protein concentration prior to shipping to OLINK. The readout of normalised protein expressions values (NPX) were obtained from OLINK following the assay for statistical analysis. The NPX value indicates the relative quantification for that protein and thus can only be used for comparison between samples for each protein and cannot be used for comparing one protein to another. A hit was determined as significant when $p<0.05$, p values were adjusted for multiple testing using the false discovery rate method.

5.3.5. *Generation of OE33P and OE33R cell supernatants for LIF ELISA*

Cells were seeded at a density of 2.5 x 10^5 cells/well in 6-well plates and allowed to adhere overnight at 37°C in 5% CO_2/95% air. After 48 h, OE33P and OE33R were either mock irradiated or irradiated with 2 Gy irradiation. Twenty-four hours later supernatant was removed and stored at -20°C. Cells were washed twice with 300 µL of ice-cold PBS. RIPA cell lysis buffer was supplemented on day of use with 100 µL phenylmethylsulfonyl fluoride (PMSF) (Sigma-Aldrich) per 10 mL cell lysis buffer and one protease inhibitor cocktail tablet (Roche) per 10 mL cell lysis buffer. 200 µL of supplemented ice-cold RIPA cell lysis buffer was added to each well and left on ice for 20 min. Cell solutions were pipetted up and down following incubation to aid cell lysis. Lysis buffer solute was incubated for 20 min at 13,400 x g at 4°C. Lysates were aspirated and stored at -80°C. Protein concentration was determined by BCA assay (Pierce) as previously described in 4.3.7.

5.3.6. *Irradiation*

Irradiation was performed using a Gulmay Medical X-ray generator, (RS225) (Gulmay Medical), at a dose rate of 3.25 Gray (Gy) per min.

5.3.7. *Patient samples*

Following ethical approval (Joint St James's Hospital/AMNCH ethical review board) and written informed consent, diagnostic biopsy specimens were taken from patients with a diagnosis of operable OAC, by a qualified endoscopist prior to neo-adjuvant therapy. Histologic confirmation of tumour tissue in biopsies was performed by a pathologist using routine haematoxylin and eosin staining. Patients with a subsequent TRG score received a complete course of neo-adjuvant therapy. All patient samples in the qPCR study received neo-CRT according to the CROSS regimen [44]. In the serum study, 16 patients received neo-CRT according to the CROSS regimen and 10 patients received neo-adjuvant chemotherapy only according to the MAGIC regimen [44]. All patient tumour and serum samples used in this study were taken prior to initiation of treatment.

5.3.8. *Generation of tumour conditioned media (TCM)*

Following informed consent, biopsies were collected at endoscopy, immediately placed on saline-soaked gauze and were transported within 10 minutes to the laboratory. Biopsies were placed in culture as follows: biopsies were placed into a well of a 12 well plate containing 1 mL M199 medium (Gibco) supplemented with 10% FBS (Gibco), 1 µg/mL insulin and 1% penicillin/streptomycin. Following 24 h culture in 0.1% DMSO in complete M199, tumour

conditioned media (TCM) was collected stored at -80°C.The remaining tissue was snap-frozen in liquid nitrogen and stored at -80°C.

5.3.9. *Protein isolation from OAC treatment-naïve biopsies*

OAC patients biospies previously treated with 0.1% DMSO in the generation of TCM were defrosted on ice. 200 µL of RIPA buffer supplemented with a protease inhibitor cocktail tablet (1 tablet per 10 mL, Roche) was added to each 2 mL tube containing one biopsy each. A metal bead was also placed in each tube. Biopsies were homogenised using the Qiagen tissue lyser (Qiagen, CA, USA) at a speed of 30 Hz for 30-45 seconds depending on biopsy size until fully homogenised. Biopsies were centrifuged at 13,000 x g for 20 min at 4°C. Cell lysate was removed and placed in new 2 mL tube, 10 µL/well of protein lysate was required to quantify protein concentration using the BCA assay (Pierce) as previously described in section 4.3.7.

5.3.10. *Serum sampling*

Following informed, written consent, OAC patient treatment-naïve serum was collected using Z-clot activator serum tubes (Greiner Bio-One, Gloustershire, United Kingdom). Samples were centrifuged at 1150 ×g for 10 min, the serum decanted, aliquoted, and subsequently stored at -80°C in a designated biobank.

5.3.11. *LIF ELISA*

To assess the secretion of LIF from OE33P and OE33R cell supernatants, patient serum and TCM a singleplex sandwich LIF ELISA was carried out as per manufacturer's instructions using 100 uL of neat OE33P or OE33R cellular supernatant, OAC treatment-naïve patient serum or 0.1% DMSO treated OAC TCM.

5.3.12. *RNA isolation from OE33P and OE33R cells and OAC treatment-naïve biopsies*

Cells were seeded at a density of 2.5 x 10^5 cells/well in 6-well plates and allowed to adhere overnight. 24 h later OE33P and OE33R were either mock irradiated or irradiated with 2 Gy irradiation. RNA was isolated as previously described in section 3.3.15. RNA from patient tumour tissue samples was isolated using a miRNeasy RNA isolation kit (Qiagen), as per the manufacturer's instructions. Total RNA was quantified spectrophotometrically using a Nanodrop 1000 spectrophotometer v3.3 (Thermo Fisher Scientific). Total RNA (1.5 µg) was reverse transcribed to cDNA using a High Capacity cDNA RT Kit (Thermo Fisher Scientific).

5.3.13. *RNA quantification of cell lines and OAC patient mRNA*

RNA quantification was determined as previously described in section 3.3.16.

5.3.14. *cDNA synthesis from cell lines and OAC patient mRNA*

For cell line samples, cDNA synthesis was carried out as previously described in section 3.3.17. For patient samples, total RNA (1.5 µg) was reverse transcribed to cDNA using a High Capacity cDNA RT Kit (Thermo Fisher Scientific).

5.3.15. *Quantitative Real-Time PCR of cell lines and OAC patient samples.*

qPCR was performed using TaqMan primer probes (*LIF, LIFR* Thermofisher) and a Quant Studio 5 real-time thermal cycler (Thermo Fisher Scientific). *18S* (Applied Biosystems) was used as an endogenous control for data normalization. PCR data were analyzed by the $2^{-\Delta\Delta Ct}$ Livak method [378].

5.3.16. *Multiplex ELISA using OAC TCM*

TCM from 6 different patients previously treated with 0.1% DMSO in M199 were defrosted on ice. The secretion of cytokines and angiogenic growth factors were analysed by ELISA as per the manufacturer's instructions. To assess angiogenic and inflammatory cytokine release in TCM, 2 multiplex kits were used (Meso Scale Diagnostics, USA). For angiogenic markers, a 7-plex ELISA was used to quantify levels of b-FGF (basic), Flt-1/VEGFR-1, PIGF, Tie-2, VEGF-A, VEGF-C, VEGF-D. For inflammatory cytokines, a 10-plex assay was used to quantify IFN-γ, IL-10, IL-12p70, IL-13, IL-1β, IL-2, IL-4, IL-6, IL-8 and TNF-α. ICAM secretions were detected by a separate ELISA (R&D Systems). Secretion data for all factors was normalised appropriately explant protein content using the BCA assay (Pierce) as previously described in section 4.3.7 for TCM secretions. Data was analysed using MSD Discovery Workbench software version 4.0.

5.3.17. *Evaluation of inflammatory infiltrate in OAC pre-treatment biopsies*

Routine haematoxylin and eosin stained sections from diagnostic biopsy material were reviewed by a pathologist who was blinded to clinical outcomes. Inflammatory cell density and tumour stroma percentage were assessed in tissue fragments containing invasive carcinoma. The inflammatory cell density was classified as either absent, low-grade (mild/patchy increase in inflammatory cells) or high-grade (prominent inflammatory infiltrate and/or involvement and destruction of cancer cell islands). The presence of eosinophils, neutrophils, lymphocytes and plasma cells was also assessed and similarly classified as either absent, low-grade or high-grade. The tumour stroma percentage (TSP) was assessed by estimating the proportion of stroma as a

percentage of the visible field from an area of carcinoma, excluding areas of mucin deposition or necrosis. Tumours were classified as low-TSP if stroma accounted for 50% of the visible field or high-TSP if stroma accounted for 50% of the visible field.

5.3.18. *Multiplex ELISA in OE33P and OE33R cells*

OE33P and OE33R cells were seeded at 2.5 x 10^3 for 24 h, following which they were treated with either 0.1% DMSO or 10 µM of Pyrazinib (P3) for 24 h following which supernatants and cell lysates were removed and stored at -80°C. Supernatants from OE33R and OE33P cells were defrosted on ice. The secretion of cytokines and angiogenic and inflammatory growth factors were analysed by ELISA as per the manufacturer's instructions. To assess angiogenic, vascular injury, inflammatory cytokine and chemokine secretions, a 54 multiplex kit spread across 7 plates was used (Meso Scale Diagnostics, USA). The 54 multiplex kit was used to quantify the secretions of CRP, Eotaxin, Eotaxin-3, FGF (basic), GM-CSF, ICAM-1, IFN-γ, IL-10, IL-12/IL-23p40, IL-12p70, IL-13, IL-15, IL-16, IL-17A, IL-17A/F, IL-17B, IL-17C, IL-17D, IL-1RA, IL-1α, IL-1β, IL-2, IL-21, IL-22, IL-23, IL-27, IL-3, IL-31, IL-4, IL-5, IL-6, IL-7, IL-8, IL-8 (HA), IL-9, IP-10, MCP-1, MCP-4, MDC, MIP-1α, MIP-1β, MIP-3α, PIGF, SAA, TARC, Tie-2, TNF-α, TNF-β, TSLP, VCAM-1, VEGF-A, VEGF-C, VEGF-D and VEGFR-1/Flt-1 from OE33P and OE33R cell supernatants previously treated with 10 µM Pyrazinib (P3) or vehicle control (0.1% DMSO) for 24 h. Secretion data for all factors was normalised appropriately to cell lysate protein content using the BCA assay (Pierce). Data was analysed using MSD Discovery Workbench software version 4.0.

5.3.19. *Statistical analysis*

Statistical analysis was performed using GraphPad Prism version 5 software (GraphPad Software, CA, USA). Scientific data were expressed as ±SEM. SEM was calculated as the standard deviation of the original samples divided by the square root of the sample size. Specific statistical tests used are indicated in figure legends. Correlations were carried out using R software version 3.4.1. Graphical representations of correlations were generated with the R package 'corrplot'. For all statistical analysis, differences were considered to be statistically significant at $p<0.05$.

5.4. Results

5.4.1. *Proteomic screening identifies alterations in intracellular and secreted protein levels in OE33P compared to OE33R cells*

To investigate the role of inflammatory mediators in radioresistance of OAC, we carried out a comprehensive proteomics screen using the previously described isogenic *in-vitro* model of OAC radioresistance [150]. Our isogenic cell line provides a unique model to investigate cellular and molecular mediators involved in radioresistance in OAC [150].

Given the multifaceted role of inflammation in cancer progression, we investigated the levels of 184 oncogenic and inflammatory proteins in the supernatants and cell lysates of isogenic OE33P and OE33R cells using a multiplex system.

This broad screen of 184 inflammatory and oncogenic proteins found 3 proteins significantly downregulated and 21 proteins significantly upregulated intracellularly in cell lysates in OE33R; radiation-resistant cells, compared to radiation-sensitive OE33P cells. Proteins significantly downregulated were linked with immune signalling, hydrolysis and growth signalling **(Figure 5-1A)**. A greater number of proteins were significantly upregulated in cell lysates of OE33R compared to OE33P cells and are involved in different biological processes with the majority of those identified in this specific study linked with interleukin and chemokine signalling **(Figure 5-1B)**. Of the 184 proteins screened in the supernatant of OE33P and OE33R cells, 71 proteins were found to be significantly altered between the two cell lines, 18 were significantly downregulated in the supernatant of OE33R cells whilst 53 were significantly upregulated in OE33R cells compared to matched radiosensitive OE33P cells ($p<0.05$). Using Panther pathway analysis the 18 downregulated proteins were linked with 9 pathways **(Figure 5-1C)**. The majority of the significantly altered secreted proteins were upregulated in OE33R cells and the 53 proteins secreted at higher levels from OE33R compared to OE33P cells were linked to 21 signalling pathways hits **(Figure 5-1D)**. Interestingly different mediators tightly linked to pro-tumorigenic pathways including angiogenesis, inflammation and interleukin signalling were found to be both upregulated and downregulated in OE33R cells compared to OE33P cells. One secreted protein LIF and its intracellular receptor LIFR were found to be significantly altered in OE33R compared to OE33P cells and were further validated *in-vitro* and *ex-vivo* following this screen.

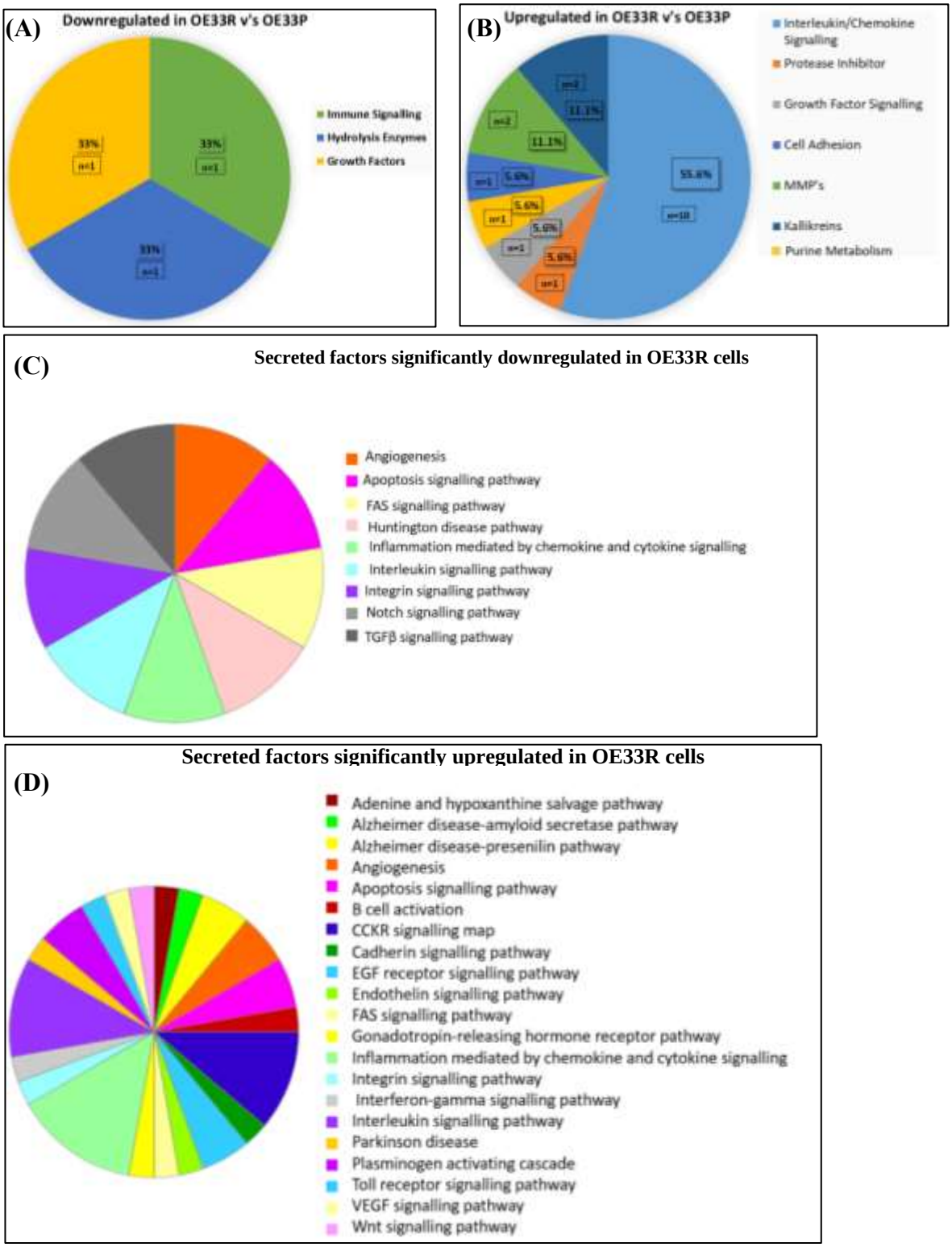

Figure 5-1 Proteomic screening identifies significant differences in intracellular and secreted proteins between OE33P and OE33R cells.

(A) Pie chart illustrating factors significantly downregulated intracellularly in OE33R (radioresistant) cells versus OE33P (radiation-sensitive) cells. **(B)** Pie chart illustrating factors significantly upregulated intracellularly in OE33R cells versus OE33P cells. **(C)** Pie chart illustrating factors significantly downregulated in the supernatant of OE33R cells versus OE33P cells. **(D)** Pie chart illustrating factors significantly upregulated in the supernatant of OE33R cells versus OE33P cells. ($p<0.05$), (n=3).

5.4.2. *LIF and LIFR expression is elevated in radioresistant OAC cells*

From our initial proteomic screen of 184 proteins of both the supernatant and cell lysates generated from passage matched OE33P and OE33R cells we selected one protein and its receptor as lead hits to further investigate as a potential mediator of radioresistance in OAC, LIF and LIFR.

Of particular interest, the inflammatory profile generated in this screen found that the interleukin 6 type cytokine, LIF, was significantly upregulated in the supernatant of OE33R cells (p=0.007), when compared to OE33P cells **(Figure 5-2A)**. In addition, intracellular expression of LIF was significantly higher in OE33R cells compared to OE33P cells, (p=0.006), **(Figure 5-2B)**.

We also found, the LIF receptor, LIFR, was significantly upregulated (p=0.022) intracellularly in OE33R cells relative to OE33P cells **(Figure 5-2C)**. This data indicated that the *in-vitro* expression of LIF is associated with a radioresistant phenotype in OAC and warranted further validation and investigation *in-vitro* and *ex-vivo*.

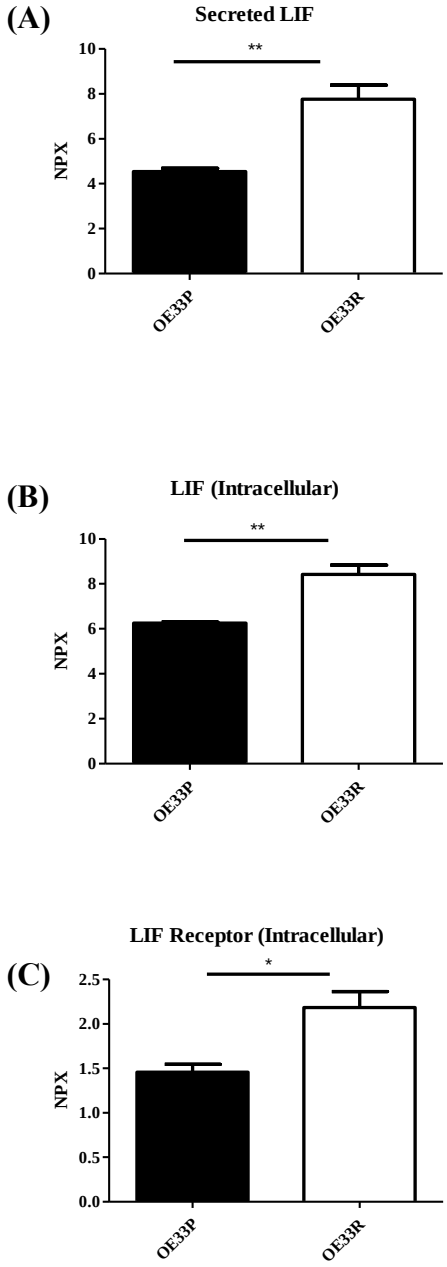

Figure 5-2 Secreted LIF and intracellular levels of LIF and LIF receptor (LIFR) are significantly higher in OE33R; radioresistant OAC cells compared to OE33P; radiation-sensitive cells.

Proteomic screening results of **(A)** Normalised protein expression (NPX) levels of secreted LIF in supernatant from OE33P radiation-sensitive and OE33R; radiation-resistant OAC cells (n=3) **(B)** NPX levels of LIF intracellularly in OE33P and OE33R cell lysates (n=3). **(C)** NPX levels of LIFR intracellularly in OE33P and OE33R cell lysates (n=3). Unpaired t-test, *p<0.05, **p<0.01. Data expressed as +SEM.

5.4.3. *Secreted LIF and intracellular LIF and LIFR expression is increased in radioresistant OAC cells*

We sought to validate the data generated in the multiplex proteomic screen and to investigate secretion and intracellular expression profiles of LIF and LIFR when OE33P and OE33R cells which were mock irradiated (0 Gy) or irradiated with 2 Gy X-ray radiation.

Secreted levels of LIF protein were evaluated by ELISA. Secreted levels of *LIF* from OE33R cells were significantly higher when compared to OE33P cells at 0 Gy (p=0.012) and 24 h post 2 Gy X-ray radiation (p=0.001), **(Figure 5-3A)**. This result validated the screen data and illustrated that radiation significantly increased the secretion of LIF specifically in the radiation-resistant OE33R cells (p=0.008) but no significant change was seen following 2 Gy irradiation in radiation-sensitive OE33P cells.

Following on from the protein data, *LIF* mRNA expression, was evaluated by RT-PCR and was found to be higher although not significant in OE33R cells compared to OE33P cells (p=0.059) **(Figure 5-3B)**. Interestingly, 24 h after the cells were exposed to one dose of 2 Gy irradiation, the levels of *LIF* mRNA expression significantly decreased in both OE33P (p=0.034) and OE33R cells (p=0.013). Similar to our findings from the proteomics screen, *LIFR* expression was higher although this was not significant in OE33R cells and no significant change in expression was observed following 2 Gy irradiation **(Figure 5-3C)**. Our findings suggest that *LIF* and *LIFR* may be expressed at higher levels in radiation-resistant OAC cells when compared to radiation-sensitive cells although this is not significant, and that radiation treatment significantly increases the secretion of LIF by OE33R cells.

Given that baseline LIF secretion is higher in OE33R cells and that radiation significantly induces LIF secretion in OE33R cells indicates LIF is an important molecular mediator of response to radiation in OAC.

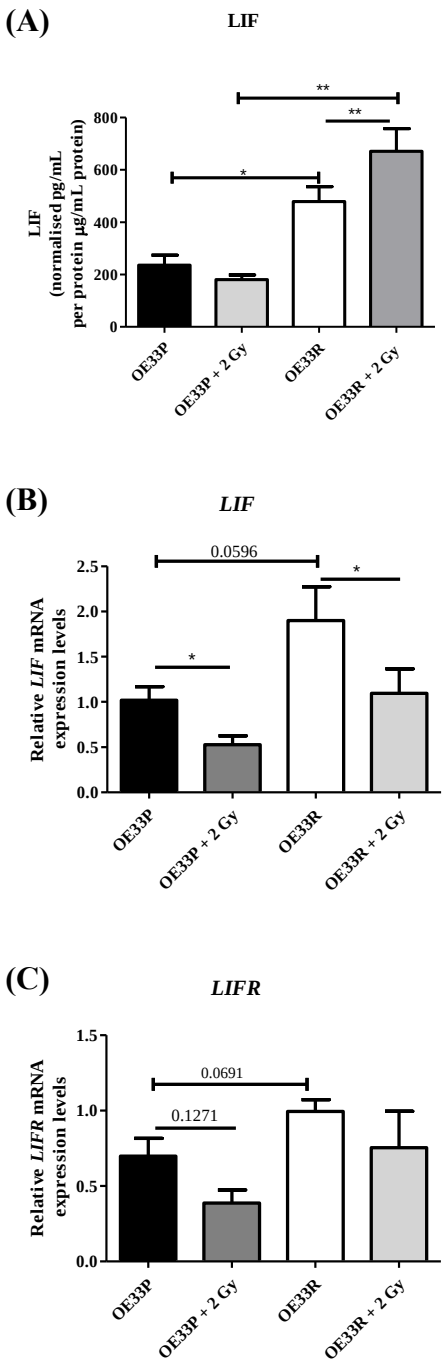

Figure 5-3 Validation of LIF and LIFR expression data from OLINK screen and investigation of expression and secretion profile of LIF and LIFR at 0 Gy and 24 hours post 2 Gy irradiation. **(A)** Secreted LIF protein from OE33P and OE33R cells which have been-mock irradiated and following 2 Gy X-ray irradiation was evaluated by ELISA, (n=4). **(B)** Relative expression of LIF mRNA in OE33P and OE33R cells at baseline and following 2 Gy irradiation was evaluated by qPCR, (n=5). **(C)** Relative mRNA expression levels of LIFR at baseline in OE33R and OE33P cells and post 2 Gy irradiation was evaluated by qPCR, (n=5). Unpaired t-test used to compare OE33P and OE33R cell lines. Paired t-test used to compare within same cell line, *p<0.05, **p<0.01. Data expressed as +SEM.

5.4.4. *Significantly increased levels of circulating LIF and decreased levels of tumoural LIFR expression are associated with a poor response to neo-adjuvant treatment in OAC*

Following on from our *in-vitro* screens we sought to investigate both the levels of circulating LIF and intra-tumoural *LIF* and *LIFR* expression *ex-vivo* in OAC treatment-naïve patient serum and OAC treatment-naïve biopsies respectively. The levels of circulating LIF in the serum of treatment-naïve patients was evaluated in 26 OAC patient samples by ELISA, the patient cohort is outlined in **Table 5-1.** Circulating levels of LIF were significantly elevated in patients who went on to have a subsequent poor pathological response following neo-adjuvant treatment (neoCT or neo-CRT), with TRG of 3-5, compared to patients who had a subsequent good pathological response to neo-adjuvant treatment, with a TRG of 1-2 (p=0.037) **(Figure 5-4A)**. Circulating levels of LIF were not significantly associated with other patient clinical characteristics, such as tumour stage, nodal status and stage of differentiation **(Figure 5-5A-D)**. In contrast to circulating levels of LIF in serum, there was no significant difference in *LIF* mRNA expression in pre-treatment OAC tumour biopsies from good and poor responders to neo-adjuvant treatment **(Figure 5-4B)** indicating that LIF in the circulation may be a more important predictive marker of treatment response than expression levels of *LIF* within the tumour. Furthermore, *LIF* expression was not significantly associated with other patient characteristics such as tumour stage, nodal status, stage of differentiation or body mass index **(Figure 5-6A-F)**.

LIFR expression (detected in 16 of 24 patients all of whom received neo-CRT) was significantly reduced in tumour biopsies from patients having a subsequent poor pathological response to neo-CRT (p<0.001), when compared to good responders **(Figure 5-4C)**. Patient cohort for mRNA expression of *LIF* and *LIFR* is outlined in **Table 5-2**. Circulating LIF and intra-tumoural expression of *LIFR* was associated with neo-CRT treatment response but not with other patient clinical characteristics **(Figure 5-6A-F, Figure 5-7 A-F)**. This suggests that circulating LIF and intra-tumoural *LIFR* expression may function as valuable pre-treatment predictive indicators of response to neo-adjuvant therapy.

Table 5-1 Patient characteristics of patient cohort for serum study.

Table detailing patient characteristics including gender, median age, median body mass index (BMI), tumour stage, nodal status, treatment received and tumour regression grade of the 26 patients whose samples were used in the serum study.

	n=26
Male	23
Female	3
Median Age at diagnosis	64.5 (58-80)
Median BMI at diagnosis	27 (23-36.8)
Tumour Stage at diagnosis	
1	1
2	2
3	20
4	1
Not Specified	2
Nodal Status at diagnosis	
0	14
1	8
2	2
Not Specified	2
Treatment	
CROSS	18
MAGIC	8
Tumour Regression Grade	
1	5
2	5
3	9
4	6
5	1

Table 5-2 Patient characteristics of patient cohort for RT-PCR study.
Table detailing patient characteristics including gender, median age, median body mass index (BMI), tumour stage, nodal status, treatment received and tumour regression grade of the 24 patients whose samples were used in the RT-PCR study.

	n=24
Male	20
Female	4
Median Age at diagnosis	62.5 (43-75)
Median BMI at diagnosis	27.34 (20.04-36.61)
Tumour Stage at diagnosis	
2	3
3	21
Nodal Status at diagnosis	
0	12
1	11
2	1
Treatment	
CROSS	24
Tumour Regression Grade	
1	4
2	8
3	6
4	6

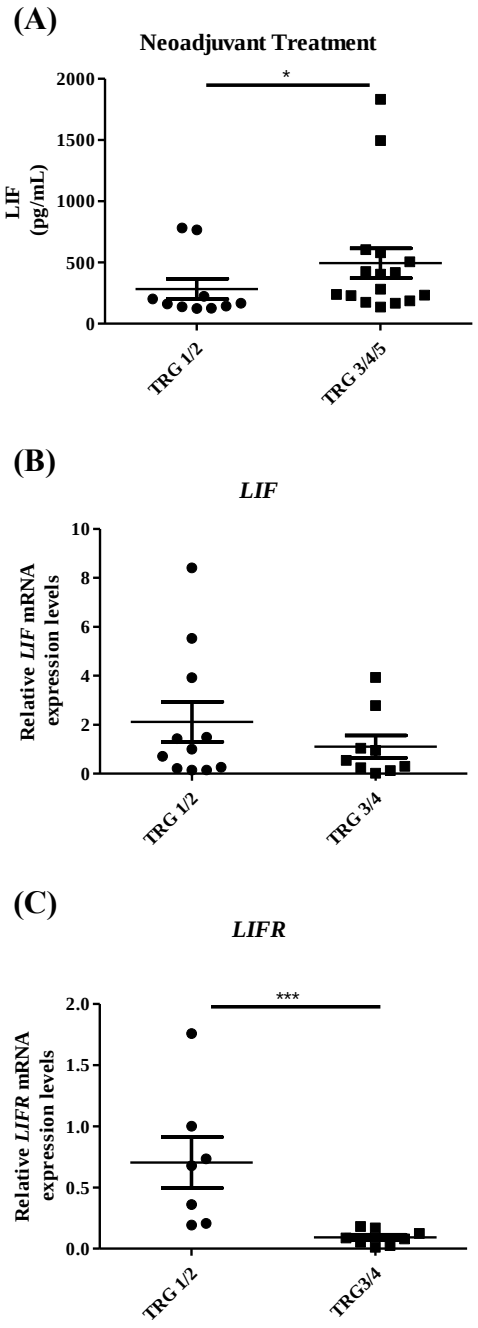

Figure 5-4 Circulating levels of LIF and tumoural levels of LIFR are significantly altered in OAC patients with a subsequent poor response to neo-adjuvant treatment.

(A) Circulating LIF in pre-treatment serum of OAC patients was assessed by ELISA. Patients were divided into good (TRG 1/2) (n=10) and poor responders (TRG 3/4/5) (n=16) based on pathological response to neo-adjuvant treatment. **(B)** Relative mRNA expression of tumoural *LIF* in OAC pre-treatment biopsies from good (TRG 1/2) (n=11) and poor (TRG 3/4) (n=9) responders (n=20). **(C)** Relative mRNA expression of tumoural *LIFR* in OAC pre-treatment biopsies from good (TRG 1/2) (n=6) and poor (TRG 3/4) (n=10) responders. Statistical analysis was performed by Mann-Whitney U test. *p<0.05, ***p<0.001. Data expressed as ±SEM.

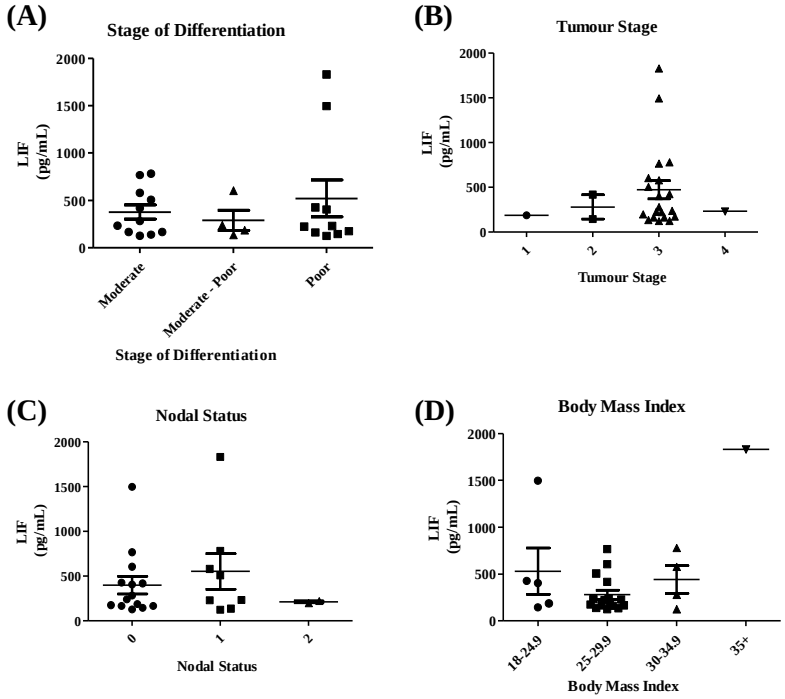

Figure 5-5 Circulating LIF in serum from treatment-naïve oesophageal adenocarcinoma patients, divided according to pathological parameters.
Circulating LIF in serum was assessed by ELISA and divided according to **(A)** Stage of Differentiation (n=25), **(B)** Tumour stage (n=26), **(C)** Nodal status (n=26) and **(D**) Body Mass Index (n=26). Mann-Whitney t-test. Data are expressed as mean ± SEM.

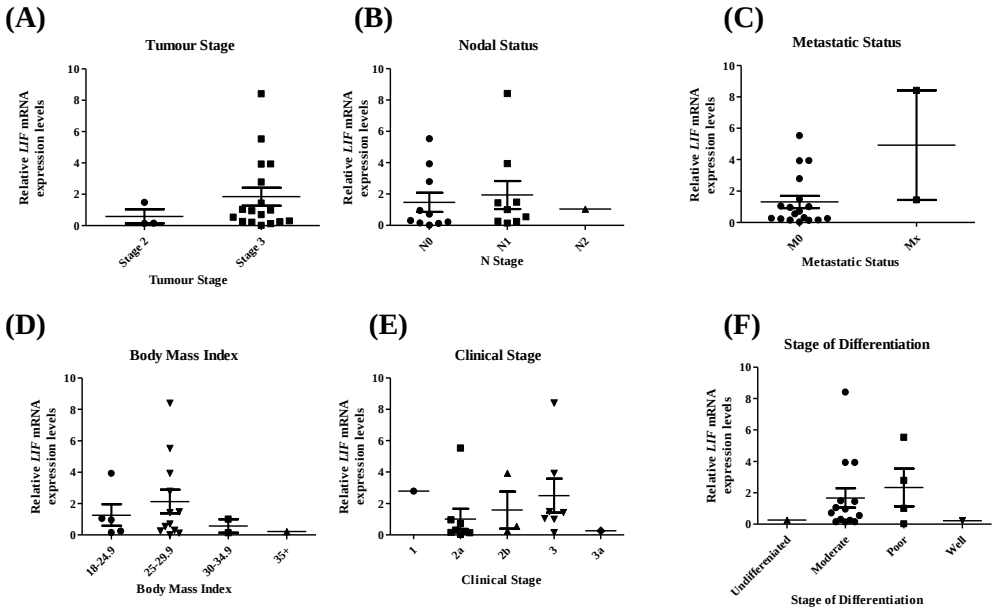

Figure 5-6 Relative expression of LIF in OAC pre-treatment biopsies.
Relative expression of LIF mRNA in treatment-naïve patient biopsies was divided according to clinical characteristics **(A)** Tumour Stage (n=20), **(B)** Nodal Status (n=20), **(C)** Presence of Metastasis (n=20), **(D)** Body Mass Index (n=20), **(E)** Clinical Stage (n=20) and **(F)** Stage of Differentiation (n=20). Mann Whitney U test. Data expressed as mean ± SEM.

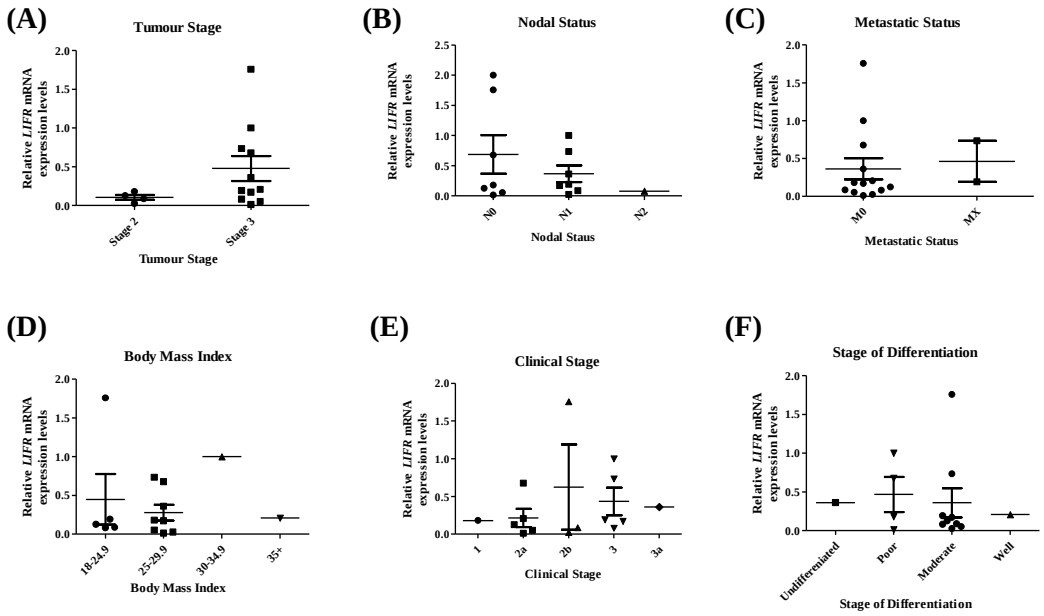

Figure 5-7 Relative expression of LIFR in OAC pre-treatment biopsies.
Expression of LIFR mRNA in patient biopsies was divided according to clinical patient characteristics **(A)** Tumour Stage (n=15) **(B)** Nodal Status (n=15) **(C)** Presence of Metastasis (n=15) **(D)** Body Mass Index (n=15) **(E)** Clinical Stage (n=15) and **(F)** Stage of differentiation (n=15).Mann-Whitney U test. Data expressed as mean ± SEM.

5.4.5. *LIF secretions were significantly correlated with the levels of b-FGF, VEGF-A and IL-8 in OAC treatment-naïve human tumour explants ex-vivo*

Given the importance of circulating LIF as a predictive marker of treatment response we further sought to investigate the secreted levels of LIF from OAC patient tumours using treatment-naïve OAC patient tumour biopsies (patient cohort outlined in **Table 5-3**). This unique model most closely recapitulates the tumour microenvironment, encompassing multiple cell types as seen *in-vivo*.

Ex-vivo treatment-naïve human explant tissue was cultured for 6 OAC patients, and the secretions of LIF and a panel of inflammatory (n=10) and angiogenic (n=8) secretions in this TCM were evaluated by ELISA. The secreted levels of these mediators were correlated in order to ascertain what other mediators in the *ex-vivo* tumour microenvironment were associated with LIF. We demonstrated for the first time that LIF is actively secreted from OAC tumour biopsies (range: 24.61-1137.36 pg/mL) and significantly correlated with the levels of basic fibroblast growth factor (bFGF), VEGF-A and IL-8 ($p<0.05$, R=1) ($p<0.05$, R=0.9429) ($p<0.05$, R=1) respectively, **(Figure 5-8A, Table 5-4)**.

Our studies *ex-vivo* have importantly demonstrated that LIF is secreted into the tumour microenvironment in OAC and is significantly positively correlated with pro-angiogenic and growth factors secretions.

Table 5-3 Patient characteristics of patient cohort for ex-vivo study.
Table detailing patient characteristics including gender, median age, median body mass index (BMI), tumour stage, nodal status, treatment received and tumour regression grade of the 6 patients whose samples were used in the *ex-vivo* study.

	n=6
Male	5
Female	1
Median Age	68.5 (61-83)
Median BMI at diagnosis	30.15 (25.5-38.5)
Tumour Stage at diagnosis	
2	2
3	3
4	1
Nodal Status at diagnosis	
0	1
1	3
2	2
Treatment	
CROSS	3
MAGIC	1
Other Chemotherapy	2
Tumour Regression Grade	
3	1
4	1
5	1
Not Specified	3

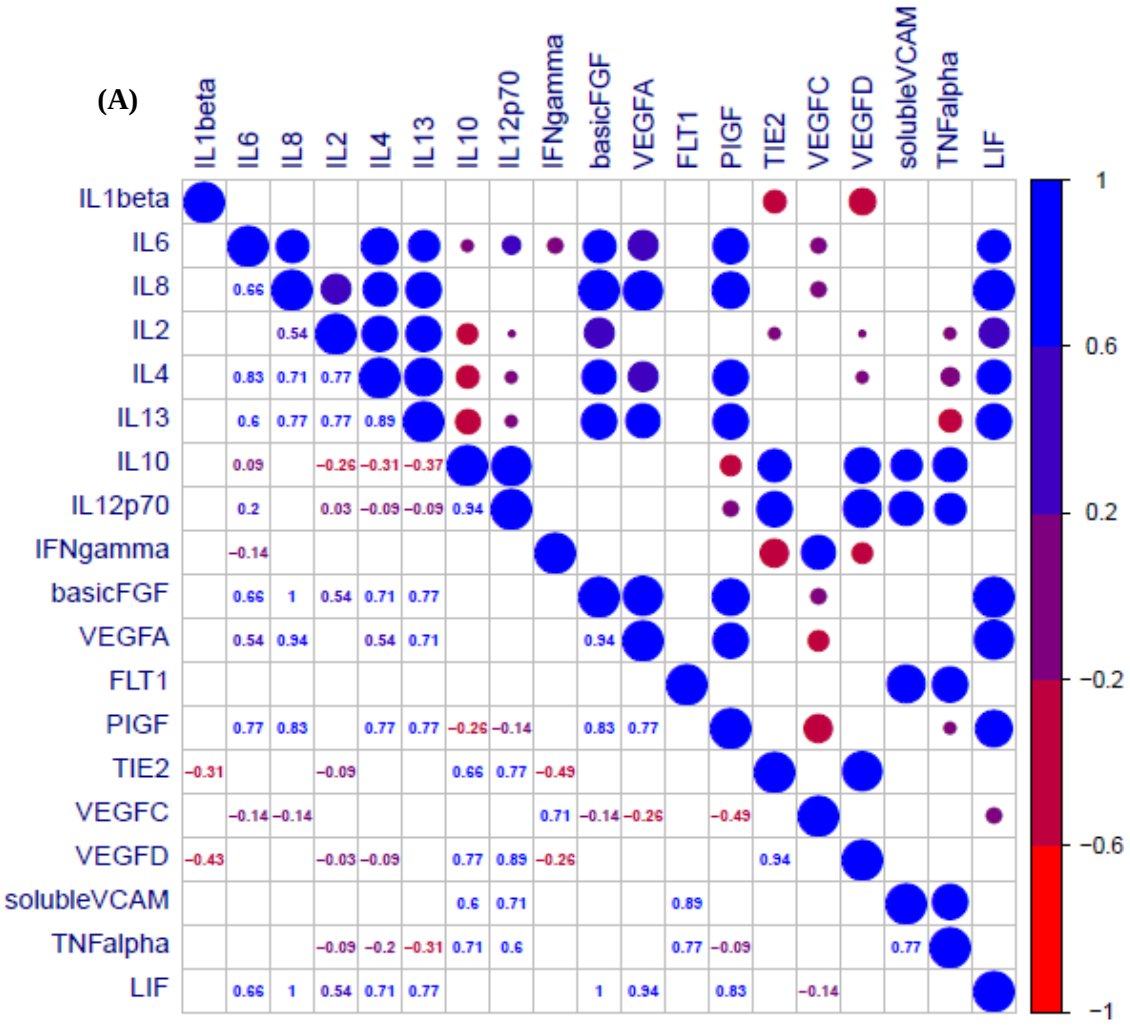

Figure 5-8 LIF secretions are significantly associated with the secretion bFGF, VEGF-A and IL-8 ex-vivo.

(A) CorrPlot illustrating the correlation values of secreted LIF to secreted angiogenic and inflammatory secretions evaluated by ELISA from OAC treatment-naïve tumour biopsies cultured *ex-vivo* (n=6). Blue indicates a positive correlation, red indicates negative correlation.

Table 5-4 LIF secretion is significantly correlated with IL-8, bFGF and VEGF-A secretion in OAC treatment-naïve biopsies.

Table showing correlation of secreted LIF secreted angiogenic and inflammatory secretions in OAC treatment-naïve biopsies cultured *ex-vivo* (n=6)**.** Secretion of inflammatory and angiogenic mediators was determined by ELISA. Correlation to LIF secretions where Spearman r 0.4-0.59 moderate, 0.6-0.79 strong and 0.8-1 very strong.*$p<0.05$, **$p<0.01$.

Factor	**Spearman r**	**P value (two-tailed)**	**P value summary**
IL-1β	-0.02857	1	ns
IL-6	0.6571	0.175	ns
IL-8	**1**	**0.0028**	****
IL-2	0.5429	0.2972	ns
IL-4	0.7143	0.1361	ns
IL-13	0.7714	0.1028	ns
IL-10	0.08571	0.9194	ns
IL-12p70	0.2571	0.6583	ns
IFN-γ	0.1429	0.8028	ns
bFGF	**1**	**0.0028**	****
VEGF-A	**0.9429**	**0.0167**	*
FLT1	0.7143	0.1361	ns
PIGF	0.8286	0.0583	ns
TIE-2	0.2	0.7139	ns
VEGF-C	-0.1429	0.8028	ns
VEGF-D	0.2571	0.6583	ns
sVCAM	0.6571	0.175	ns
TNF-α	0.3143	0.5639	ns

5.4.6. *Elevated secreted LIF negatively correlates with lymphocyte infiltration in human OAC pre-treatment biopsies*

Following our *ex-vivo* studies using TCM generated from 6 patient OAC pre-treatment biopsies, we investigated the association of secreted LIF with immune cell infiltrate and patient clinical characteristics. It is critical to understand the role of LIF in the tumour microenvironment, the association of LIF with other secreted growth factors and cytokines and to understand how LIF secretion is associated with immune cell infiltration of tumours. Immune cell infiltrates were determined by a pathologist using matched diagnostic H&E slides prepared from pre-treatment biopsies of 6 patients (patient cohort is outlined in **Table 5-3**).

We observed that LIF secretion was significantly negatively correlated with lymphocytic infiltration whereby lower LIF secretion was associated with greater lymphocyte infiltration in matched biopsies (p=0.0333, r=-0.8783) but no significant association was seen with other types of infiltrating cells, including eosinophils, neutrophils, plasma cells **(Figure 5-9A)(Table 5-5)**.

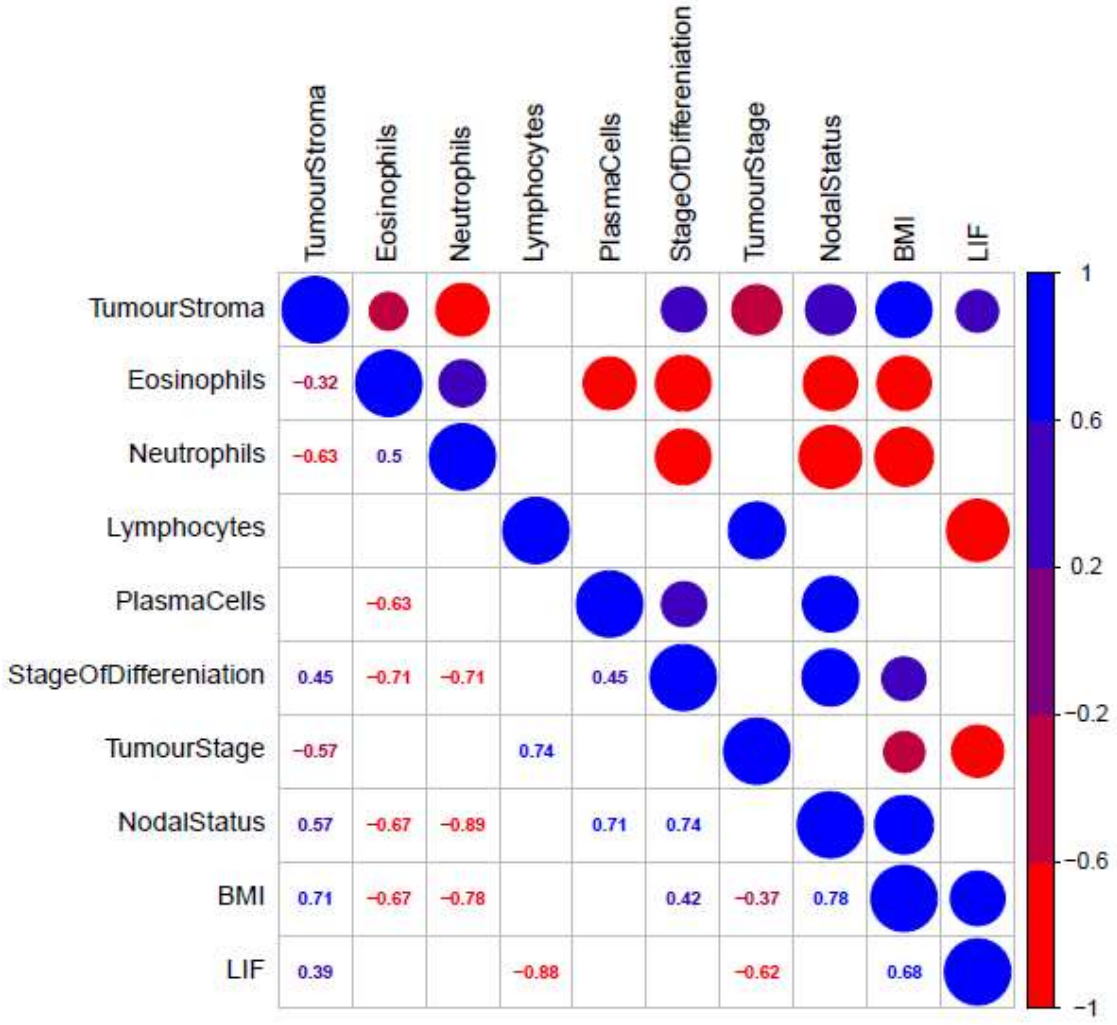

Figure 5-9 Elevated levels of secreted LIF negatively correlates with lymphocyte infiltration in human OAC pre-treatment biopsies.

(A) CorrPlot illustrating the correlation values of secreted LIF from OAC treatment-naïve biopsies cultured *ex-vivo* to patient clinical characteristics (Stage of Differentiation, Tumour Stage, Nodal Status and BMI) and percentage tumour stroma immune cell infiltrations (Neutrophils, Eosinophils, Lymphocytes and plasma cells). Blue indicates a positive correlation, red negative correlation, (n=6).

Table 5-5 LIF negatively correlates with lymphocyte infiltration in human OAC pre-treatment biopsies.

Table showing correlation values of secreted LIF to patient clinical characteristics and immune cell infiltrate (n=6). Spearman correlation to LIF secretions where Spearman r 0.4-0.59 moderate, 0.6-0.79 strong and 0.8-1 very strong.*p<0.05.

Factor	Spearman r	P value (two-tailed)	P value summary
% Tumour Stroma	0.3928	0.4194	ns
% Eosinophils Infiltrate	-0.414	0.4194	ns
% Neutrophils Infiltrate	-0.207	0.7139	ns
% Lymphocytes Infiltrate	-0.8783	0.0333	*
% Plasma Cells Infiltrate	-0.1309	0.8028	ns
Stage of differentiation	-0.09759	0.9194	ns
Tumour stage	-0.6172	0.175	ns
Nodal status	0.09258	0.9194	ns
Body mass index	0.6789	0.1361	ns

5.4.7. *Pyrazinib (P3) significantly alters the secretion of IL-6, IL-4, IL-8 and IL-13 in OE33R radioresistant cells*

Following on from our proteomics screen, we investigated the difference in inflammatory protein secretions from our OE33P and OE33R cells and evaluated the effect of treatment with our radiosensitiser Pyrazinib (P3) on inflammatory protein secretions in our isogenic model. We measured the effects of Pyrazinib (P3) on the protein secretions of 54 angiogenic factors, growth factors and inflammatory cytokines in OE33P and OE33R cells following treatment with 10 µM Pyrazinib (P3) or 0.1%DMSO control.

Of the 54 factors analysed, 30 were detected within the range of detection in our isogenic radioresistant OAC model. Of the 30 factors detected, statistical testing could be carried out for 25 proteins **(Figure 5-10A-X)**. 9 factors were secreted at significantly higher levels in OE33R radioresistant cells when compared to OE33P cells; IL-6, IL-4, IL-8, IL-13, ICAM, IL-12p70, IL-2, IL-10, IP-10 and MCP-1 **(Figure 5-10A-J)**. Pyrazinib (P3) significantly reduced the secretions of IL-6 (p=0.0006) **(Figure 5-10A)**, IL-4 (p=0.0111) **(Figure 5-10B)**, IL-8 (p=0.0488**) (Figure 5-10C)** and IL-13 (p=0.0204) **(Figure 5-10D)** *in-vitro* in OE33R cells. Two factors were significantly down regulated in OE33R compared to OE33P cells, IL-1RA (p=0.0013) (**Figure 5-10M)** and GM-CSF (p=0.0018)(**Figure 5-10N)**.

This study supported our findings in the proteomic study highlighting the altered inflammatory secretome of OE33R compared to OE33P cells and the anti-inflammatory action of Pyrazinib (P3) through its inhibition of IL-6, IL-8, IL-4 and IL-13 secretion from OE33R cells.

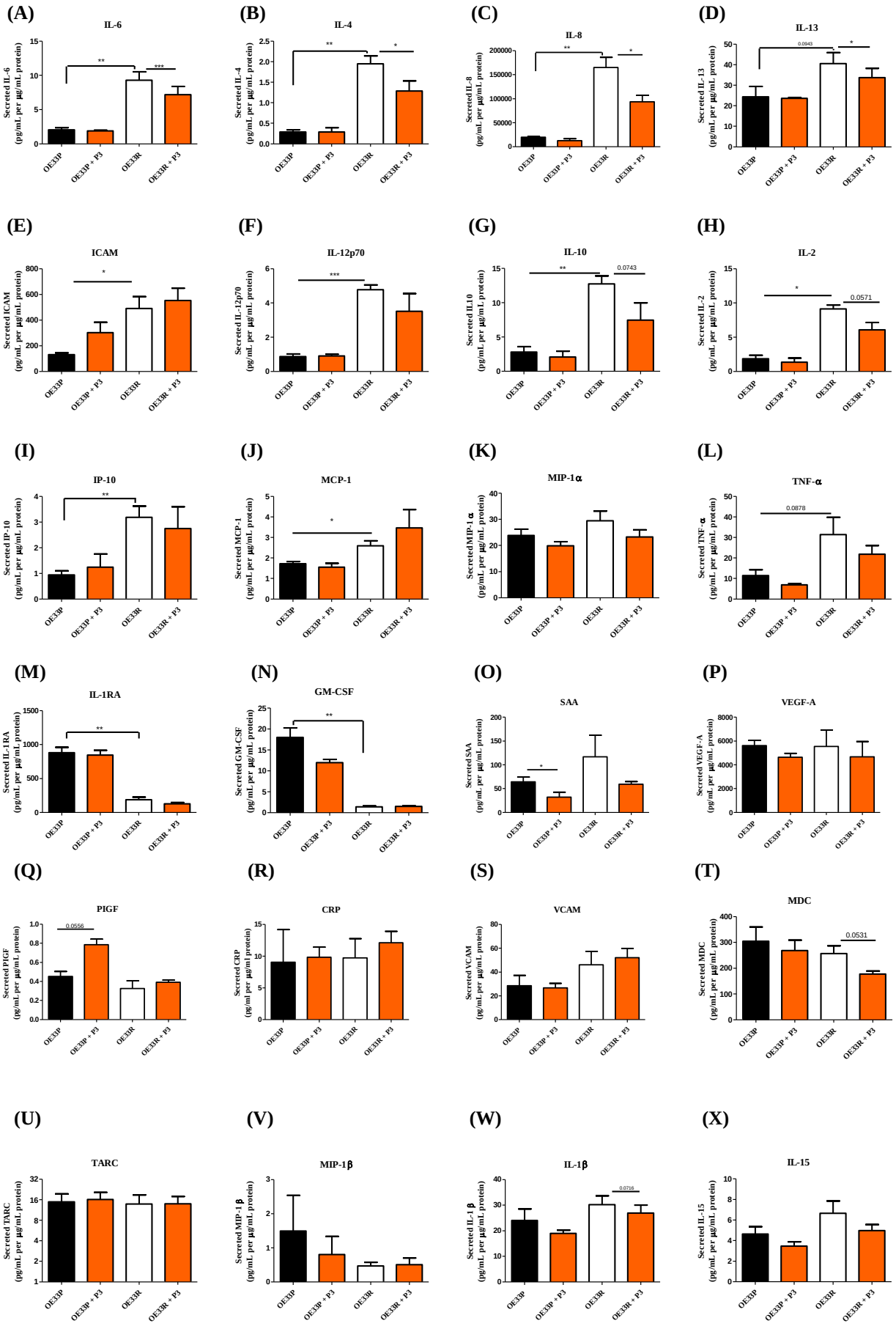
(A)
IL-6
Secreted IL-6 (pg/mL per µg/mL protein)
(B)
IL-4
Secreted IL-4 (pg/mL per µg/mL protein)
(C)
IL-8
Secreted IL-8 (pg/mL per µg/mL protein)
(D)
IL-13
Secreted IL-13 (pg/mL per µg/mL protein)
0.0943
(E)
ICAM
Secreted ICAM (pg/mL per µg/mL protein)
(F)
IL-12p70
Secreted IL-12p70 (pg/mL per µg/mL protein)
(G)
IL-10
Secreted IL10 (pg/mL per µg/mL protein)
0.0743
(H)
IL-2
Secreted IL-2 (pg/mL per µg/mL protein)
0.0571
(I)
IP-10
Secreted IP-10 (pg/mL per µg/mL protein)
(J)
MCP-1
Secreted MCP-1 (pg/mL per µg/mL protein)
(K)
MIP-1α
Secreted MIP-1 α (pg/mL per µg/mL protein)
(L)
TNF-α
Secreted TNF- α (pg/mL per µg/mL protein)
0.0878
(M)
IL-1RA
Secreted IL-1RA (pg/mL per µg/mL protein)
(N)
GM-CSF
Secreted GM-CSF (pg/mL per µg/mL protein)
(O)
SAA
Secreted SAA (pg/mL per µg/mL protein)
(P)
VEGF-A
Secreted VEGF-A (pg/mL per µg/mL protein)
(Q)
PIGF
Secreted PIGF (pg/mL per µg/mL protein)
0.0556
(R)
CRP
Secreted CRP (pg/ml per µg/mL protein)
(S)
VCAM
Secreted VCAM (pg/mL per µg/mL protein)
(T)
MDC
Secreted MDC (pg/mL per µg/mL protein)
0.0531
(U)
TARC
Secreted TARC (pg/mL per µg/mL protein)
(V)
MIP-1β
Secreted MIP-1 β (pg/mL per µg/mL protein)
(W)
IL-1β
Secreted IL-1 β (pg/mL per µg/mL protein)
0.0716
(X)
IL-15
Secreted IL-15 (pg/mL per µg/mL protein)
OE33P
OE33P + P3
OE33R
OE33R + P3

Figure 5-10 Pyrazinib (P3) significantly reduces the secretion of pro-inflammatory cytokines IL-6, IL-4, IL-8 and IL-13 in OE33R radioresistant OAC cells.
The secreted levels of 54 proteins in OE33P and OE33R cells were quantified by multiplex ELISA. Of these, 25 proteins were detected in sufficient samples to carry out statistical analysis. Protein secretions in OE33P and OE33R cells following treatment with 0.1% DMSO or 10 μM Pyrazinib (P3) **(A)** Interleukin 6 (IL-6), **(B)** Interleukin 4 (IL-4), **(C)** Interleukin 8 (IL-8), **(D)** Interleukin 13 (IL-13), **(E)** Intracellular Adhesion Molecule 1 (ICAM-1), **(F)** Interleukin 12p70 (IL-12p70), **(G)** Interleukin 10 (IL-10), **(H)** Interleukin 2 (IL-2), **(I)** Interferon gamma-induced protein 10 (IP-10), **(J)** Monocyte chemoattractant protein 1 (MCP-1), **(K)** Macrophage Inflammatory Protein -1 alpha (MIP-1α), **(L)** Tumour necrosis factor alpha (TNF-α), **(M)** Interleukin 1 receptor antagonist (IL-1RA), **(N)** Granulocyte-macrophage colony-stimulating factor (GM-CSF), **(O)** Serum amyloid A (SAA), **(P)** Vascular endothelial growth factor A (VEGF-A), **(Q)** Placental growth factor (PIGF), **(R)** C reactive protein (CRP), **(S)** Vascular cell adhesion molecule 1 (VCAM-1), **(T)** Macrophage derived chemokine (MDC), **(U)** Thymus and Activation Regulated Chemokine (TARC), **(V)** Macrophage inflammatory protein-1β (MIP-1β), **(W)** Interleukin 1 beta (IL-1β) and **(X)** Interleukin 15 (IL-15). All secretions were normalised to protein content. Unpaired t-test was used to compare different cell lines, paired t-test to compare within same cell line, (n=3), *$p<0.05$, **$p<0.01$, ***$p<0.001$. Data expressed as +SEM.

5.5. Summary of main findings of chapter 5

- OE33R radioresistant cells have significantly altered intracellular and secreted levels of inflammatory and oncogenic proteins compared to OE33P cells.

- LIF and its receptor LIFR were identified as lead hits which were secreted and/or expressed at significantly higher levels from OE33R cells.

- Circulating levels of LIF were significantly higher in the treatment-naïve serum of OAC patients who have a subsequently poor response to neo-adjuvant CRT.

- *LIFR* was expressed at significantly lower levels in the mRNA of OAC treatment-naïve biopsies of patients who had a subsequent poor response to neo-CRT.

- LIF secretions from OAC tumour conditioned media were significantly correlated with the levels of secreted basic fibroblast growth factor (bFGF), vascular endothelial growth factor (VEGF-A) and IL-8 in matched OAC treatment-naïve human tumour explants *ex-vivo*.

- Secreted levels of LIF negatively correlated with lymphocyte infiltration in human OAC pre-treatment biopsies.

- Pyrazinib (P3) significantly reduced the secretion of IL-6, IL-4, IL-8 and IL-13 in OE33R radioresistant cells.

5.6. Discussion

We carried out a large proteomics screen of 184 proteins to compare the inflammatory profiles of an isogenic radioresistant *in-vitro* model of OAC. We found that LIF, an IL-6 type cytokine, was significantly elevated in radioresistant OAC cells. Furthermore, significantly higher circulating levels of LIF were present in the serum from treatment-naïve OAC patients who had a subsequent poor pathological response to neo-adjuvant therapy. Quantitative PCR analysis revealed expression of LIF receptor (*LIFR*) may function as a predictive indicator of response to neo-adjuvant chemoradiation therapy in OAC. LIF was demonstrated to be actively secreted from human OAC treatment-naïve biopsies and significantly correlated with the secretion of bFGF, VEGF-A and IL-8. Importantly, LIF secretion negatively correlated with tumour infiltrating lymphocytes in pre-treatment OAC patient biopsies. Elevated circulating LIF is a marker of poor response to neo-adjuvant treatment in OAC and secretion of this chemokine from the tumour is tightly linked with pro-tumorigenic mediators including bFGF, VEGF-A and IL-8. Targeting this pathway may be a novel mechanism to enhance response to neo-adjuvant treatment in OAC.

LIF is a multi-functional cytokine which under non-pathological conditions plays an essential role in embryonic implantation, bone formation and neuronal development [377, 379]. In cancer, previous studies have demonstrated the role of LIF as an oncogenic mediator which stimulates cancer growth, proliferation and metastasis, and have associated LIF with both resistance to radiation and chemotherapy treatments [228, 369, 372]. To our knowledge this is the first study to investigate the role of LIF in OAC. OAC is an aggressive disease with a poor prognosis, currently over 70% of patients do not show a beneficial response to neo-adjuvant therapy [43]. A complete pathological response to treatment is associated with increased survival, thus it is critical to gain further insight into the molecular mediators which play a role in treatment response in OAC.

In-vitro, both in our screen and validation study, LIF and LIFR expression were elevated in radiation-resistant OE33R cells relative to radiation-sensitive OE33P cells. Overexpression of LIF at the mRNA level has been previously shown in a number of cell lines such as breast cancer where LIF expression was found to be significantly higher in breast cancer cells with greater metastatic capability [369]. *In-vivo*, targeting of the LIF/LIFR pathway through inhibition of LIFR with small interfering RNA was shown to inhibit metastasis in rhabdomyosarcoma xenografts, further highlighting both the role of LIF in tumorigenesis and therapeutic targeting potential of this pathway [380]. Furthermore in NPC, treatment with soluble LIFR, an antagonist of LIF or rapamycin, an mTOR inhibitor of LIF, was found to reduce cell survival and tumour growth following irradiation *in-vitro* and *in-vivo* [228]. Given these findings in the literature in

addition to our studies in OAC, the potential of targeting this pathway to enhance radiosensitivity in OAC must be investigated in future studies.

LIF secretion was significantly higher in OE33R cells than OE33P cells, complementing our findings at the gene level. An important finding from this result was the differential secretion of LIF in OE33P and OE33R cells following one dose of 2 Gy radiation, the response to radiation was cell line specific, with elevated levels of secreted LIF identified in radioresistant OE33R cells only. In contrast at the gene level *LIF* expression was reduced in both cell lines 24 hours following 2 Gy irradiation, it would be interesting to evaluate the levels of LIF at an earlier time point following irradiation to see if LIF expression is altered. Higher LIF secretion in the OE33R cells may result in increased activation of the LIF/LIFR pathway in OE33R cells and could be contributing to the radioresistant phenotype. *In-vivo*, LIF was previously shown to significantly enhance radioresistance in a NPC xenograft model whereby the administration of soluble LIF following one dose of 7 Gy irradiation significantly enhanced resistance to radiation and promoted tumour growth [228]. The enhanced tumour growth following LIF administration is supported by other studies in both breast and pancreatic cancer, where LIF administration and ectopic expression was shown to promote tumour growth and tumour progression *in-vitro* [369, 373]. Our findings, along with the current literature, indicate that LIF may play a role in treatment resistance in OAC. Enhanced cell growth and tumour progression as a result of LIF pathway activation has been linked to downstream activation of the JAK/STAT3 and Akt/mTOR pathways. In these studies, mTOR expression has been identified in both OE33P and OE33R cells previously (data not shown) but the actual pathway through which LIF signals in OAC requires further investigation, especially since inhibition of mTOR has previously been shown to enhance radiosensitivity in oesophageal SCC, lung and pancreatic cancer [369, 381, 382].

In OAC patient pre-treatment serum, circulating LIF was found at significantly higher levels in OAC treatment-naïve patients who went on to have a subsequent poor pathological response to neo-adjuvant treatment with a TRG of 3-5. This result complements our findings *in-vitro* whereby elevated LIF protein secretion was associated with radiation resistance. This result was similar to that seen by Liu *et al.*, in NPC where elevated levels of circulating LIF in serum were positively associated with a poor response to treatment and subsequent local tumour recurrence [228]. Our study demonstrates that elevated circulating levels of LIF is associated with poor response to neo-adjuvant treatment (MAGIC or CROSS) and may contribute to subsequent disease progression in OAC. Circulating LIF may therefore have important value as predictive marker of treatment response and as a therapeutic target to halt tumour progression. This is supported by a study which showed that elevated IL-6 in serum, a key oncogenic cytokine from the same family was shown

to predict a two-fold increased risk of progression to malignancy from Barrett's oesophagus (BO), a chronic inflammatory condition and pre-disposing risk factor of OAC [383].

LIFR mRNA expression was significantly reduced in treatment-naïve OAC tumour biopsies from patients having a subsequent poor pathological response to treatment, suggesting that a loss in receptor expression is associated with poor treatment response. This result may seem surprising given that elevated circulating LIF was demonstrated to be associated with a poor response. However, several other studies support this data. LIFR expression has previously been identified in breast cancer, CRC, gastric cancer, liver cancer and pancreatic cancer [373, 375, 384, 385]. In hepatocellular carcinoma (HCC), LIFR was found to negatively regulate the metastasis via the PI3K/Akt pathway and downregulated expression of LIFR was an indicator of poor prognosis [386]. A previous study in a large cohort of metastatic breast cancer patients also found loss of LIFR to be associated with poor clinical outcome [375]. LIFR was found to promote membrane localisation factor Scribble which in turn led to the activation of Hippo signalling and phosphorylation and functional inactivation of the transcriptional co-activator Yes-associated protein 1 (YAP1) and subsequent suppression of tumour metastasis [375]. It has been suggested that LIFR may be reduced in tumour tissues as a result of the promoter undergoing hypermethylation [370]. Furthermore, in pancreatic cancer tissue microarrays, downregulated LIFR was significantly associated with Tumour Node Metastasis (TNM) stage and lymph node metastasis, and silencing of LIFR *in-vitro* reduced colony formation and metastatic potential of pancreatic cancer cells [384].

The significantly lower levels of *LIFR* expression in OAC patients with a poor response to neo-CRT highlights the loss of LIFR as a predictive indicator of poor outcome, similar to findings in other cancers. LIFR may act as an additive predictive indicator for treatment response in OAC, however this result would need to be validated in a larger patient cohort.

Therapeutic targeting of this receptor in OAC warrants further investigation, particularly given that *in-vivo* in pancreatic cancer xenografts, primary tumour volume and lung metastasis were increased by LIFR silencing and tumour volume and metastasis were reduced and inhibited respectively when LIFR was overexpressed in primary implanted pancreatic cancer cells [384]. These studies support our data, which suggests that decreased LIFR in pre-treatment OAC tumour biopsies is a predictive marker of poor response to neo-adjuvant treatment. However, this requires further validation in a larger independent patient cohort.

Given the predictive importance of LIF as a circulating mediator, we then investigated the role of secreted LIF in the tumour microenvironment from human pre-treatment OAC tumour biopsies

which we cultured *ex-vivo*. We demonstrated for the first time that LIF is secreted from OAC tumours. The angiogenic and inflammatory factors produced by OAC tumours play an important role disease progression and response to treatment. Secreted LIF was significantly correlated with the secreted levels of bFGF, VEGF-A and IL-8 in the matched TCM of treatment-naïve OAC tumour explants. Basic FGF, similar to LIF, is a pleiotropic factor which was shown to promote cell growth, angiogenesis and differentiation and to prevent apoptosis in cancer [387]. Interestingly, in patients with bone sarcomas, increased serum levels of tumour-promoting cytokines, including IL-6, IL-8 and VEGF significantly correlated with poor overall survival [388]. LIF and bFGF are potent growth factors which have been previously shown to stimulate cancer growth in osteosarcoma [369, 389]. In osteosarcoma cells, bFGF was found to enhance cancer growth through hyper-activation of ERK 1/2 [389]. Both alone and in combination, LIF and bFGF were found to significantly enhance cell growth of osteosarcoma cells. Importantly, when they were administered together, this produced an additive effect on tumour growth, highlighting a synergistic interplay between both factors [389]. Anti-bFGF antibodies were shown to enhance radiosensitivity in oesophageal SCC through a reduction in colony formation *in-vitro* [382]. In addition, targeting of bFGF by a peptide has been shown to improve chemo-sensitivity in CRC [390]. These findings in the literature and within our study show that LIF and bFGF together both play important roles in cancer progression and treatment response in many cancers and may influence both OAC cells and host immunity by functioning as part of the active cytokine network. Given the ability of both bFGF and LIF to enhance radiosensitivity in previous studies and the strong correlation between both factors in OAC, the potential of the combined targeting to enhance radiosensitivity in OAC strongly warrants further investigation.

Furthermore, secreted VEGF-A was significantly correlated with LIF in the OAC tumour microenvironment. VEGF-A is a well-known tumorigenic mediator which plays a key role in angiogenesis, a process tightly linked with treatment resistance. Targeting of VEGF-A *in-vivo* was shown to enhance radiation response in a head and neck xenograft model [107]. It is unsurprising that LIF, a potent tumorigenic growth factor is strongly associated with VEGF-A, given the necessity of tumour vasculature to promote tumour growth and survival. Given the significant relationship we have shown between LIF and treatment resistance in OAC, and the known role of VEGF-A in tumorigenesis and treatment response, the potential of targeting both mediators to enhance response should be explored in future.

In addition, LIF was found to significantly correlate with IL-8, a pro-inflammatory cytokine which signals through the CXCR1/2 receptors. This signalling results in PI3K, MAPK and JAK2 pathway activation, and has been found to promote cell proliferation, angiogenesis and metastasis in xenograft models where administration of an anti-IL-8 monoclonal antibody attenuated tumour

growth and metastatic potential [137]. IL-8 expression has previously been correlated with LIF expression in other inflammatory diseases such as psoriasis [391]. Furthermore, both IL-8 and VEGF-A have been shown to play an important role in tumour angiogenesis, a key process involved in treatment resistance which, when inhibited with targeted therapy, can enhance radiation response *in-vivo* [107, 137].

Given the pivotal role of LIF, bFGF, VEGF-A and IL-8 in tumorigenesis and their correlated secretion in OAC, the potential of targeting these growth factors and cytokines to improve patient response to neo-adjuvant treatment and to inhibit tumour progression in OAC must be investigated in future studies. Whilst targeting all 4 mediators simultaneously may not be clinically feasible, this study offers insight into potential mediators which could be targeted to enhance radiosensitivity and possible compensatory mediators which may be upregulated in response to such targeting, possibly providing novel mechanistic insight into resistance mechanisms that may arise following targeting of one of the mediators in isolation. This study also highlights the potential of sequential targeting of these factors to overcome resistance and improve treatment response.

OAC tumours do not function in isolation and interaction of the tumour with the host plays a significant role in tumour progression. The recent successes of immunotherapies in the clinic highlight the key role of the host immune system in tumour control, thus we investigated the relationship between LIF and immune cell tumour infiltration. LIF secretion from the tumour microenvironment was negatively correlated to percentage of lymphocyte infiltrate in matched OAC pre-treatment biopsies. The negative correlation between LIF and lymphocyte infiltration, where LIF secretion from the tumour microenvironment is increased in patients with low tumour infiltrating lymphocytes (TILs) is a significant finding, given that high lymphocyte infiltration has been previously associated with improved patient outcome in SCC and many other cancer types. TILs are thought to play a pivotal role in tumour control through activation of the host anti-tumour immune response [392]. In addition, higher TILs have been associated with improved prognosis in breast, colon, ovarian and lung cancer [393-395]. The relationship between LIF secretion and immune activation is relatively under-explored in cancer, and it is unknown whether elevated LIF secretion in biopsies with reduced lymphocyte infiltrate is a causal relationship or if this is just an association which could have the potential to determine response of patients to treatment [392, 396]. It is however important to note that immune cell infiltration analysis was carried out on pre-treatment diagnostic OAC biopsies which only represent a very small portion of tumour and the invasive edge was not represented in these biopsies and thus inflammatory infiltrate of the invasive edge could not be analysed. It will be critical to evaluate the effect of

targeting the LIF pathway, not only in terms of treatment response but also on immune cell activation and infiltration in OAC.

Furthermore, using a multiplex ELISA approach we sought to investigate differences in inflammatory protein secretions in our isogenic model of OAC radioresistance and importantly the effect of Pyrazinib (P3) treatment on inflammatory secretions. Nine of 30 detected inflammatory and angiogenic factors were secreted at significantly higher levels in OE33R radioresistant cells when compared to OE33P cells; IL-8, IL-4, IL-6, IL-2, IL-12p70, IL-10, MCP-1, IP-10 and ICAM highlighting the potential importance of these inflammatory and angiogenic mediators in radioresistance in OAC. Pyrazinib (P3) significantly reduced the secretions of IL-6, IL-8, IL-4 and IL-13 *in-vitro* in OE33R cells. Inflammation plays a critical role in disease outcome in OAC, given the increased risk of cancer development and poor outcome for obese patients where altered secretion of adipokines and cytokines from adipose tissue contributes a pro-tumorigenic environment [397, 398]. A previous study by our group showed a significant increase in oesophageal and colorectal tumour cell proliferation following culture with conditioned media from visceral adipose tissue of centrally obese patients which may be linked to the higher levels of IL-6 and VEGF found in this tissue [399]. IL-6 and its family members have been repeatedly linked with radioresistance in multiple tumour types including nasopharyngeal, liver, prostate, oral, and oesophageal cancer [228, 400-404]. In a prostate cancer model, IL-6 inhibition enhanced radiosensitivity, an effect which was associated with increased IR-induced ROS and oxidative DNA damage *in-vitro* and inhibition of IL-6 protein expression in combination with ionising radiation attenuated angiogenesis and decreased tumour regrowth *in-vivo* [402]. In addition, IL-6 signalling was reported to promote radioresistance through enhanced DNA repair and prevention of apoptosis in CD133+ stem-like cells of lung cancer after radiation [400]. Furthermore, IL-8 has also previously been linked with tumour radioresistance and in our study both in the proteomic screen and multiplex ELISA IL-8 was secreted at significantly higher levels from OE33R cells than OE33P cells [140]. Let-7c, a tumour suppressor microRNA, was shown to restore radiosensitivity and impair stemness of oral cancer cells through inhibition of IL-8 secretion [140]. In another study, in a radioresistant nu61 oral squamous cell carcinoma xenograft, the administration of IL-8 and IL-6 neutralising antibodies sensitised the tumours to irradiation which supports our findings that inhibition of both IL-6 and IL-8 can enhance radiosensitivity [405]. In addition, similar to our findings, IL-6 and IL-8 were present at higher levels in radioresistant tumours when compared to the parental radiosensitive oral SCC tumours, further supported by our findings where IL-8 is positively correlated with radioresistant mediator LIF *ex-vivo* [405]. Furthermore, IL-4 and IL-13 are closely related cytokines which have also been previously linked with radioresistance, where the blockade of IL-4/IL-13 mediated phosphorylation of STAT6 produced a decrease in M2 polarization of macrophages and was

protective against macrophage-mediated radioresistance of inflammatory breast cancer [406]. Given the association of IL-6, IL-8, IL-4 and IL-13 with tumour growth and treatment resistance in the literature, the inhibition of secretion of these cytokines by Pyrazinib (P3) may further augment its anti-cancer effect. In summary, Pyrazinib (P3), a novel anti-angiogenic and anti-metabolic compound, can significantly enhance radiosensitivity in an isogenic model of OAC radioresistance and is associated with anti-inflammatory activity through its inhibition of IL-6, IL-8, IL-4 and IL-13 secretion from OE33R cells. IL-1RA is an anti-inflammatory cytokine which was secreted at significantly lower levels from OE33R cells compared to OE33P. The administration of IL-1RA to osteosarcoma cells was found to significantly decrease IL-1 induced secretion of IL-8 and IL-6 and was associated with reduced angiogenesis and invasiveness [388], although Pyrazinib (P3) did not directly affect IL-1RA secretion, it would be of interest to further investigate the action of Pyrazinib (P3) on the IL-1 pathway in the future.

In this chapter we have shown an association between expression of the IL-6 family member LIF and treatment response in OAC, both in *in-vitro* cell line models, and in pre-treatment OAC patient serum and biopsies. LIF secretion and expression is elevated in radioresistant cells *in-vitro*. Importantly, circulating LIF is elevated in patients with a subsequent poor response to neo-adjuvant treatment, implicating this pathway in treatment resistance in OAC. LIF secreted *ex-vivo*, from human OAC treatment-naïve biopsies, correlates with the secretion of key tumorigenic growth factors, including bFGF, VEGF-A and IL-8, indicating that these factors are tightly associated with one another in the tumour microenvironment of OAC. A significant finding of this study is the negative correlation of LIF, which we have identified as a poor prognostic factor in OAC, with percentage of tumour infiltrating lymphocytes which have been reported to play a key role in the host response to tumour and serve as a marker of prognosis in multiple cancer types [396]. The use of LIF as a circulating marker of treatment response in OAC needs to be validated in a larger patient cohort following this pilot study. Furthermore, given the increased secretion of LIF from our radioresistant cells following irradiation, and the tight association of secreted LIF with other pro-tumorigenic factors from our OAC patient tumours, targeting of the LIF pathway to boost treatment response warrants investigation in future studies in OAC. In addition, Pyrazinib (P3) was shown to have significant anti-inflammatory activity through its inhibition of IL-6, IL-8, IL-4 and IL-13 inflammatory cytokine secretions in OE33R cells. Importantly, *in-vitro* studies utilise tumour cells grown in a monolayer without the supporting stromal cells, endothelial cells and immune cells and it is possible the action of our novel dual action compounds may be altered in the complex *in-vivo* tumour microenvironment. To further progress our studies, it will be critical to evaluate the effect of our lead radiosensitising compound, Pyrazinib (P3), *ex-vivo* in human pre-treatment OAC biopsies which is the focus of the next chapter.

Aspects of this chapter have been published in *Oncotarget* and *Cancer Letters* see **Figure 5-11** and **Figure 5-12** .

www.oncotarget.com Oncotarget, 2018, Vol. 9, (No. 72), pp: 33634-33647

Research Paper

Leukaemia inhibitory factor is associated with treatment resistance in oesophageal adenocarcinoma

Amy M. Buckley[1], Niamh Lynam-Lennon[1], Susan A. Kennedy[1], Margaret R. Dunne[1], John J. Aird[2], Emma K. Foley[1], Niamh Clarke[1], Narayanasamy Ravi[1], Dermot O'Toole[3], John V. Reynolds[1], Breandán N. Kennedy[4] and Jacintha O'Sullivan[1]

[1]Department of Surgery, Trinity Translational Medicine Institute, Trinity College Dublin, Dublin, Ireland
[2]Department of Histopathology and Morbid Anatomy, School of Medicine, Trinity College Dublin, Dublin, Ireland
[3]Department of Clinical Medicine, Trinity Translational Medicine Institute, Trinity College Dublin, Dublin, Ireland
[4]UCD Conway Institute & UCD School of Biomolecular and Biomedical Science, University College Dublin, Dublin, Ireland

Correspondence to: *Jacintha O'Sullivan,* ***email:*** *OSULLIJ4@tcd.ie*

Keywords: *LIF; oesophageal cancer; LIFR; treatment resistance; radiation*

Received: *May 05, 2018* ***Accepted:*** *July 13, 2018* ***Published:*** *September 14, 2018*

Copyright: Buckley et al. This is an open-access article distributed under the terms of the Creative Commons Attribution License 3.0 (CC BY 3.0), which permits unrestricted use, distribution, and reproduction in any medium, provided the original author and source are credited.

Figure 5-11 Leukaemia inhibitory factor is associated with treatment resistance in oesophageal adenocarcinoma.
Aspects of this chapter have been published in *Oncotarget* [235].

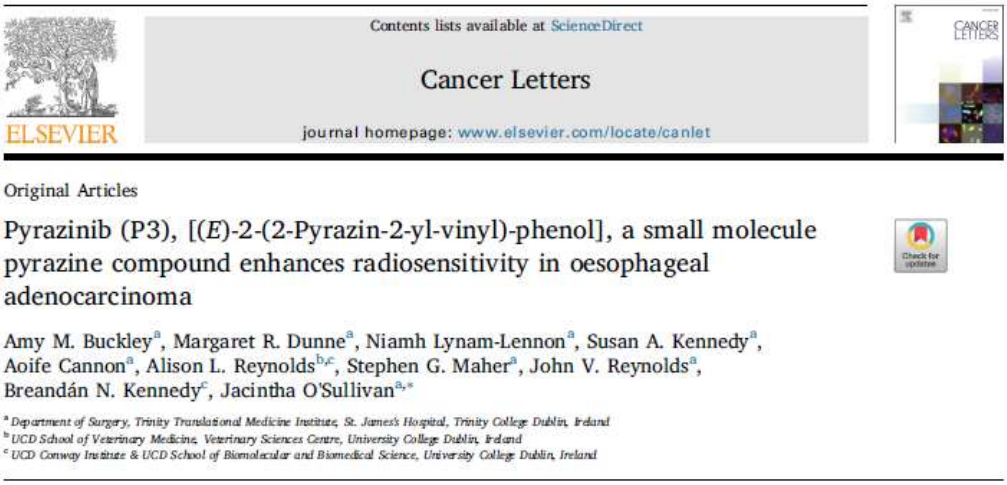

Contents lists available at ScienceDirect

Cancer Letters

journal homepage: www.elsevier.com/locate/canlet

Original Articles

Pyrazinib (P3), [(*E*)-2-(2-Pyrazin-2-yl-vinyl)-phenol], a small molecule pyrazine compound enhances radiosensitivity in oesophageal adenocarcinoma

Amy M. Buckley[a], Margaret R. Dunne[a], Niamh Lynam-Lennon[a], Susan A. Kennedy[a], Aoife Cannon[a], Alison L. Reynolds[b,c], Stephen G. Maher[a], John V. Reynolds[a], Breandán N. Kennedy[c], Jacintha O'Sullivan[a,*]

[a] *Department of Surgery, Trinity Translational Medicine Institute, St. James's Hospital, Trinity College Dublin, Ireland*
[b] *UCD School of Veterinary Medicine, Veterinary Sciences Centre, University College Dublin, Ireland*
[c] *UCD Conway Institute & UCD School of Biomolecular and Biomedical Science, University College Dublin, Ireland*

Figure 5-12 Pyrazinib (P3), [(E)-2-(2-Pyrazin-2-yl-vinyl)-phenol], a small molecule pyrazine compound enhances radiosensitivity in oesophageal adenocarcinoma.
Aspects of this chapter have been published in *Cancer Letters* [285].

6. Chapter 6 Real-time metabolic profiling reveals an altered and adaptive metabolic phenotype of oesophageal adenocarcinoma tumours

6.1. Introduction

In the previous chapters we have repeatedly alluded to the altered metabolic phenotype identified both *in-vitro* in an isogenic model of OAC radioresistance and *ex-vivo* in fixed OAC tumour tissue [82]. However, to date, metabolic rate has not yet been assessed in real-time in OAC biopsies *ex-vivo*. Understanding the real-time metabolic rate of human OAC treatment-naïve biopsies may provide novel insight into the detailed metabolic phenotype of OAC tumours and possible mechanisms of treatment resistance. Furthermore, by assessing metabolism in real-time *ex-vivo* there is the added opportunity to evaluate novel anti-metabolic agents in this human *ex-vivo* model system. In addition, we investigated whether Pyrazinib (P3) altered inflammatory protein secretions and the expression of dendritic cell maturation markers.

Whilst Warburg initially found cancer cells to be reliant on aerobic glycolysis numerous studies also support the functional role of oxidative phosphorylation in tumorigenesis [119]. Real-time metabolic profiling of OAC biopsies may support the findings at the *in-vitro* level which demonstrated mitochondrial respiration is a predominant metabolic pathway used by OAC cancer cells [82]. Numerous studies have evaluated the mitochondrial function of tumour cells and reported that tumour cells predominantly have functional mitochondria which have retained the ability to carry out oxidative phosphorylation. Furthermore, the depletion of mitochondrial DNA was shown to reduce the tumorigenic potential of cancer cells both *in-vitro* and *in-vivo* [121, 407, 408]. Of note, it has been suggested that the 'Warburg effect' could in fact be a regulated metabolic pathway in cancer cells which can be used during periods of increased metabolic demand as opposed to an adaption to defective respiration [122].

In addition to investigating the effect of Pyrazinib (P3) on metabolic rate *ex-vivo*, in this chapter we also investigated the effect of Pyrazinib (P3) on inflammatory secretions. Inflammation has been shown to play a critical role in both tumour progression and treatment resistance. In addition, inflammation and metabolism are tightly linked biological processes as inflammatory cells rely on metabolites generated from the metabolic cycle to maintain their function. Thus we investigated whether any anti-metabolic activity of Pyrazinib (P3) was accompanied by changes in inflammatory secretions *ex-vivo*.

Solid malignancies trigger an intrinsic inflammatory response that builds up a pro-tumorigenic microenvironment, through the production of chemokines and cytokines which can then recruit inflammatory cell such as neutrophils, macrophages, dendritic cells and lymphocytes to the tumour microenvironment [409]. Of which, TAMs and T cells are often the most prominent leukocytes present in a tumour [126, 410]. Pro-tumorigenic cytokines promote tumour

inflammation through several different mechanisms. For example, TNF-α produced by tumour cells or inflammatory cells in the tumour microenvironment can promote tumour cell survival through the induction of genes encoding NF-κB–dependent anti-apoptotic molecules and can also stimulate tissue remodelling [411]. IL-6 is a pleiotropic cytokine which actively promotes inflammation through the activation of signal transducer and activator of transcription 3 (STAT3) which protects cancer cells from apoptosis [412].

Furthermore, inflammation has also been shown to act as a negative regulator of neo-adjuvant treatment response in OAC [15, 234]. In the previous chapter we demonstrated circulating levels of leukaemia inhibitory factor in pre-treatment serum of OAC patients was higher in patients with a subsequent poor pathological response to neo-adjuvant treatment [235]. Additionally, as previously mentioned C3a and C4a, components of the complement system are upregulated in the pre-treatment serum of OAC patients having a poor pathological response to neo-CRT, when compared to patients having a favourable response to treatment [15]. In this chapter, following on from our *in-vitro* work in chapter 5 we sought to characterise the inflammatory secretome of TCM generated from OAC treatment-naïve biopsies and correlate this to the metabolic profile of matched OAC patient samples.

In this chapter for the first time we have demonstrated in real-time that OAC tumour biopsies have a significantly higher OCR, a measure of oxidative phosphorylation compared to ECAR, a measure of glycolysis highlighting the importance of aerobic respiration in OAC. Furthermore, biopsies from OAC tumours can adapt their metabolic rate to their environment to cope with severe levels of hypoxia. Pyrazinib (P3), an anti-metabolic small molecule radiosensitiser significantly inhibited oxygen consumption rate in OAC biopsies. Furthermore, under hypoxic conditions, Pyrazinib (P3) produced a simultaneous and significant reduction in both OCR and ECAR in OAC treatment-naïve biopsies. The inflammatory secretome profile from OAC treatment-naïve biopsies is highly heterogeneous. OCR was significantly correlated with three secreted factors in the TCM: VEGF-A, IL-1RA and TSLP. Extracellular acidification rate was significantly correlated with VEGF-A, IL-1RA, TSLP, IL-13, MIP-3α and TNF-α. Pyrazinib (P3) significantly inhibited IL-1β secretion and increased IL-3 and IL-17B secretion from treatment-naïve biopsies from OAC patients. Circulating levels of TNF-α, IL-6, IL-8 and IL-1β in OAC treatment-naïve serum are not significantly correlated with patient clinical characteristics. Critically Pyrazinib (P3) did not directly alter the expression of dendritic cell maturation markers indicating Pyrazinib (P3) does not negatively affect dendritic cell functions. We present a new method for profiling the metabolic rate of tumour biopsies in real-time and demonstrate the novel anti-metabolic and anti-inflammatory action of Pyrazinib (P3) *ex-vivo* in OAC treatment-naïve biopsies.

6.2. Overall Objective and specific aims of chapter 6

The overall objective of chapter 6 was to evaluate the effect of Pyrazinib (P3) treatment on real–time metabolic rate and inflammatory secretions in human OAC treatment-naïve biopsies.

The specific aims of chapter 6 were:

1. Evaluate real-time metabolic rate of OAC treatment-naïve biopsies to establish the metabolic nature of OAC tumours.
2. Evaluate the effect of Pyrazinib (P3) treatment on real-time metabolic rate in OAC patient biopsies.
3. Evaluate the effect of hypoxic culture on the metabolic rate of human OAC biopsies and evaluate the effect of Pyrazinib (P3) treatment under these conditions.
4. Measure lactate secretion from OAC pre-treatment biopsies.
5. Determine inflammatory protein secretions from OAC treatment-naïve biopsies by multiplex ELISA.
6. Investigate the effect of Pyrazinib (P3) treatment on inflammatory protein secretions *ex-vivo* from OAC treatment-naïve biopsies.
7. Correlate real-time metabolic rate with inflammatory protein secretions of matched OAC pre-treatment biopsies.
8. Evaluate the levels of circulating IL-8, IL-6, IL-1β and TNF-α in serum of treatment-naïve OAC patients and correlate with patient characteristics.
9. Investigate the effect of Pyrazinib (P3) treatment and the OAC tumour microenvironment on the expression of dendritic cell maturation markers, to further understand the crosstalk between the tumour microenvironment and immune cell function.

6.3. Methods

6.3.1. *Patient samples*

Following ethical approval (Joint St James's Hospital/AMNCH ethical review board) and written informed consent, diagnostic biopsy specimens were taken from patients with a diagnosis of operable OAC, by a qualified endoscopist, prior to neo-adjuvant therapy. Histologic confirmation of tumour tissue in biopsies was performed by a pathologist using routine haematoxylin and eosin staining. All patient tumour used in this study were taken prior to the initiation of neo-adjuvant treatment.

6.3.2. *Real-time metabolic profiling of OAC tumour biopsies*

Following informed consent, 3 biopsies per patient were collected at endoscopy, immediately placed on saline-soaked gauze and were transported within 10 min to the laboratory. Each biopsy was placed into a separate well of a 24 well XF24 Islet Capture Microplate (Agilent Technologies, Santa Clara, CA, USA) containing 1 mL M199 medium (Gibco) supplemented with 10% FBS (Gibco), 1 μg/mL insulin (Sigma) and 1% penicillin/streptomycin (Gibco). 1 mL of complete M199 was placed in the four background control wells. A XF24 capture screen was placed over each biopsy to prevent the biopsy touching utility plate probes during assay. The XF24 microplate was placed at 37°C for 30 min to allow biopsies to equilibrate. Three basal measurements of OCR and ECAR were taken over 24 min consisting of three repeats of mix (3 min) / wait (2 min) / measurement (3 min) to establish basal respiration, using a Seahorse Biosciences XFe24 analyser (Agilent Technologies, Santa Clara, CA, USA). Basal respiration of each patient was established by taking the average OCR and ECAR, readout from the three individual biopsies obtained from same patient. Following basal metabolic profiling of biopsies, capture screens were removed and biopsies and corresponding media were transferred to a new XF24 islet capture microplate and treated with one of the following; 0.1% DMSO (control), 6 μM of oligomycin (positive control) or 10 μM of our compound Pyrazinib (P3). Following treatment biopsies were cultured for 24 h at 37°C in 5% CO_2/95% air. Following 24 h culture, a capture screen was placed on each biopsy and three basal measurements of OCR and ECAR were taken over 24 min consisting of three repeats of mix (3 min) / wait (2 min) / measurement (3 min) to establish the effect of drug treatment with our novel small molecule Pyrazinib (P3) on OCR and ECAR. The effect of treatment was determined as the percentage change in metabolic rate readout from the baseline reading of each individual biopsy to the reading following treatment of that individual biopsy. The metabolic rate of each biopsy was normalised to protein content using the BCA assay (Pierce).

6.3.3. *Real-time metabolic profiling of OAC tumour biopsies under hypoxia (0.5% O_2)*

Basal metabolic rate was determined as described in the previous section. Following evaluation of basal OCR and ECAR using the Seahorse Biosciences XFe24 analyser; biopsies and corresponding media were transferred to a new XF24 islet capture microplate and cultured in the Whitley H35 hypoxystation (Don Whitley Scientific) at 0.5% O_2 at 37°C in 5% CO_2 for 6 h. Following 6 h culture, capture screens were placed over each biopsy in each well and the plate was transferred to Whitley i2 workstation containing the XFe24 Seahorse analyser being maintained at 0.5% O_2. Real-time OCR and ECAR were assessed under 0.5% O_2, three measurements of OCR and ECAR were taken over 24 min consisting of three repeats of mix (3 min) / wait (2 min) / measurement (3 min) to establish the effect of a 6 h hypoxia culture on real-time metabolic rate in OAC patient biopsies. Following metabolic profiling of biopsies, capture screens were removed and biopsies and corresponding media were transferred to a new XF24 islet capture microplate and treated with one of the following; 0.1% DMSO (control), 6 µM of Oligomycin (positive control) or 10 µM of our novel compound Pyrazinib (P3) for 14 h under 0.5% O_2 at , 37°C in 5% CO_2 . Following 14 h treatment, real-time OCR and ECAR measurements were taken over 24 min consisting of three repeats of mix (3 min) / wait (2 min) / measurement (3 min) whilst the Seahorse Biosciences XFe24 analyser was maintained under 0.5% O_2 to establish the effect of treatment on metabolic rate of OAC biopsies maintained under 0.5% O_2. Following metabolic profiling, capture screens were removed and biopsies were snap frozen and both biopsies and TCM were stored at -80°C.

6.3.4. *Generation TCM from OAC treatment-naïve biopsies*

Biopsies were placed in culture as follows: biopsies were placed into a well of a 12 well plate containing 1 mL complete M199 medium (Gibco). Biopsies were treated with 0.1% DMSO or 10 µM of Pyrazinib (P3). Following 24 h culture, TCM was collected and stored at -80°C.The remaining tissue was snap-frozen in liquid nitrogen and stored at -80°C.

6.3.5. *Lactate assay*

Lactate levels were assessed in TCM using a colorimetric lactate assay kit which measures L(+)-lactate concentration in biological samples. The highest standard was prepared by diluting the lactate standard to 1nmol/µL in lactate assay buffer. A 2-fold serial dilution was carried out to generate 7 standards, with the 8th standard being lactate assay buffer alone. Samples were diluted 1:20 in lactate assay buffer and 50µL/well standard or sample was added in duplicate. 50µL/well reaction mix (46µL lactate assay buffer, 2µL lactate probe, 2µL lactate enzyme mix) was added and mixed well. The reaction was incubated for 30 min at RT in the dark. The absorbance was measured at 570nm using a VersaMax microplate reader (Molecular Devices, Sunnyvale, CA,

USA). A standard curve was generated and sample values were interpolated. Values were normalised to protein content as determined by the BCA assay (Pierce).

6.3.6. *Multiplex Enzyme Linked Immunosorbent Assay (ELISA) of 54 proteins*

OAC patient treatment-naïve TCM were defrosted on ice. The secretion of cytokines and angiogenic growth factors were analysed by ELISA as per the manufacturer's instructions. To assess angiogenic, vascular injury, inflammatory cytokine and chemokine secretions, a 54 multiplex kit spread across 7 plates was used (Meso Scale Diagnostics, USA). The 54 multiplex kit was used to quantify the secretions of CRP, Eotaxin, Eotaxin-3, FGF (basic), GM-CSF, ICAM-1, IFN-γ, IL-10, IL-12/IL-23p40, IL-12p70, IL-13, IL-15, IL-16, IL-17A, IL-17A/F, IL-17B, IL-17C, IL-17D, IL-1RA, IL-1α, IL-1β, IL-2, IL-21, IL-22, IL-23, IL-27, IL-3, IL-31, IL-4, IL-5, IL-6, IL-7, IL-8, IL-8 (HA), IL-9, IP-10, MCP-1, MCP-4, MDC, MIP-1α, MIP-1β, MIP-3α, PIGF, SAA, TARC, Tie-2, TNF-α, TNF-β, TSLP, VCAM-1, VEGF-A, VEGF-C, VEGF-D and VEGFR-1/Flt-1 from OAC TCM previously treated with 10 μM Pyrazinib (P3) or vehicle control (0.1% DMSO) for 24 h. Secretion data for all factors was normalised appropriately to protein content using the BCA assay (Pierce). Data was analysed using MSD Discovery Workbench software version 4.0.

6.3.7. *Multiplex Enzyme Linked Immunosorbent Assay (ELISA) of TNF-α, IL-6, IL-8 and IL-1β*

OAC patient treatment-naïve serum samples were defrosted on ice. The secretion of TNF-α, IL-6, IL-8 and IL-1β were analysed by ELISA as per the manufacturer's instructions using a 4-plex kit (Meso Scale Diagnostics, USA). Data was analysed using MSD Discovery Workbench software version 4.0.

6.3.8. *Dendritic cell isolation and culture*

Human monocyte-derived immature dendritic cells were generated from peripheral blood mononuclear cells (PBMCs) obtained from buffy coat preparations (National Blood Centre, St. James's Hospital, Dublin) by density gradient centrifugation (Lymphoprep) as described [413, 414]. Briefly, monocytes were isolated by positive selection using anti-CD14 magnetic microbeads as described by the manufacturer (Miltenyl Biotec) and seeded at a density of 1 x 10^6 cells/mL in 6-well plates in 3 mL of RPMI-1640 medium containing 10% defined HyClone FBS (Thermo Scientific), 1% penicillin/streptomycin, 1% fungizone, human granulocyte macrophage colony-stimulating factor (50 ng/mL; Immunotools), and human IL-4 (70 ng/mL; Immunotools) in a humidified atmosphere with 5% CO_2 at 37°C. Cells were fed at day 3 by replacing half the medium, made up with fresh cytokines. At day 6, CD11c+ cells exhibited an immature dendritic cell phenotype capable of upregulating maturation markers following LPS stimulation.

6.3.9. *Stimulation of monocyte-derived dendritic cells*

Freshly generated dendritic cells were plated in 96-well plates at 2 x 10^5 cells in 200 µL RPMI-1640 media supplemented with 10% dened Hyclone FBS (Thermo Scientific) and stimulated with a 1:2 dilution of TCM from tumour explants or cell culture supernatants for 4-5 hours before exposure to 10 µg/ml of ultrapure TLR4 agonist *Escherichia coli* lipopolysaccharide (LPS-EB; Invivogen) overnight. Supernatants were harvested and frozen, and cells were assessed for expression of surface markers.

6.3.10. *Flow cytometry*

Dendritic cells were stained with the following antibodies: Pe-Cy7- anti-CD83, Brilliant Violet 421- anti-PD-L1, Brilliant Violet 510- anti-CD11c, allophycocyanin (APC)- anti-CD54, and APC-Cy7- anti-HLA-DR (Biolegend). Samples were acquired on DAKO CyAn flow cytometer (Beckman Coulter) with compensation performed with positive and negative compensation beads (BD Biosciences) stained with the antibodies and the data were analyzed with FlowJo software (Tree Star Inc.) [413, 414].

6.3.11. *Statistical analysis*

Statistical analysis was performed using GraphPad Prism version 5 software (GraphPad Software, CA, USA). Scientific data were expressed as mean ±SEM. SEM was calculated as the standard deviation of the original samples divided by the square root of the sample size. Specific statistical tests used are indicated in figure legends. For all statistical analysis, differences were considered to be statistically significant at $p<0.05$.

6.4. Results

6.4.1. *Oxidative Phosphorylation was significantly higher than glycolysis in OAC treatment-naïve biopsies*

ATP5B, a marker of oxidative phosphorylation was previously shown to be expressed at higher levels in OAC treatment-naïve biopsies of patients who had a subsequent poor response to treatment [82]. In this chapter for the first time we investigated real-time metabolic rate to understand the importance of aerobic respiration in live OAC biopsies. Real-time metabolic rate was measured in fresh OAC treatment-naïve biopsies using the Seahorse Biosciences XFe24 analyser. Real-time metabolic profiling of 17 live OAC pre-treatment biopsies demonstrated that biopsies from OAC treatment-naïve tumours have a significantly higher oxygen consumption rate (OCR), a measure of oxidative phosphorylation, compared to extracellular acidification rate (ECAR), a measure of glycolysis (p=0.0005), highlighting the importance of aerobic respiration in OAC tumours **(Figure 6-1A,B)**. The rate of OCR and ECAR was heterogeneous across our patient cohort. Clinical patient characteristics of patient cohort used in this study are outlined **Table 6-1** and **Table 6-2**.

To investigate the relationship between real-time metabolic rate and clinical patient characteristics, OCR and ECAR were divided according to nodal status, tumour stage, stage of differentiation, body mass index, TRG, age at diagnosis and gender of the 17 patients evaluated in this study. OCR and ECAR were shown to be independent of clinical patient characteristics, **(Figure 6-2A-F, Figure 6-3A-F)**. Furthermore, no significant differences in the OCR: ECAR ratio were identified when divided according to clinical patient characteristics **(Figure 6-4A-F).**

In summary, OAC treatment-naïve biopsies have a significantly higher rate of OCR, a measure of oxidative phosphorylation than, ECAR, a measure of glycolysis and real-time metabolic rate is not significantly associated with clinical patient characteristics.

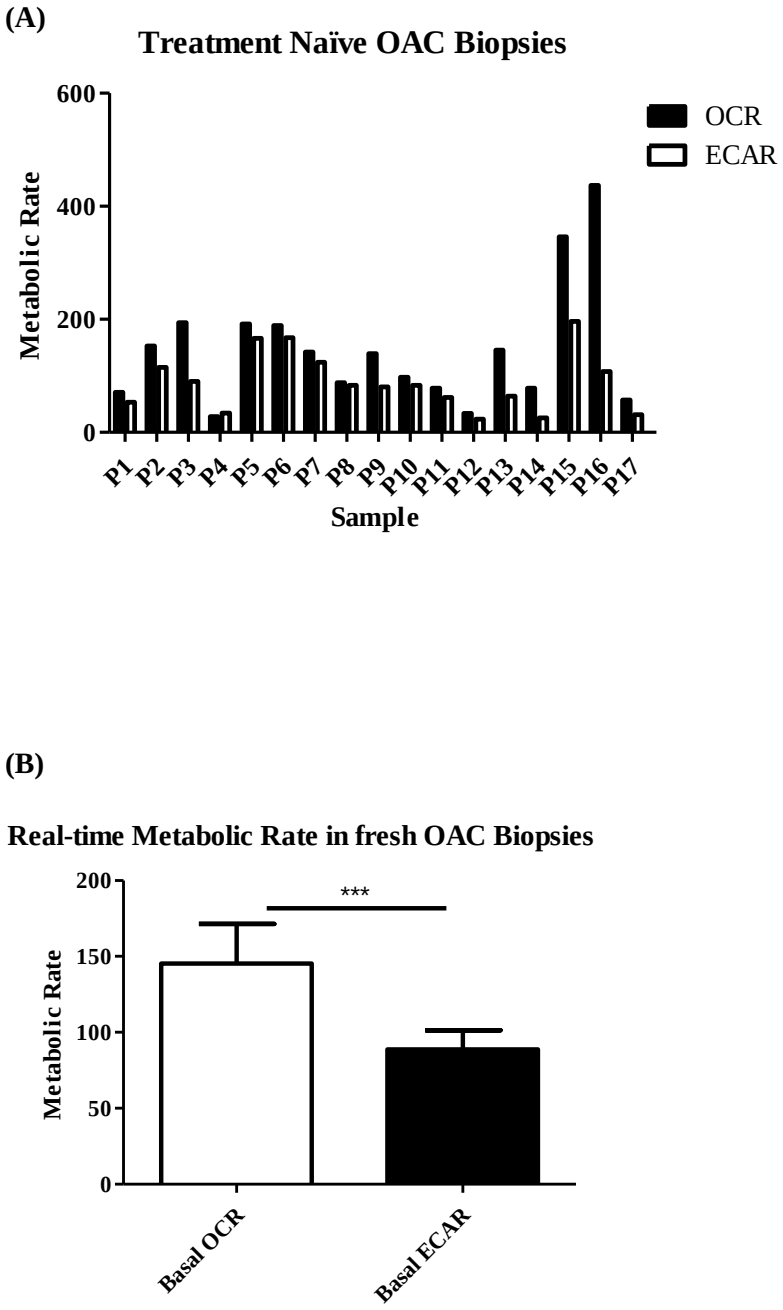

Figure 6-1 Oxygen consumption rate is significantly higher than extracellular acidification rate in OAC treatment-naïve biopsies.

OCR a measure of oxidative phosphorylation and ECAR, a measure of glycolysis were assessed in real-time in OAC treatment-naïve biopsies using the Seahorse BiosciencesXFe24 Analyser. **(A)** Basal OCR and ECAR rates in OAC pre-treatment biopsies, (n=17). **(B)** OCR is significantly elevated in OAC treatment-naïve biopsies, (n=17), paired t-test, ***$p<0.001$. Data expressed as +SEM.

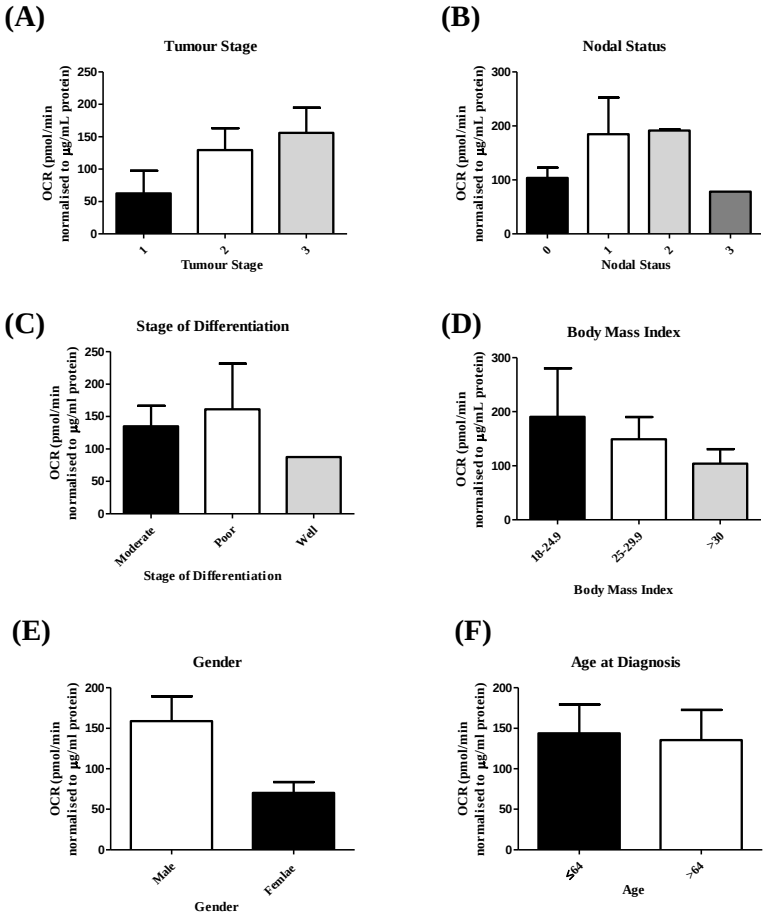

Figure 6-2 Real-time oxygen consumption rate is not significantly linked with clinical patient characteristics in OAC pre-treatment biopsies.

Baseline OCR readings of OAC treatment-naïve biopsies divided according to **(A)** Tumour Stage (n=16), **(B)** Nodal Status, (n=17), **(C)** Stage of Differentiation, (n=16), **(D)** Body Mass Index, (n=16), **(E)** Gender (n=17) and **(F)** Age at Diagnosis, (n=17). Mann Whitney U test. Data expressed as +SEM.

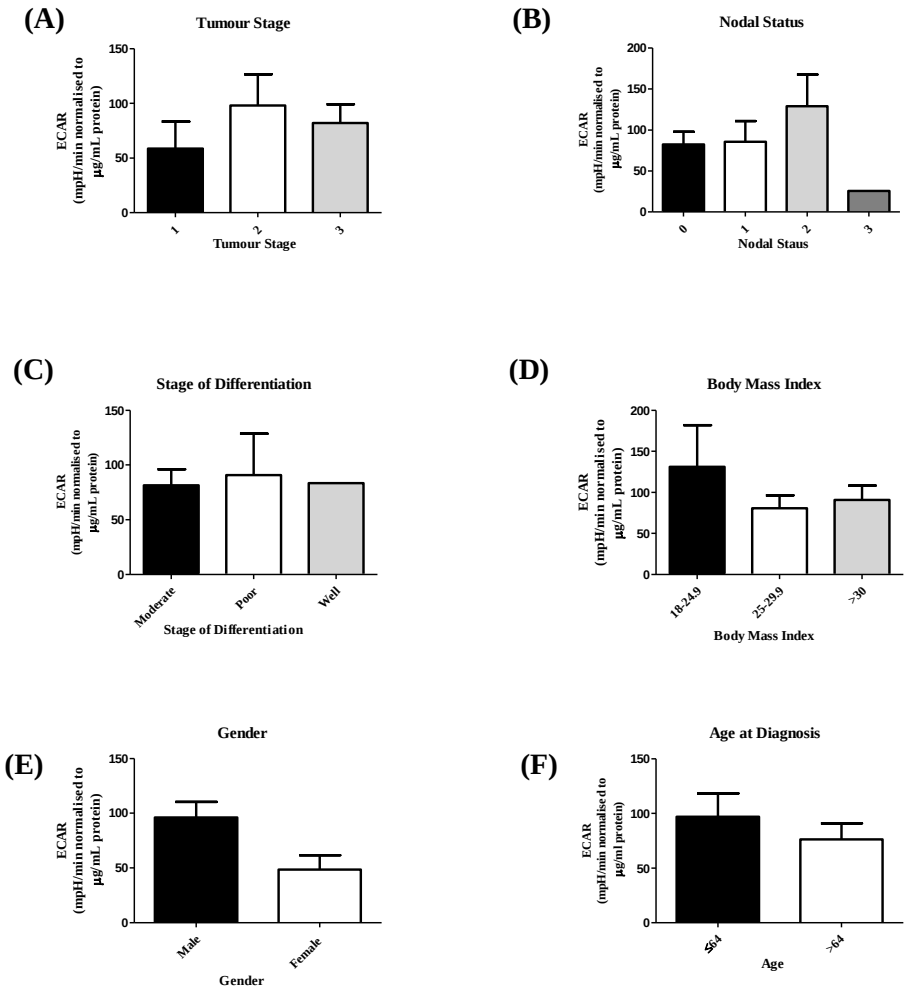

Figure 6-3 Real-time extracellular acidification rate is not significantly linked with clinical patient characteristics in OAC pre-treatment biopsies.

Baseline ECAR readings of OAC treatment-naïve biopsies divided according to **(A)** Tumour Stage (n=16), **(B)** Nodal Status, (n=17), **(C)** Stage of Differentiation, (n=16), **(D)** Body Mass Index, (n=16), **(E)** Gender (n=17) and **(F)** Age at Diagnosis, (n=17). Mann Whitney U test. Data expressed as +SEM.

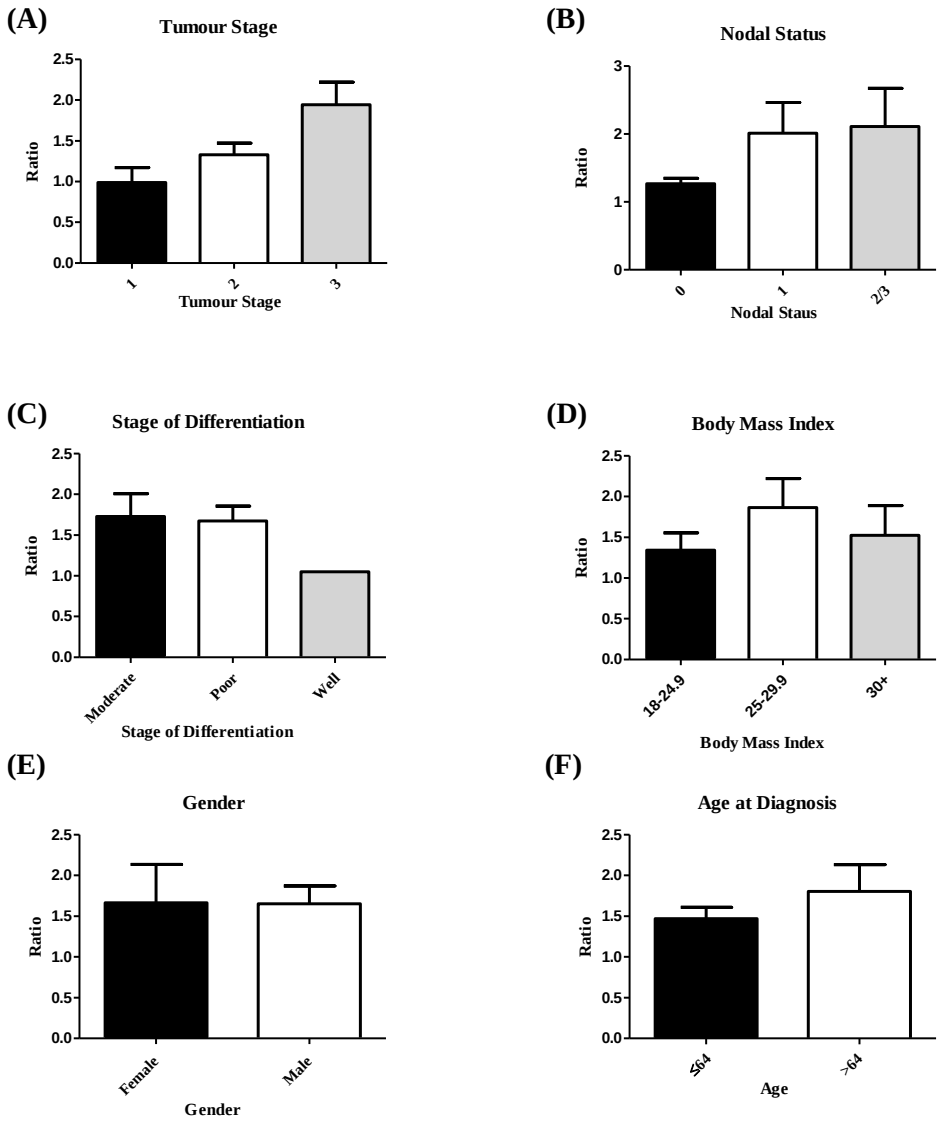

Figure 6-4 The OCR: ECAR ratio of OAC treatment-naïve biopsies is not significantly correlated with clinical patient characteristics.

Baseline OCR: ECAR ratio of OAC treatment-naïve biopsies divided according to **(A)** Tumour Stage (n=16), **(B)** Nodal Status, (n=17), **(C)** Stage of Differentiation, (n=16), **(D)** Body Mass Index, (n=16), **(E)** Gender, (n=17), and **(F)** Age at diagnosis, (n=17). Mann Whitney U test. Data expressed as +SEM.

6.4.2. *Pyrazinib (P3) significantly inhibited oxygen consumption rate in OAC treatment-naïve biopsies*

In the previous section we demonstrated in real-time the OAC treatment-naïve biopsies are metabolically active. In this section we investigated the effect of Pyrazinib (P3) on real-time metabolic rate in OAC treatment-naïve biopsies and we evaluated the difference between baseline metabolic rate and metabolic rate following 24 h treatment with Pyrazinib (P3) in OAC treatment-naïve biopsies in 10 of 17 patients samples evaluated in **Figure 6-1**, patient characteristics of the patient cohort evaluated in this study are outlined in **Table 6-1**.

Pyrazinib (P3) significantly inhibited OCR in OAC treatment-naïve biopsies (p=0.0039) **(Figure 6-5A)**. Pyrazinib (P3) produced a ~ 35% reduction in OCR compared to the baseline OCR reading. Oligomycin, an ATP synthase inhibitor, was used as a positive control in this experiment and produced a significant reduction in OCR (p=0.0098) **(Figure 6-5A)**. No significant change in metabolic rate was seen following treatment with the 0.1% DMSO control from baseline OCR **(Figure 6-5A)**. To determine if the reduction in OCR following treatment with Pyrazinib (P3) was dependant on certain clinical patient characteristics, the percentage reduction in OCR was divided according to the following clinical patient characteristics: nodal status, tumour stage, stage of differentiation and body mass index **(Figure 6-6A,C,E,G)**. The percentage reduction in OCR was independent of clinical patient characteristics.

Treatment with Pyrazinib (P3) did not significantly alter ECAR in OAC treatment-naïve biopsies **(Figure 6-5B)**. Percentage change in ECAR following treatment with Pyrazinib (P3) was independent of clinical patient characteristics: nodal status, tumour stage, stage of differentiation and body mass index **(Figure 6-6B,D,F,H)**.

Pyrazinib (P3) significantly inhibits OCR in OAC treatment-naïve biopsies and this effect is independent of clinical patient characteristics.

Table 6-1 Clinical patient characteristics of patient cohort used in normoxia metabolism study. This table details the clinical patient characteristics of the 10 patients whose biopsies were used to investigate the effective of Pyrazinib (P3) on real-time metabolic rate under normoxic conditions.

	n=10
Male	8
Female	2
Median age at diagnosis	70.5 (57-80)
Median BMI at diagnosis	27.7 (24.3-30.8)
Tumour Stage	
1	2
2	3
3	4
Not Specified	1
Nodal Status	
0	7
1	1
2	2
Not Specified	
Stage of Differentiation	
Poor	3
Moderate	5
Well	1
Not Specified	1
Tumour Regression Grade	
3	4
4	1
Not specified	5

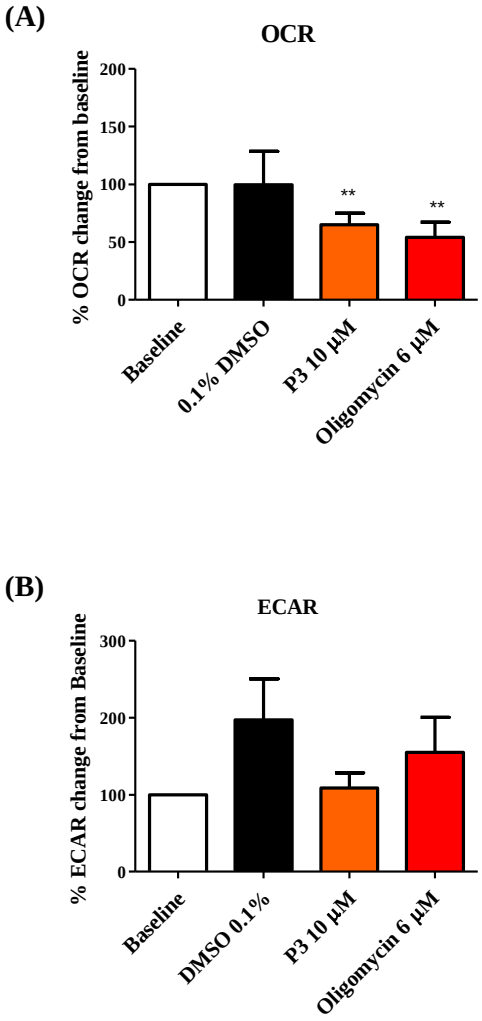

Figure 6-5 Pyrazinib (P3) significantly reduces oxygen consumption rate in OAC treatment-naïve biopsies.

OCR and ECAR were measured in real-time using Seahorse Biosciences XFe24 analyser. **(A)** Percentage change from baseline of OCR following treatment with 0.1% DMSO control, 10 µM Pyrazinib (P3) or 6 µM oligomycin for 24 h, (n=10), Wilcoxon paired t-test, *p<0.05. **(B)** Percentage change from baseline of ECAR following treatment with 0.1% DMSO control, 10 µM Pyrazinib (P3) or 6 µM Oligomycin for 24 h, (n=10), Wilcoxon paired t-test. Data are expressed as +SEM.

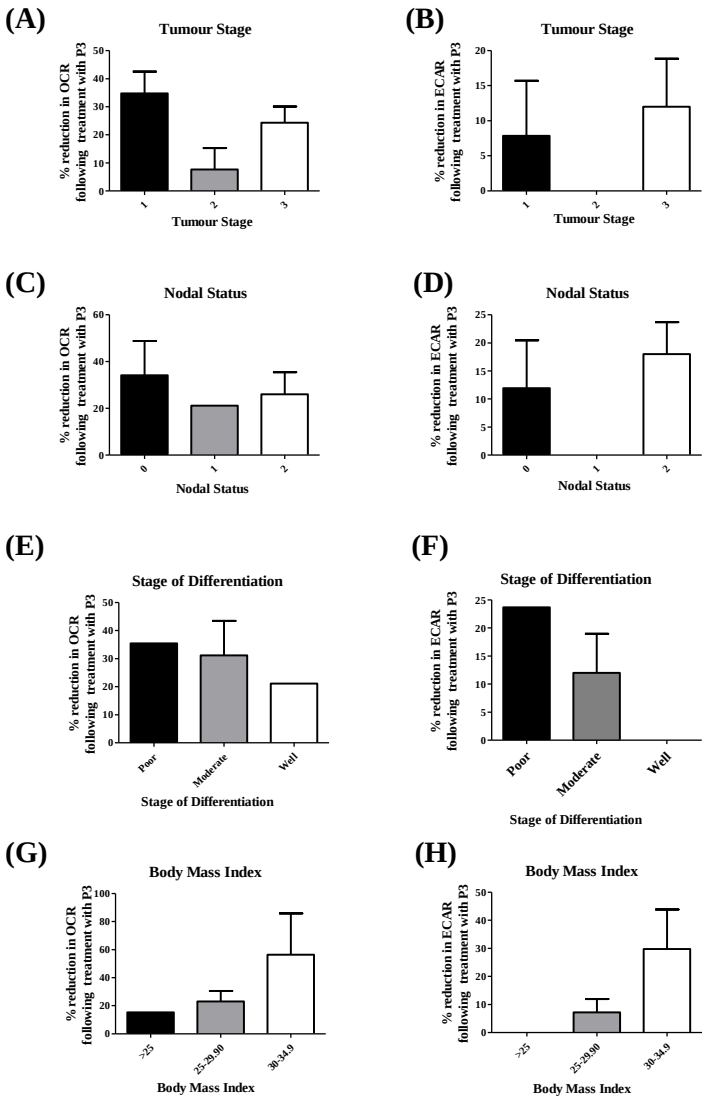

Figure 6-6 The anti-metabolic activity of Pyrazinib (P3) is not dependant on clinical patient characteristics.

OCR and ECAR were measured in real-time using Seahorse Biosciences XFe24 analyser. Percentage reduction of OCR following 24 h treatment with Pyrazinib (P3) was divided according to **(A)** Tumour Stage, (n=9), **(C)** Nodal Status (n=9), **(E)** Stage of differentiation (n=9), and **(G)** Body Mass Index (n=9). Percentage reduction of ECAR following 24 h treatment with P3 was divided according to **(D)** Tumour Stage, (n=9), **(F)** Nodal Status, (n=9), **(H)** Stage of differentiation, (n=9) and **(I)** Body Mass Index, (n=9). Mann-Whitney U test. Data are expressed as +SEM.

6.4.3. *Pyrazinib (P3) significantly inhibited real-time metabolic rate in OAC treatment-naïve biopsies cultured under hypoxia (0.5% O_2)*

Hypoxic tumours are inherently resistant to treatment thus we investigated both real-time metabolic rate and the action of Pyrazinib (P3) under hypoxic conditions of 0.5% O_2 in OAC treatment-naïve patient biopsies.

To determine if OAC biopsies adapt their metabolic rate to changes in oxygen levels we evaluated real-time basal metabolic rate under normoxia and real-time metabolic rate of the same biopsies again following culture in 0.5% O_2 for 6 h. Basal metabolic rate of 7 patients which were also evaluated in **Figure 6-1**, demonstrates OCR is significantly higher than ECAR under normoxic conditions (p=0.0156) **(Figure 6-7A)**. Clinical patient characteristics of the patient cohort used in this study are outlined in **Table 6-2**. In contrast to OAC biopsies cultured under normoxic conditions, following culture of OAC treatment-naïve biopsies under 0.5% O_2 no significant differences were observed between OCR and ECAR **(Figure 6-7A)**. The ratio of OCR:ECAR was significantly higher in OAC treatment-naïve biopsies at baseline under normoxic conditions compared to the same biopsies cultured under hypoxia for 6 h (p=0.0469) **(Figure 6-7B)**. Furthermore the ECAR:OCR ratio was significantly higher in the OAC treatment-naïve biopsies following culture in hypoxia compared to when the same biopsies were analysed at baseline under normoxia (p=0.0469) **(Figure 6-7C)**. The shift in metabolic phenotype in conditions of different oxygen concentrations highlights the ability of the OAC treatment-naïve biopsies to adapt to their local microenvironment whereby there is a shift from oxidative phosphorylation to glycolysis under hypoxic conditions.

Pyrazinib (P3) significantly inhibited OCR under hypoxia, producing a ~41% reduction real-time oxygen consumption compared baseline metabolic rate under hypoxia in OAC treatment-naïve patient biopsies (p=0.0022) **(Figure 6-8A)**. Additionally, Pyrazinib (P3) simultaneously and significantly inhibited real-time ECAR, a measure of glycolysis under hypoxia (p=0.0313) **(Figure 6-8B)**. Pyrazinib (P3) produced a ~52% reduction in ECAR under hypoxia. In summary, our studies demonstrate the ability of OAC patient biopsies to dynamically adapt their metabolic rate in real-time to cope with changes in oxygen concentration in their local environment. Additionally, Pyrazinib (P3) can significantly reduce OCR and ECAR under hypoxic conditions *ex-vivo* in OAC treatment-naïve patient biopsies.

Table 6-2 Clinical patient characteristics of patient cohort used in hypoxia metabolism study and hypoxia multiplex ELISA study

This table details the clinical patient characteristics of the 7 patients whose biopsies were used to investigate real-time metabolic rate under normoxic and hypoxic conditions, only 6 of these patients biopsies were used to evaluate the effect of Pyrazinib (P3) on real-time metabolic rate under hypoxic conditions due to limited patient material for one patient.

	n=7
Male	7
Female	0
Median Age at diagnosis	68 (54-83)
Median BMI at diagnosis	27.2(21.2-30)
Tumour Stage	
3	7
Nodal Status	
0	2
1	4
3	1
Stage of Differentiation	
Poor	2
Moderate	5
Tumour Regression Grade	
1	1
2	1
3	0
4	1
5	1
Not specified	3

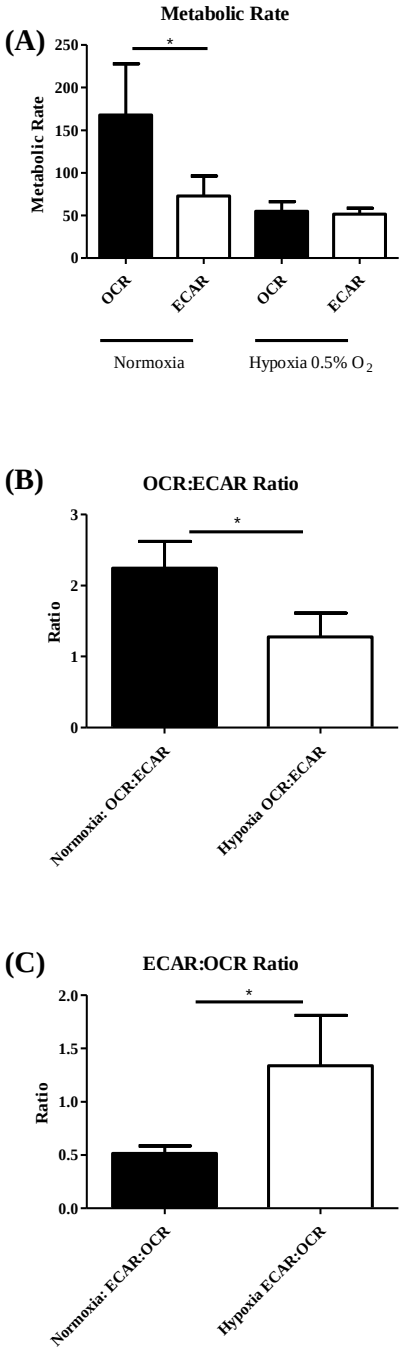

Figure 6-7 OAC treatment-naïve patient biopsies have an altered metabolic phenotype under hypoxic conditions (0.5% O_2).

OCR and ECAR were measured in real-time using Seahorse Technology. **(A)** Basal OCR and ECAR at baseline and post 6 h incubation under hypoxia 0.5% O_2, (n=7). **(B)** OCR:ECAR ratio of OAC pre-treatment biopsies cultured under normoxic and then hypoxic conditions, (n=7). **(C)** ECAR:OCR ratio of OAC treatment-naïve biopsies cultured under normoxic and then hypoxic conditions, (n=7). Wilcoxon signed rank t-test, *p<0.05. Data expressed as +SEM.

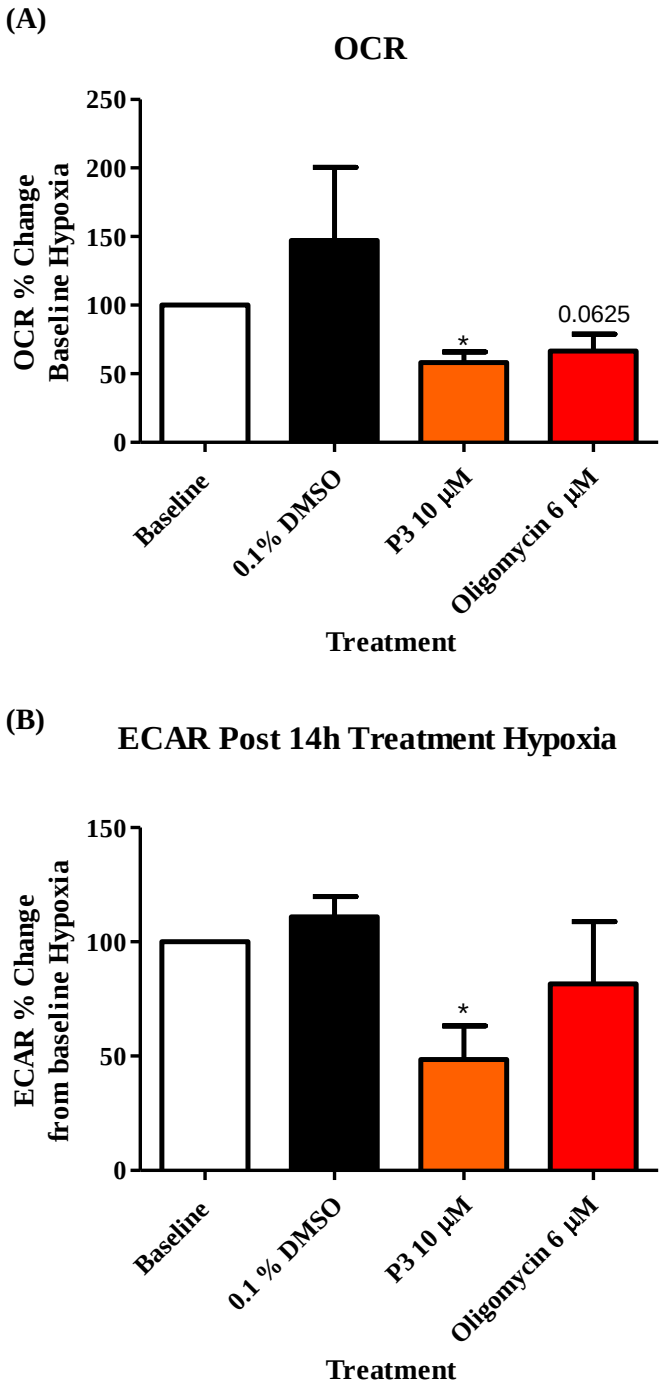

Figure 6-8 Pyrazinib (P3) significantly inhibits OCR and ECAR in OAC patient biopsies cultured under hypoxia (0.5% O_2).
(A) Percentage change from baseline OCR under hypoxia (0.5% O_2) to OCR following treatment with 0.1% DMSO control, 10 µM Pyrazinib (P3) or 6 µM Oligomycin under 0.5 % O_2, (n=6). **(B)** Percentage change from baseline ECAR under hypoxia to ECAR following treatment with 0.1% DMSO control, 10 µM Pyrazinib (P3) or 6 µM Oligomycin under 0.5 % O_2, (n=6). Wilcoxon signed rank t-test,*p<0.05. Data expressed as mean +SEM.

6.4.4. *Pyrazinib (P3) treatment does not significantly alter lactate secretion from treatment-naïve OAC patient biopsies*

As previously described, an altered metabolic phenotype is associated with treatment resistance and a more aggressive tumour type. Given the altered metabolic phenotype observed in OAC treatment-naïve biopsies in the previous results sections, we investigated the effect of Pyrazinib (P3) treatment on lactate secretion and if lactate secretion, a surrogate marker of aerobic glycolysis, was associated with clinical patient parameters in OAC patients.

Treatment with 10 μM Pyrazinib (P3) did not significantly alter lactate secretion from OAC treatment-naïve biopsies compared to 0.1% DMSO control treated biopsies **(Figure 6-9A)**. Furthermore, secreted levels of lactate were not significantly associated with clinical patient characteristics including tumour stage, nodal status, stage of differentiation and body mass index **(Figure 6-9B-E)**.

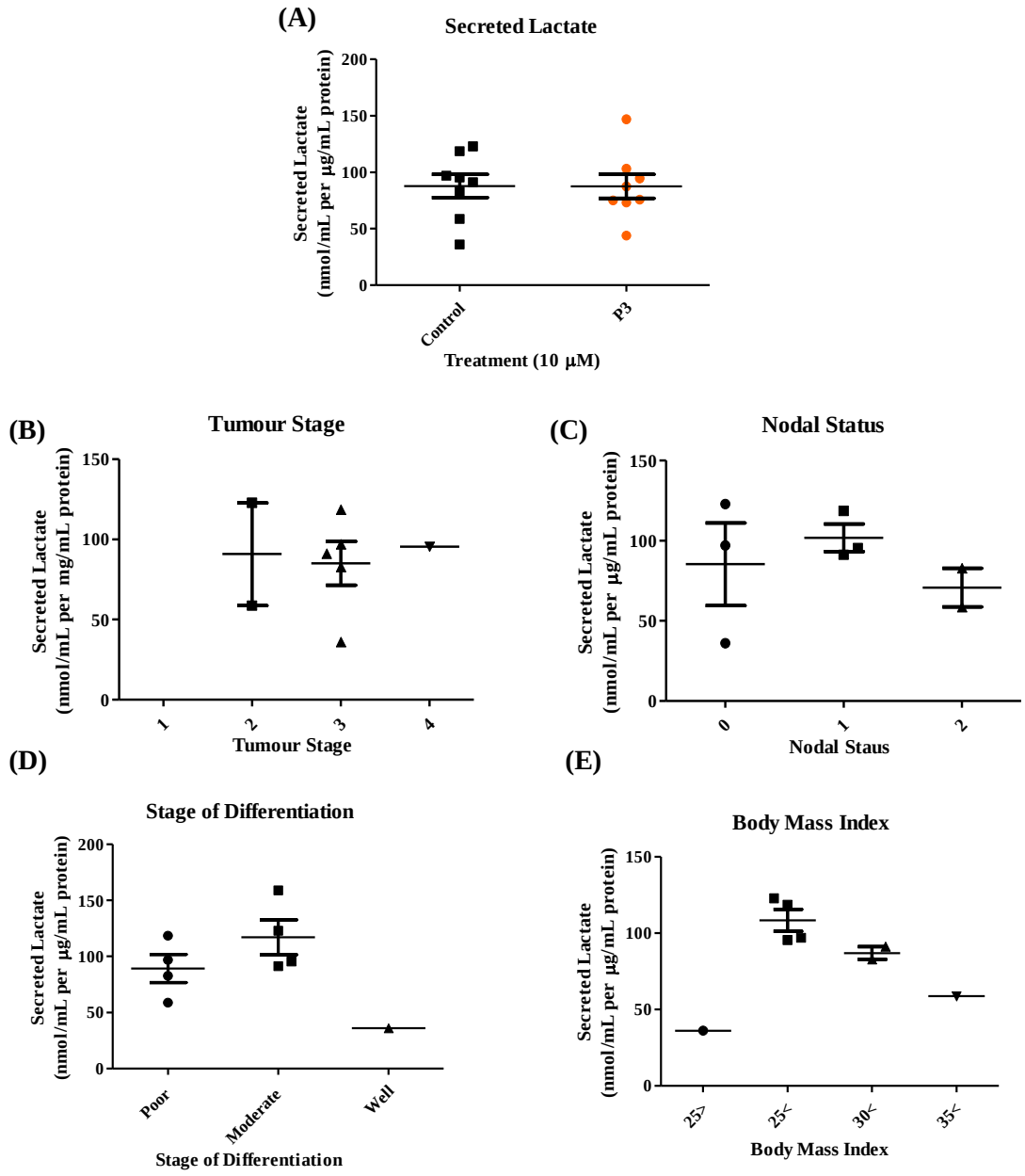

Figure 6-9 Pyrazinib (P3) does not significantly alter the secretion of lactate from OAC patient biopsies.

(A) Secreted lactate levels in OAC treatment-naïve biopsies treated with 0.1% DMSO or 10 µM Pyrazinib (P3), Wilcoxon signed rank t-test, (n=9). Secreted levels of lactate divided according to **(B)** Tumour Stage, **(C)** Nodal Status, **(D)** Stage of Differentiation and **(E)** Body Mass Index, (n=9). Mann Whitney U test. Data expressed as ±SEM.

6.4.5. *OAC treatment-naïve biopsies have a heterogeneous inflammatory secretome*

In addition to an altered metabolic phenotype, inflammation has also been reported to play a significant role in the progression and treatment response of OAC tumours [234, 415]. To profile the inflammatory secretome of OAC treatment-naïve biopsies we cultured 22 patient biopsies for 24 h and evaluated the secreted levels of 54 proteins in the TCM by multiplex ELISA. The clinical patient characteristics for the patient cohort used in this study are outlined in **Table 6-3**. The secreted levels of 54 proteins were separated into five different panels including inflammatory, angiogenesis and vascular injury, chemokine, cytokine and TH17 proteins. Secreted levels of inflammatory proteins IL-13, IFN-γ, TNF-α, IL-6, IL-8, IL-12p70, IL-4, IL-10, IL-2 and IL-1β from OAC treatment-naïve biopsies are shown in **Figure 6-10A**. Secreted levels of angiogenic and vascular injury proteins Flt-1, VEGF-A, b-FGF, PIGF, VEGF-C, TIE-2, VEGF-D, VCAM, SAA, CRP and ICAM from OAC treatment-naïve biopsies are shown in **Figure 6-10B**. Chemokine protein secretion including MIP-1α, MIP-1β, MCP, TARC, MCP-4, IP-10, Eotaxin, Eotaxin-3, MDC, and IL-8(HA) from OAC treatment-naïve biopsies are illustrated in **Figure 6-10C**. Secreted levels of cytokine proteins IL-12/IL-23p40, IL-17D, IL-17A, IL-17C, IL-17-A/F, IL-23,IL-3, IL-9, IL-17B, GM-CSF, IL-7, IL-15, TNFβ, IL-1RA, IL-1α, IL-15, TSLP and IL-5 from OAC treatment-naïve biopsies are shown in **Figure 6-10D**. TH17 pathway protein secretions of TH17/IL-17, IL-31, IL-21, IL23, IL-22, IL-27 and MIP-3α from OAC treatment-naïve biopsies are shown in **Figure 6-10E**.

Notably there is a high level of variability of the secreted levels of the proteins detected in this screen, highlighting the high level of heterogeneity between OAC treatment-naïve patient biopsies. Five proteins were notably detected at very high levels in OAC treatment-naïve patient biopsies including IL-6 **(Figure 6-10A)**, IL-8 **(Figure 6-10A)**, intracellular adhesion molecule-1 (ICAM-1) **(Figure 6-10B)**, C - reactive protein (CRP) **(Figure 6-10B)** and interleukin-1 receptor antagonist (IL1-RA) (**Figure 6-10D**). The inflammatory profile of OAC tumour biopsies generated from these OAC samples highlights the complex nature of OAC tumours which have an active inflammatory phenotype.

Furthermore, no significant associations were seen when secreted inflammatory factors were divided according to clinical patient characteristics.

Table 6-3 Clinical patient characteristics of patient cohort used in multiplex ELISA and dendritic cell study.
This table details the clinical patient characteristics of the 22 patients whose biopsies were used to investigate the inflammatory secretions from control and Pyrazinib (P3) treated TCM.

	n=22
Male	18
Female	4
Median age at diagnosis	67 (43-84)
Median BMI at diagnosis	27.9 (23.5-38.5)
Tumour Stage	
1	3
2	5
3	12
4	1
Not Specified	1
Nodal Status	
0	7
1	11
2	4
Stage of Differentiation	
Poor	9
Moderate	10
Well	2
Not Specified	1
Tumour Regression Grade	
1	1
2	0
3	6
4	2
5	2
Not specified	11

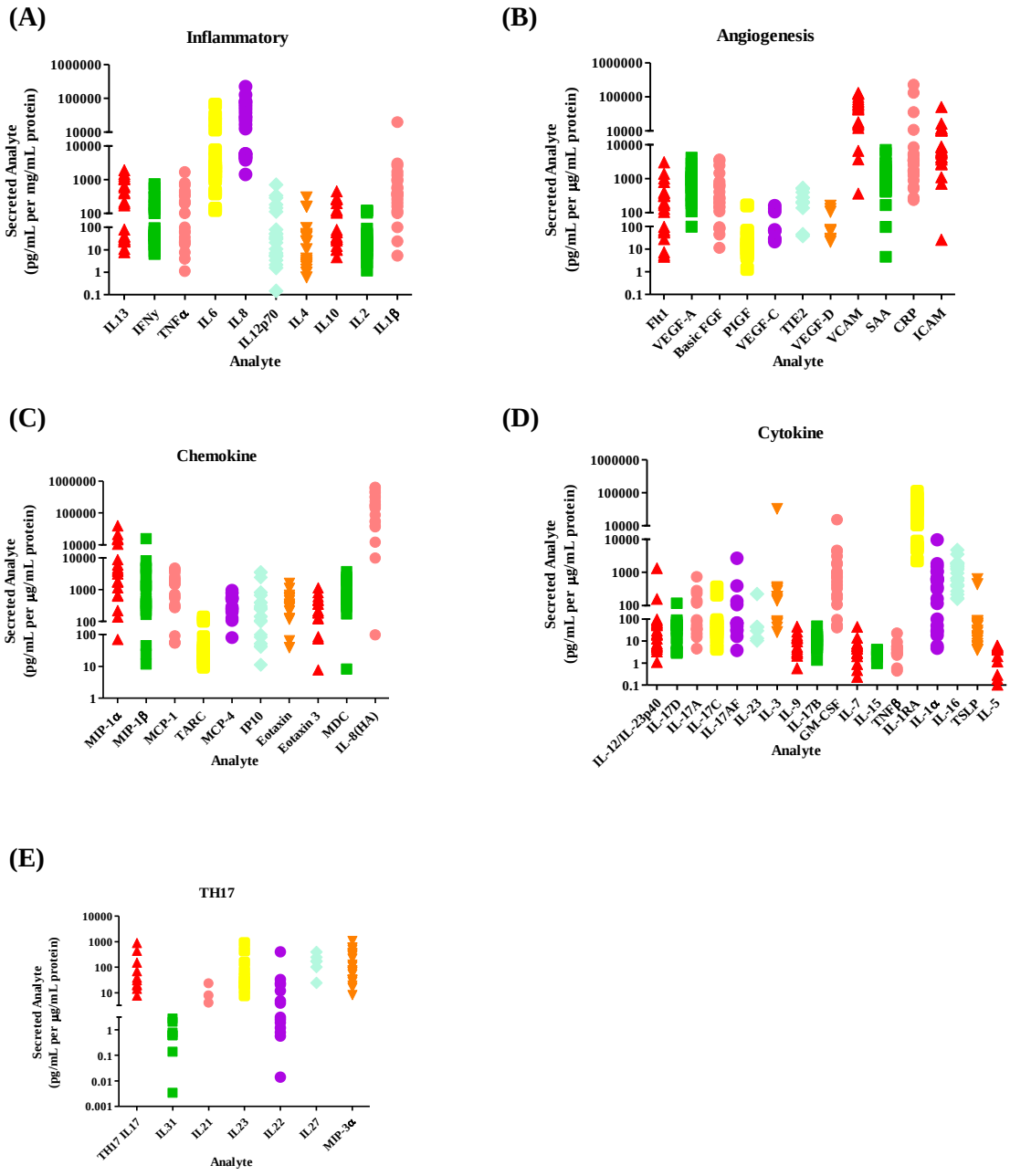

Figure 6-10 Secreted levels of 54 proteins from n=22 OAC treatment-naïve biopsies cultured for 24 h were evaluated by multiplex ELISA.

(A) Secreted levels of inflammatory proteins IL-13, IFN-γ, TNF-α, IL-6, IL-8, IL-12p70, IL-4, IL-10, IL-2 and IL-1β from OAC treatment-naïve biopsies. **(B)** Secreted levels of angiogenic and vascular injury proteins Flt1, VEGF-A, BasicFGF, PIGF, VEGF-C, TIE-2, VEGF-D, VCAM, SAA, CRP and ICAM from OAC treatment-naïve biopsies**. (C**) Secreted levels of chemokine proteins MIP-1α, MIP-1β, MCP, TARC, MCP-4, IP10, Eotaxin, Eotaxin-3, MDC, and IL-8(HA) from OAC treatment-naïve biopsies**. (D**) Secreted levels of cytokine proteins IL-12/IL-23p40, IL-17D, IL-17A, IL-17C, IL-17-A/F, IL-23,IL-3, IL-9, IL-17B, GM-CSF, IL-7, IL-15, TNF-β, IL-1RA, IL-1α, IL-15, TSLP and IL-5 from OAC treatment-naïve biopsies**. (E)** Secreted levels TH17 pathway proteins TH17/IL-17, IL-31, IL-21, IL23, IL-22, IL-27 and MIP3α from OAC treatment-naïve biopsies, (n=22). Data normalised to protein content.

6.4.6. *Real-time metabolic rate is significantly correlated with inflammatory secretions in OAC tumour biopsies*

To investigate the relationship between real-time metabolic rate (OCR and ECAR) and the inflammatory protein secretions in OAC treatment-naïve biopsies we correlated basal metabolic rate to inflammatory secretions in 10 matched patients. The patient characteristics of the patient samples used in this study are outlined in **Table 6-1.**

OCR was significantly correlated with ECAR, (r=0.8505, $p<0.0001$). In addition, OCR was significantly correlated with the secreted levels of 3 proteins in the TCM including VEGF-A (r=0.7091, $p=0.0268$), IL-1RA (r=0.7939, $p=0.0088$) and Thymic stromal lymphopoietin (TSLP) (r=.6727, $p=0.0390$) shown in **Table 6-4A**. ECAR, a measure of glycolysis, was significantly correlated with oxygen consumption rate (r=0.8505, $p<0.0001$) and the secreted levels of 6 proteins in the TCM including VEGF-A (r=0.8303,p=0.0047), IL-1RA (r=0.7455,p=0.0174), TSLP, (r=0.6727, $p=0.0390$), IL-13 (IL-13) (r=0.7212, $p=0.0234$), Tumour necrosis factor alpha (TNF-α) (r=0.6606, $p=0.0438$) and Macrophage Inflammatory Protein 3 Alpha (MIP-3α) (r=0.6606, $p=0.0438$) shown in **Table 6-4B.** (IL-13 was below the level of detection in one patient so correlation could only be calculated in 9 of 10 matched patients).

Inflammatory protein secretions are significantly correlated with the real-time measures of metabolic rate; OCR and ECAR.

Table 6-4 Correlation of Metabolic rate with protein secretions in matched OAC treatment-naïve biopsies.

The protein secretions of 54 mediators analysed by multiplex ELISA were correlated with real-time metabolic rate readouts; OCR and ECAR of matched patient biopsies. **(A)** OCR was significantly correlated with rate of ECAR and the secreted levels of 3 of 54 proteins including VEGF-A, IL-1RA and TSLP in matched OAC treatment-naïve biopsies (n=10) **(B)** ECAR, a measure of glycolysis, was significantly correlated with rate of ECAR and the secreted levels of 6 of 54 proteins including VEGF-A, IL-1RA, MIP-3α, TNF-α, IL13 and TSLP in matched OAC treatment-naïve biopsies. Secretions from explant tissue and metabolic rate were normalised to protein content. Spearman correlations; Spearman r 0.4-0.59 moderate, 0.6-0.79 strong, 0.8-1.0 very strong; *p<0.05, **p<0.01.

(A) Correlation with Oxygen Consumption Rate

Factor	R Value	P Value	Significance	n
ECAR	0.8505	<0.0001	***	17
VEGF-A	0.7091	0.0268	*	10
IL-1RA	0.7939	0.0088	**	10
TSLP	0.6727	0.0390	*	10

(B) Correlation with Extracellular Acidification Rate

Factor	R Value	P Value	Significance	n
OCR	0.8505	<0.0001	***	17
VEGF-A	0.8303	0.0047	**	10
IL-1RA	0.7455	0.0174	*	10
MIP-3α	0.6606	0.0438	*	10
TNF-α	0.6606	0.0438	*	10
IL-13	0.7212	0.0234	*	10
TSLP	0.7697	0.0126	**	9

6.4.7. *Pyrazinib (P3) significantly altered the secretion of IL-1β, IL-3 and IL-17B in OAC treatment-naïve biopsies*

As previously mentioned, OAC is an inflammatory driven cancer and altering inflammatory secretions may have an anti-tumour effect. To investigate if our anti-metabolic pyrazine compound Pyrazinib (P3) also altered inflammatory secretions *ex-vivo*, we cultured OAC treatment-naïve biopsies with 10 μM Pyrazinib (P3) or 0.1% DMSO for 24 h and compared the inflammatory secretions from the OAC treatment-naïve biopsies of the same patient.

Of the 54 factors screened for in the multiplex ELISA, Pyrazinib (P3) treatment was found to significantly alter the secretions of 3 proteins: IL-1β, IL-3 and IL-17B. Treatment with Pyrazinib (P3) significantly reduced the secretions of IL-1β from OAC treatment-naïve tumour biopsies (p=0.0377) **(Figure 6-11A)**. In contrast Pyrazinib (P3) significantly increased the secretions of IL-3 (p=0.0020) and IL-17B (p=0.0181) *ex-vivo* in OAC treatment-naïve biopsies (**Figure 6-11B,C**).

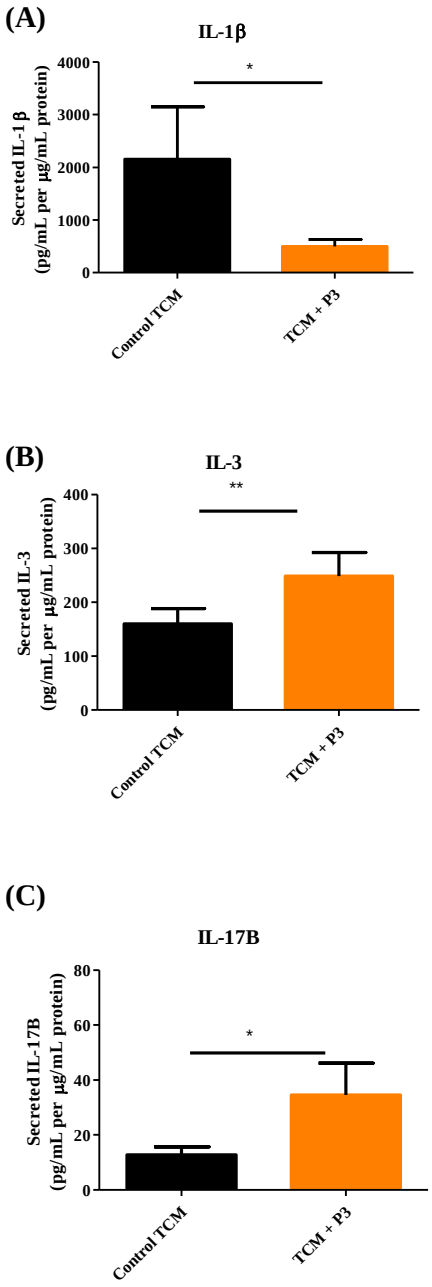

Figure 6-11 Pyrazinib (P3) significantly reduces secretion of IL-1β and increases secretion of IL-3 and IL-17B from OAC treatment biopsies.

The effect of 24 h treatment of OAC treatment-naïve biopsies with 0.1% DMSO or 10 µM Pyrazinib (P3) on protein secretion was assessed by multiplex ELISA. **(A)** Pyrazinib (P3) significantly reduced the secretion of IL-1β from OAC treatment-naïve biopsies, (n=22). **(B)** Pyrazinib (P3) significantly increases the secretion of IL-3 from OAC pre-treatment biopsies, (n=15). **(C)** Pyrazinib **(**P3) significantly increases the secretion of IL-17B from OAC pre-treatment biopsies, (n=15). Wilcoxon signed rank t-test,*p<0.05, **p<0.01. All data normalised to protein content. Data expressed as +SEM.

6.4.8. *Pyrazinib (P3) does not significantly alter the secretion of inflammatory proteins from OAC treatment-naïve biopsies cultured under hypoxia (0.5% O_2)*

Hypoxia can significantly alter the inflammatory secretome thus we investigated the inflammatory profile of OAC treatment-naïve biopsies cultured under hypoxia (0.5% O_2) following treatment with 0.1% DMSO control or 10 μM Pyrazinib (P3).

The clinical patient characteristics for the 5 patients used in this study are outlined in **Table 6-2**. The secreted levels of 54 proteins were separated into 4 different panels including inflammatory, angiogenesis and vascular injury, chemokine, TH17 proteins and cytokine proteins. Secreted levels of inflammatory proteins from OAC treatment-naïve biopsies are shown **Figure 6-12**. Secreted levels of angiogenic and vascular injury proteins from OAC treatment-naïve biopsies are shown in **Figure 6-13**. Chemokine and TH17 protein secretions from OAC treatment-naïve biopsies are illustrated in **Figure 6-14**. Secreted levels of cytokine from OAC treatment-naïve biopsies are shown in **Figure 6-15**.

No significant differences in protein secretions from OAC treatment-naïve biopsies were observed following treatment with Pyrazinib (P3) including inflammatory, angiogenic, chemokine and cytokine proteins. Of note this study consisted of a small sample size and thus it was not surprising no significant changes were observed.

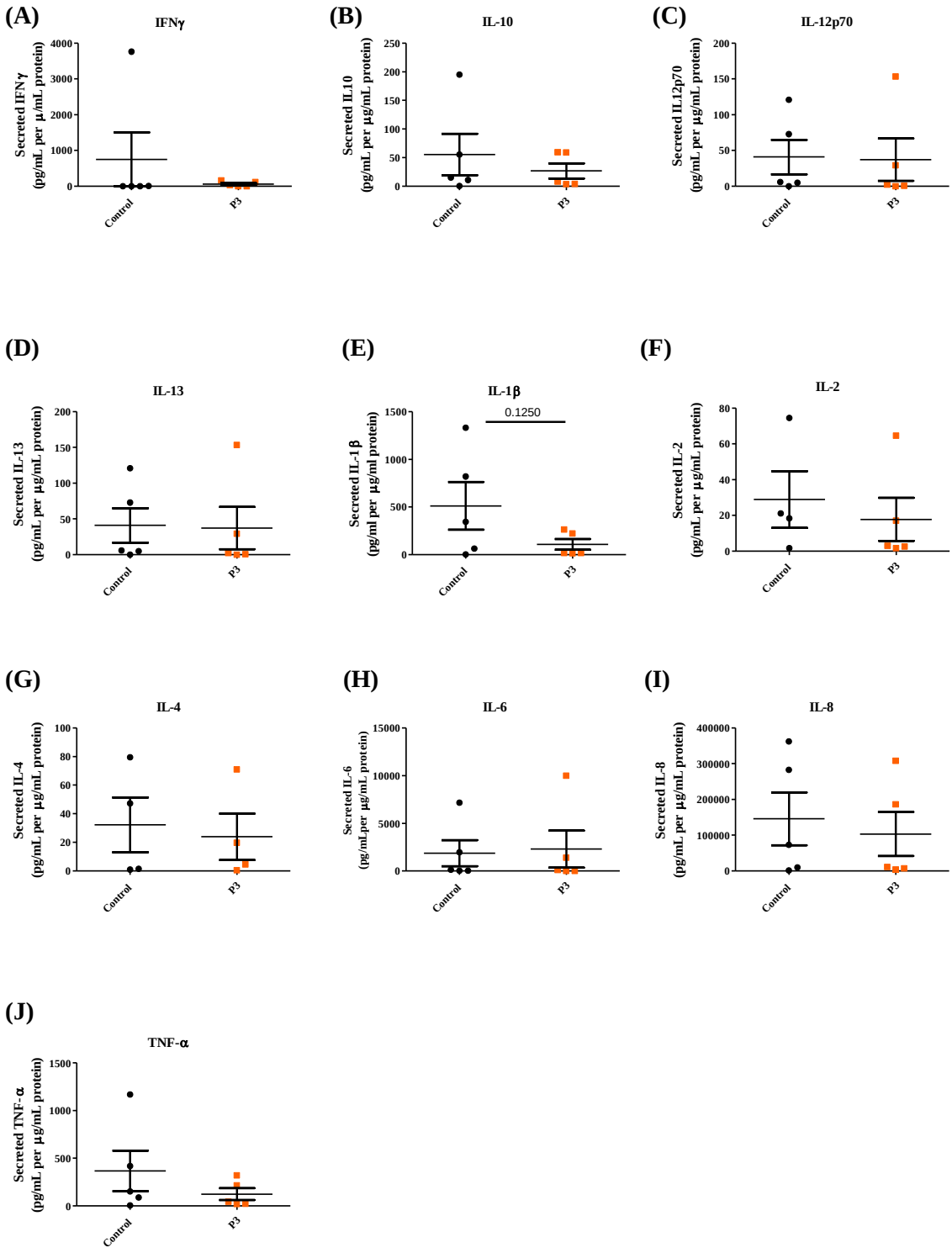

Figure 6-12 Inflammatory protein secretions in OAC biopsies cultured under hypoxia (0.5% O_2).

Inflammatory protein secretions from OAC treatment-naïve biopsies cultured under hypoxia (0.5% O_2) with 0.1% DMSO or 10 µM Pyrazinib (P3) including **(A)** IFN-γ **(B)** IL-10 **(C)** IL-12p70 **(D)** IL-13 **(E)** IL-1β **(F)** IL-2 **(G)** IL-4 **(H)** IL-6 **(I)** IL-8 and **(J)** TNF-α, (n=5)**.** Wilcoxon signed rank t-test. Data expressed as ±SEM.

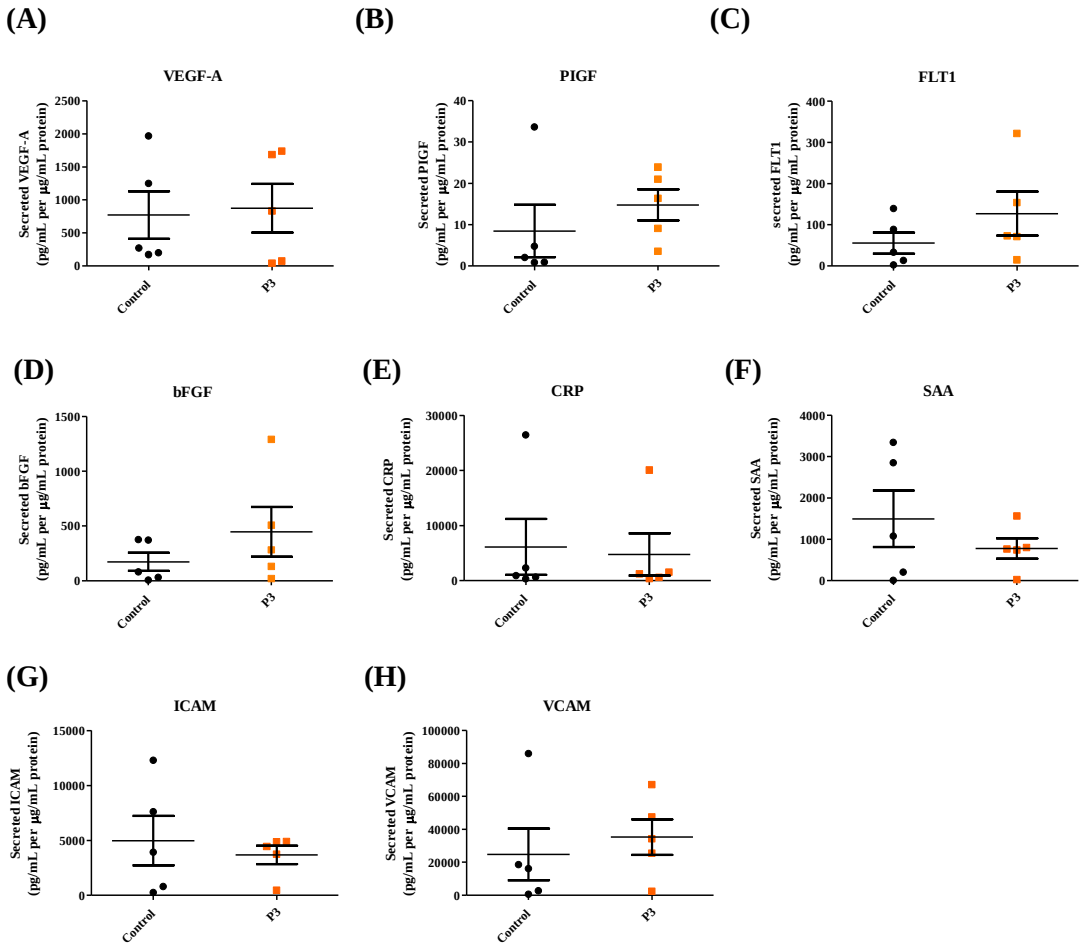

Figure 6-13 Angiogenic and vascular injury protein secretions from OAC biopsies cultured under hypoxia.

Angiogenic and vascular injury protein secretions from OAC treatment-naïve biopsies cultured under hypoxia (0.5% O_2) with 0.1% DMSO or 10 µM Pyrazinib (P3) including **(A)** VEGF-A **(B)** PIGF **(C)** flt1 **(D)** b-FGF **(E)** CRP **(F)** SAA **(G)** ICAM and **(H)** VCAM, (n=5)**.** Wilcoxon signed rank t-test. Data expressed as ±SEM.

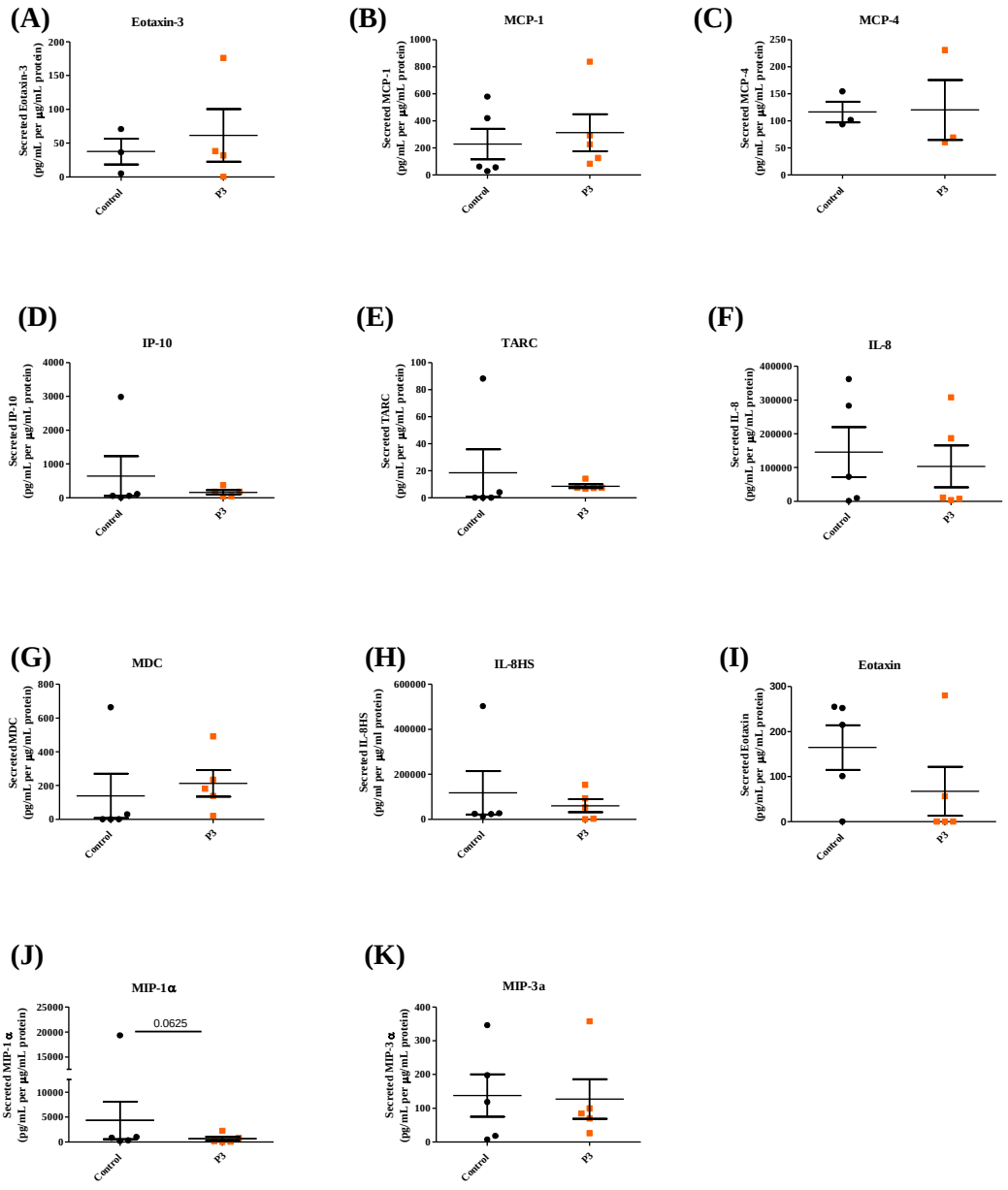

Figure 6-14 Chemokine and Th17 protein secretions from OAC treatment-naïve biopsies cultured under hypoxia.

Chemokine and Th17 protein secretions from OAC treatment-naïve biopsies cultured under hypoxia (0.5% O_2) with 0.1% DMSO or 10 µM Pyrazinib (P3) including **(A)** Eotaxin-3 **(B)** MCP-1 **(C)** MCP-4 **(D)** IP-10 **(E)** TARC **(F)** IL-8 **(G)** MDC **(H)** IL-8HS **(I)** Eotaxin **(J)** MIP-1α and **(K)** MIP-3α, (n=5)**.** Wilcoxon signed rank t-test. Data expressed as ±SEM.

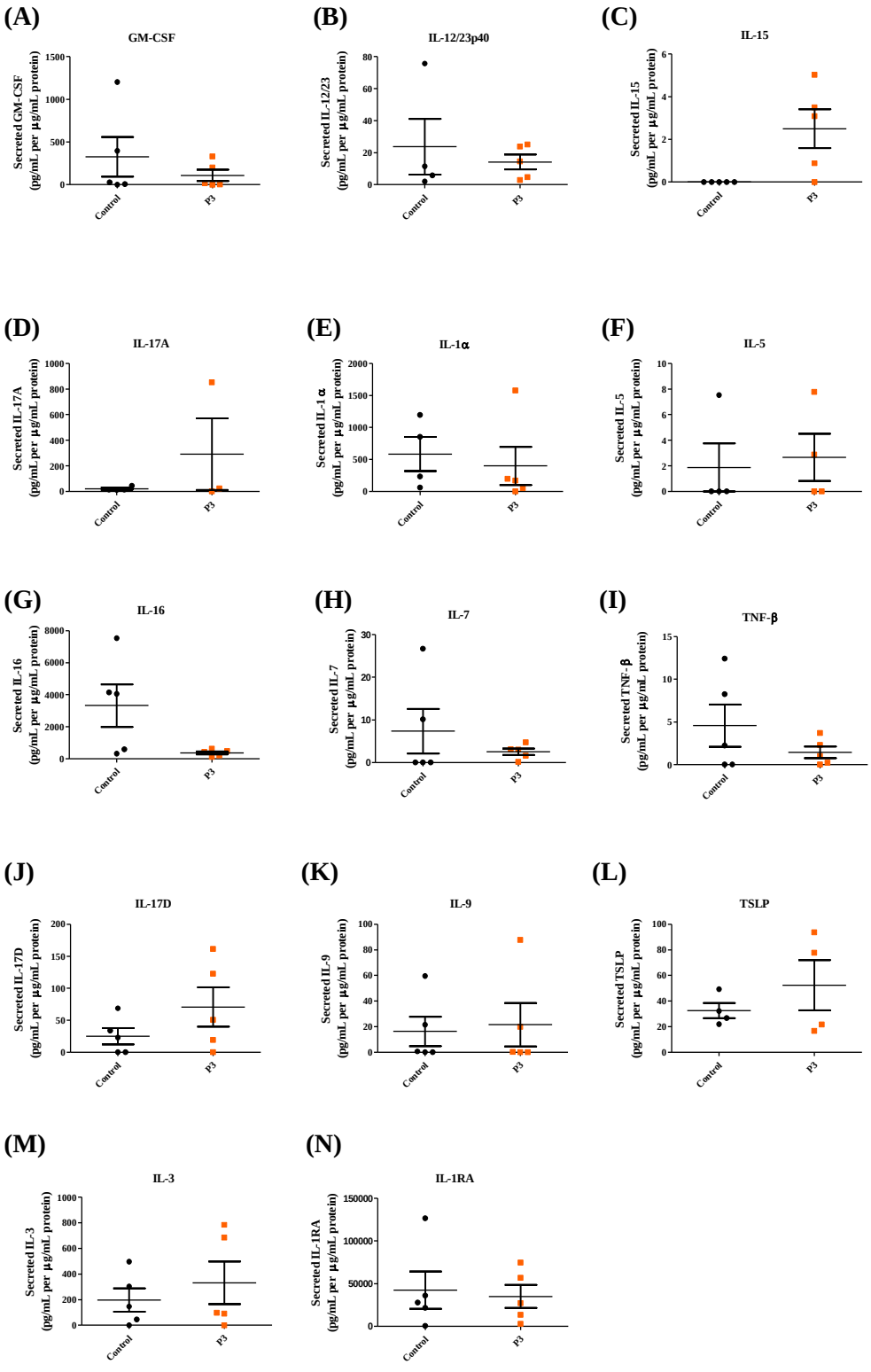

Figure 6-15 Cytokine protein secretions from OAC treatment-naive biopsies cultured under hypoxia.

Cytokine protein secretions from OAC treatment-naïve biopsies cultured under hypoxia (0.5% O_2) with 0.1% DMSO or 10 µM Pyrazinib (P3) including **(A)** GM-CSF, **(B)** IL-12/23p40, **(C)** IL-15, **(D)** IL-17A, **(E)** IL-1α, **(F)** IL-5, **(G)** IL-16, **(H)** IL-7, **(I)** TNF-β, **(J)** IL-17D, **(K)** IL-9, **(L)** TSLP, **(M)** IL-3 and **(N)** IL-1RA (n=5)**.** Wilcoxon signed rank t-test. Data expressed as ±SEM.

6.4.9. *Circulating levels of IL-6, IL-8, IL-1β and TNF-α are not significantly linked with TRG*

In both this chapter and the previous chapter we have identified a number of inflammatory factors which are linked with the resistant phenotype and/or are altered by Pyrazinib (P3) treatment. IL-8 and IL-6 were previously shown to be secreted at higher levels from OE33R cells compared to OE33P cells and their secreted levels were reduced by Pyrazinib (P3) treatment. In addition, IL-8 secretion was significantly correlated with LIF, a cytokine which is significantly higher in serum of patients with a poor pathological response to treatment. Furthermore, in this chapter Pyrazinib (P3) was shown to significantly reduce the secretion of IL-1β from treatment-naïve OAC patient biopsies and TNF-α was correlated with ECAR. Thus, given the potential role of IL-6, IL-8, IL-1β and TNF-α in both carcinogenesis and treatment resistance of OAC, we evaluated the circulating levels of these 4 cytokines in the serum of OAC patients who were treatment-naïve. The circulating levels of TNF-α, IL-6, IL-8 and IL-1β were divided according to tumour stage, nodal status, stage of differentiation, TRG, body mass index and gender **(Figure 6-16 – Figure 6-19).**

No significant differences were seen in the circulating levels of TNF-α, IL-6, IL-8 and IL-1β when divided according to clinical characteristics.

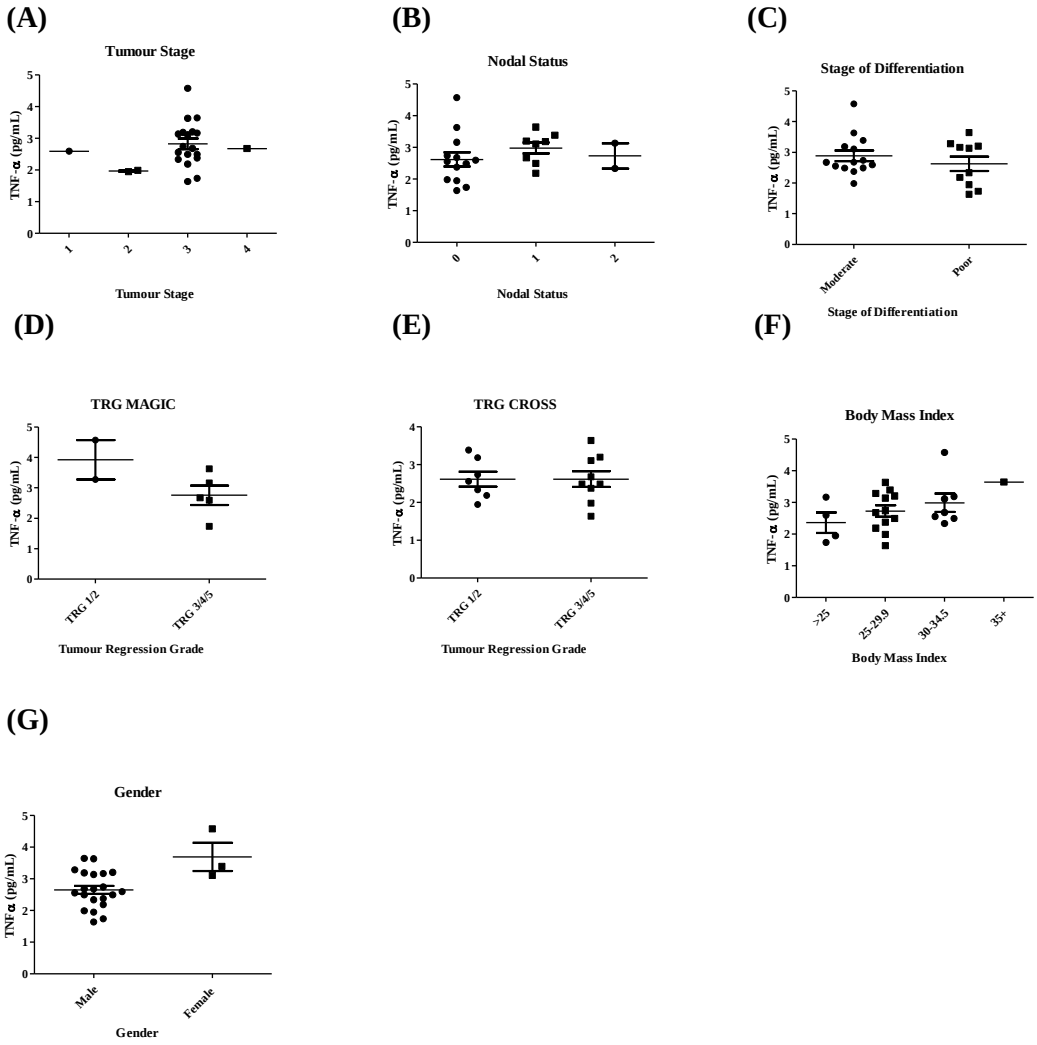

Figure 6-16 Circulating levels of TNF-α in OAC pre-treatment serum divided according to clinical patient characteristics.

Levels of circulating TNF-α in serum of OAC treatment-naïve patients divided according to **(A)** tumour stage, **(B)** nodal status, **(C)** stage of differentiation, **(D)** TRG following MAGIC, **(E)** TRG following CROSS, **(F)** body mass index and **(G)** gender, (n=26). Mann Whitney U test. Data expressed as ±SEM.

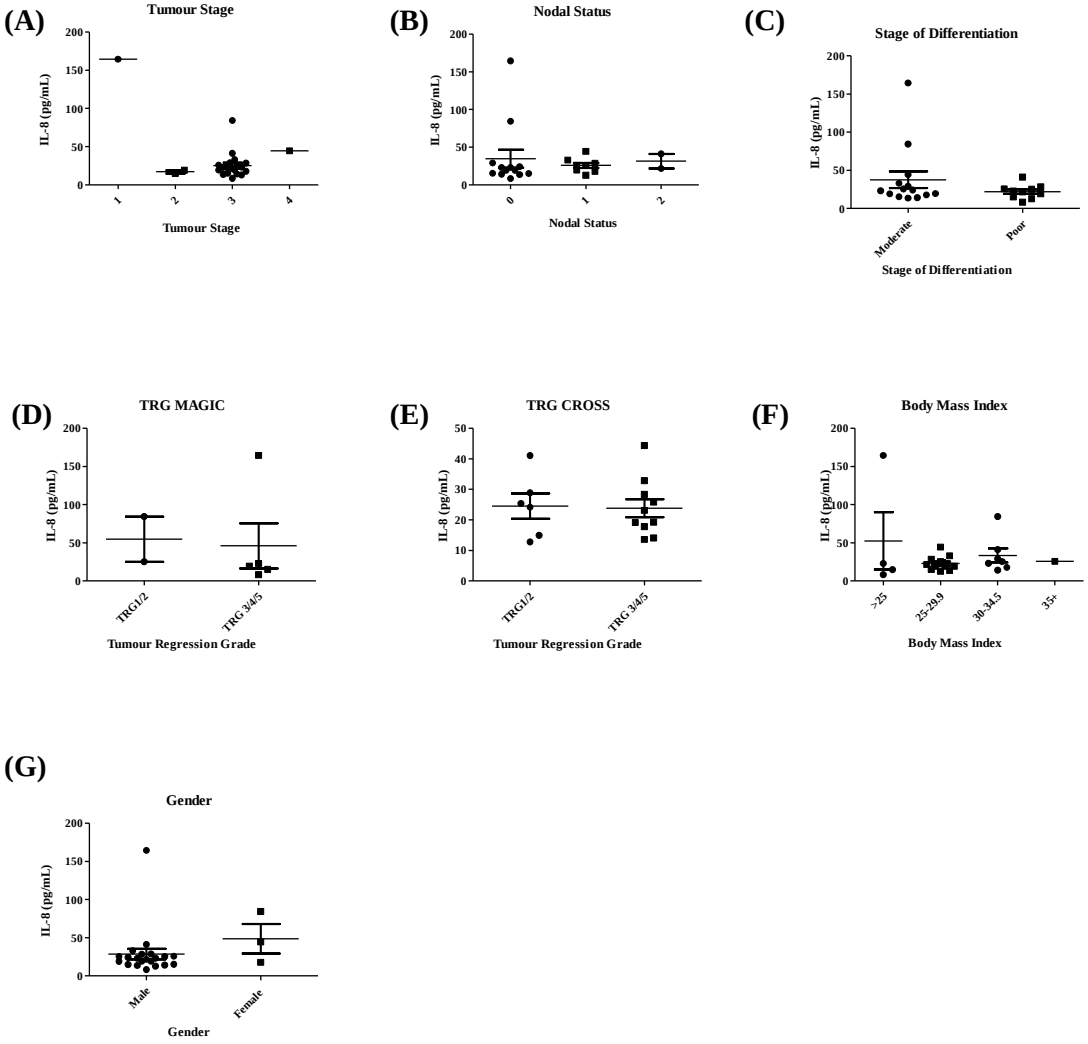

.

Figure 6-17 Circulating levels of IL-8 in OAC pre-treatment serum divided according to clinical patient characteristics.

Levels of circulating IL-8 in serum of OAC treatment-naïve patients divided according to **(A)** tumour stage, **(B)** nodal status, **(C)** stage of differentiation, **(D)** TRG following MAGIC, **(E)** TRG following CROSS, **(F)** body mass index and **(G)** gender, (n=26). Mann Whitney U test. Data expressed as ±SEM.

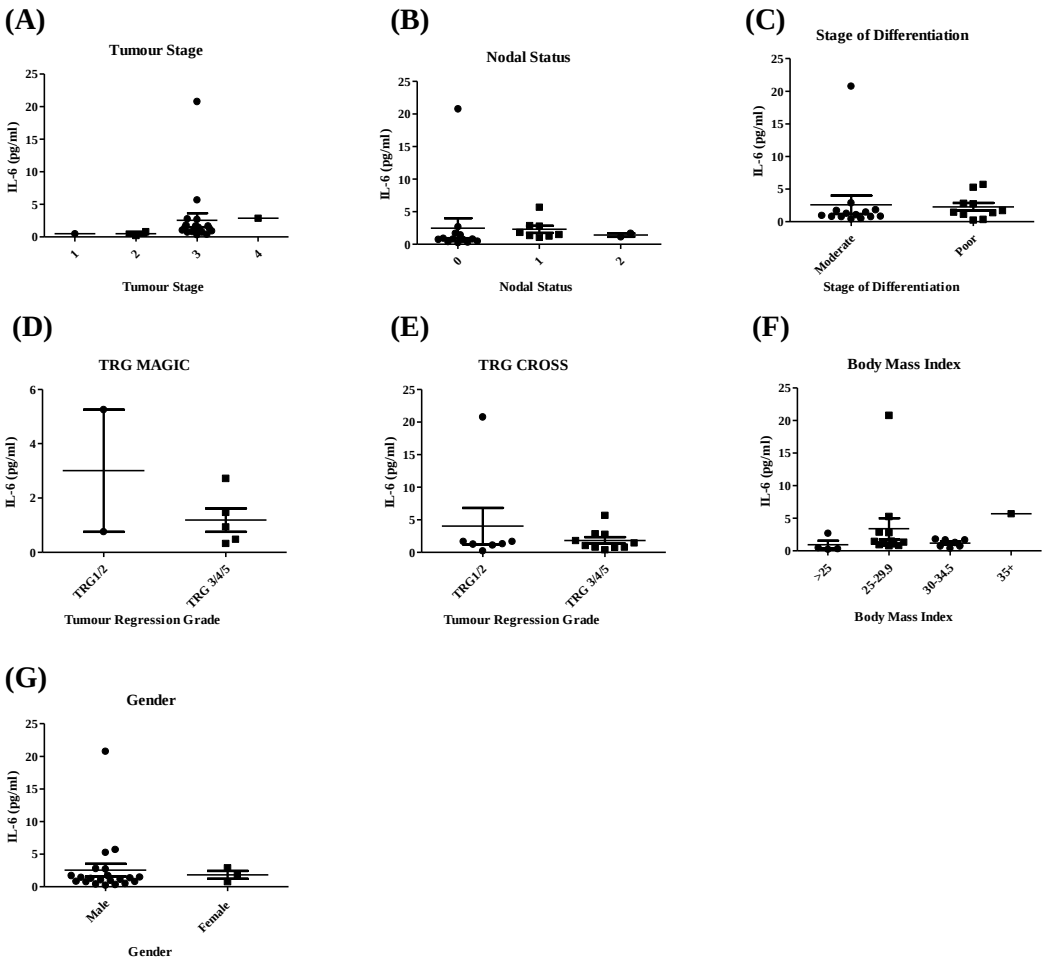

Figure 6-18 Circulating levels of IL-6 in OAC pre-treatment serum divided according to clinical patient characteristics.

Levels of circulating IL-6 in serum of OAC treatment-naïve patients divided according to **(A)** Tumour stage, **(B)** nodal status, **(C)** stage of differentiation, **(D)** TRG following MAGIC, **(E)** TRG following CROSS, **(F)** body mass index and **(G)** gender, (n=26). Mann Whitney U test. Data expressed as ±SEM.

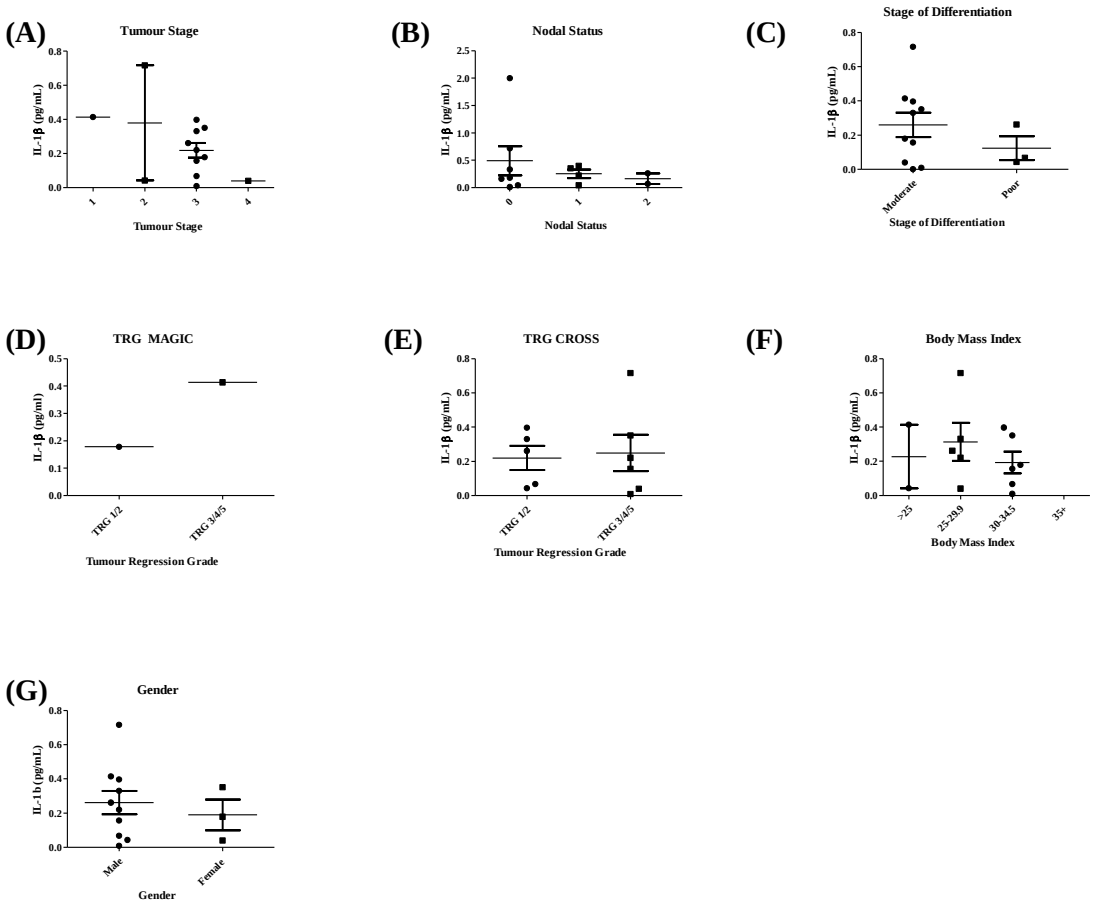

Figure 6-19 Circulating levels of IL-1β in OAC pre-treatment serum divided according to clinical patient characteristics.

Levels of circulating IL-1β in serum of OAC treatment-naïve patients divided according to **(A)** tumour stage, **(B)** nodal status, **(C)** stage of differentiation, **(D)** TRG following MAGIC, **(E)** TRG following CROSS, **(F)** body mass index and **(G)** gender, (n=26). Mann Whitney U test. Data expressed as ±SEM.

6.4.10. *Pyrazinib (P3) does not directly alter the expression of dendritic cell maturation markers on CD11+ cells*

In the previous sections of this chapter we have demonstrated that Pyrazinib (P3) significantly reduces OCR and IL-1β secretion and, thus, we investigated whether the effects of Pyrazinib (P3) negatively altered the expression of dendritic cell maturation markers. Dendritic cells are professional antigen presenting cells which play a key role in anti-tumour response. In the development of a new compound it is crucial to determine if such treatment will affect the function of important anti-tumour immune cells such as dendritic cells as this could hinder the clinical potential of our compound. OAC treatment-naïve biopsies were obtained from 22 OAC cancer patients. **Table 6-3** shows the clinical patient information of patient samples used in this study. Immature dendritic cells were pre-incubated with either control TCM or TCM which had been treated with 10 µM Pyrazinib (P3) for 24 h before LPS was added to induce dendritic cell maturation. To assess the effect of Pyrazinib (P3) alone, control OAC TCM and OAC TCM pre-treated with Pyrazinib the expression of dendritic cell maturation markers CD83, PD-L1, CD40, HLA-DR and CD54 on CD11+ cells was assessed by flow cytometry**.** Direct treatment of dendritic cells with either 0.1% DMSO or 10 µM Pyrazinib (P3) following LPS stimulation did not significantly alter the expression of CD83, PD-L1, CD40, HLA-DR and CD54 dendritic cell maturation markers (**Figure 6-20A-E**). Both 0.1% DMSO treated OAC TCM (p=0.0252) and Pyrazinib (P3) treated (p=0.0004) OAC TCM significantly reduced the expression of CD83 on dendritic cells **(Figure 6-20A)**. TCM pre-treated with Pyrazinib (P3) produced a 15% greater reduction in CD83 expression on dendritic cells compared to control treated TCM (p=0.0100). No significant differences in PD-L1, CD40, HLA-DR and CD54 expression on dendritic cells were seen following treatment with either control or Pyrazinib (P3) TCM (**Figure 6-20B-E**). In summary, Pyrazinib (P3) does not directly affect the expression of dendritic cell maturation makers CD83, PD-L1, CD40, HLA-DR and CD54. Secreted factors from OAC tumour biopsies can significantly reduce CD83 expression on dendritic cells but not the expression of PD-L1, CD40, HLA-DR and CD54.

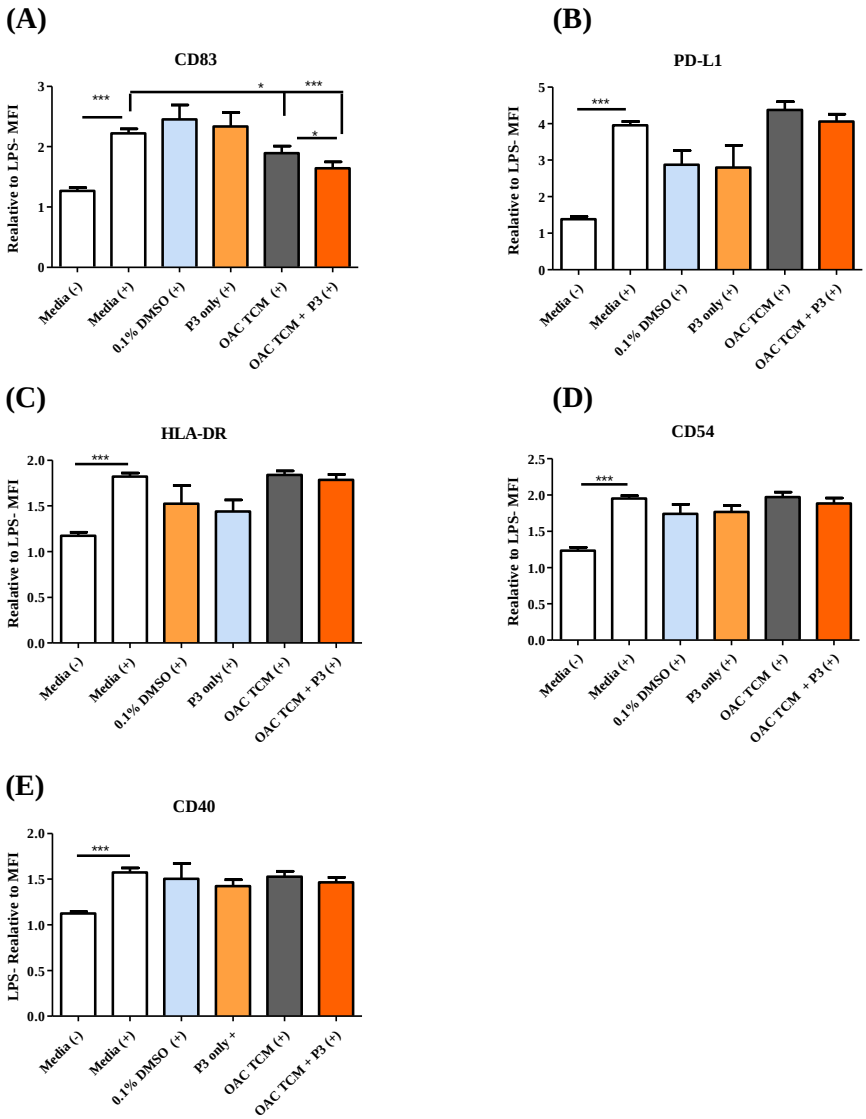

Figure 6-20 OAC TCM and Pyrazinib (P3) treated TCM significantly reduced expression of CD83 but did not alter the expression of PD-L1, CD40, HLA-DR or CD54 expression on monocyte derived dendritic cells following stimulation with LPS.

The effect Pyrazinib (P3) and Pyrazinib (P3) treated TCM on the expression of dendritic cells maturations markers was assessed by flow cytometry. **(A)** CD83 expression on monocyte derived dendritic cells following incubation with LPS – and LPS + M199, 0.1% DMSO + LPS, 10 µM Pyrazinib (P3) + LPS, 0.1% DMSO treated OAC TCM+ LPS and OAC TCM treated with Pyrazinib (P3) + LPS. **(B)** PD-L1 expression on monocyte derived dendritic cells following incubation with LPS – and LPS + M199, 0.1% DMSO + LPS, 10 µM Pyrazinib (P3) + LPS, 0.1% DMSO treated OAC TCM + LPS and OAC TCM treated with 10 µM Pyrazinib (P3) + LPS. **(C)** CD40 expression on monocyte derived dendritic cells following incubation with LPS – and LPS + M199, 0.1% DMSO + LPS, 10 µM Pyrazinib (P3) + LPS, 0.1% DMSO treated OAC TCM + LPS and OAC TCM treated with 10 µM Pyrazinib (P3) + LPS. **(D)** HLA-DR expression on monocyte derived dendritic cells following incubation with LPS – and LPS + M199, 0.1% DMSO + LPS, 10 µM Pyrazinib (P3) + LPS, 0.1% DMSO treated OAC TCM + LPS and OAC TCM treated with 10 µM P3 + LPS. **(E)** CD54 expression on monocyte derived dendritic cells following incubation with LPS – and LPS + M199, 0.1% DMSO + LPS, 10 µM Pyrazinib (P3) + LPS, 0.1 DMSO treated OAC TCM + LPS and OAC TCM treated with 10 µM Pyrazinib (P3) + LPS. LPS stimulation indicated by (+).Wilcoxon signed rank t-test, *p<0.05,***p<0.001. Data expressed as +SEM.

6.5. Summary of main findings of chapter 6

- Real-time OCR, a measure of oxidative phosphorylation, is significantly higher than ECAR, a measure of glycolysis in OAC treatment-naïve biopsies.

- Pyrazinib (P3) treatment significantly reduced real-time OCR in OAC treatment-naïve biopsies.

- OAC treatment-naïve biopsies quickly and significantly adapted their metabolic rate to changes in oxygen concentration.

- Pyrazinib (P3) significantly reduced OCR and ECAR in OAC treatment-naïve biopsies cultured under 0.5% O_2.

- Pyrazinib (P3) significantly reduced the secretion of IL-1β and increased the secretion of IL-3 and IL-17B in OAC treatment-naïve biopsies.

- OCR is significantly correlated with ECAR, VEGF-A, IL-1RA and TSLP.

- Pyrazinib (P3) did not significantly alter the secretion of inflammatory proteins from OAC treatment-naïve biopsies cultured under hypoxia (0.5% O_2).

- Circulating levels of IL-6, IL-8, IL-1β and TNF-α were not significantly linked with clinical patient characteristics.

- Pyrazinib (P3) treatment did not directly alter the expression dendritic cell maturation markers on CD11+ cells, indicating dendritic cells should maintain their function even in the presence of this compound.

6.6. Discussion

The overall goal of this chapter was to evaluate the effect of Pyrazinib (P3) treatment on real–time metabolic rate and inflammatory secretions in human OAC treatment-naïve biopsies. Furthermore, we investigated whether Pyrazinib (P3) altered the expression of dendritic cell maturation markers. Our findings highlight for the first time the real-time importance of aerobic mitochondrial respiration in OAC patient tumours and oxidative phosphorylation is an emerging target in cancer treatment which warrants investigation in OAC based on our findings in this study [416].

Ex-vivo, real-time metabolic profiling demonstrated that OCR, a measure of oxidative phosphorylation, is significantly higher in OAC treatment-naïve biopsies compared to ECAR, a measure of glycolysis. This supports previous findings by our group which have reported the importance of oxidative phosphorylation as a metabolic pathway in OAC where oxidative phosphorylation was previously associated with resistance to radiation treatment *in-vitro* [82]. The metabolic rate of OAC biopsies including OCR and ECAR were shown to be independent of clinical patient characteristics.

Furthermore, when we assessed the basal real-time metabolic rate of 10 different treatment-naïve OAC patient biopsies and then treated them with Pyrazinib (P3) for 24 h and reassessed their metabolic rate, we found Pyrazinib (P3) significantly inhibited OCR in these biopsies compared to baseline with no significant feedback upregulation of ECAR. Importantly, Pyrazinib (P3) significantly inhibited OCR independent of patient characteristics. Notably, this was a small cohort and the activity of Pyrazinib (P3) requires further validation in a larger study. The significant effect of Pyrazinib (P3) on OAC tumour oxidative phosphorylation rate is not only likely to have an anti-cancer effect given the prominent utility of oxidative phosphorylation in OAC tumours, it may also enhance the radioresponse of these tissues as seen *in-vitro* in an isogenic model of OAC radio-resistance in chapters 3 and 4. Targeting oxidative phosphorylation has been reported in a number of studies as a novel mechanism to enhance radiosensitivity [123, 229]. A study by Benej *et al.* demonstrated that targeting mitochondrial respiration with the ergot alkaloid papaverine significantly inhibited mitochondrial respiration and enhanced tumour oxygenation and subsequently enhanced radiosensitivity in pulmonary adenocarcinoma cells [229]. Of importance to note, in an *in-vivo* model, only treatment with papaverine prior to radiation enhanced radioresponse, the same effect was not seen when papaverine was administered after irradiation highlighting the importance of treatment scheduling for the best outcome when combining novel radiosensitising agents with X-ray radiation [229]. An interesting study carried out by Bol *et al.* demonstrated reprogramming of tumour mitochondria improves

responses to radiation, a mitochondrial dysfunctional cell line which were exclusively glycolytic were found to be more radiosensitive than wild type oxidative phosphorylation proficient cells [295]. A novel *in-vivo* model of oncogenic ablation-resistant pancreatic cancer cells which were responsible for tumour relapse were reported to depend on mitochondrial function for survival [123]. Targeting oxidative phosphorylation in this subpopulation of surviving pancreatic cells was found to significantly decrease tumour spheroid growth [123]. Furthermore, oxidative phosphorylation is significantly upregulated in breast cancers deficient in RB1, a protein lost in 20-30% of basal-like breast cancers, [417, 418]. Tigecycline, a mitochondrial translational inhibitor attenuated growth of RB1-deficient breast tumours *in-vivo* [418]. Taken together with our studies this highlights the potential of not only targeting oxidative phosphorylation in the neo-adjuvant setting to enhance radiosensitivity in OAC but also in the adjuvant setting to target any remaining surviving cancer cells, especially given the predominance of the oxidative phosphorylation pathway in OAC explants, such a therapeutic strategy strongly warrants investigation in the future.

Hypoxia promotes the transformation of tumour cell metabolism from oxidative metabolism to anaerobic glycolysis, which protects tumour cells and induces the development of radioresistance and drug resistance in tumour stem cells [419]. We sought to investigate how OAC treatment-naïve biopsies can adapt their metabolic profile to conditions of hypoxia and if Pyrazinib (P3) can inhibit mitochondrial respiration under hypoxic conditions of 0.5% O_2. Metabolic rate assessment of 7 OAC patient biopsies as shown before at baseline had a significantly higher rate of OCR than ECAR, again highlighting the importance of mitochondrial respiration in these tumour samples. OAC treatment-naïve biopsies adapted to their altered microenvironment and the previous dependence we had seen on oxidative phosphorylation was lost as under hypoxic conditions there was no significant difference in OCR compared to ECAR. The OCR:ECAR ratio was significantly higher in OAC treatment-naïve biopsies under normoxia versus hypoxia and the ECAR:OCR ratio was significantly higher in hypoxic versus normoxic biopsies highlighting a metabolic shift under hypoxic conditions and the adaptability of these biopsies to their environment. Pyrazinib (P3) significantly inhibited both oxidative phosphorylation and glycolysis. The ability of Pyrazinib (P3) to inhibit both oxidative phosphorylation and glycolysis under hypoxic conditions is a critical finding which shows OAC tumours have metabolic flexibility and thus they are not reliant on oxidative phosphorylation alone especially under hypoxic conditions where the ECAR:OCR ratio is significantly increased. In a study by Wang *et al*. in genetically modified macrophages overexpressing HIF1α the OCR:ECAR ratio was dramatically decreased compared to non-HIF1α overexpressing macrophages demonstrating a shift to glycolysis metabolism compared to mitochondrial oxidation in HIF1α overexpressing macrophages [420]. Oxygen is a potent radiosensitiser and solid tumours with areas of hypoxia

are the most aggressive and difficult tumours to treat [237]. A number of strategies which have attempted to increase oxygen delivery to the tumour have failed in the clinic largely due to the heterogenic nature of tumour vasculature [421]. In a pancreatic xenograft, the selective HIF-1α inhibitor PX-478 was found to potentiate the effect of fractioned chemoradiation therapy [242]. Targeting intra-tumoural oxygen consumption with compounds targeting oxidative phosphorylation may present a novel means to overcome tumour hypoxia and enhance anti-cancer activity in tumours in which oxidative phosphorylation is upregulated but also to improve treatment response rates in hypoxic treatment resistant tumours [229]. Notably elevation of oxygen by as little as 2% is sufficient to produce oxygen enhancement [416]. Targeting oxidative phosphorylation in mammary tumours with papaverine was found to enhance hypoxic tumour oxygenation and sensitise tumours to radiation therapy [229]. Taken together with our findings this suggests Pyrazinib (P3) has the potential to function as a radiosensitiser *in-vivo* given our previous findings *in-vitro* in chapter 4.

Pyrazinib (P3) did not significantly alter the secretion of lactate from treatment-naïve OAC biopsies and secreted lactate levels in the TCM were not associated with clinical patient characteristics, although a limitation is the small sample size of only 8 patients. Lactate produced by aerobic glycolysis is released into the tumour microenvironment, conferring advantages of tumour survival and growth. Whilst it would have been favourable for Pyrazinib (P3) to reduce lactate secretion this result is not surprising as Pyrazinib (P3) did not significantly alter ECAR in OAC pre-treatment biopsies under normoxic conditions [422].

OAC is an inflammatory driven upper gastrointestinal cancer [234] and we sought to characterise the inflammatory profile of the TCM of 22 OAC treatment-naïve biopsies. A 54 multiplex ELISA demonstrated the heterogeneity of secreted factors from OAC biopsies across 5 panels including inflammatory, angiogenic and vascular injury, chemokine, cytokine and TH17 related proteins. None of the secreted factors were significantly associated with clinical patient characteristics. To investigate a potential relationship between metabolic rate and the OAC secretome profile we correlated protein secretions in 10 patients which for whom we had matched TCM and baseline real-time metabolic rate. OCR was significantly correlated with ECAR in all patients at baseline. Both OCR and ECAR were significantly positively correlated with the secretion of VEGF-A, IL-1RA and TSLP in OAC treatment-naïve biopsies. In addition, ECAR was also correlated with IL-13, MIP-3α and TNF-α. Oxidative phosphorylation and glycolysis are known to be influenced by systemic inflammation thus it is not surprising that metabolic rate correlated with a number of inflammatory mediators [423]. The significant correlation between VEGF-A secretion and OCR and ECAR highlights the tight links which exist between the two biological processes of angiogenesis and metabolism whereby there are increasing levels of the angiogenic marker

VEGF-A in tumours with higher levels of oxidative phosphorylation [424]. TNF-α was only significantly correlated with ECAR and not OCR in OAC treatment-naïve biopsies. TNF-α was previously shown to induce aerobic metabolism in prostate epithelial cells and glycolytic reliance in mammary carcinoma cells [425, 426].

Treatment of OAC treatment-naïve biopsies with Pyrazinib (P3) was found to significantly inhibit IL-1β secretion and increase IL-3 and IL-17B secretion. The significant reduction of IL-1β secretion following treatment is a critical finding which may contribute to its anti-cancer effect, previous work by our department found elevated levels of IL-1β in tumour samples compared to squamous epithelium from the same patients. In addition, IL-1β levels were significantly decreased in the TCM of tumours who achieved a complete pathological response to neo-CRT [415]. IL-1β was previously shown to be significantly correlated with clinical outcome in oesophageal SCC, whereby patients with IL-1β positive tumours had a poor response to treatment compared to patients with IL-1β negative tumours [142]. In addition inhibition of IL-1β was shown to attenuate tumour growth and invasion and ameliorate treatment resistance [142]. Furthermore, in a study by Deans *et al.* tumoural IL-1β expression levels were significantly correlated with systemic inflammation, which is a marker of reduced survival in oesophageal-gastrointestinal cancer patients [427]. In an *in-vivo* melanoma model IL-1β inhibition was shown to stably reduce tumour growth by limiting inflammation and inducing the maturation of immature myeloid cells into M1 macrophages. Furthermore, in an *in-vitro* model of pancreatic chemoresistance, administration of an IL-1 receptor blocking antibody as a means of targeting IL-1β signalling reduced NF-κB activation and the acquisition of chemoresistance in these cells [428]. Reports from the literature suggest the significant inhibition of IL-1β produced by Pyrazinib (P3) is a positive effect which may contribute to the anti-cancer activity of this drug in addition to its effects on oxidative phosphorylation *in-vitro* and *ex-vivo* and radiosensitivity *in-vitro*. IL-3 has been reported to exert paradoxical effects in cancer including pro-tumorigenic as well as anti-tumorigenic cellular responses [429, 430]. Importantly, IL-3 has been reported to play an important role in anti-tumoural immunity, IL-3 is able to enhance antigen presentation by dendritic cells and activate macrophages to increase the expression of class II MHC molecules and interleukin-1 (IL-1) [431]. Elevated gene expression of IL-3 in fibrosarcoma xenografts (FSA-JmIL-3 tumours) was associated with enhanced response to radiation compared to parental tumours, where FSA-JmIL-3 tumours were associated with increased lymphocyte infiltration and elicited immune response [430], suggesting that the enhanced secretion of IL-3 following Pyrazinib (P3) treatment may support the function of this small molecule as a radiosensitiser.

Circulating levels of TNF-α, IL-8, IL-6 and IL-1β were not significantly associated with clinical patient characteristics including TRG, a marker of treatment response. Notably IL-1β was only

identified in the serum of 13 of 26 patients whereas it was detected in the TCM of all 22 patients we evaluated which may indicate intra-tumoural IL-1β is of more importance than circulating levels in serum to tumorigenesis. In the previous chapter IL-8 was shown to be secreted at significantly higher levels from OE33R cells. IL-8 has been reported in the literature to play a pivotal role in supporting tumour treatment resistance through the stimulation of an immunosuppressive microenvironment and activation of epithelial to mesenchymal transition, despite this circulating levels of IL-8 could not segregate responders and non-responders [432]. In the previous chapter we found LIF, an IL-6 type cytokine to be significantly upregulated in serum of patients with a poor response to neo-adjuvant treatment and IL-6 secretion was significantly higher in OE33R radioresistant cells, however there was no significant correlation between circulating IL-6 and TRG. In an SCC study, intra-tumoural IL-6 was expressed at significantly higher levels in the tumour than adjacent epithelium and immunohistochemical analysis found there was a positive correlation between IL-6 overexpression and cancers developing loco-regional failure or distant metastasis [236].

Immune cells such as dendritic cells play a crucial role in the induction of anti-tumoural immunity and host immune-surveillance in oesophageal cancer [433]. Dendritic cells are professional antigen presenting cells which are responsible for induction of antigen specific T cell responses, thus it is critical that function of dendritic cells remains intact even in the presence of our small molecule compound Pyrazinib (P3). In this study, we sought to investigate both the effect of the secretions from the TCM and Pyrazinib (P3) on the expression of dendritic cell maturation markers. Increased expression of several cell surface markers including CD54, PD-L1, CD40, CD83, and HLA-DR, on dendritic cells is associated with dendritic cell maturation and T-cell activation [434] . We assessed the ability of control and Pyrazinib (P3) treated TCM from cultured human OAC treatment-naïve explants to alter the function of dendritic cells. Both control TCM , and Pyrazinib (P3) treated TCM significantly reduced the expression of CD83 on CD11c+ cells. Direct treatment with Pyrazinib (P3) had no effect on CD83 expression suggesting that mediators secreted from the tumour specifically had an inhibitory effect on dendritic cell maturation. This is positive finding which demonstrates Pyrazinib (P3) treatment does not negatively affect the expression of dendritic cell maturation markers indicating the function of these cells remains intact even in presence of this compound, although more functional assays will need to be conducted in the future to support this finding. In a previous study it was reported that TCM from colorectal explants significantly inhibited the expression of dendritic cell maturation markers, however this was only seen in the case of CD83 in OAC [414].

The immune system can inhibit tumorigenesis with acute infiltration of effector innate and adaptive immune cells and cytokines such as IFN-γ which results in a Th1 T cell phenotype [435,

436]. In a separate study by our lab Pyrazinib (P3) did not have any toxic effect on Jurkat T cells. This is an important finding which highlights the potential to use Pyrazinib (P3) within the clinical setting because it does not deplete or kill $CD4^+$ T cells. The effect of Pyrazinib (P3) on Jurkat T cell activation status was also examined using pre-activated Jurkats. Pyrazinib (P3) has been previously shown to enhance radiosensitivity *in-vitro* and a study by Voos *et al*. demonstrated that radiation doses of ≥2 Gy activate Jurkat T cells and stimulate pro-inflammatory immune responses, through upregulation of IL-2, IFN-γ and CD25 surface expression [437]. Importantly, Pyrazinib (P3) did not affect the activation status of the naïve T cell markers expressed on the activated and inactivated Jurkats, demonstrating that Pyrazinib (P3) does not affect the activation status of T cells. Therefore if administered in the clinical setting, Pyrazinib (P3) may not cause T cell exhaustion within the tumour microenvironment, via continuous stimulation and upregulated of PD-1 and CTLA-4 leading to exhaustion of tumour infiltrating T cells and radioresistance [438]. $CD8^+$ T cells are more susceptible to becoming exhausted upon constitutive activation than $CD4^+$ T cells [439] and one of the limitations to this study is the use of $CD4^+$ T cells in an *in-vitro* setting. Further research is required in relation to this study both in patient derived PBMCs and the *in-vivo* setting to gain a better understanding of the effect Pyrazinib (P3) may have on other immune cells.

In summary we report a new method for profiling the metabolic rate of OAC tumour biopsies in real-time, highlighting the importance of the oxidative phosphorylation pathway in these samples and metabolic adaptability to environmental conditions of OAC tumours. In addition, we have demonstrated the novel anti-metabolic and anti-inflammatory action of Pyrazinib (P3) *ex-vivo* in OAC treatment-naïve biopsies. Pyrazinib (P3) which was previously shown to function as a robust radiosensitiser in an isogenic model of OAC radioresistance. It will be critical to further evaluate the anti-cancer potential of Pyrazinib (P3) in a murine model of OAC.

7. Chapter 7 – Conclusion and Future Directions

7.1. Concluding discussion

Radiotherapy is used in the treatment of over 50% of human malignancies including OAC [440]. Chemoradiation therapy prior to surgery is increasingly becoming the standard of care for OAC in order to debulk the tumour prior to surgery [43]. However, resistance to therapy is a major limitation whereby only ~30% of patients achieve a complete pathological response to neo-adjuvant therapy [43]. This is a major clinical challenge, as a good pathological response to neo-adjuvant treatment is associated with best clinical outcomes. Thus, there is a clinical need for the development of novel compounds which could enhance response to neo-adjuvant treatments such as radiotherapy to improve clinical outcomes and patient survival for OAC patients.

Radioresistance is a process in which the tumour cells or tissues adapt to the radiotherapy-induced changes and develop resistance to the X-ray irradiation. Resistance to radiotherapy is complex and associated with multiple factors including the alteration of multiple biological processes including alterations in mitochondrial function and energy metabolism, altered DNA repair, pathological angiogenesis, inflammation and inflammation-associated hypoxia, altered cell cycle and cell cycle checkpoints and resistance to apoptosis. Our previous work demonstrated that radioresistant OAC cells have a significantly higher rate of oxygen consumption, a measure of oxidative phosphorylation compared to matched OAC radiosensitive cells, furthermore ATP5B was shown to be expressed at significantly higher levels in OAC pre-treatment biopsies of patients who had a poor response to neo-adjuvant treatment compared to patients who achieved a good response [82]. No biological process acts in isolation and metabolism and angiogenesis have a highly interdependent relationship, whereby blood vessels which form as a result of angiogenesis supply the required nutrients and oxygen to tumour cells to carry out metabolism and in conditions of low oxygen, metabolic regulators can promote the expression of angiogenic mediators to increase tumour angiogenesis. In this thesis, using a phenotype-based approach we sought to identify a small molecule compound, using an *in-vivo* zebrafish model which could inhibit both oxidative phosphorylation and angiogenesis, two processes both tightly linked with one another and the radioresistant phenotype in order to enhance radiosensitivity in OAC.

In chapter 2, using phenotype-based screens and a zebrafish animal model we screened a panel of 23 compounds and identified Pyrazinib (P3), P2 and P4 which could significantly inhibit both angiogenesis and metabolism in zebrafish embryos. Pyrazinib (P3) and P4 produced significantly greater anti-angiogenic activity than the parent compound of Pyrazinib (P3), Quininib (Q1), highlighting the more potent anti-angiogenic nature of these compounds. This was a critical finding given that Quininib (Q1) was previously shown to inhibit colorectal tumour growth *in-vivo* highlighting the anti-tumour potential of these compounds [272]. In addition, we also found

Pyrazinib (P3) and two P series compounds P2 and P4 that could significantly inhibit oxygen consumption rate, with Pyrazinib (P3) and P4 also significantly reducing extracellular acidification rate, a measure of glycolysis. From our phenotypic screen we identified 5 potent anti-angiogenic compounds of which 3 also had significant anti-metabolic activity. Importantly, we also found that the compounds which had no anti-angiogenic activity also had no anti-metabolic activity *in-vivo* in zebrafish. We decided to further test these 7 compounds, and Quininib (Q1) in *in-vitro* screens to determine if our phenotype-based screen had identified any small molecule compounds with radiosensitising activity.

In chapter 3 we sought to further investigate the anti-metabolic action of Pyrazinib (P3) and P series compounds in an isogenic *in-vitro* model of OAC radioresistance. Pyrazinib (P3) produced the most potent anti-metabolic activity *in-vitro* significantly inhibiting oxygen consumption rate in both OE33P and OE33R cells and simultaneously reducing extracellular acidification rate in OE33R radioresistant cells. Pyrazinib (P3) was found to significantly reduce ATP turnover in OE33R cells only. The anti-metabolic activity was not coupled with major changes in mitochondrial function, Pyrazinib (P3) did not significantly alter ROS levels, mitochondrial membrane potential or mitochondrial mass in OE33R cells. A small but significant reduction in ROS levels was seen following treatment in OE33P cells. P2 significantly inhibited oxygen consumption rate in OE33R cells only. Quininib (Q1) which was shown to have no anti-metabolic activity *in-vivo* in zebrafish significantly reduced ECAR in OE33P cells only. Clonogenic assays were performed to determine if Quininib (Q1) or any of our P series compounds which we brought forward from chapter 2 (P3, P2, P4, P18, P20, P8 and P23) could enhance radiosensitivity *in-vitro* in our isogenic model of radioresistance. Pyrazinib (P3) and P4 could significantly reduce the surviving fraction of OE33P and OE33R cells. P2 was shown to significantly reduce the surviving fraction in OE33P cells only. Quininib (Q1), P18 and P20 which were previously shown to inhibit angiogenesis *in-vivo* but did not alter real-time oxygen consumption rate in OE33P or OE33R cells and could not significantly alter radiosensitivity. In addition, P8 and P23 which were shown to have no anti-angiogenic or anti-metabolic activity did not significantly reduce the surviving fraction of OE33P or OE33R cells. The findings of this chapter confirmed the importance of oxidative metabolism in governing resistance in OAC whereby only compounds which could inhibit both angiogenesis and oxidative metabolism could significantly enhance radioresponse in OAC. From the results generated in this chapter, Pyrazinib (P3) was chosen as our lead compound to bring forward in future experiments given its robust anti-angiogenic and anti-metabolic activity in both model systems and due to its significant reduction in surviving fraction of both OE33P and OE33R cells following 2 Gy irradiation. Our lead compound Pyrazinib (P3) significantly

reduced the surviving fraction of OE33P and OE33R cells following 2, 4 and 6 Gy X-ray radiation doses compared to vehicle control treated cells.

In chapter 4, we sought to further investigate the ability of Pyrazinib (P3) to inhibit metabolic rate and enhance radiosensitivity under different environmental conditions. In addition, we sought to investigate whether Pyrazinib (P3) alters chemosensitivity using an isogenic model of OAC chemoresistance. Hypoxia is a well-known mediator of radioresistance given the important function of oxygen as a radiosensitiser. Both OE33P and OE33R cells were significantly more resistant to radiation therapy following culture under hypoxic conditions of 0.5% O_2. Pyrazinib (P3) significantly reduced the surviving fraction of OE33R cells cultured under hypoxia (0.5% O_2) following 4 Gy X-ray radiation. This result further highlighted the therapeutic potential of Pyrazinib (P3) as a novel radiosensitiser as it can improve radioresponse to both increasing doses of irradiation and can maintain its function under low oxygen conditions. To determine if the ability of Pyrazinib (P3) to enhance response to treatment was specific to radiotherapy alone we investigated whether Pyrazinib (P3) could augment the sensitivity of OE33 cells to cisplatin using an isogenic model of cisplatin resistance and 5-FU in OE33P and OE33R cells. Pyrazinib (P3) could not significantly enhance sensitivity of either OE33 Cis P or OE33 Cis R cells to cisplatin or OE33P and OE33R cells to 5-FU. This finding highlights the robust and significant ability of Pyrazinib (P3) to specifically enhance radiosensitivity in OAC cells. Having further demonstrated the radiosensitising activity of Pyrazinib (P3) in this chapter, we sought to investigate the action of Pyrazinib (P3) on another pro-tumorigenic process which has previously been linked with radioresistance, inflammation.

OAC has been demonstrated to be an inflammatory driven cancer and increased levels of certain inflammatory markers including C3a, C4a and IL-1β have been previously linked with treatment resistance in OAC [234, 415]. In this chapter using our *in-vitro* model of OAC radioresistance we investigated whether we could identify molecular markers of radioresistance using a proteomics-based approach. Proteomic profiling of OE33P and OE33R cells identified a number of molecular mediators to be significantly altered between OE33P and OE33R cells. Of the hits identified in this study, LIF and its receptor LIFR were validated in further studies both *in-vitro* and *ex-vivo*. LIF was found at significantly higher levels in treatment-naïve serum of OAC patients who subsequently had a poor response to treatment compared to patients who responded well to treatment. Evaluation of protein secretions from OE33P and OE33R cells found 9 factors to be significantly upregulated in OE33R cells compared to OE33P cells including IL-6, IL-4, IL-8, ICAM, IL-12p70, IL-2, IL-10, IP-10 and MCP-1, two factors were secreted at significantly lower levels from OE33R compared to OE33P cells including IL-1RA and GM-CSF. Pyrazinib (P3) significantly reduced the secretion of IL-4, IL-6, IL-8 and IL-13 from OE33R cells. A

number of the factors identified at higher levels in OE33R cells have been previously linked with radioresistance in multiple cancer types, thus the inhibition of IL-4, IL-6, IL-8 and IL-13 may contribute to the radiosensitising effect of Pyrazinib (P3) or could just be an additive effect which may contribute to anti-cancer activity of this agent. In-depth mechanism of action studies will be required to further elucidate the relationship between the inhibition of the secretion of these interleukins and the radiosensitising effect of Pyrazinib (P3).

Resistance to cisplatin is relatively under investigated in OAC, we sought to investigate the inflammatory secretome of an isogenic model of OAC cisplatin resistance. 18 proteins were secreted at significantly different levels from OE33 Cis P versus OE33 Cis R cells, IL-7 was the only one factor that was secreted at significantly higher levels from OE33 Cis R cells. Interestingly IL-7 was previously linked with cisplatin resistance in glioma cancer cell line and therapeutic targeting was associated with improved response, thus this may a novel a therapeutic targeting to overcome cisplatin resistance in OAC which requires further investigation in the future.

To progress our studies with Pyrazinib (P3) to the next stage of pre-clinical evaluation in chapter 6 we used an *ex-vivo* human model of OAC treatment-naïve biopsies to determine the effect of Pyrazinib (P3) on real-time metabolic rate, inflammatory secretions and immune cell function. Similar to our *in-vitro* findings, oxidative metabolism is an important energy pathway *ex-vivo*, relative oxygen consumption rate was significantly higher than relative ECAR in OAC treatment-naïve biopsies. Pyrazinib (P3) significantly reduced OCR in OAC treatment-naïve biopsies, this inhibition was independent of patient characteristics. OAC treatment-naïve biopsies were shown to adapt to changing oxygen conditions, under conditions of low oxygen (0.5% O_2) the ECAR:OCR ratio was significantly higher compared to normoxic conditions. Pyrazinib (P3) maintained its function under hypoxic conditions significantly inhibiting both OCR and ECAR in OAC biopsies cultured and treated under 0.5% O_2. This result was a critical finding demonstrating Pyrazinib (P3) maintains its action in an *ex-vivo* setting under both normoxic and hypoxic conditions. In addition, we profiled the inflammatory and angiogenic secretome of OAC treatment-naïve biopsies which demonstrated the inflammatory secretome of OAC treatment-naïve biopsies is highly heterogeneous. Pyrazinib (P3) treatment significantly reduced the secretion of IL-1β and promoted the secretion of IL-3 and IL-17B from OAC tumour biopsies. IL-1β has previously been linked to poor survival and treatment resistance in other cancer types so this inhibitory action may contribute to the anti-cancer effect of Pyrazinib (P3) which requires further investigation in *in-vivo* studies in the future. To position Pyrazinib (P3) as a potential radiosensitiser it is critical to understand how Pyrazinib (P3) interacts with immune cell function. Direct treatment with Pyrazinib (P3)

did not significantly alter the expression of dendritic cell maturation markers indicating that Pyrazinib (P3) is unlikely to affect the function of these professional antigen presenting cells however this requires further evaluation in functional assays.

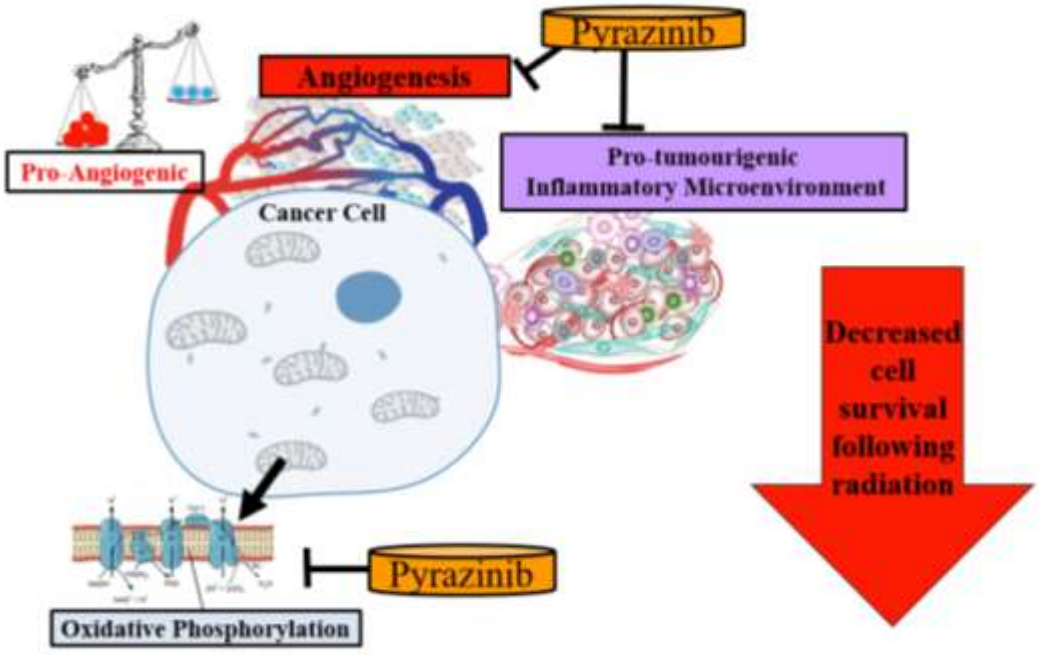

Figure 7-1 Concept diagram of main findings from thesis.
Schematic illustrating that Pyrazinib (P3) inhibits angiogenesis, oxidative phosphorylation and inflammatory protein secretions such as IL-1β. The inhibition of these biological processes was coupled with enhanced radiosensitivity shown by a significant reduction in cell survival of OAC cells following either 2, 4 or 6 Gy X-ray radiation.

The findings of this thesis have identified the small molecule compound Pyrazinib (P3) with anti-angiogenic, anti-metabolic and anti-inflammatory action which can enhance radiosensitivity both under normoxic and hypoxic conditions *in-vitro* in an isogenic model of OAC radioresistance **(Figure 7-1)**. For the first time we have identified a novel small molecule compound which robustly enhances radiosensitivity in a model of OAC radioresistance. There is currently an unmet clinical need for radiosensitisers which could be administered in combination with neo-adjuvant CRT to OAC patients to improve treatment response and further investigation of Pyrazinib (P3) in this field is warranted.

7.2. Future directions

The results generated from the research carried out in this Ph.D. thesis have generated a number of future research possibilities which are described below.

1. Previous research by our collaborators has identified Quininib (Q1) as a cysteinyl leukotriene receptor 2 antagonist. However, protein binding studies have revealed that Pyrazinib (P3) has <30% affinity for this receptor and Pyrazinib (P3) is not a CYSTLR2 antagonist. Mass spectrometry studies are currently ongoing to identify potential molecular targets of Pyrazinib (P3). Any hits identified from the mass spectrometry studies should be further validated *in-vitro* and *in-vivo* and manipulated to investigate their potential as molecular targets which play a role in the mechanism of action of Pyrazinib (P3).

2. We have demonstrated the anti-metabolic activity of Pyrazinib (P3) through its inhibition specifically of oxidative phosphorylation *in-vivo* in zebrafish, *in-vitro* in our isogenic model of OAC radioresistance and *ex-vivo* in OAC patient samples. It would also be of interest in the future to investigate how Pyrazinib (P3) is inducing this effect which may be linked to one of its major molecular targets. It would also be of interest to investigate if Pyrazinib (P3) has any effect on the pentose phosphate pathway which has also previously been linked with tumorigenesis. A major limitation of our studies was limited availability of tumour regression grades for each patient, it would be of interest in the future to determine if the metabolic rate of pre-treatment biopsies is correlated with treatment response, especially given the previous findings by our group showing ATP5B expression is significantly different in good responders compared to poor responders.

3. It will also be critical in the future to assess the effect of Pyrazinib (P3) on normal cell functions to determine whether the anti-angiogenic and anti-metabolic activity of Pyrazinib (P3) induces unwanted effects in normal cell function.

4. In our studies we have demonstrated the ability of Pyrazinib (P3) to enhance radiosensitivity *in-vitro* in an isogenic model of OAC radioresistance both under normoxic and hypoxic conditions (0.5 % O_2). In the future the radiosensitising action of Pyrazinib (P3) needs to be investigated in the *in-vivo* setting. OE33P and OE33R cells don't form large enough subcutaneous tumours for radiosensitising experiments (>100 mm^3) *in-vivo* thus an orthotropic and/or patient derived xenografts will be required for such studies, these studies have now begun with Xenopath (www.xenopat.com).

5. Nanoparticles are becoming an increasingly popular field of research in cancer treatment. In particular gold nanoparticles have been shown to enhance radiosensitivity in various cancer models. It would be of interest in the future to couple Pyrazinib (P3) to gold nanoparticles and evaluate if this has a synergistic effect in terms of enhancing radiosensitivity in our isogenic model of radioresistance. Prof O'Sullivan's lab has now received HRB-MRCG funding to conduct this work.

6. We reported for the first time a significant association between LIF secretion and LIFR expression and response to radiation treatment in OAC. It would be of interest in the future to investigate whether therapeutic targeting of the LIF pathway with specific inhibitors would alter radiosensitivity in OAC. Initially, it would be useful to investigate whether knockdown of LIF alters the radiosensitivity of our isogenic model of radioresistance *in-vitro* and *in-vivo*.

7. We have briefly investigated the effect of Pyrazinib (P3) treatment on dendritic cells by assessing the action of the direct treatment with Pyrazinib (P3) and Pyrazinib (P3) treated TCM on the expression of dendritic cell maturation markers, a surrogate measurement of dendritic cell function. Dendritic cells are professional antigen presenting cells which play a key role in anti-tumour immunity thus it will be critical in the future to also evaluate the action of Pyrazinib (P3) directly dendritic cell function. In addition, it will also be critical to evaluate the effect of Pyrazinib (P3) treatment on both T cell and natural killer cell function.

8. Immunotherapies are increasingly becoming the standard of care in many cancers whilst their utility in the treatment of OAC both alone and in combination with radiotherapy is currently being investigated in clinical trials Thus it would be critical in the future to evaluate the feasibility of Pyrazinib (P3) in combination with immunotherapies if they are adopted as part of the standard treatment regimen in OAC. The combination of Pyrazinib (P3) with immunotherapies if feasible, may have an additive effect in terms of enhancing radiosensitivity, as immunotherapies have previously been linked with enhanced radioresponse in many cancer models.

Publications

www.oncotarget.com Oncotarget, 2018, Vol. 9, (No. 72), pp: 33634-33647

Research Paper

Leukaemia inhibitory factor is associated with treatment resistance in oesophageal adenocarcinoma

Amy M. Buckley[1], Niamh Lynam-Lennon[1], Susan A. Kennedy[1], Margaret R. Dunne[1], John J. Aird[2], Emma K. Foley[1], Niamh Clarke[1], Narayanasamy Ravi[1], Dermot O'Toole[3], John V. Reynolds[1], Breandán N. Kennedy[4] and Jacintha O'Sullivan[1]

[1]Department of Surgery, Trinity Translational Medicine Institute, Trinity College Dublin, Dublin, Ireland

[2]Department of Histopathology and Morbid Anatomy, School of Medicine, Trinity College Dublin, Dublin, Ireland

[3]Department of Clinical Medicine, Trinity Translational Medicine Institute, Trinity College Dublin, Dublin, Ireland

[4]UCD Conway Institute & UCD School of Biomolecular and Biomedical Science, University College Dublin, Dublin, Ireland

Correspondence to: Jacintha O'Sullivan, **email:** OSULLJ4@tcd.ie

Keywords: LIF; oesophageal cancer; LIFR; treatment resistance; radiation

Received: May 05, 2018 **Accepted:** July 13, 2018 **Published:** September 14, 2018

Copyright: Buckley et al. This is an open-access article distributed under the terms of the Creative Commons Attribution License 3.0 (CC BY 3.0), which permits unrestricted use, distribution, and reproduction in any medium, provided the original author and source are credited.

ABSTRACT

Oesophageal cancer is an aggressive disease with a poor 5 year survival rate of <20% of diagnosed patients. Unfortunately, only 20-30% Oesophageal Adenocarinoma (OAC) patients show a beneficial response to neoadjuvant therapy (neoCT). Inflammation influences OAC given the increased risk of cancer development and poor outcome for obese patients where altered secretion of adipokines and cytokines from adipose tissue contributes a pro-tumourigenic environment. We carried out a large proteomics screen of 184 proteins to compare the inflammatory and oncogenic profiles of an isogenic radioresistant *in-vitro* model of OAC. We found that leukaemia inhibitory factor (LIF), an IL-6 type cytokine, was significantly elevated in radioresistant OAC cells (p=0.007). Furthermore, significantly higher circulating levels of LIF were present in the serum from treatment-naive OAC patients who had a subsequent poor pathological response to neo-adjuvant therapy, (p=0.037). Quantitative PCR analysis revealed expression of LIF receptor (LIFR) may function as a predictive indicator of response to neo-adjuvant chemoradiation therapy in OAC. LIF was demonstrated to be actively secreted from human OAC treatment-naïve biopsies and significantly correlated with the secretion of bFGF, VEGF-A and IL-8 (p<0.05, R=1), (p<0.05, R=0.9429), and (p<0.05, R=1) respectively. Importantly, LIF secretion negatively correlated with tumour infiltrating lymphocytes in pre-treatment OAC patient biopsies, (r=-0.8783, p=0.033). Elevated circulating LIF is a marker of poor response to neo-adjuvant treatment in OAC and secretion of this chemokine from the tumour is tightly linked with pro-tumourigenic mediators including bFGF, VEGF-A and IL-8. Targeting this pathway may be a novel mechanism enhance neoadjuvant treatment responses in OAC.

INTRODUCTION

Oesophageal cancer is the 8th most common cancer worldwide with approximately 456,000 new cases diagnosed annually [1]. Oesophageal cancer is an aggressive disease and the 6th most common cause of cancer related death, accounting for approximately 400,000 deaths annually [1]. Oesophageal cancer is classified into two histological subtypes, squamous cell carcinoma (SCC) and oesophageal adenocarcinoma (OAC) [2]. Whilst SCC is the predominant subtype globally in western populations, the incidence of OAC has

increased by approximately 48% over the past 15 years [1, 2]. The best outcomes are associated with early disease diagnosis [1, 2].

The current standard of care for OAC focuses on neoadjuvant treatment with chemotherapy (neoCT) alone or in combination with radiation; neoadjuvant chemoradiation (neoCRT) for locally advanced tumours, prior to surgery [3]. The MAGIC chemotherapy protocol consists of the administration of Epirubicin, Cisplatin or Oxaliplatin, and 5-Fluorouracil/or Capecitabine chemotherapy pre- and post-operatively, the CROSS protocol consists of the administration of carboplatin and paclitaxel chemotherapy with fractionated radiotherapy of 41.4 Gy over five weeks [4, 5]. A Cancer Trials Ireland-sponsored randomised, phase III clinical trial, Neo-AEGIS, is comparing neoadjuvant and adjuvant chemotherapy (MAGIC protocol) to neoadjuvant CRT (CROSS protocol) in OAC [6]. Surgery offers the best chance of loco-regional control and neoadjuvant treatment aims to reduce tumour burden prior to surgery to improve post-operative outcome, neoCRT in combination with surgery has been associated with higher rates of overall survival [3, 7, 8]. Unfortunately, only 20-30% of patients show a complete pathological response (pCR) to neo-adjuvant therapy with 70-80% of patients receiving a toxic treatment with little to no therapeutic gain and a subsequent delay to surgery [9–11]. Importantly, there are currently no clinico-pathological markers available to stratify patients who will achieve a beneficial response to radiation therapy.

Ionizing radiation (IR) is a crucial treatment modality used to exert local tumour control in over 50% of human malignancies [9]. IR primarily aims to exert local control through the induction of cellular DNA damage including critical double strand breaks (DSB) [9]. Response to radiation plays a central role in patient outcome in OAC, sensitivity of IR is inversely correlated to tumour burden [12]. Resistance to radiation therapy is polymodal and associated with a number of biological alterations both within the tumour itself and the surrounding microenvironment including; altered cell cycle [13] accelerated repopulation [14, 15], hypoxia [16], evasion of apoptosis [17], altered DNA damage response and enhanced DNA repair [18], and altered mitochondrial function and cellular energetics [19]. In OAC, altered mitochondrial function and DNA repair have been specifically linked to with a radio-resistant phenotype [18, 19]. Furthermore, OAC has been identified as an inflammatory-driven upper gastrointestinal cancer and previous studies have reported the role of inflammation as a negative regulator of response to radiation treatment in OAC [20, 21]. C3a and C4a, components of the complement system, were previously found to be upregulated in the pre-treatment serums of OAC patients having a subsequent poor pathological response to neoCRT, when compared to patients having a good response treatment [21].

A study by Liu *et al.* reported a potential role of the inflammatory cytokine leukaemia inhibitory factor (LIF) pathway in radioresistance of nasopharyngeal cancer (NPC), elevated serum levels were associated with significantly poorer recurrence-free survival [22]. LIF is an IL-6 type cytokine which signals through the leukaemia inhibitory factor receptor (LIFR) and glycoprotein (gp)-130 [23]. Other members of this family include IL-6, IL-11, cardiotrophin-1, cardiotrophin-like cytokine, ciliary neutrophic factor and oncostatin M [23]. Activation of the LIFR pathway is associated with the activation of a number of downstream pathways including the ERK1/2, JAK/STAT3 pathway, MAPK pathway and PI3K/AKT pathway [22, 24, 25]. Differential expression of LIF and/or LIFR is reported in a number of cancers including breast cancer, colorectal cancer (CRC), NPC, osteosarcoma, pancreatic cancer, melanoma, cholangiocarcinoma and cervical cancer [22, 24, 26–31].

LIF is a multifunctional protein and its role is often context-dependent. For example, in non-pathological conditions LIF plays an important role in embryonic implantation where dysregulated LIF expression links to implantation failure [32]. Furthermore in cancer, the role of LIF is complex and linked to both pro- and anti-tumorigenic functions dependent on the cancer type [26, 27, 29]. In breast cancer, LIF can promote tumour growth and migration *in-vitro* and *in-vivo* [24]. In addition, ectopic over-expression of LIF in CRC reduces chemotherapy-induced apoptosis in a p53-dependent manner [27]. In contrast, in cervical cancer, elevated LIF expression is associated with a reduction in cellular proliferation mediated by the downregulation of human papillomavirus-16 (HPV-16) oncogene expression [29]. However the role of LIF in OAC disease progression and treatment response has not yet been explored.

This study aimed to investigate the association of the pro-inflammatory cytokine LIF with response to neo-adjuvant treatment in OAC, in both *in-vitro* settings and in pre-treatment OAC patient serum and biopsies. We profiled the expression and secretion of LIF *in-vitro, in-vivo and ex-vivo*. LIF expression and secretion was upregulated in radioresistant cells of an isogenic model of OAC radioresistance *in-vitro*. *In-vivo*, circulating LIF was significantly elevated in pre-treatment serum from OAC patients with a subsequent poor response to neo-adjuvant treatment. *Ex-vivo*, LIF secretions from treatment naïve biopsies were positively correlated with secretions of IL-8, bFGF and VEGF-A. LIF secretions *ex-vivo* were negatively correlated with percentage lymphocyte infiltration into the tumour biopsies. In addition to LIF, downregulated LIFR expression is significantly associated with poor response to neoCRT in OAC pre-treatment biopsies. Our findings both *in-vitro* and in patient samples strongly implicate the LIF/LIFR pathway in treatment response in OAC which warrants further investigation as a therapeutic target.

RESULTS

LIF and LIFR expression is elevated in radioresistant OAC cells

To investigate the role of inflammatory and oncogenic mediators in radioresistance of OAC, we carried out a comprehensive proteomics screen using a previously described isogenic *in-vitro* model of OAC radioresistance [18]. The radioresistant OE33R cells, which were previously chronically irradiated, show significant resistance to radiation when compared to the parental OE33P cells, radiation sensitive cells. This isogenic cell line provides a unique model to investigate cellular and molecular mediators involved in radioresistance in OAC [18].

Given the multifaceted role of inflammation in cancer progression, we investigated the levels of 184 oncogenic and inflammatory proteins in the supernatants and cell lysates of isogenic OE33P and OE33R cells using a multiplex system. This broad screen of 184 inflammatory and oncogenic proteins found 3 proteins significantly downregulated and 21 proteins significantly upregulated intracellularly in cell lysates in OE33R; radioresistant cells, compared to radiation sensitive OE33P cells (Figure 1A, 1B). Proteins significantly downregulated were linked with immune signalling, hydrolysis and growth signalling (Figure 1A). A greater number of proteins were significantly upregulated in OE33R; radioresistant cells and are involved in different biological processes with the majority of those identified in this specific study linked with interleukin and chemokine signalling (Figure 1B). In particular, the inflammatory profile generated in this screen found that the interleukin 6 type cytokine, LIF, was significantly upregulated in radioresistant OE33R cells in terms of both secretion and intracellular expression ($p=0.007$, $p=0.006$), respectively, when compared to OE33P cells (Figure 1C, 1D). In addition, the LIF receptor, LIFR, was significantly upregulated ($p=0.022$) intracellularly in OE33R cells relative to OE33P cells (Figure 1E). This data indicates that the *in-vitro* expression of LIF is associated with a radioresistant phenotype in OAC.

Secreted LIF and intracellular LIF and LIFR expression is increased in radioresistant OAC cells

We sought to validate the data generated in the multiplex screen and to investigate secretion and intracellular expression profiles of LIF and LIFR post-irradiation. Secreted levels of LIF protein from OE33R cells were significantly higher when compared to OE33P cells at 0 Gy ($p=0.012$) and 24 hours post 2 Gy X-ray radiation ($p=0.001$), (Figure 2A). This result validated the screen data and illustrated that radiation significantly increased the secretion of LIF specifically in the radiation resistant OE33R cells ($p=0.008$) but no significant change was seen following 2 Gy irradiation in radiation sensitive OE33P cells. Given that baseline LIF expression is higher in OE33R cells and that radiation significantly induces LIF secretion in OE33R cells this result indicates LIF is an important molecular mediator of response to radiation in OAC. Supporting the protein data, LIF mRNA expression, as evaluated by RT-PCR, was elevated

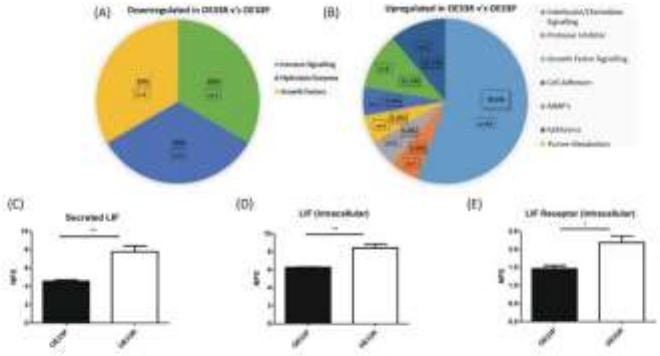

Figure 1: Secreted LIF and intracellular levels of LIF and LIF receptor (LIFR) are significantly higher in OE33R, radioresistant OAC cells compared to OE33P, and radiation sensitive cells. (A) Pie chart illustrating factors significantly downregulated intracellularly in OE33R (radioresistant) cells versus OE33P (radiation sensitive) cells ($p<0.05$). **(B)** Pie chart illustrating factors significantly upregulated intracellularly in OE33R cells versus OE33P cells ($p<0.05$). **(C)** Expression levels of secreted LIF in supernatant from OE33P radiation sensitive and OE33R, radiation resistant OAC cells (n=3) **(D)** Expression levels of LIF intracellularly in OE33P and OE33R cell lysates (n=3). **(E)** Expression levels of the LIFR intracellularly in OE33P and OE33R cell lysates (n=3). Unpaired t-test, $^{*}p<0.05$, $^{**}p<0.01$. NPX: Normalised Protein Expression.

in OE33R cells compared to OE33P cells (p=0.059) (Figure 2B). Interestingly, 24 hours after the cells were exposed to one dose of 2 Gy irradiation, the levels of LIF mRNA expression significantly decreased in both OE33P (p=0.034) and OE33R cells (p=0.013). Similar to our findings from the proteomics screen, LIFR expression was higher in OE33R cells and no significant change in expression was observed following 2 Gy irradiation (Figure 2C). Our findings suggest that LIF and LIFR may be expressed at higher levels in radiation-resistant OAC cells when compared to radiation sensitive cells although this is not significant, and that radiation treatment significantly increases the secretion of LIF by OE33R cells.

Significantly increased levels of circulating LIF and decreased levels of tumoural LIFR expression are associated with a poor response to neoadjuvant treatment in OAC

The levels of circulating LIF in the serum of treatment-naïve patients was evaluated in 26 OAC patient samples by ELISA, the patient cohort is outlined in Supplementary Table 1. Circulating levels of LIF were significantly elevated in patients who went on to have a subsequent poor pathological response following neo-adjuvant treatment (neoCT or neoCRT), with a Mandard tumour regression grade (TRG) of 3-5, compared to patients who had a subsequent good pathological response to neo-adjuvant treatment, with a TRG of 1-2 (p=0.037) (Figure 3A). Circulating levels of LIF were not significantly associated with other patient clinical characteristics, such as tumour stage, nodal status and stage of differentiation (Supplementary Figure 1). In contrast to circulating levels of LIF in serum, there was no significant difference in LIF mRNA expression in pre-treatment OAC tumour biopsies from good and poor responders to neoadjuvant treatment (Figure 3B) indicating that LIF in the circulation may be a more important predictive marker of treatment response than expression levels of LIF within the tumour. Furthermore, LIF expression was not significantly associated with other patient characteristics such as tumour stage, nodal status, stage of differentiation or body mass index (Supplementary Figure 2). LIFR expression (detected in 16 of 24 patients all of whom received neoCRT) was significantly reduced in tumour biopsies from patients having a subsequent poor pathological response to neoCRT (p<0.001), when compared to good responders (Figure 3C). Patient cohort for mRNA expression of LIF and LIFR is outlined in Supplementary Table 2. Circulating LIF and intra-tumoural LIFR expression was associated with neoCRT treatment response but not with other patient clinical characteristics (Supplementary Figures 1 and 3). This suggests that circulating LIF and intra-tumoural LIFR expression may function as valuable pre-treatment predictive indicators of response to neoadjuvant therapy.

LIF secretions were significantly correlated with the levels of secreted basic fibroblast growth factor (bFGF), vascular endothelial growth factor (VEGF-A) and IL-8 in OAC treatment-naïve human tumour explants *ex-vivo*

Given the importance of circulating LIF as a predictive marker of treatment response we further sought to investigate secreted levels of LIF from OAC patient tumours using a human *ex-vivo* model using treatment-naïve OAC patient tumour biopsies (patient cohort outlined in Supplementary Table 3). This unique model most closely recapitulates the tumour microenvironment, encompassing multiple cell types as seen *in-vivo*. *Ex-vivo* treatment-naïve human explant tissue was cultured for 6 OAC patients, and the secretions of LIF and a panel of inflammatory (n=10) and angiogenic (n=8) secretions in this Tumour Conditioned Media (TCM) were evaluated by ELISA. The secreted levels of these mediators were correlated in order to ascertain what other mediators in the *ex-vivo* tumour microenvironment were associated with LIF. We

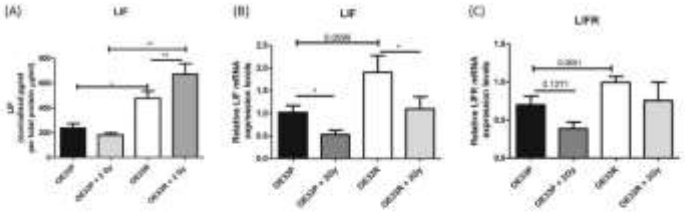

Figure 2: Validation of LIF and LIFR expression data from OLINK screen and investigation of expression and secretion profile of LIF and LIFR at 0 Gy and 24 hours post 2 Gy irradiation. (A) Secreted LIF protein from OE33P and OE33R cells which have been-mock irradiated and following 2 Gy X-ray irradiation was evaluated by ELISA, (n=4). **(B)** Relative expression of LIF mRNA in OE33P and OE33R cells at baseline and following 2 Gy Irradiation was evaluated by qPCR, (n=5). **(C)** Relative expression of LIFR mRNA at baseline in OE33R and OE33P cells and post 2 Gy irradiation was evaluated by qPCR, (n=5). Unpaired t-test used to compare OE33P and OE33R cell lines. Paired t-test used to compare within same cell lines. *p<0.05, **p<0.01.

demonstrate for the first time that LIF is actively secreted from OAC tumour biopsies (range: 24.61 1137.36 pg/mL) and significantly correlates with the levels of basic fibroblast growth factor (bFGF), VEGF-A and IL-8 ($p<0.05$, $R=1$) ($p<0.05$, $R=0.9429$) ($p<0.05$, $R=1$) respectively, (Figure 4A, 4B). Our studies *ex-vivo* have importantly demonstrated that LIF is secreted into the tumour microenvironment in OAC and is significantly positively correlated with pro-angiogenic and growth factors secretions.

Elevated secreted LIF negatively correlates with lymphocyte infiltration in human OAC pre-treatment biopsies

Following our *ex-vivo* studies using TCM generated from 6 patient OAC pre-treatment biopsies, we sought to investigate the association of secreted LIF with immune cell infiltrate and patient clinical characteristics. It is critical to understand the role of LIF in the tumour microenvironment, its association with other secreted growth factors and cytokines, and how LIF secretion is associated with immune cell infiltration of tumours. Immune cell infiltrates were determined by a pathologist using matched diagnostic H&E slides prepared from pre-treatment biopsies of 6 patients (patient cohort is outlined in Supplementary Table 3). We observed that LIF secretion was significantly negatively correlated with lymphocytic infiltration whereby lower LIF secretion was associated with greater lymphocyte infiltration in matched biopsies ($p=0.0333$, $r=-0.8783$) but no significant association was seen with other types of infiltrating cells, e.g. cosinophils, neutrophils, plasma cells (Figure 5A, 5B).

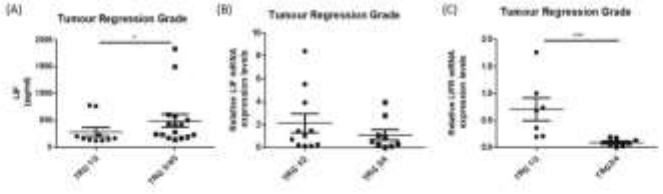

Figure 3: Circulating levels of LIF and tumoural levels of LIFR are significantly altered in OAC patients with a subsequent poor response to neo-adjuvant treatment. (A) Circulating LIF in pre-treatment serum of OAC patients was assessed by ELISA. Patients were divided into good (TRG 1/2) (n=10) and poor responders (TRG 3/4/5) (n=16) based on pathological response to neo-adjuvant treatment. **(B)** Relative mRNA expression of tumoural LIF in OAC pre-treatment biopsies from good (TRG 1/2) (n=11) and poor (TRG 3/4) (n=9) responders (n=20). **(C)** Relative mRNA expression of tumoural LIFR in OAC pre-treatment biopsies from good (TRG 1/2) (n=6) and poor (TRG 3/4) (n=10) responders. Statistical analysis was performed by Mann-Whitney U test. *p<0.05, **p<0.001.

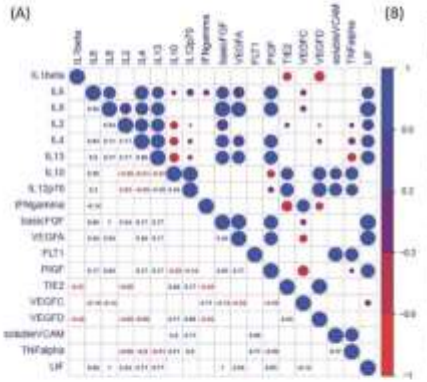

Factor	Spearman r	P value (two-tailed)	P value summary
IL1β	-0.02857	1	ns
IL6	0.6571	0.175	ns
IL8	**1**	**0.0028**	**
IL2	0.5429	0.2972	ns
IL4	0.7143	0.1361	ns
IL13	0.7714	0.1028	ns
IL10	0.08571	0.9194	ns
IL12p70	0.2571	0.6583	ns
IFNγ	0.1429	0.8028	ns
bFGF	**1**	**0.0028**	**
VEGF-A	**0.9429**	**0.0167**	*
PLT1	0.7143	0.1361	ns
PlGF	0.8286	0.0583	ns
TIE 2	0.2	0.7139	ns
VEGF-C	-0.1429	0.8028	ns
VEGF-D	0.2571	0.6583	ns
sVCAM	0.6571	0.175	ns
TNFα	0.3143	0.5639	ns

Figure 4: LIF secretions are significantly associated with the secretion bFGF, VEGF-A and IL-8 *ex-vivo*. (A) CorrPlot illustrating the correlation values of secreted LIF to secreted angiogenic and inflammatory secretions evaluated by ELISA from OAC treatment naive tumour biopsies cultured *ex-vivo* (n=6). Blue indicates a positive correlation, red negative correlation. **(B)** Table showing Correlation of secreted LIF secreted angiogenic and inflammatory secretions in OAC treatment naive biopsies cultured *ex-vivo* (n=6). Secretion of inflammatory and angiogenic mediators was determined by ELISA. Spearman correlation to LIF secretions where Spearman r 0.4-0.59 moderate, 0.6-0.79 strong and 0.8-1 very strong. *p<0.05, **p<0.01.

DISCUSSION

LIF is a multi-functional cytokine which under non-pathological conditions plays an essential role in embryonic implantation, bone formation and neuronal development [32, 33]. In cancer, previous studies have demonstrated the role of LIF as an oncogenic mediator which stimulates cancer growth, proliferation and metastasis, and have associated LIF with both resistance to radiation and chemotherapy treatments [22, 24, 27]. To our knowledge this is the first study to investigate the role of LIF in OAC. OAC is an aggressive disease with a poor prognosis, currently over 70% of patients don't show a beneficial response to neo-adjuvant therapy [11]. A complete pathological response to treatment is associated with increased survival, thus it is critical to gain further insight into the molecular mediators which play a role in treatment response in OAC.

In-vitro, both in our screen and validation study, LIF and LIFR expression was elevated in radioresistant OE33R cells relative to radiation sensitive OE33P cells. Overexpression of LIF at the mRNA level has been previously shown in a number of cell lines such as breast cancer where LIF expression was found to be significantly higher in breast cancer cells with greater metastatic capability [24]. *In-vivo*, targeting of the LIF/LIFR pathway through inhibition of LIFR with small interfering RNA was shown to inhibit metastasis in rhabdomyosarcoma xenografts, further highlighting both the role of LIF in tumourigenesis and therapeutic targeting potential of this pathway [34]. Furthermore in NPC, treatment with soluble LIFR, an antagonist of LIF or rapamycin, an mTOR inhibitor of LIF, was found to reduce cell survival and tumour growth following irradiation *in-vitro* and *in-vivo* [22]. Given these findings in the literature in addition to our studies in OAC, the potential of targeting this pathway to enhance radiosensitivity in OAC must be investigated in future studies.

LIF secretion was significantly higher in OE33R cells than OE33P cells, complementing our findings at the gene level. An important finding from this result was the differential secretion of LIF in OE33P and OE33R cells following one dose of 2 Gy radiation, the response to radiation was cell line specific, with elevated levels of secreted LIF identified in radioresistant OE33R cells only. In contrast, at the gene level LIF expression was reduced in both cell lines 24 hours following 2 Gy irradiation, the response to radiation was cell line specific, with elevated levels of secreted LIF identified in radioresistant OE33R cells only, it would be interesting to evaluate the levels of LIF at an earlier time point following irradiation to see if initially LIF expression is elevated in response to irradiation. Higher LIF secretion in the OE33R cells may result in increased activation of the LIF/LIFR pathway in OE33R cells and could be contributing to the radioresistant phenotype. *In-vivo*, LIF was previously shown to significantly enhance radioresistance in a NPC xenograft model whereby the administration of soluble LIF following one dose of 7 Gy irradiation significantly enhanced resistance to radiation and promoted tumour growth [22]. The enhanced tumour growth following LIF administration is supported by other studies in both breast and pancreatic cancer, where LIF administration and ectopic expression was shown to promote tumour growth and tumour progression *in-vitro* [24, 28]. Our findings, along with the current literature, indicate that LIF may

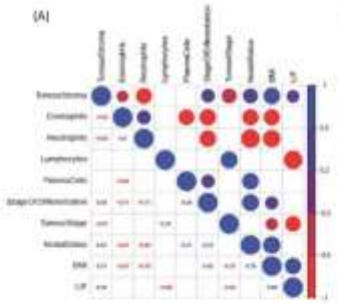

(B)

Factor	Spearman r	P value (two-tailed)	P value summary
% Tumour Stroma	0.3018	0.4194	ns
% Eosinophils Infiltrate	-0.414	0.4194	ns
% Neutrophils Infiltrate	-0.207	0.7139	ns
% Lymphocytes Infiltrate	**-0.8783**	**0.0333**	*
% Plasma Cells Infiltrate	-0.1309	0.8028	ns
Stage Of Differentiation	0.09759	0.9194	ns
Tumour Stage	-0.6172	0.175	ns
Nodal Status	0.09258	0.9194	ns
BMI	0.6789	0.1361	ns

Figure 5: Elevated levels of secreted LIF negatively correlates with lymphocyte infiltration in human OAC pre-treatment biopsies. (A) CorrPlot illustrating the correlation values of secreted LIF from OAC treatment naïve biopsies cultured *ex-vivo* to patient clinical characteristics (stage of differentiation, tumour stage, nodal status and BMI) and percentage tumour stroma immune cell infiltrations (neutrophils, eosinophils, lymphocytes and plasma cells). Blue indicates a positive correlation, red negative correlation, (n=6) **(B)** Table showing Correlation values of secreted LIF to patient clinical characteristics and immune cell infiltrate (n=6). Spearman correlation to LIF secretions where Spearman r 0.4-0.59 moderate, 0.6-0.79 strong and 0.8-1 very strong. *p<0.05.

play a role in treatment resistance in OAC. Enhanced cell growth and tumour progression as a result of LIF pathway activation has been linked to downstream activation of the JAK/STAT3 and Akt/mTOR pathways. In these studies, mTOR expression has been identified in both OE33P and OE33R cells previously (data not shown) but the actual pathway through which LIF signals in OAC requires further investigation, especially since inhibition of mTOR has previously been shown to enhance radiosensitivity in oesophageal SCC, lung and pancreatic cancer [24, 35, 36].

In OAC patient pre-treatment serum, circulating LIF was found at significantly higher levels in OAC treatment-naïve patients who went on to have a subsequent poor pathological response to neoadjuvant treatment with a TRG of 3-5. This result complements our findings *in-vitro* whereby elevated LIF protein secretion was associated with radiation resistance. This result was similar to that seen by Liu *et al.*, in NPC where elevated levels of circulating LIF in serum were positively associated with a poor response to treatment and subsequent local tumour recurrence [22]. Our study demonstrates that elevated circulating levels of LIF is associated with poor response to neoadjuvant treatment (MAGIC or CROSS) and may contribute to subsequent disease progression in OAC. Circulating LIF may therefore have important value as predictive marker of treatment response and as a therapeutic target to halt tumour progression, in the future screening with a larger number of patients in each arm of the trial is warranted for validation of these preliminary observations. Our findings are supported by a study which showed that elevated IL-6 in serum, a key oncogenic cytokine from the same family was shown to predict a two-fold increased risk of progression to malignancy from Barrett's oesophagus (BO), a chronic inflammatory condition and pre-disposing risk factor of OAC [37].

LIFR mRNA expression was significantly reduced in treatment naïve OAC tumour biopsies from patients having a subsequent poor pathological response to treatment, suggesting that a loss in receptor expression is associated with poor treatment response. This result may seem surprising given that elevated circulating LIF was demonstrated to be associated with a poor response. However, several other studies support this data. LIFR expression has previously been identified in breast cancer, CRC, gastric cancer, liver cancer and pancreatic cancer [28, 30, 38, 39]. In hepatocellular carcinoma (HCC), LIFR was found to negatively regulate metastasis via the PI3K/Akt pathway and downregulated expression of LIFR was an indicator of poor prognosis [40]. A previous study in a large cohort of metastatic breast cancer patients also found loss of LIFR to be associated with poor clinical outcome [30]. LIFR was found to promote membrane localisation factor Scribble which in turn led to the activation of Hippo signalling and phosphorylation and functional inactivation of the transcriptional co-activator Yes-associated protein 1 (YAP1) and subsequent suppression of tumour metastasis [30]. It has been suggested that LIFR may be reduced in tumour tissues as a result of the promoter undergoing hypermethylation [25]. Furthermore, in pancreatic cancer tissue microarrays, downregulated LIFR was significantly associated with Tumour Node Metastasis (TNM) stage and lymph node metastasis, and silencing of LIFR *in-vitro* reduced colony formation and metastatic potential of pancreatic cancer cells [38].

The significantly lower levels of LIFR expression in OAC patients with a poor response to neoCRT highlights the loss of LIFR as a predictive indicator of poor outcome, similar to findings in other cancers. This result did not reflect our findings *in-vitro* however tumour biopsies reflect the *ex-vivo* tumour microenvironment to a greater extent consisting of multiple cell types and thus more efficiently reflect what is going on in a tumour *in-vivo*. LIFR may act as an additive predictive indicator for treatment response in OAC, however this result would need to be validated in a larger patient cohort.

Therapeutic targeting of this receptor in OAC warrants further investigation, particularly given that *in-vivo* in pancreatic cancer xenografts, primary tumour volume and lung metastasis were increased by LIFR silencing and tumour volume and metastasis were reduced and inhibited respectively when LIFR was overexpressed in primary implanted pancreatic cancer cells [38]. These studies support our data, which suggests that decreased LIFR in pre-treatment OAC tumour biopsies is a predictive marker of poor response to neoadjuvant treatment. However, this requires further validation in a larger independent patient cohort.

Given the predictive importance of LIF as a circulating mediator, we then sought to investigate the role of secreted LIF in the tumour microenvironment from human pre-treatment OAC tumour biopsies which we cultured *ex-vivo*. We demonstrated for the first time that LIF is secreted from OAC tumours. The angiogenic and inflammatory factors produced by OAC tumours play an important role in disease progression and response to treatment. Secreted LIF was significantly correlated with the secreted levels of bFGF, VEGF-A and IL-8 in the matched TCM of treatment naïve OAC tumour explants. bFGF, similar to LIF, is a pleiotropic factor which was shown to promote cell growth, angiogenesis and differentiation and to prevent apoptosis in cancer [41]. LIF and bFGF are potent growth factors which have been previously shown to stimulate cancer growth in osteosarcoma [24, 42]. In osteosarcoma cells, bFGF was found to enhance cancer growth through hyper activation of ERK 1/2 [42]. Both alone and in combination, LIF and bFGF were found to significantly enhance cell growth of osteosarcoma cells. Importantly, when they were administered together, this produced an additive effect on tumour growth, highlighting a synergistic interplay between both factors [42]. Anti-bFGF antibodies were

shown to enhance radiosensitivity in oesophageal SCC through a reduction in colony formation *in-vitro* [36]. In addition, targeting of bFGF by a peptide has been shown to improve chemo-sensitivity in CRC [43]. These findings in the literature and within our study show that LIF and bFGF together both play important roles in cancer progression and treatment response in many cancers and may influence both OAC cells and host immunity by functioning as part of the active cytokine network. Given the ability of both bFGF and LIF to enhance radiosensitivity in previous studies and the strong correlation between both factors in OAC, the potential of the combined targeting to enhance radiosensitivity in OAC strongly warrants further investigation.

Furthermore, secreted VEGF-A was significantly correlated with LIF in the OAC tumour microenvironment. VEGF-A is a well-known tumourigenic mediator which plays a key role in angiogenesis, a process tightly linked with treatment resistance. Targeting of VEGF-A *in-vivo* was shown to enhance radiation response in a head and neck xenograft model [44]. It is unsurprising that LIF, a potent tumourigenic growth factor is strongly associated with VEGF-A, given the necessity of tumour vasculature to promote tumour growth and survival. Given the significant relationship we have shown between LIF and treatment resistance in OAC, and the known role of VEGF-A in tumourigenesis and treatment response, the potential of targeting both mediators to enhance response should be explored in future.

In addition, LIF was found to significantly correlate with IL-8, a pro-inflammatory cytokine which signals through the CXCR1/2 receptors. This signalling results in PI3K, MAPK and JAK2 pathway activation, and has been found to promote cell proliferation, angiogenesis and metastasis in xenograft models where administration of an anti-IL-8 monoclonal antibody attenuated tumour growth and metastatic potential [45]. IL-8 expression has previously been correlated with LIF expression in other inflammatory diseases such as psoriasis [46]. Furthermore, both IL-8 and VEGF-A have been shown to play an important role in tumour angiogenesis, a key process involved in treatment resistance which, when inhibited with targeted therapy, can enhance radiation response *in-vivo* [44, 45].

Given the pivotal role of LIF, bFGF, VEGF-A and IL-8 in tumourigenesis and their correlated secretion in OAC, the potential of targeting these growth factors and cytokines to improve patient response to neoadjuvant treatment and to inhibit tumour progression in OAC must be investigated in future studies. Whilst targeting all 4 mediators simultaneously may not be clinically feasible, this study offers insight into potential mediators which could be targeted to enhance radiosensitivity and possible compensatory mediators which may be upregulated in response to such targeting, possibly providing novel mechanistic insight to resistance to mechanisms that may arise following targeting of one of the mediators in isolation. This study also highlights the potential of sequential targeting of these factors to overcome resistance and to improve treatment response.

OAC tumours do not function in isolation and interaction of the tumour with the host plays a significant role in tumour progression. The recent successes of immunotherapies in the clinic highlight the key role of the host immune system in tumour control, thus we sought to investigate the relationship between LIF and immune cell tumour infiltration. LIF secretion from the tumour microenvironment was negatively correlated to percentage of lymphocyte infiltrate in matched OAC pre-treatment biopsies. The negative correlation between LIF and lymphocyte infiltration, where LIF secretion from the tumour microenvironment is increased in patients with low tumour infiltrating lymphocytes (TILs) is a significant finding, given that high lymphocyte infiltration has previously been associated with improved patient outcome in SCC and many other cancer types TILs are thought to play a pivotal role in tumour control through activation of the host anti-tumour immune response [47].In addition, higher TILs have been associated with improved prognosis in breast, colon, ovarian and lung cancer [48–50]. The relationship between LIF secretion and immune activation is relatively under-explored in cancer, and it is unknown whether elevated LIF secretion in biopsies with reduced lymphocyte infiltrate is a causal relationship or if this is just an association which could have the potential to determine response of patients to treatment [47, 51]. It is however important to note that immune cell infiltration analysis was carried out on pre-treatment diagnostic OAC biopsies which only represent a very small portion of tumour and the invasive edge was not represented in these biopsies and thus inflammatory infiltrate of the invasive edge could not be analysed. It will be critical to evaluate the effect of targeting the LIF pathway, not only in terms of treatment response but also on immune cell activation and infiltration in OAC.

In this study we have shown an association between expression of the IL-6 family member LIF and treatment response in OAC, both in *in-vitro* cell line models, and in pre-treatment OAC patient serum and biopsies. LIF secretion and expression is elevated in radioresistant cells *in-vitro*. Importantly, circulating LIF is elevated in patients with a subsequent poor response to neo-adjuvant treatment, implicating this pathway in treatment resistance in OAC. LIF secreted *ex-vivo*, from human OAC treatment-naïve biopsies, correlates with the secretion of key tumourigenic growth factors, including bFGF, VEGF-A and IL-8, indicating that these factors are tightly associated with one another in the tumour microenvironment of OAC. A significant finding of this study is the negative correlation of LIF, which we have identified as a poor prognostic in OAC, with percentage of tumour infiltrating lymphocytes which have been reported

to play a key role in the host response to tumour and serve as a marker of prognosis in multiple cancer types [51]. The use of LIF as a circulating marker of treatment response in OAC needs to be validated in a larger patient cohort following this pilot study. Furthermore, given the increased secretion of LIF from our radioresistant cells following irradiation, and the tight association of secreted LIF with other pro-tumourigenic factors from our OAC patient tumours, targeting of the LIF pathway to boost treatment response warrants investigation in future studies in OAC.

MATERIALS AND METHODS

Generation of the OE33P and OE33R cell lines

The human OE33 oesophageal adenocarcinoma cell line was obtained from the European Collection of Authenticated Cell Cultures. The isogenic model of radioresistant OAC; OE33P (radiosensitive) and OE33R (radioresistant) cells was generated, characterised and cultured in our department as previously described [18].

Preparation of OE33P and OE33R cell lysates for OLINK proseek proteomics analysis

OE33P and OE33R cells were seeded at a density of 2.5 x10^5 in 6 well plates in 1.5 mL complete Roswell Park Memorial Institute medium (RPMI) (supplemented with 10% FBS and 1% penstrep) at 37°C in 5% CO_2. At 48 h supernatant was removed and stored at -20°C. Cells were washed twice with 300 µL of ice cold PBS. NP40 cell lysis buffer (Invitrogen) was supplemented on day of use with 100 µL PhenylImethylsulfonyl fluoride (PMSF) (Sigma-Aldrich) per 10 mL cell lysis buffer and 1000 µL protease inhibitor (Sigma-Aldrich) per 10 mL cell lysis buffer. Supplemented ice cold NP40 cell lysis buffer (200 uL) was added to each well and left on ice for 20 min. Cell lysate solutions were pipetted up and down following incubation to aid lysis process. Lysis buffer solute was centrifuged for 20 min at 13,400 x g at 4°C. Lysates was aspirated off and stored at -80°C. 20 µL of each supernatant and cell lysate of equal protein concentration was determined using the Pierce Bicinchoninic acid (BCA) assay and was placed in a MicroAmp plate (Applied Biosystems) and sealed and shipped on dry ice to OLINK proteomics (Uppsala, Sweden).

Proseek proteomics assay

OLINK proteomics conducted a proseek proteomics screen of our samples, including supernatants and cell lysates from 3 independent experiments obtained from OE33P and OE33R cells. Samples were run on both their Inflammatory I and oncology II platform, with samples screened for expression of a total 184 proteins (92 per panel). All samples were of equal protein concentration prior to shipping to OLINK. The readout of normalised protein expressions values (NPX) was obtained from OLINK following the assay for statistical analysis. The NPX value indicates the relative quantification for that protein and thus can only be used for comparison between samples for each protein and cannot be used for comparing one protein to another. A hit was determined as significant when $p<0.05$, p values were adjusted for multiple testing using the false discovery rate method.

Irradiation

Irradiation was performed using a Gulmay Medical X-ray generator, (RS225) (Gulmay Medical), at a dose rate of 3.25 Gray (Gy) per min.

Patient samples

Following ethical approval (Joint St James's Hospital/AMNCH ethical review board) and written informed consent, diagnostic biopsy specimens were taken from patients with a diagnosis of operable OAC, by a qualified endoscopist prior to neoadjuvant therapy. Histologic confirmation of tumour tissue in biopsies was performed by a pathologist using routine hematoxylin and eosin staining. Patients with a subsequent TRG score received a complete course of neo-adjuvant therapy. All patient samples in the qPCR study received neoCRT according to the CROSS regimen [6]. In the serum study, 16 patients received neoCRT according to the CROSS regimen and 10 patients received neoadjuvant chemotherapy only according to the MAGIC regimen [6]. All patient tumour and serum samples used in this study were taken prior to initiation pre-treatment.

RNA isolation from OE33P and OE33R cells

RNA was isolated from cell lines using the TRI Reagent®, as per the manufacturer's instructions. Cells were seeded at a density of 2.5 x 10^5 cells/well in 6-well plates and allowed to adhere overnight. 24 h later OE33P and OE33R were either mock irradiated or irradiated with 2 Gy irradiation. RNA was isolated from cells at 24 h post irradiation using TRI Reagent® (Molecular Research Centre, Montgomery Road, OH, USA), as per the manufacturers instructions. The RNA pellet was re-suspended in 30 µL RNAase free molecular grade H_20 and stored at -80°C.

RNA isolation from OAC pre-treatment biopsies

RNA from patient tumour tissue samples was isolated using a miRNeasy RNA isolation kit (Qiagen), as per the manufacturer's instructions. Total RNA was quantified spectrophotometrically using a Nanodrop 1000 spectrophotometer v3.3 (Thermo Fisher Scientific).

Total RNA (1.5 µg) was reverse transcribed to cDNA using a High Capacity cDNA RT Kit (Thermo Fisher Scientific).

RNA quantification of cell lines and OAC patient mRNA

RNA quantification was determined spectrophotometrically, using a Nanodrop 1000 spectrophotometer (version 3.1.0, Nanodrop technologies, DE, USA). 1 µL RNase-free water was used to blank the instrument prior to RNA analysis. 1 µL of each sample of isolated RNA was loaded onto the instrument and concentration was measured in ng/µL. 260:280 and 260/230 ratios were also recorded to evaluate RNA quality.

cDNA synthesis from cell lines and OAC patient mRNA

For cell line samples, total RNA (1 µg total RNA) was reverse transcribed to cDNA using the following method. To anneal the primers to the RNA, the sample was heated for 10 min at 70°C, and immediately chilled for at least 1 min at 4°C. A master mix containing RNaseOUT (Invitrogen, Carlsbad, CA, USA) recombinant ribonuclease inhibitor (1unit/µl), dNTPs (Invitrogen, Carlsbad, CA, USA) (10 mM, prepared as a 1:1:1:1 ratio of dATP, dGTP, dTTP and dCTP), Bioscript reverse transcriptase (200units/µl) (Bioline, Kilkenny, Ireland) and 5X Bioscript Reaction Buffer (Bioline, Kilkenny, Ireland) in RNase-free water was added to each sample. Samples were incubated for 1 h at 37°C then 10 min at 70°C and held at 4°C. The resulting cDNA was stored at -20°C. For patient samples, total RNA (1.5 µg) was reverse transcribed to cDNA using a High Capacity cDNA RT Kit (Thermo Fisher Scientific).

Quantitative real time PCR of cell lines and OAC patient samples

qPCR was performed using TaqMan primer probes and a Quant Studio 5 real-time thermal cycler (Thermo Fisher Scientific). 18S was used as an endogenous control for data normalization. PCR data were analyzed by the $2^{-\Delta\Delta Ct}$ Livak method [52].

Generation of OE33P and OE33R cell supernatants for ELISA

Cells were seeded at a density of 2.5 x 10^5 cells/well in 6-well plates and allowed to adhere overnight at 37°C in 5% CO_2. After 24 hours, OE33P and OE33R were either mock irradiated or irradiated with 2 Gy irradiation. 24 h later supernatant was removed and stored at -20°C. Cells were washed twice with 300 µL of ice cold PBS. RIPA cell lysis buffer was supplemented on day of use with 100 µL phenylmethylsulfonyl fluoride (PMSF) (Sigma-Aldrich) per 10 mL cell lysis buffer and one protease inhibitor cocktail tablet (Roche) per 10 mL cell lysis buffer. 200 µL of supplemented ice cold RIPA cell lysis buffer was added to each well and left on ice for 20 min. Cell solutions were pipetted up and down following incubation to aid cell lysis. Lysis buffer solute was incubated for 20 min at 13,400 x g at 4°C. Lysates were aspirated and stored at -80°C. Protein concentration was determined by BCA assay (Pierce).

Serum sampling

Following informed, written consent, OAC patient treatment naïve serum was collected using Z-clot activator serum tubes (Greiner Bio-One, Gloustershire, United Kingdom). Samples were centrifuged at 1150 ×g for 10 min, the serum decanted, aliquoted, and subsequently stored at -80°C in a designated biobank.

Generation of tumour conditioned media

Following informed consent, biopsies were collected at endoscopy, immediately placed on saline-soaked gauze and were transported within 10 minutes to the laboratory. Biopsies were placed in culture as follows: biopsies were placed into a well of a 12 well plate containing 1 mL M199 medium (Gibco) supplemented with 10% FBS (Gibco), 1 µg/mL insulin and 1% penicillin/streptomycin. Following 24 hour culture, Tumour conditioned media (TCM) was collected stored at -80°C. The remaining tissue was snap-frozen in liquid nitrogen and stored at -80°C.

Enzyme linked immunosorbent assay (ELISA)

Supernatant from OE33R and OE33P cells, OAC patient treatment naïve TCM and OAC treatment naïve serums were defrosted on ice. The secretion of cytokines and angiogenic growth factors was analysed by ELISA as per the manufacturer's instructions. To assess the secretion of LIF from OE33P and OE33R cell supernatants, patient serum and TCM, an individual LIF ELISA kit was used (LifeSpan Biosciences). To assess angiogenic and inflammatory cytokine release, 2 multiplex kits were used (Meso Scale Diagnostics, USA). For angiogenic markers, a 7-plex ELISA was used to quantify levels of bFGF (basic), Flt-1/VEGFR-1, PlGF, Tie-2, VEGF-A, VEGF-C, VEGF-D. For inflammatory cytokines, a 10-plex assay was used to quantify IFN-γ, IL-10, IL-12p70, IL-13, IL-1β, IL-2, IL-4, IL-6, IL-8 and TNF-α. ICAM secretions were detected by a separate ELISA (R&D Systems). Secretion data for all factors was normalised appropriately to cell lysate protein content and explant protein content using the BCA assay (Pierce) for cell supernatant and TCM secretions, respectively.

Evaluation of inflammatory infiltrate in OAC pre-treatment biopsies

Routine haematoxylin and eosin stained sections from diagnostic biopsy material were reviewed by a pathologist who was blinded to clinical outcomes. Inflammatory cell density and tumour stroma percentage were assessed in tissue fragments containing invasive carcinoma. The inflammatory cell density was classified as either absent, low-grade (mild/patchy increase in inflammatory cells) or high-grade (prominent inflammatory infiltrate and/or involvement and destruction of cancer cell islands). The presence of eosinophils, neutrophils, lymphocytes and plasma cells was also assessed and similarly classified as either absent, low-grade or high-grade. The tumour stroma percentage (TSP) was assessed by estimating the proportion of stroma as a percentage of the visible field from an area of carcinoma, excluding areas of mucin deposition or necrosis. Tumours were classified as low-TSP if stroma accounted for 50% of the visible field or high-TSP if stroma accounted for 50% of the visible field.

Statistical analysis

Statistical analysis was performed using GraphPad Prism version 5 software (GraphPad Software, CA, USA). Scientific data were expressed as mean ± standard error of the mean (SEM). SEM was calculated as the standard deviation of the original samples divided by the square root of the sample size. Specific statistical tests used are indicated in figure legends. Correlations were carried out using R software version 3.4.1. Graphical representations of correlations were generated with the R package 'corrplot'. For all statistical analysis, differences were considered to be statistically significant at $p<0.05$.

Abbreviations

bFGF: Basic Fibroblast Growth Factor; CRC: Colorectal Cancer; IL-8: Interleukin 8; LIF: Leukemia Inhibitory Factor; LIFR: Leukemia Inhibitory Factor Receptor; HCC: Hepatocellular Carcinoma; ICAM: Intracellular Adhesion Molecule 1; mTOR: Mammalian Target of Rapamycin; OAC: Oesophageal Adenocarcinoma; NeoCRT: Neoadjuvant Chemoradiation Therapy; NPC: Nasopharyngeal Cancer; SCC: Squamous Cell Carcinoma; TRG: Tumour Regression Grade; TCM: Tumour Conditioned Media; VEGF: Vascular Endothelial Growth Factor.

Author contributions

Experiments Designed by: AB JOS. Performed the experiments: AB, NLL, SK, JA. Analysed the data: AB, NLL, SK, JA, MD, JOS. Contributed reagents/materials/analysis tools: DOT NR JVR. Fresh sample acquisition: NC, EF. Wrote the paper: AB, BK, JOS.

ACKNOWLEDGMENTS

The authors would like to thank all patients who consented for their specimens and data to be used for this study.

CONFLICTS OF INTEREST

The authors declare no conflicts of interest.

FUNDING

Funding for this work was provided by the Irish Cancer Society (Grant: CRS15BUC) and Science Foundation Ireland; (Grant: 16/TIDA/4063).

REFERENCES

1. Ferlay J, Soerjomataram I, Dikshit R, Eser S, Mathers C, Rebelo M, Parkin DM, Forman D, Bray F. Cancer incidence and mortality worldwide: sources, methods and major patterns in GLOBOCAN 2012. Int J Cancer. 2015; 136:E359–86. https://doi.org/10.1002/ijc.29210.
2. Arnold M, Soerjomataram I, Ferlay J, Forman D. Global incidence of oesophageal cancer by histological subtype in 2012. Gut. 2015; 64:381–87. https://doi.org/10.1136/gutjnl-2014-308124.
3. Cools-Lartigue J, Spicer J, Ferri LE. Current status of management of malignant disease: current management of esophageal cancer. J Gastrointest Surg. 2015; 19:964–72. https://doi.org/10.1007/s11605-014-2701-3.
4. Cunningham D, Allum WH, Stenning SP, Thompson JN, Van de Velde CJ, Nicolson M, Scarffe JH, Lofts FJ, Falk SJ, Iveson TJ, Smith DB, Langley RE, Verma M, et al, and MAGIC Trial Participants. Perioperative chemotherapy versus surgery alone for resectable gastroesophageal cancer. N Engl J Med. 2006; 355:11–20. https://doi.org/10.1056/NEJMoa055531.
5. van Hagen P, Hulshof MC, van Lanschot JJ, Steyerberg EW, van Berge Henegouwen MI, Wijnhoven BP, Richel DJ, Nieuwenhuijzen GA, Hospers GA, Bonenkamp JJ, Cuesta MA, Blaisse RJ, Busch OR, et al, and CROSS Group. Preoperative chemoradiotherapy for esophageal or junctional cancer. N Engl J Med. 2012; 366:2074–84. https://doi.org/10.1056/NEJMoa1112088.
6. Reynolds JV, Preston SR, O'Neill B, Baeksgaard L, Griffin SM, Mariette C, Cuffe S, Cunningham M, Crosby T, Parker I, Hofland K, Hanna G, Svendsen LB, et al. ICORG 10-14: NEOadjuvant trial in Adenocarcinoma of the oEsophagus and oesophagoGastric junction International Study

(Neo-AEGIS). BMC Cancer. 2017; 17:401. https://doi.org/10.1186/s12885-017-3386-2.

7. Walsh TN, Noonan N, Hollywood D, Kelly A, Keeling N, Hennessy TP. A comparison of multimodal therapy and surgery for esophageal adenocarcinoma. N Engl J Med. 1996; 335:462–67. https://doi.org/10.1056/NEJM199608153350702.

8. Jin HL, Zhu H, Ling TS, Zhang HJ, Shi RH. Neoadjuvant chemoradiotherapy for resectable esophageal carcinoma: a meta-analysis. World J Gastroenterol. 2009; 15:5983–91. https://doi.org/10.3748/wjg.15.5983.

9. Lord CJ, Ashworth A. The DNA damage response and cancer therapy. Nature. 2012; 481:287–94. https://doi.org/10.1038/nature10760.

10. Pasini F, de Manzoni G, Zanoni A, Grandinetti A, Capirci C, Pavarana M, Tomezzoli A, Rubello D, Cordiano C. Neoadjuvant therapy with weekly docetaxel and cisplatin, 5-fluorouracil continuous infusion, and concurrent radiotherapy in patients with locally advanced esophageal cancer produced a high percentage of long-lasting pathological complete response: a phase 2 study. Cancer. 2013; 119:939–45. https://doi.org/10.1002/cncr.27822.

11. Donohoe CL, Reynolds JV. Neoadjuvant treatment of locally advanced esophageal and junctional cancer: the evidence-base, current key questions and clinical trials. J Thorac Dis. 2017 (Suppl 8); 9:S697–S704. https://doi.org/10.21037/jtd.2017.03.159.

12. Westerterp M, van Westreenen HL, Reitsma JB, Hoekstra OS, Stoker J, Fockens P, Jager PL, Van Eck-Smit BL, Plukker JT, van Lanschot JJ, Sloof GW. Esophageal cancer: CT, endoscopic US, and FDG PET for assessment of response to neoadjuvant therapy—systematic review. Radiology. 2005; 236:841–51. https://doi.org/10.1148/radiol.2363041042.

13. Maity A, McKenna WG, Muschel RJ. The molecular basis for cell cycle delays following ionizing radiation: a review. Radiother Oncol. 1994; 31:1–13. https://doi.org/10.1016/0167-8140(94)90408-1.

14. Maciejewski BA, Skates S, Zajusz A, Lange D. Importance of tumor size and repopulation for radiocurability of skin cancer. Neoplasma. 1993; 40:51–54.

15. Shimura T. Acquired radioresistance of cancer and the AKT/GSK3β/cyclin D1 overexpression cycle. J Radiat Res. 2011; 52:539–44. https://doi.org/10.1269/jrr.11098.

16. Wilson WR, Hay MP. Targeting hypoxia in cancer therapy. Nat Rev Cancer. 2011; 11:393–410. https://doi.org/10.1038/nrc3064.

17. Igney FH, Krammer PH. Death and anti-death: tumour resistance to apoptosis. Nat Rev Cancer. 2002; 2:277–88. https://doi.org/10.1038/nrc776.

18. Lynam-Lennon N, Reynolds JV, Pidgeon GP, Lysaght J, Marignol L, Maher SG. Alterations in DNA repair efficiency are involved in the radioresistance of esophageal adenocarcinoma. Radiat Res. 2010; 174:703–11. https://doi.org/10.1667/RR2295.1.

19. Lynam-Lennon N, Maher SG, Maguire A, Phelan J, Muldoon C, Reynolds JV, O'Sullivan J. Altered mitochondrial function and energy metabolism is associated with a radioresistant phenotype in oesophageal adenocarcinoma. PLoS One. 2014; 9:e100738. https://doi.org/10.1371/journal.pone.0100738.

20. Maher SG, McDowell DT, Collins BC, Muldoon C, Gallagher WM, Reynolds JV. Serum proteomic profiling reveals that pretreatment complement protein levels are predictive of esophageal cancer patient response to neoadjuvant chemoradiation. Ann Surg. 2011; 254:809–16. https://doi.org/10.1097/SLA.0b013e31823699f2.

21. Picardo SL, Maher SG, O'Sullivan JN, Reynolds JV. Barrett's to oesophageal cancer sequence: a model of inflammatory-driven upper gastrointestinal cancer. Dig Surg. 2012; 29:251–60. https://doi.org/10.1159/000341498.

22. Liu SC, Tsang NM, Chiang WC, Chang KP, Hsueh C, Liang Y, Juang JL, Chow KP, Chang YS. Leukemia inhibitory factor promotes nasopharyngeal carcinoma progression and radioresistance. J Clin Invest. 2013; 123:5269–83. https://doi.org/10.1172/JCI63428.

23. Kishimoto T, Akira S, Narazaki M, Taga T. Interleukin-6 family of cytokines and gp130. Blood. 1995; 86:1243–54.

24. Li X, Yang Q, Yu H, Wu L, Zhao Y, Zhang C, Yue X, Liu Z, Wu H, Haffty BG, Feng Z, Hu W. LIF promotes tumorigenesis and metastasis of breast cancer through the AKT-mTOR pathway. Oncotarget. 2014; 5:788–801. https://doi.org/10.18632/oncotarget.1772.

25. Blanchard F, Tracy E, Smith J, Chattopadhyay S, Wang Y, Held WA, Baumann H. DNA methylation controls the responsiveness of hepatoma cells to leukemia inhibitory factor. Hepatology. 2003; 38:1516–28. https://doi.org/10.1016/j.hep.2003.09.029.

26. Liu B, Lu Y, Li J, Liu Y, Liu J, Wang W. Leukemia inhibitory factor promotes tumor growth and metastasis in human osteosarcoma via activating STAT3. APMIS. 2015; 123:837–46. https://doi.org/10.1111/apm.12427.

27. Yu H, Yue X, Zhao Y, Li X, Wu L, Zhang C, Liu Z, Lin K, Xu-Monette ZY, Young KH, Liu J, Shen Z, Feng Z, Hu W. LIF negatively regulates tumour-suppressor p53 through Stat3/ID1/MDM2 in colorectal cancers. Nat Commun. 2014; 5:5218. https://doi.org/10.1038/ncomms6218.

28. Kamohara H, Ogawa M, Ishiko T, Sakamoto K, Baba H. Leukemia inhibitory factor functions as a growth factor in pancreas carcinoma cells: involvement of regulation of LIF and its receptor expression. Int J Oncol. 2007; 30:977–83.

29. Bay JM, Patterson BK, Teng NN. Leukemia inhibitory factor downregulates human papillomavirus-16 oncogene expression and inhibits the proliferation of cervical

carcinoma cells. Infect Dis Obstet Gynecol. 2011; 2011:463081. https://doi.org/10.1155/2011/463081.

30. Chen D, Sun Y, Wei Y, Zhang P, Rezaeian AH, Teruya-Feldstein J, Gupta S, Liang H, Lin HK, Hung MC, Ma L. LIFR is a breast cancer metastasis suppressor upstream of the Hippo-YAP pathway and a prognostic marker. Nat Med. 2012; 18:1511–17. https://doi.org/10.1038/nm.2940.

31. Morton SD, Cadamuro M, Brivio S, Vismara M, Stecca T, Massani M, Bassi N, Furlanetto A, Joplin RE, Floreani A, Fabris L, Strazzabosco M. Leukemia inhibitory factor protects cholangiocarcinoma cells from drug-induced apoptosis via a PI3K/AKT-dependent Mcl-1 activation. Oncotarget. 2015; 6:26052–64. https://doi.org/10.18632/oncotarget.4482.

32. Salleh N, Giribabu N. Leukemia inhibitory factor: roles in embryo implantation and in nonhormonal contraception. ScientificWorldJournal. 2014; 2014:201514. https://doi.org/10.1155/2014/201514.

33. Metcalf D. The unsolved enigmas of leukemia inhibitory factor. Stem Cells. 2003; 21:5–14. https://doi.org/10.1634/stemcells.21-1-5.

34. Wysoczynski M, Miekus K, Jankowski K, Wanzeck J, Bertolone S, Janowska-Wieczorek A, Ratajczak J, Ratajczak MZ. Leukemia inhibitory factor: a newly identified metastatic factor in rhabdomyosarcomas. Cancer Res. 2007; 67:2131–40. https://doi.org/10.1158/0008-5472.CAN-06-1021.

35. Wei F, Liu Y, Guo Y, Xiang A, Wang G, Xue X, Lu Z. miR-99b-targeted mTOR induction contributes to irradiation resistance in pancreatic cancer. Mol Cancer. 2013; 12:81–81. https://doi.org/10.1186/1476-4598-12-81.

36. Brieger J, Schroeder P, Gosepath J, Mann WJ. Vascular endothelial growth factor and basic fibroblast growth factor are released by squamous cell carcinoma cells after irradiation and increase resistance to subsequent irradiation. Int J Mol Med. 2005; 16:159–64.

37. Hardikar S, Onstad L, Song X, Wilson AM, Montine TJ, Kratz M, Anderson GL, Blount PL, Reid BJ, White E, Vaughan TL. Inflammation and oxidative stress markers and esophageal adenocarcinoma incidence in a Barrett's esophagus cohort. Cancer Epidemiol Biomarkers Prev. 2014; 23:2393–403. https://doi.org/10.1158/1055-9965.EPI-14-0384.

38. Ma D, Jing X, Shen B, Liu X, Cheng X, Wang B, Fu Z, Peng C, Qiu W. Leukemia inhibitory factor receptor negatively regulates the metastasis of pancreatic cancer cells in vitro and in vivo. Oncol Rep. 2016; 36:827–36. https://doi.org/10.3892/or.2016.4865.

39. Zhao JH, Sun JX, Song YX, Chen XW, Yang YC, Ma B, Wang J, Gao P, Wang ZN. A novel long noncoding RNA-LOWEG is low expressed in gastric cancer and acts as a tumor suppressor by inhibiting cell invasion. J Cancer Res Clin Oncol. 2016; 142:601–09. https://doi.org/10.1007/s00432-015-2071-6.

40. Luo Q, Wang C, Jin G, Gu D, Wang N, Song J, Jin H, Hu F, Zhang Y, Ge T, Huo X, Chu W, Shu H, et al. LIFR functions as a metastasis suppressor in hepatocellular carcinoma by negatively regulating phosphoinositide 3-kinase/AKT pathway. Carcinogenesis. 2015; 36:1201–12. https://doi.org/10.1093/carcin/bgv108.

41. Korc M, Friesel RE. The role of fibroblast growth factors in tumor growth. Curr Cancer Drug Targets. 2009; 9:639–51. https://doi.org/10.2174/156800909789057006.

42. Shimizu T, Ishikawa T, Iwai S, Ueki A, Sugihara E, Onishi N, Kuninaka S, Miyamoto T, Toyama Y, Ijiri H, Mori H, Matsuzaki Y, Yaguchi T, et al. Fibroblast growth factor-2 is an important factor that maintains cellular immaturity and contributes to aggressiveness of osteosarcoma. Mol Cancer Res. 2012; 10:454–68. https://doi.org/10.1158/1541-7786.MCR-11-0347.

43. Luo W, Yu Y, Wang R, He D, Wang C, Zeng X, Chen X, Tan X, Huang T, Wu X. P7 peptides targeting bFGF sensitize colorectal cancer cells to CPT-11. Int J Mol Med. 2014; 33:194–200. https://doi.org/10.3892/ijmm.2013.1547.

44. Hoang T, Huang S, Armstrong E, Eickhoff JC, Harari PM. Enhancement of radiation response with bevacizumab. J Exp Clin Cancer Res. 2012; 31:37–37. https://doi.org/10.1186/1756-9966-31-37.

45. Waugh DJ, Wilson C. The interleukin-8 pathway in cancer. Clin Cancer Res. 2008; 14:6735–41. https://doi.org/10.1158/1078-0432.CCR-07-4843.

46. Szepietowski J, Walker C, Hunter JA, McKenzie RC. Elevated leukaemia inhibitory factor (LIF) expression in lesional psoriatic skin: correlation with interleukin (IL)-8 expression. J Dermatol. 2001; 28:115–22. https://doi.org/10.1111/j.1346-8138.2001.tb00104.x.

47. Jiang D, Liu Y, Wang H, Wang H, Song Q, Sujie A, Huang J, Xu Y, Zeng H, Tan L, Hou Y, Xu C. Tumour infiltrating lymphocytes correlate with improved survival in patients with esophageal squamous cell carcinoma. Sci Rep. 2017; 7:44823. https://doi.org/10.1038/srep44823.

48. Pagès F, Kirilovsky A, Mlecnik B, Asslaber M, Tosolini M, Bindea G, Lagorce C, Wind P, Marliot F, Bruneval P, Zatloukal K, Trajanoski Z, Berger A, et al. In situ cytotoxic and memory T cells predict outcome in patients with early-stage colorectal cancer. J Clin Oncol. 2009; 27:5944–51. https://doi.org/10.1200/JCO.2008.19.6147.

49. Hwang WT, Adams SF, Tahirovic E, Hagemann IS, Coukos G. Prognostic significance of tumor-infiltrating T cells in ovarian cancer: a meta-analysis. Gynecol Oncol. 2012; 124:192–98. https://doi.org/10.1016/j.ygyno.2011.09.039.

50. Dieu-Nosjean MC, Antoine M, Danel C, Heudes D, Wislez M, Poulot V, Rabbe N, Laurans L, Tartour E, de Chaisemartin L, Lebecque S, Fridman WH, Cadranel J. Long-term survival for patients with non-small-cell lung cancer with intratumoral lymphoid structures.

J Clin Oncol. 2008; 26:4410–17. https://doi.org/10.1200/JCO.2007.15.0284.

51. Gentles AJ, Newman AM, Liu CL, Bratman SV, Feng W, Kim D, Nair VS, Xu Y, Khuong A, Hoang CD, Diehn M, West RB, Plevritis SK, Alizadeh AA. The prognostic landscape of genes and infiltrating immune cells across human cancers. Nat Med. 2015; 21:938–45. https://doi.org/10.1038/nm.3909.

52. Livak KJ, Schmittgen TD. Analysis of relative gene expression data using real-time quantitative PCR and the 2(-Delta Delta C(T)) Method. Methods. 2001; 25:402–08. https://doi.org/10.1006/meth.2001.1262.

Cancer Letters 447 (2019) 115–129

Contents lists available at ScienceDirect

Cancer Letters

journal homepage: www.elsevier.com/locate/canlet

Original Articles

Pyrazinib (P3), [(*E*)-2-(2-Pyrazin-2-yl-vinyl)-phenol], a small molecule pyrazine compound enhances radiosensitivity in oesophageal adenocarcinoma

Amy M. Buckley[a], Margaret R. Dunne[a], Niamh Lynam-Lennon[a], Susan A. Kennedy[a], Aoife Cannon[a], Alison L. Reynolds[b,c], Stephen G. Maher[a], John V. Reynolds[a], Breandán N. Kennedy[c], Jacintha O'Sullivan[a,*]

[a] Department of Surgery, Trinity Translational Medicine Institute, St. James's Hospital, Trinity College Dublin, Ireland
[b] UCD School of Veterinary Medicine, Veterinary Sciences Centre, University College Dublin, Ireland
[c] UCD Conway Institute & UCD School of Biomolecular and Biomedical Science, University College Dublin, Ireland

ARTICLE INFO

Keywords:
Oesophageal cancer
Radiation
Angiogenesis
Metabolism
Inflammation

ABSTRACT

Oesophageal adenocarcinoma (OAC) is an aggressive disease with 5-year survival rates of < 20%. Only 20–30% OAC patients show a beneficial response to neoadjuvant therapy. Altered mitochondrial function is linked with radioresistance in OAC. We identified pyrazinib (P3), a pyrazine phenol small molecule drug with anti-angiogenic and anti-metabolic activity *in-vivo* in zebrafish and *in-vitro* isogenic models of OAC radioresistance. Pyrazinib (P3) significantly inhibited blood vessel development in zebrafish ($p < 0.001$). *In-vivo* in zebrafish and *in-vitro* in an isogenic model of OAC radioresistance, pyrazinib (P3) significantly reduced measures of oxidative phosphorylation and glycolysis. Pyrazinib (P3) significantly reduced the surviving fraction in OE33P; radiation-sensitive and OE33R; radiation-resistant cells following irradiation. Under hypoxic conditions pyrazinib (P3) significantly reduced OE33R cell survival following 4 Gy irradiation ($p = 0.0216$). Multiplex ELISA showed significantly higher secreted levels of 9 of 30 detected inflammatory and angiogenic factors in OE33R radioresistant cells compared to OE33P cells; IL-8, IL-4, IL-6, IL-2, IL-12p70, IL-10, MCP-1, IP-10, ICAM ($p < 0.05$). Pyrazinib (P3) significantly reduced the secretions of IL-6 ($p = 0.0006$), IL-8 ($p = 0.0488$), and IL-4 ($p = 0.0111$) in OE33R cells. Collectively, these findings support further development of pyrazinib (P3) as a novel therapeutic radiosensitiser in OAC.

1. Introduction

Oesophageal cancer is an aggressive disease and the 6th most common cause of cancer-related death, accounting for approximately 400,000 deaths annually [1]. Oesophageal cancer is classified into two histological subtypes, squamous cell carcinoma (SCC) and oesophageal adenocarcinoma (OAC) [2]. A dramatic epidemiological shift in the incidence of OAC emerged in recent years in western populations, notably OAC is now the predominant histological subtype of oesophageal cancer in both Europe and the US [2,3]. Current standard treatment regimens for OAC focus on neoadjuvant treatment with chemotherapy alone (neoCT) or in combination with radiation; neoadjuvant chemoradiation (neoCRT) for locally advanced tumours, prior to surgery [4]. Surgery is associated with increased loco-regional tumour control and neoadjuvant treatment aims to reduce tumour burden prior to surgery to improve post-operative outcome. NeoCRT in combination with surgery has been associated with higher rates of overall survival [4–6]. Unfortunately, only 20–30% of patients show a complete pathological response (pCR) to neoadjuvant treatment, meaning 70–80% of patients receive a toxic treatment with little to no therapeutic gain and a subsequent delay to surgery [7–9]. Importantly, there are currently no clinico-pathological markers available to stratify patients who will achieve a beneficial response to radiation therapy or approved radiosensitisers to enhance treatment response prior to surgery. Ionizing radiation is used to exert local tumour control in over 50% of solid cancers through the induction of double strand breaks (DSB) and cellular DNA damage [7]. Importantly, OAC sensitivity to irradiation is inversely correlated to tumour burden [10]. Resistance to radiation therapy is multifactorial and associated with a number of biological processes both within the tumour itself and the surrounding

* Corresponding author.
E-mail address: OSULLIJ4@tcd.ie (J. O'Sullivan).

https://doi.org/10.1016/j.canlet.2019.01.009
Received 1 October 2018; Received in revised form 13 November 2018; Accepted 7 January 2019
0304-3835/ © 2019 Elsevier B.V. All rights reserved.

microenvironment, including dysregulated cellular energetics, angiogenesis and inflammation [11–13].

Altered energy metabolism is an emerging hallmark of cancer which plays a critical role in radioresponse [11,14], and a feature of cancer cells which was originally alluded to in 1956 by Otto Warburg [15]. Cells produce energy primarily through two interconnected pathways; glycolysis and oxidative phosphorylation which involve the catabolism of glucose to pyruvate and the production of energy from glucose via the mitochondrial tricarboxylic acid cycle, respectively [14]. Warburg reported that cancer cells preferentially use the less efficient glycolytic pathway to metabolise glucose even in the presence of oxygen, termed "aerobic glycolysis" in order to facilitate survival and rapid cellular proliferation [15]. Warburg's observations, known as the "Warburg effect", have been repeatedly confirmed but in recent years it has also become apparent that the oxidative phosphorylation pathway in the mitochondria is still largely utilised by cancer cells and is critical to the provision of intermediates for cellular biosynthesis [14]. Lynam-Lennon et al., demonstrated that radioresistant OAC cancer cells have an altered metabolic phenotype compared to isogenic radiosensitive cells [11]. Radioresistant cells have a significantly higher rate of oxidative phosphorylation whereas no significant differences are observed in glycolytic rate between the isogenic OAC cell lines [11]. Radioresistant cells also show altered mitochondrial function [11]. The excess energy consumption in the radioresistant cells limits the availability of oxygen in the tumour microenvironment to act as a radiosensitiser in the radioresistant OE33R cells. Furthermore, *ex-vivo* examination of metabolic markers in treatment-naïve patient samples found *ATP5B*, a surrogate marker of oxidative phosphorylation to be expressed at significantly higher levels in patients with a poor response to neoCRT, further highlighting elevated metabolism as a driver of the radioresistant phenotype in OAC [11]. Targeting tumour metabolism may be a novel strategy to augment radioresponse in OAC.

Angiogenesis is another hallmark of cancer which plays a critical role in radiation sensitivity, a process tightly linked with cellular metabolism [12,16,17]. Angiogenesis supplies the oxygen and glucose required to fuel the metabolic cycle. A number of chemotherapeutic agents and radiation therapy alike rely on the formation of oxygen radical species to exert their cytotoxic effects; oxygen is a potent radiosensitiser, with oxygenated cells killed more readily than hypoxic cells [17]. As oxygen is required for maximal response to radiation it is of concern that combining anti-angiogenic agents with radiation may compromise tumour vasculature and result in a more hypoxic environment with reduced sensitivity to radiation [17]. Despite this concern, anti-angiogenic agents enhance tumour response when combined with single dose radiotherapy [18–20]. Anti-angiogenic agents may enhance radio-sensitivity through normalisation of the tumour vasculature and augmentation of endothelial cell response to injury, creating a more favourable environment for response to radiation therapy [17,21]. It is also critical to understand the effect of radiation on endothelial cell function for maximising the effect of radiotherapy. Importantly, radiation-induced changes of tumour vasculature is dependent on numerous factors, such as dose, fraction, tumour location and tumour size [22]. In this study we hypothesise that phenotype-based discovery of small molecule compounds with anti-angiogenic and anti-metabolic activity, specifically targeting oxidative phosphorylation may also function as radiosensitisers in OAC.

Furthermore, OAC is an inflammatory-driven upper gastrointestinal cancer [23,24]. Inflammation plays a crucial role in treatment response in OAC [24]. Components of the complement system C3a and C4a, were shown to be higher in the pre-treatment serum of OAC patients who had a subsequent poor pathological response to neoCRT, when compared to patients having a favourable response treatment [24]. In addition, cytokines are increasingly reported to play a role in radioresistance, e.g. LIF and IL-6 type cytokines are linked with radioresistance in nasopharyngeal carcinoma and OAC [25,26]. Additionally, in a radioresistant oral SCC xenograft, the administration of IL-8 and IL-6 neutralising antibodies sensitised the tumours to irradiation [27]. Inflammation is tightly linked to angiogenesis, with angiogenic networks responsible for sustaining inflammation through the supply of oxygen and nutrients to the inflammatory cells [28]. Inflammation is also tightly linked to metabolism as inflammatory cells rely on metabolites generated from the metabolic cycle to maintain their function. Thus, tumour inflammation, angiogenesis and metabolism form an interdependent network which plays a crucial role in radiation resistance. Given the inflammatory driven nature of OAC, we sought to investigate the effect of pyrazinib (P3) on the inflammatory secretome in addition to its effects on two primary hallmarks of cancer, angiogenesis and dysregulated metabolism. This study aimed to phenotypically identify compounds with anti-angiogenic and anti-metabolic activity specifically targeting oxidative phosphorylation which in turn may enhance radiosensitivity in both radiosensitive and radioresistant OAC cells from a series of small molecule compounds consisting of pyrazinib (P3), a pyrazine compound, and 22 compounds of the P series. Pyrazinib (P3) was synthesised as an analogue of quinini b (Q1) and in this study we sought to determine if pyrazinib or the 22 compounds of the P series could produce more potent anti-cancer activity than its parent compound quinini b in OAC. Quinini b is an anti-angiogenic quinoline compound which was previously discovered to produce significant anti-angiogenic activity and inhibit tumour growth both *in-vitro* and *in-vivo* respectively [29,30]. Pyrazinib (P3) produced significantly greater anti-angiogenic activity than quinini b *in-vivo* in zebrafish. *In-vivo*, in zebrafish embryos, pyrazinib (P3) and two P series compounds, P2 and P4, significantly reduced oxygen consumption rate (OCR), a measure of oxidative phosphorylation, with both P2 and pyrazinib (P3) producing a simultaneous significant reduction in extracellular acidification rate (ECAR), a measure of glycolysis. *In-vitro*, in an isogenic model of OAC radioresistance, pyrazinib (P3) significantly reduced OCR and ECAR. Pyrazinib (P3) significantly reduced surviving fraction in OE33P; radiation-sensitive and OE33R; radiation-resistant cells following 2, 4 and 6 Gy irradiation fractions. Furthermore, under hypoxic conditions pyrazinib (P3) significantly reduced the surviving fraction of OE33R cells following 4 Gy irradiation. Nine of thirty detected inflammatory and angiogenic factors were secreted at significantly higher levels in OE33R radioresistant cells when compared to OE33P cells; IL-8, IL-4, IL-6, IL-2, IL-12p70, IL-10, MCP-1, IP-10 and ICAM. Pyrazinib (P3) significantly reduced the secretions of IL-6, IL-8, IL-4 and IL-13 *in-vitro* in OE33R cells. Taken together, these findings support further development of our compound pyrazinib (P3) as a novel therapeutic radiosensitiser in OAC.

2. Methods

2.1. Ethical approval

The intersegmental vessel assay screen was apptroved by the UCD Animal Research Ethics Committee under protocol number AREC-P-14-69 prior to commencement of this study. The zebrafish metabolic profiling assay was approved by Trinity College Dublin Animal Research Ethics Committee prior to commencement of the study.

2.2. Small molecule compounds

Quinini b (Q1), pyrazinib (P3) and 22 P series compounds were synthesised by Celtic Catalysts (Ireland) and Onyx Scientific (UK). Compounds were dissolved in 100% DMSO.

2.3. Zebrafish husbandry

Tg(*fli1*:EGFP) zebrafish were maintained on a 14 h light/10 h dark cycle at 28 °C, in a recirculating aquaculture system, according to standard procedures [31]. Embryos were obtained through natural spawning and developmental stages were determined using time and morphological criteria [32]. Fertilised eggs were obtained from mating

adult Tg(*fli1*:EGFP) zebrafish and stored in an incubator at 28 °C. Embryos were analysed under an Olympus-SZX16 at time of collection; undeveloped-embryos were removed to prevent a delay to development of other embryos.

2.4. Intersegmental vessel assay

At 6 hours post fertilisation (hpf) Tg(*fli1*:EGFP) zebrafish embryos were plated, 5 per well in a 48-well plate, using an Olympus-SZX16 microscope in 400 µl embryo medium (EM) (5 mM NaCl, 0.17 mM KCl, 0.4 mM $CaCl_2$ and 0.16 mM $MgSO_4$). EM was removed and 400 µl containing EM and control or test compound was added to each well. 100 µM solutions, dissolved in dH_2O/1% DMSO of Q1, pyrazinib (P3) and 22 P series compounds were stored at −20°C. Compounds were defrosted to room temperature (RT) and vortexed before use. Drug treatments were carried out in duplicate and repeated three times at 10 µM. Treated larvae were incubated until 48 hpf at 28 °C on a 14 h light/10 h dark cycle.

After incubation, larvae were placed in 400 µl of phosphate-buffered-saline (PBS) and dechorionated under an Olympus-SZX16 microscope. Larvae were euthanized and fixed in 400 µl of 4% para-formaldehyde (PFA) in a paraffilm-covered plate at RT for 2 h. 400 µl of PFA was removed and larvae were washed three times at 10 min intervals with 400 µl PBS. Larvae were stored in 400 µl of PBS in a paraffin-covered 48-well plate at 4 °C until analysis.

2.5. Quantification of intersegmental vessels

Prior to analysis of intersegmental vasculature, larvae were screened using an Olympus-SZX16 microscope for morphological defects. Larvae were placed on a depression slide on their side with their head in a left pointing orientation. Anti-angiogenic activity was determined on the basis of (a) the total inhibition of intersegmental vessel (ISV) growth and (b) incomplete sprouting of the intersegmental vessel (ISV) from the dorsal aorta (DA) to the dorsal longitudinal anastomatic vessel (DLAV). Intersegmental vasculature was viewed by epi-fluorescence under an Olympus SZX16 microscope using a green fluorescent protein (GFP) filter. The number of complete intersegmental vessels was quantified for each sample and larvae were imaged using cellˆF software (Olympus, Europe).

2.6. Zebrafish metabolic profiling assay

26 hpf Tg(*fli1*:EGFP) zebrafish embryos were plated, 3 per well in a 24-well islet cell microplate (Agilent Technologies, Santa Clara, CA, USA), using an Olympus-SZX16 microscope in 700 µl EM containing a final concentration of 10 µM of test compounds; Q1, pyrazinib (P3), P2, P4, P18, P20, P8 and P23 or 0.1% DMSO as control, with 5 wells per treatment group. Four wells contained EM only to identify temperature fluctuations across the plate. Drug treated larvae were incubated for 24 h at 28 °C on a 14 h light/10 h dark cycle until 50 hpf. At 50 hpf, an islet screen (Agilent Technologies, Santa Clara, CA, USA) was inserted above the embryos in each well to prevent the embryos contacting the sensor probe during the course of the assay. The Seahorse XFe24 analyser (Agilent Technologies, Santa Clara, CA, USA) couples a sensor cartridge with a custom cell plate. Sensor probes which are close to the islet screen sense changes and measure the levels of dissolved oxygen and free protons in this microchamber at indicated intervals, giving a read-out of Oxygen Consumption Rate (OCR) and Extracellular Acidification rate (ECAR), a measure of oxidative phosphorylation and glycolysis, respectively. Prior to the assay the XFe24 cartridge plate (Agilent Technologies, Santa Clara, CA, USA) was hydrated overnight in a 37 °C non-CO_2 incubator. At 50 hpf three measurements were taken over 24 min consisting of three repeats of mix (3 min)/wait (2 min)/measurement (3 min) to establish basal respiration. Upon completion of assay, larvae were euthanized and fixed in 400 µl of 4% PFA in a paraffilm-covered plate at RT for 2 h.

2.7. Generation of the OE33P and OE33R cell lines

The human OE33 oesophageal adenocarcinoma cell line was obtained from the European Collection of Authenticated Cell Cultures. The isogenic model of radioresistant OAC; OE33P (radiosensitive) and OE33R (radioresistant) cells was generated as previously described [33].

2.8. OCR and ECAR measurements in OE33P and OE33R cells

OE33P and OE33R cells were seeded in triplicate at a density of 11,000 and 13,000 cells/well, respectively in 24-well cell culture XFe24 microplates (Agilent Technologies, Santa Clara, CA, USA) at a volume of 100 µl and allowed to adhere at 37 °C in 5% CO_2/95% air. 5 h later, an additional 150 µl/well complete cell culture Roswell Park Memorial Institute medium (RPMI) 1640 medium was added. 24 h later, OE33P and OE33R cells were treated with 10 µM of Q1, pyrazinib (P3), P2, P4, P18, P20, P8 and P23 or 0.1% DMSO control. Following 24 h treatment, media was removed and cells were washed with unbuffered Dulbecco's Modified Eagle's medium (DMEM) supplemented with 10 mM glucose (Sigma-Aldrich) and 10 mM sodium pyruvate (Sigma Aldrich), (pH 7.4) and incubated for 1 h at 37 °C in a CO_2-free incubator. OCR and ECAR were measured using a Seahorse Biosciences XFe24 Extracellular Flux Analyser (Agilent Technologies, Santa Clara, CA, USA). Three basal measurements of OCR and ECAR were taken over 24 min consisting of three repeats of mix (3 min)/wait (2 min)/measurement (3 min) to establish basal respiration. Three additional measurements were obtained over 24 min each following the injection of 3 mitochondrial inhibitors including oligomycin (2 µg·mL−1,Sigma Aldrich), an uncoupling agent Carbonyl cyanide 4-(trifluoromethoxy) phenylhydrazone (FCCP) (5 µM, Sigma Aldrich) and antimycin-A (2 µM, Sigma Adrich). ATP turnover was calculated by subtracting the OCR post oligomycin injection from baseline OCR prior to oligomycin addition. Maximal respiration was calculated by subtracting OCR post antimycin A addition from OCR post FCCP addition. Spare respiratory capacity was calculated by subtracting basal OCR from maximal respiration. All measurements were normalised to cell number using the crystal violet assay, transferring the eluted stain to a 96-well plate before reading.

2.9. Crystal violet

Cells were fixed with 1% glutaraldehyde (Sigma-Aldrich) for 15 min at RT. The fixative was removed and cells were washed with PBS and stained with 0.1% crystal violet in PBS for 30 min at RT. Plates were left to air dry and incubated with 50 µl 1% Triton X-100 in PBS on a plate shaker for 30 min at RT. Absorbance was read at 595 nm on a VersaMax microplate reader (Molecular Devices, Sunnyvale, CA, USA).

2.10. ROS levels

Reactive oxygen species levels were measured using 2,7-dichlorofluorescein (DCF) which emits a fluorescent signal linearly linked to the intracellular H_2O_2. OE33P and OE33R cells were seeded at a density of 8,000 cells/well in triplicate and allowed to adhere overnight. 24 h after seeding, OE33P and OE33R cells were treated for 24 h with µ µ0.1% DMSO control or 10 µM Q1, pyrazinib (P3), P2, P4, P18, P20, P8 and P23 in RPMI. 24 h later media was removed from wells. 50 µl of 5 µM 2,7-DCF (Invitrogen, Carlsbad, CA, USA) in PBS Mg^{++} (Sigma-Aldrich) was added to each well and incubated for 30 min at 37 °C in 5% CO_2/95% air. The probe was removed and 100 µl PBS was added to each well, fluorescence was measured FLx800 Fluorescence Microplate Reader (Mason Technology Dublin, Ireland). Fluorescence was normalised to cell number using the crystal violet assay, as previously described.

2.11. Mitochondrial membrane potential

To assess mitochondrial membrane potential, the fluorescent probe rhodamine 123 (5 μM), which is selectively taken up by mitochondria and its uptake dependent on mitochondrial membrane potential was used. OE33P and OE33R cells were seeded at a density of 8,000 cells/well in triplicate and allowed to adhere overnight. 24 h later, OE33P and OE33R cells were treated with 0.1% DMSO or 10 μM of Q1, pyrazinib (P3), P2, P4, P18, P20, P8 and P23 for 24 h. 24 h later, the media was removed from wells and cells were washed with 100 μl of PBS. 50 μl of 5 μM rhodamine 123 in PBS Mg^{++} solution was added to each well and incubated for 30 min at 37 °C in 5% CO_2/95% air. The probe was removed and 100 μl of PBS added to each well. Fluorescence was measured on FLx800 Fluorescence Microplate Reader (Mason Technology Dublin, Ireland). Fluorescence was normalised to cell number using the crystal violet assay, as previously described.

2.12. Mitochondrial mass

MitoTracker Green (0.3 μM, Invitrogen, Carlsbad, CA, USA), a mitochondrial selective dye was used to evaluate mitochondrial mass in OE33P and OE33R cells treated with 10 μM of our compounds. OE33P and OE33R cells were seeded at a density of 8,000 cells/well in triplicate in 100 μl complete RPMI and allowed to adhere overnight. 24 h later after seeding, OE33P and OE33R cells were treated with 0.1% DMSO or 10 μM Q1, pyrazinib (P3), P2, P4, P18, P20, P8 and P23. 24 h later media was removed and 50 μl of 0.3 μM MitoTracker Green in PBS Mg^{++} and incubated for 30 min at 37 °C in 5% CO_2/95% air. The probe was removed and 100 μl PBS was added to each well and fluorescence was measured on FLx800 Fluorescence Microplate Reader (Mason Technology Dublin, Ireland). Fluorescence was normalised to cell number using the crystal violet assay, as previously described.

2.13. Clonogenic assay

OE33P and OE33R cells were trypsinised, counted and seeded at the optimised densities of 1–11 × 10^3 in 1.5 ml complete RPMI in triplicate in 6 well plates and allowed to adhere overnight. 24 h later OE33P and OE33R cells were treated with 0.1% DMSO or 10 μM of Q1, pyrazinib (P3), P2 and P4. 24 h later OE33P and OE33R cells were either irradiated at 2, 4 or 6 Gy or mock irradiated. OE33P and OE33R cells were additionally treated with either 0.1% DMSO or pyrazinib at 1, 5 or 10 μM for 24 h or 10 μM for 72 h prior to irradiation. Colonies were allowed to grow for 7–14 days at which point they were fixed and stained with 0.05% crystal violet (25% methanol in dH_2O) and allowed to air dry. Clonogenics carried out under hypoxic conditions were seeded and allowed to adhere at 37 °C in 5% CO_2/95% air for 6 h before being transferred to the Whitley H35 hypoxy-station at 37 °C in 5%CO_2/0.5%O_2. Following 24 h incubation under hypoxic conditions (0.5% O_2) OE33P and OE33R cells were maintained at 0.5% O_2 and treated with 0.1% DMSO or 10 μM of pyrazinib (P3), and irradiated 24 h later at 5%CO_2/0.5%O_2. 24 h following irradiation, plates were returned to 37 °C in 5%CO_2/95% air. Colonies were allowed to grow for 7–14 days, at which point they were fixed and stained with 0.05% crystal violet and allowed to air dry. Colonies consisting of 50 cells or more were counted using a colony counter (ColCountTM, Oxford Optronix, Oxford, UK). Plating efficiency (PE), fraction of colonies formed by untreated cells, was calculated using the formula: PE = No. colonies/No. cells seeded. The surviving fraction (SF), the number of colonies formed was expressed in terms of PE, was calculated using the formula: SF = No. colonies/(No. cells seeded x PE).

2.14. Irradiation

Irradiation was performed using a Gulmay Medical X-ray generator, (RS225) (Gulmay Medical), at a dose rate of 3.25 Gray (Gy) per min.

2.15. Multiplex enzyme linked immunosorbent assay (ELISA)

Supernatants from OE33R and OE33P cells were defrosted on ice. The secretion of cytokines and angiogenic and inflammatory growth factors was analysed by ELISA as per the manufacturer's instructions. To assess angiogenic, vascular injury, inflammatory cytokine and chemokine secretions, a 54 multiplex kit spread across 7 plates was used (Meso Scale Diagnostics, USA). The 54 multiplex kit was used to quantify the secretions of CRP, Eotaxin, Eotaxin-3, FGF (basic), GM-CSF, ICAM-1, IFN-γ, IL-10, IL-12/IL-23p40, IL-12p70, IL-13, IL-15, IL-16, IL-17A, IL-17A/F, IL-17B, IL-17C, IL-17D, IL-1RA, IL-1α, IL-1β, IL-2, IL-21, IL-22, IL-23, IL-27, IL-3, IL-31, IL-4, IL-5, IL-6, IL-7, IL-8, IL-8 (HA), IL-9, IP-10, MCP-1, MCP-4, MDC, MIP-1α, MIP-1β, MIP-3α, PlGF, SAA, TARC, Tie-2, TNF-α, TNF-β, TSLP, VCAM-1, VEGF-A, VEGF-C, VEGF-D and VEGFR-1/Flt-1 from OE33P and OE33R cell supernatants previously treated with 10 μM pyrazinib (P3) or vehicle control (0.1% DMSO) for 24 h. Secretion data for all factors was normalised appropriately to cell lysate protein content using the BCA assay (Pierce) as per manufacteurs instructions. Data was analysed using MSD Discovery Workbench software version 4.0.

2.16. BrdU ELISA

Proliferation was assessed using the BrdU cell proliferation ELISA (Roche Diagnostics, Sussex, UK) as per manufactures instructions. Cells were seeded in triplicate at a density of 5,000 cells/ well in 96-well plates and allowed to adhere overnight, followed by treatment with 0.1% DMSO control or 10 μM Q1, pyrazinib (P3), P2, P4, P18, P20 , P8 and P23 for 24 or 72 h. 10 μM BrdU Labelling Solution was added to each well (except for background control wells) and cells were incubated for 1 h at 37°C in 5% CO_2/95% air. ELISA was carried out as per manufactures instructions and absorbance was measured at 450nm on a VersaMax microplate reader (Molecular Devices, Sunnyvale, CA, USA).

2.17. RNA isolation

Cells were seeded at a density of 2.5 × 10^5 cells/well in 6-well plates and allowed to adhere overnight. Following drug treatment with 10 μM of pyrazinib (P3) or 0.1% DMSO control for 24 h, RNA was isolated from cell lines using the TRI Reagent® method. The RNA pellet was re-suspended in 30 μl RNAase free molecular grade H_2O and stored at −80 °C.

2.18. RNA quantification

RNA quantification was determined spectrophotometrically, using a Nanodrop 1000 spectrophotometer (version 3.1.0, Nanodrop technologies, DE, USA). 1 μl RNase-free water was used to blank the instrument prior to RNA analysis. 1 μl of each sample of isolated RNA was loaded onto the instrument and concentration was measured in ng/μl.

2.19. cDNA synthesis

For cell line samples, total RNA (1 μg total RNA) was reverse transcribed to cDNA using the following method. To anneal the primers to the RNA, the sample was heated for 10 min at 70 °C, and immediately chilled for at least 1 min at 4 °C. A master mix containing RNaseOUT (Invitrogen, Carlsbad, CA, USA) recombinant ribonuclease inhibitor (1 unit/μl), dNTPs (Invitrogen, Carlsbad, CA, USA) (10 mM, prepared as a 1:1:1:1 ratio of dATP, dGTP, dTTP and dCTP), Bioscript reverse transcriptase (200units/μl) (Bioline, Kilkenny, Ireland) and 5X Bioscript Reaction Buffer (Bioline, Kilkenny, Ireland) in RNase-free water was added to each sample. Samples were incubated for 1 h at 37 °C then 10 min at 70 °C and held at 4 °C. The resulting cDNA was stored at −20 °C.

2.20. Quantitative real time PCR and analysis

qPCR was performed using TaqMan primer probes (*MLH1, SMUG1, PARP1, MMS19* (Roche)) and a Quant Studio 5 real-time thermal cycler (Thermo Fisher Scientific). 18S (Applied Biosystems) was used as an endogenous control for data normalization. Data analysis was performed using Thermofisher Scientific Connect qPCR application software.

2.21. Statistical analysis

Statistical analysis was performed using GraphPad Prism version 5 software (GraphPad Software, CA, USA). Scientific data were expressed as mean ± standard error of the mean (SEM). SEM was calculated as the standard deviation of the original samples divided by the square root of the sample size. Specific statistical tests used are indicated in figure legends. For all statistical analysis, differences were considered statistically significant at $p < 0.05$.

3. Results

3.1. Pyrazinib (P3) and P series compounds inhibit developmental angiogenesis in Tg(fli1:EGFP) zebrafish

Using Tg(*fli1*:EGFP) embryos, pyrazinib (P3) & P series compounds were screened for anti-angiogenic activity in a phenotype-based approach using the intersegmental vessel assay illustrated in Fig. 1A. Compounds were tested at 10 μM and their anti-angiogenic activity assessed by quantification of intersegmental vessel number at 48 hpf (Fig. 1B). This screen was carried out to identify if pyrazinib (P3) and 22 P series compounds (Table 1) produced greater anti-angiogenic activity compared to quinoline series compound quininib (Q1) from which pyrazinib (P3) was derived. Quininib (Q1) has previously been shown to inhibit both ocular and tumour angiogenesis *in-vitro* and *in-vivo* [29,30]. A dose response profile was conducted at 1, 5 and 10 μM, with the most potent anti-angiogenic effect seen at 10 μM (data for 1 & 5 μM not shown). Pyrazinib (P3) and P series compounds P2, P4, P18 and P20 produced the most potent anti-angiogenic activity ($p < 0.0001$) compared to vehicle control. The most potent anti-angiogenic compound pyrazinib (P3), reduced ISV number by −67% at 10 μM, whereas the quinoline compound quininib (Q1) produced a reduction in ISV number of −35% in this screen. Furthermore, the P series compounds, pyrazinib (P3) and P4 produced significantly greater anti-angiogenic activity when compared directly to the quinoline compound quininib (Q1) when tested at 10 μM (Fig. 1B). Fluorescent images (Fig. 1C) illustrate the potent reduction in ISV number and loss of vessel integrity following treatment with pyrazinib (P3) (white arrows indicate incomplete sprouting and absence of vessel growth) and P series compounds (P2, P4, P18, P20), compared to control and quinoline series compound quininib (Q1). No gross morphological defects or toxicities were observed following treatment with pyrazinib (P3) or any other P series compounds tested in this assay, whilst there were some alterations to skin pigmentation following treatment (Fig. 1C).

Based on this ranking of pyrazinib (P3) and 22 P series compounds, it was decided to further test P series compounds which produced significant (P2, P4, pyrazinib (P3), P18 and P20) or no (P8 and P23) anti-angiogenic activity *in-vivo* to determine if these compounds could also inhibit metabolism, in particular oxidative phosphorylation metabolism, which is strongly associated with radioresistance in OAC.

3.2. Pyrazinib (P3) inhibits metabolism in Tg(fli1:EGFP) zebrafish

Using Tg(*fli1*:EGFP) embryos, pyrazinib (P3), 6 P series compounds and quininib (Q1) of the quinoline series were screened for anti-metabolic activity as illustrated in Fig. 2A. 26 hpf embryos were treated with 10 μM of test compound and anti-metabolic activity assessed at 50 hpf using the XFe24 Seahorse analyser. Pyrazinib (P3), P2 and P4 significantly reduced oxygen consumption rate (OCR) ($p = 0.0076$, $p = 0.0088$ and $p = 0.0194$ respectively), a measure of oxidative phosphorylation, producing a reduction of between −16% and 18%

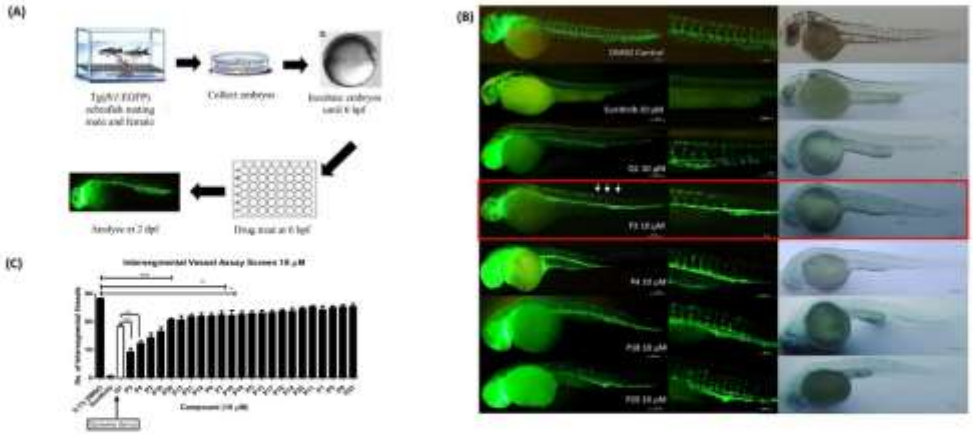

Fig. 1. Pyrazinib (P3) and P series compounds inhibit developmental angiogenesis in Tg(*fli1*:EGFP) zebrafish. **(A)** Intersegmental vessel assay schematic; 6 hours post fertilisation (hpf) Tg(*fli1:EGFP*) embryos were treated with compounds and fixed and analysed at 2 days post fertilisation (dpf) **(B)** Inhibition of intersegmental vasculature growth in Tg(*fli1*:EGFP) zebrafish. 6 hpf embryos were treated with 0.1% DMSO Control, sunitinib 10 μM, quininib (Q1), pyrazinib (P3) and 22 P series compounds at 10 μM as indicated on graph. Number of intersegmental vessels was quantified at 2 dpf. One-way ANOVA with Tukey post-tests ($n = 3$). Data expressed as mean + SEM; *$p < 0.05$, **$p < 0.01$ and ***$p < 0.001$. **(C)** Representative fluorescent images illustrating GFP-positive intersegmental vessels at low and high magnification and brightfield images of whole larvae at 2 dpf in Tg(*fli1*:EGFP) zebrafish treated with 0.1% DMSO Control, sunitinib, quininib (Q1), pyrazinib (P3), P2, P4, P18 and P20.

Table 1
Structures of P Series Compounds Table listing differences in chemical structures of P series compounds indicating where modifications were made to groups C2-C6, R1-R2, A, X and Y to yield P series of compounds.

Compound	Compound Chemical Name	A	C2	C3	C4	C5	C6	X	Y	R1	R2	Salt	Chemical Structure Skeleton
P1	(E)-2-(2-Pyridin-2-yl-vinyl)-phenol	–	N	–	–			alkene		OH			
P2	(E)-2-(2-Pyridin-2-yl-vinyl)-phenol HCl salt	–	N	–	–			alkene		OH		HCl	
P3	(E)-2-(2-Pyrazin-2-yl-vinyl)-phenol	–	N	–	–	N		alkene		OH			
P4	(E)-2-(2-Pyrazin-2-yl-vinyl)-phenol HCl salt	–	N	–	–	N		alkene		OH		HCl	
P5	(E)-2-(2-pyridin-4-yl-vinyl)-phenol	–	–	–	N			alkene		OH			
P6	(E)-2-(2-pyridin-4-yl-vinyl)-phenol HCl salt	–	–	–	N			alkene		OH		HCl	
P7	(E)-2-[2-(6-Methyl-pyridin-2-yl)-vinyl]-phenol	Me	N	–	–			alkene		OH			
P8	(E)-2-[2-(6-Methyl-pyridin-2-yl)-vinyl]-phenol HCl salt	Me	N	–	–			alkene		OH		HCl	
P9	(E)-2-(2-(pyridin-3-yl)vinyl)phenol	–	–	N	–			alkene		OH			
P10	(E)-2-(2-(pyridin-3-yl)vinyl)phenol hydrochloride	–	–	N	–			alkene		OH		HCl	
P11	(E)-2-(2-Pyrazin-2-yl-propenyl)-phenol	–	N	–	–	N		alkene	Me	OH			
P12	(E)-2-(2-Pyrazin-2-yl-propenyl)-phenol HCl salt	–	N	–	–	N		alkene	Me	OH		HCl	
P13	(E)-4-Methyl-2-(2-pyrazin-2-yl-yl-vinyl)-phenol	–	N	–	–	N		alkene		OH	Me		
P14	(E)-4-Methyl-2-(2-pyrazin-2-yl-yl-vinyl)-phenol HCl salt	–	N	–	–	N		alkene		OH	Me	HCl	
P15	(E)-2-(2-Pyrimidin-2-yl-vinyl)-phenol HCl salt	–	N	–	–		N	alkene		OH		HCl	
P16	(E)-2-(2-Pyridin-2-yl-vinyl)-pyrazine HCl salt	–	N	–	–	N		alkene		C=N		HCl	
P17	(E)-2-(2-Pyrazin-2-yl-vinyl)-benzamide HCl salt	–	N	–	–	N		alkene		CONH2		HCl	
P18	2-[2-(Pyrazin-2-yl)ethynyl]phenol	–	N	–	–	N		alkyne		OH			
P19	2-[2-(2-Methoxyphenyl) ethynyl]pyrazine	–	N	–	–	N		alkyne		Ome			
P20	2-[2-(Pyrazin-2-yl)ethynyl]phenol hydrochloride	–	N	–	–	N		alkyne		OH		HCl	
P21	(Z)-2-[2-(Pyrazin-2-yl)vinyl]phenol	–	N	–	–	N		z-alkene		OH			
P22	(E)-2-(2-(1H-imidazol-2-yl)vinyl)phenol	–	N	–	–	N	–	alkene		OH			
P23	(E)-2-(2-(1H-imidazol-2-yl)vinyl)phenol hydrochloride	–	N	–	–	N	–	alkene		OH		HCl	

(Fig. 2B), with both pyrazinib (P3) and P2 producing a simultaneous and significant reduction in extracellular acidification rate (ECAR), a measure of glycolysis, pyrazinib (P3) ($p = 0.0059$) and P2 ($p = 0.0352$) (Fig. 2C). This significant reduction of both OCR and ECAR following treatment with 10 μM of pyrazinib (P3) and P2 illustrates the ability of these P series compounds to target the two major metabolic pathways, oxidative phosphorylation and glycolysis. In summary, *in-vivo* in zebrafish we identified three compounds of the P series; pyrazinib (P3), P2 and P4 which inhibit both angiogenesis and metabolism a significant finding given the well reported role of angiogenesis and metabolism, particularly oxidative phosphorylation in radioresponse in OAC.

3.3. Pyrazinib (P3) significantly alters metabolic rates in OE33P (radiation-sensitive) and OE33R (radiation-resistant) isogenic OAC cells

To investigate if pyrazinib (P3) and P series compounds could also induce a reduction in oxidative phosphorylation and glycolysis when tested in an *in-vitro* model, we used an isogenic OAC cell line model of radioresistance, OE33P; radiationsensitive and OE33R; radioresistant cells, which was previously generated in our laboratory [33]. The effect of our compounds on two major metabolic pathways; oxidative phosphorylation and glycolysis was assessed using the Seahorse XFe24 analyser. Following 24 h treatment of OE33P and OE33R cells with our compounds, simultaneous measurements of OCR and ECAR were recorded in live cells. Radioresistant OE33R cells produced a significantly higher OCR at baseline when compared to OE33P cells ($p < 0.05$) (Fig. 3A) but no significant difference in ECAR was observed (Fig. 3D). 24 h treatment with pyrazinib (P3) significantly reduced OCR in OE33P and OE33R cells ($p = 0.0262$, $p = 0.0044$) (Fig. 3B and C), with a simultaneous reduction in ECAR in OE33R cells ($p = 0.0162$) (Fig. 3F). Treatment with P2 produced a reduction in OCR alone in OE33R cells ($p = 0.0169$). Interestingly, the non-antiangiogenic analogue P23 increased OCR in OE33P cells (Fig. 3B) and quininib (Q1) significantly reduced ECAR in OE33P cells only (Fig. 3E). No significant effect was seen following treatment with P4, the HCl salt of pyrazinib (P3), which was previously shown to have anti-angiogenic and anti-metabolic activity in zebrafish embryos in Figs. 1B and 2B. This screen demonstrated the novel anti-cancer action of pyrazinib (P3) in its ability to produce anti-metabolic activity *in-vitro* through the production of a significant reduction in OCR in both OE33P and OE33R cells and ECAR in OE33R cells only. P series compounds; P8 and P23 which produced no effect on angiogenesis or metabolism *in-vivo* in zebrafish embryos also produced no anti-metabolic activity when tested *in-vitro* in the isogenic OAC model (Fig. 3B and C,E,F). Furthermore, ATP turnover was significantly higher in OE33R cells compared to OE33P cells ($p = 0.0260$) and treatment with pyrazinib (P3) significantly reduced ATP turnover in OE33R cells ($p = 0.0168$) (Fig. 3 G). No differences were seen in maximal respiration and spare respiratory capacity between the two cell lines or following treatment with pyrazinib (P3) (Fig. 3H, I). In summary, pyrazinib (P3) a small molecule compound significantly inhibited oxidative phosphorylation in radiation-sensitive (OE33P) and radiation-resistant (OE33R) OAC cells and produced a simultaneous reduction in glycolysis in radiation-resistant OE33R cells.

3.4. Pyrazinib (P3) reduced ROS levels in radiation-sensitive OE33P cells with no effect on mitochondrial mass and mitochondrial membrane potential

Treatment with pyrazinib (P3) and P2 was previously shown to reduce metabolic rate in the isogenic model of OAC, thus, we wanted to investigate if this reduction in metabolic rate was accompanied by changes in mitochondrial function following treatment with our compounds.

To investigate if treatment with our P series compounds induced changes in mitochondrial function we assessed alterations in reactive oxygen species (ROS) levels, mitochondrial membrane potential and mitochondrial mass, three surrogate markers of mitochondrial function. OE33R cells were associated with significantly higher basal levels of ROS ($p = 0.0151$) when compared to age and passage matched OE33P cells (Fig. 4A). Treatment with our P series compounds had a notable effect on ROS production in OE33P cells (Fig. 4B) but no changes in ROS were observed following treatment in OE33R cells (Fig. 4C). 24 h treatment with pyrazinib (P3), P2 and P18, P20 significantly reduced ROS levels in OE33P cells ($p < 0.01$) with P4, P8 and P23 also inducing a modest but significant reduction in ROS levels ($p < 0.05$) in radiation-sensitive OE33P cells (Fig. 4B). There were no significant differences in the other two surrogate markers of mitochondrial function; mitochondrial membrane potential and mitochondrial mass either between the two cell lines at baseline or following treatment with 10 μM of P series compounds (Fig. 4D–I). In summary, the potent anti-metabolic activity of pyrazinib (P3) in OE33R cells is independent of

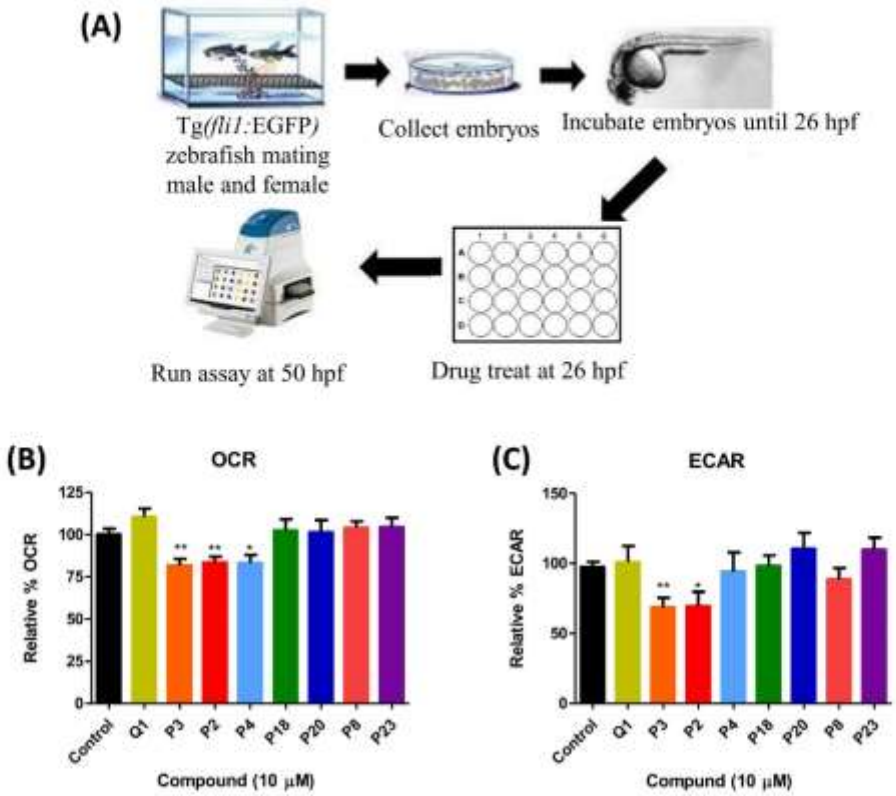

Fig. 2. Pyrazinib (P3) and P series analogues inhibit metabolism in Tg(*fli1:EGFP*) zebrafish. **(A)** Schematic of zebrafish real-time metabolic profiling assay; 26 hours post fertilisation (hpf) embryos were treated with P series compounds and metabolic profile was analysed at 50 hpf using the XFe24 Seahorse Biosciences analyser. **(B)** 26 hpf embryos were treated with 0.1% DMSO as control or 10 μM of P series compounds; quininib (Q1), pyrazinib (P3), P2, P4, P18, P20, P8 or P23, at 50 hpf basal OCR measurements were taken using Seahorse Biosciences XFe24 Analyser, (n = 5). **(C)** 26 hpf zebrafish embryos were treated with 0.1% DMSO or 10 μM of quininib (Q1), pyrazinib (P3), P2, P4, P18, P20, P8 and P23, at 50 hpf basal ECAR measurements using Seahorse Biosciences XFe24 Analyser, (n = 5). Data expressed as mean + SEM; Unpaired *t*-test. *p < 0.05, **p < 0.01.

changes to mitochondrial function including ROS production, mitochondrial membrane potential and mitochondrial mass.

3.5. Pyrazinib (P3) significantly enhanced radiosensitivity in-vitro in an isogenic model of oesophageal adenocarcinoma

Angiogenesis and metabolism are interconnected processes, tightly linked to the radioresistant phenotype [11,34]. We investigated the ability of our small molecule compounds with anti-angiogenic and anti-oxidative phosphorylation activity, pyrazinib (P3) and other P series compounds (P2, P4), to sensitise OAC cells to radiation. We carried out a clonogenic assay, the gold standard for assessing radiosensitivity [35]. Following 24 h treatment with 10 μM of quininib (Q1), pyrazinib (P3), P2 and P4 OE33P and OE33R cells were either irradiated (2 Gy) or mock irradiated (0 Gy). We also tested other P series compounds which had previously been shown to be anti-angiogenic and have no anti-metabolic activity; P18 and P20 and two compounds which were neither anti-angiogenic or anti-metabolic; P8 and P23 (data not shown).

Quininib (Q1), which produced significant anti-angiogenic activity and a modest but significant reduction in ECAR in OE33P cells had no effect on the surviving fraction in either cell line (Fig. 5 B, F) indicating that targeting OCR as opposed to ECAR may be more important to overcome radioresistance in OAC cells. Notably, pyrazinib (P3), which produced the most potent anti-angiogenic activity *in-vivo* in zebrafish embryos and significant anti-metabolic activity both *in-vivo* and *in-vitro*, could significantly reduce the surviving fraction in both radiation-sensitive ($p = 0.0395$) and radiation-resistant cells ($p = 0.0342$) (Fig. 5C, G). In addition, P4, the HCl salt of pyrazinib (P3), which was previously shown to have potent anti-angiogenic and anti-metabolic activity *in-vivo* produced a significant reduction in surviving fraction in both OE33P ($p = 0.0373$) and OEE3R cells ($p = 0.0220$) (Fig. 5 E, J). P2, a HCl salt which has a similar but distinctly different IUPAC structure from pyrazinib (P3) and P4, significantly reduced surviving fraction in OE33P cells ($p = 0.0246$) (Fig. 5D) and showed a trend, although not significant, towards a reduction in surviving fraction in the radioresistant line (Fig. 5H). This result indicated that small molecule compounds which were previously shown to inhibit angiogenesis *in-vivo* and inhibit oxidative phosphorylation either *in-vivo* or *in-vitro* or both could radiosensitise OAC cells to radiation, whereas compounds which were anti-angiogenic but do not inhibit OCR, a measure of oxidative

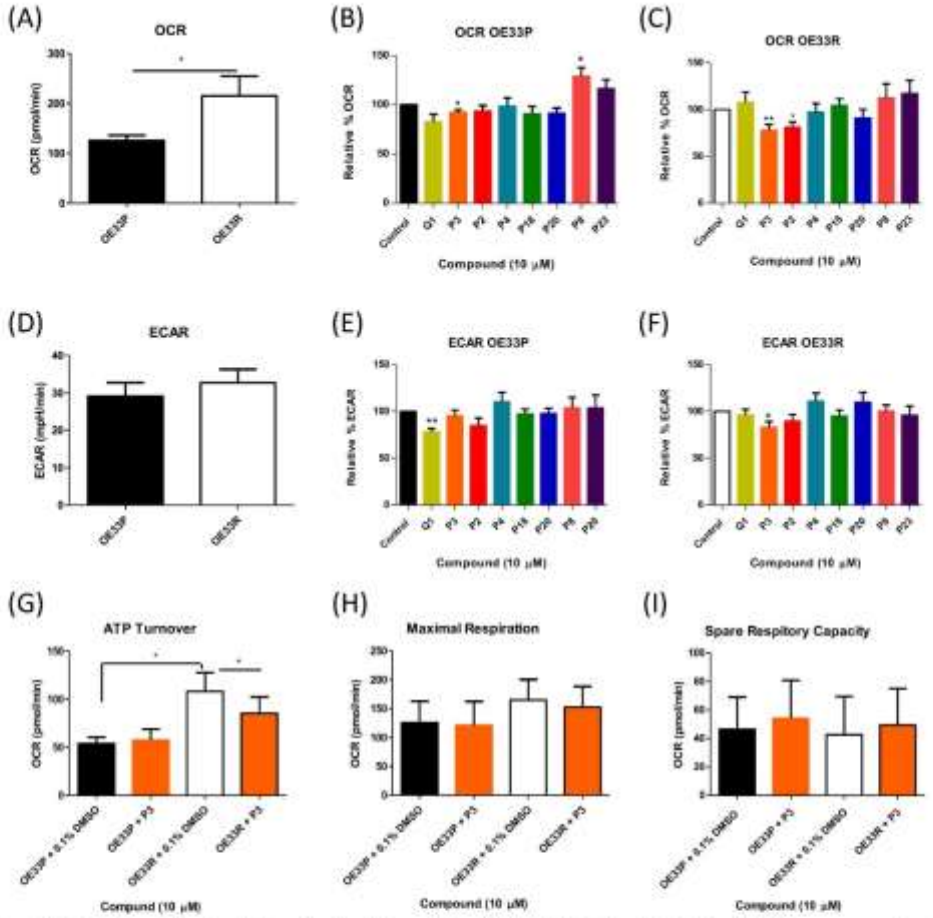

Fig. 3. Pyrazinib (P3) treatment reduced oxidative phosphorylation and glycolysis in OE33R; radioresistant OAC cells. (A) Oxygen consumption rate (OCR), a measure of oxidative phosphorylation was evaluated in OE33P and OE33R cells using the Seahorse Biosciences XFe24 analyser. OE33R cells have a significantly higher OCR when compared to OE33P, radiation sensitive cells, two-tailed unpaired *t*-test, $^{*}p < 0.05$, (n = 13). **(B)** Relative percentage OCR in OE33P cells following treatment with 0.1% DMSO control or P series compounds, (n = 7, except P3 n = 12). **(C)** Percentage relative OCR in OE33R cells following treatment with 0.1% DMSO control or novel compounds at 10 μM, (n = 7, except P3 n = 12). **(D)** Extracellular acidification rate (ECAR), a measure glycolysis was evaluated in OE33P and OE33R cells using the Seahorse Biosciences XFe24 extracellular flux analyser, (n = 7, except P3 n = 12). **(E)** Relative percentage ECAR in OE33P cells following treatment with control or 10 μM of quininib (Q1), Pyrazinib (P3), P2, P4, P18, P20, P8 and P23 (n = 7, except P3 n = 12). **(F)** Pyrazinib (P3) produced a significant reduction in relative percentage ECAR in OE33R cells (n = 7 except P3 n = 12). **(G)** ATP turnover in OE33P and OE33R cells following treatment with 0.1% DSMO or pyrazinib (P3), (n = 6). **(H)** Spare Respiratory capacity in OE33P cells and OE33R cells following treatment with 0.1% DMSO or pyrazinib (P3), (n = 6). **(I)** Maximal respiration in OE33P cells and OE33R cells following treatment with 0.1% DMSO or pyrazinib (P3), (n = 6). Data are expressed as mean + SEM. Statistical analysis was carried out using an unpaired *t*-test to compare different cell lines and paired *t*-test to compare within the same cell line. Data was normalised to cell number, as assessed by crystal violet assay. $^{*}p < 0.05$,$^{**}p < 0.01$. (For interpretation of the references to color in this figure legend, the reader is referred to the Web version of this article.)

phosphorylation (Q1, P18 and P20) could not induce this effect nor could compounds P8 and P23, which had neither anti-angiogenic or anti-metabolic activity (data not shown). Notably, treatment with 10 μM of pyrazinib for 24 h prior to radiation was found to be the optimal dose and treatment schedule to enhance radiosensitivity in OE33P and OE33R cells (Fig. 5C,G), (Supplemental Figure 2 A-D).

3.6. Pyrazinib (P3) enhanced radiosensitivity in-vitro in an isogenic model of oesophageal adenocarcinoma at 2, 4 and 6 Gy X-ray radiation

To further investigate the ability of pyrazinib (P3) to enhance radiosensitivity in OAC we evaluated the ability of pyrazinib (P3) to radio-sensitise OE33P and OE33R cells to radiation therapy at increasing doses of radiation by clonogenic assay. As previously shown pyrazinib (P3) enhanced radiosensitivity in OE33P and OE33R cells ($p = 0.0043$, $p = 0.0051$ respectively) following 2 Gy irradiation

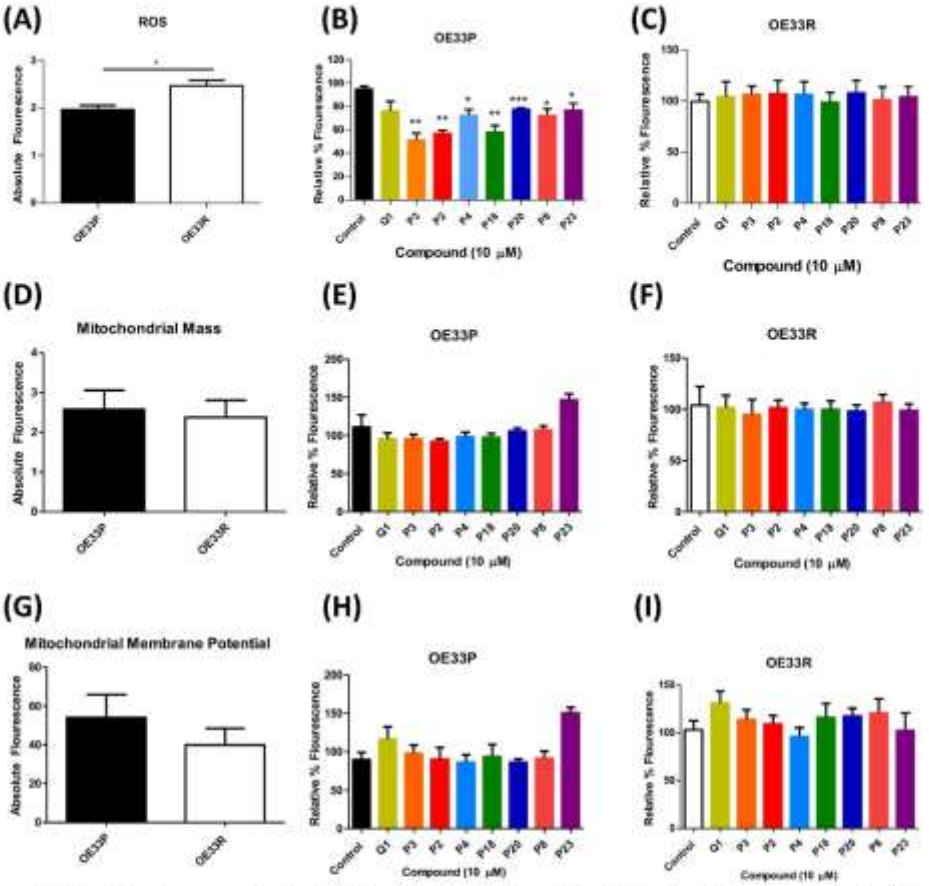

Fig. 4. Pyrazinib (P3) and P series compounds reduced ROS levels in the radiation sensitive OE33P cells with no effect on mitochondrial mass and mitochondrial membrane potential. **(A)** ROS levels are significantly higher in radiation resistant OE33R cells compared to OE33P; radiation sensitive cells, two-tailed unpaired *t*-test, (n = 4) $^{*}p < 0.05$. **(B)** 24 h treatment with pyrazinib (P3) and additional P series compounds significantly reduced ROS in OE33P cells, (n = 4). **(C)** Pyrazinib (P3) and other P series compounds tested had no effect on ROS levels in OE33R cells following treatment at 10 μM, (n = 4). **(D)** Mitochondrial mass does not differ significantly between OE33P and OE33R cells, two tailed unpaired *t*-test, (n = 4) **(E)** 24 h treatment with 10 μM of P series compounds had no effect on mitochondrial mass in OE33P cells, (n = 4) **(F)** 24 h treatment with 10 μM of P series compounds did not alter mitochondrial mass in OE33R cells, (n = 4) **(G)** Mitochondrial membrane potential does not differ significantly between OE33P and OE33R cells, unpaired *t*-test, (n = 4) **(H)** 24 h treatment with 10 μM of P series compounds had no effect on mitochondrial membrane potential in OE33P cells, (n = 4) **(I)** 24 h treatment with 10 μM of P series compounds had no effect on mitochondrial membrane potential in OE33R cells, (n = 4). Statistical analysis was carried out using an unpaired *t*-test to compare different cell lines and paired *t*-test to compare within same cell line. Data was normalised to cell number, determined by crystal violet assay. Data are expressed as mean + SEM; $^{*}p < 0.05$, $^{**}p < 0.01$, $^{***}p < 0.001$. (For interpretation of the references to color in this figure legend, the reader is referred to the Web version of this article.)

(Fig. 6 A, B). In addition, pyrazinib (P3) enhanced radiosensitivity following irradiation at 4 Gy in OE33P ($p = 0.0081$) and OE33R cells ($p = 0.0139$) and 6 Gy in OE33P and OE33R cells ($p = 0.0093$, $p = 0.0141$ respectively).

3.7. Pyrazinib (P3) enhanced radiosensitivity in-vitro in an isogenic model of oesophageal adenocarcinoma under hypoxic conditions

Hypoxic tumours are inherently radioresistant, thus we investigated the ability of pyrazinib (P3) to enhance radiosensitivity in an environment of low oxygen (0.5% O_2). Both OE33P and OE33R cells were significantly more radioresistant to both 2 and 4 Gy radiation when cultured under hypoxic conditions (0.5% O_2) when compared to matched cells cultured under normoxic conditions (Fig. 7 A, B). Pyrazinib (P3) significantly enhanced radiosensitivity of OE33R cells cultured under hypoxic conditions following 4 Gy irradiation (Fig. 7 D) ($p = 0.0216$). Pyrazinib (P3) did not alter the radiosensitivity of OE33P cells cultured under hypoxic conditions of 0.5% O_2 but could enhance radiosensitivity under normoxic conditions following 2 and 4 Gy irradiation similar to results previously shown (Fig. 7C).

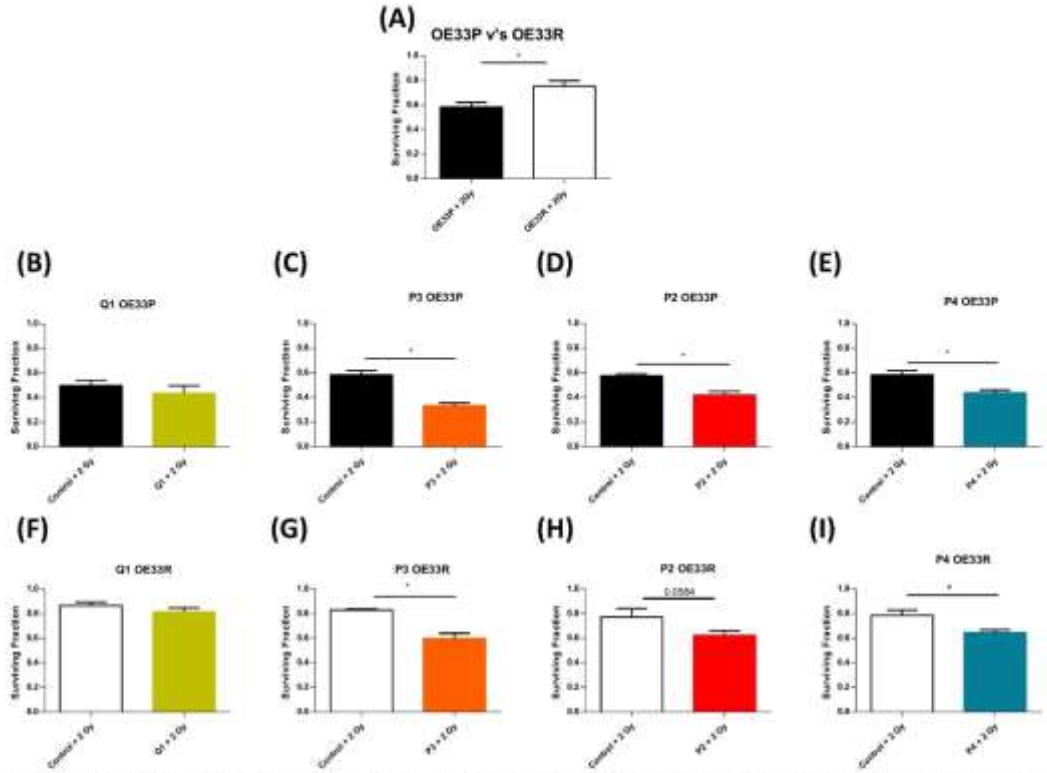

Fig. 5. Pyrazinib (P3), P2 and P4 enhanced radiosensitivity *in-vitro* in an isogenic model of Oesophageal Adenocarcinoma. The effect of 24 h treatment with P series compounds on radiosensitivity *in-vitro* was assessed by clonogenic assay. **(A)** Surviving fraction of OE33P and OE33R cells following 2 Gy radiation, OE33R radioresistant cells have a significantly higher surviving fraction when compared to OE33P radiation sensitive cells, (n = 3), unpaired *t*-test, *p < 0.05. **(B)** Surviving fraction of OE33P cells following treatment with quininib; Q1 + 2 Gy, (n = 3). **(C)** Surviving fraction of OE33P cells following treatment with pyrazinib (P3) + 2 Gy, (n = 3). **(D)** Surviving fraction of OE33P cells following treatment with P2 + 2 Gy, (n = 3) **(E)** Surviving fraction of OE33P cells following treatment with P4 + 2 Gy, (n = 3). **(F)** Surviving fraction of OE33R cells following treatment with quininib; Q1 + 2 Gy, (n = 3). **(G)** Surviving fraction of OE33R cells following treatment with pyrazinib (P3) + 2 Gy, (n = 3) **(H)** Surviving fraction of OE33R cells following treatment with P2 + 2 Gy, (n = 4). **(I)** Surviving fraction of OE33R cells following treatment with P4 + 2 Gy, (n = 4). Statistical analysis by two-tailed unpaired *t*-test to compare different cell lines and paired *t*-test to compare within same cell line. *p < 0.05. Data expressed as mean + SEM.

3.8. Pyrazinib (P3) significantly alters the secretion of IL-6, IL-4, IL-8 and IL-13 in OE33R radioresistant cells

Inflammation has previously been shown to be a negative regulator of response to radiation treatment in OAC [23,24]. We sought to investigate the difference in inflammatory protein secretions from our OE33P and OE33R cells and evaluate the effect of treatment with our radiosensitiser pyrazinib (P3) on inflammatory protein secretions in our isogenic model. We measured the effects of pyrazinib (P3) on the protein secretions of 54 angiogenic factors, growth factors and inflammatory cytokines in OE33P and OE33R cells following treatment with 10 μM pyrazinib (P3) or vehicle control. Of the 54 factors analysed, 30 were detected within the range of detection in our isogenic radioresistant OAC model. Of the 30 factors detected, 9 factors were secreted at significantly higher levels in OE33R radioresistant cells when compared to OE33P cells; IL-6, IL-4, IL-8, ICAM, IL-12p70, IL-2, IL-10, IP-10 and MCP-1 (Fig. 8A–J). Pyrazinib (P3) significantly reduced the secretions of IL-6 ($p = 0.0006$) (Fig. 8A), IL-4 ($p = 0.0111$) (Fig. 8B), IL-8 ($p = 0.0488$) (Fig. 8C) and IL-13 ($p = 0.0204$) (Fig. 8 D) *in-vitro* in OE33R cells.

4. Discussion

To date, through phenotype-based screens we have identified 3 novel small molecule compounds (pyrazinib (P3), P2 and P4) with significant anti-angiogenic and anti-metabolic activity *in-vitro* and *in-vivo*, which enhanced radiosensitivity in our isogenic model of OAC radioresistance. Pyrazinib (P3) was selected as our lead compound which significantly enhanced radiosensitivity in our isogenic model of OAC radioresistance, and was associated with significant anti-angiogenic, anti-metabolic and anti-inflammatory actions *in-vivo* in zebrafish and *in-vitro* in our isogenic model of OAC radioresistance. Importantly pyrazinib (P3) produced significantly greater anti-angiogenic and anti-metabolic activity, specifically in terms of targeting oxidative phosphorylation than its parent compound quininib, and was associated with novel radiosensitising activity in an isogenic model of OAC radioresistance.

Two of twenty-three of our P series compounds tested; pyrazinib

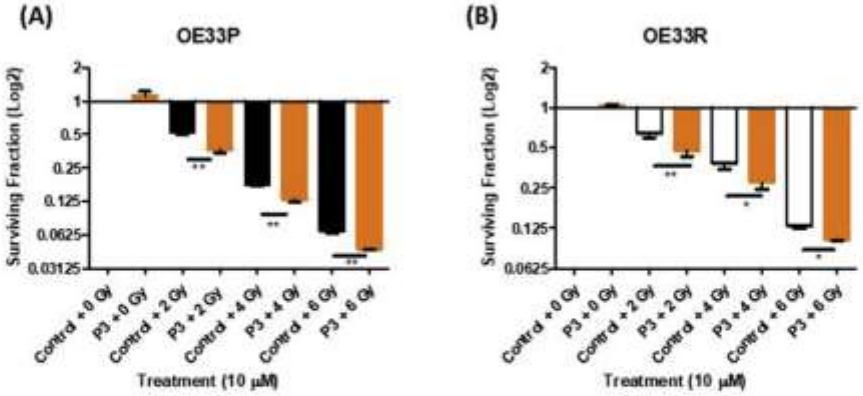

Fig. 6. Pyrazinib (P3) enhanced radiosensitivity *in-vitro* in an isogenic model of Oesophageal Adenocarcinoma at increasing fractionated doses of irradiation. The effect of treatment with pyrazinib (P3) on radiosensitivity *in-vitro* was assessed by clonogenic assay. **(A)** Surviving fraction of OE33P cells following treatment with 0.1% DMSO control or 10 μM pyrazinib (P3) and 0, 2, 4 and 6 Gy radiation, (n = 3), paired *t*-test, $^{**}p < 0.01$. **(B)** Surviving fraction of OE33R cells following treatment with 0.1% DMSO control or 10 μM pyrazinib (P3) and 0, 2, 4 and 6 Gy radiation, (n = 3), paired *t*-test, $^{*}p < 0.05$, $^{**}p < 0.01$. Data expressed as mean + SEM.

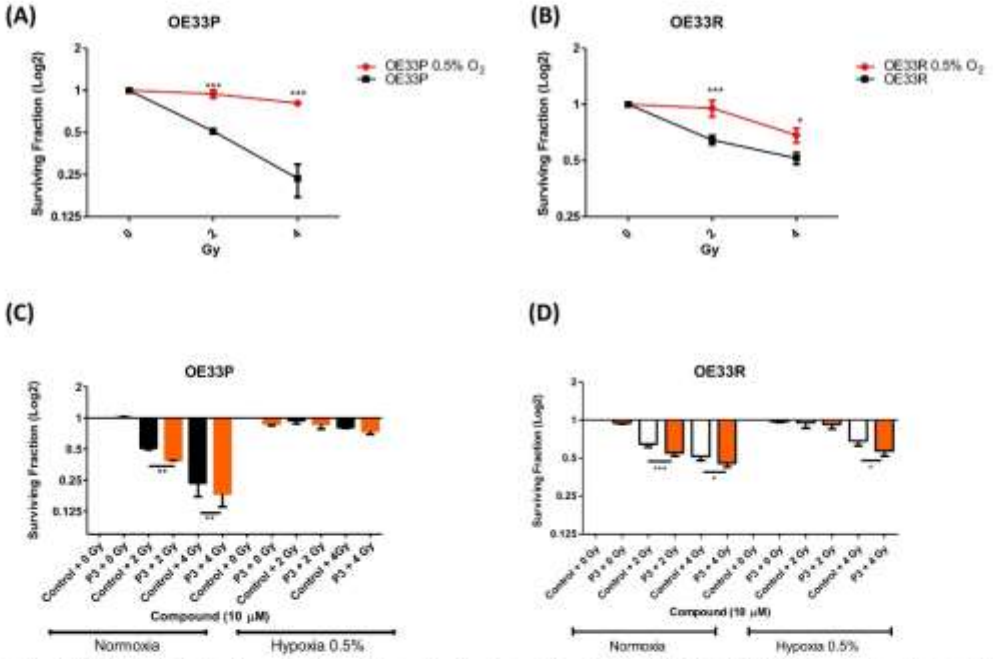

Fig. 7. Pyrazinib (P3) significantly enhanced radiosensitivity under hypoxic conditions (0.5% O_2) in OE33R; OAC radioresistant cells. The ability of pyrazinib (P3) to enhance radiosensitivity was evaluated by clonogenic assay under normoxic and hypoxic (0.5% O_2) conditions using the Whitley h35 hypoxia chamber **(A)** Surviving fraction of OE33P cells cultured under normoxic and hypoxic conditions following 0, 2 and 4 Gy irradiation, (n = 3). **(B)** Surviving fraction of OE33R cells cultured under normoxic and hypoxic conditions following 0, 2 and 4 Gy irradiation, (n = 3). **(C)** Surviving fraction of OE33P cells cultured under normoxia and hypoxia following treatment with 0.1% DMSO control or 10 μM pyrazinib (P3) and 0, 2, and 4 Gy irradiation, (n = 3). **(D)** Surviving fraction of OE33R cells cultured under normoxia or hypoxia following treatment with 0.1% DMSO control or 10 μM pyrazinib (P3) and 0, 2, and 4 Gy irradiation, (n = 3). Unpaired *t*-test to was used to compare difference cell lines and paired *t*-test was used to compare within same cell line, $^{*}p < 0.05$, $^{**}p < 0.01$, $^{***}p < 0.001$. Data expressed as ± SEM.

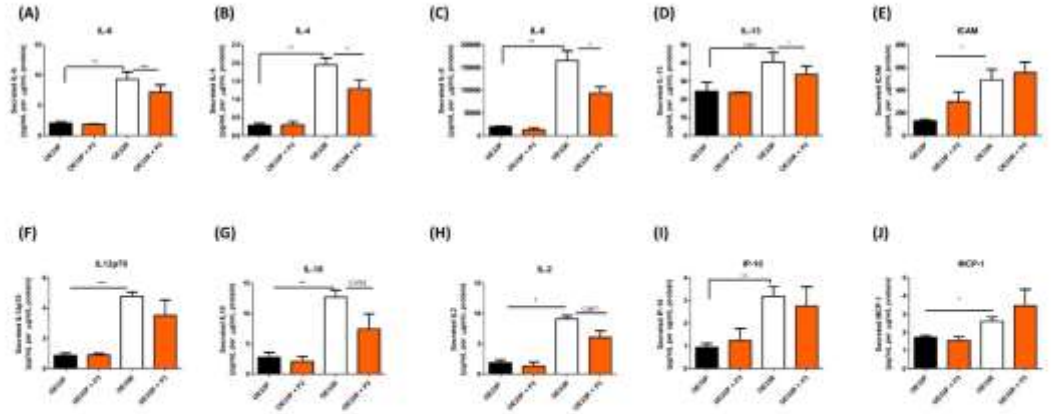

Fig. 8. Pyrazinib (P3) significantly reduced the secretion of IL-6, IL-4, IL-8 and IL-13 in OE33R; radioresistant OAC cells. The secreted levels of 54 proteins in OE33P and OE33R cells was evaluated by multiplex ELISA, 30 proteins were detected in supernatant of OE33P and OE33R cells, 9 proteins were significantly upregulated in OE33R cells. Pyrazinib (P3) significantly inhibited the secretion of IL-6, IL-4, IL-8 and IL-13 in OE33R cells. Secreted levels of **(A)** Interleukin 6 (IL-6) **(B)** Interleukin 4 (IL-4) **(C)** Interleukin 8 (IL-8) **(D)** Interleukin 13 (IL-13) **(E)** Intracellular Adhesion Molecule 1 (ICAM-1) **(F)** Interleukin 12p70 (IL-12p70) **(G)** Interleukin 10 (IL-10) **(H)** Interleukin 2 (IL-2) **(I)** Interferon gamma-induced protein 10 (IP-10) **(J)** Monocyte chemoattractant protein 1 (MCP-1) in OE33P and OE33R cells treated with either 0.1% DMSO control or 10 μM pyrazinib (P3), all secretions normalised to protein content. Unpaired *t*-test used to compare different cell lines, paired *t*-test to compare within same cell line. ($n = 3$) $^*p < 0.05$, $^{**}p < 0.01$, $^{***}p < 0.001$. Data expressed as + SEM.

(P3) and P4, demonstrated greater anti-angiogenic activity than the quinoline series compound quininib, (Q1) in the ISV assay. Pyrazinib (P3) produced the most potent anti-angiogenic activity with a −67% reduction in vessel number compared to control. The enhanced anti-angiogenic activity produced by pyrazinib (P3) and P4 of the P series was an important finding given that quininib, (Q1) a quinoline compound from which pyrazinib (P3) was derived has been previously shown to inhibit ocular and tumoural angiogenesis using *in-vitro* and *in-vivo* models and produces a potent anti-tumoural response in a colorectal murine xenograft model [29,30]. Thus, our initial findings indicated our novel small molecule compounds have more potent anti-angiogenic activity than quinoline series compound, quininib (Q1), and warrant further investigation in other model systems. The potent anti-angiogenic activity of our novel compounds is an important finding given that tumour vasculature has been recognised as a critical component of radiation response [12]. Aberrant tumour vasculature and dysregulated blood flow through tumour vasculature can promote the development of hypoxic regions which are associated with radioresistance [12]. Cells irradiated in the presence of oxygen are thought to be ~3 times more sensitive to irradiation than those located in regions of severe hypoxia [12]. In an oesophageal SCC xenograft model the administration of anti-angiogenic recombinant endostatin (rh-Endo) in combination with one dose of 8 Gy irradiation significantly delayed tumour growth which was associated with remodelling of the tumour vasculature and a reduction in tumour hypoxia in xenografts [16]. In a colon cancer xenograft model, an anti-VEGF monoclonal antibody in combination with radiation had an additive effect. The anti-VEGF antibody induced a significant tumour growth delay which was associated with a reduction in tumour microvessel density and interstitial fluid pressure [34]. These studies strongly support the development of a novel anti-angiogenic to enhance radiosensitivity. It is important to consider that the Tg*(fli1:EGFP)* zebrafish model used in this assay to identify our potent anti-angiogenic compounds is a model of developmental angiogenesis, and not pathological angiogenesis. Despite this, a large number of agents currently used in the clinic including sorafenib and regorafenib were previously shown to inhibit angiogenic activity in this zebrafish model [36]. In order to identify novel radiosensitisers with potential therapeutic benefit, it is likely that such agents will need to affect more than one biological process including metabolism to counteract the complex polymodal OAC radioresistant phenotype [11,33]. Thus, in addition to the anti-angiogenic activity produced by pyrazinib (P3) and other P series compounds, we investigated whether these compounds could also inhibit two major metabolic pathways, oxidative phosphorylation and glycolysis both *in-vivo* and *in-vitro* given the important association between oxidative phosphorylation and treatment response previously reported in OAC.

Zebrafish are becoming an increasingly popular model for cancer research and the use of this model for metabolic screening and profiling is continuing to emerge [37]. Pyrazinib (P3), P2 and P4 significantly reduced OCR, a measure of oxidative phosphorylation in zebrafish embryos, where pyrazinib (P3) and P2 produced a simultaneous reduction in ECAR, a measure of glycolysis. These findings suggest pyrazinib (P3) and P2 may be exerting their effect at an earlier point common to both metabolic pathways. Notably, Pyrazinib (P3) and P4, which were two of the most active compounds in both zebrafish assays have the same structural features including a (E)-2-(2-Pyridin-2-yl-vinyl)-phenol backbone but unlike pyrazinib (P3), P4 is a HCl salt, thus, the highly potent activity produced by P3 and P4 is likely to be attributable to these common structural features.

Additionally, *in-vitro*, pyrazinib (P3) and P2 produced a significant reduction in OCR a measure of oxidative phosphorylation of ~32% and −18% respectively in OE33R (radioresistant) cells with pyrazinib (P3) producing a simultaneous reduction in ECAR, a measure of glycolysis. Notably, only pyrazinib (P3) produced significant anti-metabolic activity in both the OE33P and radioresistant OE33R cells. We have previously shown that OAC radio-resistant cells have an increased rate of oxidative phosphorylation when compared to radiosensitive OAC cells, thus, the potent inhibition of oxidative phosphorylation produced by our compounds is a significant finding in this model [11]. The higher rate of oxidative phosphorylation in OE33R radioresistant cells may indicate these cells consume more oxygen than radiosensitive cells and is thought to be a contributing factor promoting the radio-resistant phenotype given the importance of oxygen in the radioresponse, especially given that *ATP5B*, a marker of oxidative phosphorylation, is expressed at significantly higher levels in OAC patients with a subsequent poor response to neoCRT [11]. *In-vivo*, in HCT-116 xenografts,

administration of metformin was found to produce a 7% reduction in oxygen consumption rate and to improve tumour re-oxygenation [38]. In addition, in these xenografts, pre-treatment with metformin before one dose of 15 Gy irradiation produced a significant tumour growth delay [38]. Targeting oxidative phosphorylation *in-vivo* with papaverine was found to enhance tumour oxygenation an sensitise tumours to radiation therapy [39]. These studies highlight the potential of our novel anti-metabolic agents to enhance radiosensitivity, especially as pyrazinib (P3) can produce a much higher reduction in oxidative phosphorylation than metformin did in this study. ATP turnover was significantly higher in OE33R cells when compared to OE33P cells, supporting previous findings by our group [11]. Pyrazinib (P3) could significantly inhibit ATP turnover in OE33R cells. This is an important finding given that a previous study demonstrated that the maintenance of intracellular ATP levels following irradiation was associated with a radioresistant phenotype in head and neck cancer [40]. The ability of pyrazinib (P3) to reduce ATP turnover provides insight into how pyrazinib (P3) is significantly inhibiting oxidative phosphorylation in OE33R cells. The more potent anti-angiogenic and anti-metabolic activity produced by pyrazinib (P3) than its parent compound quininib may be attributable to their different structural features and molecular targets. Quininib, a quinoline compound, is a known cysteinyl leukotriene receptor 1 and receptor 2 antagonist whereas binding studies have shown that pyrazinib (P3), a pyrazine phenol does not target this molecular pathway [29]. Furthermore, previous studies have indicated that cancer cells can switch from a predominant glycolytic phenotype to an oxidative phenotype following radiation to promote cancer cell survival under genotoxic stress via mTOR-mediated hexokinase II inhibition [41] and p53-independent mitochondrial biogenesis, which is counter-regulated by HIF1α [42]. Thus, dual inhibition of both oxidative phosphorylation and glycolysis by pyrazinib (P3) in combination with anti-angiogenic activity is favourable. The lack of feedback upregulation of ECAR following OCR inhibition suggests pyrazinib (P3) is acting at an early point common to both pathways or there is a dysregulated compensatory mechanism in this isogenic model. In a pancreatic study inhibition of OCR with oligomycin was not found to cause an upregulation in ECAR [43]. Furthermore, metabolism is tightly linked to angiogenesis, as tumour vasculature supplies glucose to the tumour which is used to fuel the tricarboxylic acid cycle [44]. Thus the use agents targeting both angiogenesis and oxidative phosphorylation may be a novel approach that could be utilised to overcome radiation resistance.

In-vitro, OE33R cells were found to have significantly higher levels of ROS when compared to their matched OE33P cells which may be linked to the increased levels of mitochondrial mutagenesis in these cells [11]. The higher levels of ROS in the OE33R line may be a product of the extensive radiation exposure these cells underwent to become radioresistant but also highlights the altered mitochondrial function in radiation-resistant cells when compared to radiation-sensitive cells. Treatment with our novel compounds pyrazinib (P3), P2, P4, P18, P20, P8 and P23 significantly reduced ROS levels in the OE33P cells but no effect was seen in the treated OE33R cells. This inhibition of ROS specifically in our OE33P but not OE33R line was interesting and may indicate pyrazinib (P3) and other P series compounds (P2, P4, P18, P20, P8) can only alter inherently lower levels of ROS, as seen in OE33P cells, with no activity on the higher ROS levels in OE33R cells. Notably only pyrazinib (P3), which produced a reduction in ROS levels in OE33P cells, could also reduce oxidative phosphorylation in OE33P cells, potentially indicating that these compounds are targeting ROS generated from other processes outside the metabolic cycle, given no simultaneous reduction in metabolism is seen despite robust reductions in ROS produced by the other compounds. This result indicated that the previous reduction in metabolic rate by pyrazinib (P3) in OE33R cells is independent of changes to mitochondrial function and the reduction of either OCR or ECAR or both by pyrazinib (P3) and P2 is possibly occurring through an alternative mechanism. ROS is critical to the DNA damage response induced by irradiation, but on the contrary can promote cellular signalling and proliferation, thus a reduction of the higher levels of ROS in the OE33R cells following treatment may confer a favourable advantage [45]. In addition, this result indicates, the radiosensitising activity produced by pyrazinib (P3) is independent of changes to ROS in OE33R cells. Our results suggest that our P series compounds may be acting directly on these metabolic pathways, independent of significant changes to mitochondrial function.

Pyrazinib (P3) and P4, significantly enhanced radiosensitivity in both radiation-sensitive and radiation-resistant OAC cells. P2 could only enhance radiosensitivity in the radiation-sensitive OAC cells. Importantly, the quinoline compound quininib, (Q1) and the P series compounds which can inhibit angiogenesis but not OCR, a measure of oxidative phosphorylation could not enhance radioresponse. Furthermore, the enhanced radiosensitising effect was independent of changes to cellular proliferation or cellular cytotoxicity (Supplemental Fig. 1). These were significant findings which demonstrated that our lead small molecule compound; pyrazinib (P3), could enhance radiosensitivity in an isogenic model of OAC radioresistance as similar agents currently do not exist in this space. In addition, our lead compound, pyrazinib (P3), could also significantly enhance radiosensitivity when given before 4 and 6 Gy irradiation doses in both our OE33P and OE33R cells. Irradiation is a critical treatment modality which is used in the treatment of over 50% of human malignancies with response to radiation often inversely correlated to a reduction in tumour size [7]. This further highlights the importance of our identification of novel small molecule compounds which can enhance radiosensitivity in an isogenic model of OAC radioresistance. Importantly, clonogenic studies have been previously used to identify radiosensitising compounds *in-vitro* which have been later translated to radiosensitising agents in the clinic, an example of which is gemcitabine [46]. Thus, the clonogenic assay is a useful tool for the identification of potential novel radiosensitising agents, but it is important to note such assays lack the complexity of the heterogeneous tumour microenvironment. Furthermore, pyrazinib (P3) significantly enhanced radiosensitivity in OE33P and OE33R cells independent of baseline changes to the expression of DNA repair genes *MLH1*, *SMUG1*, *MMS19* and *PARP1* which have been previously linked to radiation resistance in OAC (Supplemental Fig. 3) [33].

Pre-treatment with pyrazinib (P3) could significantly enhance radiosensitivity of OE33R radioresistant cells following 4 Gy irradiation cultured under hypoxic conditions. Oxygen is a potent radiosensitiser and solid tumours with areas of hypoxia are the most aggressive and difficult tumours to treat [47]. Hypoxia is heterogeneous across tumours and can change following treatment radiation [48]. Hypoxic cancer cells are generally more resistant to both chemotherapy and radiotherapy than their normoxic counterparts and contribute largely to the development of treatment resistance and thus may serve as a novel target to enhance radiosensitivity. A number of studies have reportedly developed hypoxia-targeting agents as a mechanism to enhance radioresponse, thus the ability of pyrazinib (P3) to maintain its radiosensitising effect under these conditions is a critical finding. In gastric cancer, the RNA polymerase inhibitor TAS106 was demonstrated to radiosensitise gastric cancer cells and xenografts to irradiation through its action on HIF1α [49]. The ability of pyrazinib (P3) to radiosensitise OAC radioresistant cells under normoxic and hypoxic conditions further highlights the potential of this compound to function as a novel radiosensitiser in OAC.

OAC is an inflammatory driven cancer and we sought to investigate differences in inflammatory protein secretions in our isogenic model of OAC radioresistance. Nine of 30 detected inflammatory and angiogenic factors were secreted at significantly higher levels in OE33R radioresistant cells when compared to OE33P cells; IL-8, IL-4, IL-6, IL-2, IL-12p70, IL-10, MCP-1, IP-10 and ICAM highlighting the potential importance of these inflammatory and angiogenic mediators in radioresistance in OAC. Pyrazinib (P3) significantly reduced the secretions of IL-6, IL-8, IL-4 and IL-13 *in-vitro* in OE33R cells. Inflammation plays a

critical role in disease outcome in OAC, given the increased risk of cancer development and poor outcome for obese patients where altered secretion of adipokines and cytokines from adipose tissue contributes a pro-tumourigenic environment [50,51]. A previous study by our group showed a significant increase in oesophageal and colorectal tumour cell proliferation following culture with conditioned media from visceral adipose tissue of centrally obese patients which may be linked to the higher levels of IL-6 and VEGF found in this tissue [52]. IL-6 and its family members have been repeatedly linked with radioresistance of multiple tumour types including nasopharyngeal, liver, prostate, oral, and oesophageal cancer [25,53–57]. In a prostate cancer model, IL-6 inhibition enhanced radiosensitivity an effect which was associated with increased irradiation-induced ROS and oxidative DNA damage *in-vitro* and inhibition of IL-6 protein expression in combination with irradiation attenuated angiogenesis and decreased tumour regrowth *in-vivo* [55]. In addition, IL-6 signalling was reported to promote radioresistance through enhanced DNA repair and prevention of apoptosis in CD133 + stem-like cells of lung cancer after radiation [53]. Furthermore, IL-8 has also previously been linked with tumour radioresistance [58]. Let-7c, a tumour suppressor microRNA, was shown to restore radiosensitivity and impair stemness of oral cancer cells through inhibition IL-8 secretion [58]. In another study, in a radioresistant oral SCC xenograft, the administration of IL-8 and IL-6 neutralising antibodies sensitised the tumours to irradiation which supports our findings that inhibition of both IL-6 and IL-8 could contribute to enhanced radiosensitivity [27]. Similar to our findings, IL-6 and IL-8 were present at higher levels in radioresistant tumours when compared to the parental radiosensitive oral SCC tumours [27]. Furthermore, IL-4 and IL-13 are closely related cytokines which have also been previously linked with radioresistance, where the blockade of IL-4/IL-13 mediated phosphorylation of STAT6 produced a decrease in M2 polarization of macrophages and was protective against macrophage-mediated radioresistance of inflammatory breast cancer [59]. Given the association of IL-6, IL-8, IL-4 and IL-13 with tumour growth and treatment resistance in the literature, the inhibition of secretion of these cytokines by pyrazinib (P3) may further augment its anti-cancer effect. In summary, pyrazinib (P3), a novel anti-angiogenic and anti-metabolic compound, can significantly enhance radiosensitivity in an isogenic model of OAC radioresistance and is associated with anti-inflammatory activity through its inhibition of IL-6, IL-8, IL-4 and IL-13 secretion from OE33R cells.

Through phenotype-based drug discovery screens, we have identified pyrazinib (P3) as a novel radiosensitiser in OAC which produced robust anti-angiogenic and anti-metabolic activity *in-vivo* and *in-vitro* and significantly enhanced radiosensitivity in our isogenic model of OAC radioresistance under normoxic and hypoxic conditions. In addition, pyrazinib (P3) was shown to have significant anti-inflammatory activity through its inhibition of IL-6, IL-8, IL-4 and IL-13 inflammatory cytokine secretions. Importantly, *in-vitro* studies utilise tumour cells grown in a monolayer without the supporting stromal cells, endothelial cells and immune cells and it is possible the action of our compounds may be altered in the complex *in-vivo* tumour microenvironment. To further progress our studies, it will be critical to evaluate the effect of our lead radiosensitising compound, pyrazinib (P3), *ex-vivo* in human pre-treatment OAC biopsies and *in-vivo* in a murine model of OAC radioresistance to further elucidate its therapeutic potential in the future.

Author contributions

Experiments Designed by: AMB, BNK, JOS. Performed the experiments: AMB prepared all samples and performed all *in-vivo* and *in-vitro* assays, MRD ran multiplex ELISA. AC assisted in use of Seahorse Technology. SGM assisted with use of hypoxia chamber. ALR assisted in preparation of compounds. Analysed the data: AMB, SAK, NLL, JVR, BNK, JOS. Wrote the paper: AMB, BNK, JOS.

Conflicts of interest

No conflict of interest.

Funding

Funding for this work was provided by the Irish Cancer Society (Grant: CRS15BUC) and Health Research Board (Grant: HRB ILP-POR-2017-055), Enterprise Ireland Commercialisation Fund CF-2011-1319 awarded to BK supported the synthesis of the compounds.

Abbreviations

bFGF	Basic Fibroblast Growth Factor
DMSO	Dimethyl sulfoxide
Dpf	Days post fertilisation
ECAR	Extracellular Acidification Rate
EM	Embryo Medium
Hpf	Hours post fertilisation
IL-6	Interleukin 6
IL-4	Interleukin 4
IL-8	Interleukin 8
IL-13	Interleukin 13
ISV	Intersegmental Vessel
ICAM	Intracellular Adhesion Molecule 1
mTOR	Mammalian Target of Rapamycin
OAC	Oesophageal Adenocarcinoma
OCR	Oxidative Phosphorylation
NeoCRT	Neoadjuvant Chemoradiation Therapy
SCC	Squamous Cell Carcinoma
TRG	Tumour Regression Grade
RT	Room Temperature
VEGF-A	Vascular Endothelial Growth Factor A

Appendix A. Supplementary data

Supplementary data to this article can be found online at https://doi.org/10.1016/j.canlet.2019.01.009.

References

[1] J. Ferlay, et al., Cancer incidence and mortality worldwide: sources, methods and major patterns in GLOBOCAN 2012, Int. J. Canc. 136 (5) (2015) E359–E386.
[2] M. Arnold, et al., Global incidence of oesophageal cancer by histological subtype in 2012, Gut 64 (3) (2015) 381–387.
[3] A. Pennathur, et al., Oesophageal carcinoma, Lancet 381 (9864) (2013) 400–412.
[4] J. Cools-Lartigue, J. Spicer, L.F. Ferri, Current status of management of malignant disease: current management of esophageal cancer, J. Gastrointest. Surg. 19 (5) (2015) 964–972.
[5] T.N. Walsh, et al., A comparison of multimodal therapy and surgery for esophageal adenocarcinoma, N. Engl. J. Med. 335 (7) (1996) 462–467.
[6] H.-L. Jin, et al., Neoadjuvant chemoradiotherapy for resectable esophageal carcinoma: a meta-analysis, World J. Gastroenterol.: WJG 15 (47) (2009) 5983–5991.
[7] C.J. Lord, A. Ashworth, The DNA damage response and cancer therapy, Nature 481 (7381) (2012) 287–294.
[8] F. Ferini, et al., Neoadjuvant therapy with weekly docetaxel and cisplatin, 5-fluorouracil continuous infusion, and concurrent radiotherapy in patients with locally advanced esophageal cancer produced a high percentage of long-lasting pathological complete response, Cancer 119 (5) (2013) 939–945.
[9] C.L. Donohue, J.V. Reynolds, Neoadjuvant treatment of locally advanced esophageal and junctional cancer: the evidence base, current key questions and clinical trials, J. Thorac. Dis. 9 (Suppl 8) (2017) S697–S704.
[10] M. Westerterp, et al., Esophageal cancer: CT, endoscopic US, and FDG PET for assessment of response to neoadjuvant therapy—systematic review, Radiology 236 (3) (2005) 841–851.
[11] N. Lynam-Lennon, et al., Altered mitochondrial function and energy metabolism is associated with a radioresistant phenotype in oesophageal adenocarcinoma, PloS One 9 (6) (2014) e100738.
[12] P. Wachsberger, R. Burd, A.P. Dicker, Tumor response to ionizing radiation combined with antiangiogenesis or vascular targeting agents: exploring mechanisms of interaction, Clin. Canc. Res. 9 (6) (2003) 1957–1971.
[13] W. Kim, et al., Inflammation-induced radioresistance is mediated by ROS-dependent inactivation of protein phosphatase 1 in non-small cell lung cancer cells,

Apoptosis 20 (9) (2015) 1242–1252.
[14] P.S. Ward, C.B. Thompson, Metabolic reprogramming: a cancer hallmark even warburg did not anticipate, Cancer Cell 21 (3) (2012) 297–308.
[15] O. Warburg, On the origin of cancer cells, Science 123 (3191) (1956) 309–314.
[16] H. Zhu, et al., Recombinant human endostatin enhances the radioresponse in esophageal squamous cell carcinoma by normalizing tumor vasculature and reducing hypoxia, Sci. Rep. 5 (2015) 14503.
[17] E. Ciric, G. Serra, Radiotherapy in combination with vascular-targeted therapies, Radiol. Oncol. 44 (2) (2010) 67–78.
[18] B.A. Teicher, et al., Potentiation of cytotoxic cancer therapies by TNP-470 alone and with other anti-angiogenic agents, Int. J. Canc. 57 (6) (1994) 920–925.
[19] T. Huang, et al., Enhancement of radiation response with bevacizumab, J. Exp. Clin. Canc. Res.: CR (Clin. Res.) 31 (1) (2012) 37–37.
[20] R.J. Williams, et al., Inhibition of vascular endothelial growth factor signalling using cediranib (RECENTINTM, AZD2171) enhances radiation response and causes substantial physiological changes in lung tumour xenografts, Br. J. Radiol. 81 (special_issue_1) (2008) S21–S27.
[21] R. Schmidt, et al., Combining bevacizumab with radiation or chemoradiation for solid tumors: a review of the scientific rationale, and clinical trials, Curr. Antimicrob. 1 (2) (2012) 169–179.
[22] H.J. Park, et al., Radiation-induced vascular damage in tumors: implications of vascular damage in ablative hypofractionated radiotherapy (SBRT and SRS), Radiat. Res. 177 (3) (2012) 311–327.
[23] S.G. Maher, et al., Serum proteomic profiling reveals that pretreatment complement protein levels are predictive of esophageal cancer patient response to neoadjuvant chemoradiation, Ann. Surg. 254 (5) (2011) 809–816 discussion 816-7.
[24] S.L. Picardo, et al., Barrett's to oesophageal cancer sequence: a model of its inflammatory-driven upper gastrointestinal cancer, Dig. Surg. 29 (3) (2012) 251–260.
[25] S.-C. Lin, et al., Leukemia inhibitory factor promotes nasopharyngeal carcinoma progression and radioresistance, J. Clin. Invest. 123 (12) (2013) 5269–5283.
[26] A.M. Buckley, et al., Leukaemia inhibitory factor is associated with treatment resistance in oesophageal adenocarcinoma, Oncotarget 9 (72) (2018) 33634.
[27] E.V. Efimova, et al., Radioresistance of Bcl1-myc-expressing tumour cells is associated with suppressed apoptotic response to cytotoxic agents and increased IL6-IL8 signalling, Int. J. Radiat. Biol. 85 (5) (2009) 421–431.
[28] Z. Taherzadeh, M. Khazaei, The relationship between inflammatory markers, angiogenesis, and obesity, ARYA Atheroscleosis 9 (4) (2013) 247–253.
[29] A.G. Murphy, et al., Preclinical validation of the small molecule drug quinnih as a novel therapeutic for colorectal cancer, Sci. Rep. 6 (2016) 34523.
[30] A.L. Reynolds, et al., Phenotypic-based discovery of 2-[(E)-2-(Quinolin-2-yl)vinyl] phenol as a novel regulator of ocular angiogenesis, J. Biol. Chem. 291 (14) (2016) 7242–7255.
[31] Y. Alvarez, et al., Selective inhibition of retinal angiogenesis by targeting PI3 kinase, PLoS One 4 (11) (2009) e7907.
[32] C.B. Kimmel, et al., Stages of embryonic development of the zebrafish, Dev. Dynam. 203 (3) (1995) 253–310.
[33] N. Lynam-Lennon, et al., Alterations in DNA repair efficiency are involved in the radioresistance of esophageal adenocarcinoma, Radiat. Res. 174 (6) (2010) 703–711.
[34] C.G. Lee, et al., Anti-Vascular endothelial growth factor treatment augments tumor radiation response under normoxic or hypoxic conditions, Cancer Res. 60 (19) (2000) 5565–5570.
[35] N.A. Franken, et al., Clonogenic assay of cells in vitro, Nat. Protoc. 1 (5) (2006) 2315–2319.
[36] G. Chimote, et al., Comparison of effects of anti-angiogenic agents in the zebrafish efficacy–toxicity model for translational anti-angiogenic drug discovery, Drug Des. Dev. Ther. 8 (2014) 1107–1123.
[37] Y. Gibert, S.L. McGee, A.C. Ward, Metabolic profile analysis of zebrafish embryos, JoVE (71) (2013) e4300.
[38] C.W. Song, et al., Metformin kills and radiosensitizes cancer cells and preferentially kills cancer stem cells, Sci. Rep. 2 (2012) 362.
[39] M. Sessi, et al., Papaverine and its derivatives radiosensitize solid tumors by inhibiting mitochondrial metabolism, Proc. Natl. Acad. Sci. Unit. States Am. 115 (42) (2018) 10756–10761.
[40] K. Goetze, et al., Glycolysis-related gene induction and ATP reduction during fractionated irradiation: Markers for radiation responsiveness of human tumor xenografts, Strahlenther. Onkol. 189 (9) (2013) 782–788.
[41] C.L. Lu, et al., Tumor cells switch to mitochondrial oxidative phosphorylation under radiation via mTOR-mediated hexokinase II inhibition–a Warburg-reversing effect, PLoS One 10 (3) (2015) e0121046.
[42] A. Bartoletti-Stella, et al., Gamma rays induce a p53-independent mitochondrial biogenesis that is counter-regulated by HIF1α, Cell Death Dis. 4 (6) (2013) e663.
[43] A. Viale, et al., Oncogene ablation-resistant pancreatic cancer cells depend on mitochondrial function, Nature 514 (7524) (2014) 628–632.
[44] M.G. Vander Heiden, L.C. Cantley, C.B. Thompson, Understanding the Warburg effect: the metabolic requirements of cell proliferation, Science 324 (5930) (2009) 1029–1033.
[45] S.S. Sabharwal, P.T. Schumacker, Mitochondrial ROS in cancer: initiators, amplifiers or an Achilles' heel? Nat. Rev. Canc. 14 (11) (2014) 709–721.
[46] T. Kausar, et al., Sensitization of pancreatic cancers to gemcitabine chemoradiation by WEE1 kinase inhibition depends on homologous recombination repair, Neoplasia 17 (10) (2015) 757–766.
[47] J.M. Brown, Exploiting the hypoxic cancer cell: mechanisms and therapeutic strategies, Mol. Med. Today 6 (4) (2000) 157–162.
[48] M.W. Dewhirst, Y. Cao, B. Moeller, Cycling hypoxia and free radicals regulate angiogenesis and radiotherapy response, Nat. Rev. Canc. 8 (6) (2008) 425–437.
[49] H. Yasui, et al., Inhibition of HIF-1alpha by the anticancer drug TAS106 enhances X-ray-induced apoptosis in vitro and in vivo, Br. J. Canc. 99 (9) (2008) 1442–1452.
[50] S.L. Doyle, et al., Visceral obesity, metabolic syndrome, insulin resistance and cancer, Proc. Nutr. Soc. 71 (1) (2012) 181–189.
[51] N. Ouchi, et al., Adipokines in inflammation and metabolic disease, Nat. Rev. Immunol. 11 (2) (2011) 85–97.
[52] J. Lysaght, et al., Pro-inflammatory and tumour proliferative properties of excess visceral adipose tissue, Cancer Lett. 312 (1) (2011) 62–72.
[53] Y. Chen, et al., IL-6 signaling promotes DNA repair and prevents apoptosis in CD133+ stem-like cells of lung cancer after radiation, Radiat. Oncol. 10 (2015) 227.
[54] M.F. Chen, et al., Role of interleukin-6 in the radiation response of liver tumors, Int. J. Radiat. Oncol. Biol. Phys. 84 (5) (2012) e621–e630.
[55] C.-T. Wu, et al., The role of IL-6 in the radiation response of prostate cancer, Radiat. Oncol. 8 (2013) 159–159.
[56] Y. Tamori, G. Kashino, H. Mori, Acquisition of radioresistance by IL-6 treatment is caused by suppression of oxidative stress derived from mitochondria after γ-irradiation, J. Radiat. Res. 58 (4) (2017) 412–420.
[57] Y. Masuoka, et al., IL-6 controls resistance to radiation by suppressing oxidative stress via the Nrf2-antioxidant pathway in oral squamous cell carcinoma, Br. J. Canc. 115 (2016) 1234.
[58] C.Y. Peng, et al., Let-7c restores radiosensitivity and chemosensitivity and impairs stemness in oral cancer cells through inhibiting interleukin-8, J. Oral Pathol. Med. 47 (6) (2018) 590–597.
[59] O.M. Rahal, et al., Blocking interleukin (IL) 4- and IL13-mediated phosphorylation of STAT6 (Tyr641) decreases M2 polarization of macrophages and protects against macrophage-mediated radioresistance of inflammatory breast cancer, Int. J. Radiat. Oncol. Biol. Phys. 100 (4) (2018) 1034–1043.

pharmaceuticals

MDPI

Article

Characterisation of an Isogenic Model of Cisplatin Resistance in Oesophageal Adenocarcinoma Cells

Amy M. Buckley [1], Becky AS. Bibby [2], Margaret R. Dunne [1], Susan A. Kennedy [1], Maria B. Davern [1], Breandán N. Kennedy [3], Stephen G. Maher [1,†] and Jacintha O'Sullivan [1,*,†]

[1] Department of Surgery, Trinity Translational Medicine Institute, St. James's Hospital, Trinity College Dublin, Dublin 8, Ireland; bucklea6@tcd.ie (A.M.B.); margaret.a.dunne@gmail.com (M.R.D.); KENNE521@tcd.ie (S.A.K.); DAVERNMA@tcd.ie (M.B.D.); MAHERST@tcd.ie (S.G.M.)

[2] Translational Radiobiology Group, Division of Cancer Sciences, University of Manchester, Manchester Academic Health Science Centre, Christie Hospital, Manchester M20 4BX, UK; becky.bibby@manchester.ac.uk

[3] UCD Conway Institute & UCD School of Biomolecular and Biomedical Science, University College Dublin, Dublin 4, Ireland; brendan.kennedy@ucd.ie

* Correspondence: osullij4@tcd.ie

† These authors contributed equally to this work.

Received: 19 December 2018; Accepted: 15 February 2019; Published: 20 February 2019

Abstract: Cisplatin (cis-diamminedichloroplatinum) is widely used for the treatment of solid malignancies; however, the development of chemoresistance hinders the success of this chemotherapeutic in the clinic. This study provides novel insights into the molecular and phenotypic changes in an isogenic oesophageal adenocarcinoma (OAC) model of acquired cisplatin resistance. Key differences that could be targeted to overcome cisplatin resistance are highlighted. We characterise the differences in treatment sensitivity, gene expression, inflammatory protein secretions, and metabolic rate in an isogenic cell culture model of acquired cisplatin resistance in OAC. Cisplatin-resistant cells (OE33 Cis R) were significantly more sensitive to other cytotoxic modalities, such as 2 Gy radiation ($p = 0.0055$) and 5-fluorouracil (5-FU) ($p = 0.0032$) treatment than parental cisplatin-sensitive cells (OE33 Cis P). Gene expression profiling identified differences at the gene level between cisplatin-sensitive and cisplatin-resistant cells, uncovering 692 genes that were significantly altered between OE33 Cis R cells and OE33 Cis P cells. OAC is an inflammatory-driven cancer, and inflammatory secretome profiling identified 18 proteins secreted at significantly altered levels in OE33 Cis R cells compared to OE33 Cis P cells. IL-7 was the only cytokine to be secreted at a significantly higher levels from OE33 Cis R cells compared to OE33 Cis P cells. Additionally, we profiled the metabolic phenotype of OE33 Cis P and OE33 Cis R cells under normoxic and hypoxic conditions. The oxygen consumption rate, as a measure of oxidative phosphorylation, is significantly higher in OE33 Cis R cells under normoxic conditions. In contrast, under hypoxic conditions of 0.5% O_2, the oxygen consumption rate is significantly lower in OE33 Cis R cells than OE33 Cis P cells. This study provides novel insights into the molecular and phenotypic changes in an isogenic OAC model of acquired cisplatin resistance, and highlights therapeutic targets to overcome cisplatin resistance in OAC.

Keywords: oesophageal cancer; treatment resistance; cisplatin; metabolism; inflammation; radiation

1. Introduction

Oesophageal cancer is the sixth most common cause of cancer-related mortality globally, and unfortunately, the five-year survival rates remain low at <20% [1,2]. Oesophageal cancer consists of two different histological subtypes: oesophageal squamous cell carcinoma (OSCC) and oesophageal

adenocarcinoma (OAC) [1]. In recent years, the epidemiology of oesophageal cancer dramatically shifted, wherein OAC is now the most prevalent subtype in the Western world [3]. The increasing OAC incidence in Western countries has paralleled the increasing rates of obesity, which is a known risk factor for OAC [4].

The current standard treatment of care for oesophageal cancer focusses on neoadjuvant treatment with chemotherapy alone (neoCT) or in combination with radiation, and neoadjuvant chemoradiation (neoCRT) for locally advanced tumours prior to surgery [5]. Despite the improvements demonstrated with neoadjuvant treatment versus surgery alone, only ~30% of patients achieve a complete pathological response to neoadjuvant treatment, which is a proxy for improved overall survival [6]. Surgery offers the best chance of locoregional control, and neoadjuvant treatment aims to reduce tumour burden prior to surgery to improve post-operative outcome. Thus, it is critical to improve response rates to neoadjuvant therapy to increase patient survival [5,7,8]. Treatment resistance is a major cause of treatment failure, and it is crucial to understand the molecular mechanisms and markers governing the treatment resistance phenotype.

Cisplatin is a platinum-based chemotherapy that is used to treat a wide number of solid cancers [9]. Cisplatin is administered as part of a neoadjuvant chemotherapy regimen, and is referred to as MAGIC for the treatment of OAC [10]. The MAGIC chemotherapy protocol consists of the administration of epirubicin, cisplatin, and 5-fluorouracil pre-operatively and post-operatively [11,12]. One mechanism by which cisplatin exerts its anti-cancer effect is through the generation of DNA lesions, resulting in the activation of the DNA damage response and the subsequent induction of mitochondrial-mediated apoptosis [9]. Initial responses to cisplatin are often quite promising; however, chemoresistance to cisplatin frequently develops, leading to treatment failure, and a poor response to neoadjuvant treatment is associated with poor outcome. Thus, it is critical to understand the molecular mechanisms governing resistance to cisplatin in OAC. Our first findings investigate cross-resistance and sensitivity to other cytotoxic treatments, including radiation and 5-fluorouracil (5-FU).

OAC is an inflammatory-driven upper gastrointestinal malignancy, and previous studies have reported on the role of inflammation as a negative regulator of response to radiation treatment in OAC [4,13]. Inflammation is linked with cisplatin resistance, and Cui et al. demonstrated that interleukin-7 (IL-7) upregulation was associated with cisplatin resistance in glioma cells [14]. Targeting IL-7 improved cisplatin sensitivity [14]. In the present study, we identify changes in the inflammatory secretome in an isogenic OAC model of cisplatin resistance to increase our understanding of inflammation in cisplatin resistance. Inflammation is also tightly linked to metabolism, as inflammatory cells rely on metabolites generated from the metabolic cycle to maintain their function [15]. Tumours rely on metabolism to fuel their growth, and altered energy metabolism is an emerging hallmark of cancer [16]. Metabolic alterations correlate with treatment resistance in OAC, wherein increased oxygen consumption is linked with a radioresistant phenotype in an isogenic model of OAC radioresistance [17,18]. Furthermore, in a lung cancer model, cisplatin-resistant cells have significantly elevated oxygen consumption rates compared to parental cisplatin-sensitive cells [19]. This paradigm has not yet been explored in a cisplatin-resistant model of OAC.

In this study, we examined the key differences in chemosensitivity, radiosensitivity, gene expression, inflammatory secretions, and metabolism between matched OAC cisplatin-sensitive (OE33 Cis P) cells and OAC cisplatin-resistant (OE33 Cis R) cells. Cisplatin-resistant cells are more sensitive to radiation and 5-FU treatment than cisplatin-sensitive cells. Cisplatin resistance was associated with a number of significant changes in gene expression, where KEGG pathway analysis identified four pathways upregulated in chemoresistant OE33 Cis R cells, including pathways in cancer, tumour growth factor (TGF)-beta signalling, Wnt signalling, and steroid biosynthesis. Eighteen proteins were secreted at significantly altered levels in OE33 Cis R cells compared to OE33 Cis P, with IL-7 secretion at a significantly higher level from chemoresistant OE33 Cis R cells compared with OE33 Cis P cells. Metabolic profiling revealed that the oxygen consumption rate, as a measure of oxidative phosphorylation, was significantly higher in OE33 Cis R cells under normoxic conditions ($p = 0.0040$).

In contrast, under hypoxic conditions, the oxygen consumption rate was significantly lower in OE33 Cis R cells than in OE33 Cis P cells ($p = 0.0078$). This study highlights molecular and phenotypical changes in an isogenic OAC model of acquired cisplatin resistance, and highlights key differences that could be therapeutically targeted to overcome cisplatin resistance in OAC.

2. Results

2.1. OE33 Cis R Cells Are More Sensitive to Radiation and 5-Fluorouracil (5-FU) Treatment

The relative cisplatin sensitivity of the parental cell line, OE33 Cis P, and the age and passage-matched cisplatin resistant subclone, OE33 Cis R, was evaluated by clonogenic assay. The treatment of cisplatin-sensitive OAC cells with the IC_{50} of cisplatin was previously determined in CCK8 assay (Figure 1); 1.3 µM of cisplatin significantly reduced the surviving fraction of OE33 Cis P cells to 0.303 compared to untreated OE33 Cis P cells, $p = 0.0108$ (Figure 2A). However, 1.3 µM of cisplatin did not significantly alter the surviving fraction of OE33 Cis R cells (0.944 ± 0.042 compared to untreated OE33 Cis R cells), which in itself was significantly higher than the surviving fraction of the OE33 Cis P cells treated with 1.3 µM of cisplatin, $p = 0.0011$ (Figure 2A). A ~two-fold higher concentration, 2.8 µM of cisplatin, significantly reduced the surviving fraction of OE33 Cis R cells to 0.604 ± 0.045, which was a reduction of −39%, $p = 0.0043$ (Figure 2A). Notably, OE33 Cis P cells were not clonogenically viable with 2.8 µM of cisplatin. To investigate whether OE33 cells with acquired cisplatin resistance had altered sensitivity to other treatments, we investigated the response to both clinically relevant doses of radiation and 5-FU. The basal cell survival and radiosensitivity of cisplatin-sensitive OE33 Cis P cells and cisplatin-resistant OE33 Cis R OAC cells were assessed by clonogenic assay. Basal cell survival was assessed in OE33 Cis P and OE33 Cis R to determine if in the absence of any irradiation, there was a difference in surviving fraction. No significant difference was observed between the two cell lines under basal conditions, indicating that there is no longer-term proliferation differences between these cell lines, which might correlate with the altered radiosensitivity phenotypes (Figure 2B). To assess whether acquired cisplatin resistance conferred altered radiosensitivity, OE33 Cis P and OE33 Cis R cells were either mock-irradiated or treated with a single dose of 2 Gy X-ray radiation. Interestingly, OE33 Cis R cells were significantly more radiosensitive than OE33 Cis P cells, $p = 0.0055$ (Figure 2C). Similarly, OE33 Cis R cells were significantly more sensitive to 5-FU compared to the OE33 Cis P cells following 72 h of 5-FU treatment, $p = 0.0032$ (Figure 2D). In summary, OE33 Cis R cells were more radiosensitive and 5-FU chemosensitive when compared to the parental OE33 Cis P cells.

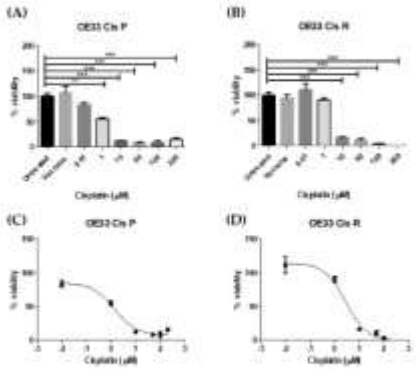

Figure 1. Oesophageal adenocarcinoma (OAC) cisplatin-sensitive (OE33 Cis P) cells were significantly more sensitive to cisplatin-induced cell death than OAC cisplatin-resistant (OE33 Cis R) cells. The toxicity to a range of increasing concentrations of cisplatin in (**A**) OE33 Cis P and (**B**) OE33 Cis R cells following 48 h of treatment was determined using a CCK-8 assay. The 48-h IC_{50} for (**C**) OE33 Cis P cells and (D) OE33 Cis R cells was 1.3 μM and 2.8 μM, respectively (n = 3). ** $p < 0.01$, *** $p < 0.001$ by an unpaired two-tailed *t*-test.

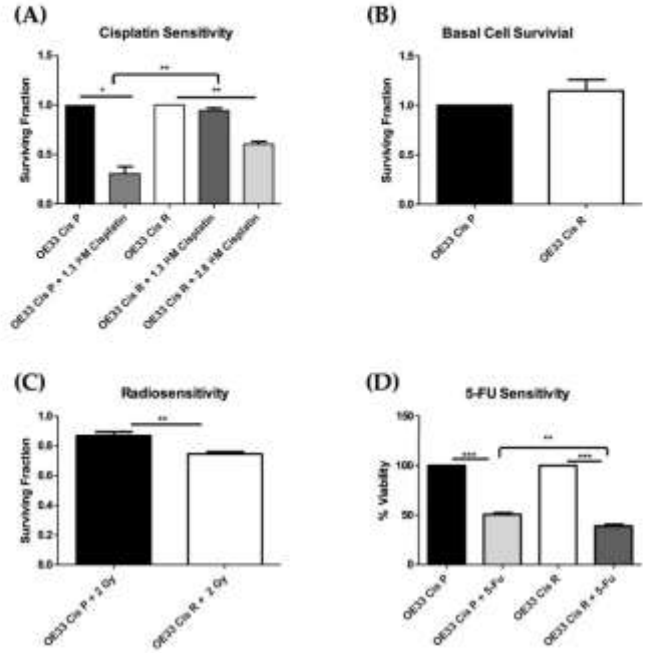

Figure 2. Cisplatin-resistant (OE33 Cis R) oesophageal adenocarcinoma cells are more radiosensitive than cisplatin-sensitive (OE33 Cis P) oesophageal adenocarcinoma (OAC) cells. (**A**) The sensitivity of cisplatin-sensitive (OE33 Cis P) and cisplatin-resistant (OE33 Cis R) OAC cells to cisplatin was assessed by clonogenic assay (n = 3). (**B**) There is no difference in the basal cell surviving fraction of cisplatin-sensitive and cisplatin-resistant OAC cells cultured in RPMI media, (n = 3). (**C**) Surviving fraction of Cis P and Cis R OAC cells following treatment of one 2 Gy fraction of irradiation, (n = 3). (**D**) The viability of the OE33 Cis R cells was significantly decreased compared to the OE33 Cis P when treated with 12 μM of 5-fluorouracil (5-FU) (n = 4). An unpaired *t*-test was used to compare between different cell lines, and a paired *t*-test was used to compare between the same cell line. Data presented as ±SEM * $p < 0.05$, ** $p < 0.01$, *** $p < 0.0001$.

2.2. Gene Expression Is Significantly Altered in OE33 Cis R Cells

OE33 Cis R cells have increased ALDH1 activity, which is a marker of stemness, compared to OE33 Cis P cells [20]. Thus, we investigated whether acquired cisplatin resistance was associated with significant changes in gene expression by whole genome digital gene expression analysis. Of the ~25,000 genes detected, 692 genes were significantly altered, 278 were upregulated, and 414 were downregulated between OE33 Cis P and OE33 Cis R cell lines. Applying a threshold of ±twofold change expression, 42 genes were upregulated (Figure 3A), and 104 genes were downregulated (Figure 3B) in the OE33 Cis R cell line compared to the OE33 Cis P cell line. Kyoto Encyclopedia of Genes and Genomes (KEGG) pathway analysis identified four pathways that were significantly upregulated in OE33 Cis R cells based on the gene expression findings, including: pathways in cancer, TGF-beta signalling, Wnt signalling, and steroid biosynthesis (Table 1A). Furthermore, eight KEGG pathways were downregulated in OE33 Cis R cells, including the MAPK signalling pathway, complement and coagulation cascades, RIG-I-like receptor signalling, sulfur metabolism, NOD-like receptor signalling, cell adhesion molecules, B cell receptor signalling, and Notch signalling (Table 1B).

In summary, OE33 Cis R cells with acquired cisplatin resistance have a significantly altered gene expression profile compared to matched cisplatin sensitive OE33 Cis P cells.

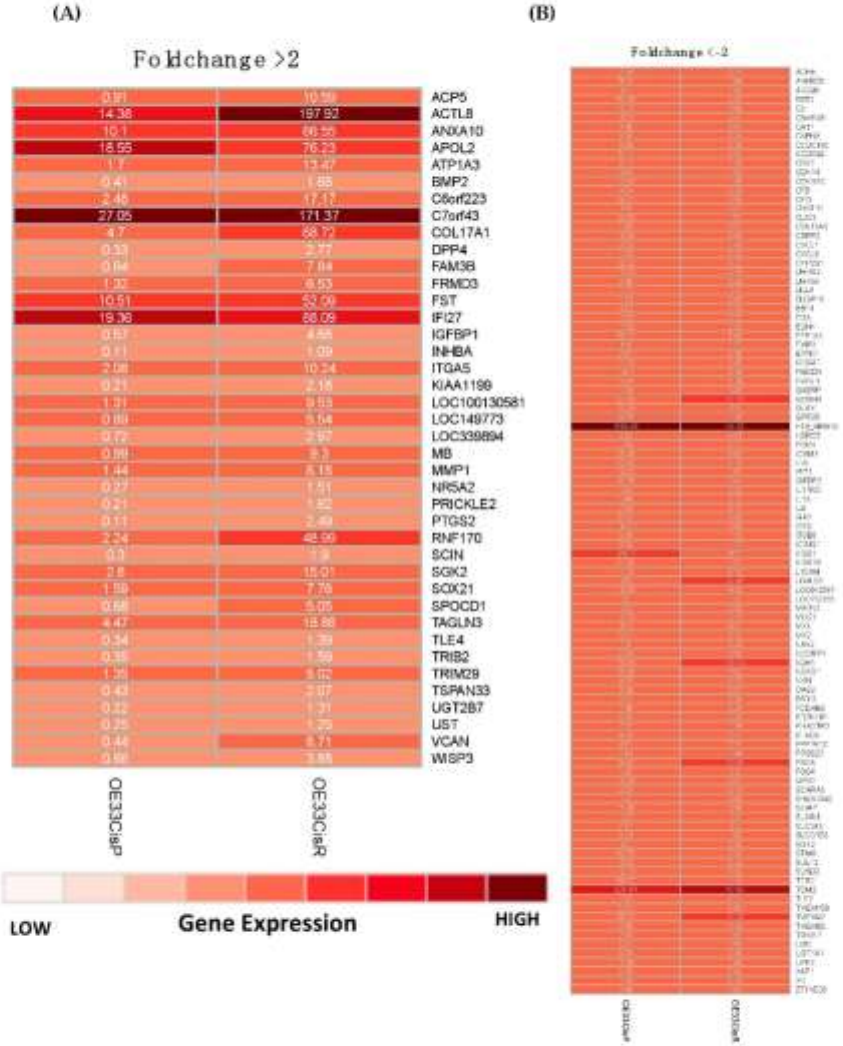

Figure 3. OE33 Cis R cells have a significantly altered gene expression profile compared to OE33 Cis P cells. Heatmaps were generated from gene expression data after applying a fold change filter ±two. (**A**) Heatmap showing 42 genes that were significantly upregulated in OE33 Cis R cells with a fold change of greater than two. (**B**) Heatmap showing 104 genes which were significantly downregulated in OE33 Cis R cells with a fold change of less than minus two. Gene expression values shown as Fragments Per Kilobase of transcript per Million mapped reads (FKPM).

Table 1. Kyoto Encyclopaedia of Genes and Genomes (KEGG) pathway analysis identifies significant pathway differences in OE33 Cis P versus OE33 Cis R cells. (**A**) KEGG pathway analysis of gene expression data identified four pathways that were significantly upregulated in OE33 Cis R cells compared to OE33 Cis P cells. (**B**) KEGG pathway analysis of gene expression data identified eight pathways that were significantly downregulated in OE33 Cis R cells compared to OE33 Cis P cells.

(**A**)

KEGG Pathway Term	Number of Identified Genes Involved	*p* Value	Gene Names
hsa05200:Pathways in cancer	13	5.29×10^{-3}	BMP4, PPARD, BMP2, BCR, PTGS2, EPAS1, PIK3CB, FOXO1, KITLG, MLH1, MMP1, RAC2, WNT9A
hsa04350:TGF-beta signalling pathway	6	1.21×10^{-2}	BMP4, INHBA, BMP2, ID2, ID1, FST
hsa00100:Steroid biosynthesis	3	2.92×10^{-2}	CYP27B1, LIPA, DHCR24
hsa04310:Wnt signalling pathway	6	9.19×10^{-2}	SENP2, PPARD, RAC2, PRICKLE2, FRAT2, WNT9A

(**B**)

KEGG Pathway Term	Number of Identified Genes Involved	*p* Value	Gene Names
hsa04010:MAPK signaling pathway	17	2.61×10^{-4}	FGFR3, PDGFA, RELB, CACNG6, CACNG4, NR4A1, STK3, JMJD7-PLA2G4B, RASGRP3, DUSP14, JMJD7, DUSP16, RRAS, HSPB1, TRAF6, GADD45B, PLA2G4B, IL1A, DUSP6
hsa04610:Complement and coagulation cascades	7	4.23×10^{-3}	PLAT, C3, CFB, SERPINA1, CFD, F2R, PLAUR
hsa04622:RIG-I-like receptor signaling pathway	6	2.09×10^{-2}	IFIH1, ISG15, IL8, IRF7, TRAF6, DHX58
hsa00920:Sulfur metabolism	3	2.84×10^{-2}	CHST11, CHST13, SULT2B1
hsa04621:NOD-like receptor signaling pathway	5	4.95×10^{-2}	CXCL1, IL8, IL18, TRAF6, BIRC3
hsa04514:Cell adhesion molecules (CAMs)	7	7.50×10^{-2}	ICAM1, CLDN9, CLDN3, ITGB8, PVRL2, CD22, L1CAM
hsa04662:B cell receptor signaling pathway	5	8.68×10^{-2}	RASGRP3, CD22, PIK3AP1, MALT1, VAV1
hsa04330:Notch signaling pathway	4	8.75×10^{-2}	HES5, DTX2, DLL4, RBPJ

2.3. Acquisition of Cisplatin Resistance Results in an Alerted Inflammatory Secretome

OAC is an inflammatory-driven upper gastrointestinal cancer, and previous studies have reported inflammation as a negative regulator of response to radiation treatment in OAC [13,21]. However, a link between inflammation and cisplatin resistance in OAC has not yet been investigated. To determine if cisplatin-resistant OE33 Cis R cells have an altered inflammatory secretome to cisplatin-sensitive OE33 Cis P OAC cells, a 47-analyte multiplex enzyme linked immunosorbent assay (ELISA) was conducted. Twenty-three proteins of 47 analytes were detected in either one or both cell lines. IL-7 was secreted at significantly higher levels from OE33 Cis R cells, $p = 0.0191$ (Figure 4A). Seventeen proteins were secreted at significantly lower levels from OE33 Cis R cells compared OE33 Cis P cells, including C-reactive protein (CRP), IL-12p70, IL-10, TNFα, macrophage-derived chemokine (MDC), intracellular adhesion molecule 1 (ICAM-1), IL-6, IL-1β, IL-13, serum amyloid A (SAA), TARC, IL-4, IL-8, IL-1RA, IL-1α, IL-2, and IP-10, as shown in Figure 4 ($p < 0.05$). There was no significant difference in the secreted levels of five of the 23 proteins detected; MCP-1, VEGF-A, VCAM, GM-CSF, and IL-15 between the cell lines (Supplemental Figure S1). OE33 Cis R cells have an altered inflammatory secretome compared to cisplatin-sensitive OE33 Cis P cells, where OE33 Cis R cells have reduced levels of a number of

inflammatory chemokines and cytokines and vascular injury proteins except for IL-7, which is secreted at significantly higher levels from OE33 Cis R OAC cells.

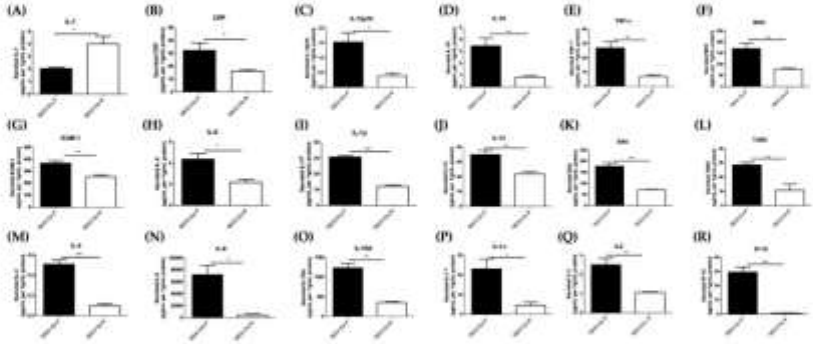

Figure 4. Inflammatory protein secretions are significantly different in cisplatin-sensitive (OE33 Cis P) versus cisplatin-resistant (OE33 Cis R) OAC cells. The secreted levels of 47 proteins in Cis P and Cis R cells was evaluated by multiplex ELISA; 23 proteins were detected in supernatant of Cis P and Cis R cells; 18 proteins were significantly different between the two cell lines, and interleukin-7 was significantly higher in Cis R cells compared to Cis P cells. Secreted levels of (**A**) Interleukin-7 (IL-7) (**B**) C-reactive protein (CRP) (**C**) Interleukin 12p70 (IL-12p70) (**D**) Interleukin 10 (IL-10) (**E**) Tumour necrosis factor α (TNF-α) (**F**) Macrophage-derived chemokine (MDC) (**G**) Intracellular adhesion molecule 1 (ICAM-1) (**H**) Interleukin 6 (IL-6) (**I**) Interleukin 1β (IL-1β) (**J**) Interleukin 13 (IL-13) (**K**) Serum amyloid A (SAA) (**L**) Thymus and activation regulated chemokine (TARC) (**M**) Interleukin 4 (IL-4) (**N**) Interleukin 8 (IL-8) (**O**) Interleukin 1 receptor antagonist (IL-1RA) (**P**) Interleukin 1α (IL-1α) (**Q**) Interleukin 2 (IL-2) (**R**) Interferon gamma-induced protein 10 (IP-10) in OE33 Cis P and OE33 Cis R cells, all secretions normalised to protein content. (n = 4). Unpaired *t*-test. * $p < 0.05$, ** $p < 0.01$, *** $p < 0.001$. Date expressed as ±SEM.

We also compared our findings from our gene expression study (Figure 3) to our inflammatory secretome data described in this section to determine if there was any overlap between the two datasets. In both our gene expression data (Figure 3B) and inflammatory secretome dataset (Figure 4G, 4N, 4P) ICAM-1, IL-8, and IL-1α were both expressed and secreted at significantly lower levels from OE33 Cis R cells compared to OE33 Cis P cells (Table 2).

Table 2. Differences in gene expression and protein secretion values of ICAM-1, IL-8, and IL-1α in OE33 Cis P and OE33 Cis R cells. This table shows the mean values of data that were used to calculate the significant differences in gene expression and protein secretions previously illustrated in Figures 3B and 4G, 4N, 4P. Fragments Per Kilobase of transcript per Million mapped reads (FKPM).

Protein	OE33 Cis P Mean Gene Expression (FPKM)	OE33 Cis R Mean Gene Expression (FPKM)	OE33 Cis P Mean Protein Secretion (pg/mL per µg/mL Protein)	OE33 Cis R Mean Protein Secretion (pg/mL per µg/mL Protein)
ICAM-1	25.26	6.08	365.64	254.39
IL-8	7.68	0.73	71822.10	4611.60
IL-1$^{\alpha}$	1.49	0.27	23.10	4.56

2.4. OE33 Cis R Cells Have an Altered Metabolic Phenotype Compared to the Parental OE33 Cis P Cells

Altered mitochondrial function is linked with treatment resistance in OAC; thus, we wanted to investigate the association between cisplatin resistance and metabolism in our model of OAC-acquired

cisplatin resistance [17]. To investigate whether cisplatin-resistant OE33 Cis R cells have altered energy metabolism, we measured the two major energy pathway—oxidative phosphorylation and glycolysis—using the Seahorse XFe24 analyser under normoxic and hypoxic conditions. OE33 Cis R cells have a significantly higher ($p = 0.0040$) oxygen consumption rate (OCR), which is a measure of oxidative phosphorylation compared to OE33 Cis P cells, under normoxia. However, the oxygen consumption rate of OE33 Cis R cells was significantly lower than OE33 Cis P cells under low oxygen conditions (0.5% O_2), $p = 0.0078$, (Figure 5A). There was no significant difference in the extracellular acidification rate (ECAR), which is a measure of glycolysis, between the two cell lines under normoxic or hypoxic conditions (Figure 5B). To further investigate changes in cellular energetics both OE33 Cis P and OE33 Cis R cells were treated with oligomycin (a mitochondrial complex V inhibitor and antimycin A (a mitochondrial complex III inhibitor), which inhibit specific processes in the electron transport chain. Oligomycin and antimycin produced a similar level of OCR inhibition in both OE33 Cis P and OE33 Cis R cells, and there was no significant difference in the rate of ATP production or proton leak between cisplatin-sensitive and cisplatin-resistant cells under normoxic or hypoxic conditions (Figure 5C,D). Furthermore, treatment of OE33 Cis P and OE33 Cis R cells with the uncoupling agent carbonyl cyanide-*p*-trifluoromethoxyphenylhydrazone (FCCP) showed no significant difference in maximal respiration rate between the cell lines (Figure 5E). In addition, the rate of non-mitochondrial respiration was not significantly altered between the two cell lines (Figure 5F). In summary, OE33 Cis R cells have an alerted metabolic phenotype whereby they have a significantly elevated OCR compared to parental OE33 Cis P cells under normoxic conditions, and OE33 Cis R cells have significantly lower OCR under hypoxic conditions.

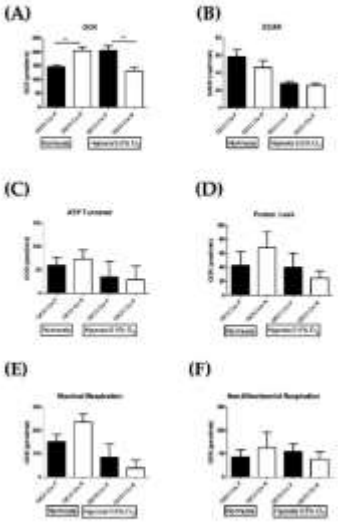

Figure 5. Cisplatin-resistant (OE33 Cis R) oesophageal adenocarcinoma cells have an altered metabolic phenotype compared to cisplatin-sensitive (OE33 Cis P) cells under normoxic and hypoxic conditions (0.5% O_2). (**A**) The oxygen consumption rate (OCR), which is a measure of oxidative phosphorylation, was evaluated in OE33 Cis P and OE33 Cis R OAC cells using the Seahorse Biosciences XFe24 extracellular flux analyser cultured under normoxic and hypoxic conditions (0.5% O_2). OE33 Cis R cells have a significantly higher OCR when compared to OE33 Cis P; cisplatin-sensitive cells, under normoxic conditions (n = 5), unpaired *t*-test, ** $p < 0.01$. (**B**) The extracellular acidification rate (ECAR), which is a measure glycolysis, was evaluated in OE33 Cis P and OE33 Cis R cells using the Seahorse Biosciences XFe24 extracellular flux analyser cultured under normoxic and hypoxic conditions (0.5% O_2), (n = 5), unpaired *t*-test. (**C**) Difference in the rate of ATP production in OE33 Cis P and OE33 Cis R cells cultured under normoxic and hypoxic conditions (0.5% O_2), (n = 5), unpaired *t*-test. (**D**) Difference in the rate of proton leak in OE33 Cis P and OE33 Cis R cells cultured under normoxic and hypoxic conditions (0.5% O_2), (n = 5), unpaired *t*-test. (**E**) Difference in maximal respiration rate in OE33 Cis P and OE33 Cis R cells cultured under normoxic and hypoxic conditions (0.5% O_2), (n = 5), unpaired *t*-test. (**F**) Difference in non-mitochondrial respiration in OE33 Cis P and OE33 Cis R cells cultured under normoxic and hypoxic conditions (0.5% O_2), (n = 5), unpaired *t*-test. Data presented as ±SEM.

3. Discussion

Cisplatin is a widely use chemotherapeutic drug for the treatment of solid cancers, including OAC; however, the development of chemoresistance to cisplatin hinders the success of this agent [9]. Previous studies in cisplatin-resistant cancer cell lines of various tissue origin report multiple mechanisms responsible for enhanced resistance, and that the cisplatin-resistant phenotype is the result of multiple microRNA, gene, and protein expression changes [22–24]. Molecular mechanisms commonly associated with cisplatin resistance include alterations in DNA repair, drug influx/efflux, drug detoxification, cell cycle dysregulation, and evasion of apoptosis [25]. In this study, we sought to characterise the key differences linked to resistance in an isogenic model of OAC cisplatin resistance, including relative chemosensitivity and radiosensitivity, whole gene expression, inflammatory protein secretions, and metabolic phenotype.

Chemoresistant OE33 Cis R cells have a significant acquired resistance to cisplatin compared to cisplatin-sensitive OE33 Cis P cells. Interestingly, cisplatin-resistant OE33 Cis R cells are more

radiosensitive than matched OE33 Cis P cells. Cisplatin is often administered in combination with radiation for the treatment of numerous solid cancers, including oesophageal, head, neck, and cervical cancer [26–29]. Cisplatin has been widely shown to enhance radiosensitivity, which is potentially through the non-homologous end joining (NHEJ) DNA repair pathway [30,31]. As cisplatin is often given in combination with radiation to improve response, it was surprising that OE33 Cis R cells are more radiosensitive than OE33 Cis P cells. OE33 Cis R cells can overcome cytotoxic insult from cisplatin to a greater degree than OE33 Cis P cells, but cannot overcome radiation-induced DNA damage as efficiently as they could before the acquisition of cisplatin resistance. Whilst it was unexpected that OE33 Cis R cells are more radiosensitive, as DNA is the common target of both cisplatin and radiation, the mechanisms of action in yielding lethal events, delivery methods, and repair systems as a result of both treatments are very different. Cisplatin has to cross the plasma membrane and traffic to the nucleus; this is a process during which it can be affected in several ways, such as influx via CTR1, efflux via ABC transporters, detoxification by glutathione, trapping in lysosomes, altered trafficking between the plasma membrane and the nucleus, as well as DNA repair proficiency [32,33]. Radiation, on the other hand, largely influences DNA damage through water radiolysis (70%), and has direct effects on DNA bases (30%), but is also subject to energy transfer, glutathione scavenging, oxygen fixation, and DNA repair proficiency [34]. Radiation is responsible for the induction of double-strand breaks in DNA, whereas cisplatin treatment results in the formation of DNA adducts as a result of covalent bonds [31]. Additionally, cisplatin largely employs homologous recombination and nucleotide excision repair as its major pathways of repair, while radiation employs non-homologous end joining, base excision repair, single-strand break repair and, to a much lesser extent, homologous recombination. Thus, the DNA repair mechanics that were employed by cancer cells following either radiation or cisplatin treatment are quite different, and the significance of DNA repair in potentially driving this phenotype requires further mechanistic investigation in the future. Furthermore, OE33 Cis R cells were found to be more sensitive to 5-FU treatment compared to OE33 Cis P cells. A previous study established cisplatin-resistant and 5-FU-resistant OAC OE19 cell lines [35]. Interestingly, miRNA expression profiling in the OE19 cisplatin-resistant cell line and the OE19 5-FU-resistant cell line identified a large number of miRNA that were significantly differentially expressed in comparison to the relatively chemosensitive controls [23,31]. In the OE19 cisplatin-resistant cells 18 miRNAs were significantly dysregulated compared to controls (13 downregulated, five upregulated), of which 11 were validated including: miR-455-3p, miR-200b-3p, let-7e-5p, miR-181b-5p, miR-125a-5p, miR-181a-5p, miR-200b-5p, miR-31-5p, miR-200a-3p, miR-638, and miR-191-5p. Interestingly, the miRNA expression profile of the cisplatin-resistant cell line differed from the miRNA expression profile of the 5-FU-resistant cell line [23,31]. The differential miRNA expression profiles may be associated with the different mechanisms by which cisplatin and 5-FU induce cytotoxic damage.

The gene expression data that were presented in this study provide indications as to the potential mechanisms associated with enhanced resistance to cisplatin in the OE33 Cis R cells compared to the OE33 Cis P cells. Cell membrane transporter genes *ATP1A3*, *ABCA12*, *TMEM199*, and *TMEM22* were upregulated in the OE33 Cis R, and *TMEM156* and *TMEM42* were downregulated. The existing literature is limited with regards to these genes; however, they are members of cell membrane transporter families, some of which are associated with transport and the cellular accumulation of cisplatin, such as ATP7A/B and TMEM205 [25]. Upregulated Wnt signalling and the EMT pathway are also associated with cisplatin resistance [36,37]. The upregulation of the *PRICKLE2* gene may contribute to an increase in Wnt signalling in the OE33 Cis R cell line [38]. The *CDKN1C* gene produces the cyclin-dependent kinase inhibitor p57, which functions as a tumour suppressor in multiple cancer types [39]. Furthermore, the overexpression of p57 has been shown to enhance cisplatin sensitivity in-vitro via intrinsic mitochondrial apoptosis [40]. The downregulation of the *CDKN1C* gene in the OE33 Cis R cell line may contribute to the evasion of apoptosis and cellular resistance to cisplatin. Interestingly, TGF-β signalling, which was identified by KEGG pathway analysis to be upregulated in OE33 Cis R cells, has previously been linked to cisplatin resistance in nasopharyngeal and head and

neck cancer; it would be of interest in the future to further understand the role Of TGF-β signalling in cisplatin resistance in OAC [41,42].

KEGG pathway analysis also revealed that the complement pathway was downregulated in cisplatin-resistant cells; this was an interesting finding, as levels of complement C3a and C4a of the classically activated pathway have previously been shown to be predictive of response to neoadjuvant chemoradiation therapy in OAC [13]. Considering this, we sought to investigate the larger inflammatory secretome of OAC cisplatin-resistant OE33 Cis R cells compared to that of cisplatin-sensitive OE33 Cis P cells. OAC is an inflammatory-driven cancer; thus, it is vital to understand the potential contributions of inflammatory secretions to cisplatin resistance. OE33 Cis R cells have a significantly altered inflammatory profile; only one protein, IL-7, was secreted at higher levels from OE33 Cis R cells. Whereas, 17 proteins (CRP, IL-12p70, IL-10, TNFα, MDC, ICAM-1, IL-6, IL-1β, IL-13, SAA, TARC, IL-4, IL-8, IL-1RA, IL-1α, IL-2, and IP-10) were secreted at significantly lower levels from in OE33 Cis R cells compared OE33 Cis P cells. Three of the proteins detected—ICAM-1, IL-1α and IL-8—were also found to be altered at the gene level, where they were both expressed and secreted at significantly lower levels from OE33 Cis R cells compared with OE33 Cis P cells. In a human glioma cancer model, the expression of IL-7 was positively correlated with the IC_{50} of cisplatin in both cell lines and glioma patient samples, and the overexpression of IL-7 further increased cisplatin resistance in glioma cancer cells [14]. This study supports our findings and further highlights IL-7 as a potential mediator of cisplatin resistance in OAC. IL-7 may be a useful therapeutic target for enhancing cisplatin sensitivity in OAC, and this warrants further investigation in the future.

Interleukin-1 alpha (IL-1α) is a potent inflammatory cytokine that plays a pivotal role in the inflammatory response [43]. IL-1α was both expressed and secreted at significantly lower levels from OE33 Cis R cells when compared to OE33 Cis P cells. Interestingly, IL-1α has previously been shown to play a key role in cisplatin sensitivity in human ovarian cancer cells, whereby IL-1α was shown to enhance sensitivity to cisplatin [44]. IL-1α given in combination with cisplatin was shown to enhance the anti-proliferative effect of cisplatin, increase cisplatin uptake, and increase DNA-platination in human ovarian OVCAR-3 cells [44]. Given that we have shown IL-1α to be expressed and secreted at a lower level in cisplatin resistant cells, it would be of interest to evaluate the potential chemosensitising effect of combining IL-1α with cisplatin in OE33 Cis R cells.

Similarly, intracellular adhesion molecule-1 (ICAM-1) was found to be both expressed and secreted at significantly lower levels from OE33 Cis R cells compared to cisplatin-sensitive OE33 Cis P cells. The role of ICAM-1 in carcinogenesis and drug resistance is often dependent on the cancer and cell type. ICAM-1 has previously been shown to have anti-cancer activity in numerous studies through its recruitment of immune cells to the tumour [45–47]. Furthermore, cisplatin treatment has been shown to induce ICAM-1 expression in cancer cells; thus, it is not surprising that ICAM-1 is found at lower levels in the cisplatin-resistant cells compared to the OAC cisplatin-sensitive cells [48]. On the other hand, in an oesophageal SCC cancer study, ICAM-1 was reported to enhance cisplatin resistance and tumourigenicity in-vivo. However, it is important to note that this study was carried out in immunodeficient mice [49]. Thus, the potential of targeting ICAM-1 to alter cisplatin sensitivity in OAC needs further exploration, as it has direct effects on numerous cell types, including both cancer and endothelial cells, and is reliant on interactions with the tumour microenvironment.

Inflammation and metabolism are tightly interlinked biological processes whereby inflammatory cells rely on metabolites generated from the metabolic cycle to maintain their function. Given the significant differences in inflammatory protein secretions from OE33 Cis R cells compared to OE33 Cis P cells, we sought to investigate the metabolic profile of our model of acquired cisplatin resistance. Cisplatin-resistant OE33 Cis R cells have an altered metabolic phenotype compared to matched OE33 Cis P cisplatin-sensitive cells. OE33 Cis R cells have an ~40% higher rate of oxygen consumption rate than OAC cisplatin-sensitive cells. Interestingly, a previous study by Lynam-Lennon et al. demonstrated that increased oxygen consumption rate was linked with a radioresistant phenotype in OAC [17]. However, to date, the role of oxidative phosphorylation in cisplatin resistance in OAC

has been underexplored. In a human ovarian cancer model of cisplatin resistance, SKOV3/DPP cisplatin-resistant cells had a significantly higher oxygen consumption rate when compared to SKOV3 cisplatin-sensitive cells [50]. The treatment of ovarian cisplatin-resistant cells with a Bcl-2 inhibitor was found to reduce the oxygen consumption rate and enhance cisplatin sensitivity [50]. Additionally, a study by Catanzaro et al. demonstrated that the inhibition of glucose-6-phosphate dehydrogenase could sensitise cisplatin-resistant ovarian cancer cells to cytotoxic death, further highlighting the role of the oxidative phosphorylation pathway in cisplatin resistance [51]. An elevated oxygen consumption rate has also been linked to chemoresistance with other chemotherapies, such as 5-FU. A study by Denise et al. demonstrated that 5-FU-resistant colorectal cancer cells have a significantly higher oxygen consumption rate compared to parental 5-FU sensitive cells. Furthermore, an increased oxygen consumption rate has also been linked to chemoresistance in docetaxel-resistant prostate cancer cells, where treatment with metformin to inhibit oxygen consumption was found to increase chemosensitivity [52]. Thus, it would be of interest to target oxidative phosphorylation in OAC OE33 Cis R cells as a potential mechanism to enhance cisplatin sensitivity. Metabolism is also tightly influenced by environmental conditions, whereby low oxygen conditions can result in the upregulation of hypoxia-inducible glucose transporters [53]. Thus, we investigated the metabolic rate of OE33 Cis P and Cis R cells under hypoxic conditions. The metabolic profile of OE33 Cis R cells is significantly altered under moderate hypoxic conditions (0.5% O_2), where OE33 Cis R cells have a significantly lower oxygen consumption rate than parental OE33 Cis P cells. This result highlights the flexible nature of OE33 Cis R cells, whereby they are able to adapt to environmental conditions and reduce oxygen consumption rate in low oxygen conditions. Hypoxia plays a critical role in cisplatin resistance, and hypoxic tumours often display a high level of resistance to cisplatin [54,55]. Studies in lung cancer have reported that hypoxia can promote the activation of autophagy, resulting in chemoresistance [55]. In addition, cisplatin-resistant lung cancer cells display a hypoxia-induced upregulation of p53, resulting in the activation of p21 transcription, which results in the arrest of the cell cycle at the G0–G1 phase, ultimately reducing the effect of cisplatin [54]. As dynamic regions of hypoxia are found in most solid tumours, including OAC, it is critical to understand how OE33 Cis R cells adapt to their tumour microenvironment to determine the best method to target this cell population. The reduced OCR that is seen in OE33 Cis R under hypoxic conditions is something that needs to be further evaluated in future studies.

This study has investigated a number of key differences in an isogenic model of OAC cisplatin resistance. Importantly, OE33 Cis R cells have a significantly altered gene expression and inflammatory secretome profile compared to cisplatin-sensitive cells. In addition, cisplatin-resistant cells have an altered metabolic profile under normal and low oxygen conditions. The molecular differences identified in this study, including the increased sensitivity to radiation and 5-FU of cisplatin-resistant cells, provides novel insight into cisplatin resistance in OAC, and has identified molecular processes that could be targeted in the future as a means to overcome cisplatin resistance and improve therapeutic outcomes for OAC.

4. Materials and Methods

4.1. Generation of the OE33 Cis P and OE33 Cis R Cell Lines

The human OE33 oesophageal adenocarcinoma cell line was obtained from the European collection of cell cultures. The isogenic model of cisplatin-resistant OAC; Cis P (cisplatin-sensitive) and Cis R (cisplatin-resistant) cells was generated as previously described [20]. Briefly, the original OE33 cells were split to generate two passage-matched flasks of OE33 cells. One flask was mock treated, and the other was treated with a metronomic dosing of cisplatin. Both lines were developed side-by-side and treated identically, differing only in being treated with vehicle or cisplatin until cisplatin-resistant cells were developed.

4.2. Preparation of Chemotherapeutic Drugs

Stock solutions of cis-diamminedichloroplatinum (cisplatin) and 5-flurouracil (5-FU) were prepared in phosphate-buffered saline (PBS) and dimethyl sulfoxide (DMSO), respectively. Solutions were sterile filtered and then aliquoted and stored at −20 °C. Prior to use, the solution was incubated at 37 °C and mixed thoroughly.

4.3. Determining IC_{50} of Cisplatin for OE33 Cis P and OE33 Cis R Cells at Using Cell Counting kit-8 (CCK8) Assay

OE33 Cis P and OE33 Cis R cells were seeded at 5×10^3 cells/200 µL in complete Roswell Park Memorial Institute (RPMI) 1640 medium supplemented with 10% fetal calf serum (Lonza, Basal, Switzerland) and 1% penicillin-streptomycin (Lonza, Basal, Switzerland) in a 96-well flat-bottomed plate and incubated at 37 °C, 5% CO_2 overnight. Media was replaced with 180 µL of fresh complete RPMI and cells were treated with 20 µL of cisplatin at a range of increasing concentrations (0, 0.01, 1, 10, 50, 100, 200 µM). Cells were incubated for 48 h at 37 °C, 5% CO_2/95% air. 10 µL of cell counting kit-8 (CCK8) assay solution (Sigma-Aldrich, Missouri, USA) was added to each well after 48 h. Cells were incubated at 37 °C, 5% CO_2 for 1.5 to 2 h until appropriate colour development was observed. The absorbance was measured at 450 nm using a VersaMax microplate reader (Molecular Devices, Sunnyvale, CA, USA).

4.4. Clonogenic Assay

OE33 Cis P and OE33 Cis R cells were trypsinised, counted, and seeded at the optimised densities of 1–2.5 × 10^3 in 1.5 mL of complete RPMI, in triplicate in six-well plates and allowed to adhere overnight. For chemosensitivity assays, cells were allowed to adhere for 24 h following which time they were treated with vehicle control or cisplatin. OE33 Cis P cells were treated with 1.3 µM of cisplatin, and OE33 Cis R cells were treated with either 1.3 µM or 2.8 µM of cisplatin. For radiosensitivity assays, cell were seeded and allowed to adhere for 48 h following which time OE33 Cis P and OE33 Cis R cells were either irradiated with 2 Gy (dose rate 1.73 Gy/min 195 KV 15 mA) or mock irradiated. Colonies were allowed to grow for 7 to 14 days, at which point they were fixed and stained with crystal violet (0.5%/ 25% *v*/*v* methanol) and allowed to air dry. Colonies consisting of 50 cells or more were counted using a colony counter (GelCount, Oxford Optronix, Oxford, UK). Plating efficiency (PE), which is the fraction of colonies formed by untreated cells, was calculated using the formula: PE = No. colonies/No. cells seeded. The surviving fraction (SF), which was the number of colonies formed following treatment, and was expressed in terms of PE, was calculated using the formula: SF = No. colonies/(No. cells seeded × PE).

4.5. Irradiation

Irradiation was performed using a XStrahl X-ray generator, (RS225), at a dose rate of 1.75 Gray per min.

4.6. RNA Extraction from Cell Lines

For total RNA extraction and purification, including miRNA, the RNeasy Mini Kit was used as per the manufacturer's instructions (Qiagen, UK). Sterile RNase and DNase-free filter tips were used throughout all of the RNA experiments (TipOne Starlab, UK). Cell pellets (<5 × 10^4 cells) were resuspended in 350 µl of RLT lysis buffer and pellets >five × 104 cells were resuspended in 600 µL of RLT lysis buffer. One volume of 70% ethanol was added to the lysate and mixed well by pipetting. RNeasy mini columns were inserted into the top of two-mL collection tubes. Up to 700 µL of the lysate was added to the columns, which were then centrifuged at 8000× *g* for 15 seconds at room temperature (RT). A 700-µL volume of RW1 buffer was added to the column, and centrifuged 8000× *g* for 15 seconds at RT. The flow through was discarded, and 500 µL of RPE buffer was added to the

column and centrifuged at 8000× *g* for 15 s at RT. The flow through was discarded, and 500 µL of buffer RPE was added to the column and centrifuged at 8000× *g* for 2 min at RT. The flow through was subsequently discarded, and the column was transferred to a new 1.5-mL collection tube. A 30 to 50-µL volume of RNase-free water was pipetted directly onto the column membrane and centrifuged for 1 min at 8000× *g* to elute the RNA from the silica membrane of the column. The concentration and purity of the eluted RNA was measured on the NanoDrop ND-1000 (Thermo Scientific, Delaware, USA). Then, RNA extracts were stored at −20 °C in the short term (<one month) or −80 °C in the long term (>one month).

4.7. Digital Gene Expression Sequencing

The gene expression sequencing was outsourced to LC Sciences (Texas, USA). Briefly, six µg total RNA from three biological replicates was prepared in 50-µL of DEPC (diethylpyrocarbonate) water, five µL of 3M of NaOAc, pH 5.2 and 150 µL of absolute ethanol to give a final volume of 205 µL. Samples were stored at −80 °C prior to shipping on dry ice. High-throughput sequencing was performed using Illumina sequencing by synthesis technology. LC Sciences provided analysed gene expression data and KEGG (Kyoto Encyclopaedia of Genes and Genomes) analysis. Gene expression abundance was normalised and evaluated in FPKM (Fragments Per Kilobase of transcript per Million reads) using the Cuffdiff module of Cufflinks_v2.2.1. The q-value was representative of a false discovery rate (FDR) adjusted *p*-value < 0.05. The fold change in gene expression was calculated from the equation: log2 (OE33 Cis R FPKM/OE33 Cis P PMK). Pathway analysis was performed with EASE (Expression Analysis Systematic Explorer). The KEGG pathway *p*-value is based on the EASE score: a modified Fisher exact *p*-value that measures if the probability of the (count/list total) is more than random chance compared to the background list (pop hits/pop total), where 'count' is the number of significant genes in a pathway, 'list total' is the number of genes in the submitted list associated with the category (e.g., KEGG pathway), 'pop hits' is the number of genes in the background list associated with the term, and 'pop total' is the number of genes in the background list associated with the category. Fold enrichment was calculated as (count/list total)/(pop hits/pop total). The lower the *p*-value, the more enrichment of the term. Gene expression changes were considered significant if the *p* value was <0.05. Heatmaps were generated using the 'pheatmap' package for the R project for statistical computing (version 3.5.1) [56,57].

4.8. Multiplex Enzyme Linked Immunosorbent Assay (ELISA)

Supernatant from OE33 Cis P and OE33 Cis R cells were defrosted on ice. The secretion of cytokines and angiogenic growth factors was analysed by ELISA as per the manufacturer's instructions. To assess angiogenic, vascular injury, inflammatory cytokine and chemokine secretions, a 47 multiplex kit spread across seven plates was used (Meso Scale Diagnostics, USA). The multiplex kit was used to quantify the secretions of CRP, Eotaxin, Eotaxin-3, GM-CSF, ICAM-1, IFN-γ, IL-10, IL-12/IL-23p40, IL-12p70, IL-13, IL-15, IL-16, IL-17A, IL-17A/F, IL-17B, IL-17C, IL-17D, IL-1RA, IL-1α, IL-1β, IL-2, IL-21, IL-22, IL-23, IL-27, IL-3, IL-31, IL-4, IL-5, IL-6, IL-7, IL-8, IL-8 (HA), IL-9, IP-10, MCP-1, MCP-4, MDC, MIP-1α, MIP-1β, MIP-3α, SAA, TARC, TNF-α, TNF-β, TSLP, VCAM-1, VEGF-A from OE33 Cis P and OE33 Cis R cell supernatants from cells that had been seeded at 250,000 cells per well for 48 h. Secretion data for all of the factors was normalised appropriately to cell lysate protein content using the BCA assay (Pierce).

4.9. OCR and ECAR Measurements in Cis P and Cis R Cells

OE33 Cis P and OE33 Cis R cells were seeded in five wells per treatment group at a density of 18,000 and 20,000 cells/well, respectively, in 24-well cell culture XFe24 microplates (Agilent Technologies, Santa Clara, CA, USA) at a volume of 100 µL and allowed to adhere at 37 °C in 5% CO_2/95% air. Five hours later, an additional 150 µL/well complete cell culture RPMI medium was added. Following 48 h of incubation, media was removed and cells were washed with unbuffered

Dulbecco's Modified Eagle's medium (DMEM) supplemented with 10 mM of glucose and 10 mM of sodium pyruvate, (pH 7.4) and incubated for one hour at 37 °C in a CO_2-free incubator. The oxygen consumption rate (OCR) and extracellular acidification rate (ECAR) were measured using a Seahorse Biosciences XFe24 Extracellular Flux Analyser (Agilent Technologies, Santa Clara, CA, USA). Three basal measurements of OCR and ECAR were taken over 24 min consisting of three repeats of mix (three min)/wait (2 min)/measurement (3 min) to establish basal respiration. Three additional measurements were obtained following the injection of three mitochondrial inhibitors including oligomycin (Sigma Aldrich, Missouri, USA), antimycin-A (Sigma Aldrich, Missouri, USA) and an uncoupling agent Carbonyl cyanide 4-(trifluoromethoxy)phenylhydrazone (FCCP) (Sigma Aldrich, Missouri, USA). ATP turnover was calculated by subtracting the OCR post oligomycin injection from baseline OCR prior to oligomycin addition. Proton leak was calculated by subtracting OCR post antimycin-A addition from OCR post oligomycin addition. Maximal respiration was calculated by subtracting OCR post antimycin addition from OCR post FCCP addition. Non-mitochondrial respiration was determined as the OCR value post antimycin-A addition. All of the measurements were normalised to cell number using the crystal violet assay, transferring the eluted stain to a 96-well plate before reading. For seahorse experiments carried out under (0.5% O_2) hypoxia, cells were seeded under normoxic conditions and allowed to adhere for 6 h at 37 °C 5% CO_2/95% air, following which time they were placed at 37 °C 0.5% O_2 5% CO_2 in the H35 Don whitley hypoxstation for 48 h, and seahorse measurements were carried out under hypoxia (0.5% O_2) in the i2 Whitley station using the same protocol for measuring rate as described for normoxic conditions.

4.10. Crystal Violet

Cells were fixed with 1% glutaraldehyde (Sigma-Aldrich, Missouri, USA) for 15 min at RT. The fixative was removed, and cells were washed with PBS and stained with 0.1% crystal violet for 30 min at RT. Plates were left to air dry and incubated with 50 µL of 1% Triton X-100 in PBS on a plate shaker for 30 min at RT. Absorbance was read at 595 nm on a VersaMax microplate reader (Molecular Devices, Sunnyvale, CA, USA).

4.11. Statistical Analysis

Statistical analysis was performed using GraphPad Prism version 5 software (GraphPad Software, CA, USA). Scientific data were expressed as mean ± standard error of the mean (SEM). SEM was calculated as the standard deviation of the original samples divided by the square root of the sample size. Specific statistical tests used are indicated in figure legends. For all of the statistical analysis, differences were considered statistically significant at $p < 0.05$.

Supplementary Materials: The following are available online at http://www.mdpi.com/1424-8247/12/1/33/s1, Figure S1: Inflammatory protein in cisplatin sensitive (OE33 Cis P) versus cisplatin resistant (OE33 Cis R) OAC cells. The secreted levels of 47 proteins in Cis P and Cis R cells was evaluated by multiplex ELISA, 23 proteins were detected in supernatant of Cis P and Cis R cells, there was no significant difference in secreted levels of (**A**) Monocyte chemoattractant protein-1 (MCP-1) (**B**) Vascular endothelial growth factor (VEGF-A) (**C**) Vascular adhesion molecule 1 (VCAM-1) (**D**) Granulocyte-macrophage colony-stimulating factor (GM-CSF) (**E**) Interleukin 15 (IL-15) in OE33 Cis P and OE33 Cis R cells, all secretions normalised to protein content. (n = 4). Unpaired *t*-test. Date expressed as ± SEM.

Author Contributions: Conceptualisation, A.M.B., B.A.S.B., S.G.M. and J.O.S.; Data curation, A.M.B. and B.A.S.B.; Formal analysis, A.M.B., B.A.S.B., S.G.M. and J.O.S.; Funding acquisition, M.R.D. and J.O.S.; Investigation, A.M.B., B.A.S.B. and M.R.D.; Methodology, A.M.B., B.A.S.B. and M.R.D.; Software, S.A.K.; Supervision, B.N.K., S.G.M. and J.O.S.; Visualisation, S.A.K.; Writing—original draft, A.M.B.; Writing—review & editing, A.M.B., M.R.D., S.A.K., B.N.K., S.G.M. and J.O.S.

Funding: Funding for this work was provided by the Irish Cancer Society (Grant: CRS15BUC) and Health Research Board (Grant: HRB ILP-POR-2017-055).

Conflicts of Interest: The authors declare no conflicts of interest.

Abbreviations

5-FU	Fluorouracil
Cis	Cisplatin
ECAR	Extracellular Acidification Rate
ELISA	Enzyme Linked Immunosorbent assay
DMEM	Dulbecco's Modified Eagle's medium
IL-1α	Interleukin 1 alpha
IL-7	Interleukin 7
IL-8	Interleukin 8
ICAM-1	Intracellular Adhesion Molecule 1
KEGG	Kyoto Encyclopedia of Genes and Genomes
MiRNA	Micro ribonucleic acid
NeoCRT	Neoadjuvant Chemoradiation Therapy
NHEJ	Non Homologous end joining
OAC	Oesophageal Adenocarcinoma
OCR	Oxidative Phosphorylation
PE	Plating Efficiency
RMPI	Roswell Park Memorial Institute medium
SCC	Squamous Cell Carcinoma
SF	Surviving Fraction
TGF-β	Transforming Growth Factor Beta
VEGF	Vascular Endothelial Growth Factor

References

1. Arnold, M.; Soerjomataram, I.; Ferlay, J.; Forman, D. Global incidence of oesophageal cancer by histological subtype in 2012. *Gut* **2015**, *64*, 381–387. [CrossRef] [PubMed]
2. Ferlay, J.; Soerjomataram, I.; Dikshit, R.; Eser, S.; Mathers, C.; Rebelo, M.; Parkin, D.M.; Forman, D.; Bray, F. Cancer incidence and mortality worldwide: Sources, methods and major patterns in GLOBOCAN 2012. *Int. J. Cancer* **2015**, *136*, E359–E386. [CrossRef] [PubMed]
3. Abbas, G.; Krasna, M. Overview of esophageal cancer. *Ann. Cardiothorac. Surg.* **2017**, *6*, 131–136. [CrossRef] [PubMed]
4. Picardo, S.L.; Maher, S.G.; O'Sullivan, J.N.; Reynolds, J.V. Barrett's to oesophageal cancer sequence: A model of inflammatory-driven upper gastrointestinal cancer. *Digest. Surg.* **2012**, *29*, 251–260. [CrossRef] [PubMed]
5. Cools-Lartigue, J.; Spicer, J.; Ferri, L.E. Current status of management of malignant disease: Current management of esophageal cancer. *J. Gastrointest. Surg. Off. J. Soc. Surg. Aliment. Tract.* **2015**, *19*, 964–972. [CrossRef] [PubMed]
6. Donohoe, C.L.; Reynolds, J.V. Neoadjuvant treatment of locally advanced esophageal and junctional cancer: The evidence-base, current key questions and clinical trials. *J. Thorac. Dis.* **2017**, *9*, S697–S704. [CrossRef] [PubMed]
7. Walsh, T.N.; Noonan, N.; Hollywood, D.; Kelly, A.; Keeling, N.; Hennessy, T.P.J. A Comparison of Multimodal Therapy and Surgery for Esophageal Adenocarcinoma. *N. Engl. J. Med.* **1996**, *335*, 462–467. [CrossRef] [PubMed]
8. Jin, H.-L.; Zhu, H.; Ling, T.-S.; Zhang, H.-J.; Shi, R.-H. Neoadjuvant chemoradiotherapy for resectable esophageal carcinoma: A meta-analysis. *World J. Gastroenterol. WJG* **2009**, *15*, 5983–5991. [CrossRef] [PubMed]
9. Galluzzi, L.; Senovilla, L.; Vitale, I.; Michels, J.; Martins, I.; Kepp, O.; Castedo, M.; Kroemer, G. Molecular mechanisms of cisplatin resistance. *Oncogene* **2012**, *31*, 1869–1883. [CrossRef] [PubMed]
10. Reynolds, J.V.; Preston, S.R.; O'Neill, B.; Baeksgaard, L.; Griffin, S.M.; Mariette, C.; Cuffe, S.; Cunningham, M.; Crosby, T.; Parker, I.; et al. ICORG 10-14: NEOadjuvant trial in Adenocarcinoma of the oEsophagus and oesophagoGastric junction International Study (Neo-AEGIS). *BMC Cancer* **2017**, *17*, 401. [CrossRef]
11. Cunningham, D.; Allum, W.H.; Stenning, S.P.; Thompson, J.N.; Van de Velde, C.J.H.; Nicolson, M.; Scarffe, J.H.; Lofts, F.J.; Falk, S.J.; Iveson, T.J.; et al. Perioperative Chemotherapy versus Surgery Alone for Resectable Gastroesophageal Cancer. *N. Engl. J. Med.* **2006**, *355*, 11–20. [CrossRef]

12. Van Hagen, P.; Hulshof, M.C.C.M.; van Lanschot, J.J.B.; Steyerberg, E.W.; Henegouwen, M.I.V.B.; Wijnhoven, B.P.L.; Richel, D.J.; Nieuwenhuijzen, G.A.P.; Hospers, G.A.P.; Bonenkamp, J.J.; et al. Preoperative Chemoradiotherapy for Esophageal or Junctional Cancer. *N. Engl. J. Med.* **2012**, *366*, 2074–2084. [CrossRef] [PubMed]
13. Maher, S.G.; McDowell, D.T.; Collins, B.C.; Muldoon, C.; Gallagher, W.M.; Reynolds, J.V. Serum proteomic profiling reveals that pretreatment complement protein levels are predictive of esophageal cancer patient response to neoadjuvant chemoradiation. *Ann. Surg.* **2011**, *254*, 809–816. [CrossRef] [PubMed]
14. Cui, L.; Fu, J.; Pang, J.C.-S.; Qiu, Z.-K.; Liu, X.-M.; Chen, F.-R.; Shi, H.-L.; Ng, H.-K.; Chen, Z.-P. Overexpression of IL-7 enhances cisplatin resistance in glioma. *Cancer Biol. Therapy* **2012**, *13*, 496–503. [CrossRef] [PubMed]
15. Andrejeva, G.; Rathmell, J.C. Similarities and Distinctions of Cancer and Immune Metabolism in Inflammation and Tumors. *Cell Metabol.* **2017**, *26*, 49–70. [CrossRef] [PubMed]
16. Hanahan, D.; Weinberg, R.A. Hallmarks of cancer: The next generation. *Cell* **2011**, *144*, 646–674. [CrossRef] [PubMed]
17. Lynam-Lennon, N.; Maher, S.G.; Maguire, A.; Phelan, J.; Muldoon, C.; Reynolds, J.V.; O'Sullivan, J. Altered Mitochondrial Function and Energy Metabolism Is Associated with a Radioresistant Phenotype in Oesophageal Adenocarcinoma. *PLoS ONE* **2014**, *9*, e100738. [CrossRef] [PubMed]
18. Lynam-Lennon, N.; Reynolds, J.V.; Pidgeon, G.P.; Lysaght, J.; Marignol, L.; Maher, S.G. Alterations in DNA repair efficiency are involved in the radioresistance of esophageal adenocarcinoma. *Radiat. Res.* **2010**, *174*, 703–711. [CrossRef]
19. Wangpaichitr, M.; Theodoropoulos, G.; Wu, C.; You, M.; Feun, L.; Kuo, M.T.; Savaraj, N. The Relationship of Thioredoxin-1 and Cisplatin Resistance: Its Impact on ROS and Oxidative Metabolism in Lung Cancer Cells. *Mol. Cancer Ther.* **2012**. [CrossRef]
20. Lynam-Lennon, N.; Heavey, S.; Sommerville, G.; Bibby, B.A.S.; Ffrench, B.; Quinn, J.; Gasch, C.; O'Leary, J.J.; Gallagher, M.F.; Reynolds, J.V.; et al. MicroRNA-17 is downregulated in esophageal adenocarcinoma cancer stem-like cells and promotes a radioresistant phenotype. *Oncotarget* **2017**, *8*, 11400–11413. [CrossRef]
21. Buckley, A.M.; Lynam-Lennon, N.; Kennedy, S.A.; Dunne, M.R.; Aird, J.J.; Foley, E.K.; Clarke, N.; Ravi, N.; O'Toole, D.; Reynolds, J.V.; et al. Leukaemia inhibitory factor is associated with treatment resistance in oesophageal adenocarcinoma. *Oncotarget* **2018**, *9*, 33634–33647. [CrossRef] [PubMed]
22. Stordal, B.; Davey, M. Understanding cisplatin resistance using cellular models. *IUBMB Life* **2007**, *59*, 696–699. [CrossRef] [PubMed]
23. Hummel, R.; Sie, C.; Watson, D.I.; Wang, T.; Ansar, A.; Michael, M.Z.; Van der Hoek, M.; Haier, J.; Hussey, D.J. MicroRNA signatures in chemotherapy resistant esophageal cancer cell lines. *World J. Gastroenterol. WJG* **2014**, *20*, 14904–14912. [CrossRef] [PubMed]
24. Xie, X.-Q.; Zhao, Q.-H.; Wang, H.; Gu, K.-S. Dysregulation of mRNA profile in cisplatin-resistant gastric cancer cell line SGC7901. *World J. Gastroenterol.* **2017**, *23*, 1189–1202. [CrossRef]
25. Shen, D.W.; Pouliot, L.M.; Hall, M.D.; Gottesman, M.M. Cisplatin resistance: A cellular self-defense mechanism resulting from multiple epigenetic and genetic changes. *Pharmacol. Rev.* **2012**, *64*, 706–721. [CrossRef] [PubMed]
26. Adelstein, D.J.; Li, Y.; Adams, G.L.; Wagner, H., Jr.; Kish, J.A.; Ensley, J.F.; Schuller, D.E.; Forastiere, A.A. An Intergroup Phase III Comparison of Standard Radiation Therapy and Two Schedules of Concurrent Chemoradiotherapy in Patients With Unresectable Squamous Cell Head and Neck Cancer. *J. Clin. Oncol.* **2003**, *21*, 92–98. [CrossRef]
27. Keys, H.M.; Bundy, B.N.; Stehman, F.B.; Muderspach, L.I.; Chafe, W.E.; Suggs, C.L.; Walker, J.L.; Gersell, D. Cisplatin, Radiation, and Adjuvant Hysterectomy Compared with Radiation and Adjuvant Hysterectomy for Bulky Stage IB Cervical Carcinoma. *N. Engl. J. Med.* **1999**, *340*, 1154–1161. [CrossRef]
28. Tu, L.; Sun, L.; Xu, Y.; Wang, Y.; Zhou, L.; Liu, Y.; Zhu, J.; Peng, F.; Wei, Y.; Gong, Y. Paclitaxel and cisplatin combined with intensity-modulated radiotherapy for upper esophageal carcinoma. *Radiat. Oncol.* **2013**, *8*, 75. [CrossRef]
29. Ilson, D.H.; Minsky, B.; Kelsen, D. Irinotecan, cisplatin, and radiation in esophageal cancer. *Oncology* **2002**, *16*, 11–15.
30. Myint, W.K.; Ng, C.; Raaphorst, G.P. Examining the non-homologous repair process following cisplatin and radiation treatments. *Int. J. Radiat. Biol.* **2002**, *78*, 417–424. [CrossRef]

31. Boeckman, H.J.; Trego, K.S.; Henkels, K.M.; Turchi, J.J. Cisplatin sensitizes cancer cells to ionizing radiation via inhibition of non-homologous end joining. *Mol. Cancer Res. MCR* **2005**, *3*, 277–285. [CrossRef] [PubMed]
32. Eljack, N.D.; Ma, H.Y.; Drucker, J.; Shen, C.; Hambley, T.W.; New, E.J.; Friedrich, T.; Clarke, R.J. Mechanisms of cell uptake and toxicity of the anticancer drug cisplatin. *Metall. Integr. Biomet. Sci.* **2014**, *6*, 2126–2133. [CrossRef] [PubMed]
33. Kilari, D.; Guancial, E.; Kim, E.S. Role of copper transporters in platinum resistance. *World J. Clin. Oncol.* **2016**, *7*, 106–113. [CrossRef]
34. Baskar, R.; Dai, J.; Wenlong, N.; Yeo, R.; Yeoh, K.-W. Biological response of cancer cells to radiation treatment. *Front. Mol. Biosci.* **2014**, *1*, 24. [CrossRef] [PubMed]
35. Hummel, R.; Watson, D.I.; Smith, C.; Kist, J.; Michael, M.Z.; Haier, J.; Hussey, D.J. Mir-148a improves response to chemotherapy in sensitive and resistant oesophageal adenocarcinoma and squamous cell carcinoma cells. *J. Gastrointest. Surg. Off. J. Soc. Surg. Aliment. Tract.* **2011**, *15*, 429–438. [CrossRef] [PubMed]
36. Singh, A.; Settleman, J. EMT, cancer stem cells and drug resistance: An emerging axis of evil in the war on cancer. *Oncogene* **2010**, *29*, 4741–4751. [CrossRef]
37. Piskareva, O.; Harvey, H.; Nolan, J.; Conlon, R.; Alcock, L.; Buckley, P.; Dowling, P.; O'Sullivan, F.; Bray, I.; Stallings, R.L. The development of cisplatin resistance in neuroblastoma is accompanied by epithelial to mesenchymal transition in vitro. *Cancer Lett.* **2015**, *364*, 142–155. [CrossRef] [PubMed]
38. Katoh, M. Networking of WNT, FGF, Notch, BMP, and Hedgehog signaling pathways during carcinogenesis. *Stem Cell Rev.* **2007**, *3*, 30–38. [CrossRef] [PubMed]
39. Matsuoka, S.; Edwards, M.C.; Bai, C.; Parker, S.; Zhang, P.; Baldini, A.; Harper, J.W.; Elledge, S.J. p57KIP2, a structurally distinct member of the p21CIP1 Cdk inhibitor family, is a candidate tumor suppressor gene. *Genes Dev.* **1995**, *9*, 650–662. [CrossRef]
40. Vlachos, P.; Nyman, U.; Hajji, N.; Joseph, B. The cell cycle inhibitor p57(Kip2) promotes cell death via the mitochondrial apoptotic pathway. *Cell Death Differ.* **2007**, *14*, 1497–1507. [CrossRef]
41. Oshimori, N.; Oristian, D.; Fuchs, E. TGF-β Promotes Heterogeneity and Drug Resistance in Squamous Cell Carcinoma. *Cell* **2015**, *160*, 963–976. [CrossRef] [PubMed]
42. Bissey, P.-A.; Law, J.H.; Bruce, J.P.; Shi, W.; Renoult, A.; Chua, M.L.K.; Yip, K.W.; Liu, F.-F. Dysregulation of the MiR-449b target TGFBI alters the TGFβ pathway to induce cisplatin resistance in nasopharyngeal carcinoma. *Oncogenesis* **2018**, *7*, 40. [CrossRef]
43. Di Paolo, N.C.; Shayakhmetov, D.M. Interleukin 1α and the inflammatory process. *Nat. Immunol.* **2016**, *17*, 906. [CrossRef]
44. Benchekroun, M.N.; Parker, R.; Dabholkar, M.; Reed, E.; Sinha, B.K. Effects of interleukin-1 alpha on DNA repair in human ovarian carcinoma (NIH:OVCAR-3) cells: Implications in the mechanism of sensitization of cis-diamminedichloroplatinum(II). *Mol. Pharmacol.* **1995**, *47*, 1255–1260. [PubMed]
45. Webb, D.S.; Mostowski, H.S.; Gerrard, T.L. Cytokine-induced enhancement of ICAM-1 expression results in increased vulnerability of tumor cells to monocyte-mediated lysis. *J. Immunol.* **1991**, *146*, 3682–3686.
46. Jonjic, N.; Alberti, S.; Bernasconi, S.; Peri, G.; Jilek, P.; Anichini, A.; Parmiani, G.; Mantovani, A. Heterogeneous susceptibility of human melanoma clones to monocyte cytotoxicity: Role of ICAM-1 defined by antibody blocking and gene transfer. *Eur. J. Immunol.* **1992**, *22*, 2255–2260. [CrossRef] [PubMed]
47. Guo, P.; Huang, J.; Wang, L.; Jia, D.; Yang, J.; Dillon, D.A.; Zurakowski, D.; Mao, H.; Moses, M.A.; Auguste, D.T. ICAM-1 as a molecular target for triple negative breast cancer. *Proc. Natl. Acad. Sci. USA* **2014**, *111*, 14710–14715. [CrossRef]
48. Takizawa, K.; Kamijo, R.; Ito, D.; Hatori, M.; Sumitani, K.; Nagumo, M. Synergistic induction of ICAM-1 expression by cisplatin and 5-fluorouracil in a cancer cell line via a NF-κB independent pathway. *Br. J. Cancer* **1999**, *80*, 954. [CrossRef]
49. Tsai, S.T.; Wang, P.J.; Liou, N.J.; Lin, P.S.; Chen, C.H.; Chang, W.C. ICAM1 Is a Potential Cancer Stem Cell Marker of Esophageal Squamous Cell Carcinoma. *PLoS ONE* **2015**, *10*, e0142834. [CrossRef]
50. Xu, Y.; Gao, W.; Zhang, Y.; Wu, S.; Liu, Y.; Deng, X.; Xie, L.; Yang, J.; Yu, H.; Su, J.; et al. ABT737 reverses cisplatin resistance by targeting glucose metabolism of human ovarian cancer cells. *Int. J. Oncol.* **2018**, *53*, 1055–1068. [CrossRef]
51. Catanzaro, D.; Gaude, E.; Orso, G.; Giordano, C.; Guzzo, G.; Rasola, A.; Ragazzi, E.; Caparrotta, L.; Frezza, C.; Montopoli, M. Inhibition of glucose-6-phosphate dehydrogenase sensitizes cisplatin-resistant cells to death. *Oncotarget* **2015**, *6*, 30102–30114. [CrossRef] [PubMed]

52. Ippolito, L.; Marini, A.; Cavallini, L.; Morandi, A.; Pietrovito, L.; Pintus, G.; Giannoni, E.; Schrader, T.; Puhr, M.; Chiarugi, P.; et al. Metabolic shift toward oxidative phosphorylation in docetaxel resistant prostate cancer cells. *Oncotarget* **2016**, *7*, 61890–61904. [CrossRef]
53. Zhao, F.Q.; Keating, A.F. Functional properties and genomics of glucose transporters. *Curr. Genomics* **2007**, *8*, 113–128. [CrossRef] [PubMed]
54. Guo, Q.; Lan, F.; Yan, X.; Xiao, Z.; Wu, Y.; Zhang, Q. Hypoxia exposure induced cisplatin resistance partially via activating p53 and hypoxia inducible factor-1alpha in non-small cell lung cancer A549 cells. *Oncol. Lett.* **2018**, *16*, 801–808. [PubMed]
55. Wu, H.M.; Jiang, Z.F.; Ding, P.S.; Shao, L.J.; Liu, R.Y. Hypoxia-induced autophagy mediates cisplatin resistance in lung cancer cells. *Sci. Rep.* **2015**, *5*, 12291. [CrossRef] [PubMed]
56. Kolde, R. Pheatmap: Pretty Heatmaps. R Package Version 1.0.10. 2018. Available online: https://CRAN.R-project.org/package=pheatmap (accessed on 4 January 2019).
57. Team, R.C. *R: A Language and Environment for Statistical Computing*; R Foundation for Statistical Computing: Vienna, Austria, 2018.

© 2019 by the authors. Licensee MDPI, Basel, Switzerland. This article is an open access article distributed under the terms and conditions of the Creative Commons Attribution (CC BY) license (http://creativecommons.org/licenses/by/4.0/).

8. Bibliography

1. Ferlay, J., et al., *Cancer incidence and mortality worldwide: Sources, methods and major patterns in GLOBOCAN 2012.* International Journal of Cancer, 2015. **136**(5): p. E359-E386.
2. Berger, B. and C. Belka, *Evidence-based radiation oncology: oesophagus.* Radiotherapy and Oncology, 2009. **92**(2): p. 276-290.
3. Mariette, C., et al., *Esophageal carcinoma: prognostic differences between squamous cell carcinoma and adenocarcinoma.* World journal of surgery, 2005. **29**(1): p. 39-45.
4. Siewert, J.R., et al., *Histologic tumor type is an independent prognostic parameter in esophageal cancer: lessons from more than 1,000 consecutive resections at a single center in the Western world.* Annals of surgery, 2001. **234**(3): p. 360.
5. Arnold, M., et al., *Global incidence of oesophageal cancer by histological subtype in 2012.* Gut, 2015. **64**(3): p. 381-7.
6. Napier, K.J., M. Scheerer, and S. Misra, *Esophageal cancer: A Review of epidemiology, pathogenesis, staging workup and treatment modalities.* World J Gastrointest Oncol, 2014. **6**(5): p. 112-20.
7. Registry, N.C. *16. Oesophageal Cancer*. 2019 [cited 2019 27/05/2019].
8. Castro, C., et al., *Patterns and trends in esophageal cancer mortality and incidence in Europe (1980-2011) and predictions to 2015.* Ann Oncol, 2014. **25**(1): p. 283-90.
9. Cronin-Fenton, D.P., et al., *Reproductive and sex hormonal factors and oesophageal and gastric junction adenocarcinoma: a pooled analysis.* Eur J Cancer, 2010. **46**(11): p. 2067-76.
10. Chen, Q., H. Zhuang, and Y. Liu, *The association between obesity factor and esophageal caner.* J Gastrointest Oncol, 2012. **3**(3): p. 226-31.
11. Hur, C., et al., *Trends in esophageal adenocarcinoma incidence and mortality.* Cancer, 2013. **119**(6): p. 1149-1158.
12. Fang, Y., et al., *Cellular origins and molecular mechanisms of Barrett's esophagus and esophageal adenocarcinoma.* Ann N Y Acad Sci, 2013. **1300**: p. 187-199.
13. Denlinger, C.E. and R.K. Thompson, *Molecular basis of esophageal cancer development and progression.* Surg Clin North Am, 2012. **92**(5): p. 1089-103.
14. Jankowski, J.A., et al., *Barrett's metaplasia.* Lancet, 2000. **356**(9247): p. 2079-85.
15. Picardo, S.L., et al., *Barrett's to oesophageal cancer sequence: a model of inflammatory-driven upper gastrointestinal cancer.* Dig Surg, 2012. **29**(3): p. 251-60.
16. Solaymani-Dodaran, M., et al., *Risk of oesophageal cancer in Barrett's oesophagus and gastro-oesophageal reflux.* Gut, 2004. **53**(8): p. 1070-4.
17. Theisen, J., J.H. Peters, and H.J. Stein, *Experimental evidence for mutagenic potential of duodenogastric juice on Barrett's esophagus.* World J Surg, 2003. **27**(9): p. 1018-20.
18. Schneider, J.L. and D.A. Corley, *A review of the epidemiology of Barrett's oesophagus and oesophageal adenocarcinoma.* Best Pract Res Clin Gastroenterol, 2015. **29**(1): p. 29-39.
19. de Jonge, P.J., et al., *Risk of malignant progression in patients with Barrett's oesophagus: a Dutch nationwide cohort study.* Gut, 2010. **59**(8): p. 1030-1036.
20. Sharma, P., *Barrett's esophagus.* New England journal of medicine, 2009. **361**(26): p. 2548-2556.
21. Yousef, F., et al., *The incidence of esophageal cancer and high-grade dysplasia in Barrett's esophagus: a systematic review and meta-analysis.* American journal of epidemiology, 2008. **168**(3): p. 237-249.
22. Drahos, J., et al., *Metabolic syndrome increases risk of Barrett esophagus in the absence of gastroesophageal reflux: an analysis of SEER-Medicare Data.* Journal of clinical gastroenterology, 2015. **49**(4): p. 282-288.
23. Ryan, A.M., et al., *Barrett esophagus: prevalence of central adiposity, metabolic syndrome, and a proinflammatory state.* Ann Surg, 2008. **247**(6): p. 909-15.
24. Corley, D.A., et al., *Surveillance and survival in Barrett's adenocarcinomas: a population-based study.* Gastroenterology, 2002. **122**(3): p. 633-40.

25. Kubo, A. and D.A. Corley, *Body mass index and adenocarcinomas of the esophagus or gastric cardia: a systematic review and meta-analysis.* Cancer Epidemiology and Prevention Biomarkers, 2006. **15**(5): p. 872-878.
26. Turati, F., et al., *A meta-analysis of body mass index and esophageal and gastric cardia adenocarcinoma.* Ann Oncol, 2013. **24**(3): p. 609-17.
27. Chen, Q., H. Zhuang, and Y. Liu, *The association between obesity factor and esophageal caner.* Journal of gastrointestinal oncology, 2012. **3**(3): p. 226.
28. Kubo, A., et al., *Sex-specific associations between body mass index, waist circumference and the risk of Barrett's oesophagus: a pooled analysis from the international BEACON consortium.* Gut, 2013: p. gutjnl-2012-303753.
29. Sweed, M.R., D. Edmonson, and S.J. Cohen. *Tumors of the esophagus, gastroesophageal junction, and stomach*. in *Seminars in oncology nursing*. 2009. Elsevier.
30. Layke, J.C. and P.P. Lopez, *Esophageal cancer: a review and update.* Am Fam Physician, 2006. **73**(12): p. 2187-94.
31. Foley, K.G., et al., *N-staging of oesophageal and junctional carcinoma: is there still a role for EUS in patients staged N0 at PET/CT?* Clin Radiol, 2014. **69**(9): p. 959-64.
32. Khanna, L.G. and F.G. Gress, *Preoperative evaluation of oesophageal adenocarcinoma.* Best Pract Res Clin Gastroenterol, 2015. **29**(1): p. 179-91.
33. Downey, R.J., et al., *Whole body 18FDG-PET and the response of esophageal cancer to induction therapy: results of a prospective trial.* J Clin Oncol, 2003. **21**(3): p. 428-32.
34. O'Neill, H., et al., *Can the Efficacy of [18F]FDG-PET/CT in Clinical Oncology Be Enhanced by Screening Biomolecular Profiles?* Pharmaceuticals, 2019. **12**(1): p. 16.
35. Luketich, J.D., et al., *Role of positron emission tomography in staging esophageal cancer.* Ann Thorac Surg, 1997. **64**(3): p. 765-9.
36. Berry, M.F., *Esophageal cancer: staging system and guidelines for staging and treatment.* Journal of Thoracic Disease, 2014. **6**(Suppl 3): p. S289-S297.
37. Rice, T.W., et al., *Cancer of the esophagus and esophagogastric junction: data-driven staging for the seventh edition of the American Joint Committee on Cancer/International Union Against Cancer Cancer Staging Manuals.* Cancer, 2010. **116**(16): p. 3763-73.
38. Ajani, J.A., et al., *Esophageal and esophagogastric junction cancers.* J Natl Compr Canc Netw, 2011. **9**(8): p. 830-87.
39. Enzinger, P.C. and D.H. Ilson, *Irinotecan in esophageal cancer.* Oncology (Williston Park), 2000. **14**(12 Suppl 14): p. 26-30.
40. Cools-Lartigue, J., J. Spicer, and L.E. Ferri, *Current status of management of malignant disease: current management of esophageal cancer.* J Gastrointest Surg, 2015. **19**(5): p. 964-72.
41. Walsh , T.N., et al., *A Comparison of Multimodal Therapy and Surgery for Esophageal Adenocarcinoma.* New England Journal of Medicine, 1996. **335**(7): p. 462-467.
42. Jin, H.-L., et al., *Neoadjuvant chemoradiotherapy for resectable esophageal carcinoma: A meta-analysis.* World Journal of Gastroenterology : WJG, 2009. **15**(47): p. 5983-5991.
43. Donohoe, C.L. and J.V. Reynolds, *Neoadjuvant treatment of locally advanced esophageal and junctional cancer: the evidence-base, current key questions and clinical trials.* Journal of Thoracic Disease, 2017. **9**(Suppl 8): p. S697-S704.
44. Reynolds, J.V., et al., *ICORG 10-14: NEOadjuvant trial in Adenocarcinoma of the oEsophagus and oesophagoGastric junction International Study (Neo-AEGIS).* BMC Cancer, 2017. **17**: p. 401.
45. Cunningham , D., et al., *Perioperative Chemotherapy versus Surgery Alone for Resectable Gastroesophageal Cancer.* New England Journal of Medicine, 2006. **355**(1): p. 11-20.
46. van Hagen, P., et al., *Preoperative Chemoradiotherapy for Esophageal or Junctional Cancer.* New England Journal of Medicine, 2012. **366**(22): p. 2074-2084.

47. Schulz, C., et al., *NeoFLOT: Multicenter phase II study of perioperative chemotherapy in resectable adenocarcinoma of the gastroesophageal junction or gastric adenocarcinoma-Very good response predominantly in patients with intestinal type tumors.* Int J Cancer, 2015. **137**(3): p. 678-85.
48. Reedijk, J., *The mechanism of action of platinum antitumor drugs.* Pure and Applied Chemistry, 1987. **59**(2): p. 181-192.
49. Malhotra, V. and M.C. Perry, *Classical chemotherapy: mechanisms, toxicities and the therapeutic window.* Cancer Biol Ther, 2003. **2**(4 Suppl 1): p. S2-4.
50. Horwitz, S.B., et al., *Taxol: mechanisms of action and resistance.* Journal of the National Cancer Institute. Monographs, 1993(15): p. 55-61.
51. Parker, W.B., *Enzymology of purine and pyrimidine antimetabolites used in the treatment of cancer.* Chem Rev, 2009. **109**(7): p. 2880-93.
52. Longley, D.B., D.P. Harkin, and P.G. Johnston, *5-fluorouracil: mechanisms of action and clinical strategies.* Nat Rev Cancer, 2003. **3**(5): p. 330-8.
53. Hortobagyi, G., *Anthracyclines in the treatment of cancer.* Drugs, 1997. **54**(4): p. 1-7.
54. Nitiss, J.L., *Targeting DNA topoisomerase II in cancer chemotherapy.* Nat Rev Cancer, 2009. **9**(5): p. 338-50.
55. Lord, C.J. and A. Ashworth, *The DNA damage response and cancer therapy.* Nature, 2012. **481**(7381): p. 287-94.
56. Shapiro, J., et al., *Neoadjuvant chemoradiotherapy plus surgery versus surgery alone for oesophageal or junctional cancer (CROSS): long-term results of a randomised controlled trial.* The lancet oncology, 2015. **16**(9): p. 1090-1098.
57. Ychou, M., et al., *Perioperative chemotherapy compared with surgery alone for resectable gastroesophageal adenocarcinoma: an FNCLCC and FFCD multicenter phase III trial.* Journal of clinical oncology, 2011. **29**(13): p. 1715-1721.
58. Pasini, F., et al., *Neoadjuvant therapy with weekly docetaxel and cisplatin, 5-fluorouracil continuous infusion, and concurrent radiotherapy in patients with locally advanced esophageal cancer produced a high percentage of long-lasting pathological complete response.* Cancer, 2013. **119**(5): p. 939-945.
59. Gillham, C.M., J. Reynolds, and D. Hollywood, *Predicting the response of localised oesophageal cancer to neo-adjuvant chemoradiation.* World journal of surgical oncology, 2007. **5**(1): p. 97.
60. Ancona, E., et al., *Only pathologic complete response to neoadjuvant chemotherapy improves significantly the long term survival of patients with resectable esophageal squamous cell carcinoma: final report of a randomized, controlled trial of preoperative chemotherapy versus surgery alone.* Cancer: Interdisciplinary International Journal of the American Cancer Society, 2001. **91**(11): p. 2165-2174.
61. Geh, J.I., A.M. Crellin, and R. Glynne-Jones, *Preoperative (neoadjuvant) chemoradiotherapy in oesophageal cancer.* Br J Surg, 2001. **88**(3): p. 338-56.
62. Mandard, A.M., et al., *Pathologic assessment of tumor regression after preoperative chemoradiotherapy of esophageal carcinoma. Clinicopathologic correlations.* Cancer, 1994. **73**(11): p. 2680-6.
63. Wahl, D.R. and T.S. Lawrence, *Integrating chemoradiation and molecularly targeted therapy.* Adv Drug Deliv Rev, 2015.
64. Allum, W.H., et al., *Long-term results of a randomized trial of surgery with or without preoperative chemotherapy in esophageal cancer.* Journal of clinical oncology, 2009. **27**(30): p. 5062-5067.
65. Al-Batran, S.-E., et al., *Perioperative chemotherapy with docetaxel, oxaliplatin, and fluorouracil/leucovorin (FLOT) versus epirubicin, cisplatin, and fluorouracil or capecitabine (ECF/ECX) for resectable gastric or gastroesophageal junction (GEJ) adenocarcinoma (FLOT4-AIO): A multicenter, randomized phase 3 trial.* Journal of Clinical Oncology, 2017. **35**(15_suppl): p. 4004-4004.
66. Wang, V.E., J.R. Grandis, and A.H. Ko, *New strategies in esophageal carcinoma: Translational insights from signaling pathways and immune checkpoints.* Clinical Cancer Research, 2016. **22**(17): p. 4283-4290.

67. Gowryshankar, A., V. Nagaraja, and G.D. Eslick, *HER2 status in Barrett's esophagus & esophageal cancer: a meta analysis.* Journal of gastrointestinal oncology, 2014. **5**(1): p. 25-35.
68. Bang, Y.-J., et al., *Trastuzumab in combination with chemotherapy versus chemotherapy alone for treatment of HER2-positive advanced gastric or gastro-oesophageal junction cancer (ToGA): a phase 3, open-label, randomised controlled trial.* The Lancet, 2010. **376**(9742): p. 687-697.
69. Tabernero, J., et al., *616OPertuzumab (P) + trastuzumab (H) + chemotherapy (CT) for HER2-positive metastatic gastric or gastro-oesophageal junction cancer (mGC/GEJC): Final analysis of a Phase III study (JACOB).* Annals of Oncology, 2017. **28**(suppl_5).
70. Hecht, J.R., et al., *Lapatinib in Combination With Capecitabine Plus Oxaliplatin in Human Epidermal Growth Factor Receptor 2-Positive Advanced or Metastatic Gastric, Esophageal, or Gastroesophageal Adenocarcinoma: TRIO-013/LOGiC--A Randomized Phase III Trial.* J Clin Oncol, 2016. **34**(5): p. 443-51.
71. Satoh, T., et al., *Lapatinib plus paclitaxel versus paclitaxel alone in the second-line treatment of HER2-amplified advanced gastric cancer in Asian populations: TyTAN--a randomized, phase III study.* J Clin Oncol, 2014. **32**(19): p. 2039-49.
72. Waddell, T., et al., *Epirubicin, oxaliplatin, and capecitabine with or without panitumumab for patients with previously untreated advanced oesophagogastric cancer (REAL3): a randomised, open-label phase 3 trial.* Lancet Oncol, 2013. **14**(6): p. 481-9.
73. Dutton, S.J., et al., *Gefitinib for oesophageal cancer progressing after chemotherapy (COG): a phase 3, multicentre, double-blind, placebo-controlled randomised trial.* Lancet Oncol, 2014. **15**(8): p. 894-904.
74. Fuchs, C.S., et al., *Ramucirumab monotherapy for previously treated advanced gastric or gastro-oesophageal junction adenocarcinoma (REGARD): an international, randomised, multicentre, placebo-controlled, phase 3 trial.* The Lancet, 2014. **383**(9911): p. 31-39.
75. Fuchs, C.S., et al., *Biomarker analyses in REGARD gastric/GEJ carcinoma patients treated with VEGFR2-targeted antibody ramucirumab.* Br J Cancer, 2016. **115**(8): p. 974-982.
76. Shen, L., et al., *Bevacizumab plus capecitabine and cisplatin in Chinese patients with inoperable locally advanced or metastatic gastric or gastroesophageal junction cancer: randomized, double-blind, phase III study (AVATAR study).* Gastric Cancer, 2015. **18**(1): p. 168-76.
77. Lennerz, J.K., et al., *MET amplification identifies a small and aggressive subgroup of esophagogastric adenocarcinoma with evidence of responsiveness to crizotinib.* J Clin Oncol, 2011. **29**(36): p. 4803-10.
78. Catenacci, D.V.T., et al., *Rilotumumab plus epirubicin, cisplatin, and capecitabine as first-line therapy in advanced MET-positive gastric or gastro-oesophageal junction cancer (RILOMET-1): a randomised, double-blind, placebo-controlled, phase 3 trial.* Lancet Oncol, 2017. **18**(11): p. 1467-1482.
79. Shah, M.A., et al., *METGastric: A phase III study of onartuzumab plus mFOLFOX6 in patients with metastatic HER2-negative (HER2-) and MET-positive (MET+) adenocarcinoma of the stomach or gastroesophageal junction (GEC).* Journal of Clinical Oncology, 2015. **33**(15_suppl): p. 4012-4012.
80. Janjigian, Y.Y., et al., *CheckMate-032 Study: Efficacy and Safety of Nivolumab and Nivolumab Plus Ipilimumab in Patients With Metastatic Esophagogastric Cancer.* J Clin Oncol, 2018. **36**(28): p. 2836-2844.
81. Westerterp, M., et al., *Esophageal Cancer: CT, Endoscopic US, and FDG PET for Assessment of Response to Neoadjuvant Therapy—Systematic Review.* Radiology, 2005. **236**(3): p. 841-851.
82. Lynam-Lennon, N., et al., *Altered Mitochondrial Function and Energy Metabolism Is Associated with a Radioresistant Phenotype in Oesophageal Adenocarcinoma.* PLOS ONE, 2014. **9**(6): p. e100738.

83. Wachsberger, P., R. Burd, and A.P. Dicker, *Tumor response to ionizing radiation combined with antiangiogenesis or vascular targeting agents: exploring mechanisms of interaction.* Clin Cancer Res, 2003. **9**(6): p. 1957-71.
84. Kim, W., et al., *Inflammation-induced radioresistance is mediated by ROS-dependent inactivation of protein phosphatase 1 in non-small cell lung cancer cells.* Apoptosis, 2015. **20**(9): p. 1242-52.
85. Wang, H., et al., *Cancer radiosensitizers.* Trends in pharmacological sciences, 2018. **39**(1): p. 24-48.
86. Janssens, G.O., et al., *Accelerated radiotherapy with carbogen and nicotinamide for laryngeal cancer: results of a phase III randomized trial.* Journal of Clinical Oncology, 2012. **30**(15): p. 1777-1783.
87. Dische, S., et al., *A trial of Ro 03-8799 (pimonidazole) in carcinoma of the uterine cervix: an interim report from the Medical Research Council Working Party on advanced carcinoma of the cervix.* Radiotherapy and Oncology, 1993. **26**(2): p. 93-103.
88. Coleman, C.N., et al., *Final report of the phase I trial of the hypoxic cell radiosensitizer SR 2508 (etanidazole) Radiation Therapy Oncology Group 83-03.* International Journal of Radiation Oncology• Biology• Physics, 1990. **18**(2): p. 389-393.
89. Overgaard, J., et al., *Plasma osteopontin, hypoxia, and response to the hypoxia sensitiser nimorazole in radiotherapy of head and neck cancer: results from the DAHANCA 5 randomised double-blind placebo-controlled trial.* The lancet oncology, 2005. **6**(10): p. 757-764.
90. Overgaard, J., *Improving radiotherapy of squamous cell carcinoma of the head and neck (HNSCC) through a continuous process of biological based clinical trials− a 40-year experience from the Danish Head and Neck Cancer Group− DAHANCA.* European Journal of Cancer, 2017. **72**: p. S102.
91. Mistry, I.N., et al., *Clinical Advances of Hypoxia-Activated Prodrugs in Combination With Radiation Therapy.* International Journal of Radiation Oncology*Biology*Physics, 2017. **98**(5): p. 1183-1196.
92. Mierzwa, M.L., et al., *Recent advances in combined modality therapy.* Oncologist, 2010. **15**(4): p. 372-81.
93. Hanahan, D. and R.A. Weinberg, *The hallmarks of cancer.* Cell, 2000. **100**(1): p. 57-70.
94. Potente, M., H. Gerhardt, and P. Carmeliet, *Basic and Therapeutic Aspects of Angiogenesis.* Cell, 2011. **146**(6): p. 873-887.
95. Folkman, J. *Role of angiogenesis in tumor growth and metastasis*. in *Seminars in oncology*. 2002. Elsevier.
96. Ucuzian, A.A., et al., *Molecular mediators of angiogenesis.* Journal of burn care & research : official publication of the American Burn Association, 2010. **31**(1): p. 158-175.
97. Ribatti, D., et al., *The history of the angiogenic switch concept.* Leukemia, 2006. **21**: p. 44.
98. Bouck, N., V. Stellmach, and S.C. Hsu, *How tumors become angiogenic*, in *Advances in cancer research*. 1996, Elsevier. p. 135-174.
99. Bergers, G. and L.E. Benjamin, *Angiogenesis: tumorigenesis and the angiogenic switch.* Nature reviews cancer, 2003. **3**(6): p. 401.
100. Bejarano, M.T. and J.R. Merchan, *Targeting tumor vasculature through oncolytic virotherapy: recent advances.* Oncolytic virotherapy, 2015. **4**: p. 169.
101. Kerbel, R.S., *Tumor angiogenesis: past, present and the near future.* Carcinogenesis, 2000. **21**(3): p. 505-515.
102. Carmeliet, P., *Developmental biology: controlling the cellular brakes.* Nature, 1999. **401**(6754): p. 657.
103. Carmeliet, P. and R.K. Jain, *Angiogenesis in cancer and other diseases.* nature, 2000. **407**(6801): p. 249.
104. Huang, Y., et al., *Vascular normalization as an emerging strategy to enhance cancer immunotherapy.* Cancer research, 2013. **73**(10): p. 2943-2948.

105. Schmidt, B., et al., *Combining Bevacizumab with Radiation or Chemoradiation for Solid Tumors: A Review of the Scientific Rationale, and Clinical Trials.* Current angiogenesis, 2012. **1**(3): p. 169-179.
106. Scappaticci, F.A., *Mechanisms and future directions for angiogenesis-based cancer therapies.* Journal of Clinical Oncology, 2002. **20**(18): p. 3906-3927.
107. Hoang, T., et al., *Enhancement of radiation response with bevacizumab.* Journal of Experimental & Clinical Cancer Research : CR, 2012. **31**(1): p. 37-37.
108. Jain, R.K., *Normalization of tumor vasculature: an emerging concept in antiangiogenic therapy.* Science, 2005. **307**(5706): p. 58-62.
109. Lee, C.G., et al., *Anti-Vascular endothelial growth factor treatment augments tumor radiation response under normoxic or hypoxic conditions.* Cancer Res, 2000. **60**(19): p. 5565-70.
110. Winkler, F., et al., *Kinetics of vascular normalization by VEGFR2 blockade governs brain tumor response to radiation: role of oxygenation, angiopoietin-1, and matrix metalloproteinases.* Cancer cell, 2004. **6**(6): p. 553-563.
111. Fraisl, P., et al., *Regulation of angiogenesis by oxygen and metabolism.* Developmental cell, 2009. **16**(2): p. 167-179.
112. Hagberg, C.E., et al., *Vascular endothelial growth factor B controls endothelial fatty acid uptake.* Nature, 2010. **464**(7290): p. 917.
113. Hsu, P.P. and D.M. Sabatini, *Cancer Cell Metabolism: Warburg and Beyond.* Cell, 2008. **134**(5): p. 703-707.
114. Gatenby, R.A. and R.J. Gillies, *Why do cancers have high aerobic glycolysis?* Nat Rev Cancer, 2004. **4**(11): p. 891-9.
115. Devlin, T.M., *Textbook of biochemistry*. 2011: John Wiley & Sons.
116. Devlin, T.M., *Textbook of biochemistry: with clinical correlations.* 2006.
117. Levine, A.J. and A.M. Puzio-Kuter, *The control of the metabolic switch in cancers by oncogenes and tumor suppressor genes.* Science, 2010. **330**(6009): p. 1340-4.
118. Hanahan, D. and R.A. Weinberg, *Hallmarks of cancer: the next generation.* Cell, 2011. **144**(5): p. 646-74.
119. Warburg, O., *On the origin of cancer cells.* Science, 1956. **123**(3191): p. 309-14.
120. Lunt, S.Y. and M.G. Vander Heiden, *Aerobic glycolysis: meeting the metabolic requirements of cell proliferation.* Annu Rev Cell Dev Biol, 2011. **27**: p. 441-64.
121. Tan, A.S., et al., *Mitochondrial genome acquisition restores respiratory function and tumorigenic potential of cancer cells without mitochondrial DNA.* Cell metabolism, 2015. **21**(1): p. 81-94.
122. Pavlova, Natalya N. and Craig B. Thompson, *The Emerging Hallmarks of Cancer Metabolism.* Cell Metabolism, 2016. **23**(1): p. 27-47.
123. Viale, A., et al., *Oncogene ablation-resistant pancreatic cancer cells depend on mitochondrial function.* Nature, 2014. **514**(7524): p. 628-632.
124. Fiorillo, M., et al., *Repurposing atovaquone: targeting mitochondrial complex III and OXPHOS to eradicate cancer stem cells.* Oncotarget, 2016. **7**(23): p. 34084-34099.
125. LeBleu, V.S., et al., *PGC-1α mediates mitochondrial biogenesis and oxidative phosphorylation in cancer cells to promote metastasis.* Nature cell biology, 2014. **16**(10): p. 992-15.
126. Balkwill, F. and A. Mantovani, *Inflammation and cancer: back to Virchow?* Lancet, 2001. **357**(9255): p. 539-45.
127. Grivennikov, S.I. and M. Karin, *Inflammation and oncogenesis: a vicious connection.* Current opinion in genetics & development, 2010. **20**(1): p. 65.
128. Talmor, M., et al., *Generation or large numbers of immature and mature dendritic cells from rat bone marrow cultures.* Eur J Immunol, 1998. **28**(3): p. 811-7.
129. Allavena, P., et al., *The chemokine receptor switch paradigm and dendritic cell migration: its significance in tumor tissues.* Immunol Rev, 2000. **177**: p. 141-9.
130. Schoppmann, S.F., et al., *Tumor-associated macrophages express lymphatic endothelial growth factors and are related to peritumoral lymphangiogenesis.* Am J Pathol, 2002. **161**(3): p. 947-56.

131. Brigati, C., et al., *Tumors and inflammatory infiltrates: friends or foes?* Clin Exp Metastasis, 2002. **19**(3): p. 247-58.
132. Kumari, N., et al., *Role of interleukin-6 in cancer progression and therapeutic resistance.* Tumor Biology, 2016. **37**(9): p. 11553-11572.
133. Aarden, L., et al., *Differential induction of interleukin-6 production in monocytes, endothelial cells and smooth muscle cells.* European cytokine network, 1991. **2**(2): p. 115-120.
134. Eustace, D., et al., *Interleukin-6 (IL-6) functions as an autocrine growth factor in cervical carcinomas in vitro.* Gynecologic oncology, 1993. **50**(1): p. 15-19.
135. Dvorakova, K., et al., *Increased expression and secretion of interleukin-6 in patients with Barrett's esophagus.* Clinical Cancer Research, 2004. **10**(6): p. 2020-2028.
136. Qiao, Y., et al., *IL6 derived from cancer-associated fibroblasts promotes chemoresistance via CXCR7 in esophageal squamous cell carcinoma.* Oncogene, 2018. **37**(7): p. 873-883.
137. Waugh, D.J. and C. Wilson, *The interleukin-8 pathway in cancer.* Clinical cancer research, 2008. **14**(21): p. 6735-6741.
138. Collins, T.S., L.-F. Lee, and J.P.-Y. Ting, *Paclitaxel up-regulates interleukin-8 synthesis in human lung carcinoma through an NF-κB-and AP-1-dependent mechanism.* Cancer Immunology, Immunotherapy, 2000. **49**(2): p. 78-84.
139. Knall, C., G.S. Worthen, and G.L. Johnson, *Interleukin 8-stimulated phosphatidylinositol-3-kinase activity regulates the migration of human neutrophils independent of extracellular signal-regulated kinase and p38 mitogen-activated protein kinases.* Proceedings of the National Academy of Sciences, 1997. **94**(7): p. 3052-3057.
140. Peng, C.Y., et al., *Let-7c restores radiosensitivity and chemosensitivity and impairs stemness in oral cancer cells through inhibiting interleukin-8.* J Oral Pathol Med, 2018. **47**(6): p. 590-597.
141. Wang, X. and Y. Lin, *Tumor necrosis factor and cancer, buddies or foes?* Acta pharmacologica Sinica, 2008. **29**(11): p. 1275-1288.
142. Chen, M.-F., et al., *Role of interleukin 1 beta in esophageal squamous cell carcinoma.* Journal of Molecular Medicine, 2012. **90**(1): p. 89-100.
143. Li, Y., et al., *IL-1β promotes stemness and invasiveness of colon cancer cells through Zeb1 activation.* Molecular Cancer, 2012. **11**(1): p. 87.
144. Mantovani, A., I. Barajon, and C. Garlanda, *IL-1 and IL-1 regulatory pathways in cancer progression and therapy.* Immunological reviews, 2018. **281**(1): p. 57-61.
145. Maity, A., W.G. McKenna, and R.J. Muschel, *The molecular basis for cell cycle delays following ionizing radiation: a review.* Radiotherapy and Oncology, 1994. **31**(1): p. 1-13.
146. Maciejewski, B., et al., *Importance of tumor size and repopulation for radiocurability of skin cancer.* Neoplasma, 1993. **40**(1): p. 51-54.
147. Shimura, T., *Acquired radioresistance of cancer and the AKT/GSK3β/cyclin D1 overexpression cycle.* Journal of radiation research, 2011. **52**(5): p. 539-544.
148. Wilson, W.R. and M.P. Hay, *Targeting hypoxia in cancer therapy.* Nat Rev Cancer, 2011. **11**(6): p. 393-410.
149. Igney, F.H. and P.H. Krammer, *Death and anti-death: tumour resistance to apoptosis.* Nat Rev Cancer, 2002. **2**(4): p. 277-88.
150. Lynam-Lennon, N., et al., *Alterations in DNA repair efficiency are involved in the radioresistance of esophageal adenocarcinoma.* Radiat Res, 2010. **174**(6): p. 703-11.
151. Chakravarty, T., et al., *Intensity-modulated radiation therapy with concurrent chemotherapy as preoperative treatment for localized gastric adenocarcinoma.* Int J Radiat Oncol Biol Phys, 2012. **83**(2): p. 581-6.
152. Gerard, J.P., et al., *Preoperative radiotherapy with or without concurrent fluorouracil and leucovorin in T3-4 rectal cancers: results of FFCD 9203.* J Clin Oncol, 2006. **24**(28): p. 4620-5.
153. Schaue, D. and W.H. McBride, *Counteracting tumor radioresistance by targeting DNA repair.* Mol Cancer Ther, 2005. **4**(10): p. 1548-50.

154. Jackson, S.P. and J. Bartek, *The DNA-damage response in human biology and disease.* Nature, 2009. **461**(7267): p. 1071.
155. Helleday, T., et al., *DNA repair pathways as targets for cancer therapy.* Nature Reviews Cancer, 2008. **8**(3): p. 193.
156. Pires, I.M., et al., *Targeting radiation-resistant hypoxic tumour cells through ATR inhibition.* Br J Cancer, 2012. **107**(2): p. 291-9.
157. Leszczynska, K.B., et al., *Preclinical testing of an Atr inhibitor demonstrates improved response to standard therapies for esophageal cancer.* Radiother Oncol, 2016. **121**(2): p. 232-238.
158. Fokas, E., et al., *Targeting ATR in vivo using the novel inhibitor VE-822 results in selective sensitization of pancreatic tumors to radiation.* Cell death & disease, 2012. **3**(12): p. e441.
159. *Phase I Study to Assess Safety of AZD6738 Alone and in Combination With Radiotherapy in Patients With Solid Tumours (Patriot).*
160. Lin, C., et al., *Combination of quercetin with radiotherapy enhances tumor radiosensitivity in vitro and in vivo.* Radiother Oncol, 2012. **104**(3): p. 395-400.
161. Javle, M. and N.J. Curtin, *The role of PARP in DNA repair and its therapeutic exploitation.* Br J Cancer, 2011. **105**(8): p. 1114-22.
162. Beck, C., et al., *Poly(ADP-ribose) polymerases in double-strand break repair: focus on PARP1, PARP2 and PARP3.* Exp Cell Res, 2014. **329**(1): p. 18-25.
163. Poggio, F., et al., *Single-agent PARP inhibitors for the treatment of patients with BRCA-mutated HER2-negative metastatic breast cancer: a systematic review and meta-analysis.* ESMO Open, 2018. **3**(4): p. e000361.
164. Haince, J.F., et al., *PARP1-dependent kinetics of recruitment of MRE11 and NBS1 proteins to multiple DNA damage sites.* J Biol Chem, 2008. **283**(2): p. 1197-208.
165. Guillot, C., et al., *PARP inhibition and the radiosensitizing effects of the PARP inhibitor ABT-888 in in vitro hepatocellular carcinoma models.* BMC Cancer, 2014. **14**: p. 603.
166. Miura, K., et al., *The combination of olaparib and camptothecin for effective radiosensitization.* Radiat Oncol, 2012. **7**: p. 62.
167. Komaki, R., et al., *Phase I study of irinotecan and concurrent radiation therapy for upper GI tumors.* Oncology (Williston Park), 2000. **14**(12 Suppl 14): p. 34-7.
168. *Neoadjuvant Chemoradiotherapy With CRLX-101 and Capecitabine for Rectal Cancer.*
169. Porcelli, L., et al., *Optimize radiochemotherapy in pancreatic cancer: PARP inhibitors a new therapeutic opportunity.* Mol Oncol, 2013. **7**(3): p. 308-22.
170. Hastak, K., et al., *Poly (ADP-ribose) polymerase inhibitor, an effective radiosensitizer in lung and pancreatic cancers.* Oncotarget, 2017. **8**(16): p. 26344-26355.
171. Lohse, I., et al., *Effects of Combined Treatment with Ionizing Radiation and the PARP Inhibitor Olaparib in BRCA Mutant and Wild Type Patient-Derived Pancreatic Cancer Xenografts.* PLoS ONE, 2016. **11**(12): p. e0167272.
172. *Radiotherapy & Olaparib in COmbination for Carcinoma of the Oesophagus (ROCOCO).*
173. Collis, S.J., et al., *The life and death of DNA-PK.* Oncogene, 2005. **24**(6): p. 949.
174. Li, Y.H., et al., *Inhibition of non-homologous end joining repair impairs pancreatic cancer growth and enhances radiation response.* PLoS One, 2012. **7**(6): p. e39588.
175. Sun, X., et al., *Identification and characterization of a small inhibitory peptide that can target DNA-PKcs autophosphorylation and increase tumor radiosensitivity.* Int J Radiat Oncol Biol Phys, 2012. **84**(5): p. 1212-9.
176. Zhao, Y., et al., *Preclinical evaluation of a potent novel DNA-dependent protein kinase inhibitor NU7441.* Cancer Res, 2006. **66**(10): p. 5354-62.
177. Van Triest, B., et al., *A phase Ia/Ib trial of the DNA-PK inhibitor M3814 in combination with radiotherapy (RT) in patients (pts) with advanced solid tumors: Dose-escalation results*. Vol. 36. 2018. 2518-2518.

178. Stachelek, G.C., et al., *YU238259 Is a Novel Inhibitor of Homology-Dependent DNA Repair That Exhibits Synthetic Lethality and Radiosensitization in Repair-Deficient Tumors.* Mol Cancer Res, 2015. **13**(10): p. 1389-97.
179. Pilié, P.G., et al., *State-of-the-art strategies for targeting the DNA damage response in cancer.* Nature Reviews Clinical Oncology, 2019. **16**(2): p. 81-104.
180. Estrada-Bernal, A., et al., *MEK inhibitor GSK1120212-mediated radiosensitization of pancreatic cancer cells involves inhibition of DNA double-strand break repair pathways.* Cell Cycle, 2015. **14**(23): p. 3713-24.
181. Shoji, M., et al., *Valproic acid, a histone deacetylase inhibitor, enhances radiosensitivity in esophageal squamous cell carcinoma.* Int J Oncol, 2012. **40**(6): p. 2140-6.
182. Makita, N., et al., *Inhibitory effects of valproic acid in DNA double-strand break repair after irradiation in esophageal squamous carcinoma cells.* Oncol Rep, 2015. **34**(3): p. 1185-92.
183. Williams, T.M., et al., *Abstract CT088: A phase I trial combining MEK-1/2 inhibition in combination with 5-fluorouracil and radiation for locally-advanced rectal adenocarcinoma*. 2017, AACR.
184. O'Neil, B.H., et al., *A phase I study of bortezomib in combination with standard 5-fluorouracil and external-beam radiation therapy for the treatment of locally advanced or metastatic rectal cancer.* Clin Colorectal Cancer, 2010. **9**(2): p. 119-25.
185. Kleiman, L.B., et al., *Comparative analysis of radiosensitizers for K-RAS mutant rectal cancers.* PLoS One, 2013. **8**(12): p. e82982.
186. Tao, Y., et al., *Radiosensitization by Chir-124, a selective CHK1 inhibitor: effects of p53 and cell cycle checkpoints.* Cell Cycle, 2009. **8**(8): p. 1196-205.
187. Morgan, M.A., et al., *Mechanism of radiosensitization by the Chk1/2 inhibitor AZD7762 involves abrogation of the G2 checkpoint and inhibition of homologous recombinational DNA repair.* Cancer Res, 2010. **70**(12): p. 4972-81.
188. Mitchell, J.B., et al., *In Vitro and In Vivo Radiation Sensitization of Human Tumor Cells by a Novel Checkpoint Kinase Inhibitor, AZD7762.* Clinical cancer research : an official journal of the American Association for Cancer Research, 2010. **16**(7): p. 2076-2084.
189. Kausar, T., et al., *Sensitization of Pancreatic Cancers to Gemcitabine Chemoradiation by WEE1 Kinase Inhibition Depends on Homologous Recombination Repair.* Neoplasia, 2015. **17**(10): p. 757-66.
190. Geenen, J.J. and J.H. Schellens, *Molecular pathways: targeting the protein kinase Wee1 in cancer.* Clinical Cancer Research, 2017. **23**(16): p. 4540-4544.
191. Karnak, D., et al., *Combined inhibition of Wee1 and PARP1/2 for radiosensitization in pancreatic cancer.* Clinical cancer research : an official journal of the American Association for Cancer Research, 2014. **20**(19): p. 5085-5096.
192. Lu, W., et al., *Telomeres-structure, function, and regulation.* Exp Cell Res, 2013. **319**(2): p. 133-41.
193. Goytisolo, F.A., et al., *Short telomeres result in organismal hypersensitivity to ionizing radiation in mammals.* J Exp Med, 2000. **192**(11): p. 1625-36.
194. Wong, K.K., et al., *Telomere dysfunction impairs DNA repair and enhances sensitivity to ionizing radiation.* Nat Genet, 2000. **26**(1): p. 85-8.
195. Chen, X., et al., *Zidovudine, abacavir and lamivudine increase the radiosensitivity of human esophageal squamous cancer cell lines.* Oncol Rep, 2016. **36**(1): p. 239-46.
196. Leeansyah, E., et al., *Inhibition of telomerase activity by human immunodeficiency virus (HIV) nucleos(t)ide reverse transcriptase inhibitors: a potential factor contributing to HIV-associated accelerated aging.* J Infect Dis, 2013. **207**(7): p. 1157-65.
197. Wu, X., et al., *Telomerase antagonist imetelstat increases radiation sensitivity in esophageal squamous cell carcinoma.* Oncotarget, 2017. **8**(8): p. 13600-13619.
198. Wang, Y., et al., *Radiosensitization to X-ray radiation by telomerase inhibitor MST-312 in human hepatoma HepG2 cells.* Life Sci, 2015. **123**: p. 43-50.

199. Berardinelli, F., et al., *Targeting telomerase and telomeres to enhance ionizing radiation effects in in vitro and in vivo cancer models.* Mutation Research/Reviews in Mutation Research, 2017. **773**: p. 204-219.
200. Hauguel, T. and F. Bunz, *Haploinsufficiency of hTERT leads to telomere dysfunction and radiosensitivity in human cancer cells.* Cancer Biol Ther, 2003. **2**(6): p. 679-84.
201. Toulany, M. and H.P. Rodemann, *Phosphatidylinositol 3-kinase/Akt signaling as a key mediator of tumor cell responsiveness to radiation.* Semin Cancer Biol, 2015. **35**: p. 180-90.
202. Park, J.H., et al., *Radiosensitization of the PI3K inhibitor HS-173 through reduction of DNA damage repair in pancreatic cancer.* Oncotarget, 2017. **8**(68): p. 112893-112906.
203. Pal, I., et al., *Cooperative effect of BI-69A11 and celecoxib enhances radiosensitization by modulating DNA damage repair in colon carcinoma.* Tumour Biol, 2016. **37**(5): p. 6389-402.
204. Mardjuadi, F.I., et al., *Panitumumab as a radiosensitizing agent in KRAS wild-type locally advanced rectal cancer.* Target Oncol, 2015. **10**(3): p. 375-83.
205. Machiels, J.P., et al., *Phase I/II study of preoperative cetuximab, capecitabine, and external beam radiotherapy in patients with rectal cancer.* Ann Oncol, 2007. **18**(4): p. 738-44.
206. Helbling, D., et al., *Neoadjuvant chemoradiotherapy with or without panitumumab in patients with wild-type KRAS, locally advanced rectal cancer (LARC): a randomized, multicenter, phase II trial SAKK 41/07.* Ann Oncol, 2013. **24**(3): p. 718-25.
207. Rodel, C., et al., *Phase I-II trial of cetuximab, capecitabine, oxaliplatin, and radiotherapy as preoperative treatment in rectal cancer.* Int J Radiat Oncol Biol Phys, 2008. **70**(4): p. 1081-6.
208. Merx, K., et al., *Panitumumab in Combination With Preoperative Radiation Therapy in Patients With Locally Advanced RAS Wild-type Rectal Cancer: Results of the Multicenter Explorative Single-Arm Phase 2 Study NEORIT.* Int J Radiat Oncol Biol Phys, 2017. **99**(4): p. 867-875.
209. Simone, V., et al., *Targeting Angiogenesis in Biliary Tract Cancers: An Open Option.* International Journal of Molecular Sciences, 2017. **18**(2): p. 418.
210. Ciric, E. and G. Sersa, *Radiotherapy in combination with vascular-targeted therapies.* Radiol Oncol, 2010. **44**(2): p. 67-78.
211. Zhu, H., et al., *Recombinant human endostatin enhances the radioresponse in esophageal squamous cell carcinoma by normalizing tumor vasculature and reducing hypoxia.* Sci Rep, 2015. **5**: p. 14503.
212. Teicher, B.A., et al., *Potentiation of cytotoxic cancer therapies by TNP-470 alone and with other anti-angiogenic agents.* Int J Cancer, 1994. **57**(6): p. 920-5.
213. Park, H.J., et al., *Radiation-induced vascular damage in tumors: implications of vascular damage in ablative hypofractionated radiotherapy (SBRT and SRS).* Radiat Res, 2012. **177**(3): p. 311-27.
214. Cao, N., et al., *Monitoring the Effects of Anti-angiogenesis on the Radiation Sensitivity of Pancreatic Cancer Xenografts Using Dynamic Contrast-Enhanced CT.* International journal of radiation oncology, biology, physics, 2014. **88**(2): p. 412-418.
215. Wen, X., et al., *Down-regulation of XIAP enhances the radiosensitivity of esophageal cancer cells in vivo and in vitro.* Bioscience Reports, 2017. **37**(5): p. BSR20170711.
216. Park, M., et al., *MiR-338-5p enhances the radiosensitivity of esophageal squamous cell carcinoma by inducing apoptosis through targeting survivin.* Scientific Reports, 2017. **7**(1): p. 10932.
217. Morales, D.R. and A.D. Morris, *Metformin in cancer treatment and prevention.* Annu Rev Med, 2015. **66**: p. 17-29.
218. Feng, T., et al., *Metformin enhances radiation response of ECa109 cells through activation of ATM and AMPK.* Biomed Pharmacother, 2015. **69**: p. 260-6.
219. Jeong, Y.K., et al., *Metformin Radiosensitizes p53-Deficient Colorectal Cancer Cells through Induction of G2/M Arrest and Inhibition of DNA Repair Proteins.* PLoS One, 2015. **10**(11): p. e0143596.

220. Jin, H., et al., *Re-sensitization of radiation resistant colorectal cancer cells to radiation through inhibition of AMPK pathway.* Oncol Lett, 2016. **11**(5): p. 3197-3201.
221. Fasih, A., et al., *Radiosensitization of pancreatic cancer cells by metformin through the AMPK pathway.* Radiat Res, 2014. **182**(1): p. 50-9.
222. Liu, J., et al., *Enhanced cytotoxic effect of low doses of metformin combined with ionizing radiation on hepatoma cells via ATP deprivation and inhibition of DNA repair.* Oncol Rep, 2012. **28**(4): p. 1406-12.
223. Cheng, G., et al., *Mitochondria-Targeted Analogues of Metformin Exhibit Enhanced Antiproliferative and Radiosensitizing Effects in Pancreatic Cancer Cells.* Cancer Res, 2016. **76**(13): p. 3904-15.
224. Elbaz, H.A., et al., *Epicatechin stimulates mitochondrial activity and selectively sensitizes cancer cells to radiation.* PLoS One, 2014. **9**(2): p. e88322.
225. Song, C.W., et al., *Metformin kills and radiosensitizes cancer cells and preferentially kills cancer stem cells.* Scientific reports, 2012. **2**: p. 362.
226. Jeong, Y.K., et al., *Metformin Radiosensitizes p53-Deficient Colorectal Cancer Cells through Induction of G2/M Arrest and Inhibition of DNA Repair Proteins.* PLoS ONE, 2015. **10**(11): p. e0143596.
227. Jin, H., et al., *Re-sensitization of radiation resistant colorectal cancer cells to radiation through inhibition of AMPK pathway.* Oncology Letters, 2016. **11**(5): p. 3197-3201.
228. Liu, S.-C., et al., *Leukemia inhibitory factor promotes nasopharyngeal carcinoma progression and radioresistance.* The Journal of Clinical Investigation, 2013. **123**(12): p. 5269-5283.
229. Benej, M., et al., *Papaverine and its derivatives radiosensitize solid tumors by inhibiting mitochondrial metabolism.* Proceedings of the National Academy of Sciences, 2018. **115**(42): p. 10756-10761.
230. Bost, F., et al., *Energy disruptors: rising stars in anticancer therapy?* Oncogenesis, 2016. **5**: p. e188.
231. Van De Voorde, L., et al., *Can metformin improve 'the tomorrow' of patients treated for oesophageal cancer?* Eur J Surg Oncol, 2015. **41**(10): p. 1333-9.
232. Coleman, M.C., et al., *2-Deoxy-d-glucose causes cytotoxicity, oxidative stress, and radiosensitization in pancreatic cancer.* Free Radical Biology and Medicine, 2008. **44**(3): p. 322-331.
233. Multhoff, G. and J. Radons, *Radiation, Inflammation, and Immune Responses in Cancer.* Frontiers in Oncology, 2012. **2**(58).
234. Maher, S.G., et al., *Serum proteomic profiling reveals that pretreatment complement protein levels are predictive of esophageal cancer patient response to neoadjuvant chemoradiation.* Ann Surg, 2011. **254**(5): p. 809-16; discussion 816-7.
235. Buckley, A.M., et al., *Leukaemia inhibitory factor is associated with treatment resistance in oesophageal adenocarcinoma.* Oncotarget, 2018. **9**(72): p. 33634.
236. Chen, M.-F., et al., *IL-6 expression predicts treatment response and outcome in squamous cell carcinoma of the esophagus.* Molecular Cancer, 2013. **12**: p. 26-26.
237. Brown, J.M., *Exploiting the hypoxic cancer cell: mechanisms and therapeutic strategies.* Mol Med Today, 2000. **6**(4): p. 157-62.
238. Dewhirst, M.W., Y. Cao, and B. Moeller, *Cycling hypoxia and free radicals regulate angiogenesis and radiotherapy response.* Nature reviews. Cancer, 2008. **8**(6): p. 425-437.
239. Yasui, H., et al., *Inhibition of HIF-1alpha by the anticancer drug TAS106 enhances X-ray-induced apoptosis in vitro and in vivo.* Br J Cancer, 2008. **99**(9): p. 1442-52.
240. Wardman, P., *Chemical radiosensitizers for use in radiotherapy.* Clin Oncol (R Coll Radiol), 2007. **19**(6): p. 397-417.
241. Bonnet, M., et al., *Next-Generation Hypoxic Cell Radiosensitizers: Nitroimidazole Alkylsulfonamides.* J Med Chem, 2018. **61**(3): p. 1241-1254.
242. Schwartz, D.L., et al., *Radiosensitization and Stromal Imaging Response Correlates for the HIF-1 Inhibitor PX-478 Given with or without Chemotherapy in Pancreatic Cancer.* Molecular cancer therapeutics, 2010. **9**(7): p. 2057-2067.

243. Seyfried, T.N. and L.C. Huysentruyt, *On the Origin of Cancer Metastasis.* Critical reviews in oncogenesis, 2013. **18**(1-2): p. 43-73.
244. Hay, E.D., *The mesenchymal cell, its role in the embryo, and the remarkable signaling mechanisms that create it.* Dev Dyn, 2005. **233**(3): p. 706-20.
245. Josson, S., et al., *Tumor-Stromal Interactions Influence Radiation Sensitivity in Epithelial- versus Mesenchymal-Like Prostate Cancer Cells.* J Oncol, 2010. **2010**.
246. Choi, Y.-J., et al., *Smad2/3-Regulated Expression of DLX2 Is Associated with Radiation-Induced Epithelial-Mesenchymal Transition and Radioresistance of A549 and MDA-MB-231 Human Cancer Cell Lines.* PLoS ONE, 2016. **11**(1): p. e0147343.
247. Su, H., et al., *FH535 increases the radiosensitivity and reverses epithelial-to-mesenchymal transition of radioresistant esophageal cancer cell line KYSE-150R.* Journal of Translational Medicine, 2015. **13**: p. 104.
248. Fernandez, Y., et al., *Bcl-xL promotes metastasis of breast cancer cells by induction of cytokines resistance.* Cell Death Differ, 2000. **7**(4): p. 350-9.
249. Yang, J., et al., *Adenovirus-mediated siRNA targeting Bcl-xL inhibits proliferation, reduces invasion and enhances radiosensitivity of human colorectal cancer cells.* World Journal of Surgical Oncology, 2011. **9**: p. 117-117.
250. Tang, C., et al., *Combining Radiation and Immunotherapy: A New Systemic Therapy for Solid tumors?* Cancer immunology research, 2014. **2**(9): p. 831-838.
251. Azad, A., et al., *PD-L1 blockade enhances response of pancreatic ductal adenocarcinoma to radiotherapy.* EMBO Mol Med, 2017. **9**(2): p. 167-180.
252. Sharabi, A.B., et al., *Radiation and checkpoint blockade immunotherapy: radiosensitisation and potential mechanisms of synergy.* The Lancet Oncology, 2015. **16**(13): p. e498-e509.
253. Kim, K.W., et al., *Direct injection of immature dendritic cells into irradiated tumor induces efficient antitumor immunity.* Int J Cancer, 2004. **109**(5): p. 685-90.
254. Son, C.H., et al., *CTLA-4 blockade enhances antitumor immunity of intratumoral injection of immature dendritic cells into irradiated tumor in a mouse colon cancer model.* J Immunother, 2014. **37**(1): p. 1-7.
255. Dewan, M.Z., et al., *Fractionated but not single dose radiotherapy induces an immune-mediated abscopal effect when combined with anti-CTLA-4 antibody.* Clinical cancer research : an official journal of the American Association for Cancer Research, 2009. **15**(17): p. 5379-5388.
256. Welsh, J.W., et al., *Phase 2 5-Arm Trial of Ipilimumab Plus Lung or Liver Stereotactic Radiation for Patients with Advanced Malignancies.* International Journal of Radiation Oncology • Biology • Physics, 2017. **99**(5): p. 1315.
257. *Adoptive Cellular Therapy and Radiation Therapy After Surgery in Treating Patients With Esophageal Cancer.*
258. *Concurrent Chemoradiation With or Without DC-CIK Immunotherapy in Treating Locally Advanced Esophageal Cancer.*
259. *Pembrolizumab With Locally Delivered Radiation Therapy for the Treatment of Metastatic Esophageal Cancers.*
260. *Pembrolizumab and Palliative Radiation Therapy in Treating Patients With Metastatic Esophagus, Stomach, or Gastroesophageal Junction Cancer.*
261. *Study of Anti-PD-L1 in Combination With Chemo(Radio)Therapy for Oesophageal Cancer.*
262. Adams, R.H. and K. Alitalo, *Molecular regulation of angiogenesis and lymphangiogenesis.* Nat Rev Mol Cell Biol, 2007. **8**(6): p. 464-78.
263. Carmeliet, P. and R.K. Jain, *Molecular mechanisms and clinical applications of angiogenesis.* Nature, 2011. **473**(7347): p. 298-307.
264. Ferrara, N. and R.S. Kerbel, *Angiogenesis as a therapeutic target.* Nature, 2005. **438**(7070): p. 967-74.
265. Williams, K.J., et al., *Inhibition of vascular endothelial growth factor signalling using cediranib (RECENTINTM; AZD2171) enhances radiation response and causes*

substantial physiological changes in lung tumour xenografts. The British Journal of Radiology, 2008. **81**(special_issue_1): p. S21-S27.
266. Ward, P.S. and C.B. Thompson, *Metabolic reprogramming: a cancer hallmark even warburg did not anticipate.* Cancer Cell, 2012. **21**(3): p. 297-308.
267. Zon, L.I. and R.T. Peterson, *In vivo drug discovery in the zebrafish.* Nat Rev Drug Discov, 2005. **4**(1): p. 35-44.
268. Rubinstein, A.L., *Zebrafish assays for drug toxicity screening.* Expert Opin Drug Metab Toxicol, 2006. **2**(2): p. 231-40.
269. Taylor, K.L., et al., *Small molecule screening in zebrafish: an in vivo approach to identifying new chemical tools and drug leads.* Cell Commun Signal, 2010. **8**: p. 11.
270. Williams, C.H. and C.C. Hong, *Zebrafish small molecule screens: Taking the phenotypic plunge.* Computational and structural biotechnology journal, 2016. **14**: p. 350-356.
271. Schoors, S., et al., *Partial and transient reduction of glycolysis by PFKFB3 blockade reduces pathological angiogenesis.* Cell Metab, 2014. **19**(1): p. 37-48.
272. Murphy, A.G., et al., *Preclinical validation of the small molecule drug quininib as a novel therapeutic for colorectal cancer.* Scientific Reports, 2016. **6**: p. 34523.
273. MacRae, C.A. and R.T. Peterson, *Zebrafish as tools for drug discovery.* Nat Rev Drug Discov, 2015. **14**(10): p. 721-31.
274. Lawson, N.D. and B.M. Weinstein, *In vivo imaging of embryonic vascular development using transgenic zebrafish.* Dev Biol, 2002. **248**(2): p. 307-18.
275. Stoletov, K., et al., *High-resolution imaging of the dynamic tumor cell vascular interface in transparent zebrafish.* Proc Natl Acad Sci U S A, 2007. **104**(44): p. 17406-11.
276. Seth, A., D.L. Stemple, and I. Barroso, *The emerging use of zebrafish to model metabolic disease.* Disease Models & Mechanisms, 2013. **6**(5): p. 1080-1088.
277. Santoro, M.M., *Zebrafish as a model to explore cell metabolism.* Trends in Endocrinology & Metabolism, 2014. **25**(10): p. 546-554.
278. Gibert, Y., S.L. McGee, and A.C. Ward, *Metabolic profile analysis of zebrafish embryos.* J Vis Exp, 2013(71): p. e4300.
279. Galvin, O., et al., *A sustained release formulation of novel quininib-hyaluronan microneedles inhibits angiogenesis and retinal vascular permeability in vivo.* Journal of Controlled Release, 2016. **233**: p. 198-207.
280. Alvarez, Y., et al., *Selective Inhibition of Retinal Angiogenesis by Targeting PI3 Kinase.* PLoS ONE, 2009. **4**(11): p. e7867.
281. Kimmel, C.B., et al., *Stages of embryonic development of the zebrafish.* Dev Dyn, 1995. **203**(3): p. 253-310.
282. Reynolds, A.L., et al., *Phenotype-based Discovery of 2-[(E)-2-(Quinolin-2-yl)vinyl]phenol as a Novel Regulator of Ocular Angiogenesis.* J Biol Chem, 2016. **291**(14): p. 7242-55.
283. Chimote, G., et al., *Comparison of effects of anti-angiogenic agents in the zebrafish efficacy–toxicity model for translational anti-angiogenic drug discovery.* Drug Design, Development and Therapy, 2014. **8**: p. 1107-1123.
284. Kumar, M.G., et al., *Altered Glycolysis and Mitochondrial Respiration in a Zebrafish Model of Dravet Syndrome.* eNeuro, 2016. **3**(2): p. ENEURO.0008-16.2016.
285. Buckley, A.M., et al., *Pyrazinib (P3), [(E)-2-(2-Pyrazin-2-yl-vinyl)-phenol], a small molecule pyrazine compound enhances radiosensitivity in oesophageal adenocarcinoma.* Cancer Letters, 2019. **447**: p. 115-129.
286. Zheng, J.I.E., *Energy metabolism of cancer: Glycolysis versus oxidative phosphorylation (Review).* Oncology Letters, 2012. **4**(6): p. 1151-1157.
287. Zu, X.L. and M. Guppy, *Cancer metabolism: facts, fantasy, and fiction.* Biochem Biophys Res Commun, 2004. **313**(3): p. 459-65.
288. Kim, S.Y., *Cancer Energy Metabolism: Shutting Power off Cancer Factory.* Biomol Ther (Seoul), 2018. **26**(1): p. 39-44.

289. Yoshida, G.J., *Metabolic reprogramming: the emerging concept and associated therapeutic strategies.* J Exp Clin Cancer Res, 2015. **34**: p. 111.
290. Pavlides, S., et al., *The reverse Warburg effect: aerobic glycolysis in cancer associated fibroblasts and the tumor stroma.* Cell Cycle, 2009. **8**(23): p. 3984-4001.
291. Martinez-Outschoorn, U.E., et al., *Oxidative stress in cancer associated fibroblasts drives tumor-stroma co-evolution: A new paradigm for understanding tumor metabolism, the field effect and genomic instability in cancer cells.* Cell Cycle, 2010. **9**(16): p. 3256-76.
292. Lisanti, M.P., et al., *Understanding the "lethal" drivers of tumor-stroma co-evolution: Emerging role(s) for hypoxia, oxidative stress and autophagy/mitophagy in the tumor microenvironment.* Cancer Biology & Therapy, 2010. **10**(6): p. 537-542.
293. Bhatt, A.N., et al., *Transient elevation of glycolysis confers radio-resistance by facilitating DNA repair in cells.* BMC Cancer, 2015. **15**(1): p. 335.
294. Dwarkanath, B.S., et al., *Heterogeneity in 2-deoxy-D-glucose–induced modifications in energetics and radiation responses of human tumor cell lines.* International Journal of Radiation Oncology*Biology*Physics, 2001. **50**(4): p. 1051-1061.
295. Bol, V., et al., *Reprogramming of tumor metabolism by targeting mitochondria improves tumor response to irradiation.* Acta Oncol, 2015. **54**(2): p. 266-74.
296. Franken, N.A., et al., *Clonogenic assay of cells in vitro.* Nat Protoc, 2006. **1**(5): p. 2315-9.
297. Lu, C.L., et al., *Tumor cells switch to mitochondrial oxidative phosphorylation under radiation via mTOR-mediated hexokinase II inhibition--a Warburg-reversing effect.* PLoS One, 2015. **10**(3): p. e0121046.
298. Bartoletti-Stella, A., et al., *Gamma rays induce a p53-independent mitochondrial biogenesis that is counter-regulated by HIF1α.* Cell Death & Disease, 2013. **4**(6): p. e663.
299. Vander Heiden, M.G., L.C. Cantley, and C.B. Thompson, *Understanding the Warburg effect: the metabolic requirements of cell proliferation.* Science, 2009. **324**(5930): p. 1029-33.
300. Storz, P., *Reactive oxygen species in tumor progression.* Front Biosci, 2005. **10**: p. 1881-96.
301. Sabharwal, S.S. and P.T. Schumacker, *Mitochondrial ROS in cancer: initiators, amplifiers or an Achilles' heel?* Nat Rev Cancer, 2014. **14**(11): p. 709-21.
302. Liou, G.-Y. and P. Storz, *Reactive oxygen species in cancer.* Free radical research, 2010. **44**(5): p. 10.3109/10715761003667554.
303. Lynam-Lennon, N., et al., *MicroRNA-31 modulates tumour sensitivity to radiation in oesophageal adenocarcinoma.* Journal of Molecular Medicine, 2012. **90**(12): p. 1449-1458.
304. Zhang, J.-L., et al., *Methyl-methanesulfonate sensitivity 19 expression is associated with metastasis and chemoradiotherapy response in esophageal cancer.* World Journal of Gastroenterology : WJG, 2015. **21**(14): p. 4240-4247.
305. Flanagan, S.A., et al., *MLH1 deficiency enhances radiosensitization with 5-fluorodeoxyuridine by increasing DNA mismatches.* Mol Pharmacol, 2008. **74**(3): p. 863-71.
306. Davis, T.W., et al., *Defective expression of the DNA mismatch repair protein, MLH1, alters G2-M cell cycle checkpoint arrest following ionizing radiation.* Cancer Res, 1998. **58**(4): p. 767-78.
307. Bucci, B., et al., *Myc Down-Regulation Sensitizes Melanoma Cells to Radiotherapy by Inhibiting MLH1 and MSH2 Mismatch Repair Proteins*. Vol. 11. 2005. 2756-67.
308. Karnak, D., et al., *Combined inhibition of Wee1 and PARP1/2 for radiosensitization in pancreatic cancer.* Clin Cancer Res, 2014. **20**(19): p. 5085-96.
309. An, Q., et al., *C --> T mutagenesis and gamma-radiation sensitivity due to deficiency in the Smug1 and Ung DNA glycosylases.* Embo j, 2005. **24**(12): p. 2205-13.

310. Fernie, A.R., F. Carrari, and L.J. Sweetlove, *Respiratory metabolism: glycolysis, the TCA cycle and mitochondrial electron transport.* Current opinion in plant biology, 2004. **7**(3): p. 254-261.
311. Eng, C.H. and R.T. Abraham, *Glutaminolysis yields a metabolic by-product that stimulates autophagy.* Autophagy, 2010. **6**(7): p. 968-970.
312. Nordsmark, M., et al., *Prognostic value of tumor oxygenation in 397 head and neck tumors after primary radiation therapy. An international multi-center study.* Radiother Oncol, 2005. **77**(1): p. 18-24.
313. Moding, E.J., M.B. Kastan, and D.G. Kirsch, *Strategies for optimizing the response of cancer and normal tissues to radiation.* Nature reviews. Drug discovery, 2013. **12**(7): p. 526-542.
314. Peters, L. and D. Rischin, *Elusive Goal of Targeting Tumor Hypoxia for Therapeutic Gain.* Journal of Clinical Oncology, 2012. **30**(15): p. 1741-1743.
315. Galluzzi, L., et al., *Molecular mechanisms of cisplatin resistance.* Oncogene, 2012. **31**(15): p. 1869-83.
316. Wohlhueter, R.M., R.S. McIvor, and P.G. Plagemann, *Facilitated transport of uracil and 5-fluorouracil, and permeation of orotic acid into cultured mammalian cells.* J Cell Physiol, 1980. **104**(3): p. 309-19.
317. Sommer, H. and D.V. Santi, *Purification and amino acid analysis of an active site peptide from thymidylate synthetase containing covalently bound 5-fluoro-2'-deoxyuridylate and methylenetetrahydrofolate.* Biochem Biophys Res Commun, 1974. **57**(3): p. 689-95.
318. Yoshioka, A., et al., *Deoxyribonucleoside triphosphate imbalance. 5-Fluorodeoxyuridine-induced DNA double strand breaks in mouse FM3A cells and the mechanism of cell death.* J Biol Chem, 1987. **262**(17): p. 8235-41.
319. McGinn, C.J., D.S. Shewach, and T.S. Lawrence, *Radiosensitizing nucleosides.* J Natl Cancer Inst, 1996. **88**(17): p. 1193-203.
320. Bruso, C.E., D.S. Shewach, and T.S. Lawrence, *Fluorodeoxyuridine-induced radiosensitization and inhibition of DNA double strand break repair in human colon cancer cells.* Int J Radiat Oncol Biol Phys, 1990. **19**(6): p. 1411-7.
321. McGinn, C.J., et al., *The role of cell cycle redistribution in radiosensitization: implications regarding the mechanism of fluorodeoxyuridine radiosensitization.* Int J Radiat Oncol Biol Phys, 1994. **30**(4): p. 851-9.
322. Tang, M., et al., *Downregulation of SIRT7 by 5-fluorouracil induces radiosensitivity in human colorectal cancer.* Theranostics, 2017. **7**(5): p. 1346-1359.
323. Macdonald, J.S., et al., *Chemoradiotherapy after surgery compared with surgery alone for adenocarcinoma of the stomach or gastroesophageal junction.* N Engl J Med, 2001. **345**(10): p. 725-30.
324. Lynam-Lennon, N., et al., *MicroRNA-17 is downregulated in esophageal adenocarcinoma cancer stem-like cells and promotes a radioresistant phenotype.* Oncotarget, 2017. **8**(7): p. 11400-11413.
325. Smallwood, H.S., et al., *Targeting metabolic reprogramming by influenza infection for therapeutic intervention.* Cell reports, 2017. **19**(8): p. 1640-1653.
326. Hensley, C.T., A.T. Wasti, and R.J. DeBerardinis, *Glutamine and cancer: cell biology, physiology, and clinical opportunities.* J Clin Invest, 2013. **123**(9): p. 3678-84.
327. Wise, D.R. and C.B. Thompson, *Glutamine addiction: a new therapeutic target in cancer.* Trends in biochemical sciences, 2010. **35**(8): p. 427-433.
328. Wise, D.R., et al., *Myc regulates a transcriptional program that stimulates mitochondrial glutaminolysis and leads to glutamine addiction.* Proceedings of the National Academy of Sciences, 2008. **105**(48): p. 18782-18787.
329. Son, J., et al., *Glutamine supports pancreatic cancer growth through a KRAS-regulated metabolic pathway.* Nature, 2013. **496**(7443): p. 101.
330. Gao, P., et al., *c-Myc suppression of miR-23a/b enhances mitochondrial glutaminase expression and glutamine metabolism.* Nature, 2009. **458**(7239): p. 762.

331. Ahluwalia, G.S., et al., *Metabolism and action of amino acid analog anti-cancer agents.* Pharmacol Ther, 1990. **46**(2): p. 243-71.
332. Huang, Q., et al., *Caspase 3-mediated stimulation of tumor cell repopulation during cancer radiotherapy.* Nature medicine, 2011. **17**(7): p. 860-866.
333. Simon, H.U., A. Haj-Yehia, and F. Levi-Schaffer, *Role of reactive oxygen species (ROS) in apoptosis induction.* Apoptosis, 2000. **5**(5): p. 415-8.
334. Cadenas, E., *Mitochondrial free radical production and cell signaling.* Mol Aspects Med, 2004. **25**(1-2): p. 17-26.
335. Allalunis-Turner, M.J., A.J. Franko, and M.B. Parliament, *Modulation of oxygen consumption rate and vascular endothelial growth factor mRNA expression in human malignant glioma cells by hypoxia.* Br J Cancer, 1999. **80**(1-2): p. 104-9.
336. Turcotte, M., et al., *Variation in mitochondrial function in hypoxia-sensitive and hypoxia-tolerant human glioma cells.* British journal of cancer, 2002. **86**(4): p. 619.
337. Semenza, G.L., *HIF-1: upstream and downstream of cancer metabolism.* Current opinion in genetics & development, 2010. **20**(1): p. 51-56.
338. Goetze, K., et al., *Glycolysis-related gene induction and ATP reduction during fractionated irradiation. Markers for radiation responsiveness of human tumor xenografts.* Strahlenther Onkol, 2013. **189**(9): p. 782-8.
339. Heytler, P.G., *Uncouplers of oxidative phosphorylation.* Methods Enzymol, 1979. **55**: p. 462-42.
340. Tafani, M., et al., *The interplay of reactive oxygen species, hypoxia, inflammation, and sirtuins in cancer initiation and progression.* Oxidative medicine and cellular longevity, 2016. **2016**.
341. Rabbani, Z.N., et al., *Antiangiogenic action of redox-modulating Mn(III) meso-tetrakis(N-ethylpyridinium-2-yl)porphyrin, MnTE-2-PyP(5+), via suppression of oxidative stress in a mouse model of breast tumor.* Free Radic Biol Med, 2009. **47**(7): p. 992-1004.
342. Cortez, M.A., et al., *Therapeutic delivery of miR-200c enhances radiosensitivity in lung cancer.* Mol Ther, 2014. **22**(8): p. 1494-503.
343. Tohme, S., et al., *Hypoxia mediates mitochondrial biogenesis in hepatocellular carcinoma to promote tumor growth through HMGB1 and TLR9 interaction.* Hepatology, 2017. **66**(1): p. 182-197.
344. Ashton, T.M., et al., *The anti-malarial atovaquone increases radiosensitivity by alleviating tumour hypoxia.* Nature communications, 2016. **7**: p. 12308-12308.
345. Semenza, G.L., *Targeting HIF-1 for cancer therapy.* Nat Rev Cancer, 2003. **3**(10): p. 721-32.
346. Hubbi, M.E. and G.L. Semenza, *Regulation of cell proliferation by hypoxia-inducible factors.* American Journal of Physiology-Cell Physiology, 2017.
347. Stordal, B. and M. Davey, *Understanding cisplatin resistance using cellular models.* IUBMB Life, 2007. **59**(11): p. 696-9.
348. Hummel, R., et al., *MicroRNA signatures in chemotherapy resistant esophageal cancer cell lines.* World Journal of Gastroenterology : WJG, 2014. **20**(40): p. 14904-14912.
349. Xie, X.-Q., et al., *Dysregulation of mRNA profile in cisplatin-resistant gastric cancer cell line SGC7901.* World Journal of Gastroenterology, 2017. **23**(7): p. 1189-1202.
350. Shen, D.W., et al., *Cisplatin resistance: a cellular self-defense mechanism resulting from multiple epigenetic and genetic changes.* Pharmacol Rev, 2012. **64**(3): p. 706-21.
351. Adelstein, D.J., et al., *An Intergroup Phase III Comparison of Standard Radiation Therapy and Two Schedules of Concurrent Chemoradiotherapy in Patients With Unresectable Squamous Cell Head and Neck Cancer.* Journal of Clinical Oncology, 2003. **21**(1): p. 92-98.
352. Keys, H.M., et al., *Cisplatin, Radiation, and Adjuvant Hysterectomy Compared with Radiation and Adjuvant Hysterectomy for Bulky Stage IB Cervical Carcinoma.* New England Journal of Medicine, 1999. **340**(15): p. 1154-1161.
353. Tu, L., et al., *Paclitaxel and cisplatin combined with intensity-modulated radiotherapy for upper esophageal carcinoma.* Radiation Oncology, 2013. **8**(1): p. 75.

354. Ilson, D.H., B. Minsky, and D. Kelsen, *Irinotecan, cisplatin, and radiation in esophageal cancer.* Oncology (Williston Park), 2002. **16**(5 Suppl 5): p. 11-5.
355. Boeckman, H.J., et al., *Cisplatin sensitizes cancer cells to ionizing radiation via inhibition of non-homologous end joining.* Molecular cancer research : MCR, 2005. **3**(5): p. 277-285.
356. Myint, W.K., C. Ng, and G.P. Raaphorst, *Examining the non-homologous repair process following cisplatin and radiation treatments.* Int J Radiat Biol, 2002. **78**(5): p. 417-24.
357. Xu, Y., et al., *ABT737 reverses cisplatin resistance by targeting glucose metabolism of human ovarian cancer cells.* International Journal of Oncology, 2018. **53**(3): p. 1055-1068.
358. Catanzaro, D., et al., *Inhibition of glucose-6-phosphate dehydrogenase sensitizes cisplatin-resistant cells to death.* Oncotarget, 2015. **6**(30): p. 30102-30114.
359. Ippolito, L., et al., *Metabolic shift toward oxidative phosphorylation in docetaxel resistant prostate cancer cells.* Oncotarget, 2016. **7**(38): p. 61890-61904.
360. Zhao, F.Q. and A.F. Keating, *Functional properties and genomics of glucose transporters.* Curr Genomics, 2007. **8**(2): p. 113-28.
361. Wu, H.M., et al., *Hypoxia-induced autophagy mediates cisplatin resistance in lung cancer cells.* Sci Rep, 2015. **5**: p. 12291.
362. Guo, Q., et al., *Hypoxia exposure induced cisplatin resistance partially via activating p53 and hypoxia inducible factor-1alpha in non-small cell lung cancer A549 cells.* Oncol Lett, 2018. **16**(1): p. 801-808.
363. Hughes, L.L., et al., *Radiosensitization of cultured human colon adenocarcinoma cells by 5-fluorouracil: effects on cell survival, DNA repair, and cell recovery.* Int J Radiat Oncol Biol Phys, 1992. **23**(5): p. 983-91.
364. Smalley, S.R., et al., *Heterogeneity of 5-fluorouracil radiosensitivity modulation in cultured mammalian cell lines.* Int J Radiat Oncol Biol Phys, 1992. **24**(3): p. 519-25.
365. Balart, J., et al., *Treatment with 5-fluorouracil enhances radiosensitivity of the human pancreatic cancer cell line MiaPaCa-2.* Pancreatology, 2002. **2**(1): p. 40-5.
366. Buckley, A.M., et al., *Characterisation of an Isogenic Model of Cisplatin Resistance in Oesophageal Adenocarcinoma Cells.* Pharmaceuticals, 2019. **12**(1): p. 33.
367. Tahergorabi, Z. and M. Khazaei, *The relationship between inflammatory markers, angiogenesis, and obesity.* ARYA Atherosclerosis, 2013. **9**(4): p. 247-253.
368. Kishimoto, T., et al., *Interleukin-6 family of cytokines and gp130.* Blood, 1995. **86**(4): p. 1243-54.
369. Li, X., et al., *LIF promotes tumorigenesis and metastasis of breast cancer through the AKT-mTOR pathway.* Oncotarget, 2014. **5**(3): p. 788-801.
370. Blanchard, F., et al., *DNA methylation controls the responsiveness of hepatoma cells to leukemia inhibitory factor.* Hepatology, 2003. **38**(6): p. 1516-28.
371. Liu, B., et al., *Leukemia inhibitory factor promotes tumor growth and metastasis in human osteosarcoma via activating STAT3.* APMIS, 2015. **123**(10): p. 837-846.
372. Yu, H., et al., *LIF negatively regulates tumour-suppressor p53 through Stat3/ID1/MDM2 in colorectal cancers.* Nat Commun, 2014. **5**: p. 5218.
373. Kamohara, H., et al., *Leukemia inhibitory factor functions as a growth factor in pancreas carcinoma cells: Involvement of regulation of LIF and its receptor expression.* Int J Oncol, 2007. **30**(4): p. 977-83.
374. Bay, J.M., B.K. Patterson, and N.N. Teng, *Leukemia inhibitory factor downregulates human papillomavirus-16 oncogene expression and inhibits the proliferation of cervical carcinoma cells.* Infect Dis Obstet Gynecol, 2011. **2011**: p. 463081.
375. Chen, D., et al., *LIFR is a breast cancer metastasis suppressor upstream of the Hippo-YAP pathway and a prognostic marker.* Nature medicine, 2012. **18**(10): p. 1511-1517.
376. Morton, S.D., et al., *Leukemia inhibitory factor protects cholangiocarcinoma cells from drug-induced apoptosis via a PI3K/AKT-dependent Mcl-1 activation.* Oncotarget, 2015. **6**(28): p. 26052-26064.

377. Salleh, N. and N. Giribabu, *Leukemia Inhibitory Factor: Roles in Embryo Implantation and in Nonhormonal Contraception.* The Scientific World Journal, 2014. **2014**: p. 201514.
378. Livak, K.J. and T.D. Schmittgen, *Analysis of relative gene expression data using real-time quantitative PCR and the 2(-Delta Delta C(T)) Method.* Methods, 2001. **25**(4): p. 402-8.
379. Metcalf, D., *The unsolved enigmas of leukemia inhibitory factor.* Stem Cells, 2003. **21**(1): p. 5-14.
380. Wysoczynski, M., et al., *Leukemia inhibitory factor: a newly identified metastatic factor in rhabdomyosarcomas.* Cancer Res, 2007. **67**(5): p. 2131-40.
381. Wei, F., et al., *miR-99b-targeted mTOR induction contributes to irradiation resistance in pancreatic cancer.* Molecular Cancer, 2013. **12**: p. 81-81.
382. Brieger, J., et al., *Vascular endothelial growth factor and basic fibroblast growth factor are released by squamous cell carcinoma cells after irradiation and increase resistance to subsequent irradiation.* Int J Mol Med, 2005. **16**(1): p. 159-64.
383. Hardikar, S., et al., *Inflammation and oxidative stress markers and esophageal adenocarcinoma incidence in a Barrett's esophagus cohort.* Cancer epidemiology, biomarkers & prevention : a publication of the American Association for Cancer Research, cosponsored by the American Society of Preventive Oncology, 2014. **23**(11): p. 2393-2403.
384. Ma, D., et al., *Leukemia inhibitory factor receptor negatively regulates the metastasis of pancreatic cancer cells in vitro and in vivo.* Oncol Rep, 2016. **36**(2): p. 827-36.
385. Zhao, J.H., et al., *A novel long noncoding RNA-LOWEG is low expressed in gastric cancer and acts as a tumor suppressor by inhibiting cell invasion.* J Cancer Res Clin Oncol, 2016. **142**(3): p. 601-9.
386. Luo, Q., et al., *LIFR functions as a metastasis suppressor in hepatocellular carcinoma by negatively regulating phosphoinositide 3-kinase/AKT pathway.* Carcinogenesis, 2015. **36**(10): p. 1201-1212.
387. Korc, M. and R.E. Friesel, *The Role of Fibroblast Growth Factors in Tumor Growth.* Current cancer drug targets, 2009. **9**(5): p. 639-651.
388. Honicke, A.S., S.A. Ender, and J. Radons, *Combined administration of EGCG and IL-1 receptor antagonist efficiently downregulates IL-1-induced tumorigenic factors in U-2 OS human osteosarcoma cells.* Int J Oncol, 2012. **41**(2): p. 753-8.
389. Shimizu, T., et al., *Fibroblast growth factor-2 is an important factor that maintains cellular immaturity and contributes to aggressiveness of osteosarcoma.* Mol Cancer Res, 2012. **10**(3): p. 454-68.
390. Luo, W., et al., *P7 peptides targeting bFGF sensitize colorectal cancer cells to CPT-11.* Int J Mol Med, 2014. **33**(1): p. 194-200.
391. Szepietowski, J., et al., *Elevated leukaemia inhibitory factor (LIF) expression in lesional psoriatic skin: correlation with interleukin (IL)-8 expression.* J Dermatol, 2001. **28**(3): p. 115-22.
392. Jiang, D., et al., *Tumour infiltrating lymphocytes correlate with improved survival in patients with esophageal squamous cell carcinoma.* Scientific Reports, 2017. **7**: p. 44823.
393. Pages, F., et al., *In situ cytotoxic and memory T cells predict outcome in patients with early-stage colorectal cancer.* J Clin Oncol, 2009. **27**(35): p. 5944-51.
394. Hwang, W.T., et al., *Prognostic significance of tumor-infiltrating T cells in ovarian cancer: a meta-analysis.* Gynecol Oncol, 2012. **124**(2): p. 192-8.
395. Dieu-Nosjean, M.C., et al., *Long-term survival for patients with non-small-cell lung cancer with intratumoral lymphoid structures.* J Clin Oncol, 2008. **26**(27): p. 4410-7.
396. Gentles, A.J., et al., *The prognostic landscape of genes and infiltrating immune cells across human cancers.* Nature Medicine, 2015. **21**: p. 938.
397. Doyle, S.L., et al., *Visceral obesity, metabolic syndrome, insulin resistance and cancer.* Proc Nutr Soc, 2012. **71**(1): p. 181-9.

398. Ouchi, N., et al., *Adipokines in inflammation and metabolic disease.* Nat Rev Immunol, 2011. **11**(2): p. 85-97.
399. Lysaght, J., et al., *Pro-inflammatory and tumour proliferative properties of excess visceral adipose tissue.* Cancer Lett, 2011. **312**(1): p. 62-72.
400. Chen, Y., et al., *IL-6 signaling promotes DNA repair and prevents apoptosis in CD133+ stem-like cells of lung cancer after radiation.* Radiation Oncology (London, England), 2015. **10**: p. 227.
401. Chen, M.F., et al., *Role of interleukin-6 in the radiation response of liver tumors.* Int J Radiat Oncol Biol Phys, 2012. **84**(5): p. e621-30.
402. Wu, C.-T., et al., *The role of IL-6 in the radiation response of prostate cancer.* Radiation Oncology (London, England), 2013. **8**: p. 159-159.
403. Tamari, Y., G. Kashino, and H. Mori, *Acquisition of radioresistance by IL-6 treatment is caused by suppression of oxidative stress derived from mitochondria after γ-irradiation.* Journal of Radiation Research, 2017. **58**(4): p. 412-420.
404. Matsuoka, Y., et al., *IL-6 controls resistance to radiation by suppressing oxidative stress via the Nrf2-antioxidant pathway in oral squamous cell carcinoma.* British Journal Of Cancer, 2016. **115**: p. 1234.
405. Efimova, E.V., et al., *Radioresistance of Stat1 over-expressing tumour cells is associated with suppressed apoptotic response to cytotoxic agents and increased IL6-IL8 signalling.* International Journal of Radiation Biology, 2009. **85**(5): p. 421-431.
406. Rahal, O.M., et al., *Blocking Interleukin (IL) 4-and IL13-Mediated Phosphorylation of STAT6 (Tyr641) Decreases M2 Polarization of Macrophages and Protects Against Macrophage-Mediated Radioresistance of Inflammatory Breast Cancer.* International Journal of Radiation Oncology* Biology* Physics, 2018. **100**(4): p. 1034-1043.
407. Cavalli, L.R., M. Varella-Garcia, and B.C. Liang, *Diminished tumorigenic phenotype after depletion of mitochondrial DNA.* Cell growth and differentiation, 1997. **8**: p. 1189-1198.
408. Morais, R., et al., *Tumor-forming ability in athymic nude mice of human cell lines devoid of mitochondrial DNA.* Cancer research, 1994. **54**(14): p. 3889-3896.
409. Mantovani, A., et al., *Cancer-related inflammation.* Nature, 2008. **454**(7203): p. 436-44.
410. Mantovani, A., et al., *Macrophage polarization: tumor-associated macrophages as a paradigm for polarized M2 mononuclear phagocytes.* Trends Immunol, 2002. **23**(11): p. 549-55.
411. Balkwill, F., *Tumor necrosis factor or tumor promoting factor?* Cytokine Growth Factor Rev, 2002. **13**(2): p. 135-41.
412. Hodge, D.R., E.M. Hurt, and W.L. Farrar, *The role of IL-6 and STAT3 in inflammation and cancer.* European Journal of Cancer, 2005. **41**(16): p. 2502-2512.
413. Dunne, M.R., et al., *(E)-4-hydroxy-3-methyl-but-2 enyl pyrophosphate-stimulated Vgamma9Vdelta2 T cells possess T helper type 1-promoting adjuvant activity for human monocyte-derived dendritic cells.* Cancer Immunol Immunother, 2010. **59**(7): p. 1109-20.
414. Michielsen, A.J., J.N. O'Sullivan, and E.J. Ryan, *Tumor conditioned media from colorectal cancer patients inhibits dendritic cell maturation.* Oncoimmunology, 2012. **1**(5): p. 751-753.
415. Abdel-Latif, M.M., et al., *Activated nuclear factor-kappa B and cytokine profiles in the esophagus parallel tumor regression following neoadjuvant chemoradiotherapy.* Dis Esophagus, 2005. **18**(4): p. 246-52.
416. Ashton, T.M., et al., *Oxidative Phosphorylation as an Emerging Target in Cancer Therapy.* Clin Cancer Res, 2018. **24**(11): p. 2482-2490.
417. Zacksenhaus, E., et al., *Mitochondrial OXPHOS Induced by RB1 Deficiency in Breast Cancer: Implications for Anabolic Metabolism, Stemness, and Metastasis.* Trends Cancer, 2017. **3**(11): p. 768-779.
418. Jones, R.A., et al., *RB1 deficiency in triple-negative breast cancer induces mitochondrial protein translation.* J Clin Invest, 2016. **126**(10): p. 3739-3757.

419. Peitzsch, C., et al., *Hypoxia as a biomarker for radioresistant cancer stem cells.* Int J Radiat Biol, 2014. **90**(8): p. 636-52.
420. Wang, T., et al., *HIF1alpha-Induced Glycolysis Metabolism Is Essential to the Activation of Inflammatory Macrophages.* Mediators Inflamm, 2017. **2017**: p. 9029327.
421. Saunders, M. and S. Dische, *Clinical results of hypoxic cell radiosensitisation from hyperbaric oxygen to accelerated radiotherapy, carbogen and nicotinamide.* The British journal of cancer. Supplement, 1996. **27**: p. S271-S278.
422. Hirschhaeuser, F., U.G. Sattler, and W. Mueller-Klieser, *Lactate: a metabolic key player in cancer.* Cancer research, 2011. **71**(22): p. 6921-6925.
423. Dolan, R.D., et al., *The relationship between tumour glucose metabolism and host systemic inflammatory responses in patients with cancer: A systematic review.* J Nucl Med, 2018.
424. Jiménez-Valerio, G. and O. Casanovas, *Angiogenesis and Metabolism: Entwined for Therapy Resistance.* Trends in Cancer, 2017. **3**(1): p. 10-18.
425. Vaughan, R.A., et al., *Tumor necrosis factor alpha increases aerobic glycolysis and reduces oxidative metabolism in prostate epithelial cells.* Prostate, 2013. **73**(14): p. 1538-46.
426. Vaughan, R.A., et al., *Tumor necrosis factor alpha induces Warburg-like metabolism and is reversed by anti-inflammatory curcumin in breast epithelial cells.* Int J Cancer, 2013. **133**(10): p. 2504-10.
427. Deans, D.A., et al., *Elevated tumour interleukin-1beta is associated with systemic inflammation: A marker of reduced survival in gastro-oesophageal cancer.* Br J Cancer, 2006. **95**(11): p. 1568-75.
428. Arlt, A., et al., *Autocrine production of interleukin 1beta confers constitutive nuclear factor kappaB activity and chemoresistance in pancreatic carcinoma cell lines.* Cancer Res, 2002. **62**(3): p. 910-6.
429. Dentelli, P., et al., *IL-3 is a novel target to interfere with tumor vasculature.* Oncogene, 2011. **30**: p. 4930.
430. Chiang, C.S., et al., *Effects of IL-3 gene expression on tumor response to irradiation in vitro and in vivo.* Cancer Res, 1997. **57**(18): p. 3899-903.
431. Frendl, G. and D. Beller, *Regulation of macrophage activation by IL-3. I. IL-3 functions as a macrophage-activating factor with unique properties, inducing Ia and lymphocyte function-associated antigen-1 but not cytotoxicity.* The Journal of Immunology, 1990. **144**(9): p. 3392-3399.
432. David, J.M., et al., *The IL-8/IL-8R Axis: A Double Agent in Tumor Immune Resistance.* Vaccines, 2016. **4**(3): p. 22.
433. Yang, W. and J. Yu, *Immunologic Function of Dendritic Cells in Esophageal Cancer.* Digestive Diseases and Sciences, 2008. **53**(7): p. 1739-1746.
434. J Michielsen, A., J. N O'Sullivan, and E. J Ryan, *Recent advances in the development of novel therapeutics targeting dendritic cells.* Recent Patents on Endocrine, Metabolic & Immune Drug Discovery, 2010. **4**(2): p. 146-152.
435. Nicholson, S.E., N. Keating, and G.T. Belz, *Natural killer cells and anti-tumor immunity.* Mol Immunol, 2017.
436. Jiang, X. and D.J. Shapiro, *The immune system and inflammation in breast cancer.* Mol Cell Endocrinol, 2014. **382**(1): p. 673-682.
437. Voos, P., et al., *Ionizing Radiation Induces Morphological Changes and Immunological Modulation of Jurkat Cells.* Frontiers in immunology, 2018. **9**: p. 922-922.
438. Balkhi, M.Y., et al., *T cell exhaustion and Interleukin 2 downregulation.* Cytokine, 2015. **71**(2): p. 339-47.
439. Hadrup, S., M. Donia, and P. thor Straten, *Effector CD4 and CD8 T Cells and Their Role in the Tumor Microenvironment.* Cancer Microenvironment, 2013. **6**(2): p. 123-133.
440. Abbas, G. and M. Krasna, *Overview of esophageal cancer.* Annals of Cardiothoracic Surgery, 2017. **6**(2): p. 131-136.